University at Albany, State University of New York

Scholars Archive

Fall 2024

Advancements in Forensic Analysis: Development of Mass Spectrometric and Chemometric Approaches for the Identification of Synthetic New Psychoactive Substances and Plant Materials

Mónica Ventura
ventura.i.monica@gmail.com

The University at Albany community has made this article openly available.
Please share how this access benefits you.

Follow this and additional works at: https://scholarsarchive.library.albany.edu/etd

 Part of the Chemistry Commons

Recommended Citation

ADVANCEMENTS IN FORENSIC ANALYSIS: DEVELOPMENT OF MASS

SPECTROMETRIC AND CHEMOMETRIC APPROACHES FOR THE IDENTIFICATION

OF SYNTHETIC NEW PSYCHOACTIVE SUBSTANCES AND PLANT MATERIALS

by

Mónica I. Ventura

A Dissertation

Submitted to the University at Albany, State University of New York

In Partial Fulfillment of

the Requirements for the Degree of

Doctor of Philosophy

College of Arts and Sciences

Department of Chemistry

May 2024

being my first friend in the Musah Lab. I am always going to cherish our time sitting next to each other in 229. In addition, thank you to the incredible postdocs I have had the pleasure to work with: Dr. Samira Beyramysoltan, Dr. Parandaman Arathala, Dr. Victor Deklerck, Dr. Allix Coon, and Dr. Oya Urucu. Samira and Victor, thank you for teaching me everything I know about statistical analysis and coding. I would also like to express my gratitude to the current Musah Lab members. Alexa Figueroa, thank you for being one of my closest friends at UAlbany. I am grateful to have someone who is as intelligent and bubbly to share a friendship with. Niara Nichols, I will never forget thinking that you were quiet and shy, only to realize you are just as lively as everyone else in 229. Benedetta Garosi, thank you for not only being a friend, but also for helping me analyze timber samples during your training. To the other members of the Musah Lab who I have had the pleasure to work with: Nana-Hawwa Abdul-Rahman, Mark Katz, and Jessica Hayes: I'm glad to have been a part of your undergraduate/graduate education experiences.

I must also share my appreciation for a few more amazing people. Dana Schroeder and Rosa de Jesus, thank you for welcoming me to the community with open arms. Karen Schupack, thank you for creating the Albany Art Room, a place where I can truly be myself. Jayne, thank you for always motivating me at the gym. Nazaree Newton, my first roommate in community college, you have always been like a sister to me. Dr. Mindy Hair, thank you for being my first friend at UAlbany and for your guidance throughout the years.

ABSTRACT

While forensic science is a well-established discipline, a number of federal agencies have highlighted challenges that continue to plague the field and the extent to which these challenges remain unaddressed. Examples are the illegal trade of wildlife timber and the drug epidemic. Characterization of these materials requires nuanced method development for compound determination, matrix material-specific protocols, and heavy use of expensive consumables. The application of a technique such as direct analysis in real time – high-resolution mass spectrometry (DART-HRMS) provides the opportunity to circumvent many of the challenges presented by conventional methods. In general, little to no sample preparation is required and a consistent sample analysis approach can be applied to most samples. This work explored the development and application of DART-HRMS through the investigation of the identification of New Psychoactive Substances (NPSs), psychoactive plants, and trade-regulated timber. The procedure for rapid structure determination of NPSs combines neutral loss mass spectral information from DART-HRMS data acquired at multiple voltages under collision-induced dissociation (CID) conditions, thereby resulting in varying levels of molecule fragmentation. This approach falls under the umbrella of "data fusion", which is a strategy that combines the output from multiple data sets in order to improve the accuracy of the results. A second focus on psychoactive substances is the development of the Database of Psychoactive Plants (DoPP). This tool is designed to be user-friendly and includes an architecture for identifying plant unknowns. The application is based on the observation that plants display specific chemical signatures that are detectable by DART-HRMS. The subsequent automated machine learning processing of libraries of these spectra enabled the rapid discrimination and identification of species, resulting in a chemical signature database containing 57 available plant species. Another focus of this work is

the development of an analysis approach to be used in a wildlife forensics context. Depending on the species, trade in timber can be totally or heavily restricted. A current technique used by law enforcement to differentiate species of wood is DART-HRMS, coupled with multivariate statistical analysis. Although this method is useful in a laboratory setting, it is impractical in field applications (such as for the determination of timber species identity in shipping containers at ports). The added dimension of wood headspace analysis by solid phase microextraction (SPME) was used to generate data to complement that acquired using the conventional wood analysis technique to facilitate the development of "stand-off" approaches for the differentiation of wood species based on their volatiles profiles.

TABLE OF CONTENTS

TABLE OF FIGURES

LIST OF TABLES

LIST OF SCHEMES

ABBREVIATIONS

ANOVA	Analysis of Variance
ATR-FTIR	Attenuated Total Reflection-Fourier Transform Infrared Spectroscopy
CDA	Canonical Discriminant Analysis
CID	Collision-Induced Dissociation
CIS	Cooling Inlet System
CITES	Convention On International Trade in Endangered Species
CSV	Comma-Separated Values
DAPC	Discriminant Analysis of Principal Components
DART	Direct Analysis in Real-Time
DART-HRMS	Direct Analysis in Real-Time – High-Resolution Mass Spectrometry
DOJ	Department Of Justice
DoPP	Database of Psychoactive Plants
DVB/CAR/PDMS	Divinylbenzene/Carboxen/(Polydimethylsiloxane-Coated)
EI	Electron Ionization
EI-MS	Electron Ionization Mass Spectrometry
ETEC	Emerging Technology and Entrepreneurship Complex
EUTR	European Union Timber Regulation
FDA	Food and Drug Administration
FTIR	Fourier Transform Infrared
GC-MS	Gas Chromatography-Mass Spectrometry
HCA	Hierarchical Clustering Analysis
KDA	Kernel Discriminant Analysis
KNN	K-Nearest Neighbor
LC	Liquid Chromatography
LDA	Linear Discriminant Analysis
LGSR	Luminescent Gunshot Residue
LIBS	Laser-Induced Breakdown Spectroscopy
LOOCV	Leave-One-Out Cross Validation

MDMA	3,4-Methylenedioxymethamphetamine
MPS	Multipurpose Sampler
MSA	Multivariate Statistical Analysis
MSA	Mass Spectrometer
NIJ	National Institute of Justice
NIR	Near-Infrared
NMR	Nuclear Magnetic Resonance
NPS(s)	New Psychoactive Substance(s)
PCA	Principal Component Analysis
PLS-DA	Partial Least Squares-Discriminant Analysis
QTOF	Quadrupole Time-of-Flight
RF	Random Forest
RSD	Relative Standard Deviation
SPME	Solid Phase Microextraction
SVM	Support Vector Machines
SVM-SMOTE	Support Vector Machine-Synthetic Minority Oversampling Technique
TD-GC-MS	Thermal Desorption-Gas Chromatography-Mass Spectrometry
TDU	Thermal Desorption Unit
THC	Tetrahydrocannabinol
TLC	Thin Layer Chromatography
TOF-MS	Time-of-Flight Mass Spectrometer
UKTR	United Kingdom Timber Regulation
UNODC	The United Nations Office on Drugs and Crime
UPGMA	Unweighted Pair Group Method with Arithmetic Mean
USDA	United States Department of Agriculture
USFWL	U.S. Fish and Wildlife Forensic Lab
VIP	Variable Importance in Projection
WDXRF	Wavelength-Dispersive X-Ray Fluorescence

COPYRIGHT PERMISSION

A significant amount of the work presented in this dissertation has been published. Copyright permissions for inclusion of the published work appearing in Chapters 2 and 3 were obtained. The acquired permissions are reproduced below. The published content is included because it involves a significant portion of the research conducted for completion of the Ph.D. requirements.

CHAPTER 1: METHODS FOR THE FORENSIC ANALYSIS OF SYNTHETIC NEW PSYCHOACTIVE SUBSTANCES AND PLANT MATERIALS

1.1. Introduction

In an era marked by unprecedented levels in organized crime, forensic science finds itself at the forefront of combating a diverse array of emerging challenges. From the production and distribution of psychoactive plants and synthetic drugs to the environmental devastation caused by illegal logging, the landscape continues to rapidly evolve. In navigating this complex terrain, forensic scientists are tasked with developing innovative methodologies to rapidly detect, identify, and classify these materials, using various analytical techniques and data-driven approaches to address these pressing concerns. Historically, the chemical interrogation of the diversity of materials that are encountered in a forensic context has been conducted using nuanced method development approaches. This has resulted in a plethora of distinct protocols that are tailored to specific material types or compounds, the development of which is time-, cost-, and resource-intensive. Furthermore, it is not unusual for the developed methods to require several hours or even days to complete. There is also often the need for expensive consumables such as chromatography columns, solvents, and calibration and reference standards.

While the issues associated with the forensic analysis and identification of new synthetic drugs of abuse, plant-based psychoactive substances and wood materials suspected of being illegally trafficked may seem disparate, the analysis challenges that they present are remarkably similar. Accordingly, it is proposed that a unified approach can be developed that addresses the technical issues that routinely confront analysts as they seek to identify these materials. To appreciate the validity of this statement, it is helpful to consider the nature of the problem both from the perspective of the forensic importance of the materials themselves, and the manner in

which they are analyzed and identified currently.

1.1.1. New Psychoactive Substances

The United Nations Office on Drugs and Crime (UNODC) has categorized mind-altering drugs that are not currently controlled under previous drug law conventions as "new psychoactive substances" (NPSs).[1] These substances, often referred to as "legal highs" because they are not yet outlawed, are readily accessible online and pose significant public health risks. NPSs include synthetic cathinones, cannabinoids, tryptamines, opioids, and their structural variants. These designer drugs are readily available for purchase on the internet and are often labelled as "not for human consumption", a designation which not only belies their intended purpose, but shields them from Food and Drug Administration (FDA) scrutiny. The emergence of NPSs has imposed unique challenges on crime labs, primarily because law enforcement agencies have been unable to keep abreast of the rapid influx of novel structural variants that appear on the market within days to weeks after earlier generations of synthetic structures have been scheduled.[2–11] Although the UNODC has the ability to schedule and ban newly discovered psychoactive materials, the process of presenting a compelling case for scheduling can be lengthy, lasting from months to years. A major contributor to this bottleneck is the necessity that the structure of the unknown NPS be identified. This has proven to be challenging due to the rapid emergence of structural variants and the significant time, equipment and human resources required for full structural characterization. Thus, manufacturers rapidly respond to the scheduling of specific synthetics by releasing novel structural variants, knowing that there will be few if any repercussions for the marketing of these substances.[5,6,11] In the case of synthetic cathinones, the National Drug Intelligence Center has noted that "no substantial law enforcement or regulatory action has significantly prevented synthetic cathinone products from reaching distributors or consumers".[12] Among the repercussions

of the use of these substances are their impacts on human health, as well as the criminal offenses committed by individuals while under their influence. Cathinones serve as a case in point. The devastating physiological effects of synthetic cathinones include hyperthermia, severe psychosis, increased body temperature, cardiac and neurological problems and death.[2,13–21] For example, negative medical impacts (including fatalities) have been attributed to 1-phenyl-2-(1-pyrrolidinyl)-1-propanone (α-pyrrolidinopropiophenone), 2-(methylamino)-1-(4-methylphenyl)-1-propanone (mephedrone), and 1-(1,3-benzodioxol-5-yl)-2-(1-pyrrolidinyl)-1-pentanone (3,4-methylenedioxy pyrovalerone), three compounds which possess significant structural differences, while having in common the core cathinone scaffold.[15,17,18,20,21] Synthetic tryptamines, such as 5-methoxy-*N*,*N*-di-2-propen-1-yl-1H-indole-3-ethanamine (5-methoxy-DALT) also cause severe agitation and cardiac problems, even in small doses.[11,22] It has also been observed that abusers often ingest multiple classes of drugs simultaneously, such as mixtures of tryptamines and synthetic cathinones.[23] Synthetic cannabinoids that have recently appeared on the drug market have resulted in hospitalizations due to alterations in mental status, tachycardia, loss of consciousness, and death.[7,24–26] Also attributed to synthetic cannabinoids was an outbreak in New York City where 33 individuals were simultaneously all under the influence of *N*-[[1-[(4-fluorophenyl)methyl]-1H-indazol-3-yl]carbonyl]-L-valine, methyl ester (AMB-FUBINACA), which caused them to behave as "zombies".[25] In this case, a comprehensive metabolic panel and analysis of the patients' urine revealed no abnormalities or presence of amphetamines, methadone, tetrahydrocannabinol (THC), barbiturates, benzodiazepines, tricyclic antidepressants, or serum ethanol.[25] Abuse of synthetic opioids has also been on the rise, leading to fatalities, especially when ingested in combination with heroin.[10,27–29]

1.1.2. Psychoactive Plants

In addition to NPSs, the ease of access to psychoactive plants also presents various challenges. There are over 400 species of plants that are purported to be psychoactive.[30] Yet in most countries, less than 5% of these are scheduled. With the advent of internet commerce, these products are readily acquired from around the world and legally traded. Their regulation is difficult to accomplish in part because of the paucity of standardized protocols for detecting and characterizing their psychoactive constituents. These plants have diverse chemical compositions and visual resemblance to benign materials, complicating their identification. Furthermore, their chemical profiles can vary significantly depending on factors such as growing conditions and preparation methods. The broad range of these substances often requires nuanced method development for their definitive identification, projects which crime labs are often ill-equipped to undertake in terms of time and resources. This underscores the pressing need for innovative analytical strategies for the analysis of complex plant matrices.

Developing comprehensive techniques that can reliably identify the specific psychoactive constituents in these plants is crucial not only for regulatory compliance purposes, but also for ensuring public safety, and preventing the dangers that accompany the misuse of these substances. For instance, in the 2013 report "The Challenge of New Psychoactive Substances", the UNODC delineated a roster of twenty plants containing psychoactive constituents, attributing their inclusion on the list to escalating instances of recreational misuse and the potential for addiction.[1] The species as well as their common names are listed in Table 1.1. While the molecular constituents of some of these plants are not well-characterized, several are well-researched and have known psychoactive components. For example, *Piper methysticum* (Kava) (Figure 1.1) contains a group of structurally related compounds commonly known as kavalactones (Figure 1.2) including the psychoactive yangonin, in addition to major compounds such as, dihydrokawain, kawain, and

Table 1.1 Mind-altering plant species listed by the UNODC as "plants of concern".

Species Name	Common Name
Argyreia nervosa	Hawaiian Baby Woodrose
Banisteriopsis caapi	Ayahuasca
Calea zacatechichi	Dream Herb
Catha edulis	Khat
Datura stramonium	Datura
Ipomea spp.	Morning Glory
Leonotis leonurus	Lion's Tail/Wild Dagga
Lophophora williamsii	Peyote or Peyote cactus
Mimosa hostilis	Mimosa
Mitragyna speciosa	Kratom
Nymphaea caerulea	Blue Egyptian Water Lily
Peganum harmala	Syrian Rue
Picralima nitida	Akuamma seed
Piper methysticum	Kava
Psychotria viridis	Chacruna
Salvia divinorum	Salvia
Sceletium tortuosum	Kanna
Turnera diffusa	Damiana
Voacanga africana	Small-Fruit Wild Frangipani
Lactua virosa	Wild Lettuce

desmethoxyyangonin which are known to induce psychoactivity and/or have toxic liver effects. Similarly, *Mitragyna speciosa* (Kratom) (Figure 1.1) contains the psychoactive alkaloids mitragynine and 7-hydroxymitragynine. These plants are challenging to identify in a forensics context because of their visual resemblance to innocuous materials such as food and spices that do not exhibit psychoactive effects.[1,31]

Of the twenty plants identified by the UNODC, only *Catha edulis* (Khat) and *Lophophora williamsii* (Peyote or Peyote cactus) have attained controlled substance status at the federal level in the United States, leaving the remainder unregulated.[32,33] This is due in part to the absence of standardized protocols for the precise and efficient detection and characterization of the psychoactive compounds that they contain, or the fact that in some cases, the psychoactive constituents remain unknown. This means that in the case of the latter, there are no known chemical constituents that can

Figure 1.1 Photographs of the psychoactive plant materials *Piper methysticum* (left) and *Mitragyna speciosa* (right).
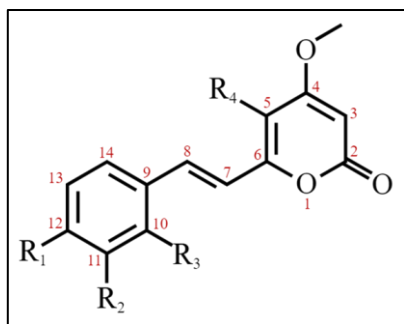
Figure 1.2 Core structure of kavalactone.

serve as the basis for positive identification of the plant material. The identification of these psychoactive plants is further complicated by the range of forms in which they are encountered, including roots, seeds, and leaves, that may have undergone further processing to generate powders, capsules, and tinctures. There is a pressing need for the development of standardized analytical protocols and comprehensive databases that can accurately identify and characterize these plants along with their psychoactive constituents. This would facilitate more effective regulation, helping to mitigate the risks associated with their misuse.

1.1.3. Timber

Another dimension to the forensic analysis of flora is the challenge of illegal logging. This leads to many global issues, including ecological and economic damage.[34] Many significant timber species around the world are economically important because of the rich beauty of their wood, in combination with favorable wood mechanical characteristics, which makes these species highly prized for furniture, musical instruments, decorative materials, and artisanal crafts.[35] Consequently, many high-value tree species are specifically targeted. Approximately 10-30% of timber is illicitly harvested worldwide, increasing to 50 to 90% when focusing on wood from tropical areas, and it is estimated to have a global cost of $52 billion to $117 billion per year.[34] Forests around the world continue to be the primary means by which to counteract climate change and support sustainable development. Deforestation is the cause of 17% of man-made emissions, which is 50% more than sea, air, and land transport combined because it releases stored carbon from trees into the atmosphere and reduces the capacity of forests to absorb CO_2.[36] Moreover, globally, only approximately 10% of natural forests remain undisturbed. Without forests, there

would be loss of water supplies, biodiversity, pharmaceuticals, recycled nutrients for agriculture, and reduction of flood prevention, all of which are imperative for a sustainable economy.[36]

The Convention on International Trade in Endangered Species (CITES) was created to address the conservation of imperiled wildlife by controlling their trade. Regulation status is defined by appendices: CITES Appendix I species are threatened with extinction, and thus, all forms of trade are illegal; CITES Appendix II species are threatened in the wild and international trade is controlled to aid in their survival; and CITES Appendix III species are regulated by a particular nation.[37] Additional regulations, such as the US Lacy Act, the European Union Timber Regulation (EUTR), and the United Kingdom Timber Regulation (UKTR) have also been devised to aid in the survival of species. Consequently, trade is either completely prohibited or heavily restricted depending on the species. These national and international laws place the onus on the importer to carry out due diligence to ensure that the timber that they procure is legal to trade.

Illegal loggers are able to avoid prosecution by falsifying documents, harvesting out of season or outside of concession boundaries, and through customs fraud in order to deceive law enforcement. For this reason, law enforcement agencies and national authorities require practical mechanisms to keep up with the complexity of these challenges. Effective management of this problem will ultimately contribute to the preservation of the world's forests and the sustainability of biodiversity and the timber trade.

1.2. Conventional Approaches for the Forensic Analysis of Complex Materials

1.2.1. Conventional Analysis—Drugs of Abuse

Conventional analysis methods, including chromatography, mass spectrometry, and various forms of spectroscopy, are essential tools in forensic laboratories, and each has specific advantages. However, for a variety of reasons, they are generally less than ideal for the

characterization of NPSs. A major issue is the difficulty of determining the structures of unknowns as they emerge, given not only the rapidity with which they flood the market, but also the time, analytical instrumentation, human resource expertise and financial investments required to accomplish this task. Crime laboratories that do undertake structure elucidation studies of suspected psychoactive unknown products rely on a variety of methods. These include colorimetric assays, thin layer chromatography (TLC), liquid chromatography (LC), gas chromatography-mass spectrometry (GC-MS), and Fourier transform infrared (FT-IR) and nuclear magnetic resonance (NMR) spectroscopies, among others.[38–45] The UNODC has created manuals of recommended methods to identify seized materials, including a guide for analysis of synthetic cathinones and synthetic cannabinoids that lists over 15 different approaches that can be employed for identification.[38,46] While these are useful, they still require optimization in terms of selecting the ideal analytical technique and conditions to be used. Other challenges associated with this effort include the amount of sample needed for analysis, and the nuanced attributes of various molecule classes when subjected to some of the most common techniques used for identification. For example, synthetic cathinones are well-known to fragment so extensively by electron ionization (EI) MS (the mainstay of most crime labs) that the data generated have limited usefulness.[47,48] Cathinones typically fragment by α-cleavage resulting in the appearance of prominent peaks representing common iminium and acylium ions, while the molecular ion peak is often absent. The result is that cathinones of very different structure can have remarkably similar but uninformative EI mass spectra.[47–49] For example, 1-(1,3-benzodioxol-5-yl)-2-(methylamino)-1-pentanone (pentylone) and 1-(1,3-benzodioxol-5-yl)-2-(ethylamino)-1-butanone (eutylone) have remarkably similar EI mass spectra as illustrated in Figure 1.3. Both spectra display base peaks at *m/z* 86 and similar fragmentation with few diagnostic fragment ions. This high degree of similarity makes it
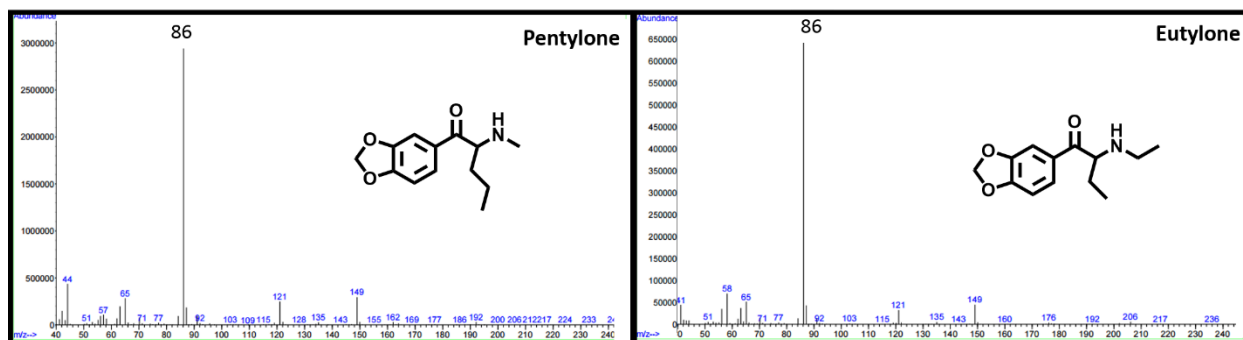
Figure 1.3 EI mass spectra of the synthetic cathinones pentylone and eutylone. The spectra share the base peak at of *m/z* 86 and are remarkably similar, with few diagnostic fragment ions that can be used to distinguish between them.

challenging to identify them based on MS fragmentation patterns. This is also true for other classes of molecules including synthetic cannabinoids. Even when MS is coupled with GC, the retention time information acquired is often of limited utility for novel compounds whose retention times have not been established. IR spectroscopy can alert the analyst to the presence of diagnostic structural features that imply the presence of a certain class of molecule, but it does not supply definitive structural information. Analysis by NMR spectroscopy, albeit a powerful structure elucidation technique, is uncommon at most crime labs because of a lack of equipment and requires relatively high concentrations of purified samples that are readily solubilized. This combination of factors remains a formidable barrier to the routine practice by crime labs of structure elucidation of NPS variants. The determination of the structure of 1-(4-fluorophenyl)-2-(pyrrolidin-1-yl)octan-1-one (4-fluoro-PV9) from samples seized by police in southern Poland is instructive. Majchrzak et al. first conducted two mass spectrometry experiments using HPLC-MS and HPLC-MS-MS.[50] After performing these analyses, they made the working assumption that the compound was a synthetic cathinone based on the appearance of an $[M+H^+ - H_2O]^+$ peak, citing this to be a "well-known characteristic of cathinone derivatives." Based on this information, GC-EI-MS was performed to piece together the structure of the new cathinone derivative. NMR was also required to determine the position of the fluorine atom on the aromatic ring.[50]

Further complicating matters is the fact that psychoactive plants and/or other psychoactive substances rarely appear on the market as purified compounds, but rather as complex plant matrices or mixtures comprised of cutting agents and diluents, among other components. To identify them, the mixture must not only be separated, but the unknown must then be structurally characterized and unequivocally identified. After receiving samples of evidence seized in criminal investigations, Shevyrin et al. determined the structures of five new derivatives of indole-3-carboxylic acid from the results of a series of MS, IR, and NMR experiments.[51] Though all five had similar fragmentation patterns, it was not immediately apparent what modifications had been made to the core scaffold. Thus, 2D NMR experiments were performed on both of the unknown compounds, and related representative compounds for comparison.[51] In one such seized product, the new drug *N*,5-dimethyl-*N*-(1-oxo-1-(*p*-tolyl)butan-2-yl)-2-(3-(*p*-tolyl)ureido)benzamide was discovered. Unable to match its GC-MS characteristics to any known compounds, Uchiyama et al. had to determine the structure via a lengthy series of NMR and MS experiments.[52] By utilizing a combination of DART-TOF-MS, 1D ^{1}H and ^{13}C NMR, DQF-COSY, HMQC, and HMBC, they were finally able to determine the structure of this new variation of 4-methylbuphedrone.[52] This example illustrates how newer MS techniques such as DART-MS are making their mark in forensic drug characterization.

1.2.2. Conventional Analysis—Timber

Various methods have been developed to address the challenge of species identification of wood samples. Among these, wood anatomical analysis stands out as the most prominent approach. A wood anatomist identifies species based on their distinctive macroscopic and microscopic features. While this method works quite well for differentiating between genera, distinguishing between species within the same genus can prove to be difficult due to similarities
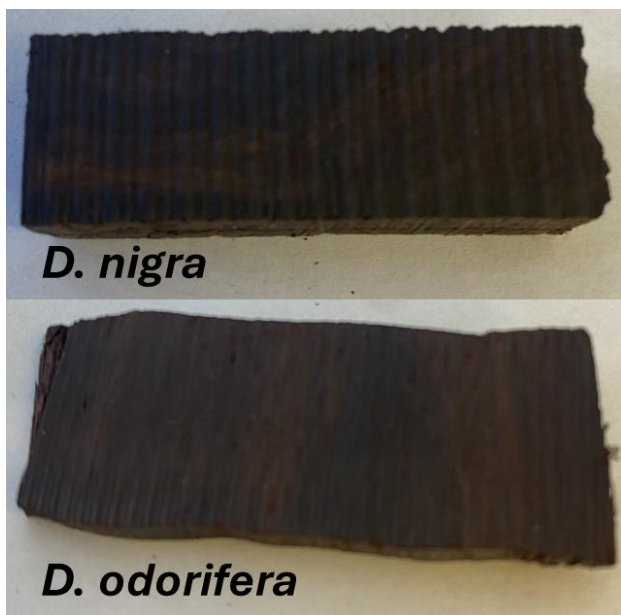
Figure 1.4 *Dalbergia nigra* (top) and *D. odorifera* (bottom), which are two endangered tree species that show visual similarities.

in their anatomical features. For example, Figure 1.4 shows an image of *Dalbergia nigra* (a CITES appendix I species) on the top and *D. odorifera* (a CITES appendix II species) on the bottom, which are too similar to visually distinguish. An alternative method is DNA analysis which, while promising, presents significant drawbacks including laborious procedures, time intensiveness, and high costs. Furthermore, the efficacy of DNA analysis hinges on the successful extraction of intact DNA from wood, a process complicated by the tendency of DNA in felled wood to be extensively fragmented, rendering it unsuitable for DNA sequence-based identification.[35,53,54]

An alternative cost-effective and rapid method for species identification involves the use of Near-Infrared (NIR) spectroscopy. This technique enables non-destructive analysis of timber, leveraging the unique spectral features of the molecules in the wood which are then further differentiated with high accuracies using multivariate statistical analysis.[55–57] Despite the promising results reported in various studies, NIR spectroscopy has several limitations, including limited spot size, wavelength range, and resolution.[55] These constraints can prevent the capture of all the spectral details necessary for differentiation, resulting in significant challenges for comprehensive species identification across a broad range of species. Additionally, the development of a more comprehensive wood identification database is hindered by the small

11

sample sizes used in existing studies, the inherent variability among wood species and the need for extensive, high-quality data collection.

One current technique employed by law enforcement agencies involves direct analysis in real time – high-resolution mass spectrometry (DART-HRMS), complemented by multivariate statistical analysis. Despite the demonstrated utility of this approach, its inability to facilitate on-site timber analysis represents a significant drawback stemming from time-consuming sample collection and transportation to off-site laboratories. Conducting analyses on site and in real time is highly desirable and would offer optimal efficiency, as it would eliminate the need to transport timber from shipping ports to laboratories for analysis, and yield considerable savings in both time and resources.

1.3. Summary and Outlook

An innovative strategy to address the aforementioned challenges involves developing a methodology that considers complex matrices and leverages the composite of a material's distinctive chemical attributes for identification, rather than relying solely on the presence of a single component, as currently practiced. The adoption of this approach has been slow due to the large volumes of complex data that would need to be produced and surveyed, and the perceived processing challenges. However, recent advances in big-data processing and the availability of the necessary computing power for developing machine learning models based on chemical profiles, offer a viable pathway to overcome these obstacles.

With regard to the type of chemical data that would lend itself to the adoption of such an approach, DART-MS provides a promising solution for the rapid screening and classification of NPSs, psychoactive plants, and wood materials. By revealing the molecular profiles of samples, DART-HRMS provides highly informative spectra. If similar substances exhibit chemically

specific molecular profiles that are distinguishable from those of other materials, then subjecting

the chemical profile data to multivariate statistical analysis (MSA) can efficiently differentiate and

identify these substances. This method leverages unique molecular signatures to provide a robust

identification mechanism. Furthermore, applying multiple analytical techniques to the same

sample can yield distinct but complementary datasets. By combining the data that is furnished by

multiple methods (i.e., fusing) and subjecting it to MSA, significant enhancement of the accuracy

of the developed prediction models can be achieved. This integrated approach maximizes the

reliability of sample identification, and these methodologies are discussed in detail below.

1.3.1. DART-HRMS

First described in the literature in 2005,[58] DART-MS was one of the two methods that

ushered in a new era for ambient ionization mass spectrometry. Prior to this development, most

mass spectrometry was performed under vacuum conditions, which greatly restricted the diversity

of analytes and sample matrices that could be analyzed. DART-MS introduced the capability to

analyze samples in their native forms under ambient conditions (i.e., room temperature and

pressure) and in open air. The "DART" refers to the ion source. This ion source can ionize

materials under standard temperature and pressure conditions, significantly extending the range of

sample types that can be interrogated, and eliminating the need for vacuum. Figure 1.5 provides

an illustration of the DART ion source. It consists of a tube containing multiple chambers. The

first has a glow discharge (i.e., a plasma) into which a gas (typically helium) is introduced. Within

the tube are a cathode and an anode where an electrical potential initiates an electrical discharge,

producing ions, electrons, and excited-state species (i.e., metastable helium states). The gas then

flows into the second chamber where a second perforated electrode removes ions from the gas

stream and the gas flow then passes through the third region that can be heated and directed toward
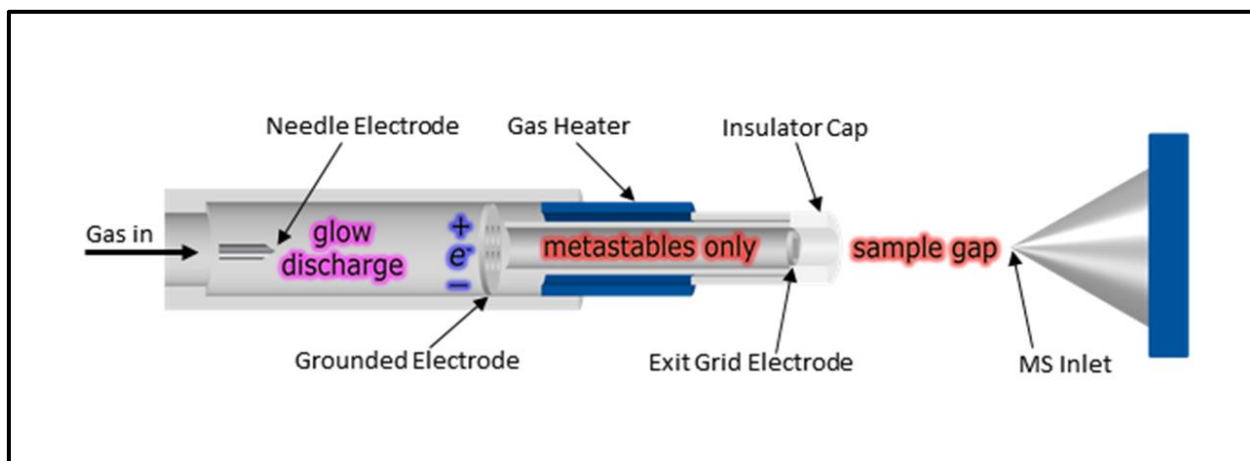
Figure 1.5. View of the DART ion source and MS inlet, illustrating the gas flow through several chambers. In the first chamber, a glow discharge between the needle electrode and the grounded electrode produces ions, electrons, and excited-state (metastable) atoms. These metastable atoms then pass through an optional heater and exit into the sample open air gap between the DART ion source and MS inlet.

the mass spectrometer sampling orifice. The metastable atoms in the gas flow that exit the ion source react with water molecules present in the atmosphere to form ionized water clusters that engage with analytes present in the sample, creating ions influenced by factors such gas composition, ion polarity, and the presence of dopants.[58]

Different ionization mechanisms can occur depending on the type of sample being analyzed and the polarity of the ions formed. In positive ion-mode, the primary mechanism involves proton transfer. The metastable helium atoms formed by the DART ion source react with atmospheric water to produce ionized water clusters. These clusters then transfer a proton to the analyte to form a protonated molecule (Figure 1.6). In negative ion mode, the primary ionization

$$He(2^3S) + H_2O \rightarrow H_2O^{+\bullet} + He(1^1S) + e^-$$

$$H_2O^{+\bullet} + H_2O \rightarrow H_3O^+ + OH^\bullet$$

$$H_3O^+ + nH_2O \rightarrow [(H_2O)_{n+1}\,H]^+$$

$$[(H_2O)_n H]^+ + M \rightarrow MH^+ + nH_2O$$
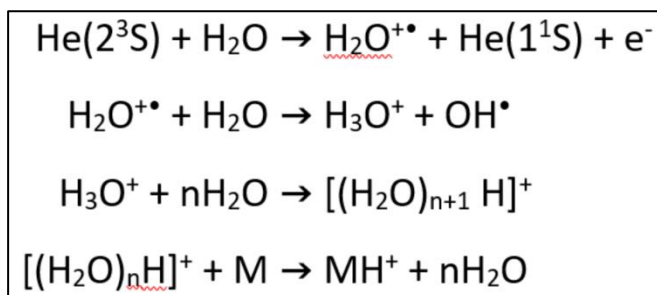
Figure 1.5 Equations illustrating formation of positive ions by proton transfer via DART, where S is the sample.

mechanism is deprotonation (see Figure 1.7). Metastable helium atoms interact with a neutral species (N) (i.e., the grid electrode) to generate electrons through Penning ionization. The resulting electrons are quickly thermalized through collisions with

$$M^* + N \rightarrow \underline{N}^{+\bullet} M + e^-$$

$$e^{-*} + G \rightarrow e^- + G^*$$

$$e^- + O_2 \rightarrow \underline{O_2}^{-\bullet}$$

$$O_2^{-\bullet} + S \rightarrow [S-H]^- + OOH^\bullet$$

$$O_2^{-\bullet} + S \rightarrow S^{-\bullet} + O_2$$

$$O_2^{-\bullet} + S \rightarrow [S + O_2]^{-\bullet*} + G \rightarrow [S + O_2]^{-\bullet} + G^*$$
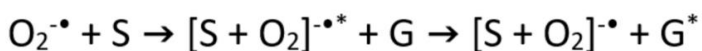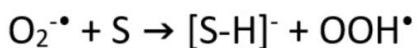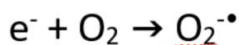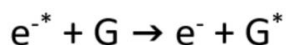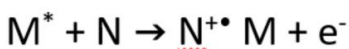
Figure 1.6 Equations illustrating formation of negative ions by DART, where N is a neutral species, G is the atmospheric gases, and S is the sample.

atmospheric gases (G) and subsequently react with gaseous oxygen to form oxygen anions. These anions then react with sample molecules (S) to generate analyte negative ions. The understanding of these different ionization mechanisms is crucial when determining which is best to use for a specific analyte and interpreting the data. For example, in positive ion mode, only analytes with proton affinities greater than that of water will be ionized, while in negative ion mode, analytes must have relatively low proton affinities to undergo deprotonation.

The DART source is commonly integrated with various mass analyzers, with a high-resolution time-of-flight mass spectrometer (TOF-MS) being a frequent choice to enhance selectivity and provide accurate elemental composition determination through exact mass measurements.[58] The difference in ionization mechanisms also means that the output from the mass spectrometer differs from that of electron ionization mass spectrometry (EI-MS). In EI-MS, ionization is typically achieved by electron collision at 70 eV, which results in formation of ion radicals, and significant fragmentation of the analyte. On the other hand, DART-MS tends to produce intact protonated or deprotonated precursor molecules due to the softer ionization process, allowing for analysis of the molecular profile of complex matrices. The output of a typical DART-MS analysis of a complex matrix is a comprehensive spectrum representing a wide range of molecules. This spectrum provides a chemical fingerprint signature of the matrix, revealing its diverse molecular components in a single experiment. Depending on the matrix, the spectrum can

include a variety of compounds, each contributing to the overall chemical profile. The detailed molecular information is essential for applications that require precise identification and characterization of complex matrices.

Several sampling methodologies are available for DART-HRMS analyses of various forms of matter, such as solids, liquids, and gases. If the appropriate mass analyzer is used, the instrument can achieve nanogram detection limits, making it highly efficient in instances where sample quantity is limited. Also, because the sampling takes place outside of the mass analyzer (as opposed to having to be transferred into the instrument, samples can be in a variety of forms. For solid irregularly-shaped samples, one approach entails introducing the material into the DART gas stream using a pair of tweezers. This is convenient for examination of bulk materials including plant components part such as roots, seeds, and leaves. Conversely, an alternative technique involves the insertion of the closed end of a glass melting capillary tube into the sample and presenting the coated surface of the tube to the open-air sampling gap between the ion source and the MS inlet (Figure 1.8). This method is effective for the analysis of liquids, powders, and homogenized materials. For analytes that have been adsorbed onto sorbent materials such as is the case when concentrating headspace volatiles using solid-phase microextraction (SPME) fibers, the fibers can be sampled by

Figure 1.7 Capillary tube suspended between the DART ion source and the MS inlet after being exposed to a powdered sample.

Figure 1.8 SPME fiber suspended between the DART ion source and the MS inlet (while being held using a SPME fiber holder. Analytes adsorbed to the fiber are desorbed in the heated DART gas stream and ionized before entering the MS inlet.

introducing them directly into the heated DART gas stream, where the compounds are desorbed and ionized prior to entering the MS inlet (Figure 1.9).

There are numerous forensic applications of DART-MS, including its use as a screening tool for psychoactive materials.[11,31,48,59–81] Analysis is rapid (in less than one minute) and numerous sample types can be analyzed with little to no sample preparation.[81] Nie et al. demonstrated that DART-MS could be used as a rapid screening method for the 11 NPSs that they analyzed in their study, including four cathinones, one phenethylamine, and six cannabinoids.[80] These NPSs were then also separated and detected using LC/QTOFMS for accurate structure determination by an independent method.[80] Gwak et al. used a DART ion source coupled to a quadrupole time-of-flight (QTOF) mass spectrometer to analyze 35 NPSs, which included a range of cannabinoids, cathinones, and one phenethylamine, with results suggesting that this method can be used for rapid screening and characterization of these types of compounds.[81] Included in the numerous forensic applications of DART-MS is its use as a screening tool for species identification based on metabolome profiles.[53,54,61,82–87] For instance, Deklerck et al. conducted direct analyses of slivers from various wood species and constructed a Random Forest classification model based on their chemical

distinctions, with an accuracy of 82%.[54] The U.S. Fish and Wildlife Forensic Lab has also embraced a similar methodology for practical use in casework scenarios, which involves screening of the DART mass spectra of seized wood samples against a comprehensive database of wood species, achieving accuracies exceeding 90%.[88,89]

1.3.2. Solid-Phase Microextraction

While the preference for minimal sample preparation steps is of recognized importance in forensic analysis, certain procedures for sample collection and pretreatment are often considered to be essential. An illustrative instance is the utilization of solid-phase microextraction (SPME) fibers, which can play a critical role in concentrating volatiles for subsequent analysis using diverse instrumental techniques.[90–92] These fibers, coated with a sorbent material, concentrate headspace volatiles within a closed system via adsorption to the sorbent. Prior to analysis, the SPME fiber must undergo a crucial conditioning step, involving exposure to a stream of inert gas (e.g., nitrogen) at an elevated temperature (i.e., 250 °C) for thirty minutes, in order to desorb any chemicals present in the environment that are not directly associated with the analysis of the material of interest. This procedure ensures that the volatiles detected in the subsequent analysis originate solely from the target sample, effectively eliminating any potential interference from extraneous analytes to which the fiber may have been exposed prior to the concentration step.

The application of SPME fiber-assisted analysis has emerged as a significant tool in facilitating the detection of headspace volatiles associated with the presence of illicit substances such as 3,4-methylenedioxymethamphetamine (MDMA) and cocaine.[93–96] Moreover, the application of SPME fiber-assisted analysis has been extended to the identification of cannabis.[97,98] Beyond the domain of illicit substances, the concentration of headspace volatiles on SPME fibers, followed by subsequent mass spectrometric and/or spectroscopic analysis, has proven valuable in

the identification of innocuous non-psychoactive plant materials.[99–102] Additionally, empirical studies have demonstrated the discriminatory capacity of headspace volatiles in distinguishing natural aromas from the fragrances of many spices.[99–101,103] These collective findings underscore the potential utility of this approach for "stand-off" analysis, where materials can be analyzed from a safe distance. The development of such methods could serve as a tool for crime scene investigators to detect hazardous compounds in a safe manner by identifying characteristic volatile compound signatures, including those associated with legal high synthetic substances and plant products.

1.3.3. Multivariate Statistical Analysis

Of key importance in the utilization of chemical data is its processing by multivariate statistical analysis (MSA), as it is a mechanism by which patterns in the data that can serve as the basis for making accurate class predictions can be accomplished. MSA is a powerful tool used to analyze complex datasets by examining multiple variables simultaneously. It facilitates the identification of patterns, relationships, and structures within the data that may not be evident when considering variables individually. MSA is essential in fields such as forensic chemistry, where data complexity and the need for accurate interpretation are of paramount importance. These techniques can be broadly categorized into two main types: unsupervised and supervised methods, as illustrated in Figure 1.10. Unsupervised methods are typically the first step in data analysis. These methods facilitate the exploration and detection of similarities and differences within data without using pre-assigned class labels. Principal Component Analysis (PCA) and Hierarchical Clustering Analysis are two examples of unsupervised methods. On the other hand, supervised methods are used for classification, where models are constructed based on labeled training data. Examples of supervised methods include Random Forest (RF), Support Vector Machines (SVM),
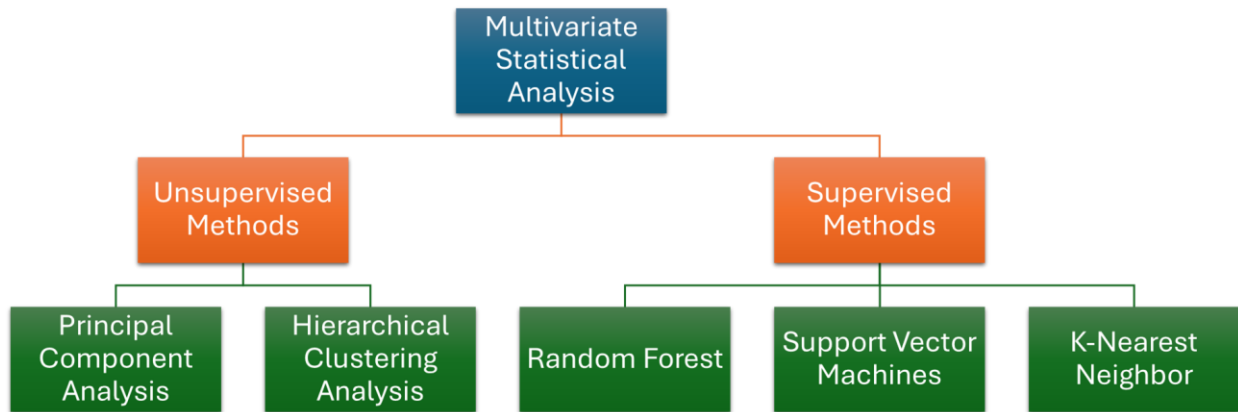
Figure 1.9 Supervised and unsupervised statistical analysis techniques.

and K-Nearest Neighbor (KNN). These methods are advantageous because they provide a systematic approach to analyzing and classifying data, making it possible to draw meaningful conclusions from complex datasets.

1.3.3.1. Forensic Applications of Multivariate Statistical Analysis Techniques

The utility of MSA for the processing of forensically relevant data has become more commonplace. It is inherently advantageous for the analysis of NPSs for characterization and classification purposes.[11,48] Setser et al. demonstrated this to be true by using MSA tools for analysis of synthetic phenethylamine and tryptamine GC-MS data.[104] It was shown that principal component analysis (PCA), an unsupervised exploratory technique that is applied to reduce the dimensionality of data, could be used as an objective method for variable selection (i.e. a method of choosing the subset of data points that can be relied upon to provide the highest prediction accuracy model). A classification model could then be created using these variables. In this case, linear discriminant analysis (LDA) was used to develop a classification model. LDA is a supervised technique, which means that the classes used in the model are assigned so that between-class variance is maximized, while within-class variance is minimized. The resulting model exhibited a prediction accuracy of 86% for the classification of phenethylamines and

tryptamines.[104] Another study applied MSA to the ion abundances observed in the electron ionization (EI) mass spectra of six phenethylamine isomers. In this case, the performance of PCA was followed by the application of the classification model "canonical discriminant analysis" (CDA), a supervised technique that determines how to separate and discriminate between groups in the most efficient way possible. Among the issues that arose in this study were that spectra created from lower concentration samples were irreproducible, and that the spectra of several of the compounds did not exhibit molecular ion peaks.[105] These challenges, which, depending on the compound class, can be quite common with EI mass spectra, can be circumvented by using alternative MS techniques like DART-MS, which can provide a more comprehensive dataset for multivariate statistical analysis. This is because DART-MS analysis is typically conducted under soft ionization conditions, and when fragmentation is induced, it can be made to occur at ionization energies well below the 70 eV used to generate conventional EI mass spectra. The molecular ion equivalent, which in the case of DART-MS (performed in positive ion mode), is usually the unfragmented protonated precursor molecule, is generally always observed. Furthermore, because samples can be analyzed directly in their native form, there is no need for them to be solubilized, and therefore the challenge of not detecting MS signals because the solution concentration of the analyte is too low, is avoided. Thus, the increased reproducibility of DART mass spectra, along with the observation of a greater number of prominent diagnostic peaks for a variety of classes of molecules, make the spectra themselves highly amenable to MSA if the purpose is sample identity prediction and pattern recognition.

There are a large number of MSA methods that have been applied to chemical data. One of the most common is partial least squares-discriminant analysis (PLS-DA), which is a machine learning classification technique that is being increasingly applied to forensic data. PLS-DA can

be viewed as a supervised version of PCA because of its dimensionality reduction attribute (but with defined class labels). In addition, it can also be used for feature selection (i.e., determination of which features in the data enable class distinctions and identity predictions to be made), and classification, unlike PCA. PLS-DA is an appropriate approach particularly when the number of features is much greater than the amount of samples.[106] As such, it yields favorable results when applied to mass spectral and spectrophotometric data, due to the high number of features (*m/z* values and wavelengths respectively). A report by Pereira et al. is illustrative.[107] The study described the classification of synthetic drugs found on seized blotter papers. When *N*-methoxybenzyl (NBOMe); 2,5-dimethoxy-benzeneethanamine (2C-H); lysergic acid diethylamine (LSD); 2-(3,5-dimethoxy-4-((2-methylallyl)oxy)phenyl)ethanamine (MAL); and blank papers were analyzed by attenuated total reflection-Fourier transform infrared spectroscopy (ATR-FTIR) and discriminated using PLS-DA, the model was able to classify the samples with relatively high accuracy. The exception was LSD, which could not be accurately classified possibly due to its low concentration on the blotter papers.[107] Overall, their results indicate that PLS-DA can be an efficient MSA tool for the classification of NPSs.

1.3.3.2. Additional Techniques That Can Be Used to Analyze Chemical Data

The Random Forest (RF) algorithm is a valuable tool in classification, employing decision trees to organize data effectively. Decision trees, a common predictive modeling technique, use a flow-chart structure to correlate the presence of particular variables with the observation of accurate conclusions, aiding in precise classification.[108] In the context of mass spectral data, each variable corresponds to a specific *m/z* value, which assists in group assignments like species identity or drug class. Decision trees in mass spectral analysis rely on the presence or absence of certain *m/z* values to accurately determine the class assignment. These trees are constructed from

distinct sample sets using bagging or bootstrap aggregation, with variables chosen randomly, enabling the creation of numerous diverse trees. RF combines multiple decision trees into a "forest," leveraging the strengths of each tree independently, thereby reducing the impact of errors within individual trees.[108] This approach is particularly advantageous for analyzing large and complex datasets, such as those obtained by mass spectrometry.[61,83,109] The collective insights from multiple trees enhance the robustness of the model, ensuring reliable classification even in the presence of errors in individual trees.

Another supervised machine learning technique suitable for sample classification and identification is Support Vector Machines (SVM).[110] In this method, boundaries are established independent of the sample vector distribution within the dataset to delineate classes. When the data exhibit linear separability, SVM constructs optimal boundaries to effectively differentiate between classes. The optimal boundary, also known as the hyperplane, is determined as the furthest point from both sets of data points, ensuring maximal separation. Support vectors, representing data points closest to the hyperplane, play a pivotal role in identifying the optimal hyperplane position amid numerous possibilities. These support vectors, often challenging to classify, exert direct influence on determining the hyperplane's optimal location for effective class separation. Furthermore, SVM is adept at performing non-linear classifications, enhancing its versatility in handling complex datasets.[110]

Nearest neighbor supervised learning is also an important tool for classification. The fundamental principle of nearest neighbor methods revolves around identifying a set number of training samples closest in proximity to a new point and using these samples to predict the label.[111] This set number can either be a fixed, user-defined constant (known as k-nearest neighbor learning) or can vary based on the local density of points (referred to as radius-based neighbor learning).[111]

Typically, any measurable metric can be used as the distance metric, with the standard Euclidean distance being the most commonly chosen.[111] These methods are classified as non-generalizing machine learning techniques, as they essentially "remember" all training data, often facilitated by transformation into a rapid indexing structure.[111] This approach has been successful across a wide range of classification and regression problems, from handwritten digits to satellite image scenes.[111] As a non-parametric method, nearest neighbors tend to perform well in classification scenarios with highly irregular decision boundaries.[111]

1.3.4. Data Fusion

While MSA provides powerful tools for analyzing and interpreting complex datasets, the integration of data from multiple sources further enhances the accuracy and reliability of classification models. "Data fusion" is a strategy that combines the data output from multiple complementary analytical techniques in order to improve the prediction accuracy of multivariate statistical analysis models that are designed to classify chemical data.[11,112–115] It can dramatically enhance the success for predicting the identity of unknowns when compared to reliance on a single technique.[113] This is due to the fact that the errors that appear when using separate techniques are usually independent of one another, which is why data from these integral approaches should be fused.[114] It has found utility in studies designed to improve classification models of forensically relevant data.[11,112,114,115] For example, in a study done to classify luminescent gunshot residue (LGSR), data from excitation and emission spectra were fused, resulting in the accuracy of the classification model improving to 100% when compared to the results using only the excitation or emission spectra alone.[115] In another study, the accuracy of a classification model for identification of human hair before and after cosmetic modification was enhanced through the use of data fusion with wavelength-dispersive X-ray fluorescence (WDXRF) and laser-induced breakdown

spectroscopy (LIBS) data.[112] Data fusion has also been shown to be useful for characterizing and comparing printing ink evidence with data collected from two complimentary methods, allowing for more thorough characterizations and more pronounced confidence distributions.[114]

1.4. Statement of the Problem

In forensic science, the emergence of new psychoactive substances (NPSs), plant-based drugs of abuse, and timber-trafficking crimes present multifaceted challenges that are global in scope. The diverse categories of the materials involved impose unique analytical challenges due to their novel nature, structural complexity and in many cases, their physical heterogeneity. With NPSs, which include opioids, cannabinoids, cathinones, and tryptamines among other compound classes, standard operating protocols for analysis are often insufficient for structure determination, leading to significant delays in the identification and classification process. This absence of established methodologies exacerbates sample testing backlogs, particularly when structural variants that deviate from known chemical structures are encountered. The problem is further compounded by the limitations of conventional analytical techniques (e.g., gas chromatography-mass spectrometry (GC-MS)), which may yield ambiguous or difficult to interpret results, such as occurs when multiple molecules exhibit seemingly identical spectra; when the molecular ion is absent from EI mass spectra; or when multiple analytes have retention time and EI-MS characteristics that are too similar to enable them to be differentiated. Moreover, the complex and resource-intensive nature of method development for GC-MS underscores the need for a more unified approach that streamlines analysis across multiple classes of materials. This is especially true for plant-based drugs, which introduce additional layers of complexity because of the high variability in plant composition, coupled with the presence of novel compounds. This necessitates the development of robust analytical techniques capable of analyzing complex matrices with high

precision and accuracy.

In parallel with the complexities surrounding analysis of NPSs and psychoactive plant materials, the forensic interrogation of timber and its derived products presents its own set of difficulties. Illegal logging and timber trafficking are pressing concerns in environmental conservation and law enforcement. The accurate identification of timber species is crucial for enforcing regulations and combating illegal logging practices. However, traditional wood identification methods often rely on subjective visual assessments or destructive sampling techniques, which are labor-intensive, time-consuming, and may yield inconclusive results for timber species identification.

Given these issues, there is a critical need for innovative analytical approaches that address the unique characteristics of NPSs, plant drugs, and timber analysis-related challenges. DART-HRMS holds promise for rapid, non-destructive interrogation of a wide range of materials due to its ability to ionize samples directly without the need for extensive sample preparation. This technique generates high-resolution mass spectra that can facilitate the efficient classification, identification, and structural elucidation of compounds. The application of multivariate statistical analysis to DART mass spectral data enables extraction of meaningful information from complex datasets, and ultimately, accurate classification. By harnessing the capabilities of advanced instrumentation and data analysis techniques, forensic scientists can overcome existing limitations and enhance their ability to address the ever-evolving landscape associated with emerging illicit substances and wildlife trafficking crimes. Moreover, the development of standardized protocols and reference databases tailored to the analysis of NPSs, plant drugs, and timber-related materials is essential for promoting consistency, precision and accuracy across forensic laboratories worldwide.

Presented in the upcoming chapters are the results of investigations into how DART-HRMS combined with multivariate statistical analysis can be applied to address challenges associated with analysis of forensically relevant materials, such as synthetic drugs, psychoactive plants, and endangered timber. Chapter 2 explores the rapid structure elucidation of unknown tryptamines, using an ambient ionization technique and high-resolution mass spectrometry to identify molecular structures of NPSs without the need for sample preparation, and highlighting the potential of the method for deployment in forensic analysis settings. Chapter 3 investigates methods to create a comprehensive database of psychoactive plants for species determination. This includes the identification of their psychoactive constituents, which could streamline the forensic identification process for plant-based substances. Chapters 4 and 5 focus on the chemical composition of endangered trees, including *Dalbergia spp.* (Chapter 4), in addition to *Swietenia spp.* (Chapter 5) for species identification. These chapters demonstrate the utility of this approach for species differentiation, which is crucial for the enforcement of regulations protecting endangered timber. In showcasing the results of the featured studies, this research demonstrates the versatility and applicability of chemometric processing of DART mass spectral data to resolve challenging concerns in forensic analysis of materials.

CHAPTER 2: FUSED DART MASS SPECTRA AND CHEMOMETRICS FOR CLASSIFICATION AND STRUCTURE ELUCIDATION OF TRYPTAMINE PSYCHOACTIVE SUBSTANCES

2.1. Introduction

Forensic laboratories across the United States continue to grapple with the challenges imposed by the unrelenting rise in the circulation of new psychoactive substances (NPSs), a term that refers to recreationally used, unscheduled products that exhibit psychoactivity.[48,116] Their unregulated status and ready accessibility make them prime targets for misuse.[117,118] Opioids in particular have received significant attention, partly because of the high toxicity of some of the compounds that fall under this category, such as fentanyl and its derivatives. However, the focus on opioids has masked the significant problems associated with the emergence of other subsets of NPSs. Tryptamines serve as a case in point. Many are structural derivatives of serotonin or *N,N*-dimethyltryptamine (DMT), and are subject to misuse because of their mind-altering effects.[119–121]

While several are scheduled compounds, there are numerous sites within their scaffolds to which structural modifications can be introduced, resulting in the continued emergence of novel variants that retain their psychoactivity.[22,122,123] There are several bottlenecks to the scheduling of these substances including: (1) the difficulty of rapidly detecting and structurally characterizing emerging compounds; and (2) development of protocols for their routine detection and identification. One obstacle encountered by crime labs that mainly use electron ionization (EI) mass spectral techniques for structure elucidation is that closely related structural variants can often exhibit nearly identical EI mass spectral fragmentation patterns, making it challenging to utilize this conventional approach for their definitive identification. Another is that some

tryptamines fragment so extensively that their EI fragmentation patterns are rendered minimally informative for identification purposes.[117,122,124,125] A number of studies that have sought to address these issues have been reported. Piorunska-Sedlak and Stypulkowska showed how attenuated total reflectance Fourier transform infrared spectroscopy (ATR-IR) can serve as a good screening method because it is rapid, there is no need for sample pre-treatment, and only a small amount of sample is needed.[126] Nevertheless, it was observed that depending on the solvent, some samples were observed to have polymorphic crystalline forms that differed from those of the reference sample, making comparisons challenging. Jones et al.[127] reported the creation of an IR and Raman spectroscopy database of NPSs, and Moorthy and Sisco[70] have created a library search algorithm for NPS identification using DART mass spectra. However, in these two cases, identification is based on matching of the spectrum of the unknown to representative spectra that are already present in the database.[70,127] Therefore, emerging compounds that are new to the database cannot be identified using these methods. In addition, while a combination of nuclear magnetic resonance (NMR) and DART-MS can be used for compound identification, as was conducted by Marino et al. for the structure determination of synthetic cannabinoids in herbal incense, fairly large amounts of sample that are soluble in a suitable solvent must be available.[128]

In principle, DART-HRMS neutral loss data can be used to circumvent the aforementioned challenges to the identification of NPSs. In previous work, DART-HRMS was used to generate highly informative mass spectra from the analysis of cathinones.[48] The observed peaks enabled the neutral loss or "dark matter" information that is essential to interpreting the spectrum, particularly in terms of elucidating the structures of new compounds, to be extracted. Here, this approach was extended to enable elucidation of new tryptamine structures. However, an added dimension was that neutral loss data derived from collision-induced dissociation (CID) spectra generated at 60 V

and 90 V, were fused to generate new virtual spectra which were then subjected to advanced statistical analysis processing.

One approach that has been found to have utility in increasing the prediction accuracy in terms of drawing inferences from chemical data is "data fusion", which improves results by combining the outputs of multiple analytical techniques.[112–115] This process was exploited in this study through the fusion of DART-HRMS 60 V and 90 V neutral loss data, which served to increase the number of mass spectral peaks that could be used for structure determination. Accordingly, using statistical analysis techniques described herein, tryptamines were clustered into groups according to the structural information embedded in their fused neutral loss data. This enabled the skeletal frameworks of the structures in each group to be revealed. The observed clusters were then used as the input for the creation of a supervised classification model that could identify unknown tryptamine structures. Thus, the developed method can be used to screen emerging tryptamines against the clusters in order to identify their skeletal frameworks and structures. This novel approach represents a significant advancement over current methodologies for the identification of novel structural variants of drugs through: (1) generation of alternative fragmentation patterns that enable retention of the protonated precursor typically not seen in their EI mass spectra; (2) utilization of data fusion which serves to provide greater amounts of interpretable information and increase the accuracy of the results; and (3) application of machine learning to fused neutral loss spectra to create a prediction model to aid in the structure elucidation of unknown NPSs with a statistical level of certainty.

2.2. Methods

2.2.1. Materials

The following fifty tryptamine standards were purchased from Cayman Chemical Company (Ann Arbor, Michigan, USA) for creating the training set for the statistical model: α-ethyl-4-methyl-1H-indole-3-ethanamine; α-ethyl-5-methoxy-1H-indole-3-ethanamine; *N*-ethyl-*N*-methyl-1H-indole-3-ethanamine; α-ethyl-1H-indole-3-ethanamine; 5,7-dichloro-1H-indole-3-ethanamine; α-methyl-1H-indole-5-ethanamine; 5-methoxy-α-methyl-1H-indole-3-ethanamine; α-methyl-1H-indole-6-ethanamine; 7-fluoro-1H-indole-3-ethanamine; 5-(nonyloxy)-1H-indole-3-ethanamine; 3-(2-aminoethyl)-1H-indol-5-ol; α-methyl-1H-indole-3-ethanamine; 3-[2-(methylamino)ethyl]-1H-indol-5-ol; *N*-methyl-1H-indole-3-ethanamine; *N*,*N*-dipropyl-1H-indole-3-ethanamine; *N*,*N*-*bis*(1-methylethyl)-1H-indole-3-ethanamine; *N*,*N*-diethyl-1H-indole-3-ethanamine; *N*,*N*-dimethyl-1H-indole-3-ethanamine; *N*-isopropyl-*N*-(2-(4-methoxy-1H-indol-3-yl)ethyl)propan-2-amine; 5-methoxy-*N*,*N*-di-2-propen-1-yl-1H-indole-3-ethanamine; *N*,*N*-dibutyl-5-methoxy-1H-indole-3-ethanamine; *N*,*N*-diethyl-5-methoxy-1H-indole-3-ethanamine; 5-methoxy-*N*,*N*-dimethyl-1H-indole-3-ethanamine; 5-methoxy-*N*,*N*-dipropyl-1H-indole-3-ethanamine; *N*-isobutyl-*N*-(2-(5-methoxy-1H-indol-3-yl)ethyl)-2-methylpropan-1-amine; 5-methoxy-*N*,*N*-*bis*(1-methylethyl)-1H-indole-3-ethanamine; *N*-ethyl-*N*-(2-(5-methoxy-1H-indol-3-yl)ethyl)propan-1-amine; *N*-ethyl-5-methoxy-*N*-(1-methylethyl)-1H-indole-3-ethanamine; 5-methoxy-*N*-methyl-*N*-(1-methylethyl)-1H-indole-3-ethanamine; 6-methoxy-*N*,*N*-*bis*(1-methylethyl)-1H-indole-3-ethanamine; *N*-isopropyl-*N*-(2-(7-methoxy-1H-indol-3-yl)ethyl)propan-2-amine; *N*-[2-(5-hydroxy-1H-indol-3-yl)ethyl]-acetamide; *N*-[2-(1H-indol-3-yl)ethyl]-acetamide; 3-[2-(diethylamino)ethyl]-1H-indol-4-ol; 3-[2-(dimethylamino)ethyl]-1H-indol-4-ol; 3-[2-(dipropylamino)ethyl]-1H-indol-4-ol; 3-[2-[*bis*(1-methylethyl)amino]ethyl]-1H-indol-4-ol; 3-[2-(ethylmethylamino)ethyl]-1H-indol-4-ol; 3-[2-(methylpropylamino)ethyl]-1H-indol-4-ol; 3-[2-[methyl(1-methylethyl)amino]ethyl]-1H-indol-4-ol; 3-[2-(dimethylamino)ethyl]-

1H-indol-4-ol 4-(dihydrogen phosphate); *N*,*N*-diethyl-6-fluoro-1H-indole-3-ethanamine; 3-[2-(dimethylamino)ethyl]-*N*-methyl-1H-indole-5-methanesulfonamide; 3-[2-(diethylamino)ethyl]-1H-indol-4-ol 4-acetate; 3-[2-(dimethylamino)ethyl]-1H-indol-4-ol 4-acetate; 3-[2-(dipropylamino)ethyl]-1H-indol-4-ol 4-acetate; 3-[2-[*bis*(1-methylethyl)amino]ethyl]-1H-indol-4-ol 4-acetate; 3-[2-(ethylmethylamino)ethyl]-1H-indol-4-ol 4-acetate; 3-[2-[methyl(1-methylethyl)amino]ethyl]-1H-indol-4-ol 4-acetate; and 3-[2-(dimethylamino)ethyl]-1H-indol-5-ol. The structures of these compounds, their assigned abbreviations and formal names are shown in Figure 2.1. To assess the prediction model's ability to identify tryptamine classes, the following four additional tryptamines were purchased from Cayman Chemical Company (Ann Arbor, Michigan, USA) for external validation: 3-(2-(allyl(methyl)amino)ethyl)-1H-indol-4-yl acetate; 3-[2-(methylpropylamino)ethyl]-1H-indol-4-ol 4-acetate; 3-(2-(allyl(methyl)amino)ethyl)-1H-indol-4-ol; and 3-[2-(dimethylamino)ethyl]-1H-indol-4-ol 4-propanoate.

2.2.2. Instrumentation

A DART-SVP ion source (IonSense, Saugus, MA, USA) interfaced with a JEOL AccuTOF mass spectrometer (JEOL USA, Peabody, MA, USA) was used to collect mass spectral data in positive-ion mode. The optimized instrument parameter settings were as follows: helium gas flow rate, 2.0 L/ min; gas temperature, 350 °C; DART ion source grid voltage, 250 V; ring lens voltage, 5 V; orifice 1 voltage, 20 V, 60 V, and 90 V; orifice 2 voltage, 5 V; and peak voltage, 400 V (to detect *m/z* values ≥40). The samples were analyzed by dipping the closed end of a melting point capillary tube into the sample and presenting the coated surface to the open-air space between the mass spectrometer inlet and ion source. Spectra were collected at a rate of one spectrum per second over the mass range *m/z* 40-1000. Each sample was analyzed by DART-HRMS three times, and the three spectra were averaged to generate a single representative spectrum. This was repeated ten

4-hydroxy DPT
3-[2-(dipropylamino)ethyl]-1H-indol-4-ol

4-hydroxy DMT
3-[2-(dimethylamino)ethyl]-1H-indol-4-ol

4-hydroxy DiPT
3-[2-(diisopropylamino)ethyl]-1H-indol-4-ol

4-hydroxy DET
3-[2-(diethylamino)ethyl]-1H-indol-4-ol

4-acetoxy MiPT
3-[2-[methyl(1-methylethyl)amino]ethyl]-1H-indol-4-ol 4 acetate

4-acetoxy MET
3-[2-(ethylmethylamino)ethyl]-1H-indol-4-ol 4-acetate

4-acetoxy DPT
3-[2-(dipropylamino)ethyl]-1H-indol-4-ol 4 acetate

4-acetoxy DMT
3-[2-(dimethylamino)ethyl]-1H-indol-4-ol 4-acetate

4-acetoxy DiPT
3-[2-[1-methylethyl)amino]ethyl]-1H-indol-4-ol 4-acetate

4-acetoxy DET
3-[2-(ethylmethylamino)ethyl]-1H-indol-4-ol 4-acetate

5-methoxy AMT
5-methoxy-α-methyl-1H-indole-3-ethanamine

5-IT
α-methyl-1H-indole-5-ethanamine

5-hydroxy-N-methyl tryptamine
3-[2-(methylamino)ethyl]-1H-indol-5-ol

5-hydroxy DMT
3-[2-(dimethylamino)ethyl]-1H-indol-5-ol

5,7-dichloro tryptamine
5,7-dichloro-1H-indole-3-ethanamine

4-methyl-α-ethyltryptamine
α-ethyl-4-methyl-1H-indole-3-ethanamine

4-methoxy DiPT
N-isopropyl-N-2-(4-methoxy-1H-indol-3-yl)ethyl)propan-2-amine

4-hydroxy MPT
3-[2-(methylpropylamino)ethyl]-1H-indol-4-ol

4-hydroxy MiPT
3-[2-[methyl(1-methylethyl)amino]ethyl]-1H-indol-4-ol

4-hydroxy MET
3-[2-(ethylmethylamino)ethyl]-1H-indol-4-ol

5-methoxy MiPT
5-methoxy-N-methyl-N-(1-methylethyl)-1H-Indole-3-ethanamine

5-methoxy EPT
N-ethyl-N-(2-(5-methoxy-1H-indol-3-yl)ethyl)propan-1-amine

5-methoxy EiPT
N-ethyl-N-(2-(5-methoxy-1H-indole-3-yl)ethyl)-1H-indole-3-ethanamine

5-methoxy DPT
5-methoxy-N,N-dipropyl-1H-indole-3-ethanamine

5-methoxy DMT
5-methoxy-N,N-dimethyl-1H-indole-3-ethanamine

5-methoxy DiPT
5-methoxy-N,N-bis(1-methylethyl)-1H-indole-3-ethanamine

5-methoxy DiBT
N-isobutyl-N-(2-(5-methoxy-1H-indol-3-yl)ethyl)-2-methylpropan-1-amine

5-methoxy DET
N,N-diethyl-5-methoxy-1H-indole-3-ethanamine

5-methoxy DBT
N,N-dibutyl-5-methoxy-1H-indole-3-ethanamine

5-methoxy DALT
N,N-di-2-propen-1-yl-1H-indole-3-ethanamine

5-methoxy-α-ethyltryptamine
α-ethyl-5-methoxy-1H-indole-3-ethanamine

N,N-DMT
N,N-dimethyl-1H-indole-3-ethanamine

N,N-DET
N,N-diethyl-1H-indole-3-ethanamine

DPT
N,N-dipropyl-1H-indole-3-ethanamine

DiPT
N,N-bis(1-methylethyl)-1H-indole-3-ethanamine

7-methoxy DiPT
N-isopropyl-N-(2-(7-methoxy-1H-indol-3-yl)ethyl)propan-2-amine

7-fluoro tryptamine
7-fluoro-1H-indole-3-ethanamine

6-methoxy DiPT
6-methoxy-N,N-bis(1-methylethyl)-1H-indole-3-ethanamine

6-IT
α-methyl-1H-indole-6-ethanamine

6-fluoro DET
N,N-diethyl-6-fluoro-1H-indole-3-ethanamine

α-methyl tryptamine
α-methyl-1H-indole-3-ethanamine

α-ethyltryptamine
α-ethyl-1H-indole-3-ethanamine

sumatriptan
3-[2-(dimethylamino)ethyl]-N-methyl-1H-indole-5-methanesulfonamide

serotonin
3-(2-aminoethyl)-1H-indol-5-ol

psilocybin
3-[2-(dimethylamino)ethyl]-1H-indol-4-ol 4-(dihydrogen phosphate)

nonyloxytryptamine
5-(nonyloxy)-1H-indole-3-ethanamine

N-methyl-N-ethyltryptamine
N-ethyl-N-methyl-1H-indole-3-ethanamine

N-methyl tryptamine
N-methyl-1H-indole-3-ethanamine

N-acetylserotonin
N-[2-(5-hydroxy-1H-indol-3-yl)ethyl]-acetamide

N-acetyl tryptamine
N-[2-(1H-indol-3-yl)ethyl]-acetamide

Figure 2.1 The structures, common names, and formal names of the tryptamines analyzed in this study.

33

times in order to produce ten replicates of each sample. PEG 600 (Sigma-Aldrich, St. Louis, MO, USA) was used as a mass calibrant. TSSPro 3 software (Shrader Analytical, Detroit, MI, USA) was used for data processing including averaging, background subtraction, and peak centroiding. The workflow for data collection by DART-HRMS is shown in Figure 2.2A. The soft ionization spectra (collected at 20 V) for the 50 tryptamines, along with their structures are presented in Figure A2.1 with their corresponding mass data tables deposited at https://rabi-musah.squarespace.com/s/Tryptamine-20-V-mass-data-tables-corresponding-to-Figure-A1-mass-spectra.xlsx. The mass data tables for the soft ionization spectra collected at 60 and 90 V are deposited at https://rabi-musah.squarespace.com/s/Tryptamine-original-60-V-mass-tables-that-were-used-to-create-the-neutral-loss-spectra-in-Figure-A2.xlsx and https://rabi-musah.squarespace.com/s/Tryptamine-original-90-V-mass-tables-that-were-used-to-create-the-neutral-loss-spectra-in-Figure-A3.xlsx, respectively. To assess the reproducibility of the results, DART-HRMS analyses were performed for 4-acetoxy MPT by three different individuals in one day and by one individual on two different days, one year apart.

2.2.3 Neutral Loss Spectra Generation

Mass Mountaineer software (RBC Software, Portsmouth, NH, USA) was used to determine the masses lost during the fragmentation that was induced when the orifice 1 voltage was raised from 20 V to 60 V, and then to 90 V. For the spectra generated at each voltage, the *m/z* values above a 0.5% relative peak intensity were subtracted from the peak representing the protonated tryptamine (as illustrated in Figure 2.2B). This furnished "neutral loss" spectra in which the peaks observed represented the high-resolution masses lost during fragmentation, and whose relative intensities were equivalent to those of the peaks in the 60 V or 90 V spectra from which they were derived. Figures A2.2 and A2.3 (corresponding mass spectral data deposited at https://rabi-

, respectively) display the neutral loss spectra

representative of the 50 tryptamines at 60 V and 90 V, respectively.

2.2.4. Multivariate Statistical Analysis

The neutral loss spectra in the form of text files were imported into MATLAB 9. 3. 0,

R2019a software (The MathWorks, Inc., Natick, MA, USA). Each text file was comprised of two

columns, with the first containing the *m/z* values and the second containing the corresponding peak

intensities. In order to reveal patterns that could serve as the basis for classifying tryptamine

structures, two procedures (shown in Figure 2.2C) were introduced. First, an unsupervised

exploratory method was applied to assess whether patterns might be present, and second, a

supervised method was conducted to create a model for discrimination.

According to Figure 2.2C—Step 1, following DART-HRMS analysis and generation of

the corresponding neutral loss spectra, the neutral loss data were aligned in a matrix according to

common *m/z* values with a bin width of 20 mmu and a relative intensity cut-off value of 0.5%. The

optimal bin width and relative intensity cutoff were determined by iterative application of

agglomerative hierarchical clustering analysis (HCA) using different bin widths and relative

intensity cutoffs. This treatment resulted in two matrices with dimensions of 500×174 and $500 \times$

368 (i.e., number of samples $\times$ number of *m/z* values) for the neutral loss spectra collected at orifice

1 voltages of 60 V and 90 V, respectively. The 60 V and 90 V spectrum of each sample was

normalized by the maximum intensity and converted to percentages. Since the neutral loss 60 V

and 90 V matrices had the same number of samples, they could be fused row wise, meaning that

the two matrices were fused together to make one matrix with the 60 V data on the left and the 90
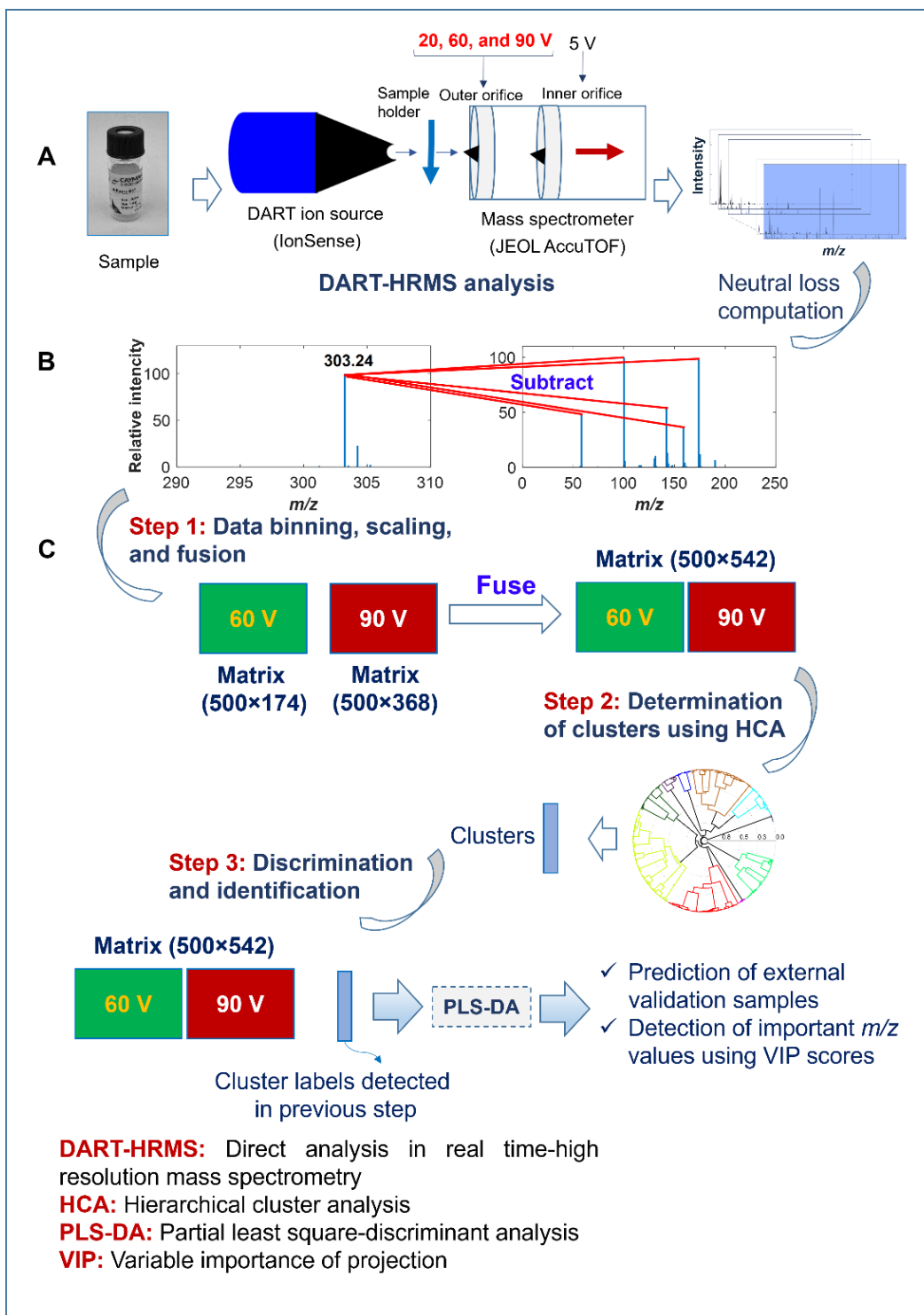
Figure 2.2 Data collection and statistical analysis workflow approach for the development of a model to enable prediction of new tryptamine variants. (A): DART-HRMS data collected at 20 V, 60 V and 90 V; (B) Generation of neutral loss spectra; and (C) Multivariate data analysis workflow: Step 1—Conversion of spectra to matrices following binning and normalization; Step 2—HCA analysis of data to define clusters; and Step 3—Creation of PLS-DA model used to discriminate between tryptamine classes.

V data on the right, in order to create a matrix with dimensions of 500×542, which could be subjected to further multivariate statistical analysis, including HCA and creation of a classification model. As shown in Figure 2.2C—Step 2, HCA, an unsupervised method, was applied to the resulting data matrix in order to reveal the presence of common patterns that might be used as a basis for classifying the data and predicting tryptamine unknowns. In this process, a correlation measure was used for assessing the proximity between objects in the dataset. Then, the objects were grouped into agglomerative hierarchal clusters using an unweighted pair group method with arithmetic mean (UPGMA). Clusters were defined by cutting branches off the dendrogram. A distance threshold of 70% of the maximum linkage was found to be optimum for the height cut-off value. If the height of a node was less than the cutoff value, all leaves at or below the node were grouped into a cluster. The optimum distance threshold and distance metrics were revealed by changing the threshold and metrics and evaluating the quality of the resulting clusters using a supervised model, which was trained by the fused matrix and the identified cluster labels. The supervised method examines how well the clusters were separated, and therefore, good clustering should result in good classification performance. Probabilistic partial least square-discriminant analysis (PLS-DA)[129] with 11 latent variables was used to create a supervised model for discrimination of tryptamines in accordance with the detected cluster labels. This is illustrated in Figure 2.2C—Step 3. The optimal latent variables for the PLS-DA model were computed using iterative application of different numbers of latent variables to see which led to higher accuracy during validation. Validation of the PLS-DA model was performed using the "leave-one-structure-out" strategy (i.e., in each step of the validation, the replicates of one tryptamine structure were left out of the training process and then subsequently predicted using the trained model). To provide a measure of reliability of classification for each prediction, probability density function

and Bayesian decision theory were applied to calculate a vector of the posterior probabilities as output, in which each coordinate corresponded to one class. For assignment of samples to each class, a probability threshold was computed for each class using the prediction results of training samples and the *Bayesian* discrimination threshold.[129,130] The sample was assigned to a class if the PLS-DA prediction output demonstrated a probability higher than that of the class threshold. The optimized discrimination model was then used for prediction of external validation samples.

A specific advantage of PLS-DA is its ability to reveal the *m/z* values that are most significant for enabling discrimination between classes through the determination of variable importance in projection (VIP) scores. Ten distinct PLS-DA discrimination models were explored. Each was used to train a one-vs-all binary model (i.e., a particular class of tryptamines was assigned a label of 1 and all the other classes were assigned a label of 0 in the training process). As such, each PLS-DA model revealed the variables that were most important for discrimination of one class from the other classes. The final VIP scores ended up being the average of the VIP scores from the ten PLS-DA models. Masses with VIP scores higher than 1 were deemed important for enabling discrimination between classes.[131]

2.3. Results

2.3.1. Generation and Processing of DART Mass Spectra

This study was conducted to develop a simple and rapid method to enable detection and identification of emerging tryptamine structures. Previous work has demonstrated the utility of extracting neutral loss information from DART mass spectra of synthetic cathinone unknowns in stitching together plausible candidate structures.[48] Here, this principle was extended to enable elucidation of new tryptamine structures. However, the approach differed from that in the cathinone work in that for cathinones, neutral loss spectra collected under CID conditions at 90 V

were utilized, while in this work, CID spectra generated at 60 V *and* 90 V were fused to generate new virtual spectra which were then subjected to advanced statistical analysis processing. The steps taken to achieve this are presented in Figure 2.2. For each of the tryptamines, spectra in replicates of 10 were collected at 20 V, 60 V and 90 V (Figure 2.2A). Analyzing the tryptamines at 20 V resulted in soft ionization spectra, meaning that by and large, only the protonated precursor peaks were observed and there was no fragmentation. 4-Acetoxy DiPT serves as a representative example. With the formula $C_{18}H_{26}N_2O_2$, its calculated monoisotopic mass is 302.1994. Its DART mass spectrum acquired at 20 V (top) in positive ion mode (see Figure 2.3) shows the unfragmented protonated precursor calculated to be at *m/z* 303.207 as a single peak (within 5 mmu). When the voltage was raised to 60 V and 90 V, fragments that appeared at the expense of the protonated precursor peak were detected (Figure 2.3). The higher the voltage, the greater the fragmentation and the lower the intensity of the protonated precursor. Therefore, the 90 V spectrum shows the greatest fragmentation, with a protonated precursor peak of lower intensity when compared to that in the 60 V spectrum. However, it is important to note that even at 90 V, the protonated precursor is still detected, which is generally not the case for EI mass

Figure 2.3 DART-HRMS spectra of 4-acetoxy DiPT analyzed at orifice 1 voltages of 20 V (top), 60 V (middle) and 90 V (bottom).

spectra (i.e. the molecular ion in these spectra is often missing). While the 60 V and 90 V spectra share several *m/z* values, there were other masses that were unique and appeared as a function of the voltage that was applied. For example, the mass spectra in Figure 2.3 show that there is a peak at nominal *m/z* 102 in the 60 V (middle) spectrum that is not present in the 90 V (bottom) spectrum. The spectra were then processed by subtracting the *m/z* values of each of the product ions from the protonated precursor to yield new neutral loss spectra. This step is summarized in Figure 2.2B, and the spectra that were generated are presented in Figures A2.2 and A2.3 for the 60 V and 90 V spectra, respectively. In these spectra, the peaks represent high-resolution masses of lost structural elements where the relative abundances are based on the fragment peaks from which they were derived. An example of the neutral loss spectra of 4-acetoxy DiPT at 60 V (top) and 90 V (bottom) is illustrated in the head-to-tail plot (Figure 2.4). They include shared masses including nominal *m/z* 114 and 160. On the other hand, the 60 V spectrum exclusively includes nominal *m/z* 129, which is absent in the 90 V spectrum. This demonstrates the importance of including both voltages
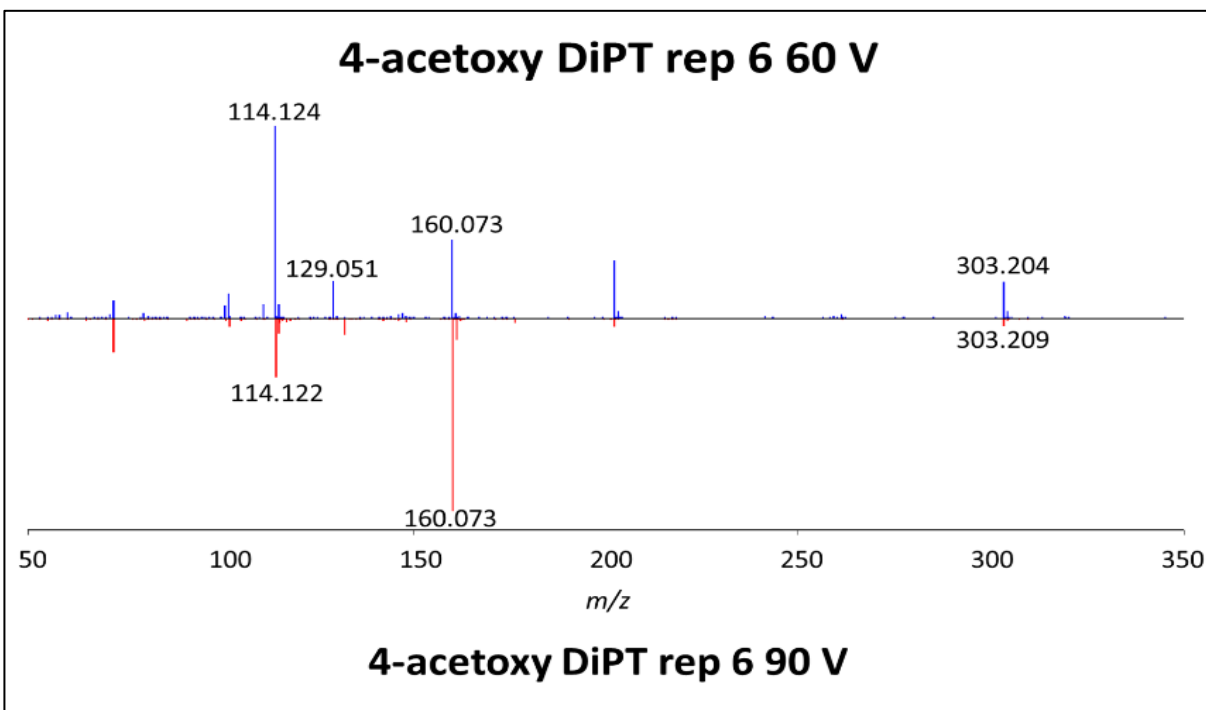
Figure 2.4 Neutral loss spectra of 4-acetoxy DiPT acquired by DART-HRMS analysis analyzed at orifice 1 voltages of 60 V (top) and 90 V (bottom).

to provide complementary information, enabling a more thorough analysis of the fragmentation patterns.

2.3.2. Determination of the Presence of Clustering of Tryptamine Spectra, Indicative of Common Structural Features

To summarize the data and assess whether the fused spectral data might exhibit patterns that could serve as the basis for being able to classify "like" structures, potential similarities between the neutral loss spectral data were determined using the "correlation" metric. This resulted in the correlation matrix shown in Figure 2.5, which illustrates the computed correlations plotted along both the x- and y-axes, arranged by similarity. It shows the correlations (with values spanning the range 0 – 1) between the two neutral loss spectra using a color gradient. The color gradient extends from dark blue to yellow, where the darkest shade of blue corresponds to the least similarity (i.e., a value of zero) and the brightest shade of yellow corresponds to the highest similarity (i.e., a value of 1). From the matrix, 10 groups emerged that each contained neutral loss spectra that were similar enough that they were grouped together and distinguished from the others. These are labeled groups 1-10 (Figure 2.5) and color-coded as follows: aqua (group 1); brown (group 2); dark blue (group 3); dark green (group 4); chartreuse (group 5); purple (group 6); red (group 7); magenta (group 8); navy (group 9) and green (group 10). The matrix revealed that the neutral loss data of like tryptamines were highly correlated, based on the bright yellow colors appearing along the diagonal which showed that each sample always perfectly correlated with itself. Moderate correlations between spectra are also revealed. For example, reading the plot from left to right, the spectral data represented by the aqua color, are shown to be moderately correlated to the spectra represented by the brown color, based on the light blue shading in the off-diagonal area where the two intersect. Furthermore, some of the spectra represented in the aqua area are also
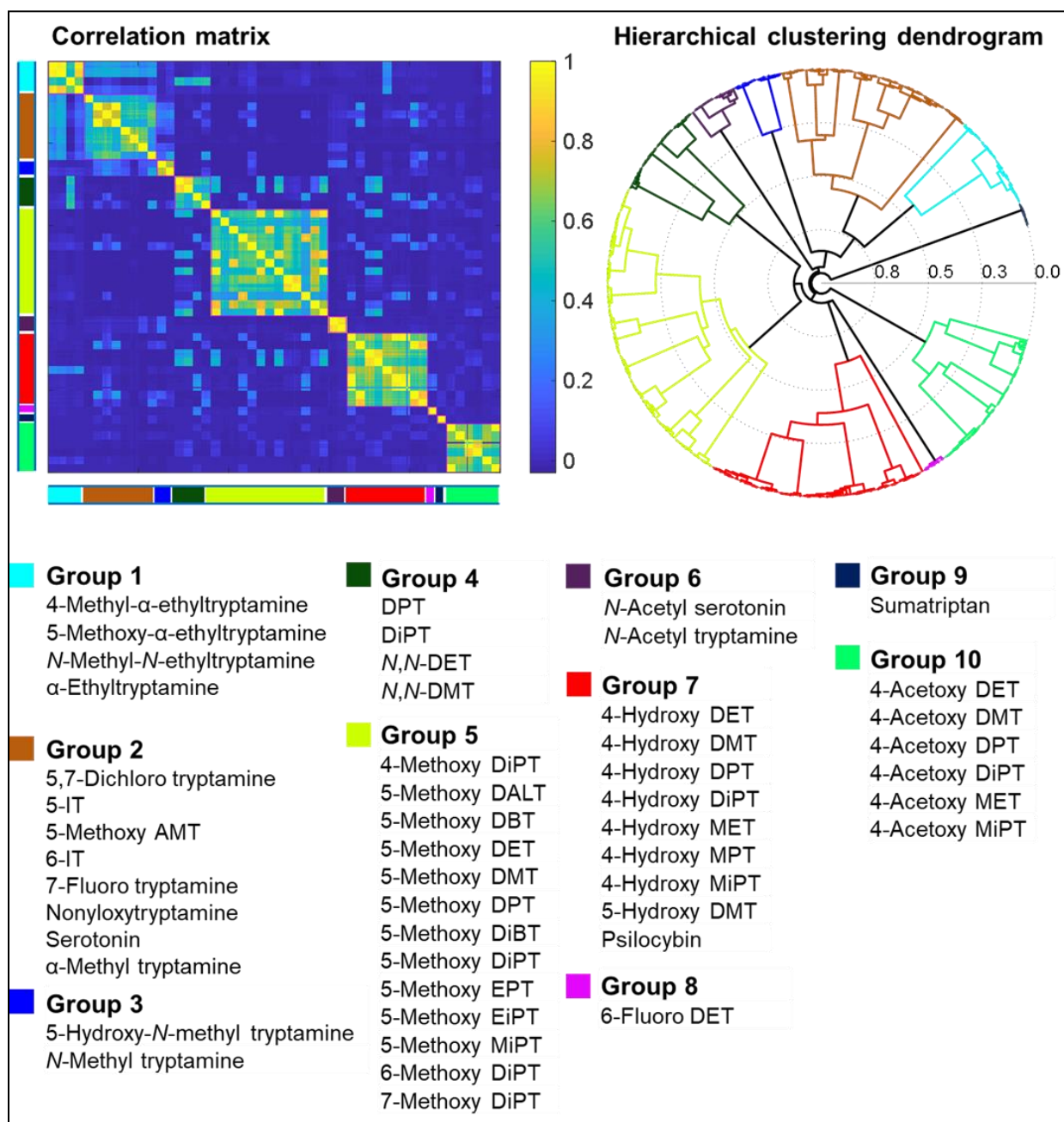
Figure 2.5 Correlation matrix showing the computed correlations between molecules, plotted along both the x- and y-axes and arranged by similarity (where yellow corresponds to the highest similarity and blue corresponds to the lowest) that were subjected to hierarchical clustering analysis (HCA). The dendrogram resulting from HCA and the ten groups that emerged are also shown (see full list of compound structures, names and their corresponding abbreviations in Figure 2.1).

correlated to data represented in red on the x-axis.

Next, the data in the correlation matrix served as the input for hierarchical clustering analysis to reveal clustering that might be used as a basis for classifying the data and predicting the structures of tryptamine unknowns. The resulting dendrogram is also presented in Figure 2.5. The axial axis in the dendrogram represents the amount of dissimilarity between clusters, and each leaf node displays a replicate of a tryptamine compound. The membership of the ten distinct groups (see full list of compound structures, names and their corresponding abbreviations presented in Figure 2.1) and their assigned numbers and colors are similar to those in the correlation matrix and are as follows: Group 1 (aqua) includes 4-methyl-α-ethyl tryptamine, 5-methoxy-α-ethyltryptamine, *N*-methyl-*N*-ethyl tryptamine, and α-ethyltryptamine; Group 2 (brown) includes 5,7-dichloro tryptamine, 5-IT, 5-methoxy AMT, 6-IT, 7-fluoro tryptamine, nonyloxytryptamine, serotonin, and α-methyl tryptamine; Group 3 (dark blue) includes 5-hydroxy-*N*-methyl tryptamine and *N*-methyl tryptamine; Group 4 (dark green) includes DPT, DiPT, *N*,*N*-DET, and *N*,*N*-DMT; Group 5 (chartreuse) includes 4-methoxy DiPT, 5-methoxy DALT, 5-methoxy DBT, 5-methoxy DET, 5-methoxy DMT, 5-methoxy DPT, 5-methoxy DiBT, 5-methoxy DiPT, 5-methoxy EPT, 5-methoxy EiPT, 5-methoxy MiPT, 6-methoxy DiPT, and 7-methoxy DiPT; Group 6 (purple) includes *N*-acetyl serotonin and *N*-acetyl tryptamine; Group 7 (red) includes 4-hydroxy DET, 4-hydroxy DMT, 4-hydroxy DPT, 4-hydroxy DiPT, 4-hydroxy MET, 4-hydroxy MPT, 4-hydroxy MiPT, 5-hydroxy DMT, and psilocybin; Group 8 (magenta) includes 6-fluoro DET; Group 9 (navy) includes sumatriptan; and Group 10 (green) includes 4-acetoxy DET, 4-acetoxy DMT, 4-acetoxy DPT, 4-acetoxy DiPT, 4-acetoxy MET, and 4-acetoxy MiPT. The dendrogram shows that five groups (1, 2, 4, 5, and 10) are at approximately the same distance on the axial axis, indicating the similarity between them.

2.3.3. Assessment of the Structural Basis of the Hierarchical Clustering Analysis-Revealed Groupings

The groupings that emerged from the clustering results revealed that there are common structural features and fragmentation pathways that are shared by the members of each group which yield similar high-resolution *m/z* values in their neutral loss spectra, and which are thereby highly correlated. The results also revealed that there are several highly correlated structures whose similarity to one another was not intuitively apparent. For example, the three compounds *N*-methyl-*N*-ethyltryptamine, *N*-methyl tryptamine and *N,N*-DET are all mono-substituted indoles in which the substituent at position 3 is comprised of a 2-carbon chain which has at its terminus a nitrogen atom with one or two alkyl groups (see Figure 2.1). Based on their highly similar structures, it might be surmised that they would have been grouped together. Yet, the clustering results show that these three compounds appeared in Groups 1, 3, and 4, respectively. Each of these compounds appears in its respective group based on the similarity of the *m/z* values in its neutral loss spectrum to the other members of the group. For example, Group 1 members all possess a nitrogen-containing three carbon unit (with *m/z* 59.07) that is lost as a neutral fragment from the indole-containing segment of the molecule. The members of Group 5, which contains the greatest diversity of structures, all possess two substituents: a methoxy moiety on the benzene ring (whose position varies), and an ethylamine substituent at position 3 of the indole ring with a range of *N*-alkyl attachments. While the structures are diverse, common fragmentation pathways result in neutral loss spectra that have *m/z* values at nominal 101, 116, 161, and 203, which were important in differentiating group 5 from the rest of the groups.

2.3.4. Creating a Structure Classification Model for Tryptamine Class Prediction

Overall, the correlation matrix and clustering results showed that each of the groups exhibited common features which in principle could serve as a basis for structure classification. To accomplish this, the groupings resulting from HCA were used as the input for PLS-DA. The "leave-one-structure-out" validation strategy was performed to evaluate the PLS-DA model using varying numbers of latent variables. This treatment revealed that eleven latent variables resulted in the lowest error in prediction. The resulting 3D PLS-DA score plot for latent variables 1, 2, and 3 is shown in Figure 2.6. The score plot shows that each group was discriminated from the others. Table 2.1 shows the confusion matrix that describes the performance of the PLS-DA discrimination model. Each column of the matrix represents the samples in the predicted class, while each row presents the samples in the actual class. The values along the diagonal in green
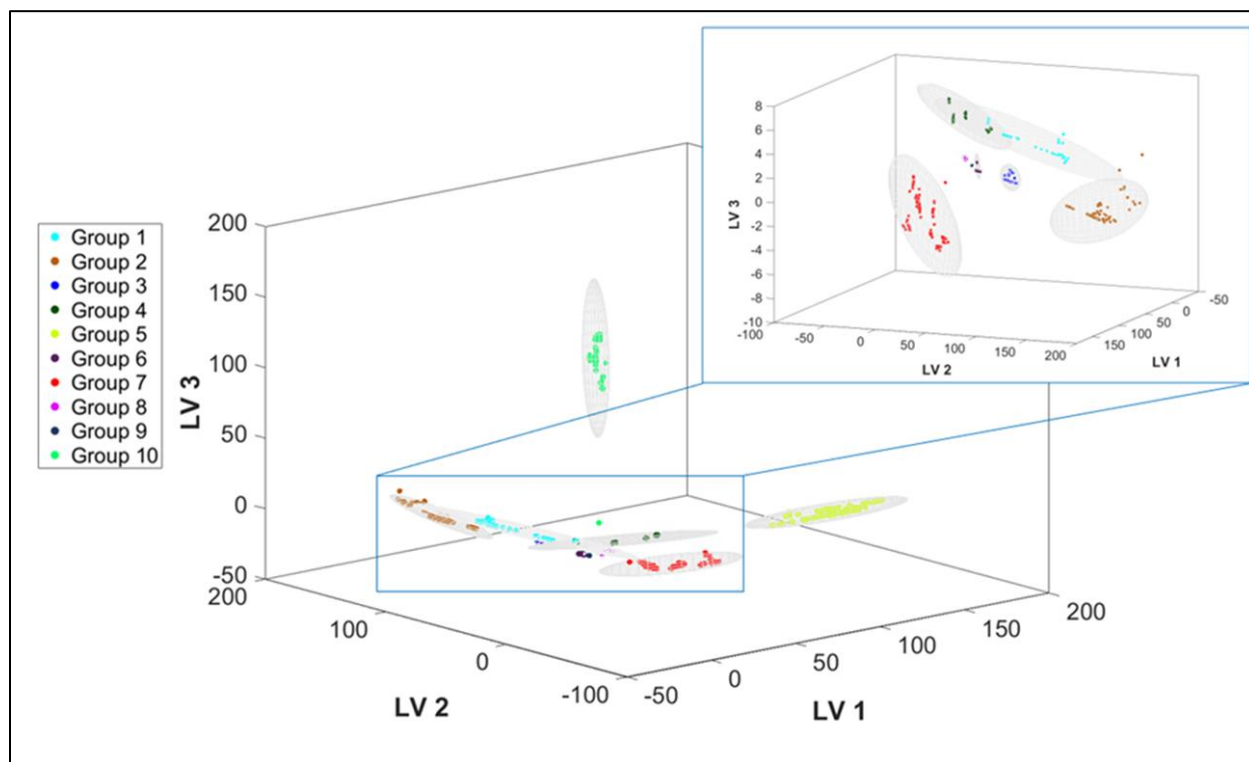
Figure 2.6 PLS-DA scores plot generated using DART-HRMS neutral loss data. Class distinctions are indicated with color coding.

illustrate the number of samples for which the predicted label matched the true label, while the non-zero values on the off-diagonal shown in red represent those that were incorrectly classified or unclassified by the discrimination model. Using class assignment thresholds that were defined by the *Bayesian* discrimination threshold, the model resulted in accuracy, error, multi-label assignment, and not-assigned rates of 1.00, 0.00, 0.05 and 0.04, respectively, in the leave-one-structure-out validation. It should be noted that multi-label and not-assigned predictions were not considered in the accuracy and error calculations.

Table 2.1 Confusion matrix resulting from the "leave-one-structure-out" validation of the PLS-DA model.

Confusion matrix		Predicted										Not assigned	Multi-label assignment
		G 1	G 2	G 3	G 4	G 5	G 6	G 7	G 8	G 9	G 10		
True	G 1 (40)	24	0	0	0	0	0	0	0	0	0	0	16
	G 2 (80)	0	80	0	0	0	0	0	0	0	0	0	0
	G 3 (20)	0	0	20	0	0	0	0	0	0	0	0	0
	G 4 (40)	0	0	0	40	0	0	0	0	0	0	0	0
	G 5 (130)	0	0	0	0	130	0	0	0	0	0	0	0
	G 6 (20)	0	0	0	0	0	20	0	0	0	0	0	0
	G 7 (90)	0	0	0	0	0	0	80	0	0	0	0	10
	G 8 (10)	0	0	0	0	0	0	0	0	0	0	10	0
	G 9 (10)	0	0	0	0	0	0	0	0	0	0	10	0
	G 10 (60)	0	0	0	0	0	0	0	0	0	60	0	0

G 1: Group 1; G 2: Group 2; G 3: Group 3; G 4: Group 4; G 5: Group 5; G 6: Group 6; G 7: Group 7; G 8: Group 8; G 9: Group 9; G 10: Group 10

Table 2.2 shows the prediction, sensitivity, specificity, and precision of the discrimination model. Sensitivity and specificity are measures of the 1-false negative rate and 1-false positive rate, respectively. As shown in the confusion matrix (Table 2.1), the off-diagonal entries for predictions in G1-G7 and G10 are zero, which reflects higher correct prediction rates, and all three figures of merit (i.e. sensitivity, specificity, and precision) are 1.00 for those classes (Table 2.2). This indicates the model to be good for predicting the classes of emerging structures. Table A2.1 shows the resulting prediction probabilities of the assignments of tryptamine structures to the classes. Of the 50 tryptamines, all except five (i.e., 5-methoxy-α-ethyltryptamine, *N*-methyl-*N*-ethyltryptamine, 6-fluoro DET, sumatriptan, and 4-hydroxy MET with their probabilities shown in red in Table A2.1) were correctly classified (i.e. probability of one). Using a significance level of 0.05 as the basis for class assignment, 5-methoxy-α-ethyltryptamine was assigned to both Group 1 and Group 2 with probabilities of 1.00 and 0.52, respectively. *N*-Methyl-*N*-ethyltryptamine was classified in Group 1 and Group 4 with an equal probability of 1.00 and 1.00, respectively. This is not surprising, since all of the compounds in Group 4 and *N*-methyl-*N*-ethyltryptamine have a fragment at nominal *m/z* 131 (Table A2.2-A2.3). 4-Hydroxy MET was placed into Group 1 and Group 7 with probabilities of 1.00 and 1.00, respectively. Given the close structural similarity between *N*-methyl-*N*-ethyltryptamine and 4-hydroxy MET, this dual classification was also not

Table 2.2 Classification performance, sensitivity, specificity and precision of the "leave-one-structure-out" validation for tryptamine discrimination using the PLS-DA model.

	G 1	G 2	G 3	G 4	G 5	G 6	G 7	G 8	G 9	G 10
Sensitivity	1.00	1.00	1.00	1.00	1.00	1.00	1.00	Not assigned	Not assigned	1.00
Specificity	1.00	1.00	1.00	1.00	1.00	1.00	1.00	1.00	1.00	1.00
Precision	1.00	1.00	1.00	1.00	1.00	1.00	1.00	Not assigned	Not assigned	1.00

surprising, since they both have the *N*-methyl-*N*-ethylamine moiety in their structures, resulting in a fragment at *m/z* 59. 6-Fluoro DET and sumatriptan had a probability of 0.00 for assignment to each cluster since these two compounds belonged to one member groups (i.e. Groups 8 and 9, respectively). This result was also unsurprising, since the structural characteristics of these compounds deviate quite significantly from the remaining compounds in the training set. Overall, the results confirm that the ability of the model to facilitate accurate prediction of tryptamine classes is dependent upon the similarities of the neutral losses observed from fragmentation of the molecule.

2.3.5. Assessment of Markers Important for Discrimination Between Groups of Structures

A specific advantage of PLS-DA is that the *m/z* values that are most important for class discrimination can be determined through the evaluation of variable importance in projection (VIP) scores. The VIP score calculation results for the PLS-DA model are presented in Figure 2.7. The solid blue points in Figure 2.7-Panel A display the VIP scores (x-axis) for *m/z* values (y-axis) that have a score >1. The higher the VIP score, the greater the impact the corresponding *m/z* value has in enabling discrimination. For example, for both the 60 V and 90 V spectra, *m/z* 161.08 has the highest VIP score, indicating that it has the highest impact on discrimination. The heatmaps shown in Figure 2.7-Panel B represent the averaged relative abundances of the most impactful neutral loss *m/z* values in each group. The color gradient of the heatmap extends from dark blue to brick red, with the darkest shade of blue indicative of a relative abundance of 0 and the darkest shade of brick red representative of a relative abundance of 100 (on an arbitrary scale). The heatmaps facilitate visualization of how the indicated *m/z* values are associated in different groups, which can be helpful in detecting unique markers. For example, the heatmap results show that the *m/z* value with the highest VIP score for the 60 V data (i.e. *m/z* 161.08) has a high relative
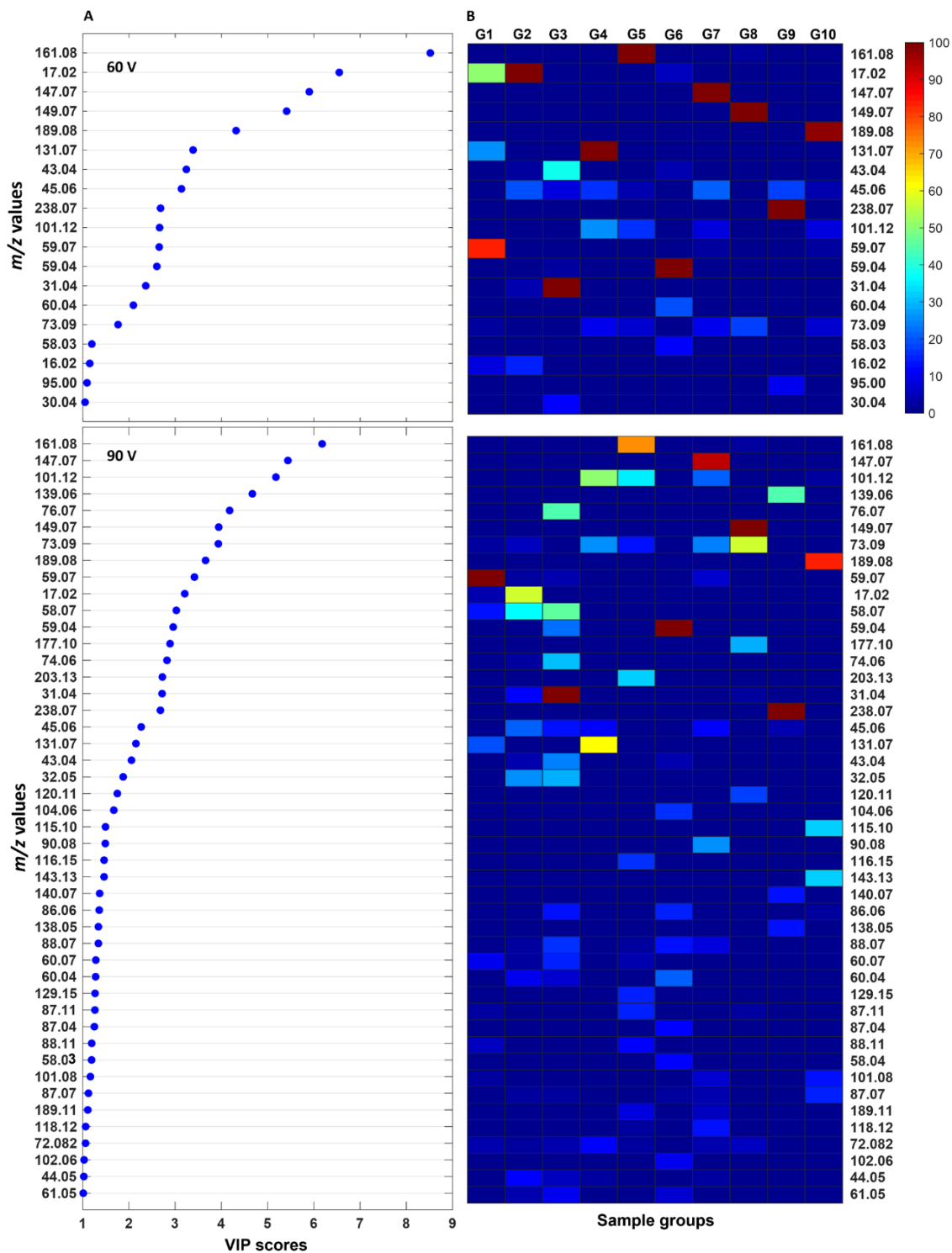
Figure 2.7 Masses determined to be most impactful in enabling differentiation of groups, based on differences in the fragmentation patterns of the represented compounds under CID conditions. Panel A: variable importance in projection (VIP) scores >1 revealed by the one-vs-all PLS-DA models for data collected at 60 V and 90 V; Panel B: neutral loss data corresponding with the indicated *m/z* values, averaged for each class and displayed as heatmaps for 60 V and 90 V spectral data.

abundance for Group 5 compounds and low relative abundances (around zero) for other groups. Therefore, *m/z* 161.08 is a unique marker that enables the model to distinguish Group 5 molecules from those in the other groups. A similar observation was made for the 90 V data, where *m/z* 161.08 remained a strong marker for Group 5. The relative intensities of the *m/z* values in the 60 V and 90 V neutral loss spectra that were found to be most highly ranked in enabling discrimination between classes are presented in Table A2.2 and Table A2.3, respectively. From the neutral loss data presented in the heatmap in Figure 2.7 and Tables A2-A3, a number of trends became apparent. First, there are neutral loss values that appear within a group that are observed for most but not all of the compounds that appear in that group. For example, for the 90 V data (Table A2.3), the neutral loss of *m/z* 90.08 appears for 6 of the 9 compounds in Group 7 (i.e. 4-hydroxy DET; 4-hydroxy DMT; 4-hydroxy MPT; 4-hydroxy MiPT; 5-hydroxy DMT and psilocybin), but not for

the other three (4-hydroxy DPT; 4-hydroxy DiPT and 4-hydroxy MET). Second, there are *m/z* values that are specific to several groups. For example, for the 60 V neutral loss data (Table A2.2), *m/z* 17.03 is found in groups 1, 2, and 6. Similarly, for the 90 V data (Table A2.3), *m/z* 59.07 appears in every group except Groups 6 and 9. Third, there were a subset of neutral losses that were observed for each

Table 2.3 Neutral loss masses (*m/z*) associated with the compounds in Groups 1 - 10 that were identified in analysis of the 60 and 90 V virtual neutral loss spectra.		
Group	**Neutral loss at 60 V**	**Neutral loss at 90 V**
Group 1	59.07	59.07
Group 2	16.02 and 17.03	17.03 and 31.05
Group 3	30.04, 31.04, 43.04 and 45.06	31.05, 32.05, 43.05, 44.05, 45.06 and 58.07
Group 4	131.07	131.08
Group 5	161.08	161.08
Group 6	17.03, 43.04, 45.06, 58.03, 59.04 and 60.04	17.03, 43.05, 58.03, 59.04, 60.05, 61.06, 86.06 and 88.07
Group 7	147.07	147.07
Group 8	73.09, 149.07 and 161.08	87.11, 101.12, 120.11, 149.07, 161.08 and 177.10
Group 9	45.06, 95.00, 149.07 and 238.08	31.05, 59.07, 138.05, 139.06 and 140.07
Group 10	189.08	189.08

compound in a given group. These are listed in Table 2.3 for the 60 V and 90 V data. For example, *m/z* 59.07 was found in all of the compounds in Group 1 in the 60 V and 90 V data. Such masses were found to be important in enabling distinctions to be made between the groups. These results show that neutral loss spectra derived from DART-HRMS can enable facile classification of tryptamine structures. They also reveal the identities of the skeletal frameworks that were the basis of the ability of the model to distinguish between classes. These are presented in Figure 2.8 for Groups 1 through 10.

2.3.6. External validation of the PLS-DA Model Using Novel Compounds

The usefulness of approaches such as those described here lies in part in their potential to correctly classify compounds that are new to the prediction model. Thus, to assess the model's prediction ability, an external validation was performed to determine if tryptamines that were not used in the creation of the model could be correctly classified. Four compounds were tested: 3-(2-(allyl(methyl)amino)ethyl)-1H-indol-4-yl acetate (4-acetoxy MALT); 3-[2-(methylpropylamino)ethyl]-1H-indol-4-ol 4-acetate (4-acetoxy MPT); 3-(2-(allyl(methyl)amino)ethyl)-1H-indol-4-ol (4-hydroxy MALT); and 3-[2-(dimethylamino)ethyl]-1H-indol-4-ol 4-propanoate (4-propanoyloxy DMT). These compounds all contain an ethylamine substituent at the 3-position of the indole scaffold, and a substituent at position 4. They differ in terms of the substituents attached to the exocyclic ring nitrogen and the benzene ring. Each external validation tryptamine was analyzed by DART-HRMS in replicates of 10. Representative neutral loss spectra acquired at 60 V and 90 V for the tryptamines used for external validation are displayed in Figure 2.9. From the neutral loss spectra presented and the information on the diagnostic *m/z* values listed in Table 2.3, it can be seen that three of the tryptamine spectra contain *m/z* values in the neutral loss 90 V spectra that the PLS-DA model revealed are common in the spectra of

Group 1

1. A,B,C = H, CH₃, CH₂CH(NH₂)CH₂CH₃
2. A,B,C = OCH₃, H, CH₂CH(NH₂)CH₂CH₃
3. A,B,C = H, H, CH₂CH(NH₂)CH₂CH₃
4. A,B,C = H, H, CH₂CH₂N(CH₃)CH₂CH₃

Group 2

1. A,B,C,D = Cl, H, Cl, CH₂CH₂NH₂
2. A,B,C,D = CH₂CH(NH₂)CH₃, H, H, H
3. A,B,C,D = OCH₃, H, H, CH₂CH(NH₂)CH₃
4. A,B,C,D = H, CH₂CH(NH₂)CH₃, H, H
5. A,B,C,D = H, F, CH₂CH₂NH₂
6. A,B,C,D = OCH₂CH₂CH₂CH₂CH₂CH₂CH₂CH₃, H, H, CH₂CH₂NH₂
7. A,B,C,D = OH, H, H, CH₂CH₂NH₂
8. A,B,C,D = H, H, CH₂CH(NH₂)CH₃

Group 3

A = OH or H

Group 4

A = CH₂CH₂CH₃, CH(CH₃)CH₃, CH₂CH₃, CH₃

Group 5

A = CH(CH₃)CH₃, CH₂CH=CH₂, CH₂CH₂CH₂CH₃, CH₂CH₃, CH₃, CH₂CH₂CH₂CH₃, CH₂CH(CH₃)CH₃

B = CH(CH₃)CH₃, CH₂CH=CH₂, CH₂CH₂CH₂CH₃, CH₂CH₃, CH₃, CH₂CH₂CH₃, CH₂CH(CH₃)CH₃

Group 6

A = OH or H

Group 7

A = CH₂CH₃, CH₃, CH₂CH₂CH₃, CH(CH₃)CH₃
B = CH₂CH₃, CH₃, CH₂CH₂CH₃, CH(CH₃)CH₃

Group 8

Group 9

Group 10

A = CH₂CH₃, CH₃, CH₂CH₂CH₃, CH(CH₃)CH₃
B = CH₂CH₃, CH₃, CH₂CH₂CH₃, CH(CH₃)CH₃

Figure 2.8 Skeletal frameworks for each of the 10 classes that emerged from PLS-DA.

52
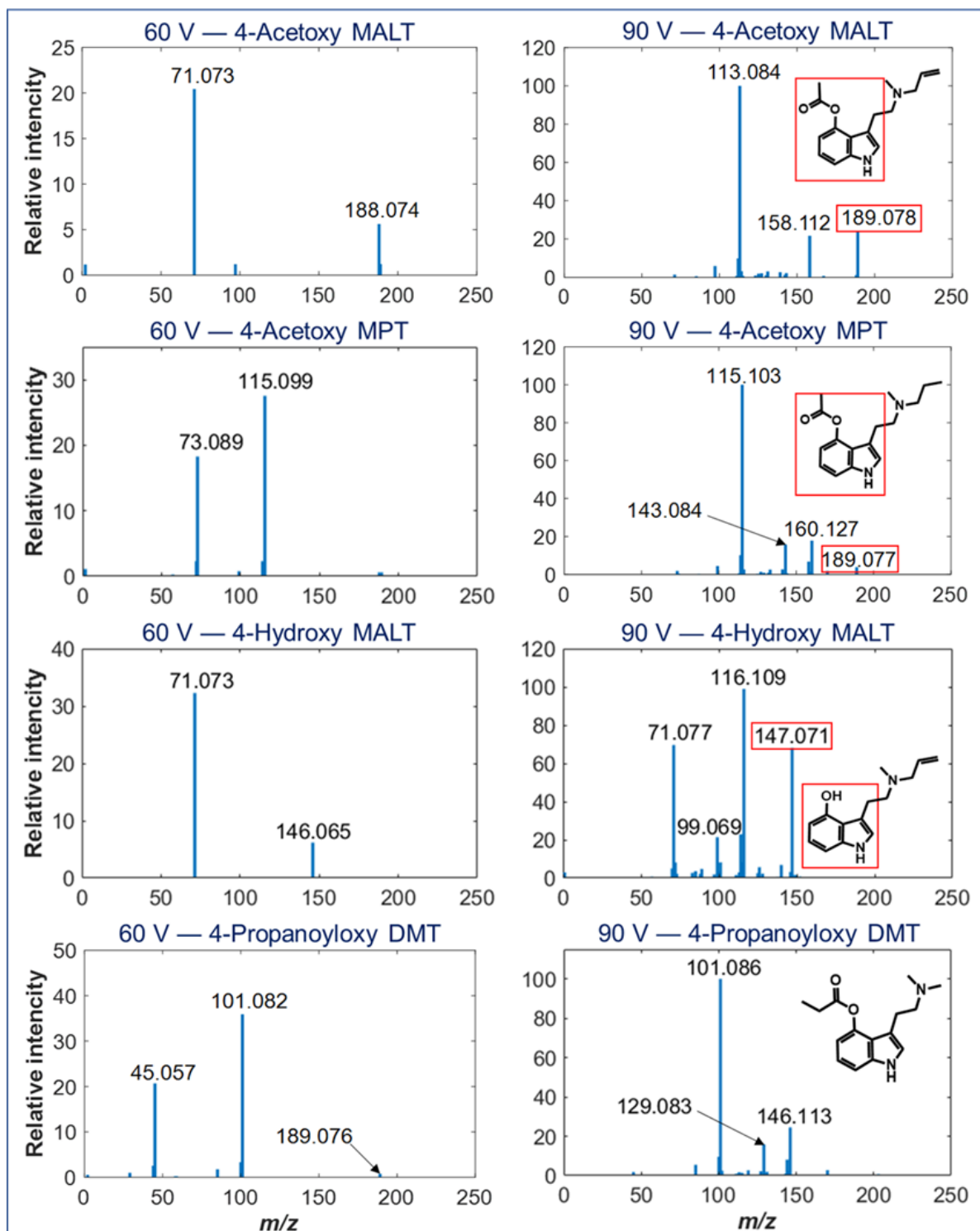
Figure 2.9 Neutral loss spectra of the four tryptamines: 4-acetoxy MALT, 4-acetoxy MPT, 4-hydroxy MALT, and 4-propanoyloxy DMT, that were used for the external validation at 60 V and 90 V. The red boxes show the *m/z* values in the neutral loss spectra that are markers for specific groups according to the PLS-DA results. Masses *m/z* 189.08 and 147.07 shown in the red boxes are markers of groups 10 and 7, respectively.

compounds in specific groups. 4-Acetoxy MALT and 4-acetoxy MPT exhibited a peak at *m/z* 89.08, which is a common *m/z* value for class 10 members. According to Table A2.3, the *m/z* value 189.08 also appears in the 90 V spectra of some compounds in groups 5 and 7. The 4-hydroxy MALT neutral loss spectrum exhibited a peak at *m/z* 147.07, a class 7 marker. The results for the screening of the four tryptamines against the previously developed hierarchical clustering dendrogram and correlation matrix, along with their corresponding groups are presented in Figure 2.10. The probabilities of a compound being assigned to a given class are shown in Table A2.4. The positioning of the unknowns within the correlation matrix is shown in Figure 2.10 for the compounds highlighted in the yellow box. Also shown in Figure 2.10 is where these unknowns fell within the dendrogram, which is indicated with blue shading. 4-Hydroxy MALT fell within the red region of the dendrogram, which represents Group 7, while 4-acetoxy MALT, 4-acetoxy MPT, and 4-propanoyloxy DMT fell within the green region, which represents Group 10. Using a significance level of >0.05, the probabilities presented in Table A2.4 show that the model was able to correctly classify 35 of the 40 external validation sample replicates. The exceptions were two replicates of 4-acetoxy MALT and three replicates of 4-hydroxy MALT, which the model did not assign to any specific group. However, for all classified replicates, the assignments made were correct. The results show that the model has the ability to correctly predict detection of new tryptamine structures and reveal indications of their core scaffolds using DART-HRMS data. This enables extraction of their features so that their shared characteristics can be detected (as shown in Table 2.3). The fusion of the 60 V and 90 V data helped to broaden the range of the fragments that could be interpreted when compared to those detected at only one of the two voltages. This effectively enhanced the prediction capacity of the model for detection of new tryptamines.
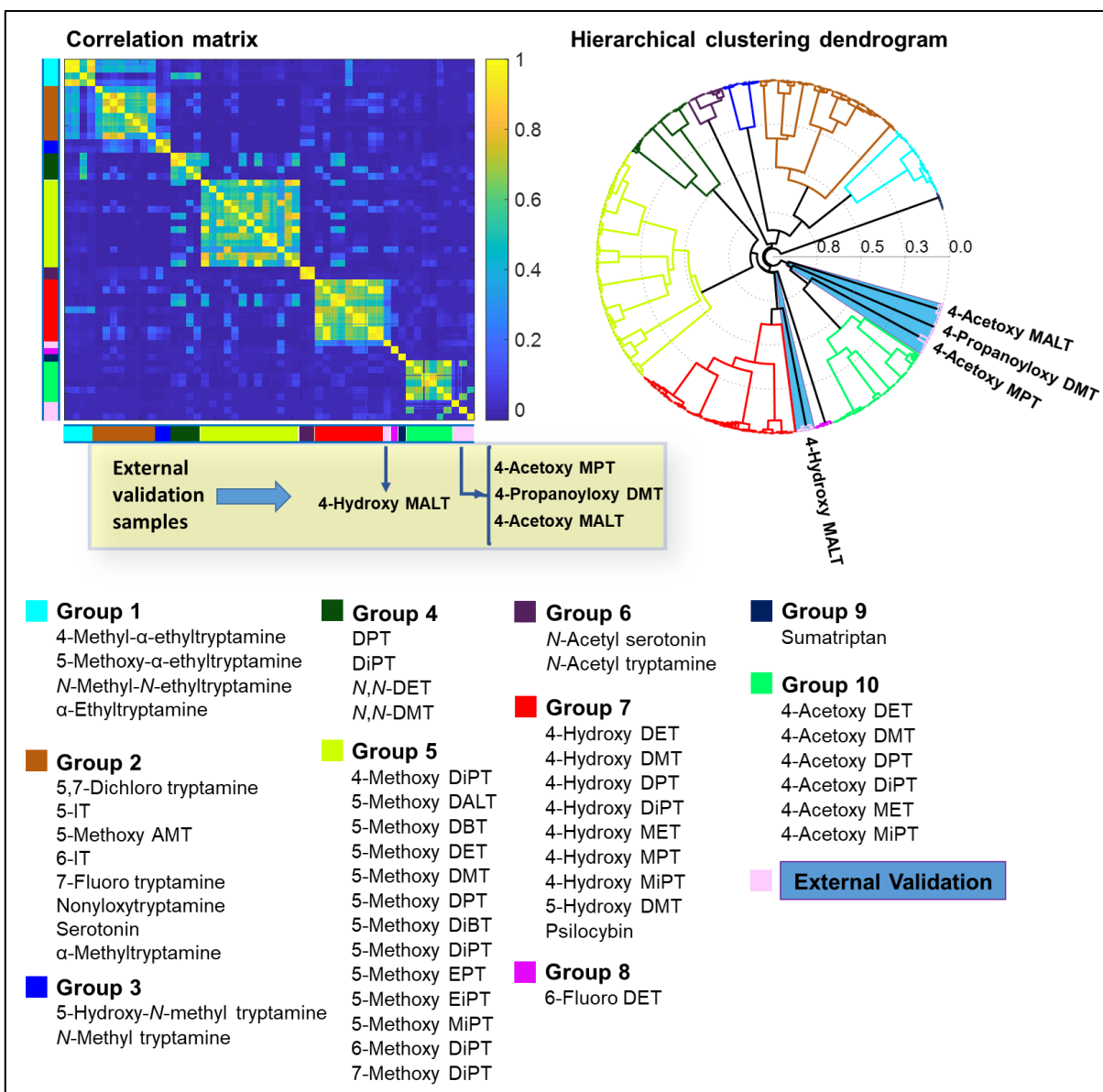
Figure 2.10. Correlation matrix and dendrogram showing the placement of the four tryptamines used for external validation. The four tryptamine external validation sample "unknowns" were: 4-Hydroxy MALT, 4-acetoxy MALT, 4-propanoyloxy DMT, and 4-acetoxy MPT. These are highlighted in the yellow box to show their placement in the correlation matrix (indicated in pink). Their placement in the dendrogram is indicated with blue shading. 4-Hydroxy MALT was correctly placed into group 7; 4-acetoxy MALT, 4-propanoyloxy DMT, and 4-acetoxy MPT were correctly placed into group 10.

2.3.7. Structure Elucidation of a Tryptamine Unknown

To illustrate how this approach can be utilized to extract information about the core tryptamine scaffold of an unknown, 4-hydroxy MALT will be used as a case in point. As indicated earlier, this molecule was not used to build the PLS-DA prediction model and therefore it can be

considered to be an unknown. From the spectrum generated from analysis of the compound at 20 V (Figure 2.11, with its corresponding mass data table shown in Table A2.5), its high-resolution monoisotopic mass (231.153) was found to correspond to the formula $C_{14}H_{19}N_2O$ for the protonated molecule (and thus a formula of $C_{14}H_{18}N_2O$ for the neutral compound). Collection and subsequent fusion of the 60 V and 90 V neutral loss data of this tryptamine and screening the resulting spectrum against the statistical model revealed it to fall into Group 7. This is mostly due to the presence of the marker m/z 147.071, with the core scaffold revealed to be a hydroxylated indole ring with an N-substituted ethylamine appendage (see Figure 2.9). The neutral loss fragment that represents this class 7 marker is illustrated in the red box in Figure 2.9 and accounts for nine carbons, nine hydrogens, one nitrogen, and one oxygen. When this is subtracted from the molecular formula of $C_{14}H_{18}N_2O$, a balance of five carbons, nine hydrogens, and one nitrogen remain (i.e. C_5H_9N) and this combination of atoms contains one double bond equivalent. Figure 2.12 illustrates what the corresponding possibilities are for the substituents on the exocyclic
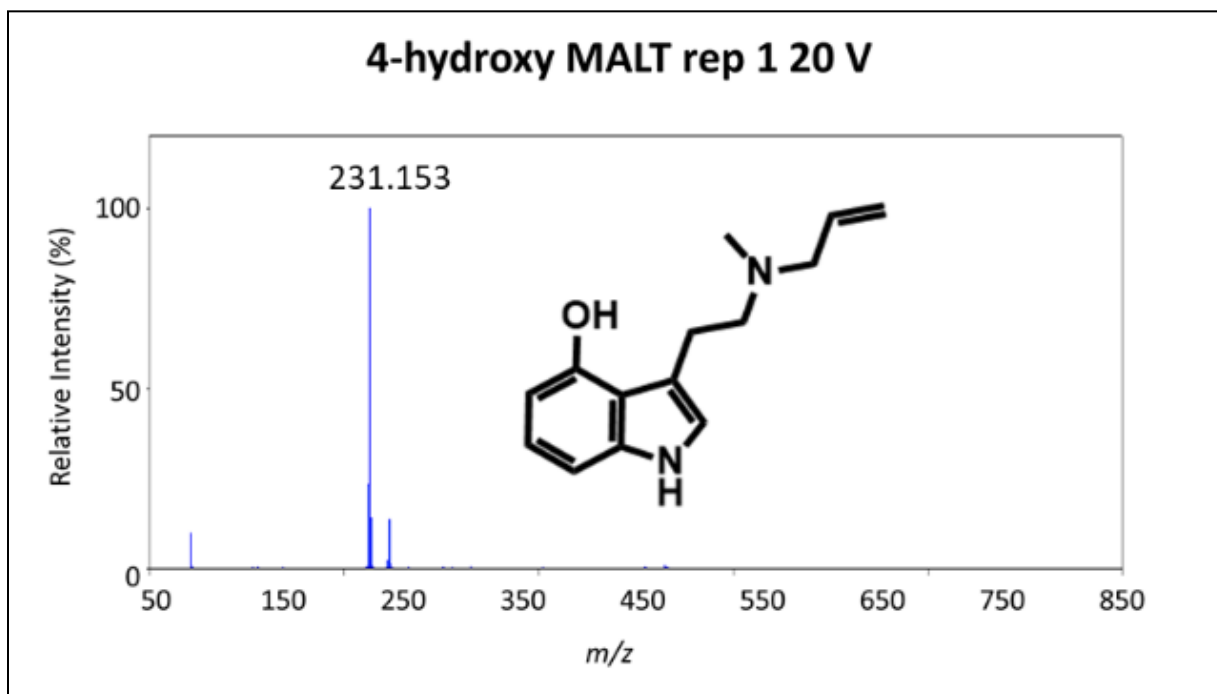
Figure 2.11. The 20 V soft ionization spectrum of 4-hydroxy MALT with the protonated precursor labeled at m/z 231.153.
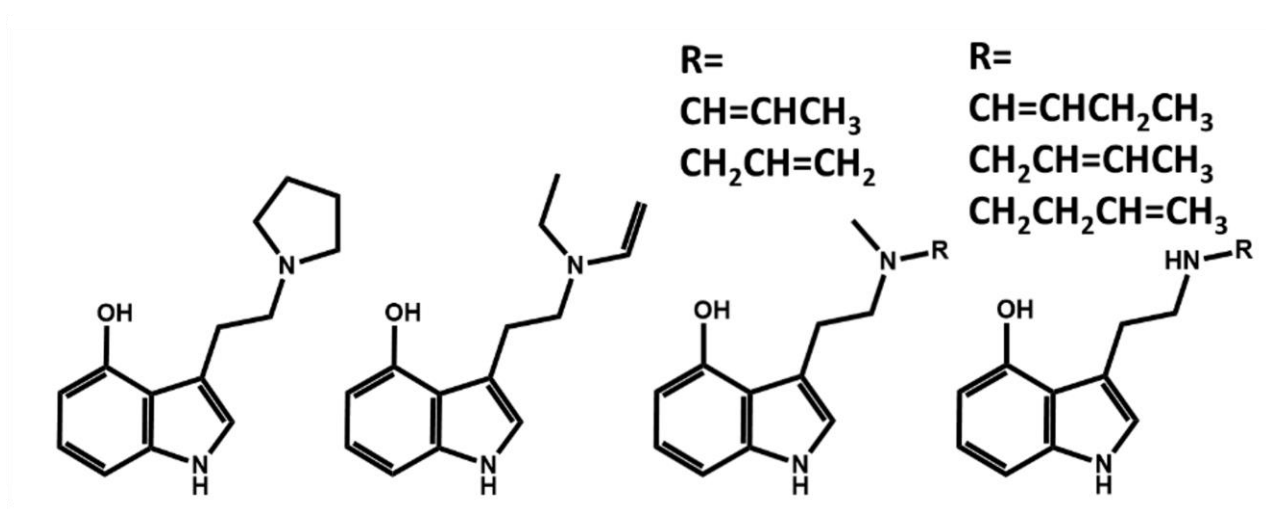
Figure 2.12. The possible tryptamine structures of the "unknown". The third structure with the R group – CH₂CH=CH₂ is the correct structure of 4-hydroxy MALT.

nitrogen, which include the nitrogen as part of a five membered ring; an ethyl and an ethylene substituent; a methyl substituent with various alkenyl substituents; and a hydrogen and a four-carbon alkenyl substituent. In the absence of the predictive model, an analyst conducting a SciFinder search of structures with the molecular formula $C_{14}H_{18}N_2O$ is confronted with a list of approximately 35,000 structures. The approach presented here decreases this number of possibilities by a thousand-fold and provides 7 plausible structures, one of which is correct.

2.3.8. Data Reproducibility

In order to assess the impact that analysis by different individuals and analysis on different days have on intra-laboratory reproducibility of the prediction results, the DART-HRMS analysis of 4-acetoxy MPT was performed by three different analysts in one day and by a fourth analyst on two different days, but one year apart. The samples were analyzed by DART-HRMS in replicates of 10. The spectra were then subjected to principal component analysis (PCA), the results of which were then examined by Q residuals and Hotelling's T^2 statistic to detect the outliers. Figure 2.13A shows a representative PCA scores plot of auto-scaled data (after removing outliers) collected by different analysts on the same day and one analyst on different days. The results show that, except

A

B
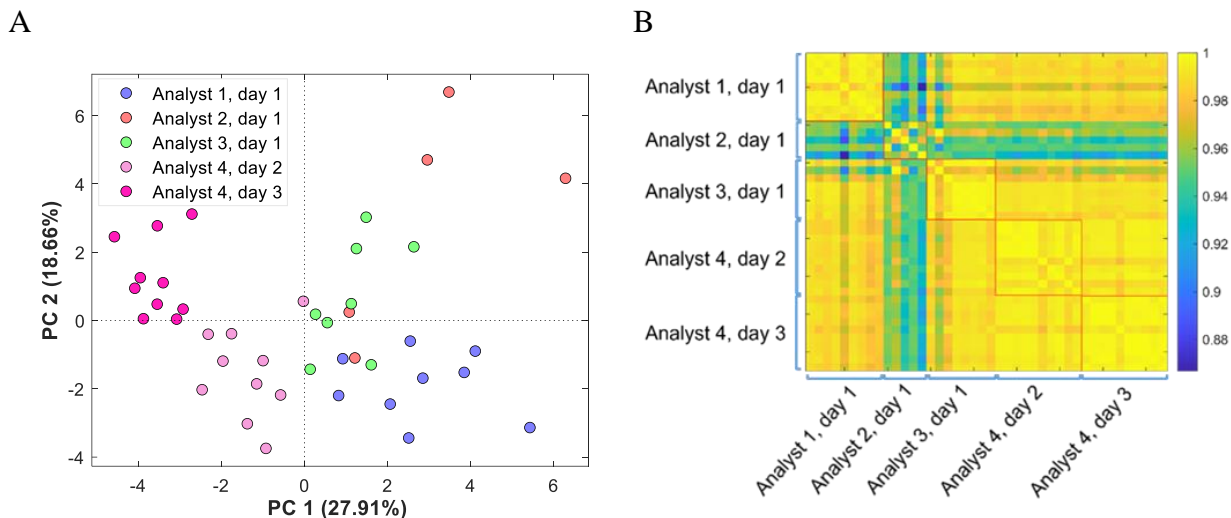
Figure 2.13 Results of the analysis of variation between DART-HRMS-derived neutral loss spectra collected by different individuals on the same day and one individual on different days. A: PCA scores plot of the collected data; B: Correlation matrix, where the yellow color shows the highest inter-spectral correlation and blue shows the lowest.

for several replicates acquired by analyst 2, the differences between multi-day versus multi- person analyses are small. Two approaches were used to quantify the variations: (1) the median of the relative standard deviation (RSD) which, according to Parsons et al.,[132] serves as a single summary statistic to reveal reproducibility in metabolomics data; and (2) the Pearson's r coefficient, which is a metric for evaluation of the reproducibility and stability of ambient ionization mass spectral data according to Zhvansky et al.[133]

Overall, the RSD values show greater reproducibility for peaks with higher intensities. The median RSD values for spectra collected for each individual analysis have variations in peak intensities between 10-28%, with a value of 24% for analyst-to-analyst variation and 13% for day-to-day variation. The correlation matrix (Figure 2.13B) shows the Pearson's r coefficient measure between DART-HRMS-derived neutral loss spectral replicates, revealing the variation between the spectra analyzed by analyst 2. No considerable variation between the chemical profiles that were analyzed by the four analysts on three different days was observed. The image also illustrates

the consistency of the results of the analyses, as there is high similarity between the data collected on two consecutive days, and that acquired one year before.

2.4. Conclusion

The prediction of the skeletal frameworks of NPS tryptamine structures can be accomplished by screening their neutral loss spectra acquired under CID conditions at 60 V and 90 V by DART-HRMS against a PLS-DA prediction model built using the neutral loss mass spectra of 50 tryptamines representing a range of structures. The model revealed 10 groups of tryptamines that were classified based on the similarities of the neutral losses observed when the molecules were fragmented under CID conditions during DART-HRMS analysis. The data generated at 60 V and 90 V were fused in order to expand the range of masses from which structural information could be extracted. "Leave-one-structure-out" validation and the screening of external validation samples (using four tryptamines that were new to the model) were used to assess the prediction capacity of the model. The results showed 100% accuracy, precision, sensitivity, and specificity for the prediction model, as well as 0% error, 5% multi-label assignment, and 4% not-assigned rates. Data from multiple analysts shows that the results are reproducible. This method provides a rubric for how to facilitate more rapid assessment of the identity of NPS tryptamines when encountering unknowns for which little information on structural identity is initially available.

CHAPTER 3: CREATION OF A <u>D</u>ATABASE <u>O</u>F <u>P</u>SYCHOACTIVE <u>P</u>LANTS (DOPP) FOR RAPID SPECIES IDENTIFICATION OF PSYCHOACTIVE PLANT MATERIALS

3.1. Introduction

One of the continuing challenges in analytical chemistry is the paucity of efficient approaches for the rapid identification of plant-derived complex matrices. This is of particular relevance in forensics where the ingestion of psychoactive plant materials can cause impairment that leads to the commission of crimes; the improper handling of machinery resulting in workplace accidents; impaired driving; agitation and disorientation leading to violence; and mental and physical health challenges that can result in death.[134–136] Because of its relevance to possible criminal activity or liability, it is essential that the species identity of the plant material that was ingested be known. While such determinations are relatively straightforward for the small number of mind-altering plants that have physical characteristics that are readily recognized by visual examination (e.g., observation of cystolithic hairs unique to *Cannabis sativa*), the vast majority of psychoactive plants and the materials derived from them (e.g., crumbled leaves and other aerial parts, seeds, tinctures and extracts, etc.) do not have distinguishing features that enable them to be readily differentiated from innocuous products such as foods and spices. Some psychoactive plants have served as sources of modern-day drugs that continue to be clinically relevant, such as atropine and scopolamine from *Datura* species plants.[66,137] However, the vast majority of known psychoactive plants are typically regarded as dangerous, with no generally accepted clinical use. It is for this reason that the active small-molecule components of many of these plants, when known, have been scheduled. Those shown to have addictive properties and no established medical use have been designated as Schedule I drugs, and those that are addictive but have clinical utility are categorized as Schedule II.[138] Examples of the former include ibogaine found in plants in the

Apocynaceae family, and *N,N*-dimethyltryptamine (DMT) found in multiple species such as *Mimosa hostilis (tenuiflora)*, *Diplopterys cabrerana*, and *Psychotria viridis*. Examples of the latter include atropine and scopolamine which are found in many plants in the *Datura* genus. Ironically, while the purified forms of most of the known addictive small-molecule natural products are scheduled, the plants from which many of them are derived are not. For instance, atropine and scopolamine are Schedule II drugs, but the *Datura spp*. plants that contain them are not. For this reason, the plants are known as "legal highs", because unlike their purified active components, in most countries and U.S. states, they can be possessed and ingested without fear of prosecution.[139,140] The exponential rise in the abuse of these dangerous materials has raised alarm and caused the United Nations Office on Drugs and Crime (UNODC) to declare 20 species as "plants of concern", including *Mitragyna speciosa* and *Salvia divinorum*.[1] An important prerequisite to the legislation of the manufacture, sale, distribution and ingestion of these substances is the ability to identify them rapidly and definitively. However, a systematic way in which to routinely accomplish this for the ever-increasing range of plant materials and their evolving forms has proven elusive. This is because: (1) the plant materials themselves often do not possess distinguishing features, making them unrecognizable in a forensic context; (2) standard well-established analytical methods (such as GC-MS and LC-MS) that are useful in the identification of purified or semi-purified substances are time-consuming to perform on whole plant material, and/or have not been developed for analysis of whole plant products; (3) there is generally no statistical reporting of the level of certainty of a positive identification of a particular plant drug based on screening it against a bona fide database; and (4) unlike the case for purified compounds for which libraries of spectroscopic and mass spectrometric data are available that can serve to facilitate confirmation of the structures of unknowns, there is no available analogous

database with accompanying software to aid in the rapid detection of plant materials. Therefore, there is an urgent need for the development of a rapid analysis approach that circumvents some of the present challenges associated with identification of dangerous psychoactive plant-derived substances.

Previous studies have shown that direct analysis in real time–high-resolution mass spectrometry (DART-HRMS), with minimal if any sample preparation required, reveals within a single analysis of the bulk material a range of detected molecules extending across the dielectric constant range.[11,48,60,69,84,141–144] Furthermore, it has been shown that when analyzed by DART-HRMS, plants exhibit species-specific chemical signatures that can be utilized to predict the identities for species within a given genus, using advanced statistical analysis tools.[61,65,66,84,87,145,146] These findings imply the possibility that the application of machine learning tools to a library of DART-HRMS-derived species-specific chemical signatures might provide a mechanism by which to predict the species identity of plant material unknowns with a statistical level of certainty. In principle, it could provide a more universal approach for the identification of new psychoactive materials, rather than relying on current conventional methods which require nuanced method development that is also time- and resource-intensive. Importantly, the analysis can be conducted in less than one minute per sample.

Reported here for the first time is the accomplishment of two main aims: (1) development of a DART-HRMS chemical signatures database of available psychoactive plants; and (2) development of a user-friendly and intuitive data analysis tool for the rapid identification of unknown materials (termed Database of Psychoactive Plants (DoPP)). The application allows users to simply import the DART-HRMS data of the unknown into the platform, which then reveals species identity with a statistical level of certainty.

3.2. Methods

3.2.1. Materials

Plant materials representing 18 families, 34 genera and 57 species, and which included various plant parts (e.g., seeds, flowers, roots, leaves, bark, roots, stems) and processed products such as resins, powders, extracts, and capsules from different vendors were analyzed. Detailed information on the analyzed plants, including order, family, genus, and species, as well as the material type and vendor, are presented in Table A3.1. Scheme 3.1 illustrates taxonomical relationships between families, genera and species of the represented plants, with the families and genera highlighted in yellow and light green boxes, respectively.

Scheme 3.1. Plant species represented in the DoPP platform and the taxonomical relationships between them.
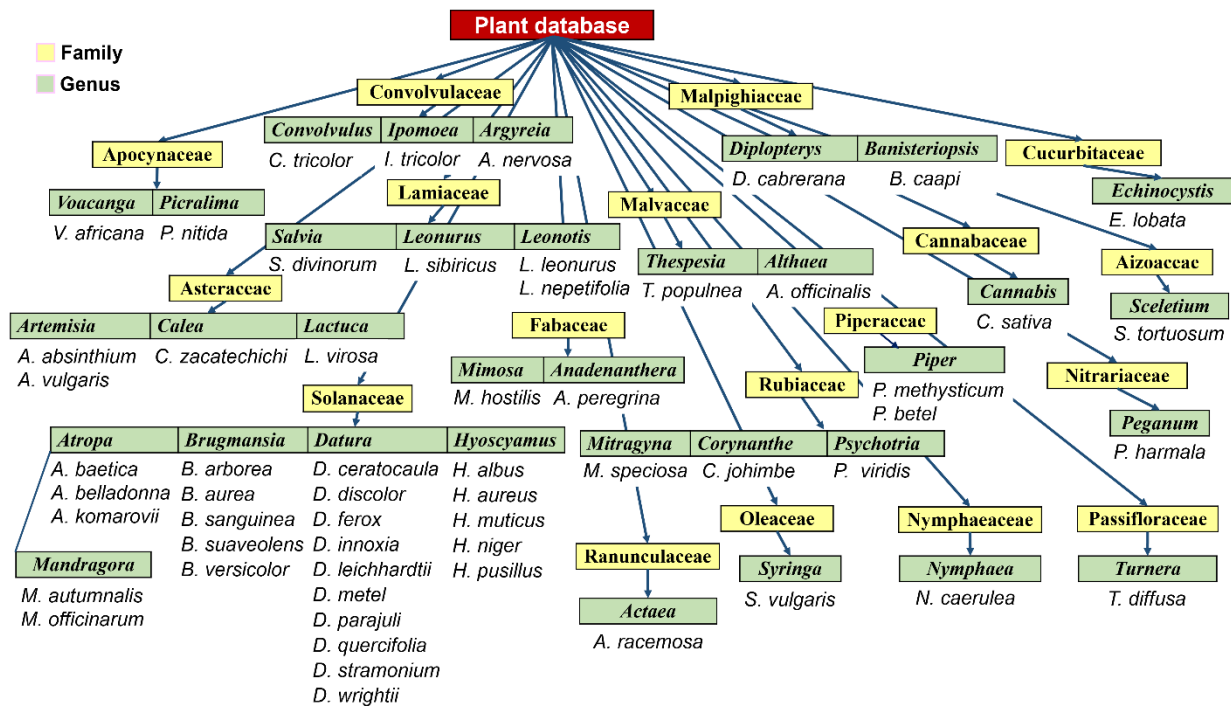
3.2.2. Instrumentation

A DART-SVP ion source (IonSense Inc., Saugus, MA, USA) coupled with a JEOL AccuTOF high-resolution time-of-flight mass spectrometer (JEOL USA, Peabody, MA, USA)

operating in positive-ion mode was used to collect spectra in the range *m/z* 40-1100 (as indicated in Scheme 3.2-Step 1). Mass spectrometer settings were as follows: gas heater temperature, 350 °C; orifice 1, 20 V; orifice 2, 5 V; ring lens, 5 V; peak voltage, 400 or 600 V; grid voltage, 50 V; and ion source helium flow rate, 2.0 L/min. For DART-HRMS analysis of seeds and bark, samples were divided into smaller segments using a razor blade, and each of the segments was suspended via tweezers directly within the path of the DART gas stream in the open-air space between the ion source and mass spectrometer inlet.

Liquids, powders, resins, extracts, crushed leaves and the pulverized content of the interiors of gelatin-based capsules were each sampled three times by suspending the closed end of a melting point capillary tube into the material and presenting the coated surface into the DART gas stream. For the seeds and bark, each of the generated DART mass spectra represented the average of the spectra of the segments, while for the liquid, powder, resin, extract, ground leaves and capsule samples, each spectrum was comprised of an average of three spectra. With each set of analyses for each product, polyethylene glycol 600, which served as a mass calibrant, was analyzed. TSSPro3 software (Schrader Software Solutions, Grosse Pointe, MI, USA) was used for processing of the mass spectra for background subtraction, mass calibration and peak centroiding. Test samples of *Mitragyna speciosa* (aka kratom) and five samples of *Datura* species were analyzed by independent laboratories using same experimental parameters. Kratom leaves were sampled by a different analyst at IonSense Inc. (Saugus, MA, USA) using a similar instrument to

Scheme 3.2. An overview of the data analysis workflow for psychoactive plant materials.
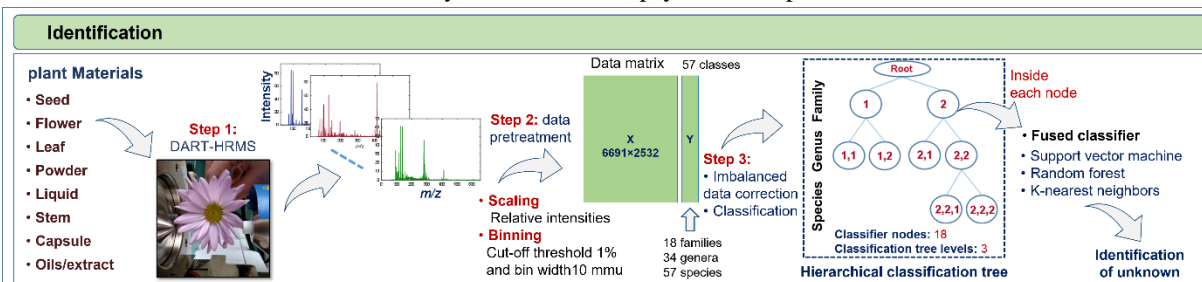
that operated in our laboratory. *Datura* species were analyzed at the Emerging Technology and Entrepreneurship Complex (ETEC) at the University at Albany by the same analysts, using a DART Ion Source SVP coupled to a JEOL JMS-T100LP AccuTOF LC-plus 4G mass spectrometer. It was found that for this instrument, increasing the detector voltage to 2200 V and adjusting the sampling interval to 0.25 ns were critical to obtaining mass spectra that could be screened against the database for external validation purposes. It should also be noted that by altering the gas temperature and/or orifice 1 voltage, the data collected can deviate enough from that of the spectra within the database to lead to false positives or negatives. There are two reasons for this: (1) the relative abundance of the peaks changes as a function of temperature. The spectra at lower temperatures are dominated by peaks from more volatile compounds and at higher temperatures, higher boiling compound peak are more prominent; and (2) increases in the orifice 1 voltage (and to a much lesser extent increases in temperature), shift the analysis from one that is conducted under soft ionization conditions (i.e., 20 V), where there is minimal fragmentation, to one where there is collision induced dissociation. This can lead to spectra that will appear quite different from those that populate the database because the spectra will be dominated by fragment peaks that appear at the expense of the protonated precursor peaks from which they are derived. Therefore, it is essential that the instrument parameters are well replicated.

3.2.3. Multivariate Data Analysis

Described here is the psychoactive plant material identification workflow that was devised, and which was based on the machine learning processing of a database of the species-specific chemical fingerprints of psychoactive plants. The sample identification aspect of this workflow is comprised of mass spectral data pre-processing, application of advanced statistical analysis, and identification of plant material unknowns. To develop the approach, the processed DART mass

spectra (6691 spectra overall), which were collected from plant materials representing 18 families, 34 genera and 57 species, were imported as text files into Python 3.7 software (Python Software Foundation, DE, USA) in the form of two column tables of *m/z* values and their corresponding relative intensities. As indicated in Scheme 3.2—Step 2, the spectra were aligned in a matrix with an optimal bin width (10 millimass units (mmu)) and a relative abundance cut-off threshold of 1%. Due to the variability of sample numbers and availability, there was significant disparity between the numbers of samples of each species. This imbalance was addressed using the support vector machine-synthetic minority oversampling technique (SVM-SMOTE),[147,148] which served to increase the number of samples in minor classes through the generation of "synthetic data". The synthetic data were randomly created along the lines adjoining each minority class support vector with several of its nearest neighbors. Since the species share taxonomical relationships (as shown in Scheme 3.1), a supervised top-down hierarchical classification tree[66,85] was designed to simplify the complex 57 flat classification problem into 18 multi-classes (as illustrated in Scheme 3.2— Step 3). The classification tree had 18 classification nodes organized in 3 levels of discrimination (family, genus, and species) and ended at 57 leaf nodes representing the individual species. Thus, samples were first categorized into families at the first level of discrimination, and subsequently discriminated by genus and then to the corresponding species at the second and third levels, respectively. To increase the performance of the classification model,[83,149,150] the results of three machine learning methods were fused using posterior probabilities. Therefore, within the classification node of each tree, random forest (RF), k-nearest neighbors (KNN) and support vector machine (SVM) were trained, and each trained model assigned a probability value to each class label for the samples in each classification node. Prediction of the sample label is based on the average of the probabilities resulting from application of the SVM, KNN and RF models. For

assignment of samples to each class in each node, a probability threshold was computed for each class using the prediction results of 100 X randomly selected test set (30 percent of data) and the precision-recall (sensitivity) curves.

3.3. Results

To develop a classification model for rapid identification of psychoactive plant-derived materials, hierarchical classification tree-based supervised methods were used. The overall approach, including data acquisition and statistical analysis, is summarized in Scheme 3.2. Assessment of mass spectra in both positive and negative ion modes revealed that much more chemical information (i.e., many more peaks) was contained in the positive-ion mode spectra. Given that the greater the number of peaks, the more refined a prediction model that can be built, we chose to use the spectra generated in positive-ion mode. Representative spectra (average of 10 DART-HRMS analysis replicates) for all 57 species are presented in Figure A3.1 for one of the forms of the material. Their corresponding mass tables are deposited at https://rabi-musah.squarespace.com/s/Psychoactive-Plant-mass-tables-corresponding-to-Figure-A4-and-Figure-35.xlsx. As an example, spectra of diverse forms of *Artemisia absinthium* are shown in Figure 3.1, with their corresponding mass data presented in Tables A3.2-A3.5. The figure displays the spectra of powders and seeds, as well as a processed form of the materials (an *A. absinthium* tincture). From the figure, similarities and differences between the spectra are noted. For example, some peaks are common to multiple sample forms (such as *m/z* 231.125). On the other hand, the seed was observed to exhibit the greatest number of peaks. The spectra of the different forms of each species were compared to remove the variables related to the plant matrix and not related to species. As indicated in Scheme 3.2—Step 2, the collected spectra were aligned along common *m/z* values using a relative abundance threshold cutoff of 1%, and binned (with a bin width of 10
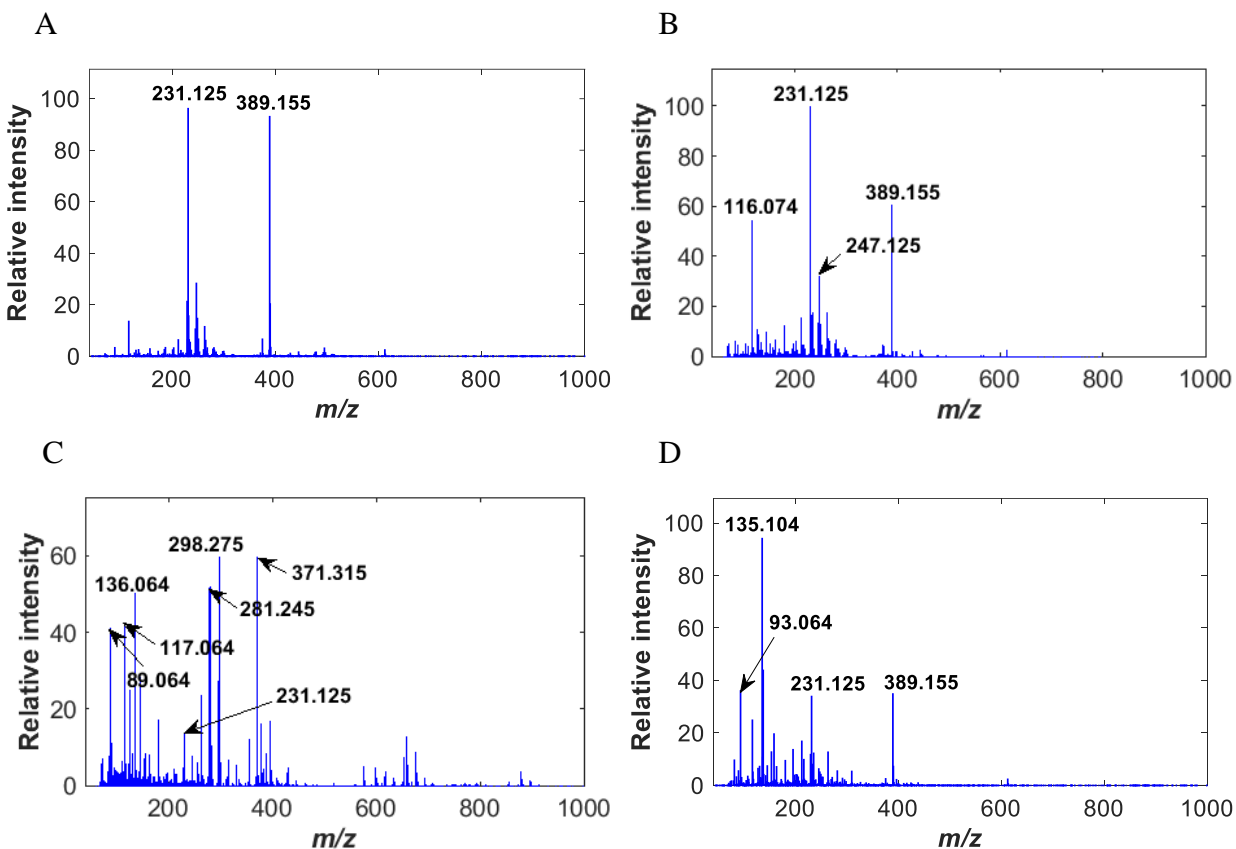
Figure 3.1. Representative 20 V soft ionization DART mass spectra of: (A) dried herb; (B) powder; (C) seed; and (D) tincture of *A. absinthium*.

mmu). The bin width and relative abundance threshold cutoff values were determined by iterative evaluation of the goodness cutoffs. The resulting matrix with dimensions of 6691×2532 was subjected to the application of SVM-SMOTE to handle the class imbalances. Species discrimination was then achieved by adopting hierarchical classification tree-based supervised methods using scikit-learn[151] and its interfaces.[152] The spectra of 30% of the samples were randomly selected to serve as external validators for the testing of the trained models, and the hierarchical classification tree was trained against a fused classifier comprised of SVM, RF, and KNN methods. The trained model was then validated using 10-fold cross validation and external validation, yielding prediction accuracies of 98% and 99%, respectively. Figure 3.2 illustrates the corresponding normalized confusion matrix for the external validation of the fused classifier. The
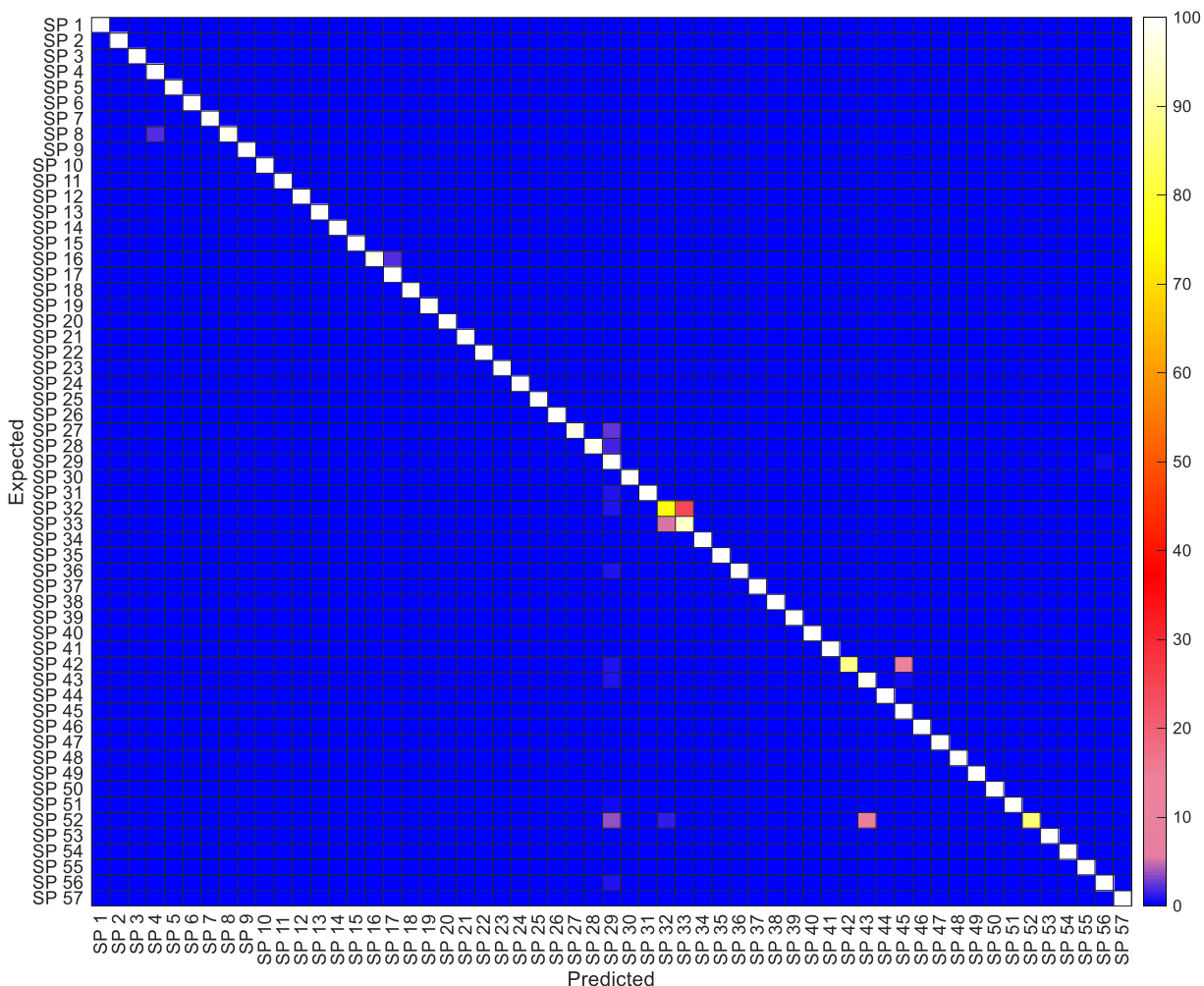
Figure 3.2 Normalized confusion matrix presenting the external validation results of the hierarchical classification tree. The color gradient extends from blue to white, where blue represents 0% and white presents 100% prediction rates. The x- and y-axes display the prediction and true values, respectively. Diagonal elements in the confusion matrix correspond to true positive rates and non-diagonal elements are indicative of false positive and false negative rates. Sp 1: *A. baetica*;Sp 2: *A. belladonna*; Sp 3: *A. komarovii*; Sp 4: *B. arborea*; Sp 5: *B. aurea*; Sp 6: *B. sanguinea*; Sp 7: *B. suaveolens*; Sp 8: *B. versicolor*; Sp 9: *D. ceratocaula*; Sp 10: *D. discolor*; Sp 11: *D. ferox*; Sp 12: *D. innoxia*; Sp 13: *D. leichhardtii*; Sp 14: *D. metel*; Sp 15: *D. parajuli*; Sp 16: *D. quercifolia*; Sp 17: *D. stramonium*; Sp 18: *D. wrightii*; Sp 19: *H. albus*; Sp 20: *H. aureus*; Sp 21: *H. muticus*; Sp 22: *H. niger*; Sp 23: *H. pusillus*; Sp 24: *M. autumnalis*; Sp 25: *M. officinarum*; Sp 26: *A. absinthium*; Sp 27: *A. vulgaris*; Sp 28: *C. zacatechichi*; Sp 29: *L. virosa*; Sp 30: *P. nitida*; Sp 31: *V. africana*; Sp 32: *A. nervosa*; Sp 33: *C. tricolor*; Sp 34: *I. tricolor*; Sp 35: *A. peregrina*; Sp 36: *M. hostilis*; Sp 37: *B. caapi*; Sp 38: *D. cabrerana*; Sp 39: *L. leonurus*; Sp 40: *L. sibiricus*; Sp 41: *L. nepetifolia*; Sp 42: *S. divinorum*; Sp 43: *M. speciosa*; Sp 44: *C. johimbe*; Sp 45: *P. viridis*; Sp 46: *A. officinalis*; Sp 47: *T. populnea*; Sp 48: *P. betel*; Sp 49: *P. methysticum*; Sp 50: *E. lobata*; Sp 51: *C. sativa*; Sp 52: *S. tortuosum*; Sp 53: *P. harmala*; Sp 54: *A. racemosa*; Sp 55: *S. vulgaris*; Sp 56: *N. caerulea*; Sp 57: *T. diffusa*. The confusion matrix reveals a prediction accuracy of 74.75%, 86.2% and 87.91% for Sp32, Sp42 and Sp52, respectively. These accuracies show that the model can still be considered to be well-fitted for Sp42 (dried herb, extract, powder and root) and Sp52 (leaf and extracts with different concentrations). However, it remains uncertain why the results are not as accurate for Sp32 (only in seed form).

69

x- and y-axes display the predicted and expected values, respectively. The color gradient extends from blue to white, with blue representing a 0% prediction rate and white, a 100% prediction rate for identification. The diagonal values in the matrix correspond to true positive rates and the off-diagonal entries represent false negative and false positive rates. As illustrated in Figure 3.2, with the exception of the three species *A. nervosa* (Sp 32), *S. divinorum* (Sp 42), and *S. tortuosum* (Sp 52), for which the true positive rates fell between 70 and 90%, all other species were predicted with ≥ 90% accuracy. To facilitate the utilization of the fused classifier model as a tool for the screening and identification of psychoactive plant material unknowns, an intuitive and user-friendly graphical interface named <u>D</u>atabase <u>o</u>f <u>P</u>sychoactive <u>P</u>lants (DoPP) was designed and developed as a stand-alone application in Windows (using the programming language Python). It is comprised of three parts termed "*Identification*", "*Quantification*" and "*Psychoactive plant directory*" which are accessible via tabs (see Figure 3.3). This chapter focuses on the content and development of the "*Identification*" and "*Psychoactive plant directory*" components. The *Identification* tab displays the species identity prediction that DoPP assigned to the DART mass spectrum of material that was screened. Using the *Psychoactive plant directory* tab, the user can access a repository of the mass spectra of different forms of the species in the database (e.g., from different areas of the plant such as the aerial parts, roots, seeds etc.), or processed forms such as extracts, in order to make comparisons and visualize the chemical structure(s) of the psychoactive component(s), among other features. Details for the plant species, such as molecule(s) of interest with their respective monoisotopic masses, chemical formulas, and structures, can be found in Table A3.6. The *Psychoactive plant directory* tab also serves as a resource of information about the plant species represented within DoPP. Clicking this tab opens the window shown in Figure 3.4A, where a list of each of the species that fall under the "*Sample Information*" section can be
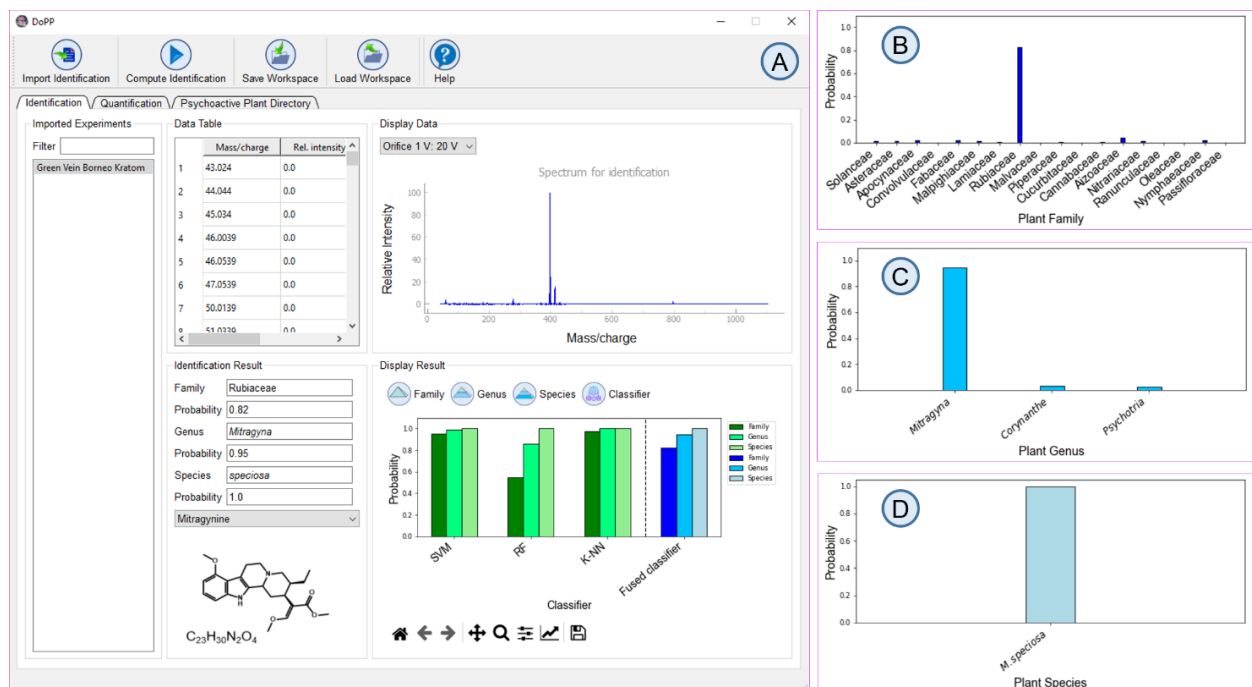
Figure 3.3. Illustration of the application of DoPP for the identification of a plant sample (*M. speciosa*) analyzed by DART-HRMS. As shown in Panel A, when the mass spectrum of the solid material is imported, the interface reveals the mass data table containing *m/z* values and the corresponding relative intensities, and the mass spectrum of the query sample. The results present: (1) the family, genus and the species of the query sample, along with the posterior probabilities from the fused classifier in the three levels of the hierarchical classification tree; (2) the identity and structure of any known psychoactive components; and (3) a bar plot showing the probabilities associated with the identification of the family, genus, and species by the embedded classifiers (i.e., SVM, RF, K-NN and a fused classifier comprised of all three) in the hierarchical classification tree. Three other bar plots (Panels B-D) display the probabilities for identification of the family, genus and species levels acquired using the fused classifier.

found. If, for example, a search of *Lactuca virosa* is performed within this tab, mass spectra of different analyzed forms of this species appear in the "Display Data" section of the tab (as shown in Figure 3.4B). Also, a link to the Wikipedia page that describes the species and the structures of its known psychoactive components appears under the "Psychoactive Compound" tab. As DoPP contains DART mass spectra of powder, leaf, flower, resin, seed, and tincture forms of *L. virosa*, representative mass spectra of each can be viewed via the "Display Data" section, where the mass spectra of each form are shown in Figure 3.4B, with their corresponding mass data tables presented in Tables A3.7-A3.12

.

71
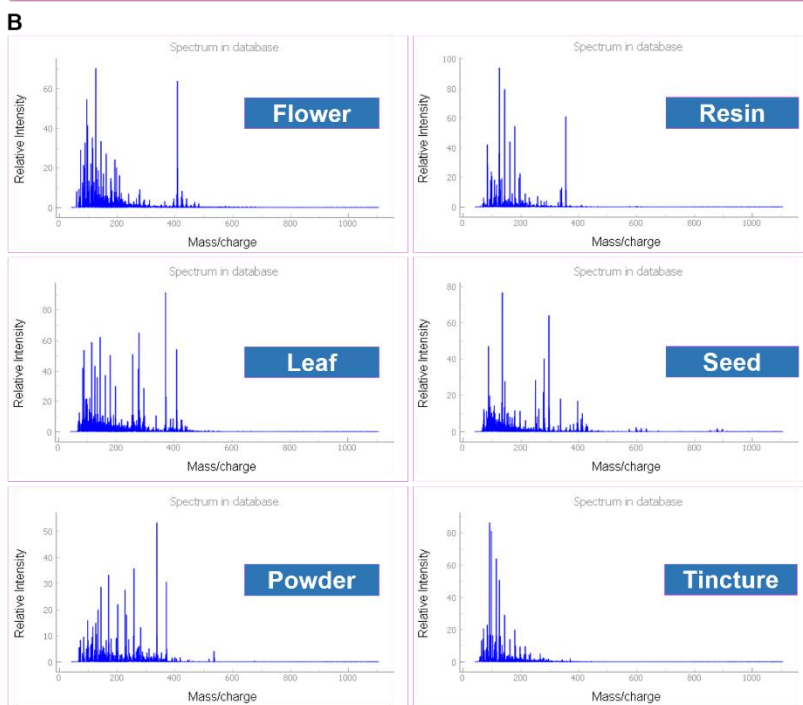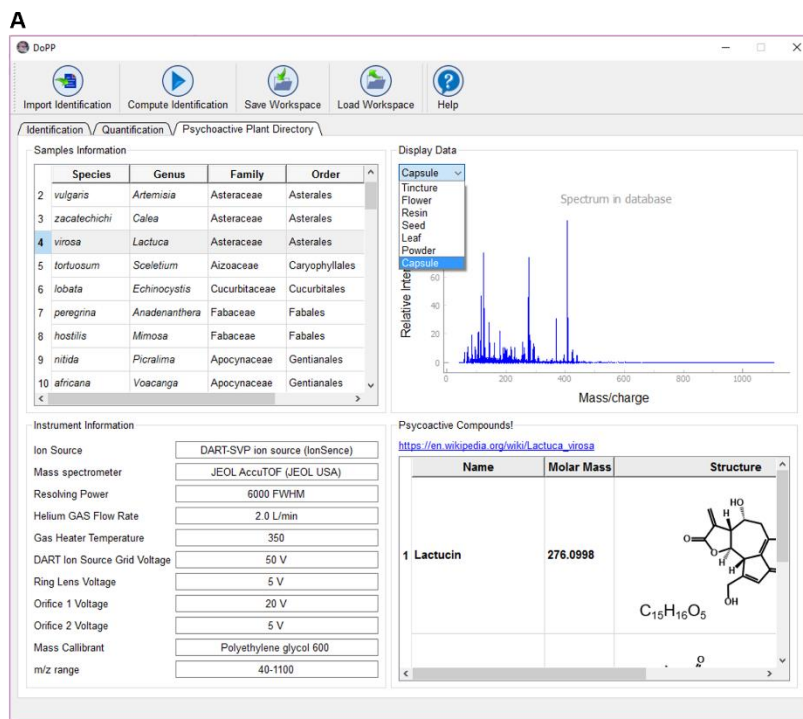
Figure 3.4. Illustration of the "Psychoactive plant directory" tab of DoPP. (A) Information about the *Lactuca virosa* species that is observed after right clicking on the species tab in the "Sample Information" section. The information includes: a link to the Wikipedia page describing the species and a table containing its known psychoactive components (names and structures) under "Psychoactive Compound" section; and the mass spectra of the various products derived from the species under "Display Data" section; (B) Retrieved mass spectra for *L. virosa* representing flower, resin, leaf, seed, powder and tincture forms.

3.3.1. Approach for the Identification of Sample Unknowns

In order to illustrate the utilization of DoPP for the identification of plant matrices, the interrogation of materials comprised of *Mitragyna speciosa* commonly known as kratom (leaf), *Datura innoxia* (seed)*, Datura wrigthii* (seed)*, Ricinus communis* in castor oil form and *Salvia miltiorrhiza* in tablet form, and a plastic bag are described here. Kratom has been identified by the UNODC as a plant of concern because of its increased recreational use, potential to cause dependence, its various adverse health effects, and because it has been implicated in drug overdose deaths.[153] Its major psychoactive component is mitragynine, which has been shown to act on various opioid receptors including the mu, delta and kappa.[153] *Datura* species are legal highs containing atropine and scopolamine, which are controlled substances in many countries. For this study, kratom and *Datura* species were also analyzed by outside independent laboratories using experimental parameters identical to those described earlier (see Methods section). This enabled determination of the utility of DoPP using data generated from a different instrument and acquired by different analysts. Figure 3.5 displays the DART mass spectra of commercially available kratom (comprised of crumbled leaves (Figure 3.5A)), and *D. innoxia* seeds (Figure 3.5B). Their corresponding mass tables can be found at https://rabi-musah.squarespace.com/s/Psychoactive-

A

B
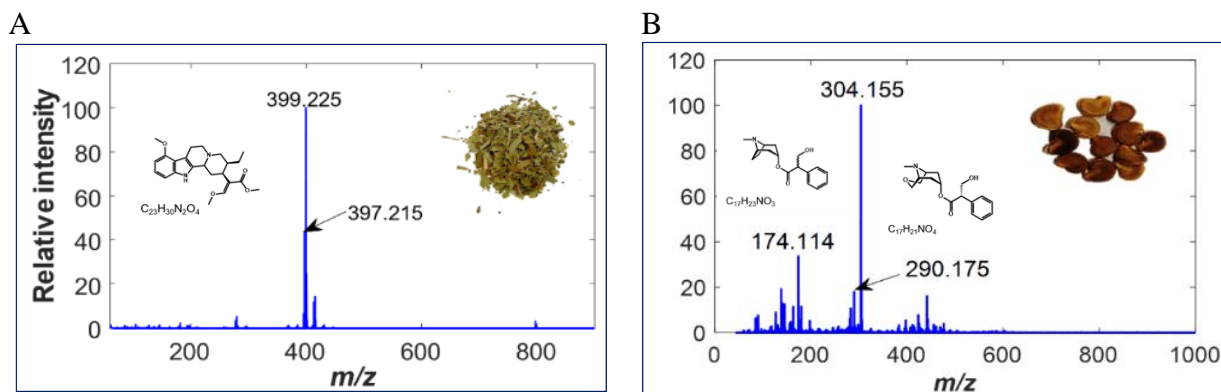
Figure 3.5 Representative 20 V soft ionization DART mass spectra of (A) *M. speciosa*, aka kratom and B. *D. innoxia*. The base peak at nominal *m/z* 399 in the kratom mass spectrum (A) corresponds to the protonated form of its psychoactive component mitragynine. Prominent peaks in the *D. innoxia* spectrum (B) correspond to the protonated forms of atropine (*m/z* 290) and scopolamine (*m/z* 304).

. Mass spectra of other samples are shown in Figure 3.6. As indicated in Figure 3.5A, the base peak at nominal m/z 399 in the kratom mass spectrum corresponds to the protonated form of mitragynine ([$C_{23}H_{30}N_2O_4$ + H]$^+$; *measured:* 399.2252). Interestingly, despite the complexity of the kratom raw material, the spectrum is relatively simple, and is dominated by the mitragynine peak. Prominent peaks in Figure 3.5B (*D. innoxia* seed) correspond to the protonated forms of atropine ([$C_{17}H_{23}NO_3$ + H]$^+$; *measured:* 290.175) and scopolamine ([$C_{17}H_{21}NO_4$ + H]$^+$; *measured:* 304.155) with the scopolamine peak being dominant. Figure 3.7 illustrates the similarities and differences in correlation coefficient for ten kratom, five *D. innoxia,* and five *D. wrightii* samples that were analyzed independently in each of two different laboratories. The brightest shade of yellow
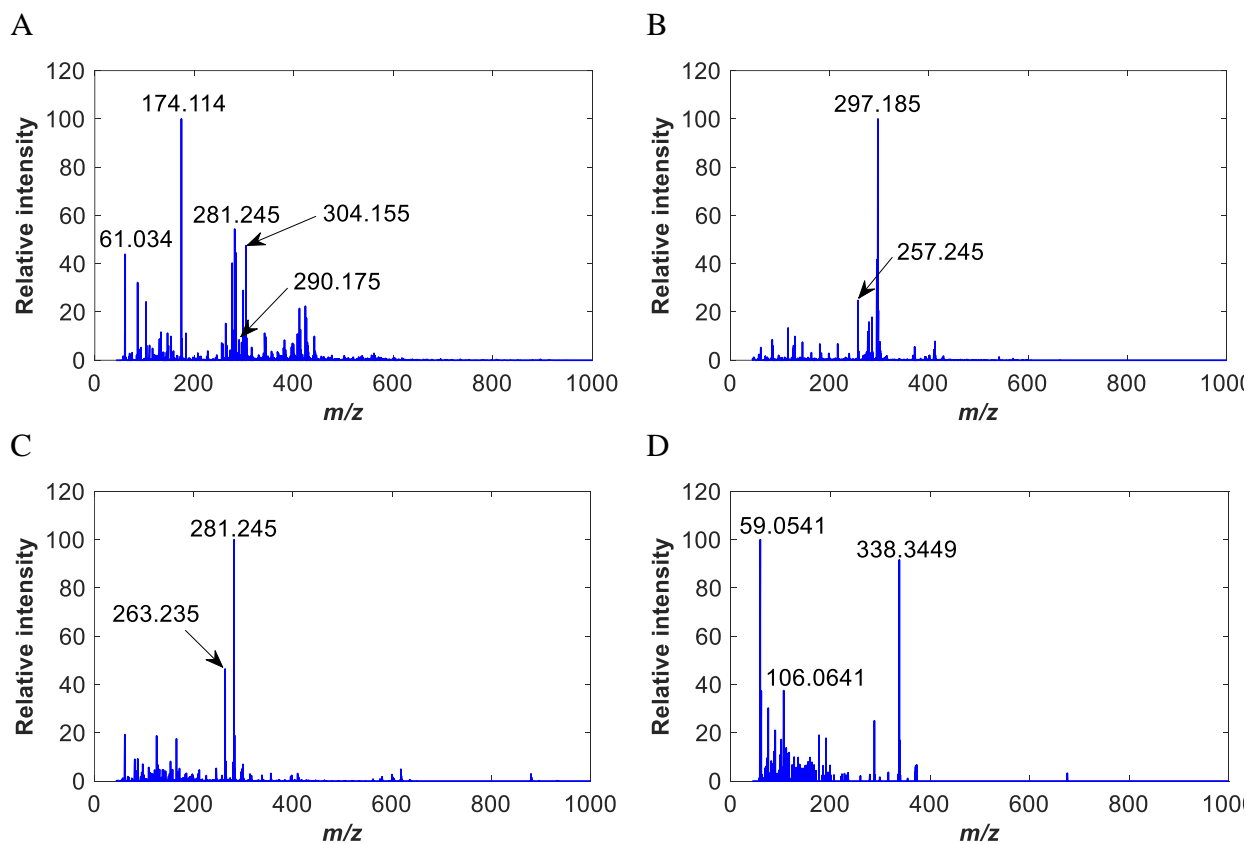
Figure 3.6 Representative 20 V soft ionization DART mass spectra of (A) *D. wrightii*; (B) *S. miltiorrhiza*; (C) *R. communis*; and (D) plastic bag which contained *Cannabis sativa* powder.

74
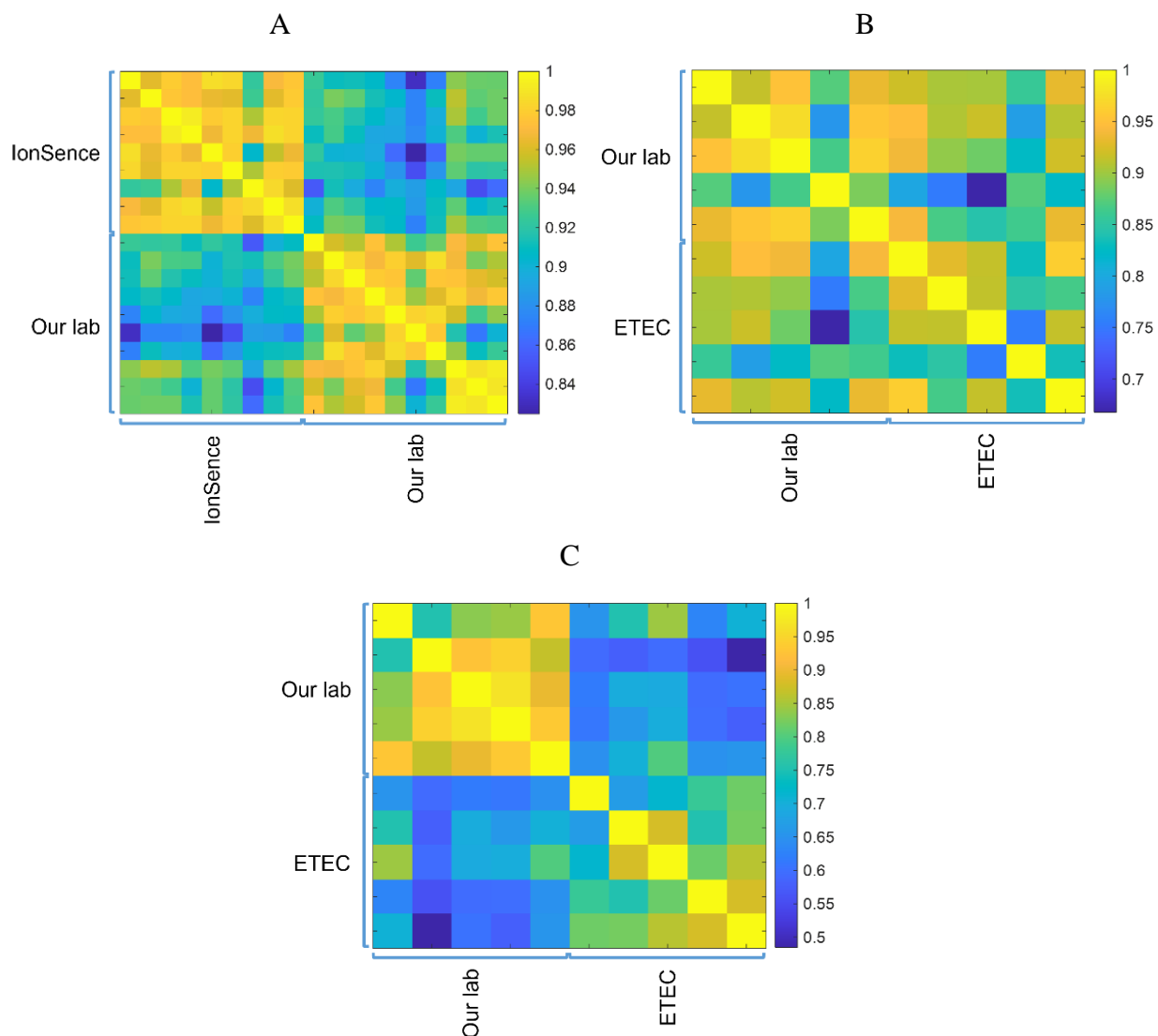
Figure 3.7 Pairwise inter-spectral similarities estimated using correlation coefficients. The plot illustrates the similarities between the DART-HR spectra of kratom (A), *D.innoxia* (B) and *D. wrightii* (C) analyzed in two different laboratories, with the brightest share of yellow representing the highest correlation (ie., 1) and the darkest share of blue representing the lowest (i.e., 0.82).

represents the highest correlation and the darkest shade of blue represents the lowest. To compare the inter-laboratory spectra for reproducibility, the inter-spectral correlation scores for the spectra were computed. Then the correlations for each spectrum were averaged. The average scores for the datasets from each laboratory for each species were examined to reveal whether they fell within the normal distribution.[154] Using the average scores of the correlation metrics along with the paired *t*-test, it was found that the spectra of the two species from the two independent laboratories were

statistically the same at the 95% confidence level. It should be noted that the mass resolving power and mass accuracy can vary between different mass analyzers, and that different types of mass analyzers may influence not only reproducibility, but also DoPP results. Future studies will be devoted to assessment of the scope and limitations of DoPP as a function differences in mass analyzer type.

In conducting classification in real-world scenarios, a classifier not only must correctly group unknown samples into the classes that are defined in the model, but must also correctly reject: (1) samples that represent novel classes against which the model was not trained; and (2) other anonymous data such as background or poor quality data. *Ricinus communis* and *Salvia miltiorrhiza*, which are species not represented in the database, were used to investigate how the classifier would handle data from species that should not be recognizable. Also, the plastic bag containing *Cannabis sativa* material, and a poor quality mass spectrum of *D. wrightii* material (by virtue of its not having been properly processed for background correction) were screened against the database to test how the model would treat data that should not be recognized, and poor quality data respectively. Screening of the spectra using DoPP resulted in a correct identification of kratom in all tested cases, as revealed in the *Identification tab* section. The prediction outcomes for all of the other samples are presented in Figure A3.2-A3.9.

3.3.2. Identification Tab

When the DART mass spectrum of unknown material is first imported into DoPP, the window that appears in the *Identification* tab is illustrated in Figure 3.3A. It displays the mass spectral data table and plot, showing *m/z* values and their corresponding relative intensities. After selecting the "*Compute identification*" tab, the material is first screened for outlier detection using principal component analysis (PCA) and Hotelling's T^2 statistic, and if it is identified as an outlier,

the result will be listed as "*Not detected*" in the "*Identification Result*" section. If it is deemed not to be an outliner, then in the "*Display Result*" section, a bar plot that reveals the prediction probabilities resulting from classification by the hierarchical classification tree based on SVM, RF, KNN and the fused classifiers for identification of the family, genus and species of the analyzed material is shown (Figure 3.3A). The four classifiers reveal the highest probability prediction results for the family, genus and species assignments. Three other bar plots (Figure 3.3B-D) display the identification results for the family, genus and species levels of the classification tree for the fused classifier. In the "*Identification result*" section, the maximum probability computed by the fused classifier for family, genus and species levels along with their corresponding class labels are shown by DoPP. When the computed probability is lower than the probability threshold for assigning a class label at each level, the background color of the cells changes to pink, indicating that these levels are not assigned. Additional information provided within this tab includes the name(s) and structure(s) of the dominant psychoactive component(s), as well as their molecular formula(s). Figure 3.3 illustrates the results for analyses performed at an independent laboratory (IonSense Inc.) for the identification of a kratom sample. Figure 3.3B shows that the probability for the assignment of the plant material to the Rubiaceae family is the highest of all the 18 families represented in the database. The material is further classified as being derived from a *Mitragyna* genus plant, and finally, as the *M. speciosa* species. These are all correct assignments. The prediction results for *D. innoxia* (Figure A3.2 and Figure A3.4) and *D. wrigthii* (Figure A3.3 and Figure A3.4) were similarly accurate for data collected in our lab and at ETEC. The screening results for *R. communis* and the plastic bag that contained the *C. sativa* sample are shown in Figures A3.6 and A3.7, respectively. Both are reported as outliers which is the expected and desired result, as the model should reject both on the grounds that they should not be recognizable. While *S.*

miltiorrhiza (Figure A3.8) and the poor-quality *D. wrigthii* spectrum (Figure A3.9) were not rejected in the outlier detection step, they were not assigned to any of the species in the database, as illustrated in the figures. The "Not-assigned" status of these samples is visually apparent from the pink background color which appears, and which signifies that the observed probability of 0.31 is lower than the threshold of 0.45 that was set for assignment of a *R. communis* sample to the Rubiaceae family, and that the observed probability of 0.26 is lower than the threshold of 0.45 for assignment of a *D. wrigthii* spectrum to the Asteraceae family. Thus, the results reveal that DoPP was successful not only in determining the identities of species contained within its database, but also in rejecting the samples that represent novel classes or poor matches with entities in the database. They further show that the hierarchical classification tree underlying the fused classifier is a well-fitted model for identification of psychoactive plant species using DART-HRMS data. In addition, DoPP provides a useful tool for interrogation of a DART-HRMS database of psychoactive plant species.

In DoPP, the approach that was developed for differentiation of plants is based on only a probabilistic model, and species-specific ions as an alternative means to distinguish between species were not considered. However, using species specific ions can provide another source of information that may be helpful in reducing the false positive rate. Plans are underway to assess the extent to which inclusion of this consideration could further enhance the utility of the application, particularly as it relates to development of a peak-matching algorithm for unknown sample pre-screening.

3.4. Conclusion

Comprised of a graphical user interface coupled to a comprehensive database of high-resolution DART mass spectra of psychoactive plant materials, DoPP enables their rapid species

identification through screening of their DART mass spectra. Eighteen families, 34 genera and 57 species are represented, including multiple species designated by the United Nations Office on Drugs and Crime as "plants of concern" due to their increased recreational use and their potential to cause addiction and negative health impacts. For identification of plant material unknowns, DoPP employs a trained hierarchical classification tree constructed from the fusion of SVM, RF and KNN models. This trained fused model provides discrimination with accuracies of 98% and 99% for 10-fold cross validation and external validation assessments, respectively. The results show the successful application of DoPP for the identification of unknown psychoactive plant materials. These features, among several others, enable facile interrogation and identification of plant materials without prior knowledge of botany, and in the absence of distinguishing plant morphological features (such as is the case when the plant materials have undergone processing such as grinding or extraction), or the need for extensive sample pre-treatment prior to analysis. DoPP will be compiled as a stand-alone desktop application for windows and mac platforms so that the user will not need to set up any specific software. It also will allow the user to submit their own entries to the host library. Following pre-processing and confirmation of the data, the spectra will be added to the database and will be used to update the trained model.

CHAPTER 4: SPECIES ATTRIBUTION OF *DALBERGIA* WOODS THROUGH HEADSPACE VOLATILES SIGNATURE ANALYSIS

4.1 Introduction

Dalbergia species, often referred to as rosewoods, belong to the Fabaceae family and encompass a diverse range of plants with notable medicinal properties.[155] Among these, *Dalbergia sissoo*, commonly known as Sheesham, is endemic to South Asia, Africa, and the Americas, and is reported to have potent therapeutic benefits.[155,156] Its prominence lies in its use in traditional medicine as an antimicrobial, antiparasitic, antidiabetic, anti-inflammatory, analgesic, and anticancer agent.[155–157] Various plant parts are used, including the heartwood, bark, leaves, and flowers.[155–157] In traditional Chinese medicine, *D. odorifera* has been used to treat liver disease, gastrointestinal disorders, inflammation, and cancer, as well as for its purported cardiovascular protective effects.[158,159] The reported biological properties of *Dalbergia spp.* have sparked considerable interest in the extraction and isolation of bioactive compounds. Isolated compound classes include flavonoids, benzophenones, styrenes, alkaloids, polyphenols, tannins, saponins, cardiac glycosides, and terpenoids.[155,156,159] In addition to their established use in traditional medicine, *Dalbergia spp.* are highly prized for their wood which is fashioned into furniture and various artifacts. As the most highly trafficked product in the world,[56,160,161] *Dalbergia spp.* have been overharvested due to their economic value. This in turn has necessitated their inclusion in CITES appendices, where all are classified as Appendix II, except for *D. nigra*, which is an Appendix I species.[37] Despite these designations, a thriving illegal trade market exists, which not only undermines conservation efforts, but also threatens the livelihoods of local communities that are reliant on these resources.

The ability of law enforcement agencies to intercept and prosecute illegal trade of

Dalbergia spp. is heavily reliant on accurate species identification. Several methodologies have been devised for species differentiation, with wood anatomical examination representing a common approach. This technique can be highly accurate for genus identification. However, distinguishing between closely related species based solely on anatomical features is challenging due to their similarities.[56] While DNA analysis might be anticipated to provide a highly accurate species identification approach, its application is impeded by cost constraints, and technical difficulties concerning the extraction of suitable DNA sequences from trees, due to the rapid fragmentation of DNA that occurs in the wood once the tree has been felled.[35,53,54] This fragmentation can complicate the analysis, making it challenging to obtain the intact DNA sequences necessary for accurate species identification. Another technique, Near-Infrared (NIR) spectroscopy enables non-destructive timber analysis with accurate species identification.[55–57] However, NIR spectroscopy has limitations, including limited spot size, wavelength range, and resolution, which hinder species identification through a comprehensive database with high quality data.[55] Given these challenges, there remains an urgent need for the development of alternative, rapid species identification methods, characterized by both accuracy and efficiency. A promising avenue in this regard is ambient ionization mass spectrometry, particularly direct analysis in real–time high-resolution mass spectrometry (DART-HRMS). This technique has demonstrated considerable potential in unveiling species-specific chemical fingerprints, which when subjected to multivariate statistical analysis, reveal species identity information. For example, Musah et al., reported on chemometric processing of DART-HRMS derived chemical fingerprints of wood to differentiate between various species, including two from the *Dalbergia* genus, with 98.98% accuracy.[82] The U.S. Fish and Wildlife Forensic Lab (USFWL) utilizes this strategy for casework applications, consistently achieving accuracies exceeding 90%.[88,89] Although this method yields

81

high accuracies, it necessitates the in-house analysis of bulk wood material using DART-HRMS. This requirement renders the technique impractical for the rapid analysis of stacked logs at ports, or other field settings. Consequently, a "stand-off" approach for species identification, which circumvents direct wood analysis in favor of utilizing headspace volatiles, presents a promising alternative. Previous work has shown that a range of psychoactive plants can be identified through chemometric processing of their species-specific headspace chemical profiles.[62] If *Dalbergia spp.* also exhibit species-specific volatiles profiles, then such a method could be developed for identifying their woods through headspace analysis, circumventing the need for direct interrogation of wood samples. In turn, such a breakthrough would lay the groundwork for the establishment of a stand-off approach for *Dalbergia spp.* identification.

Presented herein are the findings of a study examining the headspace chemical profiles of seventeen *Dalbergia spp.* Through the concentration of their volatiles using solid phase micro-extraction (SPME) followed by DART-HRMS analysis, both intraspecies similarities and interspecies differences were observed. Subsequent multivariate statistical analysis employing Support Vector Machine (SVM) effectively separated the species, yielding a prediction accuracy of 83.33% based solely on the headspace chemical signatures. The development of this approach holds immense potential for facilitating law enforcement efforts in curbing illegal logging by enabling screening and identification of timber shipments at ports of entry, border crossings, and other potential trafficking hotspots, rapidly, non-invasively, and in real-time. Ultimately, the implementation of this method could empower law enforcement agencies to combat illegal logging and trafficking activities more effectively, thereby contributing to the conservation and sustainable management of *Dalbergia spp.* and their habitats.

4.2. Methods

4.2.1. Timber Samples

All timber samples were provided by the U.S. Fish and Wildlife Laboratory (USFWL) (Ashland, OR, USA). Table 4.1 lists the species information along with the identification number assigned by the USFWL. In all, authenticated samples from each of the seventeen species *D. baronii*, *D. cearensis*, *D. oliveri*, *D. occulta*, *D. madagascariensis*, *D. latifolia, D. melanoxylon*, *D. normandii*, *D. purprascens*, *D. retusa*, *D. nigra*, *D. decipularis*, *D. stevensonii*, *D. tucurensis*, *D. spruceana*, *D. maritima*, and *D. cochinchinensis* were analyzed. At least three individuals of each species were analyzed three to five times, resulting in a comprehensive number of replicates (276).

4.2.2. Headspace Sampling by Solid-Phase Microextraction

Divinylbenzene/Carboxen/Polydimethylsiloxane-coated (DVB/CAR/PDMS) 24 Ga 50/30 μm solid-phase microextraction (SPME) fibers and SPME fiber holders for use with manual sampling were purchased from Supelco Inc. (Bellefonte, PA, USA). Fibers were conditioned for 30 min at 250 °C under a stream of helium gas before each headspace sampling. Wood samples for analysis were generated by depositing within a 20 mL scintillation vial 2 g of slivers that were produced by segmenting the bulk wood with wire cutter pliers. The mouths of the vials were covered tightly with aluminum foil, and a conditioned DVB/CAR/PDMS coated 24 Ga 50/30 µm SPME fiber was exposed to the headspace of the sample for 30 min at room temperature (Figure 4.1A). This concentration step was performed in triplicate by concentrating headspace volatiles in a vial three times under ambient conditions at approximately 23 °C

4.2.3. DART-HRMS Analysis

SPME fibers, to which headspace volatiles were adsorbed, were analyzed in positive-ion

Table 4.1 *Dalbergia spp.* analyzed, showing the U.S. Fish and Wildlife Laboratory-assigned identification number for each sample.

Species	ID Number	Species	ID Number	Species	ID Number
Dalbergia baronii	130012	*Dalbergia latifolia*	130215	*Dalbergia decipularis*	130125
	130009		130212		130124
	130001	*Dalbergia melanoxylon*	130356	*Dalbergia stevensonii*	130225
	130010		130352		130222
	130011		130348		130221
	130007		130218		130231
	130005		130353		130223
	130006	*Dalbergia normandii*	171173	*Dalbergia tucurensis*	140515
	130008		171172		140520
Dalbergia cearensis	130160		150174		140513
	130155		150168		140521
	130161		150160		140517
	130165	*Dalbergia purprascens*	150557	*Dalbergia spruceana*	130121
	130158		150034		130116
Dalbergia oliveri	131025		150035		130119
	131024	*Dalbergia retusa*	130250		130115
	131026		130251		130123
Dalbergia occulta	150170		130246	*Dalbergia maritima*	150208
	150192		130248		150227
	150198		130244		150221
Dalbergia madagascariensis	130174	*Dalbergia nigra*	130037		150228
	130173		130713		150222
	130179		171582		150175
	130172		171584	*Dalbergia cochinchinensis*	130620
	130180		162037		130672
Dalbergia latifolia	130208	*Dalbergia decipularis*	150523		130666
	130210		130129		130667
	130214		130126		130671

mode using a direct analysis in real-time (DART)-SVP ion source (IonSense, Saugus, MA, USA) interfaced with a JEOL AccuTOF mass spectrometer (JEOL USA, Peabody, MA, USA) (Figure 4.1B). The instrument parameter settings were as follows: helium gas flow rate, 2.0 L/min; gas temperature, 250 °C; ring lens voltage, 5 V; orifice 1 voltage, 20 V; orifice 2 voltage, 5 V; and peak voltage, 400 V (to detect *m/z* values ≥ 40). The mass spectrometer used has a resolving power
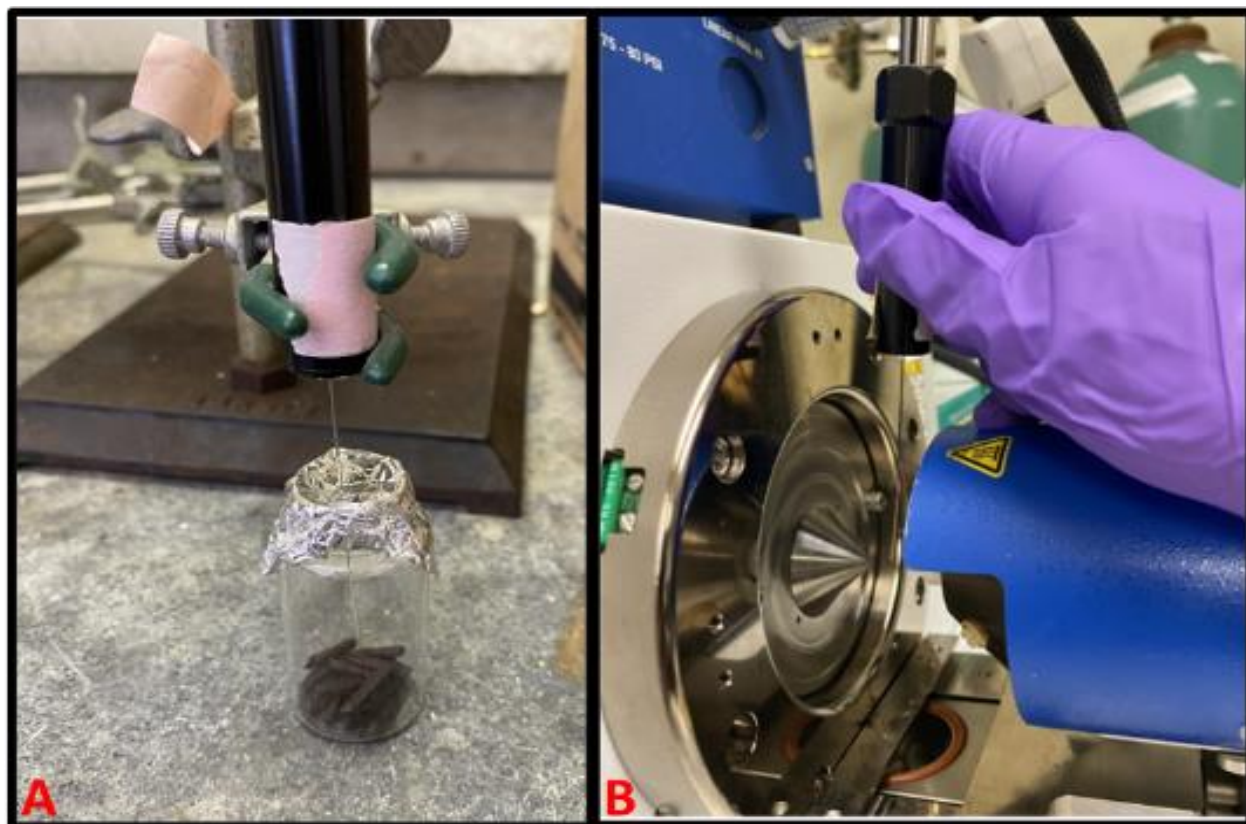
Figure 4.1. Headspace sampling of timber (A) and DART-HRMS analysis of SPME fiber (B).

of 6000 full width at half maximum (fwhm). Spectra were collected at a rate of one spectrum per second over the mass range *m/z* 40–1000. PEG 600 (Sigma-Aldrich, St. Louis, MO, USA) was used as the mass calibrant and was sampled following the analysis of each individual fiber. TSSPro 3 software (Shrader Analytical, Detroit, MI, USA) was used for data processing including averaging, background subtraction, and peak centroiding. The DART mass spectra of conditioned SPME fibers that were exposed to the headspace of an empty vial served as blanks (controls) for the SPME analyses.

4.2.4 Headspace Sampling by Thermal Desorption Coupled with Gas Chromatography – Mass Spectrometry

Following the methodology described in Dr. Meghan Appley's thesis,[162] slivers of the wood samples were analyzed using a 7890A gas chromatogram and 5977B mass spectrometer

(MS) (Agilent, Santa Clara, CA) coupled with a GERSTEL Multipurpose Sampler (MPS) thermal desorption unit (TDU) and cooling inlet system (CIS) (GERSTEL Inc. USA, Linthicum, MD). Each individual was analyzed once. Samples were placed into microvials in TDU tubes, which were desorbed in the TDU operating in splitless mode. The initial temperature was 40 °C, followed by a temperature ramp of 100 °C/min to a final temperature of 175 °C and then held for 5 min. The analytes were cryogenically trapped in the CIS inlet at -120 °C using a liner packed with glass wool. Subsequent to desorption, the analytes were transferred to the GC column by heating the CIS at 12 °C/min to a final temperature of 275 °C. This was held for 3 min. The GC column was a DB-5ms Ultra Inert column (Agilent, Santa Clara, CA) with a helium flow rate of 0.6 mL/min. The GC oven was programmed with an initial temperature of 40 °C, followed by a ramp of 15 °C/min to a final temperature of 300 °C. This was for 2 min. The MS parameters were set to scan mode, targeting a mass range of *m/z* 30 to 600. Data analysis and visualization were conducted using MassHunter Unknowns Analysis Software (Agilent, Santa Clara, CA).

4.2.5. Multivariate Statistical Analysis

The DART mass spectral data that were generated from SPME fiber analysis resulted in 2-column text files (one column containing the *m/z* values and the second containing their corresponding ion counts). These were subjected to multivariate statistical analysis using the Mass Mountaineer software suite (Version 7.1.17.0). This was done by first categorizing the samples into classes consistent with their respective species identities. Next, an iterative process was conducted to determine the optimal relative abundance threshold cutoff and mmu tolerance for the prediction model. Threshold cutoffs ranging from 1% to 10% and tolerances from 0 to 20 mmu were iteratively assessed. This revealed that a 4% threshold and 10 mmu tolerance yielded the most accurate results. Subsequently, the text files were rendered as a heat map using the 4%

threshold and 10 mmu tolerance. Next, the 256 *m/z* values with the highest relative abundances were selected. This number was ~3 percent of the total number of *m/z* values. Redundant entries were purged, and for the remaining *m/z* values, vectors were constructed to encompass all the abundances for the identified *m/z* values. This was followed by Analysis of Variance (ANOVA) for each *m/z* value. Features exhibiting statistically non-significant differences with *p*-values greater than 0.5 were flagged and excluded, resulting in a subset of 112 significant *m/z* values, which were subjected to further analysis and classification.

To mitigate the impact of the variation in relative abundances within the spectra, the data were normalized. This step ensured that the disparities in abundances did not unduly influence classification outcomes. An iterative process was then employed to determine the most optimal classification model. Various classification models available in the Mass Mountaineer software suite, such as Partial Least Squares-Discriminant Analysis (PLS-DA), Discriminant Analysis of Principal Components (DAPC), Kernel Discriminant Analysis (KDA), and Support Vector Machine (SVM) were applied to the dataset. Among these, SVM demonstrated the highest accuracy in predicting *Dalbergia spp.* identities. Therefore, SVM, a supervised multivariate statistical analysis technique, was employed to delineate class boundaries within the dataset. SVM operates by transforming the data into higher-dimensional spaces, facilitating the identification of a hyperplane that optimally separates classes. This methodology offers flexibility through the utilization of different kernels (Chi Square, Linear, and Dynamic Time Warping). Notably, the Chi Square Kernel, which leverages the chi-square distribution, was used for this study since it consistently yielded better outcomes.

4.3. Results

4.3.1. DART-MS Analysis

SPME-facilitated DART-HRMS analysis of the headspace volatiles of three to nine individuals (three to five replicates each) from each of the species *D. baronii*, *D. cearensis*, *D. oliveri*, *D. occulta, D. madagascariensis*, *D. latifolia*, *D. melanoxylon*, *D. normandii*, *D. purprascens*, *D. retusa, D. nigra, D. decipularis*, *D. stevensonii*, *D. tucurensis*, *D. spruceana*, *D. maritima*, and *D. cochinchinensis* furnished spectra, representative examples of which are shown in Figure 4.2 (with their corresponding mass spectral data tables reposited at https://rabi-musah.squarespace.com/s/Dalbergia-species-mass-data-tables-corresponding-to-Figure-42.xlsx:). The mass spectral data were then rendered as a heat map (Figure 4.3), with the *m/z* values presented on the x axis and the sample number on the y-axis. Sample numbers 1-45, 46-66, 67-75, 76-84, 85-99, 100-114, 115-128, 129-144, 145-153, 154-168, 169-183, 184-198, 199-213, 214-228, 229-243, 244-261, and 262-276 (shown on the y-axis) are representative of the replicates of *D. baronii*, *D. cearensis*, *D. oliveri*, *D. occulta, D. madagascariensis*, *D. latifolia, D. melanoxylon*, *D. normandii*, *D. purprascens*, *D. retusa, D. nigra, D. decipularis*, *D. stevensonii*, *D. tucurensis*, *D. spruceana*, *D. maritima*, and *D. cochinchinensis*, respectively. The color intensity of the bands reflects the peak relative intensity, where the darker the red, the higher the abundance of its corresponding *m/z* value. Examination of the representative mass spectra of each species (Figure 4.2) and the mass spectra rendered as a heat map (Figure 4.3), revealed a number of trends. One was the observation of intraspecies similarities between different individuals representing the same species. For example, for *D. Baronii* there were peaks that were consistently observed across all individuals including those at nominal *m/z* 61, 83, 107, 133, 134, 149, 181, 203, 221, 222, 223, and 239. This intraspecies similarity trend was also observed for the remaining sixteen species.
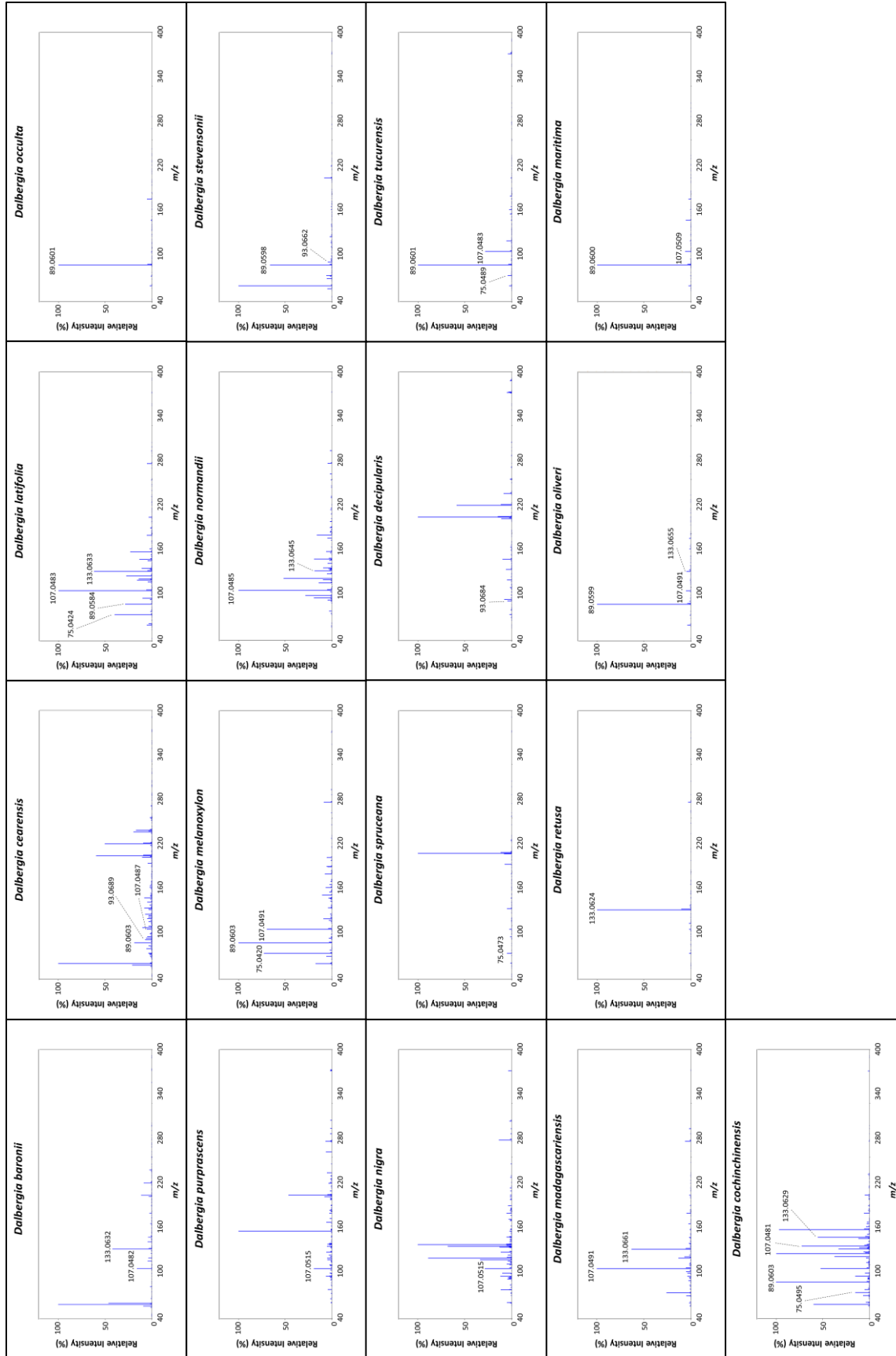
Figure 4.2 Representative DART mass spectra of the *Dalbergia spp.* analyzed in this study.

Heat Map of 17 *Dalbergia spp.*
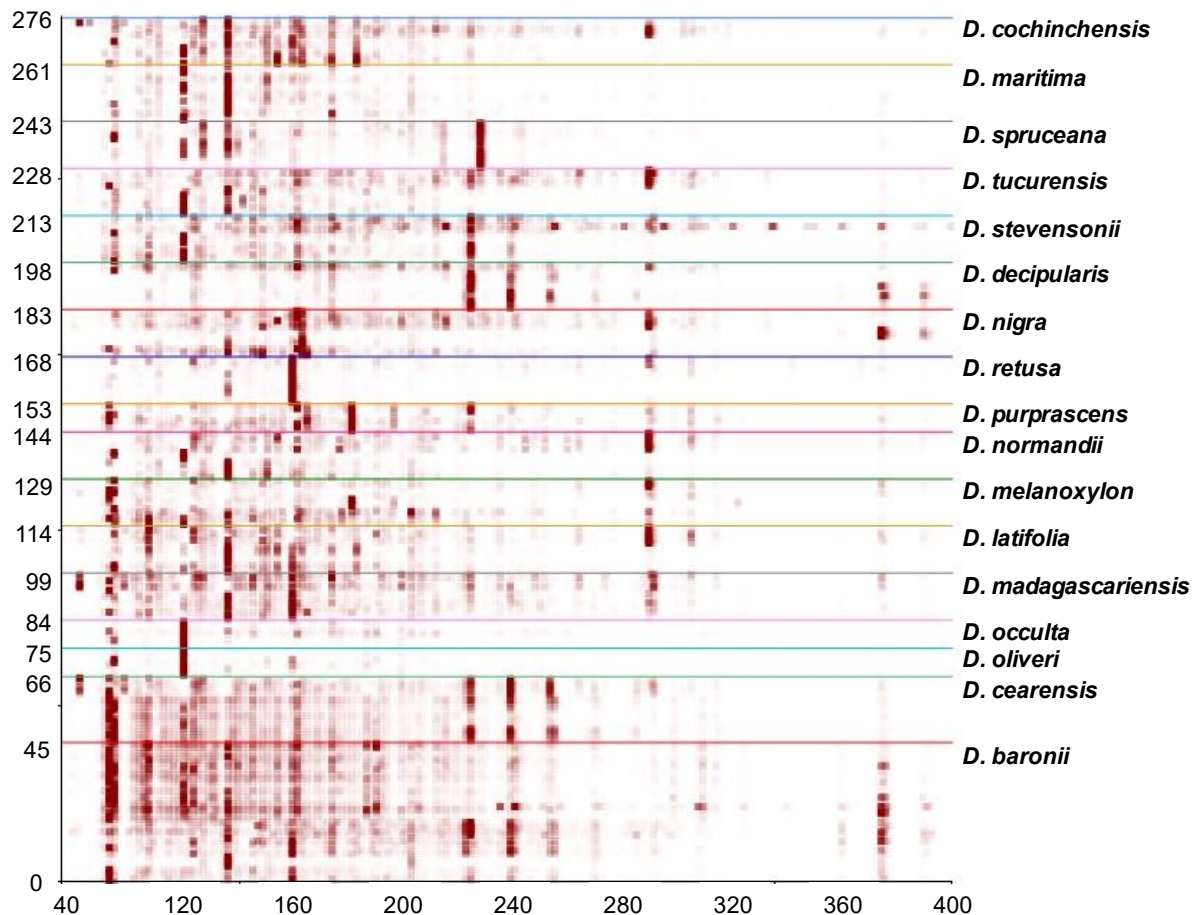
Figure 4.3. Mass spectral data rendered in the form of a heatmap of the 17 *Dalbergia spp*. The horizontal lines represent the number of replicates, and the bands correspond to the *m/z* values on the x-axis. The color intensity of the bands reflects the peak relative intensity, with darker color indicating a higher intensity.

For instance, peaks corresponding to nominal *m/z* 61, 89, 107, 133, and 177 are in the representative spectrum of *D. oliveri* shown in Figure 4.2, and these peaks are also detected in multiple individuals of this species, as illustrated in the heatmap. A second observed trend was the presence of *m/z* values that were common to individuals from different species. For example, a number of the *m/z* values characteristic of *D. oliveri* were also detected in other species, such as *D. occulta*. These included nominal *m/z* 61, 89, 107, and 177. Overall, the complexity of the spectra made species differentiation through visual assessment quite challenging and as such, multivariate

statistical analysis was explored as a means to discriminate between classes.

4.3.2. Creation of a Prediction Model

In order to determine whether there were subtle, non-visually apparent features in the DART-HRMS chemical profiles of the wood headspace that could be used to differentiate between the species, the mass spectral data were subjected to multivariate statistical analysis. The 256 most abundant masses identified from the heat map (at the $\geq$ 4% threshold cutoff) were used for the classification model. Analysis of Variance (ANOVA) revealed that 112 *m/z* values had *p*-values < 0.05, indicating statistical significance. Consequently, these 112 *m/z* values were designated as input into the model for classification. These 112 masses are listed in the first column of Table A4.1.

The data for all replicates of the individuals representing the seventeen timber species were processed as previously described (see Methods section) and subjected to Support Vector Machine (SVM) analysis. To evaluate the performance of the SVM model, internal validation was conducted using leave-one-out cross validation (LOOCV). In this approach, each spectrum in the dataset is systematically removed, treated as an unknown sample, and the model is retrained using the remaining spectra. Subsequently, the "unknown" spectrum is classified based on the retrained model, and its actual class assignment is compared to the predicted class. This iterative process is repeated until each spectrum has been assigned a class, and the accuracy of the model is assessed based on the number of correct assignments. The reported accuracy reflects the percentage of correctly classified spectra, providing insight into the model's prediction capability.

The LOOCV accuracy for this analysis was 83.33%, suggesting robust performance of the SVM classification model. Table 4.2 shows the accuracies for individual class predictions. These results demonstrate the model's effectiveness in classifying samples across different species of

Dalbergia using headspace molecular profiles. Notably, the accuracies for six of the species classes (i.e., *D. cearensis*, *D. retusa*, *D. decipularis*, *D. stevensonii*, *D. spruceana*, and *D. cochinchinensis*), were exceptionally high with values exceeding 90.00%. Conversely the *D. oliveri* and *D. occulta* classes had the lowest classification accuracies (55.56% each). Furthermore, five species classes, including *D. baronii*, *D. latifolia*, *D. melanoxylon*, *D. nigra*, and *D. maritima*, had good prediction accuracies with values above 80%. Four classes, comprising *D. madagascariensis*, *D. normandii*, *D. purprascens*, and *D. tucurensis*, exhibited more modest accuracies between 73-78%.

Table 4.2 Prediction accuracies of the SVM model used for 17 *Dalbergia spp.*	
Species	Accuracy
D. baronii	86.67%
D. cearensis	90.48%
D. oliveri	55.56%
D. occulta	55.56%
D. madagascariensis	73.33%
D. latifolia	80.00%
D. melanoxylon	80.00%
D. normandii	73.33%
D. purprascens	77.78%
D. retusa	93.33%
D. nigra	80.00%
D. decipularis	93.33%
D. stevensonii	93.33%
D. tucurensis	73.33%
D. spruceana	93.33%
D. maritima	88.89%
D. cochinchinensis	93.33%
Total	83.33%

The classification performance was explored by considering the misclassification results for each species, which are revealed in the confusion matrix depicting the prediction capabilities of the SVM model from the LOOCV analysis (Figure 4.4). This tabular representation shows the performance of a classification model by comparing the prediction results to those of the true class labels. The numerical entries along the diagonal, highlighted in green, show the number of correctly predicted samples for the indicated species, while off-diagonal entries greater than zero (highlighted in orange), indicate misclassifications. Each of the represented species is indicated by

	A	B	C	D	E	F	G	H	I	J	K	L	M	N	O	P	Q
A	39				2						2	1				1	
B	1	19										1					
C			5	3					1								
D			1	5				1						1		1	
E					11		2			1	1						
F	1					12	1	1									
G							12		1		1			1			
H	1			1			1	11								1	
I							2		7								
J							1			14							
K	1				1						12			1			
L							1					14					
M			1										14				
N					1						2			11		1	
O								1							14		
P				1								1				16	
Q														1			14

(A) *D. baronii*   **(B)** *D. cearensis*   **(C)** *D. oliveri*   **(D)** *D. occulta*   **(E)** *D. madagascariensis*   **(F)** *D. latifolia*
(G) *D. melanoxylon* **(H)** *D. normandii* **(I)** *D. purprascens* **(J)** *D. retusa* **(K)** *D. nigra*   **(L)** *D. decipularis*
(M) *D. stevensonii* **(N)** *D. tucurensis* **(O)** *D. spruceana* **(P)** *D. maritima* **(Q)** *D. cochinchinensis*

Figure 4.4 Confusion matrix created from the SVM model results, illustrating the prediction outcomes for 17 *Dalbergia* spp. obtained from the SPME-facilitated DART-HRMS analysis of 276 samples. The true species classes are represented along the left side, while the prediction outcomes are indicated across the top. The legend indicates the species to which each letter corresponds.

a letter. For example, the first class (A) corresponding to *D. baronii*, had 39 samples correctly

classify as *D. baronii* (A), with two misclassified as *D. madagascariensis* (E), two as *D. nigra* (D),

one as *D. decipularis* (L), and one as *D. maritima* (P). For the two species for which the prediction

accuracies were poor (i.e., both at 55.56%), *D. oliveri* and *D. occulta*, it was observed that only

five samples were correctly classified as *D. oliveri* (C), with three misclassified as *D. occulta* (D) and one as *D. retusa* (J). Similarly, the confusion matrix also shows that *D. occulta* (D) was also only correctly classified for five samples, with the remaining four misclassified as *D. oliveri* (C), *D. normandii* (H), *D. tucurensis* (N), and *D. maritima* (P). The misidentifications of *D. occulta* and *D. oliveri*, resulting in them being most often classified as each other, clearly arises from similarities in their DART-HRMS-derived chemical profiles. This is visually apparent in the heatmap rendering of the mass spectra (Figure 4.3). Analysis numbers 67-75, and 76-84 correspond to replicates of *D. oliveri* (three individuals) and *D. occulta* (three individuals) respectively, and the mass spectral heat map patterns are not only similar by visual inspection alone, but are significantly different from the patterns exhibited by the other 15 represented species. The native occurrence of *D. Oliveri* is Myanmar, Thailand, Laos, Cambodia, and Vietnam, while *D. occulta* is endemic to Madagascar. It is not known whether their genetic profiles have been compared to determine the extent of their relatedness, but the results here reveal that their DART-HRMS-derived chemical signatures which were acquired from analysis of multiple individuals, are highly similar. This may indicate genetically relatedness, or perhaps that the samples are actually representatives of the same species. On the other hand, the observed misclassifications may have stemmed from the limited number of representative samples. If this is the case, the model's accuracy could potentially improve with a larger dataset. However, limited sample availability precluded the exploration of this hypothesis. Nevertheless, despite the low predication accuracies for *D. occulta* and *D. oliveri*, it is noteworthy that the remaining fifteen classes exhibited good to excellent accuracies for differentiating species within the *Dalbergia* genus, simply from analysis of headspace!

The model gave a classification accuracy for *D. nigra* of 80%, clearly indicating that there

were misclassifications. Of the 15 *D. nigra* individuals, 1 was misclassified as *D. baronii*, 1 as *D. madagascariensis* and 1 as *D. tucurensis*, all of which represent false negatives. Of greater concern however, are the false positive results, because *D. nigra* is CITES Appendix 1, while the classification for all the other species is CITES Appendix II. Six samples were misclassified as *D. nigra* and such a misclassifying could lead to unwarranted legal consequences. This emphasizes the need for additional confirmatory analysis to be conducted, such a sample be identified by this approach as being *D. nigra.* The SVM model used in this study was chosen for its effectiveness in handling complex classification tasks, but these results indicate the need for larger datasets to enhance its reliability. However, these results also indicate that within the species' headspace molecular signatures are the chemical attributes that enable them to be identified with an overall accuracy of 83.33%, using the SVM classification model. Although similar studies have achieved accuracies greater than 90%,[86,163] it is important to note that these prior investigations have only analyzed two to seven species and relied on bulk analysis methods, whereas this study shows a comprehensive approach utilizing headspace signatures across seventeen species. One additional step that could be taken in direct analysis of the bulk material by DART-HRMS, which is the current approach used by USFWL for casework.

4.3.3. Identification of Chemical Constituents in Dalbergia spp.

The SVM model utilized in this study relied on a total of 112 features, each representing measured masses obtained by DART-HRMS. In an attempt at chemical identification of these masses, the samples were analyzed by thermal desorption-gas chromatography-mass spectrometry (TD-GC-MS). To illustrate the results, Figures 4.5 and 4.6 show representative TD-GC-MS chromatograms with labeled peaks corresponding to some of the identified compounds. Analysis of the gas chromatograms representing the 17 *Dalbergia* spp., revealed 28 peaks which had EI

mass spectral data consistent with those of 28 of the 112 masses utilized to generate the SVM prediction model. A list of the 112 DART-HRMS derived masses appears in the first column in Table A4.1. An entry in the second column indicates the formula corresponding to the high-resolution mass that appears in the first column, and also indicates that a mass consistent with this formula was detected by TD-GC-MS analysis of wood samples. The appearance of a "-" in the molecular formula column (i.e., column 2) indicates that a formula for the corresponding mass
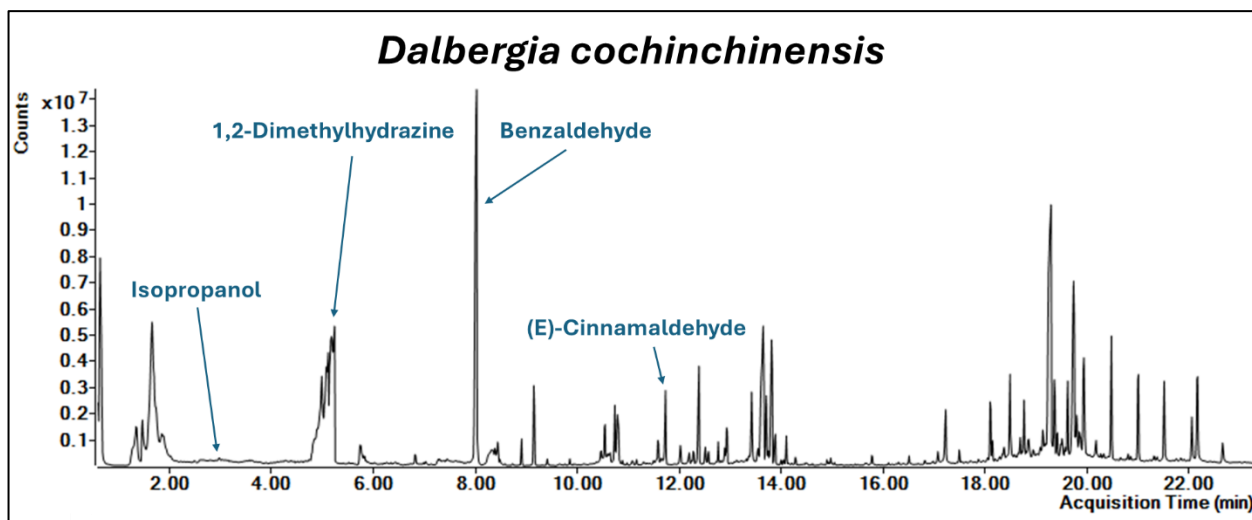
Figure 4.5 Chromatogram of *D. cochinchinensis* analyzed by TD-GC-MS. Representative peaks are labeled in blue, indicating identified compounds.
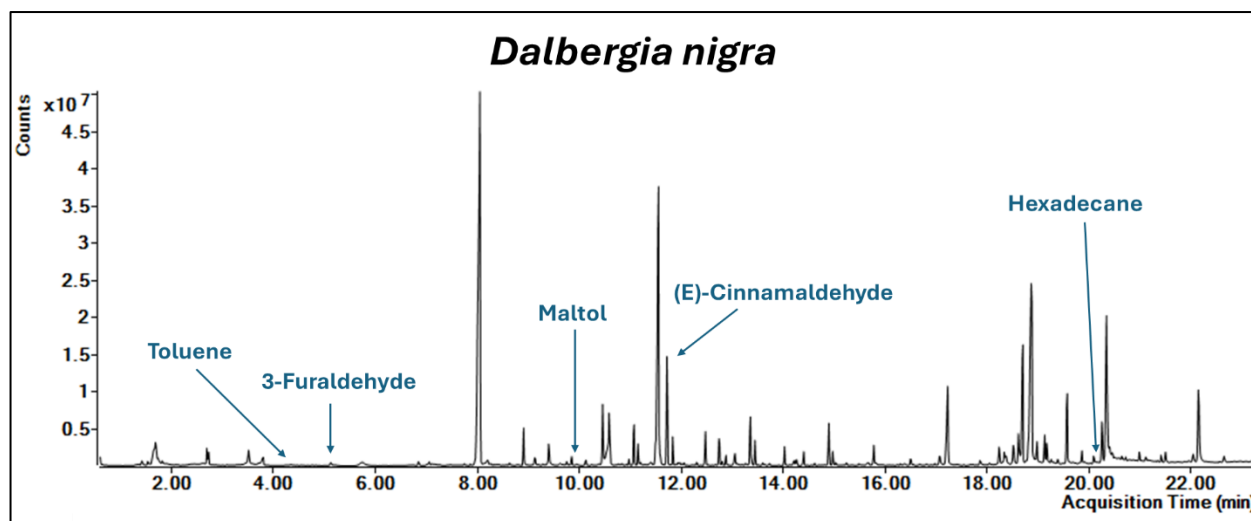
Figure 4.6 Chromatogram of *D. nigra* analyzed by TD-GC-MS. Representative peaks are labeled in blue, indicating identified compounds.

could not be definitively established. When determined, the names of tentatively identified compounds (based on mass spectral fragmentation pattern matching using the NIST 20 database) appear in column 3 (i.e., the "Compound" column). A "-" in this column indicates that no tentative identification could be made. Lastly, the fourth column of the table lists the species in which the indicated compound was detected in at least one individual of the listed species. For instance, the measured mass 61.0636, corresponds to the molecular formula $[C_3H_8O + H]^+$, identified tentatively as isopropanol by TD-GC-MS using NIST 20 mass spectral database EI fragmentation pattern matching (Figure A4.1). This mass was detected in *D. cochinchinensis*, as shown by the peak at 2.98 min in its chromatogram (Figure 4.5). While isopropanol has been documented in various plant species including *Asparagus officinalis*,[164] *Carica papaya*,[165] *Citrus aurontifolia*,[166] *C. grandis*,[166] *C. hystrix*,[166] *C. limon*[166] and *C. sinensis*[166], this is the first report of its presence in *Dalbergia spp.* Similarly, *m/z* 97.0289 was detected and tentatively identified as 3-furaldehyde ($[C_5H_4O_2 + H]^+$) as shown in its matching EI spectra (FigureA4.2) This mass was detected in multiple species including *D. baronii*, *D. cearensis*, *D. stevensonii*, *D. tucurensis*, *D. spruceana*, *D. maritima*, *D. cochinchinensis*, *D. oliveri*, *D. occulta*, *D. madagascariensis*, *D. latifolia*, *D. melanoxylon*, *D. normandii*, *D. purprascens*, *D. retusa*, *D. nigra* (as shown in its chromatogram in Figure 4.6) and *D. decipularis*. This compound has also been reported in other plants,[167,168] but never in *Dalbergia spp.* Preliminary TD-GC-MS analysis of the headspace of the 17 *Dalbergia spp.* in this study revealed the presence of the following tentatively identified compounds: dimethyl ether; cyclobutene; acetone; azomethane; 1,2-dimethylhydrazine; isopropanol; 1,2-dimethylhydrazine; 1-pentene; isobutyraldehyde; dimethylformamide; acetol; 1,4-cyclohexadiene; (*E,E*)-2,4-hexadiene; butyric acid; toluene, 3-furaldehyde; pentanoic acid; benzaldehyde; maltol; (*E*)-cinnamaldehyde; 5-methylbenzimidazole; 3-methoxycatechol; *trans*-3-

Methyl-4-octanolide; nonanoic acid; geranylacetone; β-bisabolene; humulenol II; and hexadecane. Ongoing efforts aim to identify the remainder of the 112 masses revealed by DART-HRMS to further facilitate the identification and differentiation of the *Dalbergia spp*. While the headspace volatiles are compounds that have been detected in various plant species, the specific combination of masses holds diagnostic value for species differentiation. Current efforts are focused on determining which combination of molecules is diagnostic for each species.

4.4. Conclusion

This study presents the findings of an analysis of the chemical headspace signatures of seventeen representative species of *Dalbergia*, namely: *D. baronii*, *D. cearensis*, *D. oliveri*, *D. occulta, D. madagascariensis*, *D. latifolia, D. melanoxylon*, *D. normandii*, *D. purprascens*, *D. retusa, D. nigra*, *D. decipularis*, *D. stevensonii*, *D. tucurensis*, *D. spruceana*, *D. maritima*, and *D. cochinchinensis*. Despite their DART mass spectra exhibiting visually apparent interspecies similarities, multivariate statistical analysis techniques unveiled subtle distinctions that enabled species differentiation. When their SPME-facilitated DART-HRMS-derived chemical signatures were subjected to SVM, species prediction with an overall accuracy of 83.33% was achieved. Notably, the results for certain species such as *D. cearensis*, *D. retusa*, and *D. decipularis*, exhibited exceptionally high accuracies exceeding 90%, indicating high discriminatory power. Conversely, the prediction accuracies for *D. oliveri* and *D. occulta* were poor (55.56%). Analysis of the confusion matrix derived from the SVM results provided valuable insights into misclassification patterns, and highlighting specific species prone to confusion. For instance, *D. oliveri* and *D. occulta* were often misclassified as one another. These challenges with classification may stem from interspecies similarities indicative of high genetic relatedness, or the fact that because of sample rarity, only a limited number of individuals could be analyzed. In the case of

the latter issue, accuracies may increase with the analysis of more samples as they become available, in order to give the statistical model more power. The findings underscore the need for caution when interpreting classification results and suggest avenues for future research to address misclassification challenges and enhancement of prediction accuracy when using machine learning systems.

Despite these limitations, the classification model demonstrates promising potential for species identification within the *Dalbergia* genus. The ability to accurately differentiate between timber species via headspace analysis has important implications in various areas including forestry, conservation, and trade regulation. It can inform harvesting strategies tailored to different species, facilitate targeted measures for protecting endangered species and their habitats, and promote more robust enforcement of international agreements such as CITES. Furthermore, the analysis of chemical headspace signatures revealed insights into the underlying chemical compositions of the representative *Dalbergia spp.* Moving forward, efforts to expand sample sizes could further enhance the accuracy and applicability of the classification model. In the aggregate, the results provide a foundation for future research aimed at improving species identification using headspace chemical profiles, towards the development of efficient stand-off analysis approaches.

CHAPTER 5: COMPREHENSIVE ANALYSIS OF CHEMICAL HEADSPACE SIGNATURES IN *SWIETENIA* USING MASS SPECTROMETRIC TECHNIQUES

5.1. Introduction

Mahogany is the common name used to refer to wood derived from the three species of the Swietenia genus (Meliaceae), namely *S. humilis* Zuccarini, *S. macrophylla* King, and *S. mahagoni* (Linnaeus) Jacquin.[169] These species have a rich history of use in ethnomedicine. *S. humilis*, endemic to Central America,[170] is commonly known as zopilote, cobano, gateado, caobilla, flor de venadillo, caoba and sopilocuahuilt.[170–174] Its seeds are used to treat numerous ailments including diabetes, dyslipidemia, amoebiasis, cough, cancer, diarrhea, hypertension, and intestinal worm parasitism.[169,171–175] Furthermore, extracts of the plant exhibit insecticidal activity.[176] Likewise, *S. mahagoni*, an economically important species native to the West Indies,[177,178] is traditionally used to treat a range of disorders, including malaria, eczema, diabetes, diarrhea, rheumatism, cold, anorexia, psoriasis, hypertension and as an antiseptic.[177,179–187] Similar to *S. humilis*, *S. macrophylla*, or "big-leaf mahogany"[188–192], is endemic to Central America, in addition to South America.[189–196] It is also used in folk medicine for what are believed to be its antimicrobial, anti-inflammatory, antioxidant, hypolipidemic, antifeedant, antimutagenic, antinociceptive, acaricidal, antiviral, antitumor, antidiarrheal, antifungal and antihyperglycemic effects.[188–191,195] Because of their biological properties, there has been significant interest in isolating bioactive molecules from these species. Accordingly, bioassay-guided fractionation studies have led to the discovery of flavonoids, alkaloids, phenolic compounds, terpenoids, and limonoids.[169,171,173,174,180,181,188,195,197–201] A number of fatty acids have also been isolated from the seed oil of these plants, including linoleic, elaidic, stearic, palmitic, ecosanoic, octadecanoic, oleic, arachidic, behenate, and linolenic acids.[169,181,185,191,195]

In addition to the utility of Mahogony in traditional medicine, the straight-grained and characteristic reddish-brown hue of *Swietenia* woods has made them economically important and highly prized for crafting furniture, musical instruments, decorative materials, and artisanal objects.[35,202] This has led to over-harvesting, which in turn has raised concerns that they may ultimately be threatened with extinction.[54,203] Thus, all *Swietenia spp.* are CITES regulated, where they are classified as Appendix II.[37] Accordingly, their trade is controlled. However, even though all their species are in the same appendix, meaning that they receive the same degree of protection, it is still imperative to discriminate between them because of differing country-specific regulations regarding trade.[204] Notably, the ability of law enforcement to intercept and curtail illegal logging and trade of *Swietenia spp.* depends on the availability of methods for determining the species identities of encountered timber that is suspected to be *Swietenia*.

Several approaches have been devised for the purpose of identifying wood species. The most prevalent is wood anatomical analysis, in which species attribution is made based on species-specific macroscopic and microscopic features of the wood. However, it can be challenging to distinguish between species within the same genus, such as *S. mahogani*, *S. humilis*, and *S. macrophylla* because of their anatomical similarities, and requires extensive expertise. Another species identification method is DNA analysis. However, in addition to being laborious, time-consuming, and costly, its utility is reliant on the successful extraction of DNA from the wood, which is notoriously difficult because of the tendency of the DNA extracted from felled wood to be extensively fragmented.[35,53,54]

In light of these challenges, there remains a critical need for the development of alternative approaches for the rapid determination, in a forensic context, of the species identity of woods. Both accuracy and speed would be desirable features of such a method. In this regard, one of the

developed techniques that has been applied to species identification of wood is ambient ionization mass spectrometry. Specifically, direct analysis in real – time high-resolution mass spectrometry (DART-HRMS) has been shown to reveal species-specific chemical signatures of wood, which when subjected to multivariate statistical analysis, enables accurate species identity to be determined.[53,54] For example, Deklerck et al. directly analyzed the slivers of several species (*E. angolense*, *E. candollei*, *E. cylindricum*, *E.utile*, *K. anthotheca*, *K. ivorensis*, *L. trichilioides*, *S. macrophylla*, *S. humilis*, and *S. mahagoni*) and created a Random Forest classification model based on their chemical differences. This predictive model can be used to distinguish between the 10 species with an 82% accuracy.[54] A similar approach has been adopted by the U.S. Fish and Wildlife Forensic Lab for application to casework. It involves the analysis of small segments or slivers of wood, the mass spectra of which are screened against a database of wood species' chemical signatures. The method is robust and achieves accuracies of >90%.[88,89] Despite the success of this mode of analysis for species identification, there continues to be interest, depending on the species, in the development of a "stand-off" approach that might eliminate the requirement for direct analysis of wood slivers and segments. Proof of principle for such a method was recently reported for the identification of psychoactive plants from their headspace chemical signatures.[62] The success of this approach was also used successfully for the species identification of *Dalbergia* spp. as described in Chapter 4. the headspace of *Swietenia* genus plants exhibit species-specific chemical signatures, it may be possible to identify their woods from analysis of their headspace, rather than direct analysis of the wood itself. Such an accomplishment would pave the way for the development of a stand-off approach for *Swietenia spp.* identification.

Described here are the results of an investigation of the headspace chemical profiles of all three *Swietenia spp*. When the chemicals in their headspace were concentrated using solid phase

micro-extraction (SPME) and the fibers analyzed by DART-HRMS, intraspecies similarities and interspecies differences were observed. When the mass spectra were subjected to multivariate statistical analysis via Extreme Gradient Boosting, the species were well separated, resulting in a prediction accuracy of 89% based on the headspace chemical signatures alone.

5.2. Methods

5.2.1. Timber Samples

All timber samples were provided by the U.S. Fish and Wildlife Lab (USFWL) (Ashland, OR, USA). Table 5.1 lists the species information along with the identification number assigned by the USFWL. In all, authenticated samples of five unique individuals from each of the species *S. mahagoni*, *S. humilis*, and *S. macrophylla* were analyzed.

5.2.2. Solid-Phase Microextraction

Divinylbenzene/Carboxen/(Polydi-methylsiloxane-coated (DVB/CAR/ PDMS) 24 Ga 50/30 µm solid-phase microextraction (SPME) fibers and SPME fiber holders for use with manual sampling

Table 5.1 *Swietenia spp.* analyzed, showing the U.S. Fish and Wildlife Laboratory-assigned identification number for the individual sample.

Species	Identification Number
Swietenia humilis	150635
Swietenia humilis	130980
Swietenia humilis	130984
Swietenia humilis	130726
Swietenia humilis	130898
Swietenia mahagoni	130472
Swietenia mahagoni	130473
Swietenia mahagoni	130477
Swietenia mahagoni	130474
Swietenia mahagoni	130474
Swietenia macrophylla	130748
Swietenia macrophylla	130749
Swietenia macrophylla	130744
Swietenia macrophylla	130747
Swietenia macrophylla	130751

were purchased from Supelco Inc. (Bellefonte, PA, USA). Fibers were conditioned for 30 min at 250 °C under a stream of helium gas before each headspace sampling.

5.2.3. Headspace Sampling

Wood samples for analysis were generated by depositing within a 20 mL scintillation vial 2 g of slivers that were produced by segmenting the bulk wood with wire cutter pliers. The mouths of the vials were covered tightly with aluminum foil, and a conditioned DVB/CAR/PDMS coated 24 Ga 50/30 µm SPME fiber was exposed to the headspace of the sample for 30 min at room temperature (Figure 5.1). This concentration step was performed in triplicate by concentrating headspace volatiles in a vial three times under ambient conditions at approximately 23 °C.

Figure 5.1 Headspace sampling of timber.

5.2.4. DART-HRMS Analysis

SPME fibers, to which headspace volatiles were adsorbed, were analyzed in positive-ion mode (Figure 5.2) using a direct analysis in real-time (DART)-SVP ion source (IonSense, Saugus,

Figure 5.2 DART-HRMS analysis of SPME fiber.

MA, USA) interfaced with a JEOL AccuTOF mass spectrometer (JEOL USA, Peabody, MA, USA). The instrument parameter settings were as follows: helium gas flow rate, 2.0 L/min; gas temperature, 250 °C; ring lens voltage, 5 V; orifice 1 voltage, 20 V; orifice 2 voltage, 5 V; and peak voltage, 400 V (to detect m/z values $\geq$ 40). The mass spectrometer used has a resolving power of 6000 full width at half maximum (fwhm). Spectra were collected at a rate of one spectrum per second over the mass range m/z 40–1000. PEG 600 (Sigma-Aldrich, St. Louis, MO, USA) was used as the mass calibrant and was sampled following the analysis of each individual fiber. TSSPro 3 software (Shrader Analytical, Detroit, MI, USA) was used for data processing including

averaging, background subtraction, and peak centroiding. The DART mass spectra of a conditioned SPME fiber that was exposed to the headspace of an empty scintillation vial served as a blank for the SPME analyses.

5.2.5. Multivariate Statistical Analysis

SPME fiber-facilitated DART-HRMS was used to generate mass spectra in the form of text files with one column containing the *m/z* values and the second containing their corresponding ion counts. A third column representing the relative intensities was created. In all, the mass spectra of 45 samples representing 3 different species were aligned in a matrix with dimensions of 45 x 1134 with an optimal bin width of +20 mmu and relative intensity cutoff of 0.3%. A code from Deklerk et al.[54] was used to set the bin width and relative intensity cutoff value in R 4.2.3 (Posit, Boston, MA, USA), where a range of text files can be placed into a single matrix based on the selected bin width and relative intensity cutoff value. This matrix was imported into Python 3.9.12 (Python Software Foundation, Wilmington, DE, USA) as a comma-separated values (CSV) file to be subjected to multivariate statistical analysis. The optimal bin width and relative intensity cutoff was determined by varying these values from 0 to 20 mmu and 0.1 to 5%, respectively, and screening this data through a range of classification models, including Logistic Regression, Decision Tree, Random Forest, K-Nearest Neighbors, Support Vector Machines, and Extreme Gradient Boosting to see which gave the best accuracy. The matrix was standardized using the StandardScaling function in the sklearn library and split into a training and a test set, where 80% of the samples were randomly selected for the training set and 20% were randomly selected for the test set. A supervised method, Extreme Gradient Boosting, was applied using the XGBoost Python Package. The optimal hyperparameters were investigated through an iterative process, where several models were created based on varying hyperparameters to find which values

generated the highest accuracy. These were found to be: objective, multi:softmax; num_class, 3; learning_rate, 0.3; max_depth, 1; min_child_weight, 2; n_estimators, 100; early_stopping_rounds, 10; subsample, 0.5; eval_metric, mlogloss; and scoring, accuracy. The accuracy of the prediction model was determined by screening the samples from the test set against the model to determine the percentage of correctly identified samples. Feature importance was extracted from the Extreme Gradient Boosting model by calculating their respective F scores. Features are deemed important depending on whether they are valuable when building a predictive model. In this case, the importance of a feature is represented by its F score, where the higher the score, the higher the relative importance.

5.3. Results

5.3.1. DART-MS Analysis

SPME-facilitated DART-HRMS analysis of the headspace volatiles of five individuals (three replicates each) from each of the species *S. mahagoni*, *S. humilis*, and *S. macrophylla* furnished spectra, representative examples of which are shown in Figure 5.3. where the top, middle, and bottom rows represent spectra from three individuals of *S. humilis*, *S. macrophylla*, and *S. mahagoni*, respectively. Their corresponding mass spectral data tables (with masses reported using a 0.3% relative abundance threshold), are reposited at https://rabi-musah.squarespace.com/s/Swietenia-species-mass-data-tables-corresponding-to-Figure-53.xlsx), This analysis revealed that multiple individuals of the same species exhibited similar headspace volatiles profiles. For example, the headspace spectra of *S. humilis* all contained the *m/z* values (within bin width of 20 mmu) 75.0487 and 205. 1933. This was also observed for the other species. For example, *S. macrophylla* exhibited *m/z* 61.0925 and 135.0467 and *S. mahagoni* had *m/z* 61.0925 and 167.1325 in their representative spectra within the bin width. However, the spectra
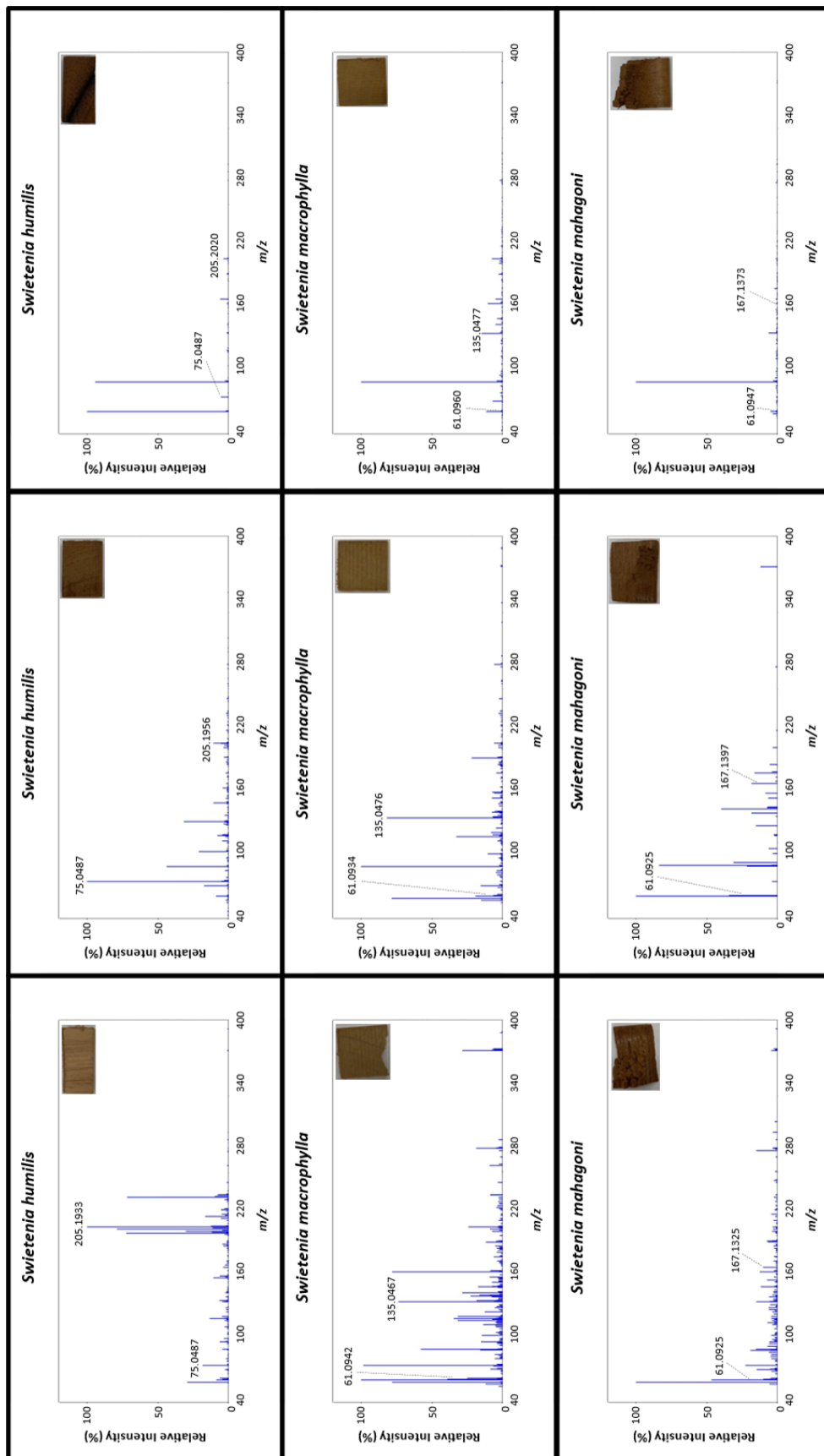
Figure 5.3 Representative DART mass spectra of *S. humilis* (top row), *S. macrophylla* (middle row), and *S. mahagoni* (bottom row).

also showed interspecies similarities which can make it difficult to visually differentiate between them. For example, Figure 5.3 shows that both *S. macrophylla* and *S. mahagoni* contain the *m/z* value 61.0925. To investigate this further, a correlation matrix featuring the mass spectral data rendered as a heat map (Figure 5.4) was generated. This table shows the correlation coefficients between the forty-five samples, plotted against one another on the x- and y-axes. Sample numbers 0-14, 15-29, and 30-44 (shown in the blue boxes) are representative of the replicates of *S. humilis*, *S. mahagoni*, and *S. macrophylla*, respectively, where every set of three sample numbers represents the three replicates that were analyzed for one individual. The values are between 1 (light orange) and -0.6 (dark purple), with values close to 1 indicate a strong correlation, and those at the other end of the continuum indicating a weak correlation. A positive correlation indicates that the variables increased together, whereas a negative correlation indicates that one increases, while the other decreases. Figure 5.4 reveals that the samples, whether of the same or of different species, are highly similar. For example, there are many *S. humilis* samples (the first blue box) that have high positive correlations of 1 or close to 1 with the other two *Swietenia spp.* (outside the first blue box). This trend was consistent across all the species for most of the samples. This low variability between the chemical profiles was so extreme, which further demonstrates that any differences that might facilitate species differentiation were not readily apparent by visual examination of their mass spectra. Therefore, multivariate statistical analysis was applied to the data to reveal any possible subtle distinctions between the spectra representative of each species, which could be used to differentiate between them.
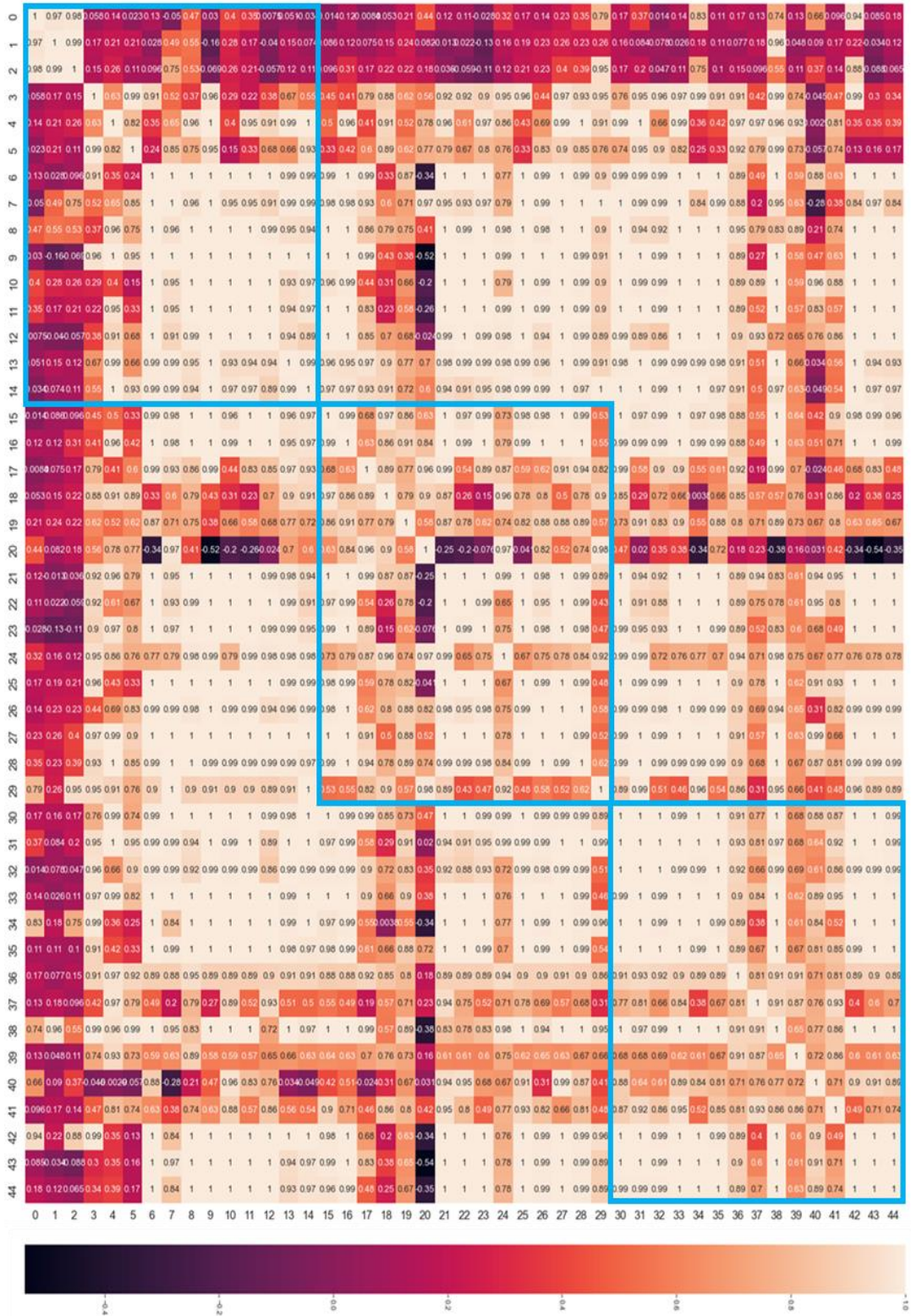
Figure 5.4 Mass spectra rendered as a correlation matrix of the forty-five spectra representing the *Swietenia spp.*

109

5.3.2. Creation of a Prediction Model

In order to determine whether there were subtle, non-visually apparent features in the DART-HRMS headspace chemical profiles that could be used to differentiate between the species, the mass spectral data were subjected to multivariate statistical analysis. The data for all replicates for the five individuals representing all three timber species were aligned along common *m/z* values using a relative abundance cutoff of 0.3% and a bin width of +20 mmu, and imported into Python to develop an Extreme Gradient Boosting classification model for the identification of *Swietenia spp*. The data were standardized by removing the mean from the relative intensities and scaling to unit variance. The data were then separated into a training and a test set. The training set was comprised of 80% of the data and was subjected to Extreme Gradient Boosting using the XGBoost scikit-learn library to create the prediction model. The remaining 20% of the data were used to test how well the model performed in discriminating between classes. Extreme Gradient Boosting is a supervised machine learning technique that creates decision tree model ensembles, where trees are added one at a time with each subsequent tree learning from the past model's errors, in order to determine the best node split for higher accuracy. The hyperparameters (presented in the methods section) were tuned to find the optimum parameter values that enabled the building of an accurate model. A confusion matrix illustrating the prediction capabilities of the resulting model for the test set samples is shown in Table 5.2. The numerical entries along the diagonal represent correct species predictions, while off diagonal entries greater than zero show misclassifications. The results show that all three of the *S. macrophylla* samples, as well as all three of the *S. mahagoni*

Table 5.2 Confusion matrix showing the prediction results of the nine samples in the test set.

Species	S. macrophylla	S. mahogoni	S. humilis
S. macrophylla	3	0	0
S. mahagoni	0	3	0
S. humilis	1	0	2

Table 5.3 The precision, recall, F1 score, and accuracy of the Extreme Gradient Boosting model were 92%, 89%, 89%, and 89%, respectively.

Classification Merits	
Precision	92%
Recall	89%
F1 Score	89%
Accuracy	89%

samples were correctly classified, and two of the *S. humilis* samples were correctly classified. However, one *S. humilis* sample was misclassified as *S. macrophylla*. The classification merits of the model are displayed in Table 5.3. They show the precision, recall, F1 score, and accuracy to be 92%, 89%, 89%, and 89%, respectively. The results indicate that within the headspace molecular signatures of *Swietenia spp.* are the chemical attributes that enable the species to be identified with an accuracy of 89%, using an Extreme Gradient Boosting Model. This approach yields results that improved upon those reported by Deklerck et al.[54] using a random forest model (82% accuracy) when differentiating between multiple species, including those of the *Swietenia* genus. Moreover, the method described here is distinguished from earlier reported approaches in that it utilizes headspace instead of direct analysis of the wood samples themselves.

5.3.3. Feature Importance Determination

An implication of the finding that the DART-HRMS-derived headspace chemical profiles of *Swietenia spp.* exhibit chemical distinctions that enabled the Extreme Gradient Boosting model to predict their identities, is that there may be chemical compounds, the presence or absence of which enable the model to accomplish species discrimination. Thus, a feature importance investigation was conducted to ascertain which masses were most impactful in enabling the model to differentiate the species from one another. The importance of a given feature (i.e., *m/z* value) in the development of a prediction model was determined, in this case, by its F score. The F score is a measurement of the discriminative power of each feature. The equation used is F = F1/F2, where F1 is the variability between groups and F2 is the variability within each group. This equation

enables determination of relative feature importance because the higher the F score of a given feature, the more important that feature is for discriminating between groups. The top twenty-eight most important features (i.e., *m/z* values) are listed in Figure 5.5 where each feature is shown on the y-axis, and its corresponding F score is shown on the x-axis. For example, the *m/z* value 61.0925 is the most important feature with an F score of 18.0, while *m/z* 61.1330, 113.1200, 117.2080, 128.1405, 146.1173, and 294.2385 all with an F score of 1.0, were the least heavily weighted of the top twenty-eight *m/z* values. Efforts are ongoing to determine what these significant features might represent, utilizing techniques such as GC- and LC-MS, as revelation of the identities of these masses will facilitate determination of whether any of them may serve as markers for *Swietenia* spp.
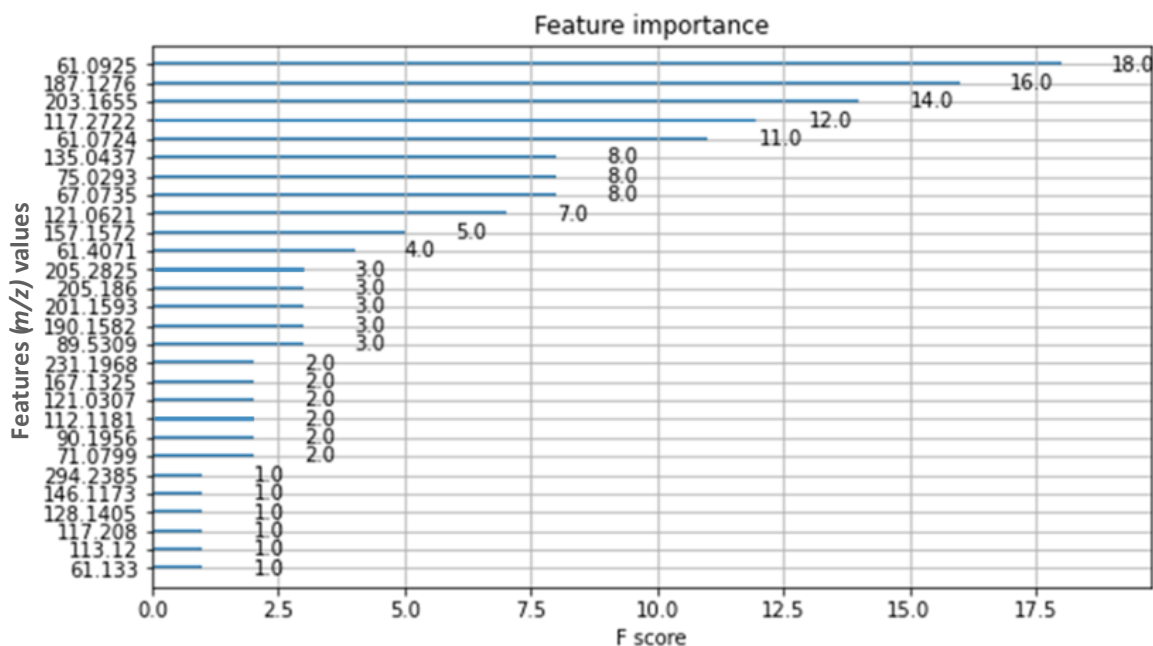
Figure 5.5 The 28 most important features (i.e., the *m/z* values presented on the y-axis) for facilitating discrimination between species, arranged in order of decreasing F score (presented on the x-axis).

5.4. Conclusion

This study presents the findings of an analysis of the chemical headspace signatures of the three representative species of *Swietenia*, namely: *S. humilis*, *S. mahagoni*, and *S. macrophylla*.

When the chemicals in their headspace were concentrated using SPME, analyzed by DART-HRMS, and the resulting data subjected to multivariate statistical analysis, interspecies similarities and intraspecies differences were observed. These were exploited using Extreme Gradient Boosting to generate a species prediction model that seemingly exhibited an accuracy of 89%, based on headspace chemical profiles alone. As these results are preliminary, future work will further assess the validity of the results by examining what features (i.e., *m/z* values) are in the data that contribute to species differentiation, and whether their chemical identities can be determined.

OVERARCHING CONCLUSIONS

In the ever-evolving landscape of global crime, forensic science plays a crucial role in combating emerging challenges, ranging from the production and distribution of psychoactive substances to the environmental devastation caused by illegal logging. The work presented here shows the development of innovative methodologies aimed at rapidly detecting, identifying, and classifying these substances, thus ensuring timely intervention and the development of robust regulatory measures to safeguard public health and environmental sustainability.

The emergence of new psychoactive substances (NPS) presents a formidable challenge to forensic laboratories worldwide. These chemically diverse compounds, marketed as "legal highs," evade regulation and pose significant public health risks. Additionally, psychoactive plants, such as Kava and Kratom, further complicate forensic analysis due to their diverse chemical compositions and visual resemblance to benign materials. The lack of standardized protocols for detecting and characterizing their psychoactive constituents underscores the need for innovative analytical strategies. Furthermore, illegal logging poses significant environmental and economic challenges worldwide. Robust analytical techniques are needed to accurately classify timber species, aiding in the enforcement of forestry regulations.

Through the integration of analytical techniques such as direct analysis in real-time high-resolution mass spectrometry (DART-HRMS) and multivariate statistical analysis, this research: (1) addresses the complexities of NPS identification and classification, facilitating more efficient regulatory enforcement; (2) demonstrates the development of a database capable of reliably identifying plants and their psychoactive constituents, thus ensuring public safety and regulatory compliance; and (3) enhances the capabilities of forensic laboratories in combating illegal logging activities, ultimately contributing to the preservation of global forests and the sustainability of the

timber trade. Therefore, this dissertation highlights the imperative of addressing the multifaceted challenges posed by NPSs, psychoactive plants, and environmental crimes. By leveraging DART-HRMS and advanced statistical methods, forensic science practitioners can adapt to the dynamic nature of organized crime, ensuring a safer and more sustainable future for society.

REFERENCES

1. United Nations Office on Drugs and Crime. *The Challenge of New Psychoactive Substances*.

2. Nelson, M. E.; Bryant, S. M.; Aks, S. E. Emerging Drugs of Abuse. *Emergency Medicine Clinics of North America* **2014**, *32* (1), 1–28.

3. Baumann, M. H.; Solis, E.; Watterson, L. R.; Marusich, J. A.; Fantegrossi, W. E.; Wiley, J. L. Baths Salts, Spice, and Related Designer Drugs: The Science Behind the Headlines. *The Journal of Neuroscience* **2014**, *34* (46), 15150–15158.

4. Rosenbaum, C. D.; Carreiro, S. P.; Babu, K. M. Here Today, Gone Tomorrow…and Back Again? A Review of Herbal Marijuana Alternatives (K2, Spice), Synthetic Cathinones (Bath Salts), Kratom, Salvia Divinorum, Methoxetamine, and Piperazines. *Journal of Medical Toxicology* **2012**, *8* (1), 15–32.

5. Seely, K. A.; Patton, A. L.; Moran, C. L.; Womack, M. L.; Prather, P. L.; Fantegrossi, W. E.; Radominska-Pandya, A.; Endres, G. W.; Channell, K. B.; Smith, N. H.; McCain, K. R.; James, L. P.; Moran, J. H. Forensic Investigation of K2, Spice, and "Bath Salt" Commercial Preparations: A Three-Year Study of New Designer Drug Products Containing Synthetic Cannabinoid, Stimulant, and Hallucinogenic Compounds. *Forensic Science International* **2013**, *233* (1–3), 416–422.

6. Shanks, K. G.; Dahn, T.; Behonick, G.; Terrell, A. Analysis of First and Second Generation Legal Highs for Synthetic Cannabinoids and Synthetic Stimulants by Ultra-Performance Liquid Chromatography and Time of Flight Mass Spectrometry. *Journal of Analytical Toxicology* **2012**, *36* (6), 360–371.

7. Barceló, B.; Pichini, S.; López-Corominas, V.; Gomila, I.; Yates, C.; Busardò, F. P.; Pellegrini, M. Acute Intoxication Caused by Synthetic Cannabinoids 5F-ADB and MMB-2201: A Case Series. *Forensic Science International* **2017**, *273*, e10–e14.

8. Dresen, S.; Ferreirós, N.; Pütz, M.; Westphal, F.; Zimmermann, R.; Auwärter, V. Monitoring of Herbal Mixtures Potentially Containing Synthetic Cannabinoids as Psychoactive Compounds. *Journal of Mass Spectrometry* **2010**, *45* (10), 1186–1194.

9. Vardakou, I.; Pistos, C.; Spiliopoulou, Ch. Spice Drugs as a New Trend: Mode of Action, Identification and Legislation. *Toxicology Letters* **2010**, *197* (3), 157–162.

10. Schneir, A.; Metushi, I. G.; Sloane, C.; Benaron, D. J.; Fitzgerald, R. L. Near Death from a Novel Synthetic Opioid Labeled U-47700: Emergence of a New Opioid Class. *Clinical Toxicology* **2017**, *55* (1), 51–54.

11. Ventura, M. I.; Beyramysoltan, S.; Musah, R. A. Revealing the Presence of Tryptamine New Psychoactive Substances Using Fused "Neutral Loss" Spectra Derived from DART High-Resolution Mass Spectra. *Talanta* **2022**, *246*, 123417.

12. U.S. Department of Justice. Synthetic Cathinones (Bath Salts): An Emerging Domestic Threat. **2011**.

13. Lee, D.; Chronister, C. W.; Hoyer, J.; Goldberger, B. A. Ethylone-Related Deaths: Toxicological Findings. *Journal of Analytical Toxicology* **2015**, *39* (7), 567–571.

14. Prosser, J. M.; Nelson, L. S. The Toxicology of Bath Salts: A Review of Synthetic Cathinones. *Journal of Medical Toxicology* **2012**, *8* (1), 33–42.

15. White, C. M. Mephedrone and 3,4-Methylenedioxypyrovalerone (MDPV): Synthetic Cathinones With Serious Health Implications. *The Journal of Clinical Pharmacology* **2016**, *56* (11), 1319–1325.

16. Wojcieszak, J.; Andrzejczak, D.; Woldan-Tambor, A.; Zawilska, J. B. Cytotoxic Activity of Pyrovalerone Derivatives, an Emerging Group of Psychostimulant Designer Cathinones. *Neurotoxicity Research* **2016**, *30* (2), 239–250.

17. Woloshchuk, C. J.; Nelson, K. H.; Rice, K. C.; Riley, A. L. Effects of 3,4-Methylenedioxypyrovalerone (MDPV) Pre-Exposure on the Aversive Effects of MDPV, Cocaine and Lithium Chloride: Implications for Abuse Vulnerability. *Drug and Alcohol Dependence* **2016**, *167*, 121–127.

18. Wright, T. H.; Harris, C. Twenty-One Cases Involving Alpha-Pyrrolidinovalerophenone (α-PVP). *Journal of Analytical Toxicology* **2016**, *40* (5), 396–402.

19. Lusthof, K. J.; Oosting, R.; Maes, A.; Verschraagen, M.; Dijkhuizen, A.; Sprong, A. G. A. A Case of Extreme Agitation and Death after the Use of Mephedrone in The Netherlands. *Forensic Science International* **2011**, *206* (1–3), e93–e95.

20. Poyatos, L.; Torres, A.; Papaseit, E.; Pérez-Mañá, C.; Hladun, O.; Núñez-Montero, M.; de la Rosa, G.; Torrens, M.; Fuster, D.; Muga, R.; Farré, M. Abuse Potential of Cathinones in Humans: A Systematic Review. *Journal of Clinical Medicine* **2022**, *11* (4), 1004.

21. Baumann, M. H.; Walters, H. M.; Niello, M.; Sitte, H. H. Neuropharmacology of Synthetic Cathinones; 2018; pp 113–142.

22. Jovel, A.; Felthous, A.; Bhattacharyya, A. Delirium Due to Intoxication from the Novel Synthetic Tryptamine 5-MeO- DALT. *Journal of Forensic Sciences* **2014**, *59* (3), 844–846.

23. Shimizu, E.; Watanabe, H.; Kojima, T.; Hagiwara, H.; Fujisaki, M.; Miyatake, R.; Hashimoto, K.; Iyo, M. Combined Intoxication with Methylone and 5-MeO-MIPT. *Progress in Neuro-Psychopharmacology and Biological Psychiatry* **2007**, *31* (1), 288–291.

24. Sasaki, C.; Saito, T.; Shinozuka, T.; Irie, W.; Murakami, C.; Maeda, K.; Nakamaru, N.; Oishi, M.; Nakamura, S.; Kurihara, K. A Case of Death Caused by Abuse of a Synthetic Cannabinoid N-1-Naphthalenyl-1-Pentyl-1H-Indole-3-Carboxamide. *Forensic Toxicology* **2015**, *33* (1), 165–169.

25.   Adams, A. J.; Banister, S. D.; Irizarry, L.; Trecki, J.; Schwartz, M.; Gerona, R. "Zombie" Outbreak Caused by the Synthetic Cannabinoid AMB-FUBINACA in New York. *New England Journal of Medicine* **2017**, *376* (3), 235–242.

26.   Alhassan, A.; Prahad, S. R.; Burk, B. G.; Fargason, R. E.; Birur, B. New-Onset Prolonged Psychosis Following Synthetic Cannabinoid Use in an Older Patient: A Case Report. *Psychopharmacology Bulletin* **2024**, *54* (1), 33—39.

27.   Mohr, A. L. A.; Friscia, M.; Papsun, D.; Kacinko, S. L.; Buzby, D.; Logan, B. K. Analysis of Novel Synthetic Opioids U-47700, U-50488 and Furanyl Fentanyl by LC–MS/MS in Postmortem Casework. *Journal of Analytical Toxicology* **2016**.

28.   Schuller, J. L.; Krantz, M. J. Synthetic Opioids and Arrhythmia Risk: A New Paradigm? *Expert Opinion on Pharmacotherapy* **2012**, *13* (13), 1825–1827.

29.   Taoussi, O.; Berardinelli, D.; Zaami, S.; Tavoletta, F.; Basile, G.; Kronstrand, R.; Auwärter, V.; Busardò, F. P.; Carlier, J. Human Metabolism of Four Synthetic Benzimidazole Opioids: Isotonitazene, Metonitazene, Etodesnitazene, and Metodesnitazene. *Archives of Toxicology* **2024**.

30.   Christian Rätsch. The Encyclopedia of Psychoactive Plants: Ethnopharmacology and Its Applications; Simon and Schuster, 2005.

31.   Beyramysoltan, S.; Chambers, M. I.; Osborne, A. M.; Ventura, M. I.; Musah, R. A. Introducing "DoPP": A Graphical User-Friendly Application for the Rapid Species Identification of Psychoactive Plant Materials and Quantification of Psychoactive Small Molecules Using DART-MS Data. *Analytical Chemistry* **2022**, *94* (48), 16570–16578.

32.   U.S. Department of Justice. KHAT Factsheet. **1992**.

33.   U.S. Department of Justice. List of Controlled Substances. **2022**.

34.   Deklerck, V. Timber Origin Verification Using Mass Spectrometry: Challenges, Opportunities, and Way Forward. *Forensic Science International: Animals and Environments* **2023**, *3*, 100057.

35.   He, T.; Marco, J.; Soares, R.; Yin, Y.; Wiedenhoeft, A. C. Machine Learning Models with Quantitative Wood Anatomy Data Can Discriminate between *Swietenia macrophylla* and *Swietenia mahagoni*. *Forests* **2020**, *11* (1).

36.   Nellemann, C.; UNEP. Green Carbon, Black Trade : Illegal Logging, Tax Fraud and Laundering in the World's Tropical Forests. A Rapid Response Assessment.

37.   Convention on International Trade in Endangered Species of Wild Fauna and Flora Appendices I, II and III. https://cites.org/eng/app/appendices.php.

38.   United Nations Office on Drugs and Crime. *Recommended Methods for the Identification and Analysis of Synthetic Cathinones in Seized Material*.

39.   Yuan, C.; Chen, D.; Wang, S. Drug Confirmation by Mass Spectrometry: Identification Criteria and Complicating Factors. *Clinica Chimica Acta* **2015**, *438*, 119–125.

40. Bijlsma, L.; Miserez, B.; Ibáñez, M.; Vicent, C.; Guillamón, E.; Ramsey, J.; Hernández, F. Identification and Characterization of a Novel Cathinone Derivative 1-(2,3-Dihydro-1H-Inden-5-Yl)-2-Phenyl-2-(Pyrrolidin-1-Yl)-Ethanone Seized by Customs in Jersey. *Forensic Toxicology* **2016**, *34* (1), 144–150.

41. Jankovics, P.; Váradi, A.; Tölgyesi, L.; Lohner, S.; Németh-Palotás, J.; Kőszegi-Szalai, H. Identification and Characterization of the New Designer Drug 4′-Methylethcathinone (4-MEC) and Elaboration of a Novel Liquid Chromatography–Tandem Mass Spectrometry (LC–MS/MS) Screening Method for Seven Different Methcathinone Analogs. *Forensic Science International* **2011**, *210* (1–3), 213–220.

42. Namera, A.; Kawamura, M.; Nakamoto, A.; Saito, T.; Nagao, M. Comprehensive Review of the Detection Methods for Synthetic Cannabinoids and Cathinones. *Forensic Toxicology* **2015**, *33* (2), 175–194.

43. Westphal, F.; Junge, T.; Klein, B.; Fritschi, G.; Girreser, U. Spectroscopic Characterization of 3,4-Methylenedioxypyrrolidinobutyrophenone: A New Designer Drug with α-Pyrrolidinophenone Structure. *Forensic Science International* **2011**, *209* (1–3), 126–132.

44. Westphal, F.; Junge, T.; Rösner, P.; Fritschi, G.; Klein, B.; Girreser, U. Mass Spectral and NMR Spectral Data of Two New Designer Drugs with an α-Aminophenone Structure: 4′-Methyl-α-Pyrrolidinohexanophenone and 4′-Methyl-α-Pyrrolidinobutyrophenone. *Forensic Science International* **2007**, *169* (1), 32–42.

45. Fakayode, S. O.; Brady, P. N.; Grant, C.; Fernand Narcisse, V.; Rosado Flores, P.; Lisse, C. H.; Bwambok, D. K. Electrochemical Sensors, Biosensors, and Optical Sensors for the Detection of Opioids and Their Analogs: Pharmaceutical, Clinical, and Forensic Applications. *Chemosensors* **2024**, *12* (4), 58.

46. United Nations Office on Drugs and Crime. Recommended Methods for the Identification and Analysis of Synthetic Cannabinoid Receptor Agonists in Seized Materials. **2013**.

47. Kerrigan, S.; Savage, M.; Cavazos, C.; Bella, P. Thermal Degradation of Synthetic Cathinones: Implications for Forensic Toxicology. *Journal of Analytical Toxicology* **2015**, bkv099.

48. Fowble, K. L.; Shepard, J. R. E.; Musah, R. A. Identification and Classification of Cathinone Unknowns by Statistical Analysis Processing of Direct Analysis in Real Time-High Resolution Mass Spectrometry-Derived "Neutral Loss" Spectra. *Talanta* **2018**, *179*, 546–553.

49. U.S. Department of Justice. Improved Detection of Synthetic Cathinones in Forensic Toxicology Samples: Thermal Degradation and Analytical Considerations. **2015**.

50. Majchrzak, M.; Rojkiewicz, M.; Celiński, R.; Kuś, P.; Sajewicz, M. Identification and Characterization of New Designer Drug 4-Fluoro-PV9 and α-PHP in the Seized Materials. *Forensic Toxicology* **2016**, *34* (1), 115–124.

51. Shevyrin, V.; Melkozerov, V.; Nevero, A.; Eltsov, O.; Shafran, Y. Analytical Characterization of Some Synthetic Cannabinoids, Derivatives of Indole-3-Carboxylic Acid. *Forensic Science International* **2013**, *232* (1–3), 1–10.

52. Uchiyama, N.; Kawamura, M.; Kikura-Hanajiri, R.; Goda, Y. URB-754: A New Class of Designer Drug and 12 Synthetic Cannabinoids Detected in Illegal Products. *Forensic Science International* **2013**, *227* (1–3), 21–32.

53. Park, G.; Lee, Y. G.; Yoon, Y. S.; Ahn, J. Y.; Lee, J. W.; Jang, Y. P. Machine Learning-Based Species Classification Methods Using DART-TOF-MS Data for Five Coniferous Wood Species. *Forests* **2022**, *13* (10).

54. Deklerck, V.; Mortier, T.; Goeders, N.; Cody, R. B.; Waegeman, W.; Espinoza, E.; Van Acker, J.; Van den Bulcke, J.; Beeckman, H. A Protocol for Automated Timber Species Identification Using Metabolome Profiling. *Wood Science and Technology* **2019**, *53* (4), 953–965.

55. Pan, X.; Qiu, J.; Yang, Z. Identification of Five Similar Cinnamomum Wood Species Using Portable Near-Infrared Spectroscopy. *Spectroscopy* **2022**, 16-23,49.

56. Chen, Z.; Xue, X.; Wu, H.; Gao, H.; Wang, G.; Ni, G.; Cao, T. Visible/near-Infrared Hyperspectral Imaging Combined with Machine Learning for Identification of Ten *Dalbergia* species. *Frontiers in Plant Science* **2024**, *15*.

57. Pan, X.; Li, K.; Chen, Z.; Yang, Z. Identifying Wood Based on Near-Infrared Spectra and Four Gray-Level Co-Occurrence Matrix Texture Features. *Forests* **2021**, *12* (11), 1527.

58. Cody, R. B.; Laramée, J. A.; Durst, H. D. Versatile New Ion Source for the Analysis of Materials in Open Air under Ambient Conditions. *Analytical Chemistry* **2005**, *77* (8), 2297–2302.

59. Longo, C. M.; Musah, R. A. An Efficient Ambient Ionization Mass Spectrometric Approach to Detection and Quantification of the Mescaline Content of Commonly Abused Cacti from the *Echinopsis* Genus. *Journal of Forensic Sciences* **2020**, *65* (1), 61–66.

60. Chambers, M. I.; Garosi, B.; Musah, R. A. DART-MS Facilitated Quantification of Cannabinoids in Complex Edible Matrices─Focus on Chocolates and Gelatin-Based Fruit Candies. *ACS Omega* **2023**, *8* (16), 14459–14469.

61. Appley, M. G.; Beyramysoltan, S.; Musah, R. A. Random Forest Processing of Direct Analysis in Real-Time Mass Spectrometric Data Enables Species Identification of Psychoactive Plants from Their Headspace Chemical Signatures. *ACS Omega* **2019**, *4* (13), 15636–15644.

62. Appley, M. G.; Beyramysoltan, S.; Musah, R. A. Random Forest Processing of Direct Analysis in Real-Time Mass Spectrometric Data Enables Species Identification of Psychoactive Plants from Their Headspace Chemical Signatures. *ACS Omega* **2019**, *4* (13), 15636–15644.

63. Chambers, M. I.; Osborne, A. M.; Musah, R. A. Rapid Detection and Validated Quantification of Psychoactive Compounds in Complex Plant Matrices by Direct Analysis in Real Time-high Resolution Mass Spectrometry – Application to "Kava" Psychoactive Pepper Products. *Rapid Communications in Mass Spectrometry* **2019**, *33* (24), 1915–1925.

64. Appley, M. G.; Chambers, M. I.; Musah, R. A. Quantification of Hordenine in a Complex Plant Matrix by Direct Analysis in Real Time–High-resolution Mass Spectrometry: Application to the "Plant of Concern" *Sceletium Tortuosum*. *Drug Testing and Analysis* **2022**, *14* (4), 604–612.

65. Lesiak, A. D.; Cody, R. B.; Ubukata, M.; Musah, R. A. Direct Analysis in Real Time High Resolution Mass Spectrometry as a Tool for Rapid Characterization of Mind-Altering Plant Materials and Revelation of Supplement Adulteration – The Case of Kanna. *Forensic Science International* **2016**, *260*, 66–73.

66. Beyramysoltan, S.; Abdul-Rahman, N.-H.; Musah, R. A. Call It a "Nightshade"—A Hierarchical Classification Approach to Identification of Hallucinogenic *Solanaceae spp.* Using DART-HRMS-Derived Chemical Signatures. *Talanta* **2019**, *204*, 739–746.

67. Chambers, M. I.; Appley, M. G.; Longo, C. M.; Musah, R. A. Detection and Quantification of Psychoactive *N*, *N*-Dimethyltryptamine in Ayahuasca Brews by Ambient Ionization High-Resolution Mass Spectrometry. *ACS Omega* **2020**, *5* (44), 28547–28554.

68. Lesiak, A. D.; Musah, R. A.; Cody, R. B.; Domin, M. A.; Dane, A. J.; Shepard, J. R. Direct Analysis in Real Time Mass Spectrometry (DART-MS) of "Bath Salt" Cathinone Drug Mixtures. *Analyst* **2013**, *138* (12), 3424–3432.

69. Sisco, E.; Forbes, T. P. Forensic Applications of DART-MS: A Review of Recent Literature. *Forensic Chemistry* **2021**, *22*, 100294.

70. Moorthy, A. S.; Sisco, E. A New Library-Search Algorithm for Mixture Analysis Using DART-MS. *Journal of the American Society for Mass Spectrometry* **2021**, *32* (7), 1725–1734.

71. Sisco, E.; Appley, M. G.; Tennyson, S. S.; Moorthy, A. S. Qualitative Analysis of Real Drug Evidence Using DART-MS and the Inverted Library Search Algorithm. *Journal of the American Society for Mass Spectrometry* **2022**, *33* (9), 1784–1793.

72. Sisco, E.; Burns, A.; Schneider, E.; Miller, C. R.; Bobka, L. Comparing Two Seized Drug Workflows for the Analysis of Synthetic Cannabinoids, Cathinones, and Opioids. *Journal of Forensic Sciences* **2022**, *67* (2), 471–482.

73. Musah, R. A.; Cody, R. B.; Domin, M. A.; Lesiak, A. D.; Dane, A. J.; Shepard, J. R. E. DART–MS in-Source Collision Induced Dissociation and High Mass Accuracy for New Psychoactive Substance Determinations. *Forensic Science International* **2014**, *244*, 42–49.

74. Sisco, E.; Verkouteren, J.; Staymates, J.; Lawrence, J. Rapid Detection of Fentanyl, Fentanyl Analogues, and Opioids for on-Site or Laboratory Based Drug Seizure Screening

Using Thermal Desorption DART-MS and Ion Mobility Spectrometry. *Forensic Chemistry* **2017**, *4*, 108–115.

75. Lesiak, A. D.; Musah, R. A.; Cody, R. B.; Domin, M. A.; Dane, A. J.; Shepard, J. R. E. Direct Analysis in Real Time Mass Spectrometry (DART-MS) of "Bath Salt" Cathinone Drug Mixtures. *The Analyst* **2013**, *138* (12), 3424.

76. Abe, H.; Takei, C.; Sakakura, M.; Yajima, D.; Iwase, H. Comprehensive Drug Screening by Thermal Desorption and Pyrolysis Combined with Direct Analysis in Real Time-Mass Spectrometry (TDP/DART-MS); 2018; pp 115–124.

77. Lesiak, A. D.; Shepard, J. R. Recent Advances in Forensic Drug Analysis by DART-MS. *Bioanalysis* **2014**, *6* (6), 819–842.

78. Peace, M. R.; Krakowiak, R. I.; Wolf, C. E.; Poklis, A.; Poklis, J. L. Identification of MDMB-FUBINACA in Commercially Available e-Liquid Formulations Sold for Use in Electronic Cigarettes. *Forensic Science International* **2017**, *271*, 92–97.

79. Lesiak, A. D.; Cody, R. B.; Dane, A. J.; Musah, R. A. Rapid Detection by Direct Analysis in Real Time-Mass Spectrometry (DART-MS) of Psychoactive Plant Drugs of Abuse: The Case of *Mitragyna speciosa* Aka "Kratom." *Forensic Science International* **2014**, *242*, 210–218.

80. Nie, H.; Li, X.; Hua, Z.; Pan, W.; Bai, Y.; Fu, X. Rapid Screening and Determination of 11 New Psychoactive Substances by Direct Analysis in Real Time Mass Spectrometry and Liquid Chromatography/Quadrupole Time-of-flight Mass Spectrometry. *Rapid Communications in Mass Spectrometry* **2016**, *30*, 141–146.

81. Gwak, S.; Almirall, J. R. Rapid Screening of 35 New Psychoactive Substances by Ion Mobility Spectrometry (IMS) and Direct Analysis in Real Time (DART) Coupled to Quadrupole Time-of-flight Mass Spectrometry (QTOF-MS). *Drug Testing and Analysis* **2015**, *7* (10), 884–893.

82. Musah, R. A.; Espinoza, E. O.; Cody, R. B.; Lesiak, A. D.; Christensen, E. D.; Moore, H. E.; Maleknia, S.; Drijfhout, F. P. A High Throughput Ambient Mass Spectrometric Approach to Species Identification and Classification from Chemical Fingerprint Signatures. *Scientific Reports* **2015**, *5* (1), 11520.

83. Deklerck, V.; Finch, K.; Gasson, P.; Van den Bulcke, J.; Van Acker, J.; Beeckman, H.; Espinoza, E. Comparison of Species Classification Models of Mass Spectrometry Data: Kernel Discriminant Analysis vs Random Forest; A Case Study of Afrormosia (*Pericopsis elata* (Harms) Meeuwen). *Rapid Communications in Mass Spectrometry* **2017**, *31* (19), 1582–1588.

84. Beyramysoltan, S.; Giffen, J. E.; Rosati, J. Y.; Musah, R. A. Direct Analysis in Real Time-Mass Spectrometry and Kohonen Artificial Neural Networks for Species Identification of Larva, Pupa and Adult Life Stages of Carrion Insects. *Analytical Chemistry* **2018**, *90* (15), 9206–9217.

85. Beyramysoltan, S.; Ventura, M. I.; Rosati, J. Y.; Giffen-Lemieux, J. E.; Musah, R. A. Identification of the Species Constituents of Maggot Populations Feeding on Decomposing Remains—Facilitation of the Determination of Post Mortem Interval and Time Since Tissue Infestation through Application of Machine Learning and Direct Analysis in Real Time-Mass Spectrometry. *Analytical Chemistry* **2020**, *92* (7), 5439–5446.

86. Lancaster, C.; Espinoza, E. Analysis of Select *Dalbergia* and Trade Timber Using Direct Analysis in Real Time and Time-of-flight Mass Spectrometry for CITES Enforcement. *Rapid Communications in Mass Spectrometry* **2012**, *26* (9), 1147–1156.

87. Lesiak, A. D.; Cody, R. B.; Dane, A. J.; Musah, R. A. Plant Seed Species Identification from Chemical Fingerprints: A High-Throughput Application of Direct Analysis in Real Time Mass Spectrometry. *Analytical Chemistry* **2015**, *87* (17), 8748–8757.

88. Lancaster, C.; Espinoza, E. Analysis of Select *Dalbergia* and Trade Timber Using Direct Analysis in Real Time and Time-of-Flight Mass Spectrometry for CITES Enforcement. *Rapid Communications in Mass Spectrometry* **2012**, *26* (9), 1147–1156.

89. McClure, P. J.; Chavarria, G. D.; Espinoza, E. Metabolic Chemotypes of CITES Protected *Dalbergia* Timbers from Africa, Madagascar, and Asia. *Rapid Communications in Mass Spectrometry* **2015**, *29* (9), 783–788.

90. Guerra-Diaz, P.; Gura, S.; Almirall, J. R. Dynamic Planar Solid Phase Microextraction−Ion Mobility Spectrometry for Rapid Field Air Sampling and Analysis of Illicit Drugs and Explosives. *Analytical Chemistry* **2010**, *82* (7), 2826–2835.

91. Custers, D.; Canfyn, M.; Courselle, P.; De Beer, J. O.; Apers, S.; Deconinck, E. Headspace–Gas Chromatographic Fingerprints to Discriminate and Classify Counterfeit Medicines. *Talanta* **2014**, *123*, 78–88.

92. de Fátima Alpendurada, M. Solid-Phase Microextraction: A Promising Technique for Sample Preparation in Environmental Analysis. *Journal of Chromatography A* **2000**, *889* (1–2), 3–14.

93. Gura, S.; Guerra-Diaz, P.; Lai, H.; Almirall, J. R. Enhancement in Sample Collection for the Detection of MDMA Using a Novel Planar SPME (PSPME) Device Coupled to Ion Mobility Spectrometry (IMS). *Drug Testing and Analysis* **2009**, *1* (7), 355–362.

94. Viana, M.; Postigo, C.; Querol, X.; Alastuey, A.; López de Alda, M. J.; Barceló, D.; Artíñano, B.; López-Mahia, P.; García Gacio, D.; Cots, N. Cocaine and Other Illicit Drugs in Airborne Particulates in Urban Environments: A Reflection of Social Conduct and Population Size. *Environmental Pollution* **2011**, *159* (5), 1241–1247.

95. Cecinato, A.; Balducci, C.; Budetta, V.; Pasini, A. Illicit Psychotropic Substance Contents in the Air of Italy. *Atmospheric Environment* **2010**, *44* (19), 2358–2363.

96. Cecinato, A.; Balducci, C.; Nervegna, G. Occurrence of Cocaine in the Air of the World's Cities. *Science of The Total Environment* **2009**, *407* (5), 1683–1690.

97. Balducci, C.; Nervegna, G.; Cecinato, A. Evaluation of Principal Cannabinoids in Airborne Particulates. *Analytica Chimica Acta* **2009**, *641* (1–2), 89–94.

98. Cicaloni, V.; Salvini, L.; Vitalini, S.; Garzoli, S. Chemical Profiling and Characterization of Different Cultivars of *Cannabis sativa L.* Inflorescences by SPME-GC-MS and UPLC-MS. *Separations* **2022**, *9* (4), 90.

99. Díaz-Maroto, M. C.; Pérez-Coello, M. S.; Cabezudo, M. D. Headspace Solid-Phase Microextraction Analysis of Volatile Components of Spices. *Chromatographia* **2002**, *55* (11–12), 723–728.

100. Asadollahi-Baboli, M.; Aghakhani, A. Headspace Adsorptive Microextraction Analysis of Oregano Fragrance Using Polyaniline-Nylon-6 Nanocomposite, GC-MS, and Multivariate Curve Resolution. *International Journal of Food Properties* **2015**, *18* (7), 1613–1623.

101. Gao, B.; Qin, F.; Ding, T.; Chen, Y.; Lu, W.; Yu, L. (Lucy). Differentiating Organically and Conventionally Grown Oregano Using Ultraperformance Liquid Chromatography Mass Spectrometry (UPLC-MS), Headspace Gas Chromatography with Flame Ionization Detection (Headspace-GC-FID), and Flow Injection Mass Spectrum (FIMS) Fingerprints Combined with Multivariate Data Analysis. *Journal of Agricultural and Food Chemistry* **2014**, *62* (32), 8075–8084.

102. Lo, M.-M.; Benfodda, Z.; Bénimélis, D.; Fontaine, J.-X.; Molinié, R.; Meffre, P. Extraction and Identification of Volatile Organic Compounds Emitted by Fragrant Flowers of Three Tillandsia Species by HS-SPME/GC-MS. *Metabolites* **2021**, *11* (9), 594.

103. Reale, S.; Biancolillo, A.; Gasparrini, C.; Di Martino, L.; Di Cecco, V.; Manzi, A.; Di Santo, M.; D'Archivio, A. A. Geographical Discrimination of Bell Pepper (*Capsicum annuum*) Spices by (HS)-SPME/GC-MS Aroma Profiling and Chemometrics. *Molecules* **2021**, *26* (20), 6177.

104. Setser, A. L.; Smith, R. W. Comparison of Variable Selection Methods Prior to Linear Discriminant Analysis Classification of Synthetic Phenethylamines and Tryptamines. *Forensic Chemistry* **2018**, *11*, 77–86.

105. Davidson, J. T.; Jackson, G. P. The Differentiation of 2, 5-Dimethoxy-N-(N-Methoxybenzyl) Phenethylamine (NBOMe) Isomers Using GC Retention Indices and Multivariate Analysis of Ion Abundances in Electron Ionization Mass Spectra. *Forensic Chemistry* **2019**, *14*, 100160.

106. Ruiz-Perez, D.; Guan, H.; Madhivanan, P.; Mathee, K.; Narasimhan, G. So You Think You Can PLS-DA? *BMC Bioinformatics* **2020**, *21* (1), 1–10.

107. Pereira, L. S. A.; Lisboa, F. L. C.; Neto, J. C.; Valladão, F. N.; Sena, M. M. Direct Classification of New Psychoactive Substances in Seized Blotter Papers by ATR-FTIR and Multivariate Discriminant Analysis. *Microchemical Journal* **2017**, *133*, 96–103.

108. *Machine Learning: A Brief Introduction to Random Forest*. Einstein Med.

109. Finch, K.; Espinoza, E.; Jones, F. A.; Cronn, R. Source Identification of Western Oregon Douglas-Fir Wood Cores Using Mass Spectrometry and Random Forest Classification. *Applications in Plant Sciences* **2017**, *5* (5).

110. *1.4 Support Vector Machines*. scikit-learn.

111. *1.6. Nearest Neighbors*. scikit-learn.

112. Santos, M.; Pereira, F. Direct Analysis of Human Hair Before and After Cosmetic Modification Using a Recent Data Fusion Method. *Journal of the Brazilian Chemical Society* **2020**.

113. Nunes, K. M.; Andrade, M. V. O.; Santos Filho, A. M. P.; Lasmar, M. C.; Sena, M. M. Detection and Characterisation of Frauds in Bovine Meat in Natura by Non-Meat Ingredient Additions Using Data Fusion of Chemical Parameters and ATR-FTIR Spectroscopy. *Food Chemistry* **2016**, *205*, 14–22.

114. Trejos, T.; Torrione, P.; Corzo, R.; Raeva, A.; Subedi, K.; Williamson, R.; Yoo, J.; Almirall, J. A Novel Forensic Tool for the Characterization and Comparison of Printing Ink Evidence: Development and Evaluation of a Searchable Database Using Data Fusion of Spectrochemical Methods. *Journal of Forensic Sciences* **2016**, *61* (3), 715–724.

115. Carneiro, C. R.; Silva, C. S.; de Carvalho, M. A.; Pimentel, M. F.; Talhavini, M.; Weber, I. T. Identification of Luminescent Markers for Gunshot Residues: Fluorescence, Raman Spectroscopy, and Chemometrics. *Analytical Chemistry* **2019**, *91* (19), 12444–12452.

116. Fabregat-Safont, D.; Barneo-Muñoz, M.; Martinez-Garcia, F.; Sancho, J. V.; Hernández, F.; Ibáñez, M. Proposal of 5-Methoxy- N -Methyl- N -Isopropyltryptamine Consumption Biomarkers through Identification of in Vivo Metabolites from Mice. *Journal of Chromatography A* **2017**, *1508*, 95–105.

117. Wohlfarth, A.; Weinmann, W.; Dresen, S. LC-MS/MS Screening Method for Designer Amphetamines, Tryptamines, and Piperazines in Serum. *Analytical and Bioanalytical Chemistry* **2010**, *396* (7), 2403–2414.

118. Meyer, M. R.; Caspar, A.; Brandt, S. D.; Maurer, H. H. A Qualitative/Quantitative Approach for the Detection of 37 Tryptamine-Derived Designer Drugs, 5 β-Carbolines, Ibogaine, and Yohimbine in Human Urine and Plasma Using Standard Urine Screening and Multi-Analyte Approaches. *Analytical and Bioanalytical Chemistry* **2014**, *406* (1), 225–237.

119. Katagi, M.; Kamata, T.; Zaitsu, K.; Shima, N.; Kamata, H.; Nakanishi, K.; Nishioka, H.; Miki, A.; Tsuchihashi, H. Metabolism and Toxicologic Analysis of Tryptamine-Derived Drugs of Abuse. *Therapeutic Drug Monitoring* **2010**, *32* (3), 328–331.

120. Kamata, T.; Katagi, M.; Tsuchihashi, H. Metabolism and Toxicological Analyses of Hallucinogenic Tryptamine Analogues Being Abused in Japan. *Forensic Toxicology* **2010**, *28* (1), 1–8.

121. Nakazono, Y.; Tsujikawa, K.; Kuwayama, K.; Kanamori, T.; Iwata, Y. T.; Miyamoto, K.; Kasuya, F.; Inoue, H. Simultaneous Determination of Tryptamine Analogues in Designer Drugs Using Gas Chromatography–Mass Spectrometry and Liquid Chromatography–Tandem Mass Spectrometry. *Forensic Toxicology* **2014**, *32* (1), 154–161.

122. S. E. Rodriguez-Cruz. Analysis and Characterization of Designer Tryptamines Using Electrospray Ionization Mass Spectrometry (ESI-MS). *Microgram Journal* **2005**, 107–112.

123. Kikura-Hanajiri, R.; Hayashi, M.; Saisho, K.; Goda, Y. Simultaneous Determination of Nineteen Hallucinogenic Tryptamines/β-Calbolines and Phenethylamines Using Gas Chromatography–Mass Spectrometry and Liquid Chromatography–Electrospray Ionisation-Mass Spectrometry. *Journal of Chromatography B* **2005**, *825* (1), 29–37.

124. Huhn, C.; Pütz, M.; Martin, N.; Dahlenburg, R.; Pyell, U. Determination of Tryptamine Derivatives in Illicit Synthetic Drugs by Capillary Electrophoresis and Ultraviolet Laser-Induced Fluorescence Detection. *Electrophoresis* **2005**, *26* (12), 2391–2401.

125. Brandt, S. D.; Tearavarich, R.; Dempster, N.; Cozzi, N. V.; Daley, P. F. Synthesis and Characterization of 5-methoxy-2-methyl- *N* , *N* -dialkylated Tryptamines. *Drug Testing and Analysis* **2012**, *4* (1), 24–32.

126. Piorunska-Sedlak, K.; Stypulkowska, K. Strategy for Identification of New Psychoactive Substances in Illicit Samples Using Attenuated Total Reflectance Infrared Spectroscopy. *Forensic Science International* **2020**, *312*, 110262.

127. Jones, L. E.; Stewart, A.; Peters, K. L.; McNaul, M.; Speers, S. J.; Fletcher, N. C.; Bell, S. E. J. Infrared and Raman Screening of Seized Novel Psychoactive Substances: A Large Scale Study of >200 Samples. *The Analyst* **2016**, *141* (3), 902–909.

128. Marino, M. A.; Voyer, B.; Cody, R. B.; Dane, A. J.; Veltri, M.; Huang, L. Rapid Identification of Synthetic Cannabinoids in Herbal Incenses with DART-MS and NMR. *Journal of Forensic Sciences* **2016**, *61* (S1).

129. Ballabio, D.; Consonni, V. Classification Tools in Chemistry. Part 1: Linear Models. PLS-DA. *Analytical Methods* **2013**, *5* (16), 3790.

130. Pérez, N. F.; Ferré, J.; Boqué, R. Calculation of the Reliability of Classification in Discriminant Partial Least-Squares Binary Classification. *Chemometrics and Intelligent Laboratory Systems* **2009**, *95* (2), 122–128.

131. Cocchi, M.; Biancolillo, A.; Marini, F. Chemometric Methods for Classification and Feature Selection; 2018; pp 265–299.

132. Parsons, H. M.; Ekman, D. R.; Collette, T. W.; Viant, M. R. Spectral Relative Standard Deviation: A Practical Benchmark in Metabolomics. *The Analyst* **2009**, *134* (3), 478–485.

133. Zhvansky, E. S.; Pekov, S. I.; Sorokin, A. A.; Shurkhay, V. A.; Eliferov, V. A.; Potapov, A. A.; Nikolaev, E. N.; Popov, I. A. Metrics for Evaluating the Stability and Reproducibility of Mass Spectra. *Scientific Reports* **2019**, *9* (1), 914.

134. Dasgupta, A. Drugs of Abuse: An Overview. In Alcohol, Drugs, Genes and the Clinical Laboratory; Academic Press, 2017.

135. Cunningham, N. Hallucinogenic Plants of Abuse. *Emergency Medicine Australasia* **2008**, *20* (2), 167–174.

136. Lo Faro, A. F.; Di Trana, A.; La Maida, N.; Tagliabracci, A.; Giorgetti, R.; Busardò, F. P. Biomedical Analysis of New Psychoactive Substances (NPS) of Natural Origin. *Journal of Pharmaceutical and Biomedical Analysis* **2020**, *179*, 112945.

137. Gurib-Fakim, A. Medicinal Plants: Traditions of Yesterday and Drugs of Tomorrow. *Molecular Aspects of Medicine* **2006**, *27* (1), 1–93.

138. U.S. Department of Justice. *In Drugs of Abuse: A DEA Resource Guide*.

139. Arunotayanun, W.; Gibbons, S. Natural Product 'Legal Highs.' *Natural Product Reports* **2012**, *29* (11), 1304.

140. Caffrey, C.; Lank, P. When Good Times Go Bad: Managing Legal High; Complications in the Emergency Department. *Open Access Emergency Medicine* **2017**, *Volume 10*, 9–23.

141. Coon, A. M.; Beyramysoltan, S.; Musah, R. A. A Chemometric Strategy for Forensic Analysis of Condom Residues: Identification and Marker Profiling of Condom Brands from Direct Analysis in Real Time-High Resolution Mass Spectrometric Chemical Signatures. *Talanta* **2019**, *194*, 563–575.

142. Hayes, J. M.; Abdul-Rahman, N.-H.; Gerdes, M. J.; Musah, R. A. Coral Genus Differentiation Based on Direct Analysis in Real Time-High Resolution Mass Spectrometry-Derived Chemical Fingerprints. *Analytical Chemistry* **2021**, *93* (46), 15306–15314.

143. Puype, F.; Ackerman, L. K.; Samsonek, J. Evaluation of Direct Analysis in Real Time – High Resolution Mass Spectrometry (DART-HRMS) for WEEE Specific Substance Determination in Polymeric Samples. *Chemosphere* **2019**, *232*, 481–488.

144. Cody, R. B.; Dane, A. J. Direct Analysis in Real Time (DART®). *Ambient Ionization Mass Spectrometry*; The Royal Society of Chemistry, **2014**; 23–57.

145. Angelis, E. De; Pilolli, R.; Bejjani, A.; Guagnano, R.; Garino, C.; Arlorio, M.; Monaci, L. Optimization of an Untargeted DART-HRMS Method Envisaging Identification of Potential Markers for Saffron Authenticity Assessment. *Foods* **2021**, *10* (6), 1238.

146. Osborne, A. M.; Beyramysoltan, S.; Musah, R. A. Distinguishing Infested Flour from Uninfested Flour through Chemometric Processing of DART-HRMS Data─Revealing the Presence of *Tribolium castaneum*, the Red Flour Beetle. *Journal of Agricultural and Food Chemistry* **2023**, *71* (22), 8613–8621.

147. Akbani, R.; Kwek, S.; Japkowicz, N. Applying Support Vector Machines to Imbalanced Datasets. *Lecture Notes in Artificial Intelligence (Subseries of Lecture Notes in Computer Science)* **2004**, *3201*, 39–50.

148. LemaˆıtreLemaˆıtre, G.; Nogueira, F.; Aridas char, C. K. Imbalanced-Learn: A Python Toolbox to Tackle the Curse of Imbalanced Datasets in Machine Learning. *Journal of Machine Learning Research* **2017**, *18*, 1–5.

149. KIM, H.-C.; Ghahramani, Z. Bayesian Classifier Combination. *Proceedings of the Fifteenth International Conference on Artificial Intelligence and Statistics* **2012**, *22*, 619–627.

150. Ruta, D.; Gabrys, B. An Overview of Classifier Fusion Methods. *Computing and Information Systems* **2000**, *7*, 1–10.

151. Pedregosa, F.; Michel, V.; Grisel, O.; Blondel, M.; Prettenhofer, P.; Weiss, R.; Vanderplas, J.; Cournapeau, D.; Pedregosa, F.; Varoquaux, G.; Gramfort, A.; Thirion, B.; Grisel, O.; Dubourg, V.; Passos, A.; Brucher, M.; Perrot and Édouardand, M.; Duchesnay, andÉdouard; Duchesnay, Fré. Scikit-Learn: Machine Learning in Python Gaël Varoquaux Bertrand Thirion Vincent Dubourg Alexandre Passos, Varoquaux, Gramfort et al. Matthieu Perrot. *Journal of Machine Learning Research* **2011**, *12*, 2825–2830.

152. GitHub Repository. *Sklearn-Hierarchical-Classification: Version = "1.3.2."* https://github.com/globality-corp/sklearn-hierarchical-classification.

153. Michael White, C. Pharmacologic and Clinical Assessment of Kratom. *American Journal of Health-System Pharmacy* **2018**, *75* (5), 261–267.

154. Sheen, D. A.; Rocha, W. F. C.; Lippa, K. A.; Bearden, D. W. A Scoring Metric for Multivariate Data for Reproducibility Analysis Using Chemometric Methods. *Chemometrics and Intelligent Laboratory Systems* **2017**, *162*, 10–20.

155. Naik, H. N.; Kanjariya, D.; Parveen, S.; Ahmed, I.; Meena, A.; Patel, H.; Meena, R.; Jauhari, S. LC–MS Profiling, in Vitro and in Silico C-ABL Kinase Inhibitory Approach to Identify Potential Anticancer Agents from *Dalbergia sissoo* Leaves. *Scientific Reports* **2024**, *14* (1), 73.

156. Thakkar, A. B.; Subramanian, Ramalingam. B.; Thakkar, V. R.; Thakor, P. Hydromethanolic Leaves Extract of *Dalbergia sissoo* Roxb. Ex DC. Induces Apoptosis in Lung Adenocarcinoma Cells. *Process Biochemistry* **2023**, *134*, 250–261.

157. Thakkar, A. B.; Subramanian, R. B.; Thakkar, V. R.; Bhatt, S. V.; Chaki, S.; Vaidya, Y. H.; Patel, V.; Thakor, P. Apoptosis Induction Capability of Silver Nanoparticles Capped with Acorus Calamus L. and *Dalbergia sissoo* Roxb. Ex DC. against Lung Carcinoma Cells. *Heliyon* **2024**, *10* (2), e24400.

158. Sun, K.; Li, Z.; Li, W.; Chi, C.; Wang, M.; Xu, R.; Gao, Y.; Li, B.; Sun, Y.; Liu, R. Investigating the Anti-Atherosclerotic Effects and Potential Mechanism of *Dalbergia odorifera* in ApoE-Deficient Mice Using Network Pharmacology Combined with Metabolomics. *Journal of Pharmaceutical and Biomedical Analysis* **2024**, *242*, 116017.

159. Wang, C.; Gong, B.; Wu, Y.; Bai, C.; Yang, M.; Zhao, X.; Wei, J. Pharmacokinetics and Molecular Docking of the Cardioprotective Flavonoids in *Dalbergia odorifera*. *Journal of Separation Science* **2024**, *47* (1).

160. Soudier, P.; Rodriguez Pinzon, D.; Reif-Trauttmansdorff, T.; Hijazi, H.; Cherrière, M.; Goncalves Pereira, C.; Blaise, D.; Pispisa, M.; Saint-Julien, A.; Hamlet, W.; Nguevo, M.; Gomes, E.; Belkhelfa, S.; Niarakis, A.; Kushwaha, M.; Grigoras, I. Toehold Switch Based Biosensors for Sensing the Highly Trafficked Rosewood *Dalbergia maritima*. *Synthetic and Systems Biotechnology* **2022**, *7* (2), 791–801.

161. The World Wildlife Seizures (World WISE) Database **2016**, 27–32.

162. Appley, M. Mass Spectral and Chemometric Analysis for The Detection and Identification of Forensically Relevant Materials, Ph.D. Thesis **2021**.

163. McClure, P. J.; Chavarria, G. D.; Espinoza, E. Metabolic Chemotypes of CITES Protected *Dalbergia* Timbers from Africa, Madagascar, and Asia. *Rapid Communications in Mass Spectrometry* **2015**, *29* (9), 783–788.

164. Creydt, M.; Arndt, M.; Hudzik, D.; Fischer, M. Plant Metabolomics: Evaluation of Different Extraction Parameters for Nontargeted UPLC-ESI-QTOF-Mass Spectrometry at the Example of White *Asparagus officinalis*. *Journal of Agricultural and Food Chemistry* **2018**, *66* (48), 12876–12887.

165. Aldrich Library of FT-IR Spectra, 1st ed. **1985**.

166. Jabalpurwala, F. A.; Smoot, J. M.; Rouseff, R. L. A Comparison of Citrus Blossom Volatiles. *Phytochemistry* **2009**, *70* (11–12), 1428–1434.

167. Arias, M. E.; Rodríguez, J.; Pérez, M. I.; Hernández, M.; Polvillo, O.; González-Pérez, J. A.; González-Vila, F. J. Analysis of Chemical Changes in *Picea abies* Wood Decayed by Different Streptomyces Strains Showing Evidence for Biopulping Procedures. *Wood Science and Technology* **2010**, *44* (2), 179–188.

168. Zhang, X. H.; da Silva, J. A. T.; Jia, Y. X.; Zhao, J. T.; Ma, G. H. Chemical Composition of Volatile Oils from the Pericarps of Indian Sandalwood (*Santalum album*) by Different Extraction Methods. *Natural Product Communications* **2012**, *7* (1), 1934578X1200700.

169. Asmara, A. P.; Nuzlia, C.; Hernawan; Maryana, R. Physicochemical, Fatty Acid Profile and Antioxidant Properties of Mahogany (*Swietenia humilis* Zucc.) Seeds Oil. In *AIP Conference Proceedings*; American Institute of Physics Inc., **2023**; Vol. 2583.

170. Jimenez, A.; Mata, R.; Pereda-Miranda, R.; Calderon, J.; Isman, M. B.; Nicol, R.; Arnason, J. T. Insecticidal Liminoids from *Swietenia humilis* and *Cedrela salvadorensis*; **1997**; Vol. 23.

171. Ovalle-Magallanes, B.; Navarrete, A.; Haddad, P. S.; Tovar, A. R.; Noriega, L. G.; Tovar-Palacio, C.; Mata, R. Multi-Target Antidiabetic Mechanisms of Mexicanolides from *Swietenia humilis*. *Phytomedicine* **2019**, *58*.

172. Ovalle-Magallanes, B.; Medina-Campos, O. N.; Pedraza-Chaverri, J.; Mata, R. Hypoglycemic and Antihyperglycemic Effects of Phytopreparations and Limonoids from *Swietenia humilis*. *Phytochemistry* **2015**, *110*, 111–119.

173. Mata, R.; Rivero-Cruz, J.-F.; Chávez, D. Bioactive Secondary Metabolites from Selected Mexican Medicinal Plants: Recent Progress.

174. Segura-Correa, R.; Mata, R.; Anaya, A. L.; Hernandez-Bautista, B.; Villena, R.; Soriano-Garcia, M.; Bye, R.; Linares, E. New Tetranortriterpenoids from *Swietenia humilis*. *Journal of Natural Products* **1993**, *56* (9), 1567–1574.

175. Ovalle-Magallanes, B.; Déciga-Campos, M.; Mata, R. Antihyperalgesic Activity of a Mexicanolide Isolated from *Swietenia humilis* Extract in Nicotinamide-Streptozotocin Hyperglycemic Mice. *Biomedicine and Pharmacotherapy* **2017**, *92*, 324–330.

176. Veni, A.; Lokeswari, T. S.; Krishna Kumari, G. N.; Gayathri, D.; Sudandiradoss, C. Bioactivity of Melianone against Salmonella and in Silico Prediction of a Membrane Protein Target. *3 Biotech* **2020**, *10* (10).

177. Yang, H.; Choi, M.; Lee, D. Y.; Sung, S. H. Anti-Differentiation Effect of B, D-Seco Limonoids of *Swietenia mahogani*. *Pharmacognosy Magazine* **2017**, *13* (50), 293–299.

178. Mohan, M. R.; Jala, R. C. R.; Kaki, S. S.; Prasad, R. B. N.; Rao, B. V. S. K. *Swietenia mahogani* Seed Oil: A New Source for Biodiesel Production. *Industrial Crops and Products* **2016**, *90*, 28–31.

179. Nugraha, A. S.; Purnomo, Y. D.; Widhi Pratama, A. N.; Triatmoko, B.; Hendra, R.; Wongso, H.; Avery, V. M.; Keller, P. A. Isolation of Antimalarial Agents From Indonesian Medicinal Plants: *Swietenia mahogani* and *Pluchea indica*. *Natural Product Communications* **2022**, *17* (1).

180. Syame, S. M.; Mohamed, S. M.; Elgabry, E. A.; Darwish, Y. A. A.; Mansour, A. S. Chemical Characterization, Antimicrobial, Antioxidant, and Cytotoxic Potentials of *Swietenia mahogani*. *AMB Express* **2022**, *12* (1).

181. Sukardiman; Ervina, M. The Recent Use of Swietenia Mahagoni (L.) Jacq. as Antidiabetes Type 2 Phytomedicine: A Systematic Review. *Heliyon*. Elsevier Ltd March 1, 2020.

182. Shi, Z.; An, L.; Yang, X.; Xi, Y.; Zhang, C.; Shuo, Y.; Zhang, J.; Jin, D. Q.; Ohizumi, Y.; Lee, D.; Xu, J.; Guo, Y. Nitric Oxide Inhibitory Limonoids as Potential Anti-Neuroinflammatory Agents from *Swietenia mahogani*. *Bioorganic Chemistry* **2019**, *84*, 177–185.

183. Zhang, W. M.; Liu, J. Q.; Deng, Y. Y.; Xia, J. J.; Zhang, Z. R.; Li, Z. R.; Qiu, M. H. Diterpenoids and Limonoids from the Leaves and Twigs of *Swietenia mahogani*. *Natural Products and Bioprospecting* **2014**, *4* (1), 53–57.

184. Abdelgaleil, S. A. M.; Doe, M.; Nakatani, M. Rings B,D-Seco Limonoid Antifeedants from *Swietenia mahogani*. *Phytochemistry* **2013**, *96*, 312–317.

185. Mostafa, M.; Jahan, I. A.; Riaz, M.; Hossain, H.; Nimmi, I.; Miah, A. S.; Chowdhury, J. U. Comprehensive Analysis of the Composition of Seed Cake and Its Fatty Oil from *Swietenia mahogani* Jacq. Growing in Bangladesh.

186. Rahman, A. K. M. S.; Chowdhury, A. K. A.; Ali, H. A.; Raihan, S. Z.; Ali, M. S.; Nahar, L.; Sarker, S. D. Antibacterial Activity of Two Limonoids from *Swietenia mahogani* against Multiple-Drug-Resistant (MDR) Bacterial Strains. *Journal of Natural Medicines* **2009**, *63* (1), 41–45.

187. Lin, B. D.; Yuan, T.; Zhang, C. R.; Dong, L.; Zhang, B.; Wu, Y.; Yue, J. M. Structurally Diverse Limonoids from the Fruits of *Swietenia mahogani* . *Journal of Natural Products* **2009**, *72* (12), 2084–2090.

188. Pamplona, S. G. S. R.; Arruda, M. S. P.; Castro, K. C. F.; Silva, C. Y. Y.; Ferreira, A. G.; Da Silva, M. F. G. F.; Ohashi, O. S.; Da Silva, M. N. Phragmalin Limonoids from *Swietenia macrophylla* and Their Antifeedant Assay against Mahogany Predator. *Journal of the Brazilian Chemical Society* **2018**, *29* (8), 1621–1629.

189. Ma, Y. Q.; Jiang, K.; Deng, Y.; Guo, L.; Wan, Y. Q.; Tan, C. H. Mexicanolide-Type Limonoids from the Seeds of *Swietenia macrophylla*. *Journal of Asian Natural Products Research* **2018**, *20* (4), 299–305.

190. Cheng, Y. Bin; Chien, Y. T.; Lee, J. C.; Tseng, C. K.; Wang, H. C.; Lo, I. W.; Wu, Y. H.; Wang, S. Y.; Wu, Y. C.; Chang, F. R. Limonoids from the Seeds of *Swietenia macrophylla* with Inhibitory Activity against Dengue Virus 2. *Journal of Natural Products* **2014**, *77* (11), 2367–2374.

191. Suliman, B. Fatty Acid Composition and Antibacterial Activity of *Swietenia macrophylla* King Seed Oil. *African Journal of Plant Science* **2013**, *7* (7), 300–303.

192. Tan, S. K.; Osman, H.; Wong, K. C.; Boey, P. L. New Phragmalin-Type Limonoids from *Swietenia macrophylla* King. *Food Chemistry* **2009**, *115* (4), 1279–1285.

193. Sun, Y. P.; Zhu, L. L.; Liu, J. song; Yu, Y.; Zhou, Z. yu; Wang, G.; Wang, G. K. Limonoids and Triterpenoid from Fruit of *Swietenia macrophylla*. *Fitoterapia* **2018**, *125*, 141–146.

194. Chen, L. C.; Liao, H. R.; Chen, P. Y.; Kuo, W. L.; Chang, T. H.; Sung, P. J.; Wen, Z. H.; Chen, J. J. Limonoids from the Seeds of *Swietenia macrophylla* and Their Anti-Inflammatory Activities. *Molecules* **2015**, *20* (10), 18551–18564.

195. Mustafa Masoud Eid, A.; Elmarzugi, A.; Ali El-Enshasy, H. A Review on The Phytopharmacological Effect of *Swietenia macrophylla*.

196. Chen, J. J.; Huang, S. S.; Liao, C. H.; Wei, D. C.; Sung, P. J.; Wang, T. C.; Cheng, M. J. A New Phragmalin-Type Limonoid and Anti-Inflammatory Constituents from the Fruits of *Swietenia macrophylla*. *Food Chemistry* **2010**, *120* (2), 379–384.

197. Fowles, R. G.; Mootoo, B. S.; Ramsewak, R.; Reynolds, W.; Lough, A. J. 3,6-Di-O-Acetylswietenolide 0.25-Hydrate. *Acta Crystallographica Section E: Structure Reports Online* **2007**, *63* (2).

198. Wakabayashi, N.; Spencer, S. L.; Waters, R. M.; Lusby, W. R. A Polyacetylene from Honduras Mahogany, *Swietenia macrophylla*. *Journal of Natural Products* **1991**, *54* (5), 1419–1421.

199. Omar, S.; Marcotte, M.; Fields, P.; Sanchez, P. E.; Poveda, L.; Mata, R.; Jimenez, A.; Durst, T.; Zhang, J.; MacKinnon, S.; Leaman, D.; Arnason, J. T.; Philogène, B. J. R. Antifeedant Activities of Terpenoids Isolated from Tropical Rutales. *Journal of Stored Products Research* **2007**, *43* (1), 92–96.

200. Jimenez, A.; Villarreal, C.; Toscano, R. A.; Cook, M.; Arnason, J. T.; Byell, R.; Mata, R. Liminoids from *Swietenia humis* and *Guarear grandiflora* (Meliaceae); 1998; Vol. 49.

201. Masendra; Purba, B. A. V.; Lukmandaru, G. Antioxidant Activity of *Swietenia macrophylla* King Bark Extracts. *Wood Research* **2021**, *66* (1), 57–69.

202. Cordeiro, J. R.; Li, R. W. C.; Takahashi, É. S.; Rehder, G. P.; Ceccantini, G.; Gruber, J. Wood Identification by a Portable Low-Cost Polymer-Based Electronic Nose. *RSC Advances* **2016**, *6* (111), 109945–109949.

203. Kometter, R. F.; Martinez, M.; Blundell, A. G.; Gullison, R. E.; Steininger, M. K.; Kometter, R. F.; Martinez, M.; Blundell, A. G.; Gullison, R. E.; Steininger, M. K.; Rice, R. E. Impacts of Unsustainable Mahogany Logging in Bolivia and Peru; 2004.

204. Grogan, J.; Barreto, P. Big-Leaf Mahogany on CITES Appendix II: Big Challenge, Big Opportunity. *Conservation Biology* **2005**, *19* (3), 973–976.

APPENDIX

TABLE OF CONTENTS

Figure A2.1 The 20 V DART-HRMS soft ionization spectra and structures for the 50 tryptamines analyzed in this study.

Figure A2.1 (continued). The 20 V DART-HRMS soft ionization spectra and structures for the 50 tryptamines analyzed in this study.

Figure A2.1 (continued). The 20 V DART-HRMS soft ionization spectra and structures for the 50 tryptamines analyzed in this study.
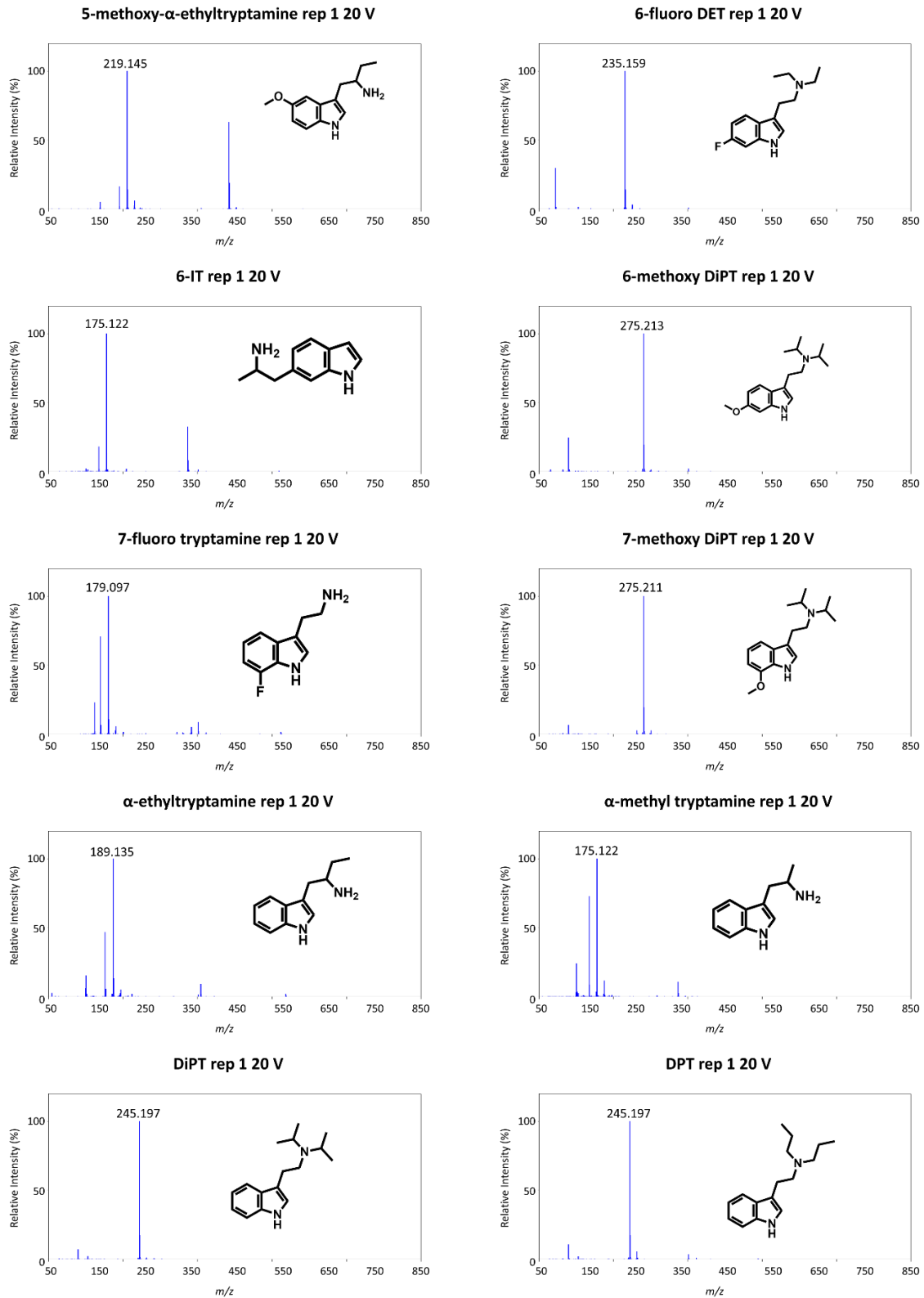
Figure A2.1 (continued). The 20 V DART-HRMS soft ionization spectra and structures for the 50 tryptamines analyzed in this study.

Figure A2.1 (continued). The 20 V DART-HRMS soft ionization spectra and structures for the 50 tryptamines analyzed in this study.
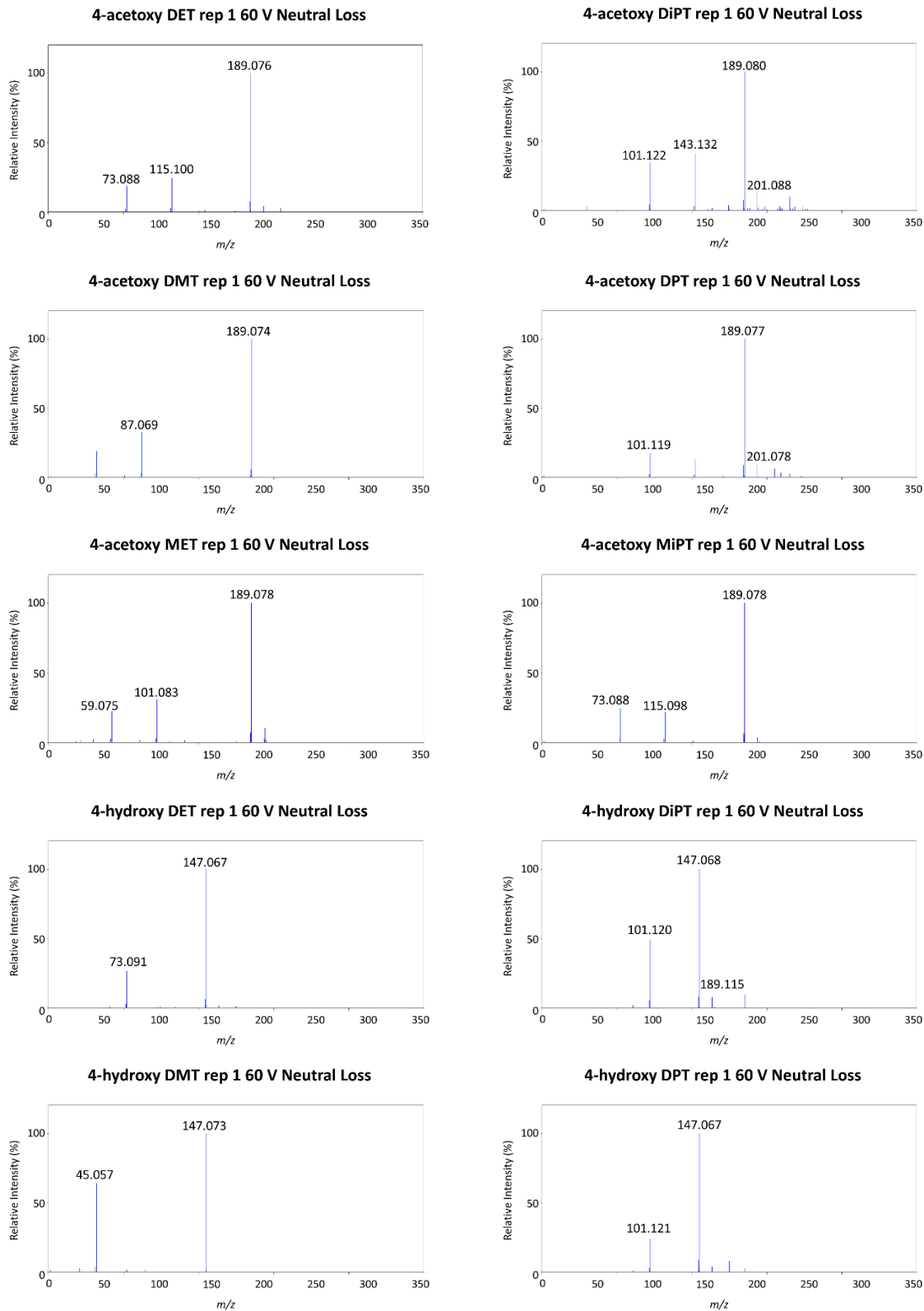
Figure A2.2 The 60 V DART-HRMS neutral loss spectra for the 50 tryptamines analyzed in this study.
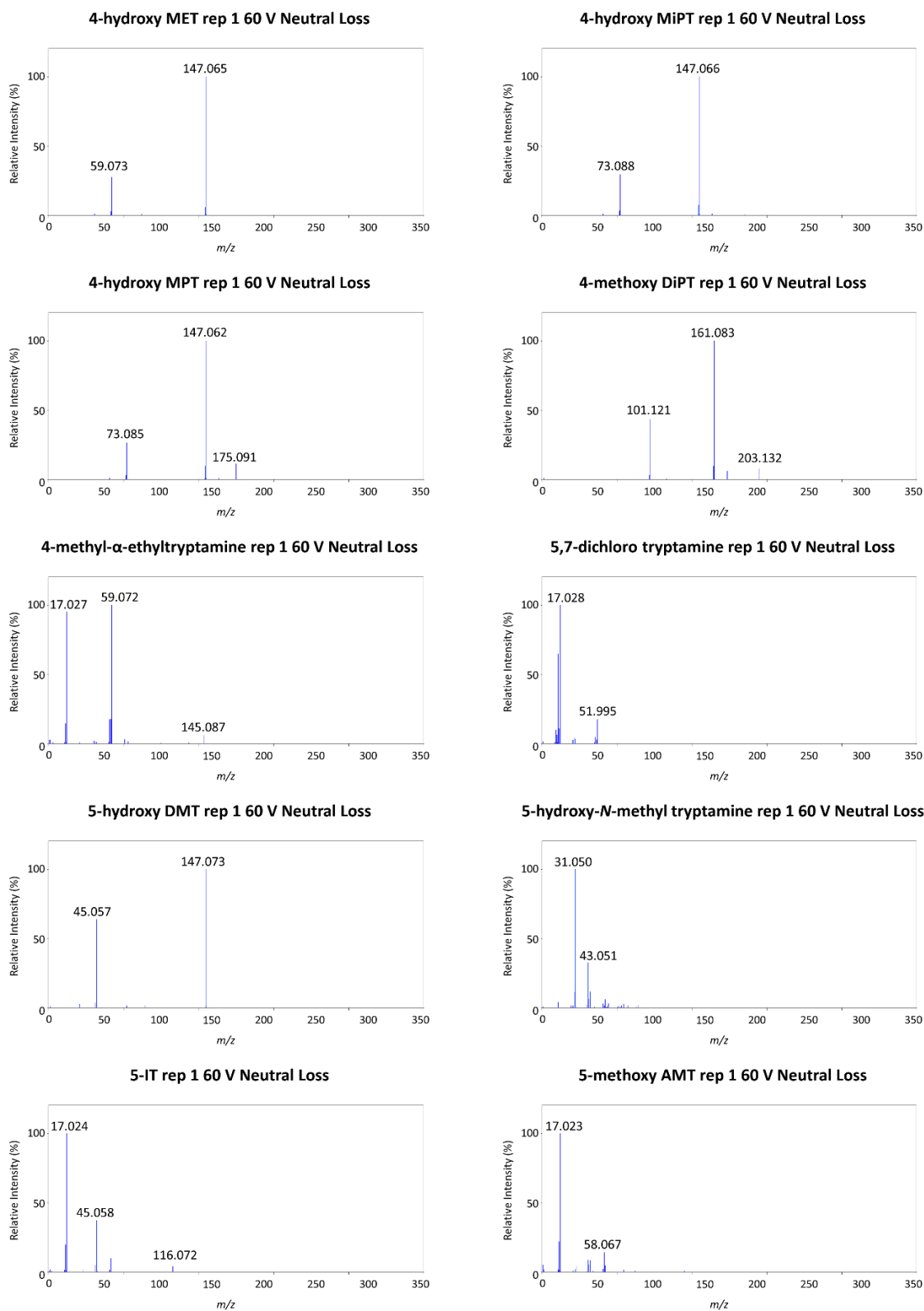
Figure A2.2 (continued). The 60 V DART-HRMS neutral loss spectra for the 50 tryptamines analyzed in this study.

5-methoxy DALT rep 1 60 V Neutral Loss

5-methoxy DBT rep 1 60 V Neutral Loss

5-methoxy DET rep 1 60 V Neutral Loss

5-methoxy DiBT rep 1 60 V Neutral Loss

5-methoxy DiPT rep 1 60 V Neutral Loss

5-methoxy DMT rep 1 60 V Neutral Loss

5-methoxy DPT rep 1 60 V Neutral Loss

5-methoxy EiPT rep 1 60 V Neutral Loss

5-methoxy EPT rep 1 60 V Neutral Loss

5-methoxy MiPT rep 1 60 V Neutral Loss

Figure A2.2 (continued). The 60 V DART-HRMS neutral loss spectra for the 50 tryptamines analyzed in this study.

144

Figure A2.2 (continued). The 60 V DART-HRMS neutral loss spectra for the 50 tryptamines analyzed in this study.

Figure A2.2 (continued). The 60 V DART-HRMS neutral loss spectra for the 50 tryptamines analyzed in this study.

4-acetoxy DET rep 1 90 V Neutral Loss

4-acetoxy DiPT rep 1 90 V Neutral Loss

4-acetoxy DMT rep 1 90 V Neutral Loss

4-acetoxy DPT rep 1 90 V Neutral Loss

4-acetoxy MET rep 1 90 V Neutral Loss

4-acetoxy MiPT rep 1 90 V Neutral Loss

4-hydroxy DET rep 1 90 V Neutral Loss

4-hydroxy DiPT rep 1 90 V Neutral Loss

4-hydroxy DMT rep 1 90 V Neutral Loss

4-hydroxy DPT rep 1 90 V Neutral Loss
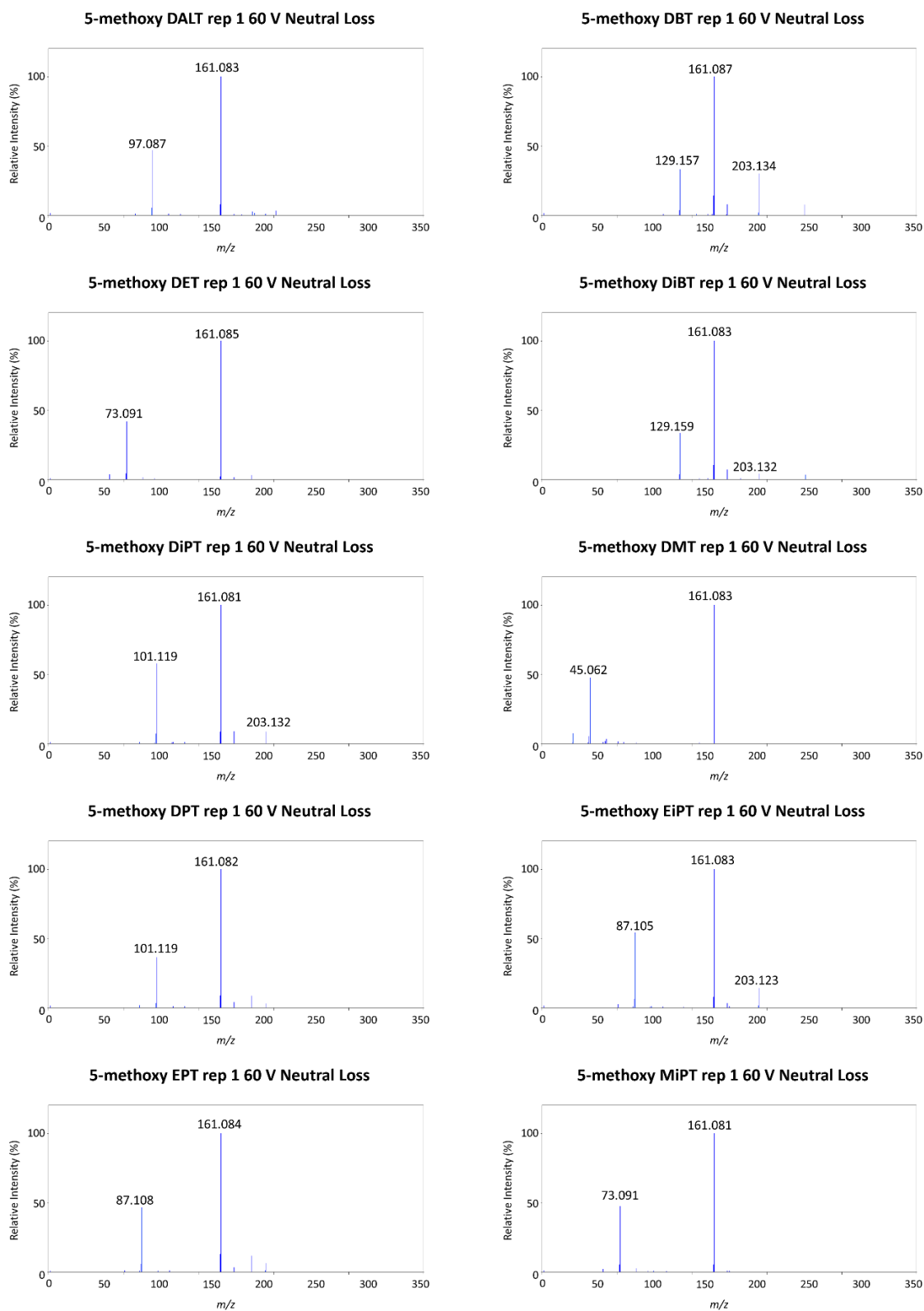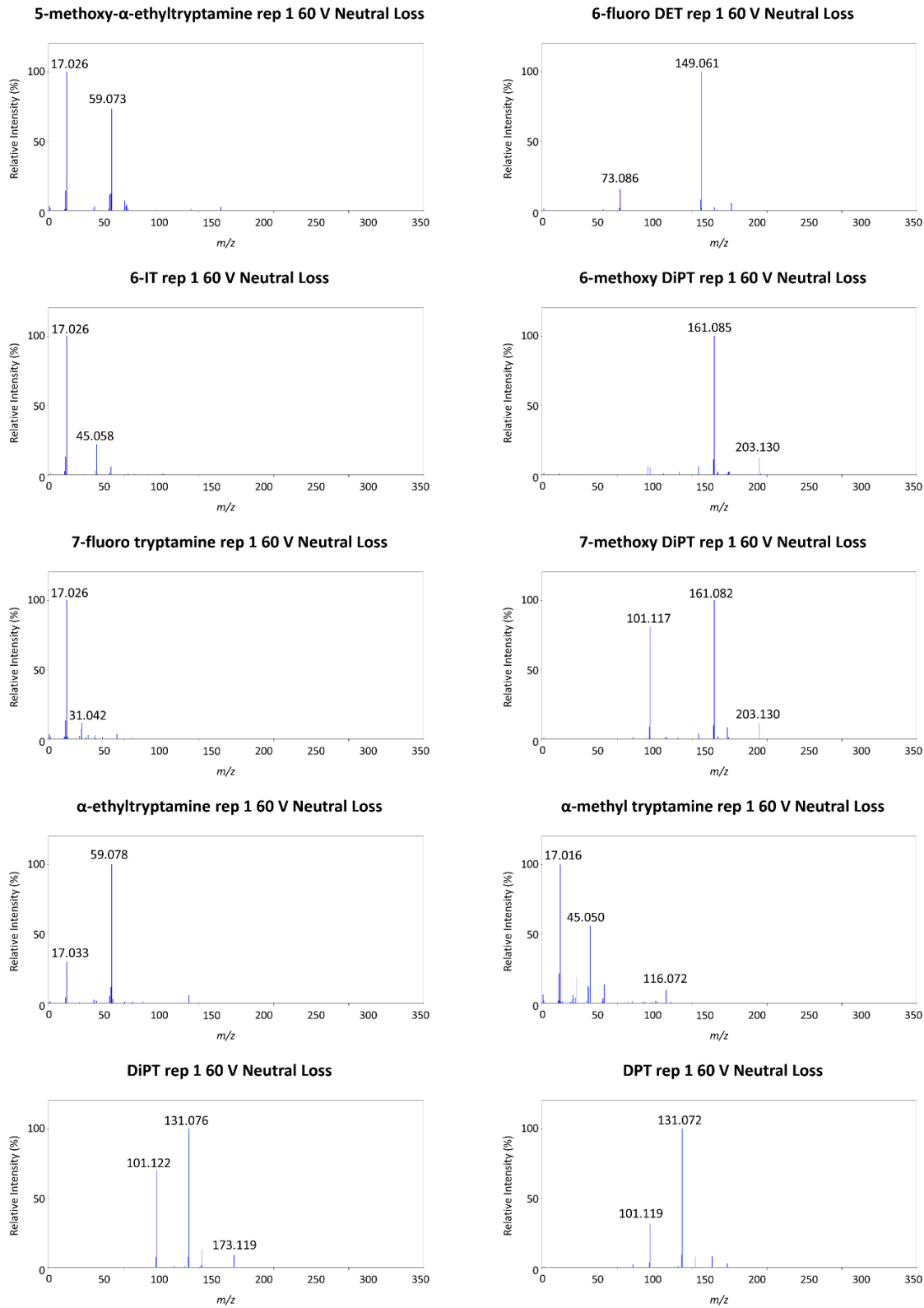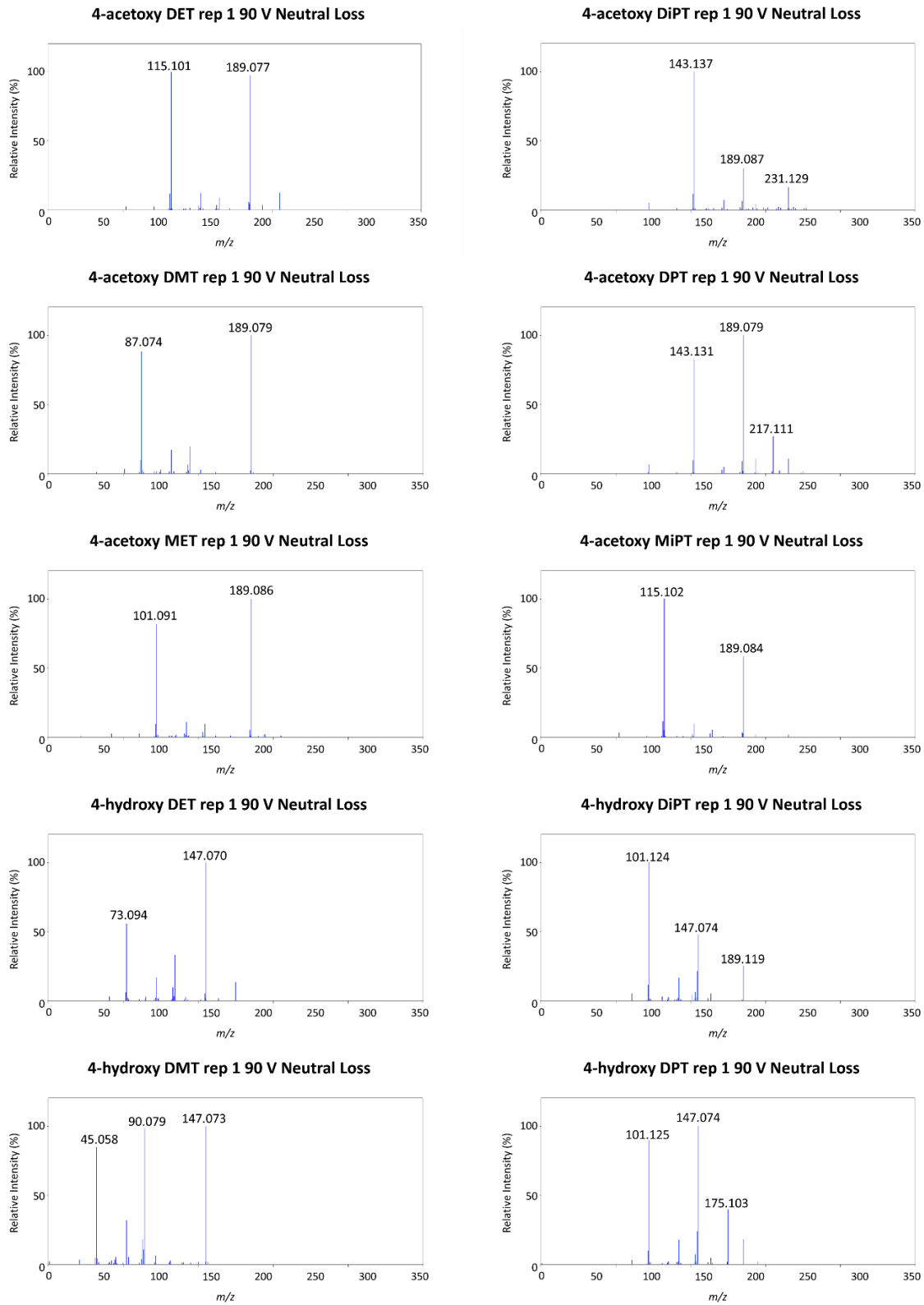
Figure A2.3 The 90 V DART-HRMS neutral loss spectra for the 50 tryptamines analyzed in this study.
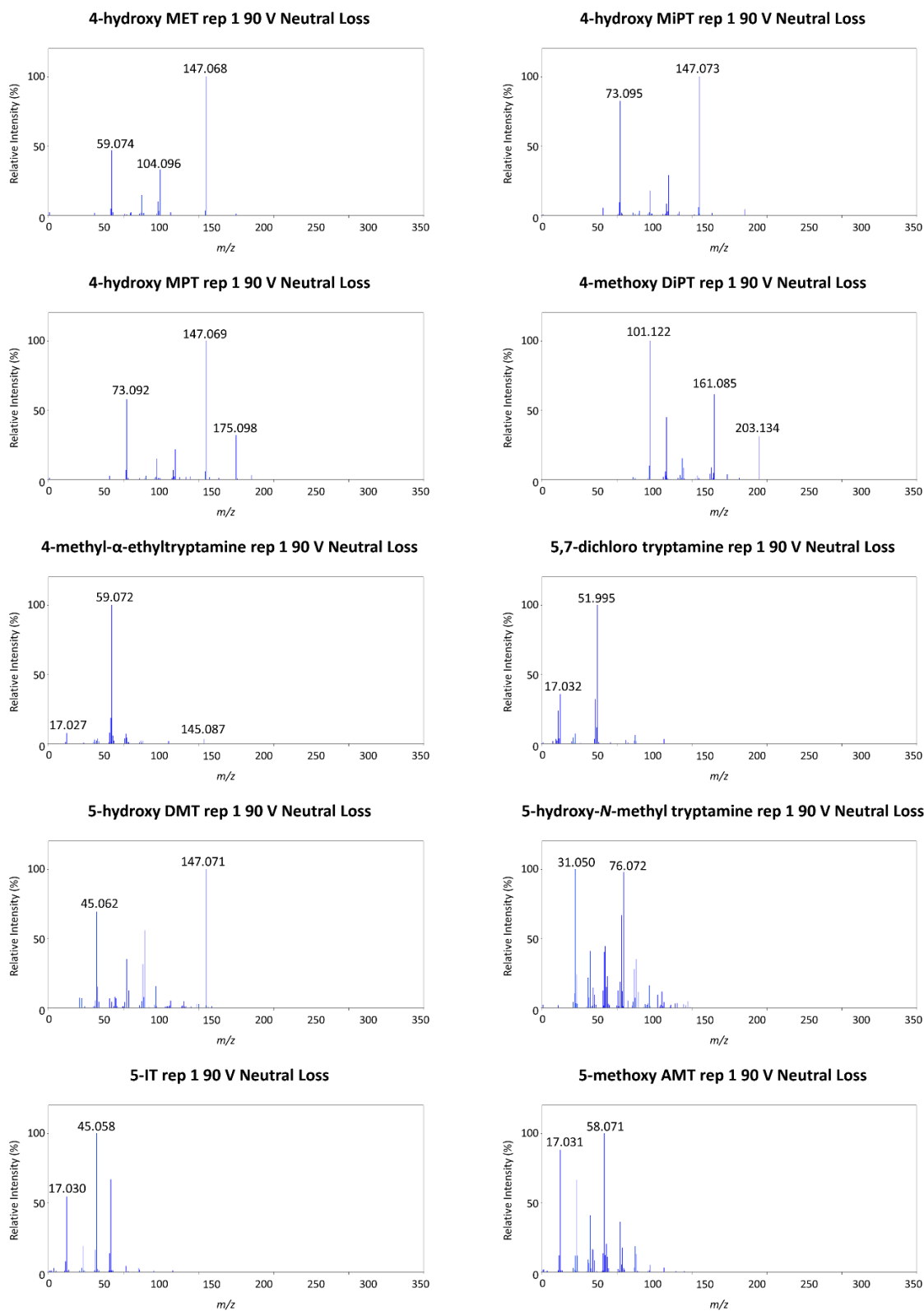
Figure A2.3 (continued). The 90 V DART-HRMS neutral loss spectra for the 50 tryptamines analyzed in this study.
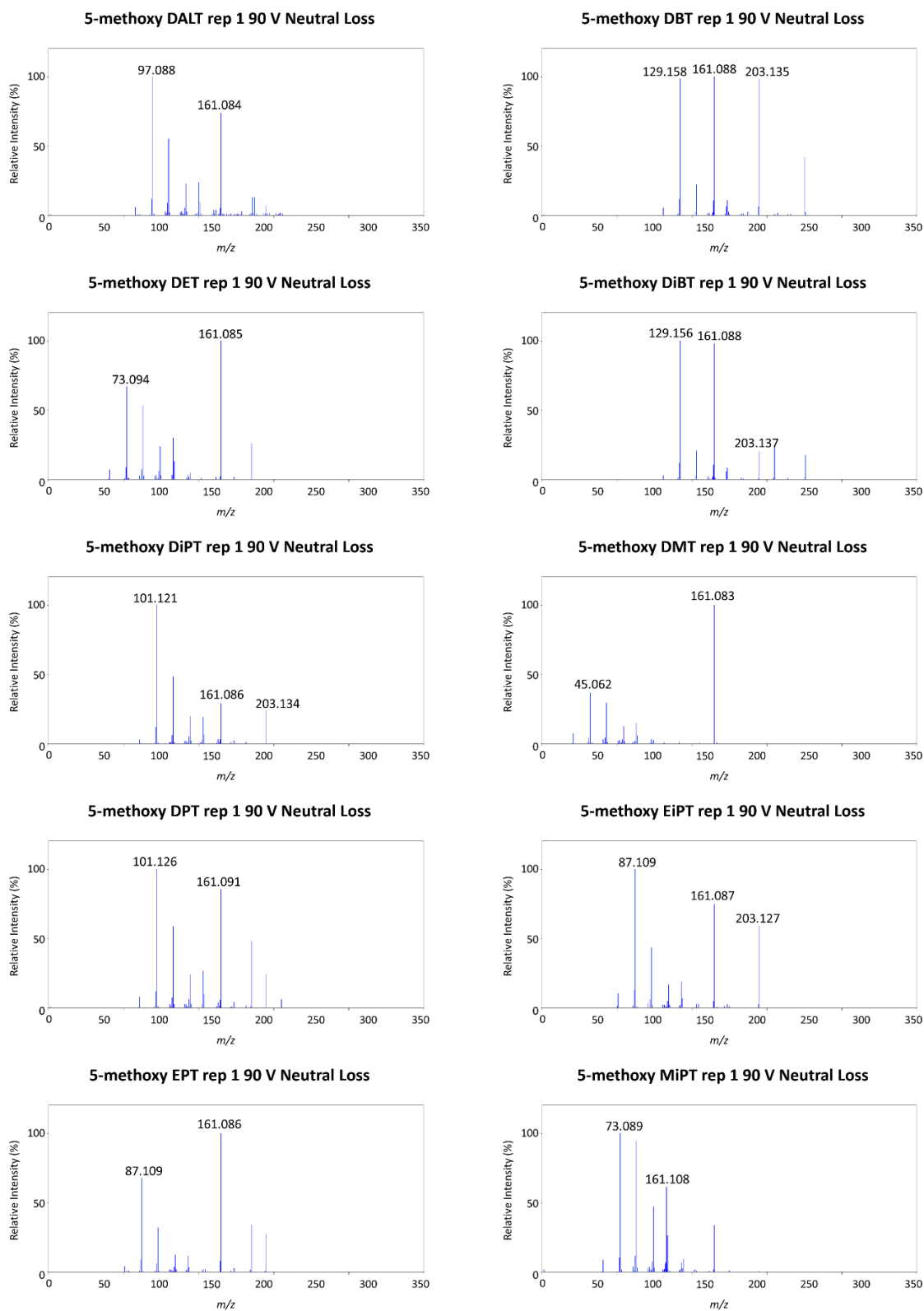
Figure A2.3 (continued). The 90 V DART-HRMS neutral loss spectra for the 50 tryptamines analyzed in this study.
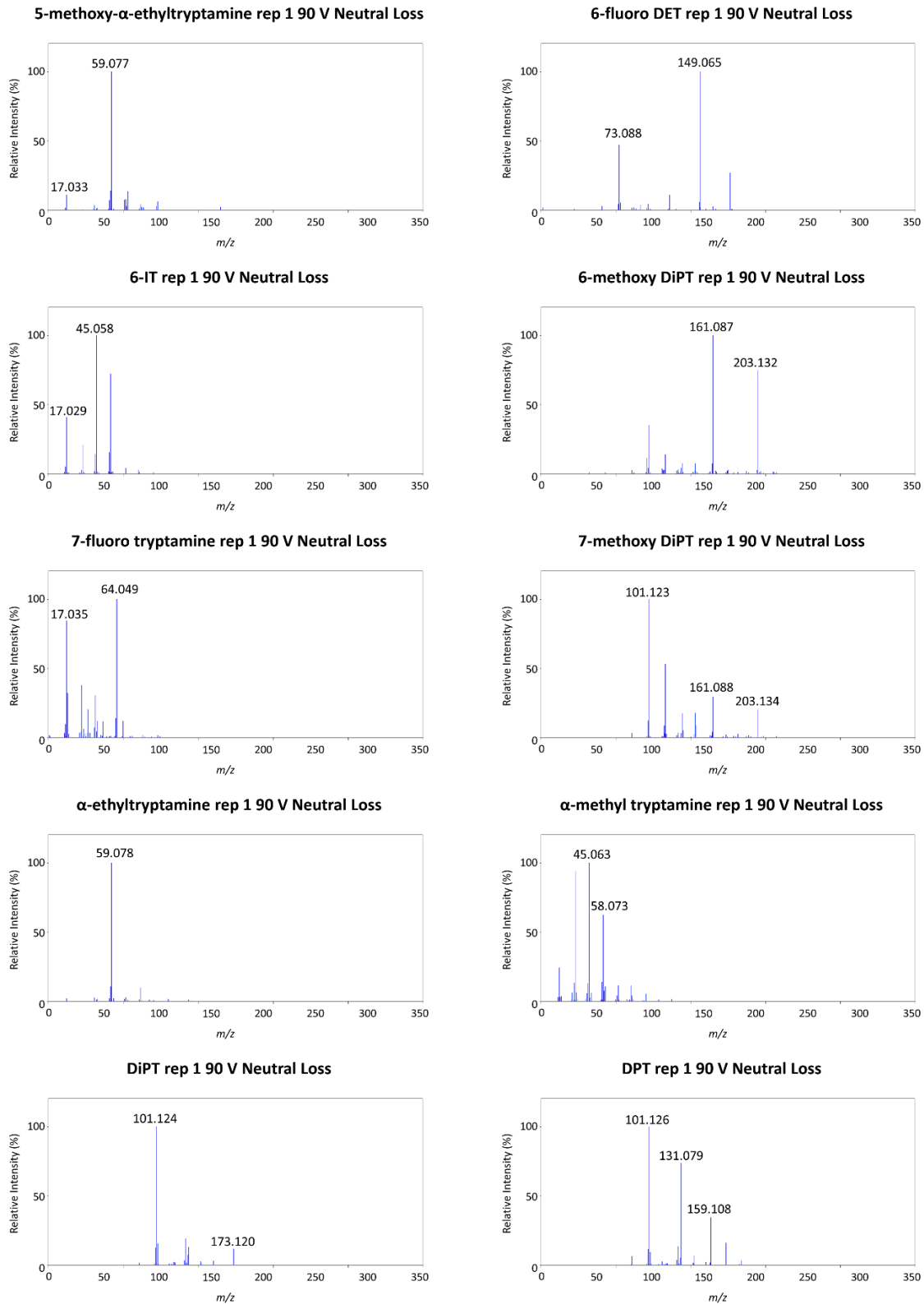
Figure A2.3 (continued). The 90 V DART-HRMS neutral loss spectra for the 50 tryptamines analyzed in this study.

Figure A2.3 (continued). The 90 V DART-HRMS neutral loss spectra for the 50 tryptamines analyzed in this study.

Table A2.1 Probability prediction assignments of the PLD-DA model for the "leave-one structure out" validation when screened against the ten groups that were identified in the cluster analysis. The correctly classified tryptamines with a probability of one are shown in blue, whereas the red numbers show the probabilities for tryptamines with multilabel assignments.

Compound	G 1	G 2	G 3	G 4	G 5	G 6	G 7	G 8	G 9	G 10
4-Methyl-α-ethyl tryptamine	1.00	0.00	0.00	0.00	0.00	0.00	0.00	0.00	0.00	0.00
5-Methoxy-α-ethyl tryptamine	1.00	0.52	0.00	0.00	0.00	0.00	0.00	0.00	0.00	0.00
N-Methyl-N-ethyltryptamine	1.00	0.00	0.00	1.00	0.00	0.00	0.00	0.00	0.00	0.00
α-Ethyltryptamine	1.00	0.00	0.00	0.00	0.00	0.00	0.00	0.00	0.00	0.00
5,7-Dichloro tryptamine	0.00	1.00	0.00	0.00	0.00	0.00	0.00	0.00	0.00	0.00
5-IT	0.00	1.00	0.00	0.00	0.00	0.00	0.00	0.00	0.00	0.00
5-Methoxy AMT	0.00	1.00	0.00	0.00	0.00	0.00	0.00	0.00	0.00	0.00
6-IT	0.00	1.00	0.00	0.00	0.00	0.00	0.00	0.00	0.00	0.00
7-Fluoro tryptamine	0.00	1.00	0.00	0.00	0.00	0.00	0.00	0.00	0.00	0.00
Nonyloxytryptamine	0.00	1.00	0.00	0.00	0.00	0.00	0.00	0.00	0.00	0.00
Serotonin	0.00	1.00	0.00	0.00	0.00	0.00	0.00	0.00	0.00	0.00
α-Methyl tryptamine	0.00	1.00	0.00	0.00	0.00	0.00	0.00	0.00	0.00	0.00
5-Hydroxy-N-methyl tryptamine	0.00	0.00	1.00	0.00	0.00	0.00	0.00	0.00	0.00	0.00
N-Methyl tryptamine	0.00	0.00	1.00	0.00	0.00	0.00	0.00	0.00	0.00	0.00
DPT	0.00	0.00	0.00	1.00	0.00	0.00	0.00	0.00	0.00	0.00
DiPT	0.00	0.00	0.00	1.00	0.00	0.00	0.00	0.00	0.00	0.00
N, N-DET	0.00	0.00	0.00	1.00	0.00	0.00	0.00	0.00	0.00	0.00
N, N-DMT	0.00	0.00	0.00	1.00	0.00	0.00	0.00	0.00	0.00	0.00
4-Methoxy DiPT	0.00	0.00	0.00	0.00	1.00	0.00	0.00	0.00	0.00	0.00
5-Methoxy DALT	0.00	0.00	0.00	0.00	1.00	0.00	0.00	0.00	0.00	0.00
5-Methoxy DBT	0.00	0.00	0.00	0.00	1.00	0.00	0.00	0.00	0.00	0.00
5-Methoxy DET	0.00	0.00	0.00	0.00	1.00	0.00	0.00	0.00	0.00	0.00
5-Methoxy DMT	0.00	0.00	0.00	0.00	1.00	0.00	0.00	0.00	0.00	0.00
5-Methoxy DPT	0.00	0.00	0.00	0.00	1.00	0.00	0.00	0.00	0.00	0.00
5-Methoxy DiBT	0.00	0.00	0.00	0.00	1.00	0.00	0.00	0.00	0.00	0.00
5-Methoxy DiPT	0.00	0.00	0.00	0.00	1.00	0.00	0.00	0.00	0.00	0.00
5-Methoxy EPT	0.00	0.00	0.00	0.00	1.00	0.00	0.00	0.00	0.00	0.00
5-Methoxy EiPT	0.00	0.00	0.00	0.00	1.00	0.00	0.00	0.00	0.00	0.00
5-Methoxy MiPT	0.00	0.00	0.00	0.00	1.00	0.00	0.00	0.00	0.00	0.00
6-Methoxy DiPT	0.00	0.00	0.00	0.00	1.00	0.00	0.00	0.00	0.00	0.00
7-Methoxy DiPT	0.00	0.00	0.00	0.00	1.00	0.00	0.00	0.00	0.00	0.00
N-Acetyl serotonin	0.00	0.00	0.00	0.00	0.00	1.00	0.00	0.00	0.00	0.00
N-Acetyl tryptamine	0.00	0.00	0.00	0.00	0.00	1.00	0.00	0.00	0.00	0.00
4-Hydroxy DET	0.00	0.00	0.00	0.00	0.00	0.00	1.00	0.00	0.00	0.00
4-Hydroxy DMT	0.00	0.00	0.00	0.00	0.00	0.00	1.00	0.00	0.00	0.00
4-Hydroxy DPT	0.00	0.00	0.00	0.00	0.00	0.00	1.00	0.00	0.00	0.00
4-Hydroxy DiPT	0.00	0.00	0.00	0.00	0.00	0.00	1.00	0.00	0.00	0.00
4-Hydroxy MET	1.00	0.00	0.00	0.00	0.00	0.00	1.00	0.00	0.00	0.00
4-Hydroxy MPT	0.00	0.00	0.00	0.00	0.00	0.00	1.00	0.00	0.00	0.00
4-Hydroxy MiPT	0.00	0.00	0.00	0.00	0.00	0.00	1.00	0.00	0.00	0.00
5-Hydroxy DMT	0.00	0.00	0.00	0.00	0.00	0.00	1.00	0.00	0.00	0.00
Psilocybin	0.00	0.00	0.00	0.00	0.00	0.00	1.00	0.00	0.00	0.00
6-Fluoro DET	0.00	0.00	0.00	0.00	0.00	0.00	0.00	0.00	0.00	0.00
Sumatriptan	0.00	0.00	0.00	0.00	0.00	0.00	0.00	0.00	0.00	0.00
4-Acetoxy DET	0.00	0.00	0.00	0.00	0.00	0.00	0.00	0.00	0.00	1.00
4-Acetoxy DMT	0.00	0.00	0.00	0.00	0.00	0.00	0.00	0.00	0.00	1.00
4-Acetoxy DPT	0.00	0.00	0.00	0.00	0.00	0.00	0.00	0.00	0.00	1.00
4-Acetoxy DiPT	0.00	0.00	0.00	0.00	0.00	0.00	0.00	0.00	0.00	1.00
4-Acetoxy MET	0.00	0.00	0.00	0.00	0.00	0.00	0.00	0.00	0.00	1.00
4-Acetoxy MiPT	0.00	0.00	0.00	0.00	0.00	0.00	0.00	0.00	0.00	1.00

Table A2.2 The relative intensities for the *m/z* values in the tryptamine 60 V neutral loss spectra ranked most important in discrimination of the ten tryptamine clusters, from the average of ten replicates.

Group	Compound	Neutral loss 60																		
		16.02	17.03	30.04	31.04	43.04	45.06	58.03	59.04	59.07	60.04	73.09	95.00	101.12	131.07	147.07	149.07	161.08	189.08	238.07
G 1	4-Methyl-α-ethyl tryptamine	13.3	80.6	0.0	0.0	0.0	0.8	0.0	0.0	100.0	0.0	0.1	0.0	0.0	0.1	0.0	0.0	0.0	0.0	0.0
	5-Methoxy-α-ethyl tryptamine	14.8	98.2	0.0	0.0	0.0	0.0	0.0	0.0	83.6	0.0	6.8	0.0	0.0	0.0	0.0	0.0	2.7	0.0	0.0
	N-Methyl-*N*-ethyltryptamine	0.0	0.0	0.0	0.0	0.0	0.0	0.0	0.0	48.7	0.0	0.0	0.0	0.0	100.0	0.0	0.0	0.0	0.0	0.0
	α-Ethyltryptamine	3.5	27.4	0.0	0.0	0.0	0.8	0.0	0.0	100.0	0.0	0.0	0.0	0.0	5.7	0.0	0.0	0.0	0.0	0.0
G 2	5,7-Dichloro tryptamine	11.2	100.0	4.4	4.6	0.0	0.0	0.0	0.0	0.0	0.0	0.0	0.0	0.0	0.0	0.0	0.0	0.0	0.0	0.0
	5-IT	19.8	100.0	0.0	0.0	0.0	53.7	0.0	0.0	0.0	0.0	0.0	0.0	0.0	0.0	0.0	0.0	0.0	0.0	0.0
	5-Methoxy AMT	16.4	100.0	0.0	1.2	6.7	8.2	0.0	0.0	3.9	0.0	0.0	0.0	0.0	0.0	0.0	0.0	0.0	0.0	0.0
	6-IT	15.5	100.0	0.0	0.0	0.1	43.7	0.0	0.0	0.0	0.0	0.0	0.0	0.0	0.0	0.0	0.0	0.0	0.0	0.0
	7-Fluoro tryptamine	12.3	100.0	6.0	10.3	0.0	0.0	0.0	0.0	0.0	0.0	0.0	0.0	0.0	0.0	0.0	0.0	0.0	0.0	0.0
	Nonyloxytryptamine	20.0	100.0	1.3	3.5	0.0	0.0	0.0	0.0	0.0	0.0	0.0	0.0	0.0	0.0	0.0	0.0	0.0	0.0	0.0
	Serotonin	13.3	100.0	0.0	5.2	0.0	0.0	0.0	0.0	0.0	1.3	0.0	0.0	0.0	0.0	0.0	0.0	0.0	0.0	0.0
	α -Methyl tryptamine	16.3	100.0	0.0	3.7	10.0	51.5	1.6	0.0	0.0	0.0	0.0	0.0	0.0	0.0	0.0	0.0	0.0	0.0	0.0
G 3	5-Hydroxy-*N*-methyl tryptamine	0.0	0.0	11.2	100.0	32.8	9.1	0.0	5.7	0.0	0.0	0.0	0.0	0.0	0.0	0.0	0.0	0.0	0.0	0.0
	N-Methyl tryptamine	0.3	0.0	13.1	100.0	42.3	7.1	0.0	0.0	0.0	0.0	0.0	0.0	0.0	0.0	0.0	0.0	0.0	0.0	0.0
G 4	DPT	0.0	0.0	0.0	0.0	0.0	0.0	0.0	0.0	0.0	0.0	0.0	0.0	29.9	100.0	0.0	0.0	0.0	0.0	0.0
	DiPT	0.0	0.0	0.0	0.0	0.0	0.0	0.0	0.0	0.0	0.0	0.0	0.0	71.9	100.0	0.0	0.0	0.0	0.0	0.0
	N,N-DET	0.0	0.0	0.0	0.0	0.0	0.0	0.0	0.0	0.0	0.0	37.5	0.0	0.0	100.0	0.0	0.0	0.0	0.0	0.0
	N,N-DMT	0.0	0.0	0.0	0.0	0.0	63.2	0.0	0.0	2.0	0.0	0.0	0.0	0.0	100.0	0.0	0.0	0.0	0.0	0.0
G 5	4-Methoxy DiPT	0.0	0.0	0.0	0.0	0.0	0.0	0.0	0.0	0.0	0.0	0.0	0.0	44.4	0.0	0.0	0.0	100.0	0.0	0.0
	5-Methoxy DALT	0.0	0.0	0.0	0.0	0.0	0.0	0.0	0.0	0.0	0.0	0.0	0.0	0.0	0.0	0.0	0.0	100.0	0.0	0.0
	5-Methoxy DBT	0.0	0.0	0.0	0.0	0.0	0.0	0.0	0.0	0.0	0.0	0.0	0.0	0.0	0.0	0.0	0.0	100.0	0.0	0.0
	5-Methoxy DET	0.0	0.0	0.0	0.0	0.0	0.0	0.0	0.0	0.0	0.0	46.7	0.0	0.0	0.0	0.0	0.0	100.0	0.0	0.0
	5-Methoxy DMT	0.0	0.0	0.0	0.0	0.0	48.2	0.0	0.0	1.2	0.0	0.0	0.0	0.0	0.0	0.5	0.0	100.0	0.0	0.0
	5-Methoxy DPT	0.0	0.0	0.0	0.0	0.0	0.0	0.0	0.0	0.0	0.0	0.0	0.0	38.0	0.0	0.0	0.0	100.0	0.0	0.0
	5-Methoxy DiBT	0.0	0.0	0.0	0.0	0.0	0.0	0.0	0.0	0.0	0.0	0.0	0.0	0.0	0.0	0.0	0.0	100.0	0.0	0.0
	5-Methoxy DiPT	0.0	0.0	0.0	0.0	0.0	0.0	0.0	0.0	0.0	0.0	0.0	0.0	59.3	0.0	0.0	0.0	100.0	0.0	0.0
	5-Methoxy EPT	0.0	0.0	0.0	0.0	0.0	0.0	0.0	0.0	0.0	0.0	0.0	0.0	0.0	0.0	0.0	0.0	100.0	0.0	0.0
	5-Methoxy EiPT	0.0	0.0	0.0	0.0	0.0	0.0	0.0	0.0	0.0	0.0	0.0	0.0	0.0	0.0	0.5	0.0	100.0	0.0	0.0
	5-Methoxy MiPT	0.0	0.0	0.0	0.0	0.0	0.0	0.0	0.0	0.0	0.0	48.8	0.0	0.0	0.0	0.0	0.0	100.0	0.0	0.0
	6-Methoxy DiPT	0.0	0.0	0.0	0.0	0.0	0.0	0.0	0.0	0.0	0.0	0.0	0.0	5.4	0.0	0.0	0.0	100.0	0.0	0.0
	7-Methoxy DiPT	0.1	0.0	0.0	0.0	0.0	0.0	0.0	0.0	0.0	0.0	0.0	0.0	75.7	0.0	0.0	0.0	100.0	0.0	0.0
G 6	*N*-Acetylserotonin	0.0	5.5	0.0	0.0	4.6	0.1	11.0	100.0	0.0	20.5	0.0	0.0	0.0	0.0	0.4	0.0	0.0	0.0	0.0
	N-Acetyl tryptamine	0.0	4.5	0.0	0.0	2.3	1.1	11.8	100.0	0.0	19.3	0.0	0.0	0.0	0.0	0.0	0.0	0.0	0.0	0.0
G 7	4-Hydroxy DET	0.0	0.0	0.0	0.0	0.0	0.0	0.0	0.0	0.0	0.0	30.5	0.0	0.0	0.0	100.0	0.0	0.0	0.0	0.0
	4-Hydroxy DMT	0.0	0.0	0.0	0.0	0.0	57.1	0.0	0.0	0.0	0.0	0.0	0.0	0.0	0.0	100.0	0.0	0.0	0.0	0.0
	4-Hydroxy DPT	0.0	0.0	0.0	0.0	0.0	0.0	0.0	0.0	0.0	0.0	0.0	0.0	24.8	0.0	100.0	0.0	0.0	0.0	0.0
	4-Hydroxy DiPT	0.0	0.0	0.0	0.0	0.0	0.0	0.0	0.0	0.0	0.0	0.0	0.0	46.6	0.0	100.0	0.0	0.0	0.0	0.0
	4-Hydroxy MET	0.0	0.0	0.0	0.0	0.0	0.0	0.0	0.0	25.5	0.0	0.0	0.0	0.0	0.0	100.0	0.0	0.0	0.0	0.0
	4-Hydroxy MPT	0.0	0.0	0.0	0.0	0.0	0.0	0.0	0.0	0.0	0.0	25.7	0.0	0.0	0.0	100.0	0.0	0.0	0.0	0.0
	4-Hydroxy MiPT	0.0	0.0	0.0	0.0	0.0	0.0	0.0	0.0	0.0	0.0	28.8	0.0	0.0	0.0	100.0	0.0	0.0	0.0	0.0
	5-Hydroxy DMT	0.0	0.0	0.0	4.7	0.0	82.8	0.0	0.0	0.2	0.0	0.0	0.0	0.0	0.0	100.0	0.0	0.0	0.0	0.0
	Psilocybin	0.0	0.0	0.0	0.1	0.0	53.4	0.0	0.0	1.3	0.0	0.0	0.0	0.0	0.1	100.0	0.0	0.0	0.0	0.0
G 8	6-Fluoro DET	0.0	0.0	0.0	0.0	0.0	0.0	0.0	0.0	0.0	0.0	17.6	0.0	0.0	0.0	0.0	100.0	2.1	0.0	0.0
G 9	Sumatriptan	0.0	0.0	0.0	0.0	0.0	18.0	0.0	0.0	0.0	0.0	0.0	10.2	0.0	0.0	0.3	0.0	0.0	0.0	100.0
G 10	4-Acetoxy DET	0.0	0.0	0.0	0.0	0.0	0.0	0.0	0.0	0.0	0.0	23.2	0.0	0.0	0.0	0.0	0.0	0.0	100.0	0.0
	4-Acetoxy DMT	0.0	0.0	0.0	0.0	0.0	20.8	0.0	0.0	0.0	0.0	0.0	0.0	0.0	0.0	0.0	0.0	0.0	100.0	0.0
	4-Acetoxy DPT	0.0	0.0	0.0	0.0	0.0	0.0	0.0	0.0	0.0	0.0	0.0	0.0	18.7	0.0	0.0	0.0	0.0	90.0	0.0
	4-Acetoxy DiPT	0.0	0.0	0.0	0.0	0.0	0.0	0.0	0.0	0.0	0.0	0.0	0.0	31.2	0.0	0.0	0.0	0.0	100.0	0.0
	4-Acetoxy MET	0.0	0.0	0.0	0.0	0.0	0.0	0.0	0.0	18.0	0.0	0.0	0.0	0.0	0.0	0.0	0.0	0.0	100.0	0.0
	4-Acetoxy MiPT	0.0	0.0	0.0	0.0	0.0	0.0	0.0	0.0	0.0	0.0	22.3	0.0	0.0	0.0	0.0	0.0	0.0	100.0	0.0

Table A2.3 The relative intensities for the *m/z* values in the tryptamine 90 V neutral loss spectra ranked most important in discrimination of the ten tryptamine clusters, from the average of ten replicates.

Group	Compound	Neutral loss 90														
		17.03	31.05	32.05	43.05	44.05	45.06	58.03	58.07	59.04	59.07	60.05	60.08	61.06	72.08	73.09
G 1	4-Methyl-α-ethyl tryptamine	7.0	0.0	0.2	0.0	0.8	1.1	0.0	17.6	0.0	100.0	0.0	6.5	0.0	6.3	5.0
	5-Methoxy-α-ethyl tryptamine	7.5	0.0	0.0	0.0	0.0	0.5	0.0	13.6	0.0	100.0	0.0	0.0	0.0	8.3	4.7
	N-Methyl-*N*-ethyltryptamine	0.0	0.0	0.0	0.0	0.0	0.0	0.0	12.7	0.0	100.0	0.0	32.1	0.0	0.0	1.1
	α-Ethyltryptamine	1.4	0.0	0.0	0.0	0.0	0.4	0.0	11.7	0.0	100.0	0.0	0.0	0.0	3.0	0.0
G 2	5,7-Dichloro tryptamine	25.1	6.8	0.0	0.0	0.0	0.0	0.0	0.0	0.0	0.0	0.0	0.0	0.0	0.0	0.0
	5-IT	45.9	2.8	17.8	1.0	14.8	50.0	0.0	63.9	0.0	0.5	0.0	1.1	0.0	5.2	0.0
	5-Methoxy AMT	77.1	11.2	72.5	7.6	5.9	20.5	0.0	100.0	0.0	13.4	25.0	0.0	15.7	2.2	48.8
	6-IT	20.7	2.3	21.9	1.1	12.1	50.0	0.0	65.8	0.0	1.7	0.0	1.9	0.0	5.4	0.0
	7-Fluoro tryptamine	91.6	29.0	0.0	6.1	29.4	1.8	0.0	0.1	0.0	0.0	0.0	0.0	0.0	0.0	0.0
	Nonyloxytryptamine	98.6	2.0	0.0	0.0	0.0	0.0	0.0	0.0	0.0	0.0	0.0	0.0	0.0	0.0	0.0
	Serotonin	99.8	29.7	1.8	5.5	15.7	0.0	0.2	0.0	10.7	0.0	54.0	0.0	11.8	0.0	0.0
	α-Methyl tryptamine	2.4	13.5	98.0	5.3	12.6	49.3	0.0	67.1	0.9	8.5	1.1	11.6	0.0	10.7	0.0
G 3	5-Hydroxy-*N*-methyl tryptamine	0.0	97.6	22.7	22.2	5.7	17.1	0.0	38.3	44.6	0.0	13.5	0.0	21.6	0.0	0.0
	N-Methyl tryptamine	0.3	100.0	35.2	25.7	4.2	10.3	0.0	53.1	0.0	6.5	0.0	29.2	0.0	6.6	0.0
G 4	DPT	0.0	0.0	0.0	0.0	0.0	0.0	0.0	0.0	0.0	0.0	0.0	0.0	0.0	0.0	0.0
	DiPT	0.0	0.0	0.0	0.0	0.0	0.0	0.0	0.0	0.0	0.0	0.0	0.0	0.0	0.0	0.0
	N,*N*-DET	0.0	0.0	0.0	0.0	0.0	0.0	0.0	0.0	0.0	0.0	0.0	0.0	0.0	11.7	100.0
	N,*N*-DMT	0.0	0.0	0.0	0.2	10.7	47.1	0.0	0.0	0.0	5.2	0.0	0.6	0.0	34.3	5.9
G 5	4-Methoxy DiPT	0.0	0.0	0.0	0.0	0.0	0.0	0.0	0.0	0.0	0.0	0.0	0.0	0.0	0.0	0.0
	5-Methoxy DALT	0.0	0.0	0.0	0.0	0.0	0.0	0.0	0.0	0.0	0.0	0.0	0.0	0.0	0.0	0.0
	5-Methoxy DBT	0.0	0.0	0.0	0.0	0.0	0.0	0.0	0.0	0.0	0.0	0.0	0.0	0.0	0.0	0.0
	5-Methoxy DET	0.0	0.0	0.0	0.0	0.0	0.0	0.0	0.0	0.0	0.0	0.0	0.0	0.0	8.0	66.9
	5-Methoxy DMT	0.0	0.0	0.0	0.0	4.4	17.5	0.0	0.0	0.0	6.0	0.0	41.7	0.0	3.9	0.4
	5-Methoxy DPT	0.0	0.0	0.0	0.0	0.0	0.0	0.0	0.0	0.0	0.0	0.0	0.0	0.0	0.0	0.0
	5-Methoxy DiBT	0.0	0.0	0.0	0.0	0.0	0.0	0.0	0.0	0.0	0.0	0.0	0.0	0.0	0.0	0.0
	5-Methoxy DiPT	0.0	0.0	0.0	0.0	0.0	0.0	0.0	0.0	0.0	0.0	0.0	0.0	0.0	0.0	0.0
	5-Methoxy EPT	0.0	0.0	0.0	0.0	0.0	0.0	0.0	0.0	0.0	0.0	0.0	0.0	0.0	0.0	0.0
	5-Methoxy EiPT	0.0	0.0	0.0	0.0	0.0	0.0	0.0	0.0	0.0	0.0	0.0	0.0	0.0	0.0	0.0
	5-Methoxy MiPT	0.0	0.0	0.0	0.0	0.0	0.0	0.0	0.0	0.0	0.0	0.0	0.0	0.0	10.6	95.7
	6-Methoxy DiPT	0.0	0.0	0.0	0.0	0.0	0.0	0.0	0.0	0.0	0.0	0.0	0.0	0.0	0.0	0.0
	7-Methoxy DiPT	0.0	0.0	0.0	0.0	0.0	0.0	0.0	0.0	0.0	0.0	0.0	0.0	0.0	0.0	0.0
G 6	*N*-Acetylserotonin	0.6	0.0	0.0	5.4	1.5	0.1	10.4	0.0	100.0	0.0	19.4	0.0	7.6	0.0	0.0
	N-Acetyl tryptamine	0.1	0.0	0.0	2.3	0.0	0.0	12.4	0.0	100.0	0.0	22.5	0.0	5.9	0.0	0.0
G 7	4-Hydroxy DET	0.0	0.0	0.0	0.0	0.0	0.0	0.0	0.0	0.0	0.0	0.0	0.0	0.0	6.6	62.3
	4-Hydroxy DMT	0.0	0.0	0.0	0.0	5.6	36.3	0.0	0.0	0.0	2.6	0.0	0.0	0.0	0.0	0.0
	4-Hydroxy DPT	0.0	0.0	0.0	0.0	0.0	0.0	0.0	0.0	0.0	0.0	0.0	0.0	0.0	0.0	0.0
	4-Hydroxy DiPT	0.0	0.0	0.0	0.0	0.0	0.0	0.0	0.0	0.0	0.0	0.0	0.0	0.0	0.0	0.0
	4-Hydroxy MET	0.0	0.0	0.0	0.0	0.0	0.0	0.0	5.5	0.0	54.4	0.0	2.3	0.0	0.0	0.0
	4-Hydroxy MPT	0.0	0.0	0.0	0.0	0.0	0.0	0.0	0.0	0.0	0.0	0.0	0.0	0.0	7.6	78.0
	4-Hydroxy MiPT	0.0	0.0	0.0	0.0	0.0	0.0	0.0	0.0	0.0	0.0	0.0	0.0	0.0	8.9	83.0
	5-Hydroxy DMT	0.0	7.6	0.0	0.0	8.1	38.0	0.0	0.2	0.0	4.2	0.0	0.0	0.8	9.2	0.0
	Psilocybin	0.0	0.1	0.0	0.0	3.9	29.1	0.0	0.1	0.0	4.6	0.0	0.0	0.0	2.8	0.0
G 8	6-Fluoro DET	0.0	2.6	0.0	0.0	0.0	0.0	0.0	0.0	0.0	0.1	0.0	0.0	0.0	5.7	56.9
G 9	Sumatriptan	0.0	0.0	0.0	0.0	0.0	3.5	0.0	0.0	0.0	0.0	0.0	0.0	0.0	0.0	0.0
G 10	4-Acetoxy DET	0.0	0.0	0.0	0.0	0.0	0.1	0.0	0.0	0.0	0.0	0.0	0.0	0.0	0.1	3.9
	4-Acetoxy DMT	0.0	0.0	0.0	0.0	0.0	0.5	0.0	0.0	0.0	0.0	0.0	0.0	0.0	0.0	0.0
	4-Acetoxy DPT	0.0	0.0	0.0	0.0	0.0	0.0	0.0	0.0	0.0	0.0	0.0	0.0	0.0	0.0	0.0
	4-Acetoxy DiPT	0.0	0.0	0.0	0.0	0.0	0.0	0.0	0.0	0.0	0.0	0.0	0.0	0.0	0.0	0.0
	4-Acetoxy MET	0.0	0.0	0.0	0.0	0.0	0.0	0.0	0.0	0.0	2.2	0.0	0.0	0.0	0.0	0.0
	4-Acetoxy MiPT	0.0	0.0	0.0	0.0	0.0	0.0	0.0	0.0	0.0	0.0	0.0	0.0	0.0	0.0	3.8

Table A2.3 (continued). The relative intensities for the *m/z* values in the tryptamine 90 V neutral loss spectra ranked most important in discrimination of the ten tryptamine clusters, from the average of ten replicates.

Group	Compound	Neutral loss 90														
		74.06	76.07	86.06	87.04	87.07	87.11	88.07	88.11	90.08	101.09	101.12	102.06	104.06	115.10	116.15
G 1	4-Methyl-α-ethyl tryptamine	0.0	0.0	0.0	0.0	0.0	0.0	0.0	2.5	0.0	0.0	0.0	0.0	0.0	0.0	0.0
	5-Methoxy-α-ethyl tryptamine	0.0	0.0	0.0	0.0	0.1	3.1	1.7	0.0	0.0	8.0	0.0	0.0	0.0	0.1	0.0
	N-Methyl-N-ethyltryptamine	0.0	0.0	0.0	0.0	0.0	4.3	0.0	19.6	0.0	0.0	0.0	0.0	0.0	0.0	0.0
	α-Ethyltryptamine	0.0	0.0	0.0	0.0	0.0	0.0	0.0	0.0	0.0	0.0	0.0	0.0	0.0	0.0	0.0
G 2	5,7-Dichloro tryptamine	0.0	0.0	0.0	0.0	0.0	0.0	0.0	0.0	0.0	0.0	0.0	0.0	0.0	0.0	0.0
	5-IT	0.0	0.0	0.0	0.0	0.0	0.0	0.0	0.0	0.0	0.0	0.0	0.0	0.0	0.0	0.0
	5-Methoxy AMT	5.2	2.7	3.3	0.0	21.8	0.0	13.6	0.0	0.1	9.9	0.0	0.0	0.0	0.0	0.0
	6-IT	0.4	0.0	0.0	0.0	0.0	0.0	0.0	0.0	0.0	0.0	0.0	0.0	0.0	0.0	0.0
	7-Fluoro tryptamine	0.0	0.0	0.0	0.0	0.0	0.0	0.0	0.0	0.2	0.0	0.0	0.2	0.0	0.0	0.0
	Nonyloxytryptamine	0.0	0.0	0.0	0.0	0.0	0.0	0.0	0.0	0.0	0.0	0.0	0.0	0.0	0.0	0.0
	Serotonin	7.8	0.0	8.0	0.0	1.0	0.0	1.1	0.0	0.0	0.0	0.0	0.0	0.0	0.0	0.0
	α-Methyl tryptamine	0.0	0.0	0.1	0.0	0.0	0.0	0.0	0.0	0.0	0.0	0.0	0.0	0.0	0.0	0.0
G 3	5-Hydroxy-N-methyl tryptamine	60.3	89.4	26.0	0.0	6.3	0.0	32.6	0.0	1.1	0.5	0.0	0.0	0.0	0.0	0.0
	N-Methyl tryptamine	0.1	0.0	0.0	0.0	0.0	0.0	0.0	0.0	0.0	0.0	0.0	0.0	0.0	0.0	0.0
G 4	DPT	0.0	0.0	0.0	0.0	0.0	0.0	0.0	0.0	0.0	0.0	100.0	0.0	0.0	0.0	0.1
	DiPT	0.0	0.0	0.0	0.0	0.0	0.0	0.0	0.0	0.0	0.0	100.0	0.0	0.0	0.0	0.0
	N,N-DET	0.0	0.0	0.0	0.0	0.0	1.2	0.0	0.0	0.0	0.0	2.8	0.0	0.0	0.0	0.0
	N,N-DMT	0.0	0.0	0.0	0.0	0.0	0.0	0.0	0.0	0.0	0.0	0.0	0.0	0.0	0.0	0.0
G 5	4-Methoxy DiPT	0.0	0.0	0.0	0.0	0.0	0.0	0.0	0.0	0.0	0.0	100.0	0.0	0.0	0.0	42.9
	5-Methoxy DALT	0.0	0.0	0.0	0.0	0.0	0.0	0.0	0.0	0.0	0.0	0.0	0.0	0.0	0.0	0.0
	5-Methoxy DBT	0.0	0.0	0.0	0.0	0.0	0.0	0.0	0.0	0.0	0.0	0.0	0.0	0.0	0.0	0.0
	5-Methoxy DET	0.0	0.0	0.0	0.0	0.0	6.5	0.0	50.8	0.0	0.1	0.0	0.0	0.0	3.0	0.0
	5-Methoxy DMT	0.1	20.2	0.0	0.0	3.4	0.0	30.3	0.0	0.0	1.2	0.0	0.0	0.0	0.8	0.0
	5-Methoxy DPT	0.0	0.0	0.0	0.0	0.0	0.0	0.0	0.0	0.0	0.0	100.0	0.0	0.0	0.0	52.0
	5-Methoxy DiBT	0.0	0.0	0.0	0.0	0.0	0.0	0.0	0.0	0.0	0.0	0.0	0.0	0.0	0.0	0.0
	5-Methoxy DiPT	0.0	0.0	0.0	0.0	0.0	0.0	0.0	0.0	0.0	0.0	100.0	0.0	0.0	0.0	50.0
	5-Methoxy EPT	0.0	0.0	0.0	0.0	0.0	67.6	0.0	0.0	0.0	0.0	5.4	1.8	0.0	0.0	0.0
	5-Methoxy EiPT	0.0	0.0	0.0	0.0	0.0	100.0	0.0	0.4	0.0	0.0	7.1	0.0	0.0	0.0	0.0
	5-Methoxy MiPT	0.1	0.0	0.0	0.4	0.0	12.2	0.0	97.9	0.0	0.4	0.8	0.4	1.2	6.8	0.0
	6-Methoxy DiPT	0.0	0.0	0.0	0.0	0.0	0.3	0.0	0.0	0.0	0.0	41.5	0.0	0.0	0.0	19.5
	7-Methoxy DiPT	0.0	0.0	0.0	0.0	0.0	0.0	0.0	0.0	0.0	0.0	100.0	0.0	0.0	0.0	51.1
G 6	N-Acetylserotonin	0.0	0.0	6.8	23.6	0.0	0.0	7.7	0.0	0.0	0.0	0.0	19.4	31.4	0.0	0.0
	N-Acetyl tryptamine	0.0	2.6	21.6	0.0	5.1	0.0	17.8	0.0	0.0	0.0	0.0	0.0	0.0	0.0	0.0
G 7	4-Hydroxy DET	0.0	0.0	0.0	0.0	0.0	0.0	0.0	0.0	1.5	17.7	0.0	0.0	0.0	1.1	0.0
	4-Hydroxy DMT	0.1	0.0	0.0	0.0	3.5	0.0	17.5	0.0	75.9	0.0	0.0	0.0	0.0	0.0	0.0
	4-Hydroxy DPT	0.0	0.0	0.0	0.0	0.0	0.0	0.0	0.0	0.0	0.0	87.3	0.0	0.0	0.0	0.0
	4-Hydroxy DiPT	0.0	0.0	0.0	0.0	0.0	0.0	0.0	0.0	0.0	0.0	100.0	0.0	0.0	0.0	0.0
	4-Hydroxy MET	0.0	1.4	2.0	0.0	16.5	0.0	1.3	0.0	0.0	1.2	0.0	0.0	0.0	0.0	0.0
	4-Hydroxy MPT	0.0	0.0	0.0	0.0	0.0	0.0	0.0	0.0	1.6	21.2	0.0	0.0	0.0	1.2	0.0
	4-Hydroxy MiPT	0.0	0.0	0.0	0.0	0.0	0.2	0.0	0.0	1.4	19.3	0.0	0.0	0.0	1.3	0.0
	5-Hydroxy DMT	5.1	0.2	0.0	0.0	4.5	0.0	35.8	0.0	58.5	1.7	0.0	0.0	0.0	0.0	0.0
	Psilocybin	2.5	0.1	0.0	0.0	7.5	0.0	20.5	0.0	87.2	1.1	0.0	0.0	0.0	0.0	0.0
G 8	6-Fluoro DET	0.0	0.0	0.0	0.0	0.0	2.6	0.0	0.0	0.0	0.0	0.1	0.0	0.0	0.0	0.0
G 9	Sumatriptan	0.0	0.0	0.0	0.0	0.0	0.0	0.0	0.0	0.0	0.0	0.0	0.0	0.0	0.0	0.0
G 10	4-Acetoxy DET	0.0	0.0	0.0	0.0	0.0	0.0	0.0	0.0	0.0	0.0	0.0	0.0	0.0	96.1	0.0
	4-Acetoxy DMT	0.0	0.0	9.6	0.0	84.6	0.0	1.6	0.0	0.0	1.3	0.0	0.0	0.0	0.0	0.0
	4-Acetoxy DPT	0.0	0.0	0.0	0.0	0.0	0.0	0.0	0.0	0.0	0.0	5.5	0.0	0.0	0.0	0.0
	4-Acetoxy DiPT	0.0	0.0	0.0	0.0	0.0	0.0	0.0	0.0	0.0	0.0	5.2	0.0	0.0	0.0	0.0
	4-Acetoxy MET	0.0	0.0	0.0	0.0	0.0	0.0	0.0	0.0	0.0	82.6	0.0	0.0	0.0	0.3	0.0
	4-Acetoxy MiPT	0.0	0.0	0.0	0.0	0.0	0.0	0.0	0.0	0.0	0.0	0.0	0.0	0.0	99.4	0.0

Table A2.3 (continued). The relative intensities for the *m/z* values in the tryptamine 90 V neutral loss spectra ranked most important in discrimination of the ten tryptamine clusters, from the average of ten replicates.

Group	Compound	Neutral loss 90															
		118.12	120.11	129.15	131.08	138.05	139.06	140.07	143.13	147.07	149.07	161.08	177.10	189.08	189.12	203.13	238.08
G 1	4-Methyl-α-ethyl tryptamine	0.0	0.1	0.0	0.0	0.0	0.0	0.0	0.0	0.0	0.0	0.0	0.0	0.0	0.0	0.0	0.0
	5-Methoxy-α-ethyl tryptamine	0.0	0.0	0.0	0.0	0.0	0.0	0.0	0.0	0.0	0.0	1.5	0.0	0.0	0.0	0.0	0.0
	N-Methyl-N-ethyltryptamine	0.0	0.8	0.0	75.1	0.0	0.0	0.0	0.0	0.0	0.0	0.0	0.0	0.0	0.0	0.0	0.0
	α-Ethyltryptamine	0.0	0.0	0.0	0.7	0.0	0.0	0.0	0.0	0.0	0.0	0.0	0.0	0.0	0.0	0.0	0.0
G 2	5,7-Dichloro tryptamine	0.0	0.0	0.0	0.0	0.0	0.0	0.0	0.0	0.0	0.0	0.0	0.0	0.0	0.0	0.0	0.0
	5-IT	0.0	0.0	0.0	0.0	0.0	0.0	0.0	0.0	0.0	0.0	0.0	0.0	0.0	0.0	0.0	0.0
	5-Methoxy AMT	0.0	0.0	0.0	0.0	0.0	0.0	0.0	0.0	0.0	0.0	0.0	0.0	0.0	0.0	0.0	0.0
	6-IT	0.0	0.0	0.0	0.0	0.0	0.0	0.0	0.0	0.0	0.0	0.0	0.0	0.0	0.0	0.0	0.0
	7-Fluoro tryptamine	0.0	0.0	0.0	0.0	0.0	0.0	0.0	0.0	0.0	0.0	0.0	0.0	0.0	0.0	0.0	0.0
	Nonyloxytryptamine	0.0	0.0	0.0	0.0	0.0	0.0	0.0	0.0	0.0	0.0	0.0	0.0	0.0	0.0	0.0	0.0
	Serotonin	0.0	0.0	0.0	0.0	0.0	0.0	0.0	0.0	0.0	0.0	0.0	0.0	0.0	0.0	0.0	0.0
	α-Methyl tryptamine	0.0	0.0	0.0	0.0	0.0	0.0	0.0	0.0	0.0	0.0	0.0	0.0	0.0	0.0	0.0	0.0
G 3	5-Hydroxy-N-methyl tryptamine	0.0	0.0	0.0	0.0	0.0	0.0	0.0	0.0	0.0	0.0	0.0	0.0	0.0	0.0	0.0	0.0
	N-Methyl tryptamine	0.0	0.0	0.0	0.1	0.0	0.0	0.0	0.0	0.0	0.0	0.0	0.0	0.0	0.0	0.0	0.0
G 4	DPT	0.0	0.0	0.3	69.3	0.0	0.0	0.0	0.0	0.0	0.0	0.0	0.0	0.0	0.0	0.0	0.0
	DiPT	0.0	0.0	1.2	16.3	0.0	0.0	0.0	0.0	0.0	0.0	0.0	0.0	0.0	0.0	0.0	0.0
	N,N-DET	0.0	0.0	0.0	67.0	0.0	0.0	0.0	0.0	0.0	0.0	0.0	0.0	0.0	0.0	0.0	0.0
	N,N-DMT	0.0	0.0	0.0	93.2	0.0	0.0	0.0	0.0	0.0	0.0	0.0	0.0	0.0	0.0	0.0	0.0
G 5	4-Methoxy DiPT	0.0	0.0	0.0	0.0	0.0	0.0	0.0	0.2	0.0	0.0	67.8	0.0	0.0	0.0	33.0	0.0
	5-Methoxy DALT	0.0	0.0	0.0	0.0	0.0	0.0	0.0	0.0	0.0	0.0	58.6	0.0	0.0	1.5	7.0	0.0
	5-Methoxy DBT	0.0	0.0	94.3	0.0	0.0	0.0	0.0	0.0	0.0	0.0	80.6	0.0	0.0	0.0	98.7	0.0
	5-Methoxy DET	0.0	0.0	0.0	0.0	0.0	0.0	0.0	0.0	0.0	0.0	100.0	0.0	1.2	23.9	0.0	0.0
	5-Methoxy DMT	0.0	0.0	0.0	0.0	0.0	0.0	0.0	0.0	0.6	0.0	100.0	0.0	0.0	0.0	0.0	0.0
	5-Methoxy DPT	0.0	0.0	0.0	0.0	0.0	0.0	0.0	2.2	0.0	0.0	90.3	0.0	2.9	45.5	21.3	0.0
	5-Methoxy DiBT	0.0	0.0	100.0	0.0	0.0	0.0	0.0	0.0	0.0	0.0	81.1	0.0	0.0	0.0	20.0	0.0
	5-Methoxy DiPT	0.0	0.0	0.1	0.0	0.0	0.0	0.0	2.3	0.0	0.0	37.2	0.0	0.0	0.0	26.3	0.0
	5-Methoxy EPT	13.1	0.0	0.0	0.0	0.0	0.0	0.0	0.0	0.0	0.0	100.0	0.0	0.8	34.0	27.6	0.0
	5-Methoxy EiPT	21.9	0.0	0.0	0.0	0.0	0.0	0.0	0.8	0.3	0.0	67.4	0.0	0.0	0.0	66.7	0.0
	5-Methoxy MiPT	0.1	0.0	0.0	0.0	0.0	0.0	0.0	1.6	0.0	0.0	33.9	0.0	0.0	0.0	0.0	0.0
	6-Methoxy DiPT	0.0	0.0	0.1	0.0	0.0	0.0	0.0	2.9	0.0	0.0	91.4	0.0	0.0	0.0	91.3	0.0
	7-Methoxy DiPT	0.0	0.0	0.0	0.0	0.0	0.0	0.0	2.4	0.0	0.0	34.1	0.0	0.0	0.0	21.1	0.0
G 6	N-Acetylserotonin	0.0	0.0	0.0	0.0	0.8	0.3	2.0	0.0	0.2	0.0	0.0	0.0	0.0	0.0	0.0	0.0
	N-Acetyl tryptamine	0.0	0.0	0.0	0.0	0.0	0.0	0.0	0.0	0.0	0.0	0.0	0.0	0.0	0.0	0.0	0.0
G 7	4-Hydroxy DET	37.7	0.0	0.0	0.0	0.0	0.0	0.0	0.0	100.0	0.0	0.0	0.0	0.0	0.0	0.0	0.0
	4-Hydroxy DMT	0.0	0.0	0.0	0.0	0.0	0.0	0.0	0.0	100.0	0.9	0.0	0.0	0.0	0.0	0.0	0.0
	4-Hydroxy DPT	0.7	0.0	0.0	0.0	0.0	0.0	0.0	0.7	94.1	0.0	0.0	0.0	0.0	16.5	2.2	0.0
	4-Hydroxy DiPT	0.1	0.0	0.0	0.0	0.0	0.0	0.0	0.1	53.7	0.0	0.0	0.0	1.7	25.3	0.0	0.0
	4-Hydroxy MET	0.0	0.0	0.0	0.0	0.0	0.0	0.0	0.0	100.0	0.0	0.0	0.0	0.0	0.0	0.0	0.0
	4-Hydroxy MPT	42.1	0.0	0.0	0.0	0.0	0.0	0.0	0.0	99.3	0.0	0.0	0.0	0.0	2.2	0.0	0.0
	4-Hydroxy MiPT	35.0	0.0	0.0	0.0	0.0	0.0	0.0	0.0	87.7	0.0	0.0	0.0	0.0	1.7	0.0	0.0
	5-Hydroxy DMT	0.0	0.0	0.0	0.0	0.0	0.0	0.0	0.0	99.7	0.0	0.0	0.0	0.0	0.0	0.0	0.0
	Psilocybin	0.0	0.0	0.0	0.0	0.0	0.0	0.0	0.0	95.2	0.8	0.0	0.0	0.0	0.0	0.0	0.0
G 8	6-Fluoro DET	0.0	17.8	0.0	0.0	0.0	0.0	0.0	0.0	0.0	100.0	1.7	29.4	0.0	0.0	0.0	0.0
G 9	Sumatriptan	0.0	0.0	0.0	0.0	12.5	43.9	12.9	0.0	0.0	0.0	0.0	0.0	0.0	0.0	0.0	100.0
G 10	4-Acetoxy DET	0.0	0.0	0.0	0.0	0.0	0.0	0.0	0.0	0.0	0.0	0.0	0.0	96.5	0.0	0.0	0.0
	4-Acetoxy DMT	0.0	0.0	0.0	1.4	0.0	0.0	0.0	0.0	0.0	0.0	0.0	0.0	100.0	0.0	0.0	0.0
	4-Acetoxy DPT	0.0	0.0	0.0	0.0	0.0	0.0	0.0	91.3	0.0	0.0	0.0	0.0	89.1	0.0	0.0	0.0
	4-Acetoxy DiPT	0.0	0.0	0.0	0.0	0.0	0.0	0.0	100.0	0.0	0.0	0.0	0.0	37.8	0.0	0.0	0.0
	4-Acetoxy MET	0.0	0.0	0.0	0.3	0.0	0.0	0.0	0.0	0.0	0.0	0.0	0.0	100.0	0.0	0.0	0.0
	4-Acetoxy MiPT	0.0	0.0	0.0	0.0	0.0	0.0	0.0	0.0	0.0	0.0	0.0	0.0	74.0	0.0	0.0	0.0

Table A2.4 Probabilities of the external validation tryptamines being assigned to each group.										
	G 1	G 2	G 3	G 4	G 5	G 6	G 7	G 8	G 9	G 10
4-Acetoxy MALT	0.00	0.00	0.00	0.00	0.00	0.00	0.00	0.00	0.00	**1.00**
4-Acetoxy MALT	0.00	0.00	0.00	0.00	0.00	0.00	0.00	0.00	0.00	**1.00**
4-Acetoxy MALT	0.00	0.00	0.00	0.00	0.00	0.00	0.00	0.00	0.00	**1.00**
4-Acetoxy MALT	0.00	0.00	0.00	0.00	0.00	0.00	0.00	0.00	0.00	**1.00**
4-Acetoxy MALT	0.00	0.00	0.00	0.00	0.00	0.00	0.00	0.00	0.00	**0.00**
4-Acetoxy MALT	0.00	0.00	0.00	0.00	0.00	0.00	0.00	0.00	0.00	**0.00**
4-Acetoxy MALT	0.00	0.00	0.00	0.00	0.00	0.00	0.00	0.00	0.00	**1.00**
4-Acetoxy MALT	0.00	0.00	0.00	0.00	0.00	0.00	0.00	0.00	0.00	**1.00**
4-Acetoxy MALT	0.00	0.00	0.00	0.00	0.00	0.00	0.00	0.00	0.00	**1.00**
4-Acetoxy MALT	0.00	0.00	0.00	0.00	0.00	0.00	0.00	0.00	0.00	**1.00**
4-Acetoxy MPT	0.00	0.00	0.00	0.00	0.00	0.00	0.00	0.00	0.00	**1.00**
4-Acetoxy MPT	0.00	0.00	0.00	0.00	0.00	0.00	0.00	0.00	0.00	**1.00**
4-Acetoxy MPT	0.00	0.00	0.00	0.00	0.00	0.00	0.00	0.00	0.00	**1.00**
4-Acetoxy MPT	0.00	0.00	0.00	0.00	0.00	0.00	0.00	0.00	0.00	**1.00**
4-Acetoxy MPT	0.00	0.00	0.00	0.00	0.00	0.00	0.00	0.00	0.00	**1.00**
4-Acetoxy MPT	0.00	0.00	0.00	0.00	0.00	0.00	0.00	0.00	0.00	**1.00**
4-Acetoxy MPT	0.00	0.00	0.00	0.00	0.00	0.00	0.00	0.00	0.00	**1.00**
4-Acetoxy MPT	0.00	0.00	0.00	0.00	0.00	0.00	0.00	0.00	0.00	**1.00**
4-Acetoxy MPT	0.00	0.00	0.00	0.00	0.00	0.00	0.00	0.00	0.00	**1.00**
4-Acetoxy MPT	0.00	0.00	0.00	0.00	0.00	0.00	0.00	0.00	0.00	**1.00**
4-Hydroxy MALT	0.00	0.00	0.00	0.00	0.00	0.00	**0.00**	0.00	0.00	0.00
4-Hydroxy MALT	0.00	0.00	0.00	0.00	0.00	0.00	**1.00**	0.00	0.00	0.00
4-Hydroxy MALT	0.00	0.00	0.00	0.00	0.00	0.00	**1.00**	0.00	0.00	0.00
4-Hydroxy MALT	0.00	0.00	0.00	0.00	0.00	0.00	**0.00**	0.00	0.00	0.00
4-Hydroxy MALT	0.00	0.00	0.00	0.00	0.00	0.00	**0.00**	0.00	0.00	0.00
4-Hydroxy MALT	0.00	0.00	0.00	0.00	0.00	0.00	**1.00**	0.00	0.00	0.00
4-Hydroxy MALT	0.00	0.00	0.00	0.00	0.00	0.00	**1.00**	0.00	0.00	0.00
4-Hydroxy MALT	0.00	0.00	0.00	0.00	0.00	0.00	**1.00**	0.00	0.00	0.00
4-Hydroxy MALT	0.00	0.00	0.00	0.00	0.00	0.00	**1.00**	0.00	0.00	0.00
4-Hydroxy MALT	0.00	0.00	0.00	0.00	0.00	0.00	**1.00**	0.00	0.00	0.00
4-Propanoyloxy DMT	0.00	0.00	0.00	0.00	0.00	0.00	0.00	0.00	0.00	**1.00**
4-Propanoyloxy DMT	0.00	0.00	0.00	0.00	0.00	0.00	0.00	0.00	0.00	**1.00**
4-Propanoyloxy DMT	0.00	0.00	0.00	0.00	0.00	0.00	0.00	0.00	0.00	**1.00**
4-Propanoyloxy DMT	0.00	0.00	0.00	0.00	0.00	0.00	0.00	0.00	0.00	**1.00**
4-Propanoyloxy DMT	0.00	0.00	0.00	0.00	0.00	0.00	0.00	0.00	0.00	**1.00**
4-Propanoyloxy DMT	0.00	0.00	0.00	0.00	0.00	0.00	0.00	0.00	0.00	**1.00**
4-Propanoyloxy DMT	0.00	0.00	0.00	0.00	0.00	0.00	0.00	0.00	0.00	**1.00**
4-Propanoyloxy DMT	0.00	0.00	0.00	0.00	0.00	0.00	0.00	0.00	0.00	**1.00**
4-Propanoyloxy DMT	0.00	0.00	0.00	0.00	0.00	0.00	0.00	0.00	0.00	**1.00**
4-Propanoyloxy DMT	0.00	0.00	0.00	0.00	0.00	0.00	0.00	0.00	0.00	**1.00**

Table A2.5 Mass data (*m/z* values and their relative intensities) for the DART-HRMS analysis of 4-hydroxy MALT.* The corresponding spectrum appears in Figure 2.11

4-Hydroxy MALT							
m/z	Rel. Int. %	*m/z*	Rel. Int. %	*m/z*	Rel. Int. %	*m/z*	Rel. Int. %
84.085	9.8335	231.487	0.2341	232.704	0.1431	248.283	0.2601
84.136	0.7674	231.524	0.2992	232.902	0.2081	248.320	0.2341
84.157	0.5333	231.560	0.2211	232.953	0.3122	249.168	0.1561
84.174	0.4032	231.767	0.1691	233.024	0.2862	263.154	0.4553
84.195	0.2992	231.807	0.2601	233.070	0.2341	291.188	0.4292
84.217	0.2732	231.873	0.4162	233.106	0.2081	299.082	0.0390
85.086	0.4943	231.946	0.3642	233.161	0.9755	314.239	0.4943
135.107	0.2081	232.012	0.2341	233.307	0.1561	373.115	0.3382
139.116	0.2732	232.053	0.2601	233.522	0.1691	457.295	0.2211
160.077	0.2081	232.088	0.2862	233.597	0.1951	458.289	0.2992
228.129	0.3122	232.155	14.2560	245.128	0.2992	473.292	0.8325
229.142	0.6764	232.373	0.6634	246.143	2.0812	473.603	0.1431
230.145	23.5822	232.453	0.3772	246.268	0.3382	474.306	0.1431
230.370	0.5723	232.499	0.3122	246.341	0.1561	474.424	0.0520
231.153	100.0000	232.578	0.3122	247.147	13.7357	475.294	0.3902
231.433	0.4292	232.614	0.2992	248.154	1.4958	475.438	0.1691
*The full name and structure are presented in Figure 2.1 in Chapter 2.							

Table A3.1 Plant materials analyzed and related taxonomical information including order, family, genus, and species, and the matrix of each.

Index	Order	Family	Genus	Species	Matrix	Vendor
1	Asterales	Asteraceae	*Artemisia*	*absinthium*	Dried herb	Brewer's Best
						Salem
					Powder	Penn Herb Co. Ltd.
					Seed	Strictly Medicinal Seeds
					Tincture	Herb Pharm
						Starwest Botanicals
2	Asterales	Asteraceae	*Artemisia*	*vulgaris*	Seed	World Seed Supply
3	Asterales	Asteraceae	*Calea*	*zacatechichi*	Leaf	World Seed Supply
					Seed pod	World Seed Supply
					Seed	World Seed Supply
					Syrup	Hawaii Pharm
					Tincture	Hawaii Pharm
4	Asterales	Asteraceae	*Lactuca*	*virosa*	Capsule	Swanson
					Leaf	Mr. Botanicals
						Schmerbals Herbals
						World Seed Supply
					Powder	Mr. Botanicals
						Schmerbals Herbal
						World Seed Supply
					Resin	World Seed Supply
					Seed	Schmerbals Herbal
						World Seed Supply
					Tincture	Schmerbals Herbal

Table A3.1 (continued). Plant materials analyzed and related taxonomical information including order, family, genus, and species, and the matrix of each.

Index	Order	Family	Genus	Species	Matrix	Vendor
5	Caryophyllales	Aizoaceae	*Sceletium*	*tortuosum*	Dried herb	eBay
						Herb Stomp
						Schmerbals Herbal
						World Seed Supply
					Extract	World Seed Supply
					Powder	Herb Stomp
						World Seed Supply
					Root	eBay
6	Cucurbitales	Cucurbitaceae	*Echinocystis*	*lobata*	Seed	Prairie Moon Nursery
7	Fabales	Fabaceae	*Anadenanthera*	*peregrina*	Seed	Herbal Flame
						World Seed Supply
8	Fabales	Fabaceae	*Mimosa*	*hostilis*	Bark	Mr. Botanicals
						Waking Herbs
					Powder	Heavenly Products
					Root	Unknown
					Seed	Heavenly Products
9	Gentianales	Apocynaceae	*Picralima*	*nitida*	Powder	World Seed Supply
					Seed	World Seed Supply
10	Gentianales	Apocynaceae	*Voacanga*	*africana*	Bark	World Seed Supply
					Powder	Amazon
						Om-Chi
					Seed	World Seed Supply
11	Gentianales	Rubiaceae	*Mitragyna*	*speciosa*	Capsule	Kratom Crazy
					Leaf	Kratom King
					Powder	Authentic Kratom
						Herbal Flame
						Kratom Underground

Table A3.1 (continued). Plant materials analyzed and related taxonomical information including order, family, genus, and species, and the matrix of each.

Index	Order	Family	Genus	Species	Matrix	Vendor
12	Gentianales	Rubiaceae	*Corynanthe*	*johimbe*	Bark	Bouncing Bear Botanicals
13	Gentianales	Rubiaceae	*Psychotria*	*viridis*	Leaf	Mr. Botanicals
					Powder	USA Botanicals
					Seed	World Seed Supply
14	Lamiales	Lamiaceae	*Leonotis*	*leonurus*	Extract	Schmerbals Herbals
					Flower	World Seed Supply
					Leaf	Herbal Fire Botanicals
					Powder	Herbal Fire Botanicals
15	Lamiales	Lamiaceae	*Leonotis*	*nepetifolia*	Flower	Schmerbals Herbals
16	Lamiales	Lamiaceae	*Leonurus*	*sibiricus*	Extract	Mr. Botanicals
17	Lamiales	Lamiaceae	*Salvia*	*divinorum*	Leaf	Arena Ethnobotanicals
						Salvia Dragon
18	Lamiales	Oleaceae	*Syringa*	*vulgaris*	Leaf	Unknown
19	Malpighiales	Malpighiaceae	*Banisteriopsis*	*caapi*	Leaf	World Seed Supply
					Powder	World Seed Supply
					Rootbark	World Seed Supply
					Seed	World Seed Supply
20	Malpighiales	Malpighiaceae	*Diplopterys*	*cabrerana*	Leaf	Herbal Flame
					Powder	USA Botanicals
21	Malpighiales	Passifloraceae	*Turnera*	*diffusa*	Capsule	Penn Herb Co. Ltd.
					Extract	Strictly Medicinal Seeds
					Leaf	Bouncing Bear Botanicals
						Monterey Bay Spice Co.
					Powder	Monterey Bay Spice Co.
22	Malvales	Malvaceae	*Althaea*	*officinalis*	Leaf	Bouncing Bear Botanicals
						World Seed Supply
23	Malvales	Malvaceae	*Thespesia*	*populnea*	Seeds	Amazon

Table A3.1 (continued). Plant materials analyzed and related taxonomical information including order, family, genus, and species, and the matrix of each.

Index	Order	Family	Genus	Species	Matrix	Vendor
24	Nymphaeales	Nymphaeaceae	*Nymphaea*	*caerulea*	Extract	Unknown
					Flower	Schmerbals Herbals
					Leaves	World Seed Supply
					Powder	Herb Stomp
						Lotus Extracts
					Resin	Etsy (Schmerbals Herbals)
					Seed	World Seed Supply
					Tincture	World Seed Supply
25	Piperales	Piperaceae	*Piper*	*betel*	Leaf	Live Plant
					Essential Oil	Healing Solutions
26	Piperales	Piperaceae	*Piper*	*methysticum*	Capsule	Starwest Botanicals
					Powder	Bouncing Bear Botanicals
						World Seed Supply
					Root	Bouncing Bear Botanicals
					Tincture	Herbal Island
						Root of Happiness
						Happy Kava Brand
27	Ranunculales	Ranunculaceae	*Actaea*	*racemosa*	Root	Bouncing Bear Botanicals
28	Rosales	Cannabaceae	*Cannabis*	*sativa*	Flower	Berkshire CBD
						Plain Jane
						Stewart Rose Farms
29	Sapindales	Nitrariaceae	*Peganum*	*harmala*	Capsule	Herb Stomp
					Seed	World Seed Supply
					Powder	Waking Herbs
30	Solanales	Convolvulaceae	*Argyreia*	*nervosa*	Seed	World Seed Supply
31	Solanales	Convolvulaceae	*Convolvulus*	*tricolor*	Seed	World Seed Supply
32	Solanales	Convolvulaceae	*Ipomoea*	*tricolor*	Seed	World Seed Supply

Table A3.1 (continued). Plant materials analyzed and related taxonomical information including order, family, genus, and species, and the matrix of each.

Index	Order	Family	Genus	Species	Matrix	Vendor
33	Solanales	Solanaceae	*Atropa*	*baetica*	Seed	eBay
34	Solanales	Solanaceae	*Atropa*	*belladonna*	Seed	World Seed Supply
					Extract	Hawaii Pharm
35	Solanales	Solanaceae	*Atropa*	*komarovii*	Seed	Strictly Medicinal Seeds
36	Solanales	Solanaceae	*Brugmansia*	*arborea*	Seed	Georgia Vines
37	Solanales	Solanaceae	*Brugmansia*	*aurea*	Seed	Seedman's
38	Solanales	Solanaceae	*Brugmansia*	*sanguinea*	Seed	Seedman's
39	Solanales	Solanaceae	*Brugmansia*	*suaveolens*	Seed	Seedman's
40	Solanales	Solanaceae	*Brugmansia*	*versicolor*	Seed	Seedman's
41	Solanales	Solanaceae	*Datura*	*ceratocaula*	Seed	World Seed Supply
						Georgia Vines
						Hudson
42	Solanales	Solanaceae	*Datura*	*discolor*	Seed	World Seed Supply
						Hudson
43	Solanales	Solanaceae	*Datura*	*ferox*	Seed	World Seed Supply
						Georgia Vines
44	Solanales	Solanaceae	*Datura*	*innoxia*	Seed	World Seed Supply
						Georgia Vines
						Horizon Herbs
45	Solanales	Solanaceae	*Datura*	*leichhardtii*	Seed	Hudson
46	Solanales	Solanaceae	*Datura*	*metel*	Seed	Georgia Vines
47	Solanales	Solanaceae	*Datura*	*parajuli*	Seed	Georgia Vines
48	Solanales	Solanaceae	*Datura*	*quercifolia*	Seed	Hirts Gardens

Table A3.1 (continued). Plant materials analyzed and related taxonomical information including order, family, genus, and species, and the matrix of each.

Index	Order	Family	Genus	Species	Matrix	Vendor
49	Solanales	Solanaceae	*Datura*	*stramonium*	Seed	World Seed Supply
						Hudson
						Horizon Herbs
						Georgia Vines
					Powder	Amazon Shopping Universe
50	Solanales	Solanaceae	*Datura*	*wrightii*	Seed	Georgia Vines
						Hudson
51	Solanales	Solanaceae	*Hyocyamus*	*albus*	Seed	eBay
52	Solanales	Solanaceae	*Hyocyamus*	*aureus*	Seed	eBay
53	Solanales	Solanaceae	*Hyocyamus*	*muticus*	Seed	eBay
54	Solanales	Solanaceae	*Hyocyamus*	*niger*	Seed	Horizon Herbs
						Amazon
55	Solanales	Solanaceae	*Hyocyamus*	*pusillus*	Seed	eBay
56	Solanales	Solanaceae	*Mandragora*	*autumnalis*	Seed	Amazon
57	Solanales	Solanaceae	*Mandragora*	*officinarum*	Seed	eBay
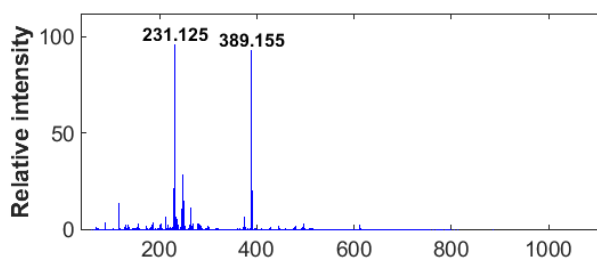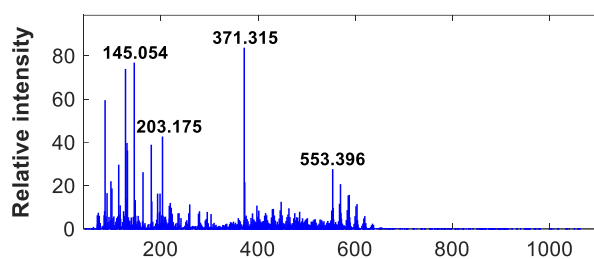
Figure A3.1 Representative DART high-resolution mass spectra of *A. absinthium*; *A. vulgaris*; *C. zacatechichi*; *L. virosa*; *S. tortuosum*; *E. lobata*; *A. peregrina*; *M. hostilis*; *P. nitida*; and *V. africana*.
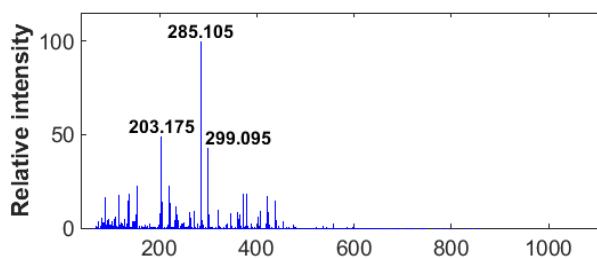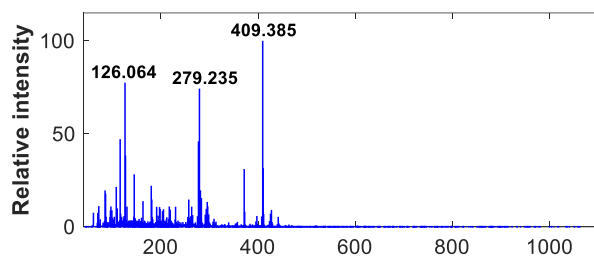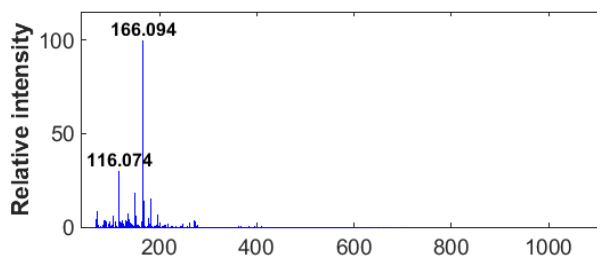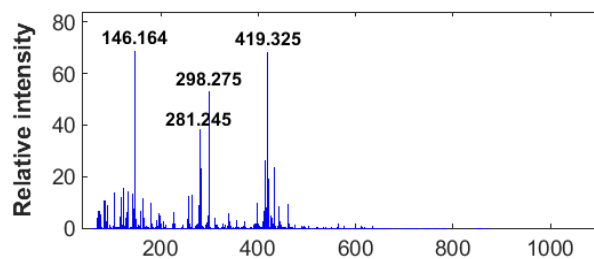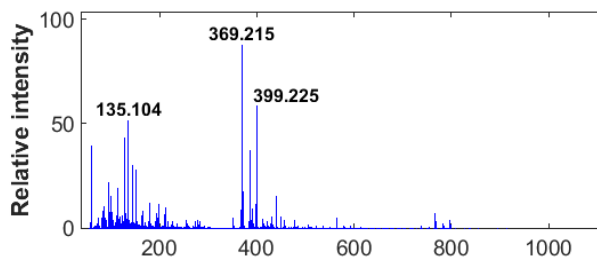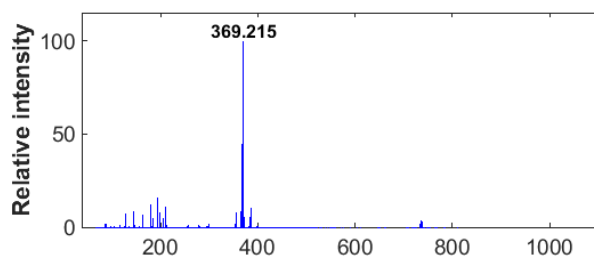
Figure A3.1 (continued). Representative DART high-resolution mass spectra of *M. speciosa*, *C. johimbe*; *P. viridis*; *L. leonurus*; L. *nepetifolia; L. sibiricus*; *S. divinorum*; *S. vulgaris*; *B. caapi* and *D. cabrerana*.
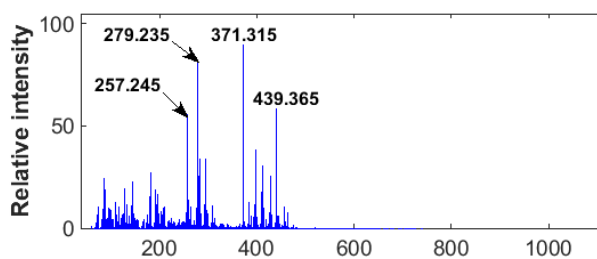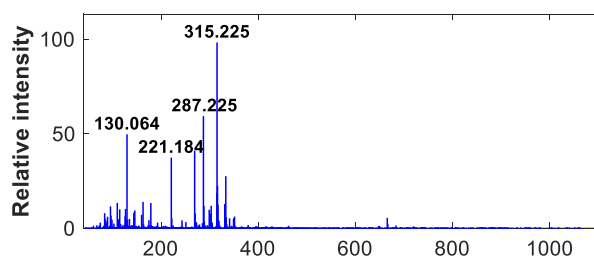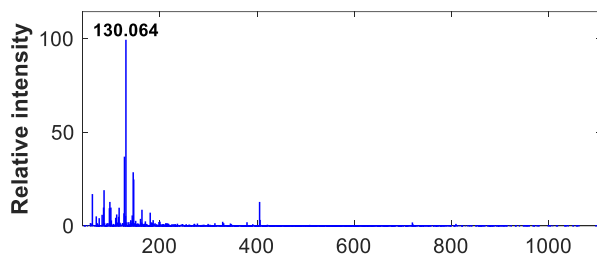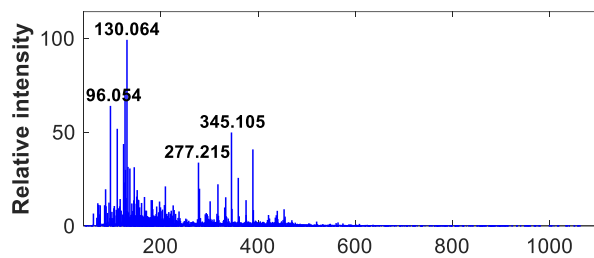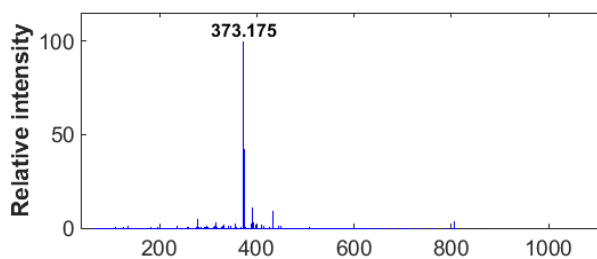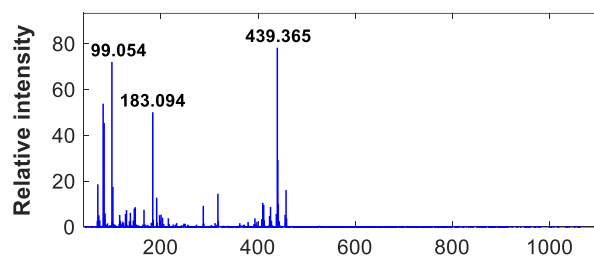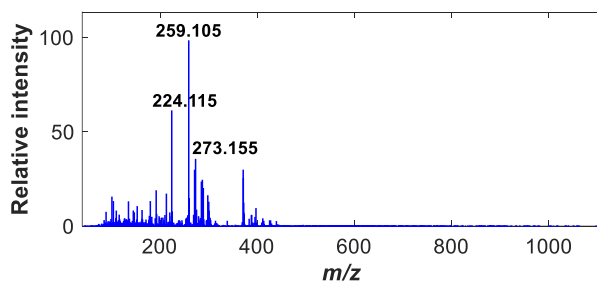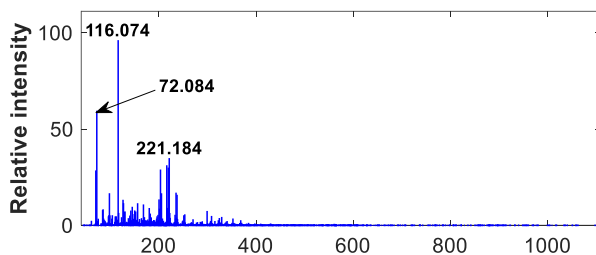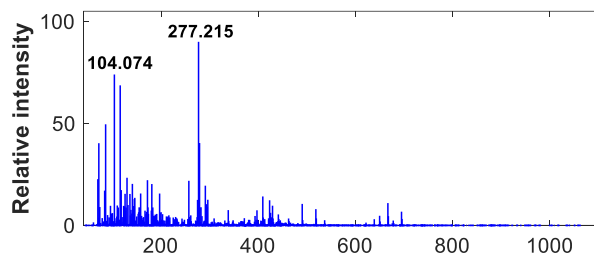
Figure A3.1 (continued). Representative DART high-resolution mass spectra of *T. diffusa*; *A. officinalis*; *T. populnea*; *N. caerulea*; *P. betel*; *P. methysticum*; *A. racemosa*; *C. sativa*; *P. harmala* and *A. nervosa*.
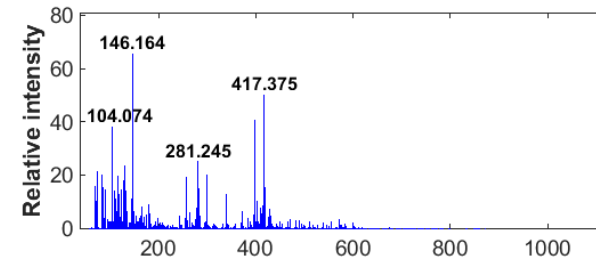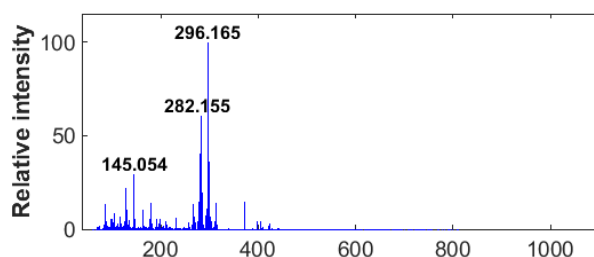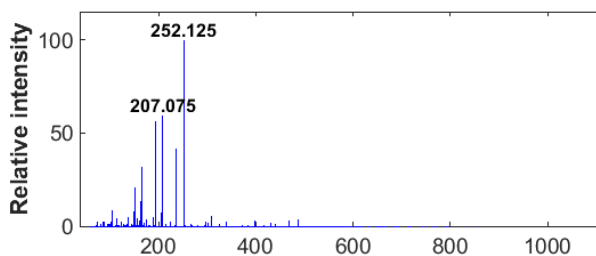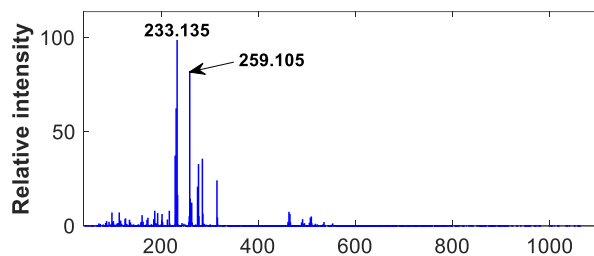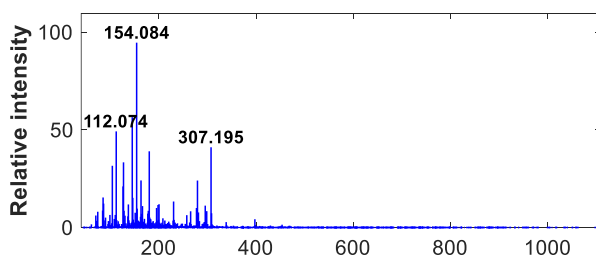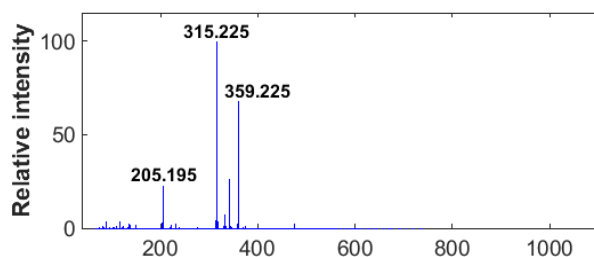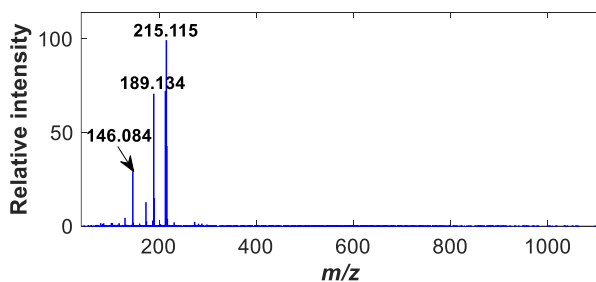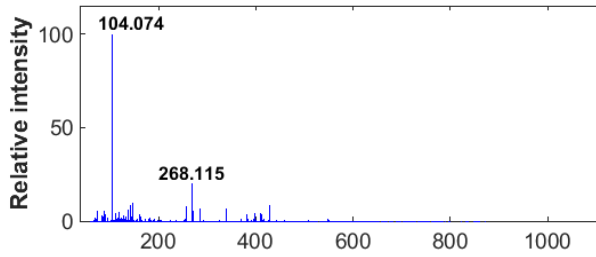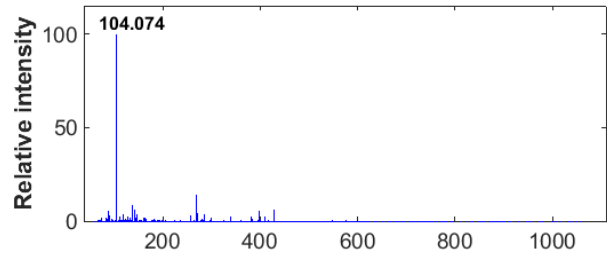
Figure A3.1 (continued). Representative DART high-resolution mass spectra of *C. tricolor*; *I. tricolor*; *A. baetica*; *A. belladonna*; *A. Komarovii*; *B. arborea*; *B. aurea*; *B. sanguinea*; *B. suaveolens* and *B. versicolor*.
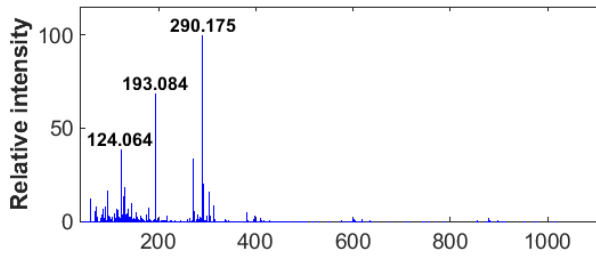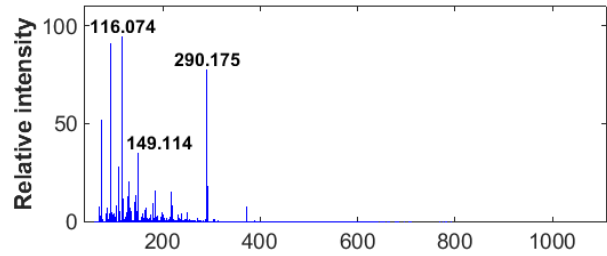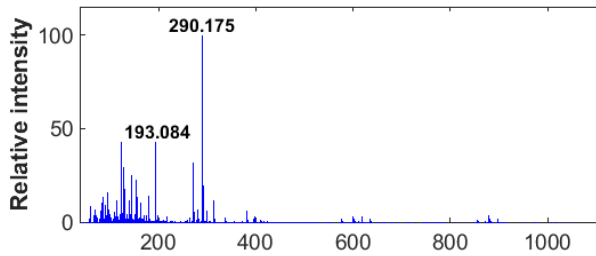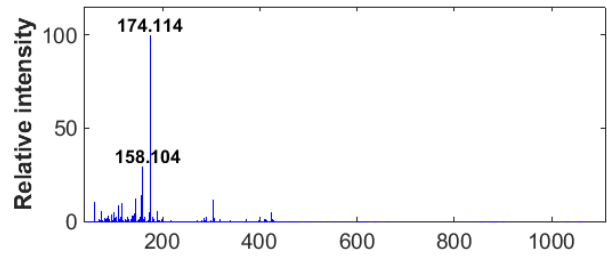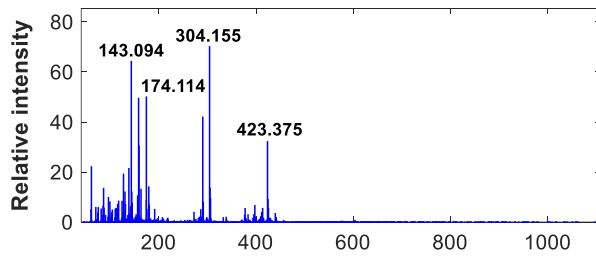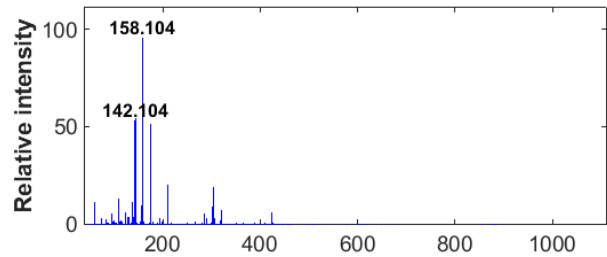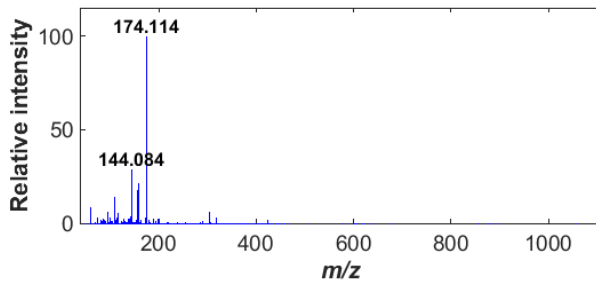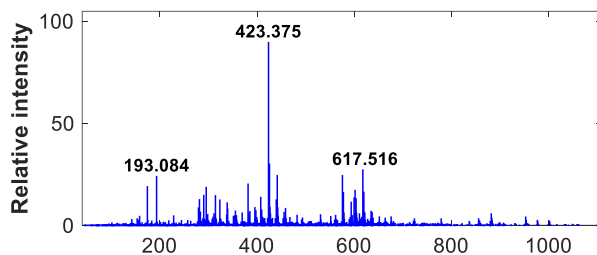
Figure A3.1 (continued). Representative DART high-resolution mass spectra of *D. ceratocaula*; *D. discolor*; *D. ferox*; *D. innoxia*; *D. leichhardtii*; *D. metel*; *D. parajuli*; *D. quercifolia*; *D. stramonium* and *D. wrightii*.
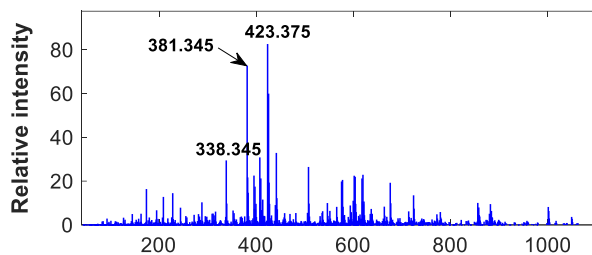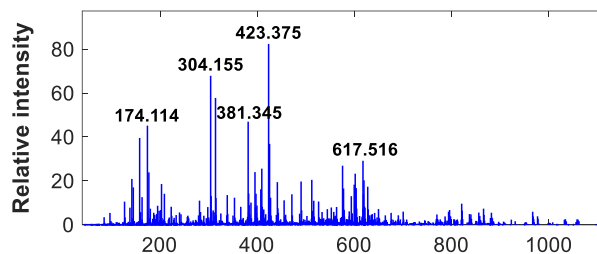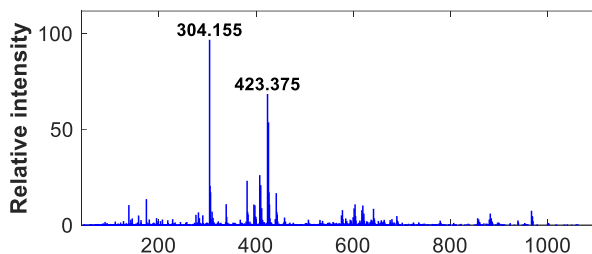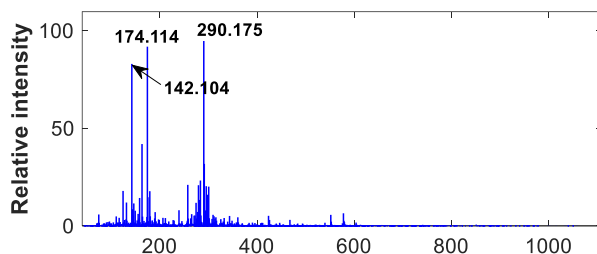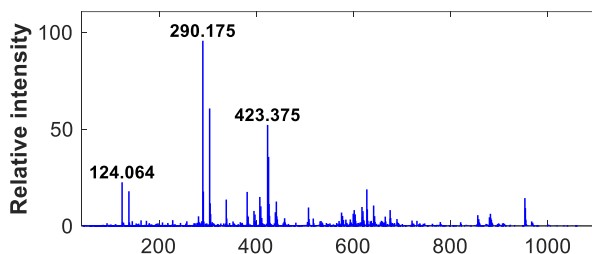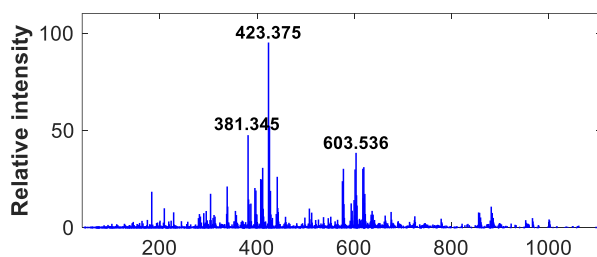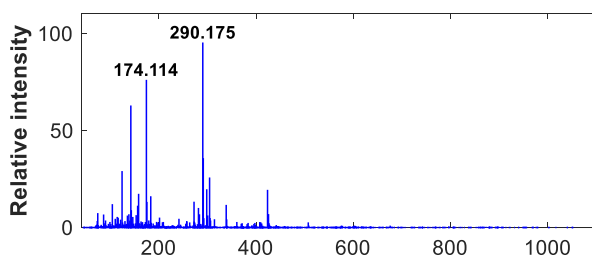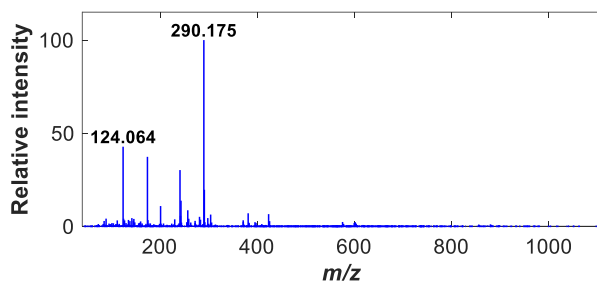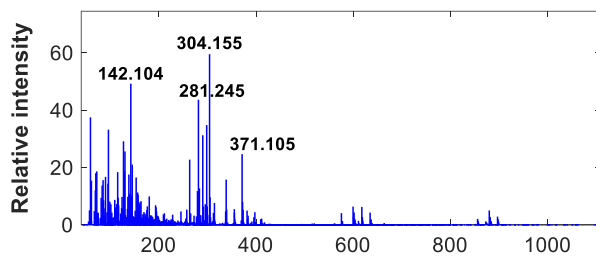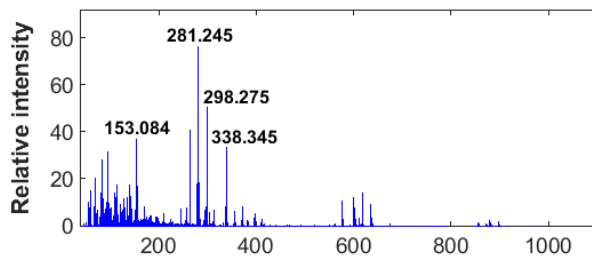
Figure A3.1 (continued). Representative DART high-resolution mass spectra of *H. albus*; *H. aureus*; *H. muticus*; *H. niger*; *H. pusillus*; *M. autumnalis*; and *M. officinarum*.
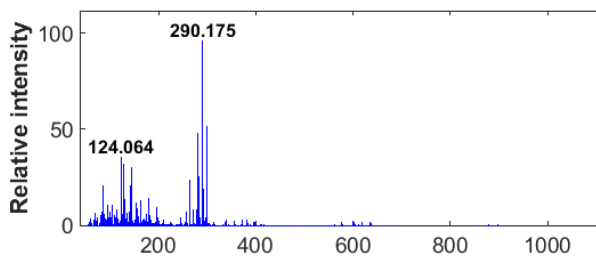
Table A3.2 Mass data (*m/z* values and their relative intensities) for the DART-HRMS analysis of *A. absinthium* dried herb. Ten replicates of one sample were averaged where the corresponding spectrum appears in Figure 3.1.

				A. Absinthium dried herb			
m/z	Rel. Int. %	*m/z*	Rel. Int. %	*m/z*	Rel. Int. %	*m/z*	Rel. Int. %
61.0339	0.0103	97.0941	0.2767	122.0742	0.0095	143.0943	0.3191
61.1041	0.0107	97.2241	0.0263	123.0942	0.3783	144.0843	0.4655
65.0541	0.0438	97.2841	0.0065	124.0642	0.2421	144.2443	0.0084
67.0540	0.0014	98.0841	0.0098	124.1844	0.0044	145.0543	0.7781
69.0440	0.0534	99.0541	0.3235	125.0942	0.3040	145.1243	0.8671
69.1440	0.0014	100.0041	0.0032	125.2144	0.0106	145.2243	0.0725
70.0640	1.1975	101.0641	0.3775	126.0642	0.1355	146.0843	0.3291
71.0640	0.0891	101.1841	0.0154	126.1542	0.0597	147.0743	0.6616
72.0840	0.7674	103.0541	0.1255	127.0442	1.4916	148.0745	0.0945
73.0640	0.6615	103.1443	0.0076	127.1142	0.3728	148.1544	0.0112
75.0440	0.1119	104.0741	0.9407	127.2342	0.0452	149.1142	0.3053
76.0640	0.0463	104.1443	0.0242	129.0641	0.1430	149.9942	0.0414
77.0440	0.0330	104.2343	0.0181	130.0643	2.5421	150.0942	0.6467
78.0440	0.0058	105.0641	0.0328	131.0643	0.3623	150.2342	0.0023
79.0440	0.0983	106.0641	0.0333	131.2243	0.0687	150.3142	0.0084
80.0540	0.0216	107.0841	0.4690	132.1041	0.7577	151.1042	0.7084
81.0540	0.1701	109.0340	0.2143	133.0643	1.0672	152.1144	0.2459
82.0642	0.0089	109.0942	0.3018	133.2543	0.0238	152.2444	0.0029
82.9442	0.0504	110.0742	0.1489	134.0843	0.1029	153.0844	1.2883
83.0840	0.1984	112.0742	0.2875	134.2543	0.0046	154.0844	0.2562
84.0640	0.3370	112.1542	0.0108	135.1043	2.7948	154.1544	0.1397
84.9540	0.0434	113.0542	0.2253	135.2443	0.0045	155.0100	0.0098
85.0342	0.3426	115.0542	0.4653	136.0643	1.2452	155.1044	0.2440
85.0942	0.2451	115.1040	0.0043	136.1343	0.0522	156.1042	0.6189
86.0740	0.0897	115.2442	0.0051	136.2843	0.0019	156.2744	0.0050
87.0539	0.4205	116.0742	13.8110	137.0743	0.1261	157.1242	3.1300
89.0641	3.6116	116.2242	0.1842	137.1243	1.3893	157.2644	0.0926
89.2541	0.0134	117.0642	0.8002	137.2843	0.0285	158.1044	0.5273
90.0641	0.4745	117.2442	0.0169	138.0843	0.0897	159.0544	0.0175
90.1641	0.0234	118.0842	0.7446	138.1643	0.1461	159.1244	1.0228
91.0541	0.2234	118.2042	0.0160	139.1043	0.1135	160.0944	0.1695
92.0641	0.0010	119.0042	0.0022	139.2643	0.0077	162.0844	0.0447
93.0641	0.5762	119.0842	1.1245	140.0843	0.1230	162.2244	0.0120
93.1341	0.0331	120.0742	0.1923	141.1043	0.4994	164.0844	0.0880
95.0841	0.0498	120.2042	0.0169	142.1043	0.2821	165.0844	0.1794
96.0541	0.0574	121.0842	0.2530	142.1843	0.0708	165.1794	0.1468

Table A3.2 (continued). Mass data (*m/z* values and their relative intensities) for the DART-HRMS analysis of *A. absinthium* dried herb. Ten replicates of one sample were averaged where the corresponding spectrum appears in Figure 3.1.

A. Absinthium dried herb							
m/z	**Rel. Int. %**	*m/z*	**Rel. Int. %**	*m/z*	**Rel. Int. %**	*m/z*	**Rel. Int. %**
165.2744	0.0382	191.0678	0.9779	212.1045	6.6367	230.1047	6.6597
166.0944	0.4472	191.1644	0.5446	212.3345	0.1007	230.3547	0.1483
166.1944	0.0225	191.3244	0.0710	213.1145	1.0094	231.1247	96.4495
167.0944	0.4670	192.1044	0.1558	213.3445	0.0028	231.3247	0.5285
167.2544	0.0224	192.1644	0.1367	213.7345	0.0059	232.0389	0.2011
168.0944	0.5062	193.0844	0.5299	214.1245	0.2000	232.1346	15.9118
168.1744	0.0028	193.1544	0.0839	214.2545	0.0669	233.1346	6.6581
168.9844	0.0152	194.0944	0.0978	215.1145	1.1508	234.1346	1.2035
169.1144	0.1279	195.0946	1.1067	215.1895	0.0345	234.3546	0.1180
170.0943	0.1279	196.0946	0.4054	215.3545	0.0732	235.1746	5.6539
170.3143	0.0017	196.2794	0.0035	216.1245	0.7341	236.1746	0.9743
171.3143	0.0122	197.1144	0.4790	216.3345	0.0046	237.1846	2.5558
173.1143	2.1475	197.3344	0.0299	217.0770	1.2351	238.1946	0.4351
174.1143	0.2684	198.1044	0.8119	217.1745	2.4711	238.3846	0.0381
174.2843	0.0047	199.1044	0.4638	217.3645	0.0084	239.2346	0.7183
175.1245	0.6912	199.1744	0.1831	218.1345	0.8625	240.2146	0.1565
176.0945	0.1618	200.1244	0.4351	219.1045	0.4969	240.3046	0.0020
177.1443	0.1193	201.1444	2.6985	219.1845	1.1242	241.1846	0.1742
178.0945	0.0611	202.1244	0.5626	220.1145	0.1135	242.1846	0.0594
178.2443	0.0028	202.2846	0.0224	220.1745	0.2415	243.1046	1.1888
179.0845	0.3001	203.1746	3.4862	220.3347	0.0304	243.4048	0.0245
180.0845	0.9556	203.3346	0.0804	221.1845	1.5384	244.1148	1.1306
181.1045	0.7530	204.0244	0.0201	222.1245	0.0279	245.1246	10.8140
182.1045	0.3731	204.1844	0.5458	222.2045	0.1876	246.1148	2.4493
183.0945	1.3478	205.1046	0.6295	223.1247	0.7173	247.1246	28.5924
184.1145	0.3584	205.1946	0.7580	224.1147	0.1773	248.1346	6.0560
185.1145	2.8489	205.4046	0.0077	224.2545	0.0076	248.3297	0.1660
185.3245	0.0452	206.1146	0.3616	225.1447	0.4686	248.4046	0.0170
186.1145	1.1025	207.1546	0.5920	226.1247	0.0910	249.1646	14.9570
187.1245	3.6293	208.1146	0.2473	226.2547	0.0173	250.0646	0.0367
188.0945	0.0541	208.2096	0.1076	227.1347	1.3462	250.1548	2.5904
188.1645	0.5228	209.1346	0.5293	227.4147	0.0055	251.1648	6.9254
188.2445	0.0251	210.1046	0.2059	228.1247	0.3376	252.1847	1.1082
189.1345	0.4723	210.3596	0.0035	228.1947	0.0074	253.1847	1.8786
189.2345	0.0260	211.1345	0.4213	229.1047	21.5507	254.1847	0.3533
190.1244	0.1646	211.3145	0.0032	230.0147	0.0432	255.2247	0.2778

Table A3.2 (continued). Mass data (*m/z* values and their relative intensities) for the DART-HRMS analysis of *A. absinthium* dried herb. Ten replicates of one sample were averaged where the corresponding spectrum appears in Figure 3.1.

				A. Absinthium dried herb			
m/z	Rel. Int. %	*m/z*	Rel. Int. %	*m/z*	Rel. Int. %	*m/z*	Rel. Int. %
256.1447	0.0979	277.1146	0.5629	293.2148	0.3523	309.2849	0.0765
256.2447	0.0013	277.2148	0.9249	294.2147	0.1845	309.3549	0.0096
257.2447	0.2926	277.4548	0.0137	294.2949	0.0122	310.2449	0.1432
258.1647	0.0056	277.5248	0.0367	295.1547	0.2914	311.2349	0.2122
258.2547	0.0382	278.1248	0.5250	295.2347	0.9490	311.2749	0.0122
258.4347	0.0120	278.2148	0.0442	296.1649	0.6648	312.1649	0.1864
259.1047	0.1386	279.1546	2.9828	296.2549	0.3916	313.2149	0.1947
259.1947	0.1312	279.2348	1.4216	296.4747	0.0346	314.1548	0.4680
260.1147	0.6115	279.4048	0.0518	296.5247	0.0414	315.2248	0.5284
260.2547	0.0740	280.1448	1.1641	297.1847	0.4220	315.4448	0.0045
261.1147	2.7603	280.2446	0.0515	297.2449	0.0293	316.2250	0.7279
261.4647	0.0334	281.1448	3.5252	298.1649	2.0457	317.2348	0.9132
262.1847	1.8883	281.2448	0.9167	298.2749	0.3801	318.2248	0.3985
263.1347	11.7712	282.1548	2.5584	298.4049	0.0497	319.2348	0.8498
263.3147	0.1482	282.5246	0.0514	298.5049	0.0844	320.2350	0.4359
263.3849	0.2582	283.1848	0.8467	299.1949	0.6079	321.2350	0.3583
264.1249	2.2729	283.2648	0.7140	299.2749	0.6170	322.2450	0.2283
265.1547	6.4006	284.1548	1.6367	300.1949	2.1376	323.2548	0.1833
266.1447	2.2691	285.2748	1.8634	300.3749	0.0190	324.1750	0.0441
267.1547	1.8474	286.0281	0.0019	300.4249	0.1467	324.2650	0.0835
268.2047	3.4775	286.2148	0.4580	301.0949	0.3497	325.1950	0.0139
269.2147	1.1767	287.0648	0.0194	301.2049	1.0255	325.2850	0.1409
270.2049	0.3680	287.3048	0.8782	301.2949	1.2389	326.1850	0.1078
270.3849	0.0184	287.4748	0.0223	302.2149	0.4476	326.2950	0.0448
271.2347	0.4174	288.2448	0.2709	302.3049	0.5182	327.1950	0.1663
272.2547	0.1377	289.1748	0.0683	303.1249	0.0374	327.2850	0.1140
272.4649	0.0017	289.2348	0.2041	303.2249	0.3298	328.2250	0.1651
273.2446	0.1538	289.4048	0.0107	303.3049	0.2373	328.3248	0.0867
274.1548	0.0199	289.4748	0.0039	304.2349	0.2258	329.2350	0.2939
274.2648	0.0858	290.1748	0.1165	305.2349	0.2478	329.3150	0.0432
274.4148	0.0129	290.2748	0.0114	306.2749	0.0442	330.1650	0.1539
275.1046	0.0288	290.4048	0.0030	307.1949	0.2504	330.2350	0.0960
275.2046	0.0707	291.1948	0.3319	307.3449	0.0110	330.3350	0.0795
275.2648	0.0243	291.4148	0.0381	308.2349	0.0703	331.0950	0.1289
276.1648	0.0641	292.1148	0.0264	308.3315	0.0049	331.2250	0.3449
276.2748	0.0127	292.1948	0.1285	309.2149	0.2255	332.2150	0.3682

Table A3.2 (continued). Mass data (*m/z* values and their relative intensities) for the DART-HRMS analysis of *A. absinthium* dried herb. Ten replicates of one sample were averaged where the corresponding spectrum appears in Figure 3.1.

A. Absinthium dried herb							
m/z	**Rel. Int. %**	*m/z*	**Rel. Int. %**	*m/z*	**Rel. Int. %**	*m/z*	**Rel. Int. %**
332.2950	0.0110	348.1851	0.2357	368.2652	0.3758	378.2651	0.0457
332.3550	0.0364	348.2949	0.0281	369.2150	0.3846	379.2651	0.2284
333.2350	0.2885	349.2151	0.4591	369.3452	0.0392	379.3451	0.1396
334.2350	0.3477	349.3351	0.0143	369.4852	0.0070	380.2051	0.5685
334.3350	0.0225	350.2351	0.3193	369.5650	0.0686	381.1951	0.4738
335.2049	0.4132	350.3751	0.0092	370.2150	0.3129	382.1951	0.5930
336.1849	0.4307	351.2451	0.2690	370.4337	0.0035	383.1951	0.2501
336.2549	0.0254	352.2451	0.3985	371.1052	0.5709	383.2951	0.2392
336.4749	0.0798	352.3251	0.0859	371.2250	0.1134	384.2051	0.2527
337.2049	0.2418	353.2651	0.3502	371.3152	1.4951	384.2751	0.0191
337.2651	0.1562	354.2651	0.3666	371.5852	0.0589	385.2151	0.6009
337.3451	0.0828	354.3351	0.0189	371.6750	0.0400	385.4851	0.0196
338.1951	0.2772	355.1950	0.0804	371.7551	0.0037	386.2153	0.2895
338.2649	0.0640	355.2950	0.1886	371.8352	0.0089	387.1053	0.2876
338.3449	0.3800	355.3550	0.0259	372.1152	0.2470	387.2253	0.2203
338.4849	0.0066	356.2850	0.2995	372.2352	0.1564	387.6051	0.0300
338.6049	0.0801	357.2050	0.3576	372.3152	0.4610	388.1351	2.5599
339.1849	0.2712	357.2950	0.0231	372.4152	0.0166	388.3451	0.3120
339.3251	0.0190	358.2152	0.2209	372.6450	0.0120	388.4351	0.0286
340.2651	0.0084	358.3650	0.0124	372.8352	0.0141	388.5351	0.1446
340.3449	0.0957	359.1350	0.6659	372.9152	0.0019	389.1553	93.3380
341.2149	0.1291	359.2250	0.2333	373.1052	0.0392	390.1353	20.6033
341.3149	0.0533	359.3850	0.0101	373.1752	0.2512	390.3351	0.0436
342.2151	0.1249	359.5150	0.0493	373.3152	0.0525	391.1753	3.6669
343.1649	0.1543	359.5850	0.0160	374.0952	0.1657	391.2951	0.5194
343.2351	0.0928	360.1550	0.0648	374.1652	0.0156	391.3901	0.1086
343.3351	0.0886	360.2252	0.2186	374.2652	0.2068	391.4851	0.2805
344.1751	0.1629	361.1550	0.2831	375.1052	6.9154	392.1851	0.5212
344.2651	0.0050	361.2352	0.2504	376.1451	1.2958	392.2853	0.0291
344.3951	0.0078	362.1652	0.3070	376.2551	0.0211	393.1853	0.1063
345.1051	0.1814	362.3750	0.0746	376.5751	0.0389	393.2652	0.1124
345.1849	0.4813	363.2452	0.2324	377.1851	0.2867	393.3451	0.2478
346.1751	0.3813	364.1952	0.6589	377.2551	0.0368	393.4453	0.1019
347.0851	0.0423	365.2750	0.4684	377.4251	0.0849	394.1853	0.2769
347.1649	0.3560	366.2652	0.5683	377.5251	0.0647	394.3353	0.1177
348.1149	0.0071	367.2750	0.5611	378.1851	0.2822	395.0553	0.0170

Table A3.2 (continued). Mass data (*m/z* values and their relative intensities) for the DART-HRMS analysis of *A. absinthium* dried herb. Ten replicates of one sample were averaged where the corresponding spectrum appears in Figure 3.1.

m/z	Rel. Int. %	*m/z*	Rel. Int. %	*m/z*	Rel. Int. %	*m/z*	Rel. Int. %
395.1953	0.3058	411.1952	0.1651	427.2253	0.1631	445.2154	1.9096
395.3653	0.2034	411.3852	0.4576	427.3953	0.3220	446.2254	0.6708
396.2053	0.6152	411.6254	0.0456	428.2353	0.2297	446.3854	0.0722
396.3753	0.0989	411.6954	0.0477	428.3955	0.1740	447.2254	0.5873
397.2152	0.3793	412.2052	0.3122	428.4953	0.0429	448.2054	0.3466
397.3852	0.4830	412.3852	0.1887	429.1653	1.3950	449.3254	0.4519
398.2152	0.7900	413.2152	0.5100	429.3853	0.5338	449.5154	0.0107
398.3950	0.1526	413.3754	0.0159	430.3853	0.1562	450.3454	0.2298
398.5452	0.0489	414.2154	0.2606	430.5553	0.0631	450.5154	0.0288
399.2252	0.5552	414.3854	0.1629	431.2253	0.5304	451.3454	0.1927
400.2352	0.2904	414.6152	0.0353	431.3853	0.0218	452.4854	0.0131
400.3552	0.0881	415.2254	0.4860	432.1853	0.2289	453.3554	0.1499
400.4452	0.0122	416.2354	0.2882	432.3153	0.0230	453.4654	0.0085
401.2252	0.3337	416.4452	0.0020	432.3955	0.0094	454.3454	0.0270
401.4652	0.0063	417.2553	0.2711	433.2555	0.5095	454.4956	0.0271
402.2252	0.1852	417.4553	0.0120	434.2653	0.1552	455.3556	0.2042
402.3352	0.0420	418.2253	0.2267	435.2253	0.2454	456.2854	0.0835
403.1952	0.0642	418.2953	0.0167	435.4655	0.0811	456.3754	0.0367
403.2952	0.1352	418.4553	0.0442	436.3353	0.1328	456.5156	0.0276
404.1552	0.1457	419.3253	0.2074	437.2753	0.1264	457.2256	0.2287
404.2952	0.0149	420.2553	0.0937	437.3455	0.0967	457.3054	0.0371
405.1952	0.0323	421.2753	0.1794	437.4755	0.0042	457.3754	0.1494
405.2752	0.2884	421.3453	0.0797	438.3552	0.1148	458.2354	0.0350
405.3752	0.1242	421.4653	0.0062	438.4852	0.0063	458.3853	0.0358
405.4552	0.0080	422.2053	0.0682	439.2903	0.1402	459.3053	0.6503
406.1952	0.1319	422.3453	0.1130	439.3652	0.2023	460.3053	0.2405
406.2852	0.1172	423.2753	0.1499	440.3654	0.0950	460.4955	0.0054
406.3854	0.0691	423.3753	0.5305	441.2154	0.0826	461.2053	0.2104
407.2652	0.1649	424.2653	0.0121	441.3754	0.2339	461.3055	0.3219
407.3652	0.1579	424.3753	0.3146	442.3054	0.1229	462.2055	0.2915
407.4652	0.0097	425.2053	0.0182	442.3854	0.1442	463.2155	0.3591
408.3752	0.0106	425.2853	0.1306	443.2954	0.1172	463.3153	0.1073
409.2052	0.1282	425.3753	0.8201	443.3854	0.2198	463.3855	0.0460
409.3852	0.5986	426.2253	0.0171	444.2354	0.1639	464.2255	0.3276
410.2252	0.2495	426.3153	0.1626	444.2954	0.0288	465.3255	0.2974
410.3854	0.1680	426.3853	0.0762	444.4054	0.0235	465.3955	0.0165

Table A3.2 (continued). Mass data (*m/z* values and their relative intensities) for the DART-HRMS analysis of *A. absinthium* dried herb. Ten replicates of one sample were averaged where the corresponding spectrum appears in Figure 3.1.

				***A. Absinthium* dried herb**			
m/z	Rel. Int. %	*m/z*	Rel. Int. %	*m/z*	Rel. Int. %	*m/z*	Rel. Int. %
465.4855	0.0101	484.3956	0.0091	507.2155	0.3584	526.5658	0.0060
466.2355	0.2080	484.5456	0.0495	507.5155	0.0248	527.2156	0.4552
466.5055	0.0139	485.3354	0.1531	508.2355	0.2107	527.3456	0.0568
467.3255	0.1847	485.4056	0.0319	508.3557	0.0648	527.5256	0.1740
467.3955	0.1999	486.3254	0.1032	509.2255	0.9064	528.3458	0.3157
468.3955	0.0060	486.3854	0.1006	509.5257	0.0790	529.2658	0.2265
468.4955	0.0123	487.3156	0.0639	510.2257	0.2398	529.3256	0.2280
469.3353	0.1448	487.3854	0.0395	510.4157	0.0195	531.3158	0.2573
470.3455	0.0528	488.4656	0.0149	511.2557	0.9316	532.3358	0.2041
470.4155	0.0419	488.5456	0.0203	511.3257	0.2488	533.3556	0.0962
470.5055	0.0340	489.1956	0.1489	512.5757	0.0652	533.4407	0.0130
471.2455	0.0834	489.3056	0.1039	513.3357	0.8361	533.5258	0.0618
471.3255	0.1393	489.3756	0.0631	514.3357	0.8057	534.3656	0.1201
471.3855	0.0120	490.2156	0.0195	515.3257	0.2751	535.3656	0.1193
471.4955	0.0578	490.3254	0.1421	515.4257	0.0264	535.5358	0.0177
472.2555	0.0151	491.2156	0.8755	516.3457	0.1715	536.3158	0.0514
472.3455	0.1317	492.2256	0.2975	516.4257	0.0115	536.3858	0.0027
473.2255	0.3139	493.2456	1.6431	517.3257	0.1648	536.5358	0.0179
473.3755	0.0371	495.2656	3.4204	517.4457	0.0222	536.6058	0.0104
474.2857	0.1962	496.3256	1.0950	518.3457	0.0859	537.3958	0.0687
474.3855	0.1687	497.3256	1.5815	518.4357	0.0060	537.5058	0.0536
475.3055	0.9827	498.3256	0.6004	518.5157	0.0272	537.6158	0.0079
475.3855	0.0141	499.3256	0.2394	519.3457	0.0192	538.3158	0.0101
477.2955	1.7277	499.4256	0.1228	519.4057	0.0990	538.3858	0.0895
477.5455	0.0938	500.3455	0.1679	519.4957	0.0114	538.5058	0.0153
478.2455	0.5623	501.3255	0.1301	520.3356	0.0998	539.3658	0.1100
478.5455	0.0812	501.3957	0.0087	521.2156	0.0284	539.4958	0.0434
479.2956	1.8615	501.4755	0.0067	521.3356	0.0900	540.4358	0.0521
480.3254	0.5116	502.3355	0.0947	521.4056	0.0090	541.3457	0.1567
480.4954	0.0179	503.3255	0.2145	521.5256	0.0644	541.5057	0.0040
481.3254	0.3928	504.2857	0.0217	523.2456	0.2069	542.3357	0.1818
482.3354	0.1169	504.4555	0.0241	523.3256	0.0066	542.4157	0.0038
482.4756	0.0436	505.3255	0.1380	523.4056	0.0035	543.2857	0.1501
482.5256	0.0059	505.3955	0.1009	524.2756	0.0918	543.4957	0.0323
483.3156	0.1864	505.5755	0.0044	525.3358	0.0268	544.3057	0.1801
483.3856	0.0390	506.2555	0.1546	525.4256	0.0187	544.3857	0.0129

Table A3.2 (continued). Mass data (*m/z* values and their relative intensities) for the DART-HRMS analysis of *A. absinthium* dried herb. Ten replicates of one sample were averaged where the corresponding spectrum appears in Figure 3.1.

				A. Absinthium dried herb			
m/z	Rel. Int. %	*m/z*	Rel. Int. %	*m/z*	Rel. Int. %	*m/z*	Rel. Int. %
544.5257	0.0296	560.4159	0.0171	572.5658	0.0334	589.4759	0.0030
545.3257	0.2080	560.4959	0.0101	572.6658	0.0086	589.5959	0.0070
545.4757	0.0067	561.3359	0.0977	573.2958	0.0157	590.3959	0.1011
545.7257	0.0389	561.4159	0.0725	573.3758	0.0276	590.4859	0.0114
546.3157	0.2550	561.4957	0.0552	573.4558	0.0241	591.3559	0.0449
547.3357	0.1253	561.5658	0.0233	573.5758	0.0243	591.4359	0.0239
547.4657	0.0688	562.3458	0.1852	574.4460	0.0259	591.4961	0.0303
548.3459	0.1774	562.4358	0.0063	575.4260	0.0714	591.5859	0.0190
549.2757	0.0356	562.5158	0.0057	576.3458	0.1214	592.3059	0.0164
549.3559	0.0791	563.3558	0.1332	576.5158	0.0242	592.3759	0.0603
549.4959	0.0598	563.5358	0.0028	577.3458	0.0781	592.4959	0.0280
550.3757	0.0816	563.6158	0.0075	577.5258	0.0653	592.5759	0.0291
550.4459	0.0082	564.3558	0.1663	578.3660	0.0552	592.6759	0.0160
550.5657	0.0284	564.4358	0.0167	578.5260	0.0723	593.3859	0.0547
551.3759	0.0795	564.5458	0.0034	579.3460	0.0599	593.5159	0.0451
552.3859	0.1057	564.6358	0.0178	579.4160	0.0205	593.6659	0.0172
552.4959	0.0586	565.3658	0.0477	579.5260	0.0509	594.3759	0.1329
552.5857	0.0102	565.5258	0.0258	581.3658	0.1203	594.5159	0.0767
553.3157	0.0664	566.3758	0.1896	581.4460	0.0132	595.3559	0.1050
553.3957	0.0030	566.4458	0.0989	581.5358	0.0127	595.5259	0.0598
553.4957	0.0483	566.5358	0.0636	582.3759	0.1352	596.5261	0.0469
554.4057	0.0641	567.3858	0.1242	582.5159	0.0069	597.3661	0.0813
554.4957	0.0570	567.5358	0.0073	583.3759	0.0710	597.4460	0.0516
554.5659	0.0052	568.3858	0.3997	583.5259	0.0074	597.5259	0.0174
555.3859	0.0815	568.5258	0.0108	583.5859	0.0180	598.3859	0.1063
555.5357	0.0070	569.3858	0.1460	584.3959	0.1673	598.4561	0.0233
556.3659	0.1294	569.4958	0.0073	585.3859	0.2081	598.5959	0.0097
556.4359	0.0019	569.5660	0.0385	586.3959	0.1405	599.3761	0.0979
557.3357	0.0700	569.6358	0.0328	586.4857	0.0039	599.5061	0.0479
557.4459	0.0032	570.4058	0.0858	586.5559	0.0602	600.3861	0.3349
557.5359	0.0280	570.5458	0.0727	587.3959	0.0074	600.5959	0.0027
558.3759	0.0846	571.3958	0.0718	587.4909	0.0525	601.3761	0.1720
558.4457	0.0208	571.4458	0.0036	587.5859	0.0357	601.5259	0.0187
559.3359	0.0989	571.5558	0.0082	588.4059	0.0615	601.5961	0.0028
559.5459	0.0124	572.3758	0.1099	588.5059	0.0614	601.8059	0.0033
560.3459	0.1645	572.4458	0.0066	589.3959	0.0609	602.3861	0.0840

Table A3.2 (continued). Mass data (*m/z* values and their relative intensities) for the DART-HRMS analysis of *A. absinthium* dried herb. Ten replicates of one sample were averaged where the corresponding spectrum appears in Figure 3.1.

A. Absinthium dried herb							
m/z	Rel. Int. %	*m/z*	Rel. Int. %	*m/z*	Rel. Int. %	*m/z*	Rel. Int. %
602.5261	0.0099	617.6460	0.0084	633.5961	0.0193	650.6060	0.0366
602.6261	0.0199	618.3960	0.0858	633.6961	0.0236	650.6862	0.0101
603.3060	0.0040	618.5260	0.0045	634.4661	0.0051	651.4160	0.0520
603.3958	0.0289	618.6762	0.0187	634.5461	0.0098	651.5462	0.0194
603.5360	0.0302	619.3860	0.0756	635.3161	0.0080	652.4062	0.0757
603.6260	0.0081	619.4560	0.0053	635.3861	0.0556	652.5462	0.0236
604.4058	0.0470	619.5360	0.0256	635.4661	0.0300	653.4162	0.0606
604.4660	0.0073	619.6660	0.0119	635.5461	0.0142	653.4962	0.0221
604.5458	0.0294	619.7560	0.0137	635.6161	0.0258	653.5660	0.0030
604.6560	0.0066	620.3260	0.0876	635.7061	0.0152	654.5662	0.0390
605.4060	0.0154	620.4560	0.0275	636.3961	0.0706	656.4962	0.0338
605.4660	0.0527	620.5360	0.0413	636.5661	0.0436	657.5062	0.0330
605.5460	0.0050	620.6660	0.0208	637.4061	0.0578	658.5062	0.0119
605.6360	0.0111	621.4060	0.0429	637.4761	0.0203	659.3862	0.0623
606.4060	0.1099	621.5460	0.0234	637.5661	0.0325	659.5262	0.0471
606.5360	0.0290	621.6660	0.0298	638.5761	0.0554	659.6162	0.0129
606.6260	0.0277	622.4062	0.0891	639.4661	0.0366	660.3962	0.0954
607.5060	0.0495	622.5460	0.0664	639.5661	0.0399	660.5362	0.0289
607.5760	0.0406	623.5659	0.0532	640.4761	0.0133	661.3962	0.0608
608.3760	0.2083	624.4759	0.0439	641.5661	0.0053	661.4762	0.0115
608.5260	0.0528	625.3961	0.0965	642.4863	0.0025	661.5562	0.0063
609.3160	0.0021	625.4861	0.0044	644.4960	0.0022	661.6517	0.0086
609.3860	0.0916	626.3359	0.4107	645.4862	0.0046	662.5662	0.0055
609.5160	0.0526	626.4061	0.0664	646.4160	0.0696	663.3862	0.0731
610.5460	0.0402	627.3361	0.2093	646.6162	0.0262	663.5562	0.0067
611.5360	0.0015	627.5061	0.0016	647.4060	0.0350	663.6262	0.0140
612.3560	2.7385	627.5861	0.0036	647.4762	0.0116	664.3862	0.0885
613.3660	1.0378	629.5059	0.0021	647.6360	0.0300	664.5662	0.0267
614.4160	0.0936	630.4161	0.1144	648.5160	0.0194	665.4161	0.0781
615.3860	0.0698	630.4961	0.0088	648.6360	0.0329	665.5161	0.0084
615.5060	0.0477	631.3959	0.0590	649.4160	0.0450	665.5961	0.0169
615.6460	0.0214	631.5059	0.0368	649.5160	0.0163	666.4161	0.0779
616.5160	0.0272	632.4161	0.1105	649.5960	0.0036	666.5561	0.0115
617.3860	0.0656	632.5361	0.0109	649.6760	0.0346	666.6461	0.0134
617.4460	0.0022	633.3961	0.0991	650.4160	0.0630	666.7161	0.0195
617.5160	0.0635	633.5161	0.0373	650.5460	0.0069	667.4561	0.0122

Table A3.2 (continued). Mass data (*m/z* values and their relative intensities) for the DART-HRMS analysis of *A. absinthium* dried herb. Ten replicates of one sample were averaged where the corresponding spectrum appears in Figure 3.1.

			A. Absinthium dried herb				
m/z	Rel. Int. %	*m/z*	Rel. Int. %	*m/z*	Rel. Int. %	*m/z*	Rel. Int. %
667.5861	0.0055	689.6462	0.0201	709.5963	0.0096	733.7864	0.0035
667.7161	0.0071	690.4762	0.0073	710.4263	0.0309	734.3964	0.0071
668.4806	0.0115	690.6564	0.0204	710.6063	0.0075	734.4964	0.0068
669.4961	0.0010	691.4062	0.0369	711.6063	0.0046	734.6864	0.0034
669.5863	0.0019	691.4962	0.0185	712.6063	0.0060	735.4064	0.0038
670.5161	0.0077	691.6662	0.0283	713.5865	0.0086	735.4864	0.0035
671.3561	0.0036	692.4764	0.0287	714.5863	0.0042	735.6764	0.0015
672.3661	0.0216	692.5564	0.0157	715.6063	0.0022	736.4066	0.0130
673.6463	0.0040	692.6462	0.0260	716.5963	0.0067	736.5164	0.0068
675.4063	0.0493	693.6164	0.0166	717.5965	0.0061	737.4164	0.0190
675.5063	0.0294	694.3962	0.0331	718.6763	0.0013	737.5064	0.0087
675.6761	0.0336	694.4762	0.0075	719.3963	0.0053	737.6364	0.0015
675.7963	0.0047	694.6064	0.0249	719.6565	0.0019	738.4264	0.0222
676.3663	0.0357	694.7462	0.0227	719.7265	0.0020	738.6364	0.0050
676.4462	0.0355	695.6264	0.0191	720.4563	0.0240	739.6464	0.0095
676.5261	0.0567	695.7464	0.0074	720.5265	0.0042	740.4664	0.0583
676.6763	0.0166	696.4462	0.0288	720.6665	0.0017	740.5366	0.0038
677.5463	0.0355	696.5964	0.0252	720.7365	0.0014	740.6364	0.0212
677.6263	0.0186	697.3964	0.0113	721.5363	0.0183	741.3664	0.0490
677.7063	0.0372	697.4664	0.0156	721.6263	0.0037	741.4664	0.0328
678.5961	0.0313	697.6262	0.0099	722.6365	0.0016	741.6266	0.0201
678.7263	0.0299	699.4762	0.0150	722.7963	0.0071	742.3564	0.0046
679.4163	0.0487	700.5264	0.0069	723.4365	0.0351	742.6164	0.0120
679.5963	0.0288	703.6464	0.0027	723.6465	0.0038	743.6164	0.0315
680.4013	0.0553	704.4064	0.0126	724.4465	0.0292	744.6166	0.0260
680.5963	0.0331	704.6564	0.0012	724.6665	0.0019	745.6266	0.0213
681.4563	0.0470	705.3964	0.0161	725.4565	0.0378	746.5464	0.0156
681.5963	0.0233	705.6664	0.0086	725.6065	0.0140	746.6264	0.0061
682.4563	0.0427	705.7564	0.0128	725.6665	0.0036	747.6265	0.0034
682.5563	0.0182	706.3963	0.0176	727.5744	0.0218	748.6463	0.0082
683.4163	0.0453	706.5863	0.0070	728.5964	0.0135	749.6365	0.0015
683.4863	0.0220	706.6563	0.0045	729.5964	0.0162	750.6863	0.0040
684.5063	0.0367	707.4063	0.0310	730.5464	0.0077	750.8165	0.0073
685.4962	0.0311	707.6463	0.0061	732.6864	0.0039	751.4665	0.0042
688.5764	0.0200	708.4363	0.0368	733.3964	0.0035	751.6863	0.0014
689.4062	0.0325	708.6463	0.0091	733.4764	0.0035	752.6765	0.0015

Table A3.2 (continued). Mass data (*m/z* values and their relative intensities) for the DART-HRMS analysis of *A. absinthium* dried herb. Ten replicates of one sample were averaged where the corresponding spectrum appears in Figure 3.1.

A. Absinthium dried herb							
m/z	Rel. Int. %	*m/z*	Rel. Int. %	*m/z*	Rel. Int. %	*m/z*	Rel. Int. %
753.4165	0.0061	768.4866	0.0141	777.6866	0.0055	793.6067	0.0086
753.6165	0.0043	769.4166	0.0019	778.6266	0.0060	794.6167	0.0167
754.6465	0.0108	770.6064	0.0044	778.6966	0.0172	795.6267	0.0032
755.6265	0.0031	771.6364	0.0043	779.6366	0.0090	796.6267	0.0089
756.5165	0.0098	772.6366	0.0112	779.7066	0.0012	796.7067	0.0053
756.6265	0.0182	773.6364	0.0080	780.7066	0.0043	797.3567	0.0026
757.6265	0.0138	775.6164	0.0151	781.6166	0.0015	797.4367	0.0185
761.3767	0.0340	776.4566	0.0418	787.4366	0.0029	798.4367	0.0230
762.4767	0.0049	776.6166	0.0123	789.3865	0.0159	806.4467	0.0100
763.4765	0.0117	776.6866	0.0099	790.6167	0.0028	812.6366	0.0062
767.4765	0.0096	777.6166	0.0091	792.6067	0.0077	885.7771	0.0077

Table A3.3 Mass data (*m/z* values and their relative intensities) for the DART-HRMS analysis of *A. absinthium* powder. Ten replicates of one sample were averaged where the corresponding spectrum appears in Figure 3.1.

A. Absinthium powder
m/z	Rel. Int. %	*m/z*	Rel. Int. %	*m/z*	Rel. Int. %	*m/z*	Rel. Int. %
61.0339	0.0017	88.0741	0.1003	111.0540	0.0217	130.1543	0.3889
62.0639	0.0060	88.2041	0.0067	111.1140	0.3157	130.2343	0.0592
65.0541	0.0418	89.0641	4.9308	111.2342	0.0341	131.0643	1.1208
67.0540	0.0300	89.2541	0.0803	112.0742	0.5919	131.2243	0.1679
68.0538	0.0182	90.0641	2.2307	113.0542	0.9095	132.1041	3.0695
68.9640	0.0436	90.1641	0.0613	114.0842	0.2834	133.0643	2.5699
69.0440	0.8062	91.0541	0.5715	114.2242	0.0121	133.2543	0.0313
70.0640	4.6129	92.0641	0.0297	115.0542	1.6189	134.0843	0.3265
70.1340	0.0484	93.0641	1.3884	115.1040	0.1999	134.1943	0.0017
71.0640	0.5466	94.0641	0.0578	115.2442	0.0635	134.2543	0.0430
72.0840	5.3919	94.1741	0.0050	116.0742	54.7874	135.1043	5.9879
72.2040	0.0759	95.0841	0.6408	116.2242	0.6204	135.2443	0.0027
72.9940	0.0322	96.0541	0.7428	117.0642	3.6290	135.9943	0.0093
73.0640	1.3401	97.0341	1.3293	117.2442	0.1142	136.0643	2.7938
74.0640	0.2253	97.0941	0.8667	118.0842	3.2803	136.1343	0.5150
74.1640	0.0071	97.2841	0.0315	118.2042	0.1606	136.2843	0.0091
75.0440	0.9216	98.0841	0.6196	119.0842	4.1093	136.4043	0.0291
76.0640	0.3093	99.0541	2.3777	120.0742	0.7624	137.0743	0.6507
77.0440	0.1141	100.0841	0.1198	120.2042	0.0573	137.1243	2.6931
78.0440	0.0033	100.2341	0.0221	121.0842	0.8966	137.2143	0.0301
79.0440	0.2757	101.0641	1.2435	122.0742	0.0992	137.2843	0.1377
79.1242	0.0056	101.1841	0.0785	123.0942	1.5863	138.0843	0.3310
80.0540	0.1091	102.0741	0.0981	124.0642	0.5116	138.1643	0.3375
81.0540	1.2838	103.0541	1.0706	124.1844	0.0220	139.1043	0.7014
81.1442	0.0095	104.0741	5.4601	125.0942	1.3765	139.2243	0.0318
82.0642	0.0739	104.2343	0.0720	125.2144	0.0409	139.2643	0.0515
82.9442	0.0506	105.0641	0.6238	126.0642	1.6122	140.0843	0.5596
83.0840	0.6394	105.1843	0.0449	126.1542	0.1369	140.3143	0.0255
84.0640	1.1107	106.0641	0.1854	127.0442	11.1922	141.1043	1.6087
84.9540	0.0557	107.0841	1.2515	127.1142	1.6663	142.1043	1.9899
85.0342	6.4045	108.0640	0.1446	127.2342	0.0241	142.1843	0.2560
85.0942	0.3430	109.0340	4.4457	128.0844	0.8781	143.0343	0.0281
86.0740	1.2786	109.0942	1.6283	128.1843	0.0766	143.0943	1.4383
86.1742	0.0037	109.2042	0.0089	129.0641	0.8430	144.0843	1.8458
87.0539	1.4816	110.0742	1.0415	129.2141	0.0053	144.1743	0.0043
87.1641	0.0543	110.2142	0.0987	130.0643	9.0599	144.2443	0.0150

Table A3.3 (continued). Mass data (*m/z* values and their relative intensities) for the DART-HRMS analysis of *A. absinthium* powder. Ten replicates of one sample were averaged where the corresponding spectrum appears in Figure 3.1.

m/z	Rel. Int. %	*m/z*	Rel. Int. %	*m/z*	Rel. Int. %	*m/z*	Rel. Int. %
145.0543	10.2977	163.0644	6.8475	183.0945	2.1110	204.1146	0.0597
145.1243	1.0410	163.1344	1.5404	184.1145	1.1476	204.1844	1.1315
145.2243	0.1806	164.0844	0.6281	185.1145	2.5841	205.0044	0.0026
145.9868	0.0033	164.1644	0.0951	185.3245	0.0106	205.1046	1.2828
146.0843	1.7296	165.0844	0.9747	186.1145	1.0852	205.1946	2.9907
147.0743	1.4222	165.1794	0.6582	187.1245	2.1322	205.4046	0.0154
147.2345	0.0032	165.2744	0.0920	188.0945	0.2066	206.1146	0.6438
148.0745	0.3261	166.0944	1.2721	188.1645	0.8306	206.2044	0.3082
149.1142	1.0160	166.1944	0.1374	189.1345	1.0700	207.1546	1.0468
149.9942	0.0477	167.0944	2.0030	189.4045	0.0078	208.1146	0.4653
150.0942	1.1647	167.2544	0.1195	190.1244	0.4931	208.2096	0.1325
150.1542	0.1218	168.0944	1.4610	191.0678	0.9317	209.1346	1.2652
150.2342	0.0065	168.1744	0.0472	191.1644	0.8660	209.2746	0.0244
150.3142	0.0438	168.9844	0.0305	191.3244	0.1436	210.1046	0.5900
151.1042	2.6041	169.1144	3.1163	192.1044	0.3768	210.1646	0.1208
152.1144	0.7102	170.0143	0.0035	192.1644	0.0314	210.3596	0.0348
153.0844	5.4541	170.0943	1.2377	192.2646	0.0183	211.0245	0.0027
153.2044	0.0612	170.1643	0.1157	193.0844	1.3417	211.1345	1.0074
154.0844	0.5804	171.1543	0.4218	193.1544	0.8520	212.1045	16.0029
154.1544	0.5387	171.3143	0.0242	194.0944	0.3799	212.3345	0.2399
155.0100	0.1094	172.1243	0.4757	195.0946	3.4363	213.0145	0.0099
155.1044	1.0659	173.1143	2.0363	196.0946	0.7657	213.1145	2.4834
156.1042	2.1936	174.1143	1.0136	196.2794	0.0128	213.3445	0.0096
156.1744	0.2103	174.2843	0.0028	197.1144	1.5898	213.7345	0.0398
156.2744	0.0295	174.9843	0.0037	197.3344	0.0627	214.0245	0.0245
157.1242	3.8769	175.1245	1.4523	198.1044	5.6610	214.1245	0.6046
157.2644	0.0815	176.0945	0.4336	199.1044	0.5942	214.2545	0.2322
158.1044	1.2304	177.1443	1.1199	199.1744	0.7578	215.1145	1.2022
159.0544	0.5742	178.0945	0.3188	199.3844	0.0025	215.2645	0.0172
159.1244	2.6671	178.1694	0.0276	199.4046	0.0073	215.3245	0.1016
160.0944	0.7079	178.2443	0.0139	200.1244	1.0553	216.1245	4.9139
160.2342	0.0029	179.0845	0.9860	201.1444	2.4637	216.3345	0.0087
161.0844	0.4566	180.0845	12.7418	202.1244	0.8159	217.1745	4.8842
161.1644	0.7974	181.0032	0.0022	202.2846	0.0717	218.0445	0.0037
162.0844	0.7494	181.1045	2.2584	203.1746	6.5781	218.1345	1.7270
162.2244	0.0432	182.1045	0.9864	204.0244	0.0296	219.1045	0.2199

	Table A3.3 (continued). Mass data (*m/z* values and their relative intensities) for the DART-HRMS analysis of *A. absinthium* powder. Ten replicates of one sample were averaged where the corresponding spectrum appears in Figure 3.1.						
A. Absinthium **powder**							
m/z	**Rel. Int. %**	*m/z*	**Rel. Int. %**	*m/z*	**Rel. Int. %**	*m/z*	**Rel. Int. %**
219.1845	3.2461	240.2146	0.2272	259.4247	0.0491	277.5248	0.0467
220.1145	0.4231	241.1846	0.4807	260.1147	0.5424	278.1248	0.3673
220.1745	0.3107	242.1048	0.0943	260.1947	0.0109	278.2148	0.5787
220.3347	0.0589	242.1846	0.1167	260.2547	0.1093	279.1546	5.5368
221.1845	3.2411	242.2846	0.0024	261.1147	3.2451	279.2348	5.0682
222.0347	0.0045	243.1046	0.8746	261.2247	0.1412	280.1448	1.6965
222.1245	0.1391	243.1648	0.0866	261.4647	0.0595	280.2446	1.1343
222.2045	0.4091	243.2498	0.0495	262.1847	1.5330	281.1448	7.1186
223.1247	0.9857	243.4048	0.0472	263.1347	17.9901	281.2448	2.4814
224.1147	0.5929	244.1148	0.7513	263.2347	1.1766	282.1548	3.5212
225.1447	0.8504	244.1946	0.0392	263.3849	0.3957	282.5246	0.0468
226.1247	0.2694	245.1246	13.5276	264.1249	3.5740	283.1848	1.2591
226.2547	0.0272	246.1148	2.7670	264.2447	0.0556	283.2648	1.4191
227.1347	1.1743	247.1246	32.3786	265.1547	7.5109	284.1548	1.8805
228.1247	0.3178	248.1346	6.6186	266.1447	3.8041	285.1048	0.1372
228.1947	0.0625	248.3297	0.2016	267.1547	2.5979	285.2048	0.0934
228.3247	0.0058	248.4046	0.1195	268.2047	6.2292	285.2748	3.2157
229.1047	20.8101	249.1646	12.2845	269.2147	2.7621	286.0281	0.0021
230.0147	0.0262	249.3148	0.1318	270.2049	0.9594	286.2148	0.2210
230.1047	6.0492	250.0646	0.0153	270.3849	0.0258	286.2748	0.6261
230.3547	0.1381	250.1548	2.4300	271.0847	0.2680	287.2248	0.0691
231.1247	100.0000	251.1648	13.3530	271.2347	1.0550	287.3048	1.7560
232.0389	0.1982	252.1847	2.0856	272.2547	0.3372	287.4748	0.0667
232.1346	16.7594	253.1847	4.8437	272.4649	0.0260	288.2448	0.6808
233.1346	12.5463	254.1847	0.8491	273.1548	0.0502	289.1048	0.0601
234.0346	0.0278	255.2247	0.8160	273.2446	0.4567	289.1748	0.1982
234.1346	3.3526	256.1447	0.1536	274.1548	0.2545	289.2348	0.2806
234.3546	0.1499	256.2447	0.0711	274.2648	0.3089	289.4048	0.0301
235.1746	17.8801	256.3447	0.0018	274.4148	0.0019	289.4748	0.0173
236.1746	3.0038	257.2447	0.7518	275.2046	0.1656	290.1748	0.2664
237.1846	3.5881	258.1647	0.0076	275.2648	0.0562	290.2748	0.0592
238.1946	0.7666	258.2547	0.1552	276.1648	0.0633	290.4048	0.0151
238.3846	0.0637	258.4347	0.0179	276.2748	0.0231	291.1948	0.4280
239.1446	0.2504	259.1047	0.0842	277.1146	0.3523	291.2750	0.0219
239.2346	0.6045	259.1947	0.2928	277.2148	3.0483	291.4148	0.0187
240.1246	0.0700	259.2647	0.0416	277.4548	0.0417	292.1948	0.1529

Table A3.3 (continued). Mass data (*m/z* values and their relative intensities) for the DART-HRMS analysis of *A. absinthium* powder. Ten replicates of one sample were averaged where the corresponding spectrum appears in Figure 3.1.

m/z	Rel. Int. %	*m/z*	Rel. Int. %	*m/z*	Rel. Int. %	*m/z*	Rel. Int. %
292.3148	0.0256	307.3449	0.0701	330.1650	0.0369	344.1751	0.1648
293.2148	0.6147	308.2349	0.0905	330.2350	0.1778	344.2651	0.1642
293.2947	0.0317	309.2149	0.2142	330.3350	0.0984	344.3951	0.0016
294.2147	0.1666	309.2849	0.0791	331.2250	0.3464	345.1849	0.3690
294.2949	0.0286	310.2449	0.2972	331.2950	0.0294	345.2749	0.0464
295.1547	0.2485	311.2349	0.3182	332.2150	0.3755	346.1751	0.4832
295.2347	1.8251	312.1649	0.1711	332.2950	0.0270	346.2749	0.0168
296.1649	0.8234	312.2749	0.1894	332.3550	0.0330	347.1649	0.2568
296.2549	1.2427	313.2149	0.2159	333.2350	0.2308	347.2851	0.0902
296.4747	0.0164	313.2749	0.0587	333.3450	0.0213	347.3651	0.0029
296.5247	0.0553	314.1548	0.6406	334.2350	0.4838	348.1851	0.1441
297.1847	0.7516	314.2448	0.0594	334.3350	0.0896	348.2949	0.1433
297.2449	0.7265	315.1148	0.0264	335.2049	0.4182	348.3751	0.0033
298.1649	3.6859	315.2248	0.6016	336.1849	0.4172	349.2151	0.5409
298.2749	2.5079	316.2250	0.9688	336.2549	0.2842	349.3351	0.1244
298.4049	0.0381	316.3048	0.0304	336.3251	0.0225	350.2351	0.5935
298.5049	0.2097	317.2348	0.7980	336.4749	0.0602	350.3151	0.0124
299.1949	0.8543	318.2248	0.4268	337.2049	0.3621	350.3751	0.0673
299.2749	0.6555	319.2348	0.9201	337.2651	0.0746	351.2451	0.3504
300.1949	3.0466	319.4450	0.0299	337.3451	0.0074	351.3351	0.0221
300.2947	0.8582	320.2350	0.5217	338.1951	0.6281	352.2451	0.9239
300.4249	0.0215	321.2350	0.4291	338.2649	0.1218	352.3251	0.0813
301.2049	1.8385	322.2450	0.3546	338.3449	0.0869	353.2651	0.4346
301.2949	1.4352	323.2548	0.2716	338.4849	0.0648	354.2651	0.9564
302.2149	0.3540	324.2650	0.2533	338.6049	0.0136	355.0751	0.0157
302.3049	1.1689	325.1950	0.0350	339.1849	0.3560	355.1950	0.1592
303.1249	0.2082	325.2850	0.1934	339.3251	0.0848	355.2950	0.2067
303.2249	0.4443	325.3862	0.0112	340.2651	0.0900	356.0750	0.0028
303.3049	0.3019	326.1850	0.0640	340.3449	0.0857	356.1950	0.0202
304.2349	0.1361	326.2950	0.1615	341.2149	0.1357	356.2850	0.2591
304.3649	0.1182	327.1950	0.0880	341.3149	0.1614	357.2050	0.5358
305.2349	0.3653	327.2850	0.1374	342.2151	0.2221	357.2950	0.0886
306.1649	0.0322	328.2250	0.2447	342.3149	0.1050	358.2152	0.2715
306.2749	0.0646	328.3248	0.0599	343.1649	0.1261	358.2950	0.0104
307.1949	0.4211	329.2350	0.4907	343.2351	0.1639	358.3650	0.0253
307.2749	0.0276	329.3150	0.0692	343.3351	0.0823	359.1350	0.4463

Table A3.3 (continued). Mass data (*m/z* values and their relative intensities) for the DART-HRMS analysis of *A. absinthium* powder. Ten replicates of one sample were averaged where the corresponding spectrum appears in Figure 3.1.

m/z	Rel. Int. %	*m/z*	Rel. Int. %	*m/z*	Rel. Int. %	*m/z*	Rel. Int. %
359.2250	0.3372	372.9152	0.0223	388.1351	1.5036	403.1952	0.0635
359.2952	0.0439	373.1052	0.0654	388.2653	0.2013	403.2952	0.1301
359.3850	0.0133	373.1752	0.2457	388.3451	0.5388	403.3652	0.0339
359.5150	0.0574	373.2452	0.0249	388.4351	0.0734	404.1552	0.0550
359.5850	0.0078	373.3152	0.1573	389.1553	60.6191	404.2952	0.0832
360.2252	0.3550	374.0952	0.0153	390.1353	12.9647	405.1952	0.0722
360.3150	0.0195	374.1652	0.0543	390.3351	0.1070	405.2752	0.2311
361.0493	0.0134	374.2652	0.1964	391.1753	2.2428	405.4552	0.0451
361.1550	0.1470	375.1052	4.2851	391.2951	0.5260	406.2852	0.1181
361.2352	0.2463	376.1451	0.7637	391.3901	0.0666	406.3854	0.0076
361.3250	0.0645	376.5751	0.0183	391.4851	0.1812	407.1754	0.1417
362.1652	0.6090	377.1851	0.2584	392.1851	0.3956	407.2652	0.0937
362.2650	0.0094	377.2551	0.0876	392.2853	0.1029	407.3652	0.1990
362.3750	0.0809	377.3351	0.0877	393.2652	0.2163	407.4652	0.0064
363.2452	0.2796	377.4251	0.0113	393.3451	0.0891	409.3852	1.1131
364.1952	1.3258	377.5251	0.0684	394.1853	0.5154	410.2252	0.5402
365.2750	0.5869	378.1851	0.5839	394.2653	0.1419	410.3854	0.3584
366.1952	0.0817	379.2651	0.2502	394.3353	0.0953	411.1952	0.0240
366.2652	1.1198	379.3451	0.1140	395.0553	0.0014	411.2952	0.0418
367.2750	0.6210	380.2051	1.2276	395.1953	0.3175	411.3852	0.5563
368.2652	1.1966	381.1951	0.5426	395.2753	0.0416	411.6254	0.0154
369.2150	0.5423	381.4153	0.0193	395.3653	0.4132	411.6954	0.0500
369.3452	0.0465	382.1951	1.1866	396.2053	2.2938	412.2052	0.8274
369.4252	0.0303	382.4351	0.0973	396.3753	0.1082	412.2954	0.0527
369.4852	0.0672	383.1951	0.5473	397.2152	0.5786	413.2152	0.3442
369.5650	0.0564	383.2951	0.0485	397.3852	1.0846	413.3754	0.2564
370.2150	0.6492	383.3651	0.1547	398.2152	2.1487	414.2154	0.6538
371.1052	0.4551	384.2051	0.5712	398.3950	0.3619	414.3854	0.1698
371.3152	4.6970	385.2151	0.5271	398.4752	0.0510	414.6152	0.0534
371.5852	0.0876	385.4851	0.0298	399.0952	0.0921	415.1554	0.1377
371.6750	0.0826	386.2153	0.5002	399.2252	0.7985	415.2254	0.4314
372.1152	0.2420	387.1053	0.0227	400.2352	0.5349	415.3004	0.0594
372.2352	0.2970	387.2253	0.1413	401.2252	0.3499	415.3754	0.1265
372.3152	1.1612	387.2853	0.0829	401.4652	0.0703	416.2354	0.3565
372.6450	0.0110	387.3353	0.0119	402.2252	0.2635	417.1753	0.1067
372.8352	0.0299	387.6051	0.0235	402.3352	0.0709	417.2553	0.2108

Table A3.3 (continued). Mass data (*m/z* values and their relative intensities) for the DART-HRMS analysis of *A. absinthium* powder. Ten replicates of one sample were averaged where the corresponding spectrum appears in Figure 3.1.

m/z	Rel. Int. %	*m/z*	Rel. Int. %	*m/z*	Rel. Int. %	*m/z*	Rel. Int. %
417.3753	0.1680	433.2555	0.2936	449.3954	0.0436	467.3955	0.0507
418.2253	0.2506	433.3253	0.0190	450.3454	0.2689	468.4955	0.0041
418.2953	0.0155	433.4753	0.0020	450.5154	0.0581	469.4055	0.1273
418.4553	0.0116	434.2653	0.1673	451.3454	0.1652	470.5055	0.0430
419.3253	0.1917	434.3353	0.0376	452.4854	0.0221	471.3255	0.0898
420.2553	0.0569	434.3955	0.0308	453.3554	0.1327	471.3855	0.0132
420.3153	0.0615	435.2253	0.1280	453.4654	0.0048	471.4955	0.0045
421.2753	0.1661	435.3553	0.0713	454.3454	0.0203	472.3455	0.1873
421.3453	0.1132	435.4655	0.0541	454.4956	0.0337	473.2255	0.1020
421.4653	0.0341	436.3353	0.1848	455.3556	0.1677	473.2955	0.0049
422.2053	0.0264	437.1955	0.0099	455.4954	0.0033	473.3755	0.1061
422.3453	0.1677	437.2753	0.0698	456.2854	0.1087	474.2857	0.1302
423.2753	0.1059	437.3455	0.0165	456.5156	0.0141	474.3855	0.0554
423.3753	0.6099	437.4755	0.0123	457.3054	0.1124	474.4655	0.0072
424.2653	0.0167	438.3552	0.1932	457.3754	0.0598	475.3055	0.3640
424.3753	0.3548	439.2903	0.0557	457.4954	0.0056	475.3855	0.0102
425.2053	0.0474	439.3652	0.1850	458.3853	0.0464	476.3155	0.0796
425.2853	0.0310	439.4554	0.0076	459.3053	0.2470	476.4055	0.0483
425.3753	0.8009	441.2154	0.0152	459.3855	0.1042	477.2955	0.5996
426.2253	0.2742	441.2954	0.0076	460.3053	0.0535	477.5455	0.0620
426.3153	0.0428	441.3754	0.2695	460.4155	0.0382	478.2455	0.2024
426.3853	0.2974	442.3054	0.2319	460.4955	0.0157	478.3255	0.1034
427.2253	0.0395	442.3854	0.2557	461.2053	0.3321	478.4355	0.0215
427.3953	0.5111	443.2954	0.0628	461.3055	0.0132	478.5455	0.0048
428.2353	0.3524	443.3854	0.2318	461.3755	0.0513	479.2956	0.5285
428.2953	0.0674	444.2354	0.1443	462.2055	0.1544	479.4854	0.0247
428.3955	0.1300	444.2954	0.0666	462.3053	0.1762	480.3254	0.2345
429.1653	2.5774	444.4054	0.0645	463.2155	0.2699	480.4954	0.0078
429.3853	0.8813	445.2154	2.6160	463.3855	0.3037	481.3254	0.2066
430.3853	0.2626	445.3754	0.2502	464.2255	0.4230	481.4956	0.0029
430.5553	0.0173	446.2254	1.2014	465.2255	0.0796	482.3354	0.1539
431.3053	0.2321	446.3054	0.0466	465.3255	0.1228	482.5256	0.0096
431.3853	0.0482	446.3854	0.0183	465.3955	0.0182	483.3156	0.1380
432.1853	0.2527	447.2254	1.3044	466.3355	0.2056	483.3856	0.0319
432.3153	0.1074	448.2054	0.5553	466.5055	0.0051	483.5356	0.0128
432.3955	0.0403	449.3254	0.2255	467.3255	0.1048	484.3956	0.0262

Table A3.3 (continued). Mass data (*m/z* values and their relative intensities) for the DART-HRMS analysis of *A. absinthium* powder. Ten replicates of one sample were averaged where the corresponding spectrum appears in Figure 3.1.

A. Absinthium powder							
m/z	Rel. Int. %	*m/z*	Rel. Int. %	*m/z*	Rel. Int. %	*m/z*	Rel. Int. %
484.5456	0.0217	505.3255	0.0914	521.5256	0.0116	538.5058	0.0077
485.3354	0.1404	505.3955	0.0268	523.2456	0.0506	539.3658	0.0679
485.4056	0.0104	505.4955	0.0078	523.3256	0.0340	539.4958	0.0466
486.3254	0.0394	506.2555	0.0706	523.4056	0.0374	540.4358	0.0063
486.3854	0.3208	506.3657	0.0503	525.3358	0.1538	541.3457	0.0858
487.3854	0.1501	507.2155	0.0334	526.4156	0.0047	541.5057	0.0020
488.3956	0.1081	507.3155	0.0553	526.5658	0.0220	542.3357	0.0799
489.3056	0.0885	507.3955	0.0452	527.3456	0.1324	542.4157	0.0307
489.3756	0.0837	507.5155	0.0126	527.4256	0.0389	543.2857	0.0198
490.3254	0.1740	508.3557	0.1410	527.5256	0.0580	543.3457	0.0465
490.4656	0.0033	508.5257	0.0027	528.3458	0.1521	543.4257	0.0235
491.2156	0.2474	509.2255	0.1316	529.2658	0.0817	543.4957	0.0110
491.3056	0.0253	509.3255	0.0912	529.3256	0.0479	544.3057	0.0558
491.3756	0.0089	509.4055	0.0413	529.4156	0.0471	544.3857	0.0694
491.4856	0.0076	509.5257	0.0540	530.2856	0.0069	544.5257	0.0217
492.3356	0.1466	510.4157	0.0316	530.4056	0.0065	545.3257	0.0975
493.2456	0.4425	511.2557	0.2641	531.4058	0.1484	545.4057	0.0165
493.3056	0.0817	511.3257	0.0595	532.3358	0.1836	545.4757	0.0051
493.5156	0.0139	511.4357	0.0046	532.4158	0.0093	545.7257	0.0093
495.2656	0.1772	512.4057	0.0244	533.1858	0.0024	546.2857	0.4584
495.3056	0.7254	513.3357	0.2336	533.3556	0.0943	546.4557	0.0254
496.3256	0.3177	513.3957	0.0121	533.5258	0.0477	547.2357	0.0595
497.3256	0.4070	514.3357	0.3456	534.2756	0.0316	547.3357	0.0804
498.3256	0.2816	515.3257	0.1505	534.3656	0.1666	547.4057	0.0981
498.5356	0.0090	515.4257	0.0062	535.3656	0.0380	547.4657	0.0523
499.3256	0.1322	516.3457	0.2552	535.4458	0.0353	548.3459	0.2034
499.4256	0.0795	516.4957	0.0046	535.5358	0.0144	549.2757	0.0535
500.3455	0.2080	517.3257	0.1235	536.3158	0.0676	549.3559	0.0515
501.3255	0.1086	517.4457	0.0188	536.3858	0.0094	549.4959	0.0430
502.2355	0.0364	518.3457	0.2829	536.5358	0.0209	550.2857	0.1164
502.3355	0.1219	519.3457	0.1457	536.6058	0.0247	550.3757	0.0171
502.4155	0.0832	519.4957	0.0186	537.3958	0.0609	550.4459	0.0209
503.3255	0.1667	520.3356	0.1305	537.5058	0.0022	550.5657	0.0046
503.4155	0.0158	520.4056	0.0109	537.6158	0.0069	551.3759	0.0795
504.2857	0.0379	521.3356	0.0512	538.3158	0.0264	551.5057	0.0031
504.4555	0.0186	521.4056	0.0284	538.3858	0.0745	552.3859	0.1083

Table A3.3 (continued). Mass data (*m/z* values and their relative intensities) for the DART-HRMS analysis of *A. absinthium* powder. Ten replicates of one sample were averaged where the corresponding spectrum appears in Figure 3.1.

								A. Absinthium powder

m/z	Rel. Int. %	*m/z*	Rel. Int. %	*m/z*	Rel. Int. %	*m/z*	Rel. Int. %
552.4959	0.0196	565.5258	0.0335	581.3658	0.0590	594.3759	0.1148
552.5857	0.0105	566.3758	0.1789	581.4460	0.0236	594.5159	0.0056
553.3157	0.0385	566.4458	0.0169	581.5358	0.0075	595.3559	0.0752
553.4957	0.0313	566.5358	0.0046	582.3759	0.1138	595.5259	0.0115
554.4057	0.0579	567.3858	0.1001	582.5159	0.0187	596.5261	0.0082
554.4957	0.0278	567.4558	0.0031	583.3759	0.0504	597.3661	0.0371
555.3859	0.0489	567.5358	0.0179	583.4557	0.0086	597.4460	0.0274
555.4559	0.0069	568.3858	0.5751	583.5259	0.0091	597.5259	0.0140
555.5357	0.0029	568.5258	0.0119	584.3959	0.1371	598.3859	0.0838
556.2459	0.0102	569.3858	0.1859	584.5759	0.0102	598.4561	0.0401
556.3659	0.0712	569.4958	0.0035	585.3859	0.1333	598.5959	0.0162
556.4359	0.0243	569.5660	0.0184	585.4759	0.0043	599.3761	0.0751
557.3357	0.0339	569.6358	0.0023	585.5859	0.0025	599.6059	0.0023
557.4459	0.0152	570.4058	0.0927	586.3959	0.1075	600.3861	0.3318
557.5359	0.0327	570.5458	0.0668	586.4857	0.0196	600.5061	0.0038
558.3759	0.0564	571.3958	0.0548	586.5559	0.0250	600.5959	0.0024
558.4457	0.0173	572.3758	0.0710	587.3959	0.0343	601.3761	0.1270
559.3359	0.0652	572.4458	0.0157	587.4909	0.0097	601.5259	0.0174
559.5459	0.0463	572.5658	0.0136	587.5859	0.0190	601.8059	0.0019
560.3459	0.1476	572.6658	0.0056	588.4059	0.0617	602.3861	0.0584
560.4159	0.0445	573.2958	0.0135	588.5059	0.0032	602.5261	0.0123
560.4959	0.0611	573.3758	0.0085	589.3959	0.0381	602.6261	0.0178
561.3359	0.0567	573.4558	0.0223	589.4759	0.0066	603.3958	0.0203
561.4159	0.0478	573.5758	0.0063	590.3959	0.0833	603.5360	0.0197
561.4957	0.0434	574.4460	0.0116	590.4859	0.0169	603.6260	0.0023
561.5658	0.0198	575.4260	0.0545	591.3559	0.0228	604.4058	0.0408
562.2558	0.8424	575.5060	0.0062	591.4961	0.0233	604.4660	0.0144
563.2758	0.2638	576.3458	0.1743	591.5859	0.0095	604.5458	0.0131
563.4858	0.0067	576.5158	0.0080	592.3059	0.0034	604.6560	0.0051
563.5358	0.0041	577.3458	0.0639	592.3759	0.0654	605.4060	0.0233
564.2758	0.1790	577.5258	0.0422	592.4959	0.0153	605.4660	0.0159
564.4358	0.0160	578.3660	0.0320	592.5759	0.0101	605.5460	0.0045
564.5458	0.0034	578.5260	0.0389	592.6759	0.0090	606.4060	0.0899
564.6358	0.0335	579.3460	0.0035	593.3859	0.0383	606.5360	0.0099
565.2958	0.0023	579.4160	0.0641	593.5159	0.0260	606.6260	0.0115
565.3658	0.0282	580.5258	0.0026	593.6659	0.0196	607.2958	0.0261

Table A3.3 (continued). Mass data (*m/z* values and their relative intensities) for the DART-HRMS analysis of *A. absinthium* powder. Ten replicates of one sample were averaged where the corresponding spectrum appears in Figure 3.1.

A. Absinthium powder							
m/z	Rel. Int. %	*m/z*	Rel. Int. %	*m/z*	Rel. Int. %	*m/z*	Rel. Int. %
607.5060	0.0149	622.4062	0.0683	638.6861	0.0064	657.5062	0.0151
607.5760	0.0161	622.5460	0.0181	639.4661	0.0126	658.5062	0.0334
608.3760	0.1499	623.4659	0.0232	639.5661	0.0068	659.3862	0.0384
608.4510	0.0413	623.5659	0.0050	640.4761	0.0022	659.5262	0.0350
608.5260	0.0170	624.4759	0.0037	640.5661	0.0062	660.3962	0.0757
609.3160	0.0024	625.3961	0.0563	641.4861	0.0047	660.5362	0.0225
609.3860	0.0612	625.4861	0.0028	641.5661	0.0089	661.3962	0.0382
609.5160	0.0289	626.3359	0.2718	642.4863	0.0022	661.6517	0.0025
610.5460	0.0411	626.4061	0.1512	643.4963	0.0182	662.5662	0.0150
611.5360	0.0019	626.5259	0.0024	645.4862	0.0063	663.3862	0.0398
612.3560	2.8563	627.3361	0.1230	646.4160	0.0386	663.4662	0.0025
613.3660	0.9564	627.5061	0.0227	646.4960	0.0273	663.5562	0.0142
614.4160	0.1711	627.5861	0.0070	646.6162	0.0210	663.6262	0.0080
614.4960	0.0033	628.5061	0.0038	647.4060	0.0090	664.3862	0.0514
615.3860	0.0637	629.5059	0.0124	647.4762	0.0123	664.5662	0.0048
615.5060	0.0444	630.4161	0.0742	647.6360	0.0057	665.4161	0.0435
615.6460	0.0124	631.3959	0.0293	648.5160	0.0390	665.5161	0.0059
616.5160	0.0465	631.5059	0.0122	648.6360	0.0128	665.5961	0.0098
617.3860	0.0136	632.4161	0.1135	649.4160	0.0243	666.4161	0.0390
617.4460	0.0407	633.3961	0.0675	649.5160	0.0025	666.5561	0.0091
617.5160	0.0029	633.5161	0.0087	649.5960	0.0082	666.6461	0.0112
617.6460	0.0035	633.5961	0.0087	649.6760	0.0093	666.7161	0.0091
618.3960	0.0685	633.6961	0.0073	650.4160	0.0451	667.4561	0.0030
618.5260	0.0108	634.4661	0.0408	650.5460	0.0048	667.5861	0.0010
618.6762	0.0116	634.5461	0.0134	650.6060	0.0196	667.7161	0.0043
619.3860	0.0422	635.3861	0.0301	650.6862	0.0088	668.5761	0.0086
619.4560	0.0271	635.4661	0.0022	651.4160	0.0327	669.4961	0.0029
619.5360	0.0026	635.5461	0.0200	651.5462	0.0216	669.5863	0.0054
619.6660	0.0020	635.6161	0.0147	652.4062	0.0492	670.5161	0.0069
619.7560	0.0077	635.7061	0.0034	652.5462	0.0206	671.3561	0.0014
620.3960	0.0560	636.3961	0.0384	653.4162	0.0297	675.4063	0.0239
620.5360	0.0291	636.5661	0.0257	653.4962	0.0172	675.5063	0.0251
620.6660	0.0186	637.4061	0.0323	653.5660	0.0136	675.6761	0.0056
621.4060	0.0200	637.4761	0.0062	654.5662	0.0248	675.7963	0.0038
621.5460	0.0170	637.5661	0.0249	656.4962	0.0316	676.3663	0.0654
621.6660	0.0157	638.5761	0.0179	657.4262	0.0079	676.4462	0.0082

Table A3.3 (continued). Mass data (*m/z* values and their relative intensities) for the DART-HRMS analysis of *A. absinthium* powder. Ten replicates of one sample were averaged where the corresponding spectrum appears in Figure 3.1.

A. Absinthium powder							
m/z	Rel. Int. %	*m/z*	Rel. Int. %	*m/z*	Rel. Int. %	*m/z*	Rel. Int. %
676.5261	0.0660	694.3962	0.0211	715.6063	0.0024	741.5264	0.0043
677.5463	0.0044	694.6064	0.0198	716.5963	0.0061	741.6266	0.0022
677.6263	0.0163	694.7462	0.0062	717.5965	0.0011	742.6164	0.0053
677.7063	0.0182	695.6264	0.0066	720.4563	0.0102	743.6164	0.0055
678.5961	0.0080	696.4462	0.0174	720.5265	0.0057	744.6166	0.0043
678.7263	0.0183	696.5964	0.0199	721.6263	0.0032	746.5464	0.0072
679.4163	0.0279	696.6562	0.0013	722.6365	0.0027	746.6264	0.0055
679.5963	0.0183	697.3964	0.0087	722.7963	0.0013	748.6463	0.0047
680.4013	0.0370	697.4664	0.0019	723.4365	0.0089	749.6365	0.0018
680.5963	0.0242	699.4762	0.0049	723.6465	0.0022	752.6065	0.0013
681.4563	0.0224	700.5264	0.0168	724.4465	0.0060	752.6765	0.0028
681.5963	0.0153	705.3964	0.0016	725.4565	0.0097	753.6165	0.0010
682.4563	0.0106	705.6664	0.0027	726.6565	0.0047	754.6465	0.0027
682.5563	0.0136	705.7564	0.0017	727.5744	0.0082	755.6265	0.0011
683.4163	0.0191	706.3963	0.0020	728.5964	0.0097	756.5165	0.0039
683.4863	0.0098	706.5863	0.0032	729.5964	0.0013	756.6265	0.0036
684.5063	0.0046	706.6563	0.0040	730.5464	0.0154	757.6265	0.0010
688.5764	0.0117	707.4063	0.0036	733.7864	0.0010	762.4767	0.0016
689.4062	0.0072	707.6463	0.0052	734.4964	0.0028	768.4866	0.0049
689.6462	0.0088	708.4363	0.0196	735.6764	0.0015	768.5766	0.0011
690.4762	0.0165	708.5863	0.0037	736.5164	0.0025	770.6064	0.0013
690.6564	0.0126	708.6463	0.0025	736.6164	0.0046	776.4566	0.0019
691.4062	0.0085	709.5963	0.0015	738.4264	0.0028	778.6266	0.0025
691.4962	0.0101	710.4263	0.0072	738.6364	0.0045	781.6166	0.0010
691.6662	0.0045	710.6063	0.0068	740.4664	0.0100	782.6766	0.0016
692.4764	0.0035	711.6063	0.0025	740.5366	0.0045	792.6067	0.0047
692.5564	0.0076	712.6063	0.0033	740.6364	0.0042	794.6167	0.0011
692.6462	0.0118	713.5865	0.0054	741.3664	0.0019		
693.6164	0.0051	714.5863	0.0035	741.4664	0.0136		

Table A3.4 Mass data (*m/z* values and their relative intensities) for the DART-HRMS analysis of *A. absinthium* seed. Ten replicates of one sample were averaged where the corresponding spectrum appears in Figure 3.1.

A. Absinthium seed							
m/z	**Rel. Int. %**	*m/z*	**Rel. Int. %**	*m/z*	**Rel. Int. %**	*m/z*	**Rel. Int. %**
61.0339	0.0077	88.0741	0.3545	110.2142	0.2002	130.0643	8.5624
61.1041	0.0045	88.2041	0.0243	111.0540	0.6201	130.2343	0.2163
62.0639	0.0245	89.0641	41.2958	111.1140	3.6292	131.0643	1.4724
67.0540	0.0962	89.2541	0.2766	111.2342	0.2857	131.2243	0.3548
68.0538	0.0164	90.0641	11.2002	112.0742	6.5991	132.1041	4.2517
68.9640	0.0328	90.1641	0.4804	113.0542	3.8696	133.0643	2.0356
69.0440	1.1626	91.0541	2.2326	115.0542	2.2760	133.2543	0.1652
69.1440	0.0515	91.1241	0.4108	115.1040	0.8205	134.0843	0.4475
70.0640	3.1145	92.0641	0.1841	115.2442	0.3061	134.1943	0.0464
71.0640	0.7515	93.0641	2.8307	116.0742	37.2390	134.2543	0.0432
72.0840	5.7430	93.1341	0.0021	116.2242	0.5961	135.1043	25.1682
72.2040	0.1155	95.0841	4.1132	117.0642	42.4009	135.2443	0.1265
72.9940	0.0322	96.0541	0.4782	117.1642	0.1152	136.0643	50.5126
73.0640	7.2213	97.0341	1.6525	117.2442	0.7127	136.1343	3.0901
74.0640	0.8635	97.0941	4.7288	118.0842	6.0764	136.2143	0.7433
75.0440	1.6586	97.2241	0.0859	118.2042	0.6559	136.2843	0.0043
76.0640	0.7205	97.2841	0.1781	119.0042	0.0111	136.4043	0.2110
77.0440	0.9092	98.0841	0.1140	119.0842	0.6754	136.9843	0.0358
78.0440	0.0144	99.0541	4.2895	120.0742	1.9076	137.0743	50.5187
79.0440	1.1858	100.0841	0.0463	120.2042	0.1437	137.1243	5.1013
79.1242	0.0588	100.2341	0.0045	121.0842	2.0223	137.2843	0.6070
80.0540	0.6966	101.0641	3.8752	122.0742	0.1122	137.9843	0.1306
81.0540	0.9623	101.1841	0.3330	122.2242	0.0106	138.0843	2.9421
81.1442	0.0367	102.0741	0.2397	123.0942	2.7865	138.1643	0.5395
82.0642	0.1540	103.0541	1.4873	124.0642	5.9249	139.0054	0.0191
82.9442	0.0120	103.1443	0.6132	124.1844	0.0764	139.1043	4.2342
83.0240	0.0328	104.0741	3.6580	125.0942	2.6624	139.2243	0.1475
83.0840	2.9215	104.1443	0.0252	125.2144	0.2966	139.2643	0.3757
84.0640	3.7901	104.2343	0.1435	126.0642	3.8396	140.0843	0.7585
84.9540	0.0813	105.0641	0.4708	126.1542	0.0411	140.2543	0.0245
85.0342	7.9050	105.1843	0.1852	127.0442	24.9968	140.3143	0.0678
85.0942	1.8724	106.0641	0.3796	127.1142	5.8769	141.1043	2.0851
86.0740	1.5450	107.0841	3.2777	127.2342	0.1503	142.1043	0.4484
86.1742	0.0170	109.0942	3.5115	128.0844	0.2317	142.1843	0.0167
87.0539	2.9484	109.2042	0.0202	129.0641	3.3483	143.0943	1.9847
87.1641	0.1018	110.0742	1.8244	129.2141	0.0882	143.1743	0.2208

Table A3.4 (continued). Mass data (*m/z* values and their relative intensities) for the DART-HRMS analysis of *A. absinthium* seed. Ten replicates of one sample were averaged where the corresponding spectrum appears in Figure 3.1.

A. Absinthium seed							
m/z	Rel. Int. %	*m/z*	Rel. Int. %	*m/z*	Rel. Int. %	*m/z*	Rel. Int. %
144.0843	3.8238	162.2244	0.3310	182.1943	0.5146	199.4046	0.0174
145.0543	28.5045	163.0644	8.2313	183.0945	2.5383	200.1244	0.1136
145.2243	0.4832	163.1344	1.2165	183.1945	0.0809	200.1844	0.0918
146.0843	14.5802	164.0844	0.3964	184.1145	0.1790	200.2346	0.5673
146.1643	12.9979	164.1644	0.2872	184.2045	0.0891	201.1444	0.9261
146.9943	0.0133	165.0844	2.6959	185.1145	1.4972	201.2244	0.0187
147.0743	2.8892	165.2744	0.2101	185.2145	0.0812	201.3044	0.1070
147.2345	0.0274	166.0944	3.2960	185.3245	0.1118	202.1244	0.4413
148.0745	1.8909	166.1944	0.1630	186.1145	0.1676	202.2846	0.1233
149.0165	1.7816	167.0944	1.7233	186.2245	0.0334	203.1746	1.5619
149.1142	1.1345	167.1744	0.1418	187.1245	0.7026	203.3346	0.1948
149.9942	0.0138	167.2544	0.1631	188.0945	0.3033	204.1844	0.2438
150.0942	2.1970	168.0944	0.2743	188.1645	0.5245	205.1046	1.9153
150.1542	0.5463	168.1744	0.2257	189.1345	0.9053	205.1946	0.6353
150.2342	0.0224	168.9844	0.0449	190.1244	2.4029	205.2646	0.0510
150.3142	0.0798	169.1144	0.7634	191.1644	0.8260	205.3346	0.2674
151.1042	2.4169	170.0943	2.4524	191.3244	0.1444	206.1146	1.3888
151.9942	0.0233	170.1643	0.7699	192.1044	0.8808	207.1546	0.6841
152.1144	1.8475	170.3143	0.0121	192.1644	0.7164	207.3046	0.0065
153.0844	7.3443	171.3143	0.0316	192.2646	0.1631	208.1146	0.1866
154.0844	0.2669	172.1243	0.0233	193.0844	1.9747	208.2096	0.2489
154.1544	0.6016	173.1143	2.5624	193.1544	1.2033	209.1346	0.6855
155.1044	4.3168	174.1143	1.6005	194.0944	0.1066	210.1046	0.5924
156.1042	0.8579	174.2843	0.0278	194.1944	0.0112	210.1646	0.4759
156.1744	0.0032	175.1245	1.0943	194.9975	0.0072	210.3596	0.0539
156.2744	0.0043	176.1694	0.3052	195.0946	3.1210	211.1345	3.0752
157.1242	8.6263	178.0945	0.1522	195.1845	0.2334	212.1045	4.5670
157.2644	0.4851	178.1694	0.1653	196.0946	0.5111	212.2245	0.0402
158.1044	0.7496	178.2443	0.0012	196.2794	0.0381	212.3345	0.1979
158.1844	0.9330	179.0845	1.2791	197.1144	1.5219	213.1145	0.9750
158.9742	0.0192	179.1743	0.2183	197.3344	0.1330	213.2095	0.1117
159.0544	0.0104	180.0845	17.4680	198.1044	3.6321	213.3445	0.0168
159.1244	1.8878	181.0032	0.0079	198.1746	0.0900	214.1245	0.0236
160.0944	0.5539	181.1045	2.1415	199.1044	0.0119	214.2545	3.1092
161.2344	0.0030	181.1945	0.0652	199.1744	1.9133	215.1145	0.0645
162.0844	2.6589	182.1045	1.2815	199.3844	0.0011	215.1895	0.3722

Table A3.4 (continued). Mass data (*m/z* values and their relative intensities) for the DART-HRMS analysis of *A. absinthium* seed. Ten replicates of one sample were averaged where the corresponding spectrum appears in Figure 3.1.

A. Absinthium seed							
m/z	Rel. Int. %	*m/z*	Rel. Int. %	*m/z*	Rel. Int. %	*m/z*	Rel. Int. %
215.2645	0.1361	231.2847	0.1691	252.1247	0.0722	272.2547	0.0314
215.3245	0.0777	232.0389	0.0108	252.1847	0.1192	272.4649	0.0261
216.1245	3.0779	232.1346	2.0151	253.1847	0.8417	273.2446	0.0113
216.1945	0.0097	233.1346	1.6849	254.1847	0.0882	274.1548	0.0543
216.3345	0.1228	234.1346	0.2621	255.2247	1.2228	274.2648	0.6870
217.0770	0.2061	234.2046	0.0143	256.1447	0.0199	274.4148	0.0208
217.1745	0.6003	234.3546	0.0237	256.2447	0.0508	275.2648	0.0807
217.3645	0.0310	235.1746	1.8698	256.3447	0.0245	277.2148	2.4102
218.1345	0.3988	236.1746	0.3679	257.2447	6.0798	277.4548	0.0804
218.2747	0.0156	237.1846	0.8437	258.2547	1.1295	277.5248	0.0903
219.1045	0.4915	238.1946	0.2835	258.4347	0.1400	278.2148	0.7028
219.1845	0.7159	238.3846	0.0303	259.1947	3.3580	279.1546	0.2520
219.3045	0.0106	239.1446	0.3931	259.4247	0.1201	279.2348	51.6559
220.1145	0.4840	239.2346	1.2640	260.1947	0.1186	280.1448	0.5290
220.1745	0.0285	240.2146	0.0678	261.1147	1.1132	280.2446	12.1284
220.2546	0.0183	241.1846	1.3675	261.2247	0.7872	281.1448	0.6879
220.3347	0.0708	242.1846	0.0738	261.4647	0.0998	281.2448	52.2017
221.1845	0.8104	242.2846	0.9462	262.1847	0.5058	282.1548	0.2286
222.1245	0.0030	243.1648	0.3973	262.2547	0.2678	282.2648	9.9797
222.2045	0.0380	243.2498	0.1048	263.1347	3.4730	282.5246	0.3523
223.1247	0.8684	243.4048	0.1022	263.2347	23.6652	283.2648	10.7828
224.1147	0.1883	244.1148	1.4705	264.1249	0.6248	284.1548	0.0445
225.1447	1.1930	244.1946	0.3537	264.2447	3.8598	284.2648	1.2786
225.2547	0.2439	245.1246	2.6048	265.1547	1.7065	285.1048	1.0515
226.1247	0.1671	245.2246	2.6123	265.2449	3.0021	285.2048	0.0320
227.1347	0.8899	246.1148	1.4909	266.1447	0.4431	285.2748	1.7000
227.4147	0.0224	246.2446	0.2136	266.2547	0.6415	286.0281	0.0177
228.1947	0.1707	247.1246	7.7799	267.1547	0.1947	286.2748	0.0845
229.1047	5.0525	247.2248	0.4967	267.2647	0.3879	287.2248	0.0410
229.2045	0.6200	248.1346	1.4966	268.1149	1.9904	287.4748	0.0276
230.1047	0.4054	248.3297	0.0359	268.2047	0.5413	288.2448	0.0189
230.1847	0.3360	248.4046	0.1176	269.2147	0.7286	289.2348	0.0142
230.2547	2.2896	249.1646	1.3545	270.2049	0.0154	289.4048	0.0212
230.3547	0.1008	249.2648	0.0525	270.3049	0.0163	290.1748	0.0218
231.1247	13.8742	250.1548	0.1091	270.3849	0.0479	291.1948	0.1849
231.2147	0.1998	251.1648	1.5220	271.2347	0.6634	291.2750	0.0113

Table A3.4 (continued). Mass data (*m/z* values and their relative intensities) for the DART-HRMS analysis of *A. absinthium* seed. Ten replicates of one sample were averaged where the corresponding spectrum appears in Figure 3.1.

				A. Absinthium seed				
m/z	Rel. Int. %	*m/z*	Rel. Int. %	*m/z*	Rel. Int. %	*m/z*	Rel. Int. %
291.4148	0.0832	315.2998	1.4832	335.3249	0.0281	351.3351	0.2121
292.1948	0.0398	315.4448	0.0561	336.1849	0.1975	352.1751	0.0504
293.2148	0.9967	316.2250	0.9076	336.2549	0.0258	352.2451	0.2253
294.2147	0.1312	316.3048	0.5518	336.3251	0.0047	352.3251	0.1651
295.2347	9.4293	317.0648	0.1872	336.4749	0.0525	353.2651	1.2844
296.2549	1.8684	317.2348	0.3283	337.2651	1.8501	354.2651	0.6474
296.4747	0.0535	318.2248	0.0360	337.3451	0.0118	355.0751	0.7350
296.5247	0.1264	319.2348	0.0190	338.2649	0.4657	355.1950	0.0180
297.2449	27.5080	319.4450	0.0373	338.3449	0.8284	355.2950	12.4215
298.2749	59.9312	320.2350	0.0712	338.4251	0.0398	356.0750	0.3558
298.5049	0.1159	321.1550	0.0171	338.4849	0.1317	356.1950	0.0600
299.1949	0.6525	321.2350	0.0688	338.6049	0.0570	356.2850	2.5877
299.2749	11.8350	322.2450	0.1498	339.1049	0.0994	357.0750	0.2243
300.1949	0.2509	323.2548	0.1215	339.3251	0.6675	357.2050	0.1532
300.2947	6.3775	324.2650	0.8082	340.2651	0.2254	357.2950	0.8318
301.2049	0.0815	325.1150	0.2831	340.3449	0.1356	358.2152	0.2412
301.2949	0.7104	325.1950	0.0218	340.4251	0.0070	358.2950	0.3693
302.3049	0.0904	325.2850	0.3584	341.3149	0.6053	358.3650	0.0425
303.0549	0.0141	326.2950	0.1338	342.2151	0.0348	359.2250	0.1099
303.3049	0.0094	327.2850	0.2446	342.3149	0.2487	359.2952	0.2346
304.2349	0.0066	328.3248	0.1111	343.1649	0.3245	359.5150	0.0483
305.2349	0.0127	329.2350	0.0531	343.3351	0.1438	360.1550	0.2815
306.2749	0.9310	329.3150	0.0897	344.2651	0.2884	360.2252	0.3296
307.2749	0.0794	330.1150	0.0131	344.3951	0.0078	360.3150	0.2263
308.2349	0.0187	330.2350	0.1414	345.2749	0.1059	361.0493	0.0122
309.2149	0.1481	330.3350	0.0255	346.2749	0.1741	361.2352	0.1395
309.2849	0.2882	331.0950	5.4222	347.0851	0.0466	361.3250	0.0565
310.2449	1.7125	331.2950	0.8723	347.1649	0.0060	362.2650	0.2136
311.2349	0.1707	332.0950	0.9401	347.2851	0.1277	363.1752	0.0036
311.2749	0.9380	332.2150	0.6975	347.3651	0.0032	363.2452	0.0606
312.2749	0.7400	332.2950	3.0123	348.2949	0.8337	364.1952	0.2067
313.1149	0.1130	333.0950	0.0945	349.3351	0.1077	364.2550	0.2474
313.2749	2.0211	333.1750	0.0882	350.2351	0.0209	365.2750	0.3536
314.2448	2.4460	333.3450	0.2980	350.3151	0.0616	365.4150	0.0174
315.1148	0.2424	334.3350	0.0439	351.1751	0.1520	366.2950	0.3276
315.2248	6.8480	335.2049	0.1016	351.2451	0.1901	367.2050	0.2876

Table A3.4 (continued). Mass data (*m/z* values and their relative intensities) for the DART-HRMS analysis of *A. absinthium* seed. Ten replicates of one sample were averaged where the corresponding spectrum appears in Figure 3.1.

A. *Absinthium* seed							
m/z	Rel. Int. %	*m/z*	Rel. Int. %	*m/z*	Rel. Int. %	*m/z*	Rel. Int. %
367.3352	0.3726	376.5751	0.0575	393.4453	0.0940	408.4554	0.0519
368.2052	0.0753	377.1851	0.0058	394.1853	0.0063	409.3852	2.3246
368.2652	0.1049	377.2551	0.2989	394.2653	0.1222	410.2952	0.3790
368.3350	0.1669	377.3351	0.0828	394.3353	0.2956	410.3854	0.6383
369.2150	0.2595	377.4251	0.0085	395.2753	1.3692	411.3852	1.4485
369.3452	0.6414	377.5251	0.1390	395.3653	5.3406	411.6254	0.0790
369.4252	2.5058	378.2651	0.4268	396.1353	0.0253	411.6954	0.1788
369.4852	0.0717	378.3351	0.0240	396.3753	2.0546	412.2954	0.1593
369.5650	0.1619	379.2651	16.3623	397.0552	0.0608	412.3852	0.5545
370.3352	0.6134	380.0651	0.1134	397.2152	0.0066	413.3052	0.3568
370.4337	0.6249	380.2851	3.6781	397.3852	17.2076	413.3754	0.9794
371.1052	13.4222	381.2851	3.2323	398.2152	0.5912	414.3154	0.2379
371.3152	59.9483	382.1251	0.0231	398.2952	0.2479	414.3854	0.9685
371.5852	0.8103	382.2951	1.2016	398.3950	4.2988	414.6152	0.1977
371.6750	0.6295	382.3551	0.0405	398.5452	0.6650	415.3754	0.5279
371.7551	0.0305	383.3651	4.6425	399.3652	0.8908	416.3652	0.5769
371.8352	0.1284	384.1251	0.0084	400.0752	0.0052	416.4452	0.0066
372.1152	5.1981	384.2051	0.0039	400.3552	0.4426	417.3753	0.2704
372.2352	0.0285	384.3751	1.1128	401.2252	0.0931	418.2253	0.1046
372.3152	15.5203	385.3151	0.7488	401.3252	0.2238	418.2953	0.1994
372.6450	0.1105	386.3351	0.7504	401.4652	0.0488	418.3653	0.1086
372.8352	0.4032	387.3353	0.4753	402.3352	1.3219	418.4553	0.0421
372.9152	0.3248	387.6051	0.0362	403.1952	0.0037	419.1853	0.0160
373.1052	2.7045	388.1351	0.3540	403.3652	0.4719	419.3253	0.9093
373.1752	0.0384	388.3451	8.7539	404.1552	0.1237	420.3153	0.1819
373.3152	2.0065	388.5351	0.0961	404.2952	0.2808	421.1953	0.1894
374.0952	0.5629	389.1553	2.6418	404.6452	0.0259	421.2753	0.1034
374.2652	0.2913	389.2653	0.9947	405.2752	0.1055	421.3453	0.1971
374.3252	0.6841	389.3453	2.2144	405.3752	0.2365	421.4653	0.2248
375.1052	0.6765	390.1353	0.4452	406.2852	0.0468	422.2053	0.0282
375.1752	0.2394	390.2551	0.0360	406.3854	0.0100	422.3453	0.1645
375.2452	0.0439	390.3351	0.6314	407.1754	0.0474	422.4851	0.0570
375.3152	0.5161	391.1753	0.1943	407.2652	0.2069	423.2753	0.0572
376.1451	0.1903	391.2951	1.1851	407.3652	0.0367	423.3753	0.2818
376.2551	0.0446	392.2853	0.2943	407.4652	0.0247	423.4753	0.0072
376.3351	0.3739	393.3451	0.5062	408.3752	0.0945	424.2053	0.0253

Table A3.4 (continued). Mass data (*m/z* values and their relative intensities) for the DART-HRMS analysis of *A. absinthium* seed. Ten replicates of one sample were averaged where the corresponding spectrum appears in Figure 3.1.

				A. Absinthium seed			
m/z	Rel. Int. %	*m/z*	Rel. Int. %	*m/z*	Rel. Int. %	*m/z*	Rel. Int. %
424.3753	0.3905	444.4054	0.0666	461.4255	0.1870	479.2956	0.0485
424.5353	0.0075	445.2154	0.0112	462.1355	0.0094	479.3754	0.3453
425.3753	0.3494	445.3754	1.3984	462.2055	0.0646	479.4854	0.0493
426.3153	0.4146	446.3854	0.8715	463.3855	0.9876	480.4954	0.0313
426.4653	0.0205	447.3854	1.6879	464.2255	0.0870	481.3254	0.1403
427.3953	0.8807	448.2054	0.0542	464.3155	0.0043	481.3954	0.0121
428.3955	0.6191	448.3854	0.3675	464.3855	0.2079	481.4956	0.0571
429.1653	0.0071	449.3954	0.2618	465.3955	0.2546	482.3354	0.0682
429.2353	0.0036	449.5154	0.0374	465.4855	0.0281	482.4756	0.0661
429.3853	3.6109	450.2154	0.0124	466.3355	0.1563	482.5256	0.0248
430.2353	0.1375	450.3454	0.1669	466.5055	0.0944	483.3856	0.2132
430.3853	3.0544	450.5154	0.0578	467.3955	0.3813	483.5356	0.0457
431.3853	5.0368	451.3454	0.2013	468.3955	0.1063	484.3956	0.1026
432.1853	0.0799	451.4254	0.0148	468.4955	0.0318	484.5456	0.0419
432.3955	1.8944	453.3554	0.1802	469.4055	0.1299	485.4056	0.1046
433.4003	0.6599	453.4654	0.0233	470.3455	0.0384	486.2256	0.0206
434.2653	0.0073	454.2154	0.0875	470.4155	0.0906	486.3854	0.5837
434.3955	0.2949	454.3454	0.0979	470.5055	0.0700	487.3854	0.2135
435.3553	0.2288	454.4956	0.0955	471.3855	0.0692	487.5256	0.0982
435.4655	0.1036	455.3556	0.1383	471.4955	0.0336	488.3956	0.2371
436.3353	0.1496	455.4354	0.0205	472.3455	0.1285	488.4656	0.0234
437.1955	0.0716	455.4954	0.0534	472.3855	0.0099	488.5456	0.0683
437.2753	0.0328	456.2854	0.0122	473.3755	0.0588	489.3756	0.1188
437.3455	0.0995	456.3754	0.0446	474.3855	0.2300	490.4656	0.0300
437.4755	0.0759	456.5156	0.1332	474.4655	0.0217	491.3056	0.0039
438.2154	0.2303	457.3754	0.1517	475.3855	0.1368	491.3756	0.3084
438.3552	0.2487	457.4954	0.0559	476.3155	0.0269	491.4856	0.0058
438.4852	0.1289	458.2354	0.1227	476.4055	0.1940	492.3356	0.0695
439.2903	0.0066	458.3853	0.1120	476.4955	0.0141	493.3856	0.2874
439.3652	0.3679	459.1855	0.0079	477.2955	0.0771	493.5156	0.0070
440.3654	0.2758	459.3855	0.1864	477.4355	0.0688	494.3656	0.0143
441.3754	0.1897	459.4855	0.0676	477.5455	0.0347	495.3856	0.2400
442.3054	0.2607	460.3053	0.2411	478.2455	0.0104	495.4456	0.0332
442.3854	0.4019	460.4155	0.0099	478.3255	0.1805	496.3256	0.0576
443.3854	0.2663	460.4955	0.0742	478.4355	0.0122	497.3956	0.1088
444.2954	0.2934	461.3755	0.2467	478.5455	0.0053	498.3256	0.0592

Table A3.4 (continued). Mass data (*m/z* values and their relative intensities) for the DART-HRMS analysis of *A. absinthium* seed. Ten replicates of one sample were averaged where the corresponding spectrum appears in Figure 3.1.

				A. Absinthium seed			
m/z	Rel. Int. %	*m/z*	Rel. Int. %	*m/z*	Rel. Int. %	*m/z*	Rel. Int. %
498.3956	0.1150	520.4056	0.0536	545.4057	0.0567	564.5458	0.0086
498.5356	0.0554	521.5256	0.2611	545.4757	0.1240	564.6358	0.0031
499.3256	0.0138	522.4256	0.1238	545.7257	0.0045	565.5258	0.0329
499.4256	0.0443	523.4056	0.0529	546.3857	0.0156	566.4458	0.0981
500.4255	0.2258	525.4256	0.2084	546.4557	0.0860	566.5358	0.0118
501.3957	0.0104	526.4156	0.1614	547.4657	0.2551	567.3858	0.1189
501.4755	0.0550	526.5658	0.0572	548.3459	0.0526	567.4558	0.0144
502.4155	0.2389	527.4256	0.1146	548.4657	0.1268	567.5358	0.0533
503.4155	0.2023	527.5256	0.0113	549.3559	0.0838	568.5258	0.0051
504.4555	0.0165	528.4256	0.1889	549.4959	0.1116	569.4958	0.0974
505.3955	0.2749	529.4156	0.0288	550.2857	0.0093	569.5660	0.0561
505.5755	0.0067	530.4056	0.0888	550.4459	0.0727	569.6358	0.0040
506.2555	0.0098	531.4058	0.2206	550.5657	0.0292	570.4058	0.1113
506.3657	0.1381	532.4158	0.1296	551.5057	0.2557	570.5458	0.0406
507.3955	0.2319	533.4407	0.1760	552.3859	0.0372	571.4458	0.0995
507.5155	0.0416	533.5258	0.0413	552.4959	0.0901	571.5558	0.0143
508.3557	0.1863	534.3656	0.0903	552.5857	0.0624	572.4458	0.0321
508.5257	0.0839	534.4858	0.0712	553.4957	0.0250	572.5658	0.0029
509.2255	0.0029	535.4458	0.1132	554.4957	0.0782	573.4558	0.1930
509.4055	0.1826	535.5358	0.0106	555.3859	0.0436	574.4460	0.1600
509.5257	0.0600	536.5358	0.0156	555.4559	0.0509	575.5060	5.3988
510.4157	0.1342	536.6058	0.0877	556.3659	0.0034	576.5158	1.7812
511.3257	0.1330	537.5058	0.2106	556.4359	0.0580	577.5258	1.4352
511.4357	0.0380	537.6158	0.0652	557.4459	0.2784	578.5260	0.5325
512.4057	0.0666	538.3858	0.0708	557.5359	0.0041	579.5260	0.4060
512.5757	0.0134	538.5058	0.0865	558.4457	0.2189	580.4360	0.1457
513.3957	0.0798	539.3658	0.0412	559.4459	0.4397	580.5258	0.0727
514.3357	0.0369	539.4958	0.0699	559.5459	0.0201	580.6060	0.0064
514.4157	0.1094	540.4358	0.1007	560.4159	0.0720	581.4460	0.0058
515.4257	0.0360	541.4257	0.1019	560.4959	0.1348	581.5358	0.0167
516.4257	0.2177	541.5057	0.0176	561.4957	0.6502	582.5159	0.0735
516.4957	0.0082	542.4157	0.0485	562.5158	0.3347	583.4557	0.0606
517.4457	0.0903	543.4257	0.0718	563.4358	0.1125	583.5259	0.0071
518.4357	0.1137	543.4957	0.0430	563.4858	0.0364	584.5759	0.0071
518.5157	0.0074	544.3857	0.2480	563.5358	0.0870	585.3859	0.0753
519.4957	0.9803	544.5257	0.0657	564.4358	0.0027	585.4759	0.0854

Table A3.4 (continued). Mass data (*m/z* values and their relative intensities) for the DART-HRMS analysis of *A. absinthium* seed. Ten replicates of one sample were averaged where the corresponding spectrum appears in Figure 3.1.

				A. Absinthium seed			
m/z	Rel. Int. %	*m/z*	Rel. Int. %	*m/z*	Rel. Int. %	*m/z*	Rel. Int. %
585.5859	0.0055	607.5760	0.0866	631.5059	0.5154	659.5262	12.9289
586.3959	0.0631	608.4510	0.0118	632.5361	0.3288	660.5362	5.5682
586.5559	0.0483	608.5260	0.0835	633.5161	2.3094	661.5562	2.9388
587.4909	0.0789	609.5160	0.1586	633.6961	0.0166	662.5662	0.7432
587.5859	0.0121	610.5460	0.7343	634.5461	1.8370	663.5562	0.2423
588.5059	0.0932	611.5360	0.2021	635.5461	1.2565	664.5662	0.1427
589.4759	0.2366	612.3560	0.0121	635.7061	0.0141	665.5161	0.0492
589.5959	0.0365	612.4760	0.1372	636.5661	0.5835	665.5961	0.0031
590.4859	0.0563	612.5460	0.1022	637.5661	0.3195	666.5561	0.1756
591.4961	0.5266	613.5060	0.1623	637.7161	0.0043	666.7161	0.0281
591.5859	0.0066	614.4960	0.1108	638.5761	0.2563	667.5861	0.0777
592.4959	0.2526	615.5060	2.5911	639.5661	0.1078	667.7161	0.0187
592.6759	0.0574	616.5160	1.2760	640.4761	0.1476	668.5761	1.0519
593.5159	0.2646	617.5160	3.8543	641.4861	0.1151	669.5863	0.4915
593.6659	0.0114	618.5260	1.1245	641.5661	0.0248	675.5063	2.0499
594.5159	0.1878	618.6762	0.3420	642.4863	0.0809	676.5261	8.8438
595.5259	0.1241	619.3860	0.0437	643.4963	0.0542	677.5463	3.5702
596.5261	0.0278	619.5360	0.4843	644.4960	0.0406	678.5961	2.3270
597.5259	0.2500	619.6660	0.0627	645.4862	0.0089	678.7263	0.1993
598.4561	0.2292	619.7560	0.1620	646.4960	0.0731	679.4163	0.0090
599.5061	4.9894	620.5360	0.1319	646.6162	0.0097	679.5963	0.9353
600.5061	1.6251	620.6660	0.0711	647.4762	0.0305	680.3263	0.0026
601.3761	0.0067	621.5460	0.0384	647.6360	0.0189	680.5963	1.0469
601.5259	2.1357	621.6660	0.0177	648.5160	0.1287	681.4563	0.0038
602.3861	0.0063	622.5460	0.0772	648.6360	0.0077	681.5963	0.3019
602.5261	0.7791	623.4659	0.0244	649.5160	0.3783	682.5563	0.1779
602.6261	0.0085	623.5659	0.0408	649.6760	0.0049	683.4863	0.0098
603.3060	0.0304	624.4759	0.3130	650.5460	0.7286	684.5063	0.0832
603.5360	1.0100	624.5459	0.0052	650.6862	0.0189	685.4962	0.0091
604.3158	0.0203	625.4861	0.1336	651.5462	1.2632	688.5764	0.1360
604.5458	0.4894	626.5259	0.1017	652.5462	7.4825	690.6564	0.0030
605.5460	0.2148	627.5061	0.0165	653.5660	2.5408	691.6662	0.0046
606.4060	0.0166	627.5861	0.0081	654.5662	1.0360	692.5564	2.1809
606.5360	0.1106	628.5061	0.0523	656.4962	0.1744	694.6064	0.8570
606.6260	0.0221	629.5059	0.1083	657.5062	4.3870	695.6264	0.1339
607.5060	0.1172	630.4961	0.1024	658.5062	2.3846	695.7464	0.0041

Table A3.4 (continued). Mass data (*m/z* values and their relative intensities) for the DART-HRMS analysis of *A. absinthium* seed. Ten replicates of one sample were averaged where the corresponding spectrum appears in Figure 3.1.

			A. Absinthium seed				
m/z	Rel. Int. %	*m/z*	Rel. Int. %	*m/z*	Rel. Int. %	*m/z*	Rel. Int. %
696.5964	0.5385	743.6164	0.2213	781.6166	0.3996	863.6170	0.0620
697.6262	0.2518	744.6166	0.2580	782.6766	0.0946	868.6470	0.0664
700.5264	0.0985	745.6266	0.1582	784.6668	0.0794	872.7669	0.6410
704.6564	0.0064	746.6264	0.4897	785.6266	0.2432	873.7669	0.3646
705.6664	0.0294	747.6265	0.3209	788.6167	0.3000	874.7669	0.4464
705.7564	0.0024	748.6463	0.5271	790.6167	0.4364	875.7769	0.2707
706.5863	0.6067	749.6365	0.2505	792.6067	0.4260	876.7869	0.1523
707.6463	0.0143	750.8165	0.0939	793.6067	0.2348	877.7269	0.8943
708.5863	0.7301	751.5965	0.3816	794.6167	0.7072	878.7369	0.7561
709.5963	0.3503	751.6863	0.0484	795.6267	0.4042	879.0569	0.0411
710.6063	0.4899	752.6065	0.5278	796.6267	0.4222	879.7369	3.8423
711.6063	0.2194	752.6765	0.0104	796.7067	0.0252	880.7371	1.9447
712.6063	0.2480	753.6165	0.3577	797.6367	0.2096	881.7469	1.4180
713.5865	0.1294	754.6465	0.3414	805.5967	0.0887	882.7471	0.5159
714.5863	0.1139	755.6265	0.1791	807.6067	0.1036	883.7571	0.3351
715.6063	0.0561	756.6265	0.1785	809.6066	0.1689	884.7571	0.2749
717.5965	0.1071	757.6265	0.1696	810.6266	0.5443	885.7771	0.1344
718.6763	0.0131	761.6165	0.1758	811.6166	0.3201	886.7871	0.0687
719.6565	0.0357	762.6165	0.3706	812.6366	0.2334	895.7370	0.5214
720.7365	0.0360	764.6765	0.1141	819.6266	0.1376	896.7570	1.6384
721.5363	0.0080	767.6067	0.2657	821.5868	0.1263	897.7570	1.1949
721.6263	0.2477	768.5766	0.4499	822.6068	0.1241	898.7670	0.9538
722.6365	0.2834	768.6666	0.0154	831.7269	0.0550	899.7770	0.4726
723.6465	0.1928	769.6066	0.3416	833.7469	0.0079	900.7970	0.3218
725.6065	0.2465	769.7011	0.0093	835.6169	0.0590	901.7970	0.0899
727.5744	0.1841	770.6064	0.8236	837.5867	0.0438	902.7970	0.0081
728.5964	0.2871	771.6364	0.5518	848.7569	0.0942	906.6772	0.0340
729.5964	0.1867	772.6366	0.3393	849.7469	0.0190	907.6770	0.0422
735.6764	0.0042	773.6364	0.1779	853.7170	0.4683	908.6872	0.0198
736.6164	0.4112	775.6164	0.2823	854.7268	0.3197	910.7072	0.0352
737.6364	0.1859	776.6166	0.3364	855.7368	1.2436	912.7569	0.6736
738.6364	0.2353	776.6866	0.0106	856.7468	0.7694	914.7771	0.2883
739.6464	0.1691	777.6166	0.1818	857.7568	0.3171	930.8371	0.0769
740.6364	0.2020	778.6266	0.4112	858.7570	0.2125	946.7772	0.0241
741.6266	0.1610	779.6366	0.2511	859.7668	0.0505	954.8371	0.0302
742.6164	0.1642	780.7066	0.0051	860.7668	0.0216	956.8473	0.0430

Table A3.4 (continued). Mass data (*m/z* values and their relative intensities) for the DART-HRMS analysis of *A. absinthium* seed. Ten replicates of one sample were averaged where the corresponding spectrum appears in Figure 3.1.

A. Absinthium **seed**							
m/z	Rel. Int. %	*m/z*	Rel. Int. %	*m/z*	Rel. Int. %	*m/z*	Rel. Int. %
957.8671	0.0093	998.8173	0.0551	1015.7774	0.1524	1035.8576	0.0191
969.7873	0.0458	1000.7873	0.0679	1016.7974	0.1985	1057.8476	0.0143
970.7773	0.0948	1001.7973	0.0282	1017.8074	0.0699	1058.8376	0.0228
974.7874	0.0021	1002.8173	0.0234	1031.8374	0.0460		
978.7674	0.0210	1007.8273	0.1162	1032.8274	0.0705		
997.8173	0.0647	1014.7875	0.1885	1034.8576	0.0286		

Table A3.5 Mass data (*m/z* values and their relative intensities) for the DART-HRMS analysis of A. *absinthium tincture*. Ten replicates of one sample were averaged where the corresponding spectrum appears in Figure 3.1.

				A. Absinthium **tincture**			
m/z	Rel. Int. %	*m/z*	Rel. Int. %	*m/z*	Rel. Int. %	*m/z*	Rel. Int. %
62.0639	0.0071	89.2541	0.0584	111.2342	0.0349	130.1543	0.5747
65.0541	0.0249	90.0641	2.0243	112.0742	0.5280	130.2343	0.0116
67.0540	0.0282	90.1641	0.0601	113.0542	0.5720	131.0643	1.0222
68.9640	0.0049	91.0541	1.0553	114.0842	0.0609	131.2243	0.0652
69.0440	0.2619	92.0641	0.0688	115.0542	0.7994	132.1041	3.2236
69.1440	0.0104	93.0641	36.3133	115.1040	0.3258	133.0643	2.9299
70.0640	1.0348	93.1341	0.2653	115.2442	0.0524	133.2543	0.0573
70.1340	0.0020	94.0641	1.6029	116.0742	25.1456	134.0843	0.3293
71.0640	0.2138	94.1741	0.2113	116.2242	0.2814	134.1943	0.0613
72.0840	0.7456	95.0241	0.0048	117.0642	5.3270	134.2543	0.0327
72.2040	0.0453	95.0841	3.2434	117.2442	0.1904	135.1043	94.3581
73.0640	1.6518	96.0541	0.0717	118.0842	2.5391	135.2443	1.0253
74.0640	0.5628	97.0341	1.0567	118.2042	0.1246	135.9943	0.0596
75.0440	0.3751	97.0941	0.5378	119.0842	0.7680	136.0643	3.7305
75.1140	1.9582	97.2241	0.0052	120.0742	0.3024	136.1343	10.9441
76.0640	0.1644	97.2841	0.0284	120.2042	0.0396	136.2143	0.7611
77.0440	0.0961	98.0841	0.2797	121.0842	0.6385	136.2843	0.0736
78.0440	0.0037	99.0541	1.2337	122.0742	0.0164	136.4043	0.1418
79.0440	1.9468	100.0841	0.0298	123.0942	0.9329	136.9843	0.0935
79.1242	0.0048	101.0641	0.8662	123.2942	0.0057	137.0743	0.3476
80.0540	0.1080	101.1841	0.0654	124.0642	0.2157	137.1243	44.1460
81.0540	9.9085	102.0741	0.0175	124.1844	0.0098	137.2143	1.2811
82.0642	0.3674	103.0541	0.6721	125.0942	0.5186	137.2843	0.5252
82.9442	0.0085	104.0741	2.0646	125.2144	0.0043	137.9843	0.1061
83.0840	0.5053	104.2343	0.0329	126.0642	1.2051	138.0843	0.0591
84.0640	0.4440	105.0641	0.4827	126.1542	0.0268	138.1643	4.4227
84.9540	0.0187	105.1843	0.0755	127.0442	6.7202	139.0054	0.0846
85.0342	3.4864	106.0641	0.0409	127.1142	0.9593	139.1043	0.2369
85.0942	0.1589	107.0841	3.7356	127.2342	0.0447	139.2243	0.0333
86.0740	0.5917	108.0640	0.1352	127.9777	0.0040	139.2643	0.0688
86.1742	0.0084	109.0340	2.5654	128.0844	1.1828	140.0043	0.0032
87.0539	0.7272	109.0942	1.3359	128.2243	0.0821	140.0843	0.4261
87.1641	0.0417	110.0742	0.4568	128.3041	0.0038	140.3143	0.0211
88.0741	0.1020	110.1640	0.0045	129.0641	0.9715	141.1043	0.6748
88.2041	0.0042	110.2142	0.0524	129.2141	0.0128	142.1043	3.9298
89.0641	5.8049	111.1140	0.3539	130.0643	7.5097	142.1843	0.0108

Table A3.5 (continued). Mass data (*m/z* values and their relative intensities) for the DART-HRMS analysis of A. *absinthium tincture*. Ten replicates of one sample were averaged where the corresponding spectrum appears in Figure 3.1.

m/z	Rel. Int. %	*m/z*	Rel. Int. %	*m/z*	Rel. Int. %	*m/z*	Rel. Int. %
143.0943	0.5855	160.0042	0.0084	178.2443	0.0055	198.1044	4.1262
144.0843	1.6581	160.0944	0.6560	179.0845	0.6239	198.1746	0.0049
144.1743	0.0598	161.1644	2.0729	180.0845	9.7425	199.0346	0.0015
144.2443	0.0360	162.0844	0.7146	181.0032	0.0012	199.1044	0.4673
145.0543	7.7067	162.2244	0.0063	181.1045	1.2993	199.1744	0.6996
145.1243	0.2423	163.0644	7.3887	181.1945	0.9694	199.4046	0.0015
145.2243	0.1180	163.1344	1.0014	182.0143	0.0045	200.1244	0.9852
146.0843	1.3336	164.0844	0.3901	182.1045	0.3788	200.1844	0.0021
147.0743	1.2831	164.1644	0.1224	182.1943	0.1325	201.1444	4.3431
147.2345	0.0022	165.0844	1.2441	183.0945	1.2663	202.1244	1.2666
148.0745	0.1662	165.2744	0.0558	184.1145	1.7788	202.2846	0.0455
149.1142	0.5606	166.0944	0.4822	185.1145	2.2092	203.1746	4.2152
149.9942	0.0209	166.1944	0.0156	186.1145	0.9693	204.0244	0.0145
150.0942	0.9642	167.0944	0.4566	187.1245	1.5630	204.1844	0.6291
150.1542	0.0897	167.2544	0.0537	188.0945	0.5427	205.1046	0.4215
150.2342	0.0123	168.0944	0.2402	188.1645	1.0170	205.1946	3.4250
150.3142	0.0248	168.1744	0.0119	189.1345	1.3725	205.4046	0.0152
151.1042	1.3554	168.2544	0.0373	189.4045	0.0156	206.1146	0.4467
151.2342	0.0553	168.9844	0.0178	190.1244	0.4748	206.2044	0.4012
152.1144	0.4844	169.1144	0.4855	191.0678	1.0660	207.0746	1.8141
153.0844	13.0097	170.0943	0.7063	191.1644	0.3300	207.1546	1.7662
154.0144	0.0032	170.1643	1.1136	191.3244	0.0863	208.1146	0.6600
154.0844	0.1222	170.3143	0.0180	192.1044	0.2391	208.2096	0.1821
154.1544	1.8085	171.1543	0.0280	192.2646	0.0169	209.1346	0.8336
155.0100	0.0085	171.3143	0.0191	193.0844	1.1384	210.1046	0.7793
155.1044	0.8417	172.1243	2.4882	193.1544	0.0954	210.1646	0.0387
156.1042	1.0748	173.1143	1.7777	194.0944	0.2435	210.3596	0.0059
156.1744	0.0039	174.1143	0.5087	195.0946	13.9189	211.1345	0.4994
156.2744	0.0183	174.2843	0.0068	195.1845	1.3034	212.1045	17.1033
157.1242	1.8408	175.0543	0.0676	195.2744	0.3006	212.1845	0.0367
157.2644	0.1131	175.1245	0.8725	196.0144	0.0347	212.3345	0.2481
158.1044	19.8836	176.0945	0.5259	196.0946	1.7477	213.0145	0.0210
158.2544	0.0204	177.0645	0.1209	196.2794	0.0488	213.1145	2.2449
158.9742	0.0305	177.1443	0.2352	197.1144	0.7177	213.3045	0.0062
159.0544	0.8624	178.0945	0.1356	197.3344	0.0783	213.3445	0.0332
159.1244	2.4850	178.1694	0.0430	198.0244	0.0075	213.7345	0.0407

Table A3.5 (continued). Mass data (*m/z* values and their relative intensities) for the DART-HRMS analysis of A. *absinthium tincture*. Ten replicates of one sample were averaged where the corresponding spectrum appears in Figure 3.1.

A. *Absinthium* tincture							
m/z	Rel. Int. %	*m/z*	Rel. Int. %	*m/z*	Rel. Int. %	*m/z*	Rel. Int. %
214.0245	0.0183	231.0247	0.0027	248.4046	0.1021	268.2047	0.5507
214.1245	0.8341	231.1247	34.1941	249.1646	4.4412	269.1347	0.5190
214.2545	0.2571	231.3247	0.3079	249.2648	0.0068	269.2147	2.4481
215.1145	0.7732	232.0389	0.0794	250.1548	0.9231	270.2049	0.7184
215.1895	0.1773	232.1346	6.6442	251.1648	3.3880	270.3849	0.0294
215.2645	0.0183	233.0346	0.0040	252.1247	0.4648	271.0847	0.5086
215.3245	0.0521	233.1346	8.2950	252.1847	0.0685	271.1597	0.0762
216.1245	10.1334	234.0346	0.0174	252.2647	0.0051	271.2347	3.2743
216.1945	0.0015	234.1346	2.4610	253.1847	3.3493	271.4147	0.0208
216.3345	0.0132	234.3546	0.0671	254.1847	0.6009	272.1349	0.0160
217.1745	2.5802	235.1746	12.5424	255.2247	0.2265	272.2547	0.5725
218.0445	0.0148	236.1746	2.0313	256.1447	0.2523	272.4649	0.0304
218.1345	1.3737	237.1846	1.8993	256.2447	0.0899	273.1548	0.3181
219.1845	2.0461	238.1146	0.0495	256.3447	0.0018	273.2446	0.7268
220.1145	0.3874	238.1946	0.4278	257.1647	0.0707	274.1548	0.1972
220.1745	0.0593	238.3846	0.0437	257.2447	0.0712	274.2648	0.1001
220.3347	0.0362	239.2346	2.3366	258.1647	0.0644	274.4148	0.0279
221.0545	0.1864	240.1246	0.1316	258.2547	0.0336	275.2046	1.4751
221.1845	1.8364	240.2146	0.4433	258.4347	0.0154	276.1648	0.2664
222.0347	0.0016	241.1046	0.5379	259.1947	0.1581	276.2748	0.0039
222.1245	0.0602	241.1846	0.1839	259.2647	0.0231	277.1146	1.0502
222.2045	0.2447	242.1048	0.2607	259.4247	0.0083	277.2148	0.1568
223.1247	0.3390	242.1846	0.0124	260.1147	0.3180	277.4548	0.0040
224.1147	0.4065	242.2846	0.0068	260.2547	0.0412	277.5248	0.0230
224.2545	0.0218	243.1046	0.8008	261.1147	1.1808	278.1248	0.6067
225.1447	0.7626	243.1648	0.0834	261.2247	0.0155	278.2148	0.0243
226.1247	0.9722	243.2498	0.0116	261.4647	0.0137	279.1546	1.6952
227.1347	0.7217	243.4048	0.0232	262.1847	0.6009	279.4048	0.0317
227.4147	0.0060	244.1148	0.5946	263.1347	12.9541	280.1448	0.5783
228.1247	0.3810	244.1946	0.0148	263.3849	0.2120	280.2446	0.5533
228.1947	0.0114	245.1246	6.5700	264.1249	2.0949	281.1448	5.7724
228.3247	0.0015	245.2246	0.0092	264.2447	0.0100	281.2448	0.0558
229.1047	12.0553	246.1148	1.5522	265.1547	1.0754	282.1548	0.9245
230.0147	0.0104	247.1246	5.3481	265.2449	0.8083	282.2648	0.0795
230.1047	2.7117	248.1346	1.3818	266.1447	0.6250	282.5246	0.0181
230.3547	0.0837	248.3297	0.0722	267.1547	0.3571	283.0948	0.0825

Table A3.5 (continued). Mass data (*m/z* values and their relative intensities) for the DART-HRMS analysis of A. *absinthium tincture*. Ten replicates of one sample were averaged where the corresponding spectrum appears in Figure 3.1.

A. Absinthium tincture							
m/z	Rel. Int. %	*m/z*	Rel. Int. %	*m/z*	Rel. Int. %	*m/z*	Rel. Int. %
283.1848	0.6651	296.4747	0.0147	311.1449	0.3086	331.0950	0.1893
283.2648	0.1322	296.5247	0.0236	311.2349	0.0182	331.2250	0.1777
284.1548	0.2164	297.1847	0.8349	311.2749	0.1541	331.2950	0.0284
284.2648	0.0797	298.1649	1.6865	312.1649	0.2420	332.2150	0.2038
284.3648	0.0059	298.2749	0.0857	312.2749	0.0112	332.2950	0.0252
285.1048	0.4050	298.4049	0.0413	313.2149	0.1712	332.3550	0.0282
285.2748	1.3377	298.5049	0.0353	314.2448	0.8044	333.1750	0.1056
286.1348	0.0329	299.0949	0.0215	315.2248	0.2066	333.2350	0.0068
286.2148	0.0747	299.1949	0.4621	315.4448	0.0062	333.3450	0.0131
286.2748	0.2475	299.2749	0.0282	316.2250	0.2173	334.2350	0.6895
287.3048	1.4514	300.1949	0.3464	317.0648	0.0438	335.2049	0.2425
287.4748	0.0388	300.4249	0.0388	317.2348	0.1038	336.1849	0.0724
288.0348	0.0011	301.0949	0.3642	318.2248	0.1289	336.2549	0.3572
288.1348	0.0825	301.2049	0.2650	319.2348	0.2313	336.4749	0.0520
288.2448	0.2800	301.2949	0.2398	319.4450	0.0018	337.2049	1.1734
289.1048	0.7724	302.1449	0.3062	320.1648	0.9176	338.1951	0.3160
289.1748	0.1048	302.3049	0.1087	320.2350	0.0316	338.2649	0.1309
289.2348	0.1561	303.1249	0.4762	321.1550	0.3739	338.4251	0.0156
289.4048	0.0108	303.3049	0.1465	321.2350	0.1662	338.4849	0.0318
289.4748	0.0151	304.1549	0.1237	322.2450	0.3132	339.1849	0.2119
290.1748	0.4913	304.2349	0.1137	323.1750	0.1782	339.3251	0.1114
290.2748	0.3719	304.3649	0.0048	323.2548	0.1491	340.3449	0.0614
290.4048	0.0371	305.1549	0.1524	323.3570	0.0025	341.1349	0.4068
291.1948	2.9599	305.2349	0.1482	324.1750	0.6040	341.2149	0.0158
291.2750	0.0105	305.3149	0.0674	324.2650	0.1990	341.3149	0.1797
291.4148	0.1011	306.1649	0.3631	325.1950	0.3243	342.2151	0.9155
292.1948	0.6580	306.2749	0.0840	325.2850	0.2215	342.3149	0.0012
293.1348	0.2885	307.1949	0.7736	326.1850	1.3670	343.1649	0.1811
293.2148	0.6379	307.2749	0.4476	326.2950	0.2031	343.2351	0.0853
293.2947	0.0201	308.2349	0.6230	327.1950	0.2139	343.3351	0.0197
294.2147	0.3665	308.3315	0.0214	327.2850	0.1452	344.1751	0.3797
294.2949	0.0213	309.2149	5.6435	328.2250	0.3963	345.1849	0.2066
295.1547	2.3359	309.2849	1.0392	328.3248	0.0086	345.2749	0.0013
296.1649	0.3693	309.3549	0.0756	329.2350	0.2988	346.1751	0.3255
296.2549	0.2825	310.1349	1.0852	330.2350	0.2077	347.0851	0.4028
296.3447	0.1253	310.2449	0.0519	330.3350	0.0579	347.1649	0.4195

Table A3.5 (continued). Mass data (*m/z* values and their relative intensities) for the DART-HRMS analysis of A. *absinthium tincture*. Ten replicates of one sample were averaged where the corresponding spectrum appears in Figure 3.1.

			A. Absinthium **tincture**				
m/z	Rel. Int. %	*m/z*	Rel. Int. %	*m/z*	Rel. Int. %	*m/z*	Rel. Int. %
347.2851	0.0037	362.3750	0.0170	374.3252	0.0052	387.2253	0.0784
348.1149	0.0492	363.2452	0.1949	375.1052	2.8164	387.2853	0.0242
348.1851	0.2599	364.1952	0.6650	375.2452	0.0019	387.6051	0.0172
348.2949	0.0060	365.2750	0.3407	376.1451	0.5084	388.1351	0.3108
349.2151	0.1332	365.4150	0.0022	376.2551	0.0017	388.2653	0.3309
349.3351	0.0383	366.2652	0.5554	376.3351	0.0014	388.3451	0.0114
350.2351	0.3809	366.2950	0.0012	376.5751	0.0202	388.4351	0.0781
350.3751	0.0042	367.2750	0.3957	377.1851	0.2251	388.5351	0.0025
351.2451	0.1283	368.2652	1.0909	377.2551	0.0318	389.1553	35.1469
351.3351	0.0017	369.2150	0.3552	377.3351	0.0526	390.1353	7.5208
352.2451	0.7292	369.4252	0.0396	377.4251	0.0182	390.2551	0.0081
352.3251	0.0079	369.4852	0.0576	377.5251	0.0415	390.3351	0.1055
353.1851	0.4032	369.5650	0.0507	378.1851	1.0607	391.1753	1.2976
354.1951	0.2643	370.2150	0.9058	378.3351	0.0035	391.2951	0.5549
354.2651	0.4743	371.1052	0.9000	379.1751	0.0518	391.3901	0.1904
355.0751	0.0428	371.2250	0.0743	379.2651	0.2646	392.1851	0.4879
355.1950	0.0115	371.3152	0.5281	379.3451	0.0110	392.2853	0.1007
355.2950	0.2377	371.4952	0.0104	380.2051	0.5292	393.2652	0.1879
356.0750	0.0209	371.5852	0.0436	380.3451	0.0038	393.3451	0.1300
356.2850	0.4206	371.6750	0.0296	381.1951	0.0855	393.4453	0.0052
357.0750	0.0081	371.7551	0.0046	381.2851	0.2354	394.2653	0.3295
357.2050	0.2786	371.8352	0.0092	381.3451	0.0020	394.3353	0.0048
357.2950	0.0039	372.1152	0.3629	381.4153	0.0056	395.0553	0.0023
357.3850	0.0010	372.2352	0.6795	382.2951	0.5853	395.1953	0.1865
358.2152	0.2039	372.3152	0.0740	382.4351	0.0523	395.2753	0.0014
359.1350	0.1084	372.6450	0.0252	383.1951	0.1259	395.3653	0.1575
359.2250	0.1795	372.8352	0.0334	383.2951	0.1363	396.2053	2.4907
359.2952	0.0063	372.9152	0.0289	383.3651	0.0395	396.2853	0.0066
359.3850	0.0205	373.1052	0.1964	384.2051	0.2584	396.3753	0.0027
359.5150	0.0296	373.1752	0.0652	384.2751	0.1508	397.0552	0.0066
360.2252	0.3244	373.2452	0.1366	385.2151	0.2363	397.2152	0.5724
361.1550	0.0679	373.3152	0.0208	385.3151	0.0073	397.3852	0.3709
361.2352	0.1908	373.4052	0.0055	385.4851	0.0120	398.2152	0.7710
361.3250	0.0366	374.0952	0.0292	386.2153	0.3277	398.3950	0.0895
362.1652	0.1732	374.1652	0.0444	386.3351	0.0589	398.4752	0.0456
362.2650	0.0603	374.2652	0.1751	387.1053	0.0838	398.5452	0.0404

Table A3.5 (continued). Mass data (*m/z* values and their relative intensities) for the DART-HRMS analysis of A. *absinthium tincture*. Ten replicates of one sample were averaged where the corresponding spectrum appears in Figure 3.1.

m/z	Rel. Int. %	*m/z*	Rel. Int. %	*m/z*	Rel. Int. %	*m/z*	Rel. Int. %
399.2252	0.3230	412.2052	0.5860	427.2253	0.0555	441.3754	0.0219
399.3652	0.0116	412.3852	0.0029	427.2953	0.1705	441.4754	0.0027
400.2352	0.8933	413.2152	0.4899	427.3953	0.1643	442.2454	0.2299
401.2252	0.1688	413.3052	0.0032	428.2353	0.2707	442.3054	0.0613
401.3252	0.0739	413.3754	0.0072	428.2953	0.0082	442.3854	0.0014
401.4652	0.0453	413.4554	0.0029	428.3955	0.0038	443.2954	0.1338
402.2252	0.2336	414.2154	0.3107	428.4953	0.0173	443.3854	0.0650
403.1952	0.0375	414.3154	0.0081	429.1653	0.4000	444.2354	0.3144
403.2952	0.0993	414.3854	0.0039	429.2353	0.0590	444.2954	0.0253
403.3652	0.0188	414.6152	0.0232	429.3853	0.5772	445.2154	0.2200
404.1552	0.0643	415.2254	0.1588	430.2353	0.0418	445.3054	0.0195
404.2952	0.0787	415.3004	0.0792	430.3853	0.2155	445.3754	0.0926
404.6452	0.0026	415.3754	0.0033	431.2253	0.2093	446.2254	0.3166
405.1952	0.1437	416.2354	1.0424	431.3053	0.0124	446.3054	0.0017
405.2752	0.0807	417.2553	0.2805	431.3853	0.0139	446.3854	0.0014
405.3752	0.1693	417.3753	0.0070	431.4753	0.0108	447.2254	0.3186
405.4552	0.0356	418.2253	0.3208	432.1853	0.0512	447.3254	0.0056
406.1952	0.0571	418.2953	0.0041	432.3153	0.1826	447.3854	0.0145
406.2852	0.1582	418.4553	0.0181	432.3955	0.0641	448.2054	0.2726
406.3854	0.0363	419.1853	0.0844	433.2555	0.1910	448.3254	0.0033
407.1754	0.1492	419.3253	0.0414	433.4003	0.0034	449.3254	0.1454
407.2652	0.0104	420.2553	0.3832	434.2653	0.1437	449.3954	0.0034
407.3652	0.0706	421.2753	0.1757	434.3353	0.0039	449.5154	0.0024
407.4652	0.0072	421.3453	0.0485	435.2253	0.1312	450.2154	0.0899
408.4554	0.0023	421.4653	0.0264	435.3553	0.0048	450.3454	0.0719
409.2052	0.0849	422.2053	0.2159	435.4655	0.0086	450.5154	0.0381
409.2752	0.0292	422.3453	0.0178	436.3353	0.0334	451.2254	0.0061
409.3852	0.1717	423.2753	0.1233	437.1955	0.0249	451.3454	0.0867
410.2252	0.9700	423.3753	0.1296	437.2753	0.0485	452.4854	0.0328
410.3854	0.0036	424.2653	1.1587	437.3455	0.0115	453.3554	0.0421
411.1952	0.0988	425.2853	0.3644	437.4755	0.0084	454.4956	0.0510
411.2952	0.1558	425.3753	0.1763	438.2154	1.2155	455.2856	0.1021
411.3852	0.2018	425.4553	0.0013	439.2903	0.3600	455.3556	0.0055
411.4754	0.0035	425.5953	0.0022	439.3652	0.0016	456.2854	0.1081
411.6254	0.0018	426.2253	0.8246	439.4554	0.0131	456.5156	0.0225
411.6954	0.0142	426.3853	0.0016	441.2954	0.1259	457.2256	0.0747

Table A3.5 (continued). Mass data (*m/z* values and their relative intensities) for the DART-HRMS analysis of A. *absinthium tincture*. Ten replicates of one sample were averaged where the corresponding spectrum appears in Figure 3.1.

m/z	Rel. Int. %	*m/z*	Rel. Int. %	*m/z*	Rel. Int. %	*m/z*	Rel. Int. %
457.3054	0.1027	476.3155	0.0264	491.4856	0.0088	511.3257	0.1402
457.3754	0.0177	476.4055	0.0011	492.2256	0.2546	511.4357	0.0011
459.3053	0.4100	477.2955	0.3728	492.3356	0.0112	512.5757	0.0039
459.3855	0.0042	477.5455	0.0428	493.2456	0.1793	513.3357	0.1931
460.3053	0.1459	478.2455	0.1956	493.3056	0.1186	514.3357	0.2355
460.4155	0.0010	478.3255	0.0134	495.3056	0.2018	515.3257	0.0988
460.4955	0.0405	478.4355	0.0013	495.4456	0.0034	515.4257	0.0045
461.3055	0.2122	479.2956	0.3893	496.3256	0.1969	516.3457	0.1346
461.3755	0.0101	479.3754	0.0058	497.3256	0.3227	516.4957	0.0049
462.1355	0.0019	479.4854	0.0112	497.3956	0.0013	517.3257	0.0784
462.3053	0.1867	480.3254	0.1972	498.3256	0.2788	517.4457	0.0016
463.3153	0.2232	480.4954	0.0044	498.5356	0.0183	518.3457	0.0893
463.3855	0.0018	481.3254	0.1635	499.3256	0.0925	518.4357	0.0069
464.2255	0.1816	481.3954	0.0023	499.4256	0.0082	519.3457	0.0797
464.3155	0.0211	481.4956	0.0015	500.3455	0.1200	519.4957	0.0048
465.3255	0.1205	482.3354	0.1312	501.2257	0.0191	520.3356	0.0083
465.3955	0.0012	482.4756	0.0197	501.3255	0.0358	521.3356	0.0814
466.2355	0.0921	482.5256	0.0128	502.3355	0.1278	521.4056	0.0043
466.3355	0.3689	483.3156	0.0962	502.4155	0.0133	521.5256	0.0028
466.5055	0.0190	483.5356	0.0118	503.3255	0.1190	523.2456	0.0842
467.3255	0.1494	484.5456	0.0530	503.4155	0.0010	523.3256	0.0033
469.3353	0.0819	485.3354	0.1172	504.2857	0.1002	523.4056	0.0040
469.4055	0.0042	485.4056	0.0013	504.4555	0.0301	524.2756	0.0728
471.3255	0.2470	486.2256	0.0329	505.3255	0.1031	525.3358	0.0900
471.3855	0.0060	486.3254	0.1202	505.3955	0.0176	525.4256	0.0063
471.4955	0.0044	487.3156	0.0699	506.2555	0.1022	526.5658	0.0145
472.2555	0.2350	487.3854	0.0101	506.3657	0.0144	527.3456	0.0660
472.3455	0.0028	487.5256	0.0028	507.3155	0.0818	527.4256	0.0116
472.3855	0.0014	488.3956	0.0015	507.3955	0.0063	527.5256	0.0063
473.2255	0.0490	488.4656	0.0048	508.2355	0.0294	528.3458	0.0949
473.2955	0.0647	488.5456	0.0201	508.3557	0.1046	529.2658	0.0549
473.3755	0.0010	489.3056	0.0960	508.5257	0.0117	529.3256	0.0051
474.2857	0.1625	489.3756	0.0077	509.3255	0.1149	529.4156	0.0031
474.3855	0.0015	490.3254	0.2219	509.5257	0.0206	530.2856	0.0016
474.4655	0.0016	490.4656	0.0017	510.4157	0.0220	530.4056	0.0098
475.3055	0.2806	491.3056	0.1947	510.5357	0.0013	531.3158	0.0459

Table A3.5 (continued). Mass data (*m/z* values and their relative intensities) for the DART-HRMS analysis of A. *absinthium tincture*. Ten replicates of one sample were averaged where the corresponding spectrum appears in Figure 3.1.

m/z	Rel. Int. %	*m/z*	Rel. Int. %	*m/z*	Rel. Int. %	*m/z*	Rel. Int. %
531.4058	0.0129	547.4657	0.0239	562.2558	0.2577	577.5258	0.0404
532.3358	0.0899	548.3459	0.0995	562.3458	0.0096	578.3660	0.0615
532.4158	0.0081	548.4657	0.0071	562.4358	0.0086	578.5260	0.0253
533.2707	0.0228	549.2757	0.0391	563.2758	0.0746	579.3460	0.0385
533.3556	0.0462	549.3559	0.0292	563.3558	0.1157	579.4160	0.0094
533.4407	0.0023	549.4959	0.0069	564.2758	0.1089	580.5258	0.0024
533.5258	0.0043	550.2857	0.0214	564.4358	0.0036	580.6060	0.0054
534.3656	0.0956	550.3757	0.0405	564.5458	0.0015	581.3658	0.0435
535.4458	0.0155	550.4459	0.0137	564.6358	0.0083	582.3759	0.0459
536.3158	0.0547	550.5657	0.0020	565.2958	0.0101	582.5159	0.0069
536.5358	0.0096	551.3759	0.0232	565.3658	0.0149	583.3759	0.0297
536.6058	0.0051	551.5057	0.0238	565.5258	0.0040	583.5259	0.0059
537.3958	0.0052	552.3859	0.0318	566.3758	0.1060	583.5859	0.0020
537.5058	0.0268	552.4959	0.0221	567.3858	0.0638	584.3959	0.0558
537.6158	0.0028	552.5857	0.0153	567.5358	0.0040	585.3859	0.0485
538.3158	0.1194	553.3157	0.0501	568.3858	0.2121	585.5859	0.0075
538.5058	0.0033	553.4957	0.0277	569.3158	0.0012	586.3959	0.0856
539.3658	0.0614	554.4057	0.0124	569.3858	0.0753	586.4857	0.0031
539.4958	0.0107	554.4957	0.0541	569.4958	0.0039	586.5559	0.0069
541.3457	0.0754	555.5357	0.0087	569.5660	0.0079	587.3959	0.0026
541.4257	0.0023	556.3659	0.1374	570.4058	0.0763	587.4909	0.0128
541.5057	0.0015	557.3357	0.0484	570.5458	0.0449	587.5859	0.0059
542.3357	0.0907	557.4459	0.0011	571.3958	0.0542	588.2659	0.0246
543.3457	0.0457	557.5359	0.0157	572.3758	0.0787	588.4059	0.0450
543.4257	0.0040	558.3759	0.1645	572.4458	0.0102	588.6059	0.0012
543.4957	0.0091	559.3359	0.0880	572.5658	0.0016	589.3959	0.0453
544.3057	0.1404	559.4459	0.0024	572.6658	0.0095	589.4759	0.0092
544.3857	0.0065	559.5459	0.0038	573.2958	0.0196	589.5959	0.0018
545.3257	0.0842	560.2259	0.0490	573.3758	0.0034	590.2959	0.0449
545.4757	0.0094	560.3459	0.0669	573.4558	0.0332	590.3959	0.0389
545.7257	0.0047	560.4159	0.0055	574.4460	0.0358	590.4859	0.0034
546.2857	0.3155	560.4959	0.0041	575.3358	0.0070	591.3559	0.0188
546.4557	0.0537	561.3359	0.0536	575.5060	0.1901	591.4961	0.0245
547.2357	0.0671	561.4159	0.0270	576.3458	0.1186	591.5859	0.0029
547.3357	0.0300	561.4957	0.0345	576.5158	0.0899	592.3059	0.0015
547.4057	0.0679	561.5658	0.0028	577.3458	0.0545	592.3759	0.0597

Table A3.5 (continued). Mass data (*m/z* values and their relative intensities) for the DART-HRMS analysis of A. *absinthium tincture*. Ten replicates of one sample were averaged where the corresponding spectrum appears in Figure 3.1.

m/z	Rel. Int. %	*m/z*	Rel. Int. %	*m/z*	Rel. Int. %	*m/z*	Rel. Int. %
592.4959	0.0357	605.3160	0.0089	620.6660	0.0088	637.4761	0.0134
592.5759	0.0067	605.4060	0.0327	621.5460	0.0188	637.5661	0.0299
592.6759	0.0061	605.5460	0.0087	621.6660	0.0096	638.5761	0.0323
593.3159	0.0153	606.4060	0.1001	622.4062	0.0705	638.6861	0.0017
593.3859	0.0286	606.5360	0.0028	622.5460	0.0280	643.4963	0.0026
593.5159	0.0355	606.6260	0.0050	623.5659	0.0020	645.4862	0.0033
594.3759	0.0865	607.2958	0.0198	624.5459	0.0011	646.4160	0.0389
594.5159	0.0039	607.5060	0.0104	625.3961	0.0644	646.4960	0.0021
595.3559	0.0629	607.5760	0.0092	626.3359	0.3283	646.6162	0.0170
595.5259	0.0120	608.3060	0.0013	626.4061	0.3054	647.4060	0.0227
596.5261	0.0178	608.3760	0.3760	626.5259	0.0015	647.4762	0.0039
597.3661	0.0226	608.4510	0.0012	627.3361	0.1877	648.5160	0.0109
597.4460	0.0059	608.5260	0.0065	628.5061	0.0011	648.6360	0.0011
597.5259	0.0234	609.3860	0.1669	629.2761	0.0012	649.4160	0.0271
598.3859	0.0536	610.5460	0.0882	629.4310	0.0219	649.5160	0.0149
598.4561	0.0419	611.5360	0.0086	629.5059	0.0039	649.5960	0.0053
598.5959	0.0066	612.3560	2.6442	630.4161	0.0532	649.6760	0.0019
599.3761	0.0041	613.3660	0.8886	630.4961	0.0196	650.4160	0.0524
599.5061	0.0538	614.4160	0.1839	631.3959	0.0315	650.6862	0.0069
599.6059	0.0018	614.4960	0.0617	631.5059	0.0186	651.4160	0.0436
600.3861	0.1700	615.3860	0.0338	632.4161	0.0395	651.5462	0.0045
600.5061	0.0013	615.5060	0.0955	632.5361	0.0025	652.4062	0.0899
601.3761	0.0635	616.5160	0.0481	633.3961	0.0892	652.5462	0.0052
601.5259	0.0229	617.3860	0.0013	633.5161	0.0199	653.4162	0.0464
601.5961	0.0016	617.4460	0.0308	633.5961	0.0017	653.4962	0.0033
601.8059	0.0016	617.5160	0.0472	633.6961	0.0124	653.5660	0.0062
602.3861	0.0370	618.3960	0.0555	634.3261	0.0022	654.5662	0.0403
602.5261	0.0152	618.5260	0.0353	634.4661	0.0031	655.4762	0.0024
602.6261	0.0121	618.6762	0.0050	634.5461	0.0323	657.4262	0.0030
603.3060	0.0073	619.3860	0.0482	635.3861	0.0447	657.5062	0.0106
603.3958	0.0110	619.4560	0.0149	635.5461	0.0202	658.5062	0.0051
603.5360	0.0209	619.5360	0.0056	635.6161	0.0126	659.3862	0.0352
604.3158	0.0631	619.7560	0.0060	635.7061	0.0017	659.5262	0.0246
604.4058	0.0020	620.3260	0.0091	636.3961	0.0672	659.6162	0.0016
604.4660	0.0033	620.3960	0.0515	636.5661	0.0290	660.3962	0.0641
604.5458	0.0263	620.5360	0.0248	637.4061	0.0144	660.5362	0.0028

Table A3.5 (continued). Mass data (*m/z* values and their relative intensities) for the DART-HRMS analysis of A. *absinthium tincture*. Ten replicates of one sample were averaged where the corresponding spectrum appears in Figure 3.1.

A. *Absinthium* tincture							
m/z	Rel. Int. %	*m/z*	Rel. Int. %	*m/z*	Rel. Int. %	*m/z*	Rel. Int. %
660.6317	0.0026	680.4013	0.0638	707.4063	0.0263	740.4664	0.0294
661.3962	0.0393	680.5963	0.0016	707.6463	0.0022	740.5366	0.0196
661.5562	0.0109	681.4563	0.0385	708.4363	0.3030	740.6364	0.0180
661.6517	0.0057	681.5963	0.0079	710.4263	0.0749	741.4664	0.0348
662.5662	0.0044	682.4563	0.0030	710.6063	0.0058	741.5264	0.0026
663.3862	0.0570	682.5563	0.0190	717.5965	0.0020	741.6266	0.0061
663.6262	0.0032	683.4163	0.0397	719.3963	0.0179	742.6164	0.0126
664.3862	0.0555	684.5063	0.0033	720.4563	0.0357	743.6164	0.0084
664.5662	0.0051	688.5764	0.0073	720.6665	0.0067	744.6166	0.0061
665.4161	0.1588	689.4062	0.0263	721.5363	0.0017	745.6266	0.0042
665.5961	0.0020	689.4762	0.0042	721.6263	0.0019	746.5464	0.0175
666.4161	0.0204	689.6462	0.0084	722.6365	0.0075	746.6264	0.0037
666.6461	0.0105	690.4762	0.0165	723.4365	0.0203	747.6265	0.0015
666.7161	0.0057	690.6564	0.0127	724.4465	0.0296	749.6365	0.0066
667.5861	0.0101	691.4062	0.0262	724.6665	0.0032	750.6863	0.0016
667.7161	0.0033	692.4764	0.0035	725.4565	0.0223	751.4665	0.0121
668.5761	0.0052	692.5564	0.0102	725.6665	0.0031	751.5965	0.0012
669.5863	0.0080	692.6462	0.0121	726.6565	0.0024	751.6863	0.0035
670.5161	0.0166	693.6164	0.0011	727.5744	0.0029	752.6065	0.0027
671.3561	0.0023	694.3962	0.0393	728.5964	0.0085	753.4165	0.0042
673.6463	0.0031	694.4762	0.0048	729.5964	0.0059	753.6165	0.0012
674.6263	0.0041	694.6064	0.0162	730.5464	0.0225	754.6465	0.0015
675.4063	0.0279	696.4462	0.0432	732.6864	0.0012	756.5165	0.0133
675.5063	0.0030	696.5964	0.0057	733.3964	0.0110	756.6265	0.0034
675.7963	0.0027	697.3964	0.0234	734.3964	0.0068	757.6265	0.0035
676.3663	0.0896	697.4664	0.0037	734.4964	0.0081	761.3767	0.0047
676.4462	0.0014	697.6262	0.0027	735.4064	0.0034	762.4767	0.0030
676.5261	0.0035	699.4762	0.0116	735.4864	0.0058	762.6165	0.0017
676.6763	0.0020	700.5264	0.0067	736.4066	0.0141	763.4765	0.0027
677.5463	0.0048	704.4064	0.0355	736.6164	0.0097	765.3965	0.0092
677.6263	0.0019	704.6564	0.0012	737.4164	0.0138	766.6665	0.0022
677.7063	0.0018	705.3964	0.0046	737.5064	0.0068	767.3967	0.0019
678.5961	0.0052	705.6664	0.0024	737.6364	0.0074	767.4765	0.0105
678.7263	0.0095	706.3963	0.0346	738.4264	0.0208	767.6067	0.0034
679.4163	0.0450	706.5863	0.0051	738.6364	0.0105	768.4866	0.0132
679.5963	0.0019	706.6563	0.0021	739.6464	0.0057	768.5766	0.0038

Table A3.5 (continued). Mass data (*m/z* values and their relative intensities) for the DART-HRMS analysis of A. *absinthium tincture*. Ten replicates of one sample were averaged where the corresponding spectrum appears in Figure 3.1.

m/z	Rel. Int. %	*m/z*	Rel. Int. %	*m/z*	Rel. Int. %	*m/z*	Rel. Int. %
				A. *Absinthium* tincture			
769.4166	0.0031	778.6966	0.0026	789.3865	0.0067	804.5667	0.0030
769.6066	0.0038	779.6366	0.0012	790.6167	0.0026	812.6366	0.0014
770.6064	0.0021	779.7066	0.0020	793.6067	0.0059	816.4266	0.0057
772.6366	0.0078	781.6166	0.0030	795.6267	0.0032	820.5668	0.0034
773.6364	0.0022	782.6766	0.0026	796.3967	0.0028	839.5569	0.0020
775.6164	0.0023	784.4266	0.0030	796.6267	0.0061	840.5569	0.0019
776.4566	0.0116	784.6668	0.0012	797.3567	0.0055	856.5368	0.0032
776.6166	0.0031	785.6266	0.0023	797.4367	0.0026	878.5569	0.0031
777.6866	0.0026	786.4266	0.0054	797.6367	0.0031	890.6471	0.0042
778.6266	0.0053	787.4366	0.0027	798.4367	0.0104		
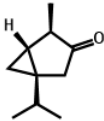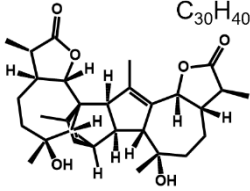
Table A3.6 Known molecules of interest in the indicated species.

Index	Species	Molecules of Interest	Monoisotopic Mass	Structure
1	*A. absinthium*	(-)–thujone	152.1201	$C_{10}H_{16}O$
		Absinthin	496.2824	$C_{30}H_{40}O_6$
2	*A. vulgaris*	None	None	None
3	*C. zacatechichi*	Sesquiterpene alkaloids	--------	--------
		Caleicines	--------	--------
		Caleochromenes	--------	--------
4	*L. virosa*	Lactucin	276.0998	$C_{15}H_{16}O_5$
		Lactucopicrin	410.1366	$C_{23}H_{22}O_7$
5	*S. tortuosum*	Mesembrenol	289.1678	$C_{17}H_{23}NO_3$
		Tortuosamine	326.1994	$C_{20}H_{26}N_2O_2$
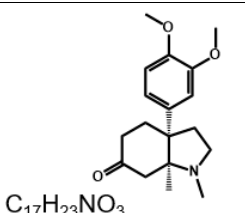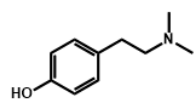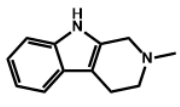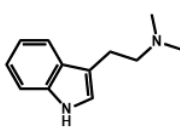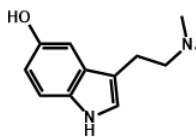
Table A3.6 (continued). Known molecules of interest in the indicated species.				
Index	**Species**	**Molecules of Interest**	**Monoisotopic Mass**	**Structure**
5	*S. tortuosum*	Mesembrine	289.1678	$C_{17}H_{23}NO_3$
		Hordenine	165.1154	$C_{10}H_{15}NO$
		Mesembrenone	287.1521	$C_{17}H_{21}NO_3$
6	*E. lobata*	None	None	None
7	*A. peregrina*	2-Methyltryptoline	186.1157	$C_{12}H_{14}N_2$
		N,N-Dimethyltryptamine (DMT)	188.1313	$C_{12}H_{16}N_2$
		Bufotenin	204.1263	$C_{12}H_{16}N_2O$
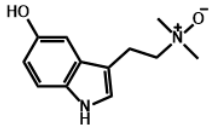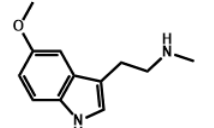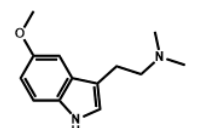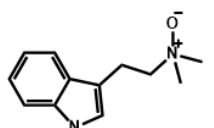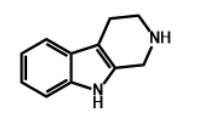
Table A3.6 (continued).	Known molecules of interest in the indicated species.			
Index	Species	Molecules of Interest	Monoisotopic Mass	Structure
7	*A. peregrina*	Bufotenin-oxide	220.1212	 $C_{12}H_{16}N_2O_2$
		5-Methoxy-*N*-methyltryptamine	204.1263	 $C_{12}H_{16}N_2O$
		N-Methyltryptamine	174.1157	 $C_{11}H_{14}N_2$
		5-Methoxy DMT	218.1419	 $C_{13}H_{18}N_2O$
		DMT-oxide	204.1263	 $C_{12}H_{16}N_2O$
		Tryptoline	172.1000	 $C_{11}H_{12}N_2$
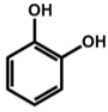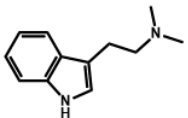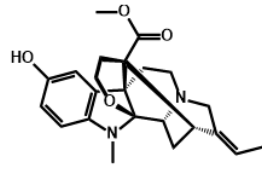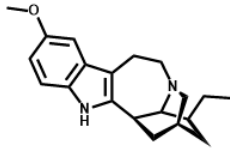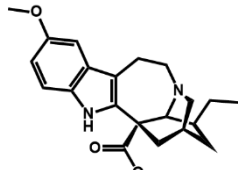
Table A3.6 (continued). Known molecules of interest in the indicated species.

Index	Species	Molecules of Interest	Monoisotopic Mass	Structure
7	*A. peregrina*	Catechol	110.0368	$C_6H_6O_2$
8	*M. hostilis*	*N,N*-Dimethyltryptamine (DMT)	188.1313	$C_{12}H_{16}N_2$
9	*P. nitida*	Pericine	278.1783	$C_{19}H_{22}N_2$
		Akuammine	382.1893	$C_{22}H_{26}N_2O_4$
10	*V. africana*	Ibogaine	310.2045	$C_{20}H_{26}N_2O$
		Voacangine	368.2100	$C_{22}H_{28}N_2O_3$
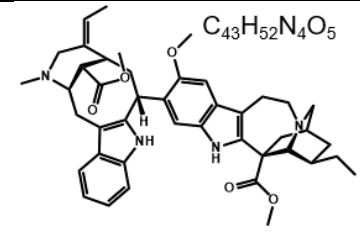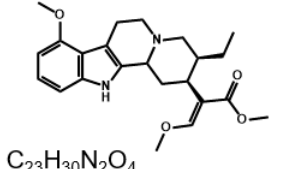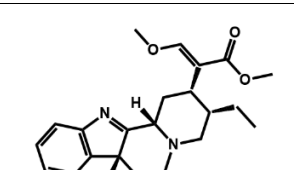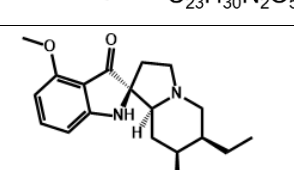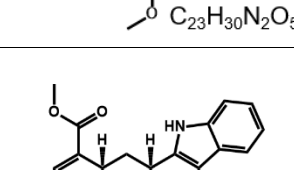
Table A3.6 (continued). Known molecules of interest in the indicated species.				
Index	Species	Molecules of Interest	Monoisotopic Mass	Structure
10	*V. africana*	Voacamine	704.3938	$C_{43}H_{52}N_4O_5$
11	*M. speciosa*	Mitragynine	398.2206	$C_{23}H_{30}N_2O_4$
		Mitraphylline	368.1736	$C_{21}H_{24}N_2O_4$
		7-Hydroxymitragynine	414.2155	$C_{23}H_{30}N_2O_5$
		Mitragynine pseudoindoxyl	414.2155	$C_{23}H_{30}N_2O_5$
		Ajmalicine	352.1787	$C_{21}H_{24}N_2O_3$
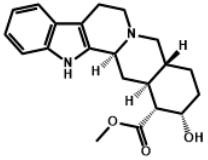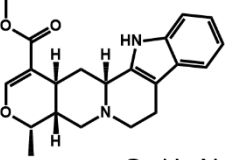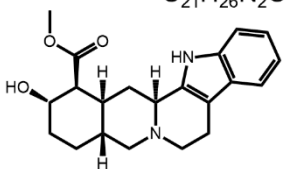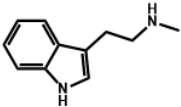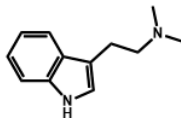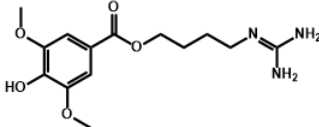
Table A3.6 (continued). Known molecules of interest in the indicated species.

Index	Species	Molecules of Interest	Monoisotopic Mass	Structure
12	*C. johimbe*	Yohimbine	354.1943	$C_{21}H_{26}N_2O_3$
		Ajmalicine	352.1787	$C_{21}H_{24}N_2O_3$
		Corynanthine	354.1943	$C_{21}H_{26}N_2O_3$
13	*P. viridis*	*N*-Methyltryptamine	174.1157	$C_{11}H_{14}N_2$
		N,N-Dimethyltryptamine (DMT)	188.1313	$C_{12}H_{16}N_2$
14	*L. leonurus*	Leonurine	311.1481	$C_{14}H_{21}N_3O_5$
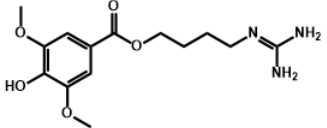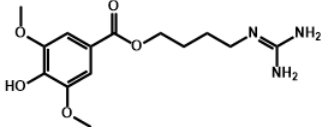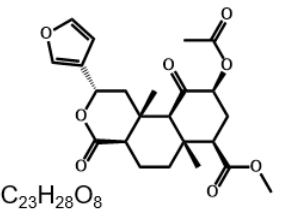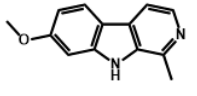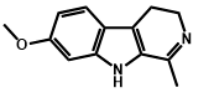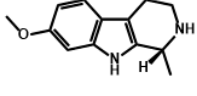
Table A3.6 (continued). Known molecules of interest in the indicated species.

Index	Species	Molecules of Interest	Monoisotopic Mass	Structure
15	*L. nepetifolia*	Leonurine	311.1481	$C_{14}H_{21}N_3O_5$
16	*L. sibiricus*	Leonurine	311.1481	$C_{14}H_{21}N_3O_5$
17	*S. divinorum*	Salvinorin A	432.1784	$C_{23}H_{28}O_8$
18	*S. vulgaris*	None	None	None
19	*B. caapi*	Harmine	212.0950	$C_{13}H_{12}N_2O$
		Harmaline	214.1106	$C_{13}H_{14}N_2O$
		Tetrahydroharmine	216.1263	$C_{13}H_{16}N_2O$
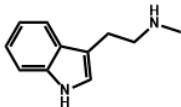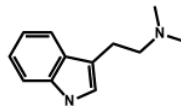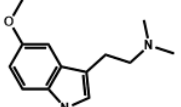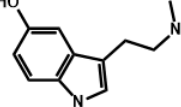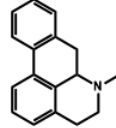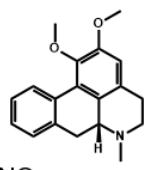
			Table A3.6 (continued). Known molecules of interest in the indicated species.			

Index	Species	Molecules of Interest	Monoisotopic Mass	Structure
20	*D. cabrerana*	*N*-Methyltryptamine	174.1157	$C_{11}H_{14}N_2$
		*N,N-*Dimethyltryptamine (DMT)	188.1313	$C_{12}H_{16}N_2$
		5-Methoxy DMT	218.1419	$C_{13}H_{18}N_2O$
		Bufotenin	204.1263	$C_{12}H_{16}N_2O$
21	*T. diffusa*	Damianin	Unknown	Unknown
22	*A. officinalis*	None	None	None
23	*T. populnea*	None	None	None
24	*N. caerulea*	Aporphine	235.1361	$C_{17}H_{17}N$
		Nuciferine	295.1572	$C_{19}H_{21}NO_2$
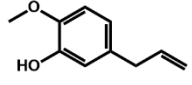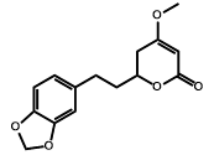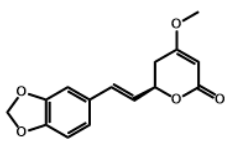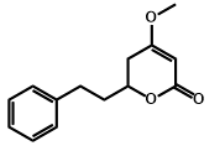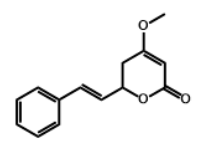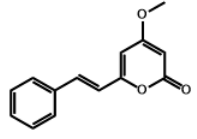
Table A3.6 (continued). Known molecules of interest in the indicated species.

Index	Species	Molecules of Interest	Monoisotopic Mass	Structure
25	*P. betel*	Chavibetol	164.0837	$C_{10}H_{12}O_2$
26	*P. methysticum*	Dihydromethysticin	276.0998	$C_{15}H_{16}O_5$
		Methysticin	274.0841	$C_{15}H_{14}O_5$
		Dihydrokavain	232.1099	$C_{14}H_{16}O_3$
		Kavain	230.0943	$C_{14}H_{14}O_3$
		Desmethoxyyangonin	228.0786	$C_{14}H_{12}O_3$
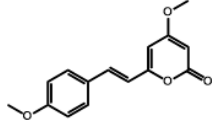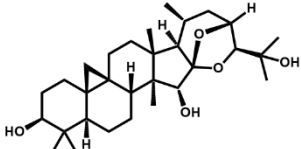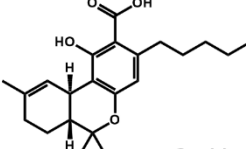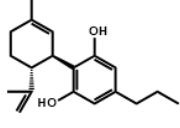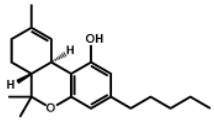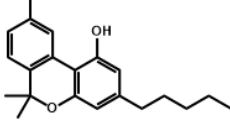
Table A3.6 (continued). Known molecules of interest in the indicated species.

Index	Species	Molecules of Interest	Monoisotopic Mass	Structure
26	*P. methysticum*	Yangonin	258.0892	$C_{15}H_{14}O_4$
27	*A. racemosa*	Cimigenol	488.3502	$C_{30}H_{48}O_5$
28	*C. sativa*	Tetrahydrocannabinolic acid (THCA)	358.2144	$C_{22}H_{30}O_4$
		Cannabidivarin (CBDV)	286.1933	$C_{19}H_{22}O_2$
		Tetrahydrocannabinol (THC)	314.2246	$C_{21}H_{30}O_2$
		Cannabinol (CBN)	310.1933	$C_{21}H_{26}O_2$

	Table A3.6 (continued). Known molecules of interest in the indicated species.			
Index	Species	Molecules of Interest	Monoisotopic Mass	Structure
28	*C. sativa*	Cannabidiol (CBD)	314.2246	$C_{21}H_{30}O_2$
		Cannabidiolic acid (CBDA)	358.2144	$C_{22}H_{30}O_4$
		Tetrahydrocannabidivar in (THCV)	286.1933	$C_{19}H_{26}O_2$
29	*P. harmala*	Vasicinone	202.0742	$C_{11}H_{10}N_2O_2$
		Harmalol	200.0950	$C_{12}H_{12}N_2O$
		Harmine	212.0950	$C_{13}H_{12}N_2O$
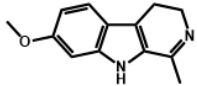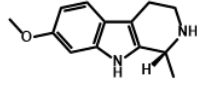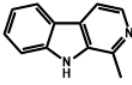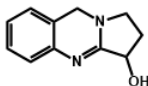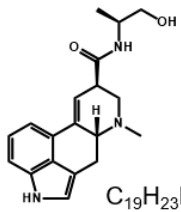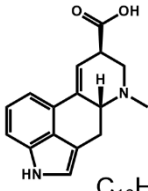
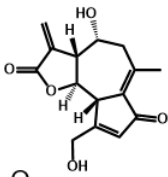**Table A3.6 (continued).** Known molecules of interest in the indicated species.

Index	Species	Molecules of Interest	Monoisotopic Mass	Structure
29	*P. harmala*	Harmaline	214.1106	$C_{13}H_{14}N_2O$
		Tetrahydroharmine	216.1263	$C_{13}H_{16}N_2O$
		Harmane	182.0844	$C_{12}H_{10}N_2$
		Vasicine (peganine)	188.0950	$C_{11}H_{12}N_2O$
30	*A. nervosa*	Ergometrine	325.1790	$C_{19}H_{23}N_3O_2$
		Lysergic acid	268.1212	$C_{16}H_{16}N_2O_2$
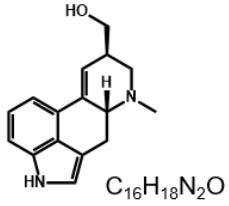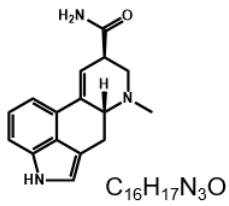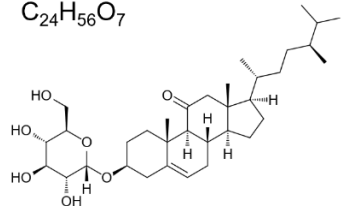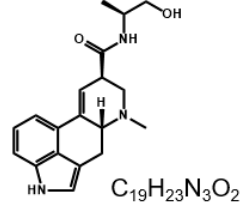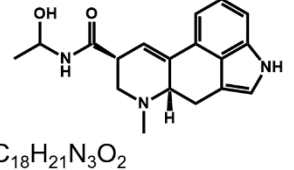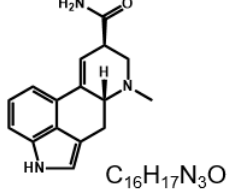
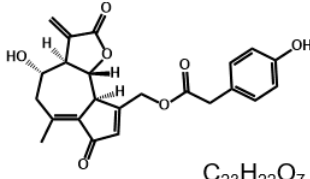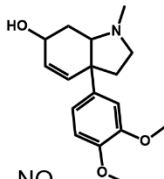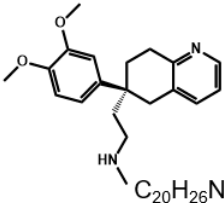**Table A3.6 (continued).** Known molecules of interest in the indicated species.

Index	Species	Molecules of Interest	Monoisotopic Mass	Structure
30	*A. nervosa*	Lysergol	254.1419	$C_{16}H_{18}N_2O$
		Ergine	267.1372	$C_{16}H_{17}N_3O$
		Argyroside	576.4026	$C_{24}H_{56}O_7$
31	*C. tricolor*	Unknown	--------	--------
32	*I. tricolor*	Ergometrine	325.1790	$C_{19}H_{23}N_3O_2$
		Lysergic acid-α-hydroxyethylamide	311.1634	$C_{18}H_{21}N_3O_2$
		Ergine	267.1372	$C_{16}H_{17}N_3O$
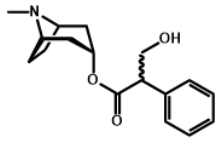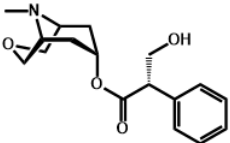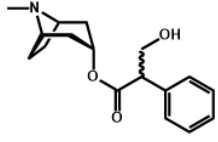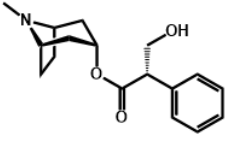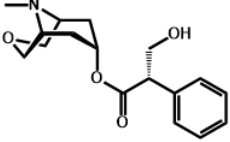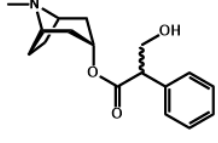
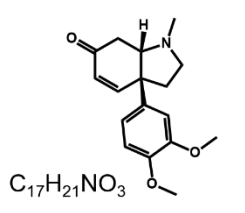| Table A3.6 (continued). Known molecules of interest in the indicated species.				
Index	Species	Molecules of Interest	Monoisotopic Mass	Structure
33	*A. baetica*	Atropine	289.1678	$C_{17}H_{23}NO_3$
		Hyoscine (Scopolamine)	303.1471	$C_{17}H_{21}NO_4$
34	*A. belladonna*	Atropine	289.1678	$C_{17}H_{23}NO_3$
34	*A. belladonna*	Hyoscyamine	289.1678	$C_{17}H_{23}NO_3$
		Hyoscine (Scopolamine)	303.1471	$C_{17}H_{21}NO_4$
35	*A. komarovii*	Atropine	289.1678	$C_{17}H_{23}NO_3$
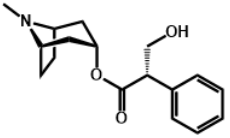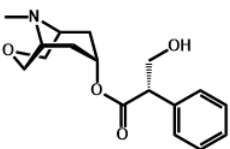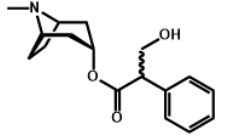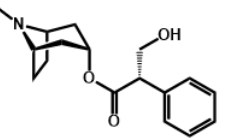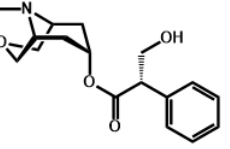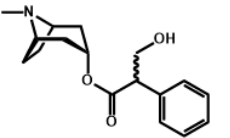
Table A3.6 (continued). Known molecules of interest in the indicated species.				
Index	Species	Molecules of Interest	Monoisotopic Mass	Structure
35	*A. komarovii*	Hyoscyamine	289.1678	$C_{17}H_{23}NO_3$
		Hyoscine (Scopolamine)	303.1471	$C_{17}H_{21}NO_4$
36	*B. arborea*	Atropine	289.1678	$C_{17}H_{23}NO_3$
		Hyoscyamine	289.1678	$C_{17}H_{23}NO_3$
		Hyoscine (Scopolamine)	303.1471	$C_{17}H_{21}NO_4$
37	*B. aurea*	Atropine	289.1678	$C_{17}H_{23}NO_3$
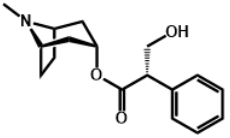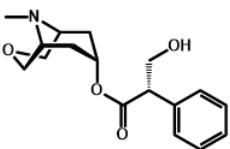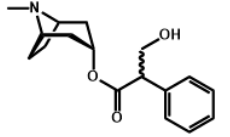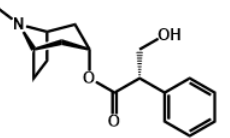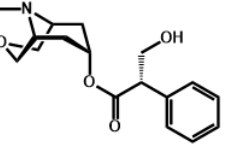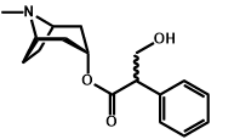
Table A3.6 (continued). Known molecules of interest in the indicated species.				
Index	**Species**	**Molecules of Interest**	**Monoisotopic Mass**	**Structure**
37	*B. aurea*	Hyoscyamine	289.1678	$C_{17}H_{23}NO_3$
		Hyoscine (Scopolamine)	303.1471	$C_{17}H_{21}NO_4$
38	*B. sanguinea*	Atropine	289.1678	$C_{17}H_{23}NO_3$
		Hyoscyamine	289.1678	$C_{17}H_{23}NO_3$
		Hyoscine (Scopolamine)	303.1471	$C_{17}H_{21}NO_4$
39	*B. suaveolens*	Atropine	289.1678	$C_{17}H_{23}NO_3$
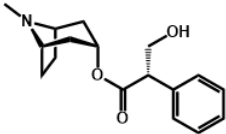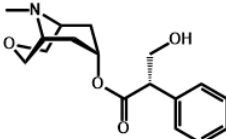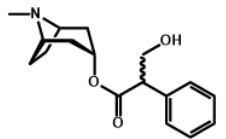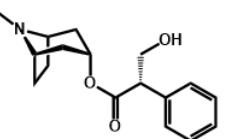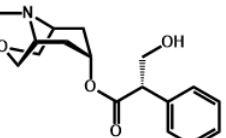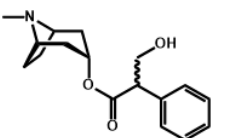
Index	Species	Molecules of Interest	Monoisotopic Mass	Structure
39	*B. suaveolens*	Hyoscyamine	289.1678	$C_{17}H_{23}NO_3$
		Hyoscine (Scopolamine)	303.1471	$C_{17}H_{21}NO_4$
40	*B. versicolor*	Atropine	289.1678	$C_{17}H_{23}NO_3$
		Hyoscyamine	289.1678	$C_{17}H_{23}NO_3$
		Hyoscine (Scopolamine)	303.1471	$C_{17}H_{21}NO_4$
41	*D. ceratocaula*	Atropine	289.1678	$C_{17}H_{23}NO_3$
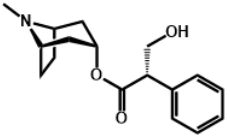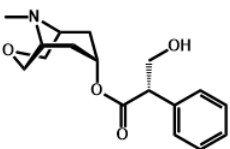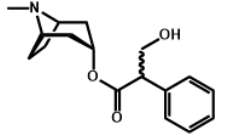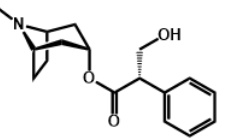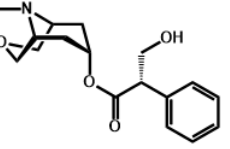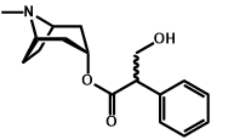
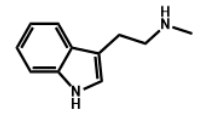**Table A3.6 (continued).** Known molecules of interest in the indicated species.

Table A3.6 (continued). Known molecules of interest in the indicated species.				
Index	**Species**	**Molecules of Interest**	**Monoisotopic Mass**	**Structure**
41	*D. ceratocaula*	Hyoscyamine	289.1678	$C_{17}H_{23}NO_3$
		Hyoscine (Scopolamine)	303.1471	$C_{17}H_{21}NO_4$
42	*D. discolor*	Atropine	289.1678	$C_{17}H_{23}NO_3$
		Hyoscyamine	289.1678	$C_{17}H_{23}NO_3$
		Hyoscine (Scopolamine)	303.1471	$C_{17}H_{21}NO_4$
43	*D. ferox*	Atropine	289.1678	$C_{17}H_{23}NO_3$
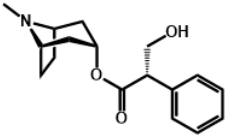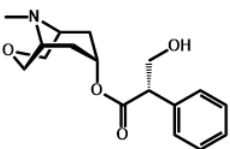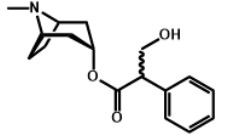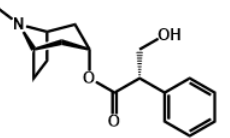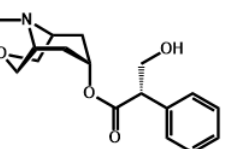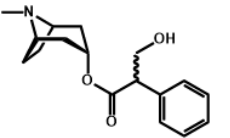
Table A3.6 (continued). Known molecules of interest in the indicated species.				
Index	Species	Molecules of Interest	Monoisotopic Mass	Structure
43	*D. ferox*	Hyoscyamine	289.1678	$C_{17}H_{23}NO_3$
		Hyoscine (Scopolamine)	303.1471	$C_{17}H_{21}NO_4$
44	*D. innoxia*	Atropine	289.1678	$C_{17}H_{23}NO_3$
		Hyoscyamine	289.1678	$C_{17}H_{23}NO_3$
		Hyoscine (Scopolamine)	303.1471	$C_{17}H_{21}NO_4$
45	*D. leichhardtii*	Atropine	289.1678	$C_{17}H_{23}NO_3$
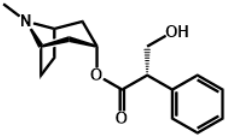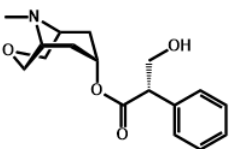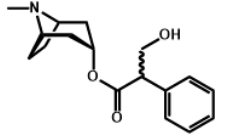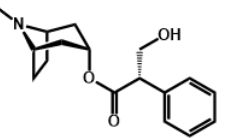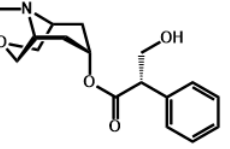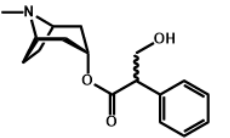
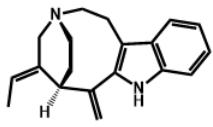| Table A3.6 (continued). Known molecules of interest in the indicated species.				
Index	Species	Molecules of Interest	Monoisotopic Mass	Structure
45	*D. leichhardtii*	Hyoscyamine	289.1678	$C_{17}H_{23}NO_3$
		Hyoscine (Scopolamine)	303.1471	$C_{17}H_{21}NO_4$
46	*D. metel*	Atropine	289.1678	$C_{17}H_{23}NO_3$
		Hyoscyamine	289.1678	$C_{17}H_{23}NO_3$
		Hyoscine (Scopolamine)	303.1471	$C_{17}H_{21}NO_4$
47	*D. parajuli*	Atropine	289.1678	$C_{17}H_{23}NO_3$
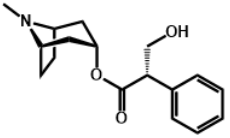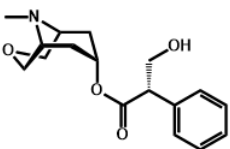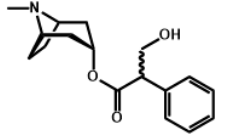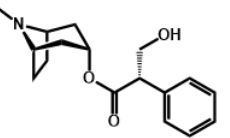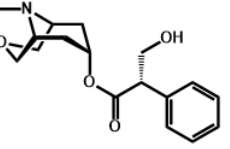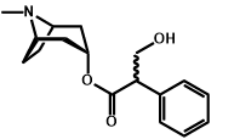
Table A3.6 (continued). Known molecules of interest in the indicated species.				
Index	**Species**	**Molecules of Interest**	**Monoisotopic Mass**	**Structure**
47	*D. parajuli*	Hyoscyamine	289.1678	$C_{17}H_{23}NO_3$
		Hyoscine (Scopolamine)	303.1471	$C_{17}H_{21}NO_4$
48	*D. quercifolia*	Atropine	289.1678	$C_{17}H_{23}NO_3$
		Hyoscyamine	289.1678	$C_{17}H_{23}NO_3$
		Hyoscine (Scopolamine)	303.1471	$C_{17}H_{21}NO_4$
49	*D. stramonium*	Atropine	289.1678	$C_{17}H_{23}NO_3$
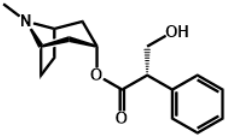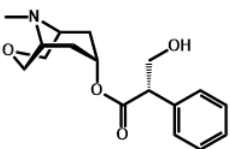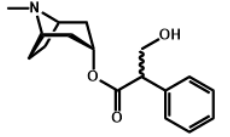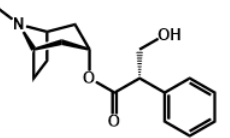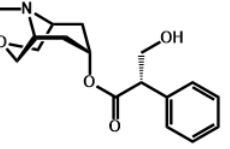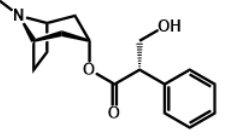
Table A3.6 (continued). Known molecules of interest in the indicated species.				
Index	**Species**	**Molecules of Interest**	**Monoisotopic Mass**	**Structure**
49	*D. stramonium*	Hyoscyamine	289.1678	$C_{17}H_{23}NO_3$
		Hyoscine (Scopolamine)	303.1471	$C_{17}H_{21}NO_4$
50	*D. wrightii*	Atropine	289.1678	$C_{17}H_{23}NO_3$
		Hyoscyamine	289.1678	$C_{17}H_{23}NO_3$
		Hyoscine (Scopolamine)	303.1471	$C_{17}H_{21}NO_4$
51	*H. albus*	Hyoscyamine	289.1678	$C_{17}H_{23}NO_3$

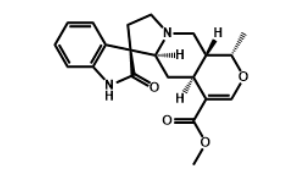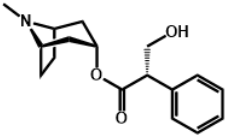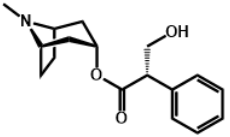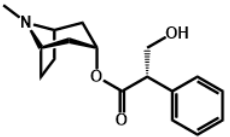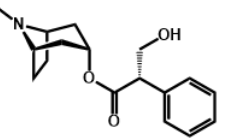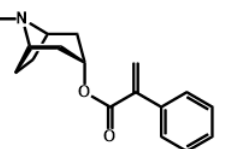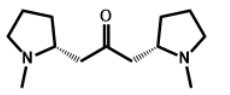| Table A3.6 (continued). Known molecules of interest in the indicated species.				
Index	**Species**	**Molecules of Interest**	**Monoisotopic Mass**	**Structure**
52	*H. aureus*	Hyoscyamine	289.1678	$C_{17}H_{23}NO_3$
53	*H. muticus*	Hyoscyamine	289.1678	$C_{17}H_{23}NO_3$
54	*H. niger*	Hyoscyamine	289.1678	$C_{17}H_{23}NO_3$
55	*H. pusillus*	Hyoscyamine	289.1678	$C_{17}H_{23}NO_3$
56	*M. autumnalis*	Apoatropine	271.1572	$C_{17}H_{21}NO_2$
		Cuscohygrine	224.1889	$C_{13}H_{24}N_2O$

Table A3.7 Mass data (*m/z* values and their relative intensities) for the DART-HRMS analysis of *L. virosa* flower. Ten replicates of one sample were averaged where the corresponding spectrum appears in Figure 3.4B.

				L. virosa flower			
m/z	Rel. Int. %	*m/z*	Rel. Int. %	*m/z*	Rel. Int. %	*m/z*	Rel. Int. %
60.0541	0.2286	86.0740	12.1543	102.0741	0.6491	121.0842	12.8068
60.1541	0.0074	86.1742	0.2380	102.1641	0.0032	122.0042	0.0017
61.0339	8.0786	87.0539	20.1001	103.0541	13.4775	122.0742	2.3519
61.1041	0.4093	87.1641	0.1657	104.0741	10.8328	122.2242	0.0811
62.0639	0.2370	88.0741	1.1695	104.1443	0.1349	123.0942	4.0858
65.0541	0.0518	88.1441	0.0312	104.2343	0.1051	124.0642	8.0340
67.0540	0.2348	88.2041	0.0077	105.0641	0.9899	124.1844	0.0767
68.0538	2.5510	89.0641	3.9929	106.0641	0.1767	125.0942	6.7076
68.1240	0.1250	89.1741	0.0780	107.0141	1.8230	125.2144	0.0679
69.0440	9.3342	90.0641	32.8085	107.0841	1.5358	126.0642	8.6720
70.0640	2.2022	90.1641	1.1082	108.0640	1.4842	127.0442	70.3863
70.1340	0.0421	90.9639	0.0395	108.1542	0.2021	127.2342	0.5208
71.0640	3.5726	91.0541	3.1266	109.0340	9.6020	127.9777	0.0090
72.0140	0.3294	91.1241	1.4243	109.0942	5.6036	128.0844	4.3861
72.0840	5.3212	92.0641	0.1300	109.2042	0.0756	128.2243	0.2134
72.2040	0.0822	93.0641	4.3745	110.0742	22.1513	128.9841	0.0346
72.9940	0.6834	93.1341	0.2548	110.2142	0.2929	129.0641	20.2923
73.0640	2.7689	94.0641	1.5865	111.0540	10.8317	129.2141	0.1459
73.1840	0.0247	94.1741	0.0720	111.1140	0.5890	130.0643	4.8195
74.0640	1.2134	95.0241	1.1282	111.2342	0.0685	130.2343	0.1893
75.0440	29.1202	95.0841	4.5441	112.0742	6.4196	131.0643	14.2362
75.1140	0.0259	96.0541	54.6389	113.0542	11.1953	131.1643	0.2241
76.0640	0.8634	96.1291	0.9630	114.0842	3.2425	131.2243	0.3927
77.0440	0.3269	97.0341	27.9648	114.2242	0.1048	132.0343	1.2999
78.0440	0.0494	97.0941	1.6962	115.0542	35.2873	132.1041	6.5688
79.0440	0.4073	97.2241	0.0462	115.2442	0.2127	132.9841	0.0091
80.0540	0.7698	97.2841	0.0909	115.9642	0.0273	133.0643	5.1109
81.0540	12.5941	97.9941	0.2914	116.0742	3.7716	133.2543	0.1070
82.0642	1.3027	98.0841	3.0402	116.2242	0.0783	134.0843	2.0447
83.0240	1.7946	99.0541	41.4203	117.0642	29.9573	134.1943	0.0753
83.0840	1.7660	99.1841	0.8789	117.2442	0.1611	134.2543	0.1619
84.0640	9.9524	100.0841	3.3293	118.0842	3.4390	135.0343	3.4028
84.1542	0.1136	100.2341	0.0283	118.2042	0.1373	135.1043	2.9000
85.0342	21.4274	100.9841	0.5710	119.0842	0.6694	135.2443	0.0329
85.0942	2.0909	101.0641	8.1433	120.0742	1.3166	136.0643	18.6590
85.1642	0.0103	101.1841	0.1076	120.2042	0.0468	136.2143	0.3715

Table A3.7 (continued). Mass data (*m/z* values and their relative intensities) for the DART-HRMS analysis of *L. virosa* flower. Ten replicates of one sample were averaged where the corresponding spectrum appears in Figure 3.4B.

| *L. virosa* flower |
m/z	Rel. Int. %	*m/z*	Rel. Int. %	*m/z*	Rel. Int. %	*m/z*	Rel. Int. %
136.2843	0.0063	150.3142	0.1130	170.0143	0.0020	191.3244	0.2765
136.4043	0.0966	151.1042	10.5445	170.0943	4.7060	192.0044	0.0018
137.0743	10.6458	151.9942	0.0035	171.1543	0.1909	192.1044	2.0417
137.1243	0.8900	152.1144	4.7175	171.3143	0.0211	192.1644	1.1487
137.2143	0.2312	153.0844	17.0492	172.1243	1.9975	193.0844	24.2045
137.2843	0.1072	154.0844	5.5130	173.1143	2.2013	193.1544	0.3486
137.9843	0.0158	155.0100	0.0062	174.1143	1.5082	194.0144	0.0608
138.0843	3.5115	155.1044	5.1401	175.0543	1.0031	194.0944	4.9224
139.0054	1.2468	155.2644	0.0424	175.1245	1.3075	194.9975	0.0066
139.1043	5.1999	156.1042	3.4559	176.0945	2.4399	195.0946	3.3197
139.2643	0.0886	156.1744	0.1816	176.1694	0.1133	195.2744	0.2261
140.0043	0.0029	156.2744	0.0174	177.0645	5.0113	196.0144	0.0051
140.0843	6.6638	157.0544	1.4219	177.1443	1.7150	196.0946	3.5807
140.2543	0.0276	157.1242	1.3602	178.0945	3.0780	196.2794	0.1864
140.3143	0.0935	157.2644	0.1241	179.0845	14.7202	197.1144	5.5468
141.1043	4.8646	158.1044	3.2886	179.2145	0.0449	197.2244	0.1596
142.1043	3.8233	159.0544	5.8899	180.0143	0.0083	197.3344	0.0873
142.1843	0.7758	159.1244	0.4003	180.0845	12.8943	198.1044	7.8548
143.0343	3.9860	160.0944	2.4160	180.2345	0.0276	199.1044	20.2048
143.0943	4.1905	160.2342	0.0124	181.0032	0.0109	199.3844	0.0218
143.9843	0.0080	161.0844	4.1312	181.1045	5.9437	200.1244	5.1994
144.0843	4.5604	162.0844	2.7875	182.0143	0.0040	201.0394	0.9549
144.1743	0.0650	162.2244	0.1633	182.1045	5.6085	201.1444	4.0136
144.2443	0.0364	163.0644	27.0958	183.0945	8.5432	201.3044	0.3041
145.0543	33.4717	163.1344	0.1963	184.1145	2.7562	202.1244	1.8829
145.2243	0.0751	163.2644	0.0376	185.1145	3.0669	202.2846	0.0598
146.0843	3.7597	164.0844	4.6281	186.1145	2.1770	203.1144	0.1284
146.1643	0.0401	164.2244	0.1078	187.1245	2.5861	203.1746	2.6795
146.2443	0.2036	164.9869	0.0053	188.0945	2.4804	203.3346	0.0697
146.9943	0.0092	165.0844	5.9265	189.0356	1.8762	204.1146	1.2655
147.0743	5.1617	166.0944	4.8991	189.1345	2.0823	204.1844	0.5133
148.0745	1.7110	167.0944	5.8499	189.2345	0.1667	205.1046	5.4658
149.0165	1.6969	167.2544	0.1688	189.3145	0.1081	205.1946	2.6313
149.1142	2.4863	168.0944	3.7961	190.1244	2.2174	205.3346	0.0280
150.0942	5.3803	168.2544	0.2205	191.0678	1.0142	205.4046	0.0711
150.2342	0.0583	169.1144	3.4586	191.1644	7.7943	206.1146	2.3775

Table A3.7 (continued). Mass data (*m/z* values and their relative intensities) for the DART-HRMS analysis of *L. virosa* flower. Ten replicates of one sample were averaged where the corresponding spectrum appears in Figure 3.4B.

				L. virosa flower			
m/z	Rel. Int. %	*m/z*	Rel. Int. %	*m/z*	Rel. Int. %	*m/z*	Rel. Int. %
206.2044	0.1331	222.2947	0.1379	241.1046	6.8763	254.3547	0.1141
207.0746	1.6385	223.1247	2.6392	241.1846	0.1869	255.1347	0.3731
207.1546	2.6818	224.1147	1.5180	241.3046	0.0491	255.2247	0.7703
208.1146	2.1770	225.0447	0.2961	242.1048	1.1922	256.1447	0.7865
209.1346	16.2431	225.1447	2.2372	243.1046	2.1909	256.2447	0.0801
210.1046	4.4357	225.2547	0.2334	243.1648	0.2112	256.3447	0.0022
210.3596	0.1012	226.1247	1.3417	243.2498	0.1423	257.0847	0.0924
211.1345	4.1664	226.2547	0.0128	243.4048	0.0374	257.1647	0.4573
211.2445	0.2487	227.1347	3.0111	244.1148	1.1628	257.2447	2.5197
211.3145	0.1109	227.4147	0.0316	244.1946	0.2126	258.0947	0.4580
212.0245	0.0112	228.1247	1.1498	245.1246	1.4157	258.1647	0.1626
212.1045	3.7479	229.1047	1.6588	245.2246	1.2429	258.2547	0.4486
212.3345	0.0852	229.2045	3.2842	246.1148	1.0856	258.4347	0.0831
213.0145	0.0075	230.1047	2.5258	246.2446	0.0913	259.1047	2.9838
213.1145	2.4455	230.1847	0.8661	247.1246	2.0369	259.1947	0.1642
213.7345	0.0038	230.3547	0.0591	247.2248	0.1047	259.2647	1.1520
214.1245	2.2874	231.1247	1.7555	248.1346	1.4877	259.4247	0.0431
215.1145	7.3372	231.2147	1.6451	248.3297	0.0988	260.1147	1.1129
215.3245	0.1606	232.1346	1.5563	248.4046	0.0298	260.1947	0.1232
215.3545	0.1632	232.2346	0.1375	249.0646	0.1484	260.2547	0.2560
216.1245	4.5358	233.1346	1.5316	249.1646	1.6517	261.1147	1.6315
216.3345	0.0454	234.1346	1.1626	249.3148	0.0278	261.2247	0.6991
217.0770	2.5775	234.2046	0.2021	250.1548	0.9319	261.4647	0.0805
217.1745	2.9787	234.3546	0.0760	251.1048	0.3947	262.1847	0.9056
217.3645	0.1428	235.0846	0.3938	251.1648	1.6170	263.1347	1.2243
218.0445	0.0038	235.1746	0.6993	251.2748	0.0074	263.2347	1.2618
218.1345	1.9293	236.1046	0.9583	252.1247	0.7741	263.3849	0.2177
219.1045	2.0860	236.1746	0.2051	252.1847	0.1453	264.1249	0.6868
219.1845	4.1079	237.1146	1.5977	252.2647	0.0292	264.2447	0.0731
220.1145	1.4774	238.1146	1.1911	253.1047	0.5372	265.1547	1.3771
220.1745	0.5701	238.1946	0.2157	253.1847	0.8833	265.2449	0.5070
220.2546	0.1826	238.3846	0.0632	253.2847	0.1316	266.1447	1.0081
220.3347	0.1646	239.1446	1.2947	254.1145	1.0688	267.1547	1.4283
221.0545	0.6098	239.2346	0.1801	254.1847	0.0503	267.2647	0.2049
221.1845	1.4070	240.1246	1.0522	254.2747	0.0485	268.1149	4.5251
222.1245	1.3077	240.2146	0.0842	254.3047	0.0732	268.2847	0.1228

Table A3.7 (continued). Mass data (*m/z* values and their relative intensities) for the DART-HRMS analysis of *L. virosa* flower. Ten replicates of one sample were averaged where the corresponding spectrum appears in Figure 3.4B.

L. virosa **flower**							
m/z	Rel. Int. %	*m/z*	Rel. Int. %	*m/z*	Rel. Int. %	*m/z*	Rel. Int. %
269.1347	0.7391	281.2448	1.9866	296.1649	0.2477	308.2349	0.2859
269.2147	0.9421	282.1548	0.6226	296.2549	1.2508	308.3315	0.0779
270.1247	0.8070	282.2648	0.8480	296.4747	0.0646	309.2149	1.5572
270.2049	0.0036	282.5246	0.1022	296.5247	0.0992	309.2849	0.0163
270.3849	0.0556	283.1848	0.9249	297.1847	0.0783	310.1349	0.2401
271.0847	1.4830	283.2648	0.2333	297.2449	1.3710	310.2449	0.5760
271.1597	0.2527	284.1548	0.6752	298.1649	0.2480	311.2349	0.7404
271.2347	0.9700	284.2648	0.2753	298.2749	0.6358	311.2749	0.5270
272.1349	0.6983	285.1048	1.0151	298.4049	0.1113	312.1649	0.2952
272.2547	0.3211	285.2048	0.0764	298.5049	0.1134	312.2749	0.3284
272.3549	0.0407	285.2748	0.7010	299.1949	0.5584	313.1149	0.0692
272.4649	0.0549	285.4148	0.0218	299.2749	0.6488	313.2749	3.7049
273.0848	0.5357	286.1348	0.6223	300.1949	0.4348	314.1548	0.2168
273.1548	0.4998	286.2148	0.2720	300.2947	0.2996	314.2448	0.8693
273.2446	0.1447	286.2748	0.0390	300.4249	0.1117	315.1148	0.2844
274.1248	0.2591	287.0648	0.3161	301.0949	1.1750	315.2248	0.5047
274.1548	0.3568	287.1248	0.4374	301.2049	0.0880	315.2998	0.1333
274.2648	0.1346	287.2248	0.2661	301.2949	0.2221	315.4448	0.1329
274.4148	0.0738	287.3848	0.0654	302.1049	0.1973	316.1150	0.1167
275.1046	0.4872	287.4748	0.0793	302.1449	0.4021	316.2250	0.3469
275.2046	1.7042	288.1348	0.5463	302.2149	0.1701	316.3048	0.0329
276.0946	0.4915	288.2448	0.1333	302.3049	0.1258	317.1250	0.0664
276.1648	0.7245	289.1048	0.8222	302.4149	0.1057	317.2348	0.5032
277.1146	1.1655	289.1748	0.4699	303.0549	0.1202	318.1048	0.0628
277.2148	6.5586	289.2348	0.3223	303.1249	0.4300	318.2248	0.3251
277.4548	0.0954	289.4048	0.0759	303.2249	0.2811	319.2348	0.5130
277.5248	0.1483	289.4748	0.0208	303.3049	0.0226	319.3050	0.0473
278.1248	0.4042	290.1748	0.7507	304.1549	0.4942	319.4450	0.0956
278.2148	1.8311	291.1948	2.3464	304.2349	0.2844	320.1648	0.1133
279.1546	1.4648	291.4148	0.2423	305.1549	0.5234	320.2350	0.2582
279.2348	9.0819	292.1148	0.4560	305.2349	0.1554	321.1550	0.1319
279.4048	0.1123	292.1948	0.5726	306.1649	0.5077	321.2350	0.3562
280.1448	0.6739	293.2148	3.2664	306.2749	0.3023	321.3150	0.0399
280.2446	1.5795	294.1098	0.3383	307.1149	0.3437	322.1748	0.2487
280.3648	0.0564	294.2147	0.7533	307.1949	1.0189	322.2450	0.3298
281.1448	0.3373	295.2347	3.9788	308.1360	0.3517	323.1750	0.4098

				L. virosa flower				
m/z	Rel. Int. %	*m/z*	Rel. Int. %	*m/z*	Rel. Int. %	*m/z*	Rel. Int. %
323.2548	0.2871	337.2049	0.2293	350.1649	0.1377	364.2550	0.2693
323.3570	0.0776	337.2651	0.7765	350.2351	0.1596	365.2750	0.6252
324.1750	0.2921	338.1951	0.0726	350.3151	0.2340	365.4150	3.0897
324.2650	0.4066	338.2649	0.5209	351.1751	0.0559	366.2652	0.0263
325.1150	0.0765	338.3449	0.1927	351.2451	0.8248	366.2950	0.1479
325.1950	0.3080	338.4849	0.0782	352.2451	0.5249	366.4150	0.8380
325.2850	0.8959	338.6049	0.0494	353.2651	1.4179	367.2050	0.2590
326.1850	0.2967	339.1849	0.0497	354.2651	0.5078	367.2750	0.1857
326.2950	0.6610	339.3251	0.8560	355.0751	0.1433	367.3352	0.1961
327.1950	0.3135	339.4249	0.0061	355.2950	0.9849	368.2052	0.2671
327.2850	0.6952	340.2651	0.4046	356.0750	0.0738	368.2652	0.0160
328.2250	0.3525	340.3449	0.0074	356.1950	0.0726	368.3350	0.1845
328.3248	0.5697	341.1349	0.1578	356.2850	0.4306	369.1252	0.0395
329.1050	0.1100	341.2149	0.1771	357.0750	0.1377	369.2150	0.7150
329.2350	0.3780	341.3149	0.5113	357.2050	0.3074	369.3452	0.5092
329.3150	0.1354	342.1451	0.1694	357.2950	0.4336	369.4252	0.0451
330.1650	0.2841	342.2151	0.1384	358.2152	0.3130	369.4852	0.0347
330.2350	0.2377	342.3149	0.2357	358.2950	0.2115	369.5650	0.1439
330.3350	0.1736	343.1649	0.3045	358.3650	0.0082	370.2150	0.0893
331.0950	0.2601	343.2351	0.5996	359.1350	0.0788	370.3352	0.3883
331.2250	0.2595	343.3351	0.4484	359.2250	0.5741	371.1052	1.2912
331.2950	1.0312	344.1751	0.3810	359.2952	0.3332	371.2250	0.3566
332.0950	0.1555	344.2651	0.1423	359.5150	0.0130	371.3152	0.2349
332.2150	0.3969	344.3951	0.0357	359.5850	0.1018	371.4052	0.2169
332.2950	0.2503	345.1849	0.5047	360.1550	0.1288	371.5852	0.0754
332.3550	0.0078	345.2749	0.3326	360.2252	0.3141	371.6750	0.0563
333.1750	0.4042	346.1751	0.2348	360.3150	0.0712	371.7551	0.0671
333.2350	0.1877	346.2749	0.2442	361.1550	0.1511	372.1152	0.4631
334.1550	0.2068	347.1649	0.1015	361.2352	0.5581	372.2352	0.4416
334.2350	0.3457	347.2851	0.4311	361.3250	0.0772	372.3152	0.1936
334.3350	0.0907	347.3651	0.0461	362.1652	0.2049	372.4152	0.0395
335.2049	0.6569	348.1851	0.1685	362.2650	0.2656	372.4902	0.0437
336.1849	0.3435	348.2949	0.3848	362.3750	0.2233	373.1052	0.2852
336.2549	0.0970	349.1101	0.1170	363.1752	0.2002	373.1752	0.1108
336.3251	0.0173	349.2151	0.5066	363.2452	0.2560	373.2452	0.3584
336.4749	0.0626	349.3351	0.0309	364.1952	0.1098	373.3152	0.1684

Table A3.7 (continued). Mass data (*m/z* values and their relative intensities) for the DART-HRMS analysis of *L. virosa* flower. Ten replicates of one sample were averaged where the corresponding spectrum appears in Figure 3.4B.

L. virosa flower							
m/z	Rel. Int. %	*m/z*	Rel. Int. %	*m/z*	Rel. Int. %	*m/z*	Rel. Int. %
374.0952	0.0078	385.2151	0.2860	399.3652	0.7697	413.3052	0.2760
374.1652	0.0259	385.3151	0.3301	400.1552	0.0114	413.3754	0.7374
374.2652	0.3142	385.4851	0.0843	400.2352	0.1290	414.2154	0.0217
374.3252	0.0840	386.2153	0.1556	400.3552	0.1573	414.3154	0.1239
375.1752	0.1269	386.3351	0.1608	400.4452	0.4823	414.3854	0.3251
375.2452	0.3294	387.1053	0.1367	401.2252	0.4244	414.6152	0.0773
375.3152	0.1447	387.2253	0.1280	401.3252	0.0639	415.0554	0.0057
376.1451	0.1007	387.2853	0.1648	401.4652	0.0948	415.2254	0.0797
376.2551	0.1279	387.3353	0.0228	402.1252	0.0193	415.3004	0.3185
376.3351	0.0496	387.6051	0.0237	402.2252	0.0871	415.3754	0.2040
376.5751	0.0064	388.1351	0.1373	402.3352	0.2601	416.3652	0.3348
377.1851	0.1128	388.2653	0.3211	403.1952	0.0752	417.1753	0.0851
377.2551	0.3010	388.4351	0.1214	403.2952	0.3690	417.2553	0.0914
377.3351	0.2358	388.5351	0.0946	403.4452	0.0186	417.3053	0.1415
377.4251	0.0154	389.2653	0.4840	404.1552	0.0721	417.3753	0.0385
377.5251	0.1328	390.1353	0.0062	404.2952	0.2094	417.4553	0.1594
378.2651	0.3336	390.2551	0.2004	404.3752	0.0209	418.2253	0.0817
379.1751	0.0241	390.3351	0.0304	404.6452	0.0060	418.2953	0.1855
379.2651	0.2172	391.1753	0.0730	405.3752	1.2255	418.3653	0.1026
379.3451	0.3643	391.2951	0.4097	406.1952	0.0268	418.4553	0.0819
380.2051	0.1949	391.3901	0.1924	406.3854	0.4390	419.3253	0.4169
380.2851	0.0196	391.4851	0.0216	407.2652	0.1124	420.2553	0.0770
380.3451	0.2240	392.2853	0.3492	407.3652	6.6078	420.3153	0.0605
381.1951	0.3662	393.3451	1.0761	408.3752	3.3015	421.3453	1.1270
381.2851	0.0260	394.1853	0.0895	409.2052	0.0344	422.2053	0.0181
381.3451	0.3048	394.3353	0.4002	409.3852	63.9548	422.3453	0.4738
381.4153	0.6704	395.2753	0.2391	410.2252	0.1028	422.4851	0.0215
382.2951	0.3057	395.3653	2.5967	410.3854	19.9172	423.3753	5.2412
382.3551	0.0431	396.2053	0.0052	411.1252	0.2148	424.3753	2.1722
382.4351	0.3887	396.3753	1.1716	411.3852	4.7150	425.2053	0.0166
383.2951	0.0499	397.2152	0.0215	411.6254	0.0785	425.3753	8.2646
383.3651	0.9655	397.3852	4.4393	411.6954	0.3171	426.3853	2.7636
384.2051	0.1463	398.2152	0.2202	412.2052	0.2213	427.3953	4.2071
384.2751	0.0846	398.2952	0.0764	412.2954	0.0744	428.2953	0.0231
384.3051	0.0723	398.3950	1.1350	412.3852	0.8829	428.3955	1.2893
384.3751	0.2193	398.5452	0.0526	413.0454	0.0739	429.1653	0.0049

Table A3.7 (continued). Mass data (*m/z* values and their relative intensities) for the DART-HRMS analysis of *L. virosa* flower. Ten replicates of one sample were averaged where the corresponding spectrum appears in Figure 3.4B.

L. virosa flower							
m/z	Rel. Int. %	*m/z*	Rel. Int. %	*m/z*	Rel. Int. %	*m/z*	Rel. Int. %
429.3853	1.6234	446.3854	0.2531	464.3155	0.1306	481.4956	0.0191
430.2353	0.1987	447.3254	0.0523	464.3855	0.1487	482.2154	0.0130
430.3053	0.0164	447.3854	0.2336	465.2255	0.0023	482.3354	0.1947
430.3853	0.3807	448.3254	0.1961	465.3955	0.4898	482.4756	0.0221
430.5553	0.1050	448.3854	0.0836	465.4855	0.0335	482.5256	0.0382
431.3853	0.5484	449.2154	0.0038	466.3355	0.0708	483.3856	1.9489
432.1853	0.0391	449.3254	0.1500	466.4055	0.3409	484.3956	0.5540
432.3153	0.1110	449.3954	0.0586	466.5055	0.0468	485.2156	0.0040
432.3955	0.1928	449.4354	0.1162	467.3955	1.7507	485.4056	0.4758
433.1855	0.0048	449.5154	0.0296	468.3955	0.5720	486.3254	0.1975
433.3253	0.3535	450.2154	0.1559	469.1855	0.0040	486.3854	0.1170
434.1953	0.0062	450.3454	0.1575	469.4055	2.7503	486.4556	0.0454
434.2653	0.0801	450.5154	0.0320	470.4155	0.9349	487.3854	0.2010
434.3353	0.0206	451.3454	0.3208	471.3855	0.4345	487.5256	0.1291
434.3955	0.0065	451.4254	0.0717	472.3455	0.2926	488.3956	0.0806
435.2253	0.0803	452.4854	0.0673	472.3855	0.0237	488.4656	0.0663
435.3553	0.3058	453.3554	0.5310	473.2255	0.0117	488.5456	0.0203
435.4655	0.1136	454.3454	0.2923	473.3755	0.2761	489.1956	0.0053
436.3353	0.1813	454.4956	0.0429	474.3855	0.2546	489.3756	0.2491
437.3455	0.6501	455.3556	1.1135	474.4655	0.0207	491.3056	0.1359
437.4755	0.0866	456.2854	0.0111	475.3055	0.1320	491.3756	0.1203
438.3552	0.4051	456.3754	0.3063	475.3855	0.0895	491.4856	0.0788
438.4852	0.0272	456.5156	0.0490	476.3155	0.0733	492.3356	0.0914
439.2154	0.0082	457.3754	0.9655	476.4055	0.1156	493.3056	0.0659
439.3652	1.7850	458.3853	0.3836	477.2955	0.1470	493.3856	0.1874
440.3654	1.0579	459.3855	0.4747	477.4355	0.0991	494.3656	0.1017
441.2154	0.0365	460.3053	0.1206	477.5455	0.0237	495.3856	0.3191
441.3754	4.4880	460.4155	0.0834	478.3255	0.0890	496.3256	0.0875
442.3854	1.4419	460.4955	0.0148	478.4355	0.1006	497.3956	0.3662
443.3854	0.9998	461.3755	0.2686	478.5455	0.0319	498.3256	0.2145
444.2954	0.2636	462.2055	0.0199	479.2956	0.0189	498.3956	0.0384
444.4054	0.0952	462.3053	0.1480	479.3754	0.2662	498.5356	0.0330
445.1154	0.0572	462.4455	0.0993	479.4854	0.1231	499.2156	0.0042
445.2154	0.0120	463.2155	0.0046	480.3254	0.1040	499.3256	0.0668
445.3754	0.5075	463.3855	0.3968	480.4954	0.0914	499.4256	0.2868
446.3054	0.1795	464.2255	0.0356	481.3954	0.5351	500.3455	0.0599

Table A3.7 (continued). Mass data (*m/z* values and their relative intensities) for the DART-HRMS analysis of *L. virosa* flower. Ten replicates of one sample were averaged where the corresponding spectrum appears in Figure 3.4B.

L. virosa **flower**							
m/z	Rel. Int. %	*m/z*	Rel. Int. %	*m/z*	Rel. Int. %	*m/z*	Rel. Int. %
500.4255	0.2310	516.3457	0.0366	535.4458	0.0325	552.4959	0.3242
501.3255	0.1440	516.4257	0.1535	535.5358	0.0298	552.5857	0.0305
501.3957	0.0565	517.3257	0.1939	536.2558	0.0157	553.3957	0.0704
501.4755	0.0056	517.4457	0.0246	536.3158	0.0154	553.4957	0.1747
502.3355	0.0294	518.3457	0.0152	536.3858	0.0073	554.4957	0.2603
502.4155	0.1213	518.4357	0.1328	536.5358	0.0581	555.4559	0.2164
503.3255	0.1365	518.5157	0.0092	536.6058	0.0467	556.3659	0.1049
503.4155	0.1158	519.4057	0.2306	537.3958	0.0377	556.4359	0.0556
504.2857	0.0715	520.3356	0.0933	537.5058	0.2089	557.4459	0.0966
504.4555	0.0689	520.4056	0.1470	538.3858	0.1418	557.5359	0.0653
505.1857	0.0025	521.4056	0.1860	538.5058	0.2095	558.4457	0.0791
505.3255	0.0073	521.5256	0.1320	539.3658	0.1846	559.4459	0.1791
505.3955	0.2498	522.4256	0.1864	539.4958	0.1199	559.5459	0.0230
506.3657	0.1619	523.3256	0.0884	540.4358	0.0884	560.3459	0.0154
507.3955	0.1902	523.4056	0.1019	541.4257	0.2082	560.4159	0.1214
507.5155	0.1035	524.2756	0.0176	542.3357	0.1123	560.4959	0.0109
508.3557	0.1029	525.4256	0.2164	542.4157	0.0386	561.4159	0.0754
508.5257	0.0347	526.4156	0.1559	543.3457	0.0240	561.4957	0.0602
509.3255	0.0547	526.5658	0.0530	543.4257	0.0443	561.5658	0.0567
509.4055	0.1542	527.3456	0.0890	543.4957	0.0318	562.2558	0.0033
509.5257	0.1513	527.4256	0.0579	544.3857	0.0803	562.4358	0.0786
510.2257	0.0038	527.5256	0.0100	544.5257	0.0543	562.5158	0.0561
510.4157	0.1537	528.4256	0.1921	545.4057	0.1590	563.4358	0.1026
510.5357	0.0129	529.3256	0.1497	545.4757	0.0928	563.4858	0.3308
511.3257	0.1701	529.4156	0.0126	545.7257	0.0125	563.6158	0.0071
511.4357	0.1259	530.4056	0.0623	546.2857	0.0028	564.3558	0.1087
512.2057	0.0264	531.4058	0.1004	546.3857	0.0806	564.4358	0.0212
512.4057	0.0745	531.4756	0.0803	546.4557	0.0709	564.5458	0.1326
512.5757	0.0156	532.3358	0.1029	547.4657	0.1149	564.6358	0.0027
513.3357	0.0352	532.4158	0.1356	548.3459	0.0308	565.2958	0.0052
513.3957	0.1451	533.2707	0.0032	548.4657	0.1447	565.5258	0.0618
514.3357	0.1987	533.3556	0.0752	549.3559	0.0472	566.4458	0.0716
514.4157	0.0791	533.4407	0.0923	549.4959	0.2394	566.5358	0.0639
515.2357	0.0103	533.5258	0.0975	550.4459	0.1782	567.4558	0.1954
515.3257	0.1546	534.4858	0.2085	550.5657	0.0698	568.3858	0.0670
515.4257	0.0275	535.3656	0.1990	551.5057	0.4275	569.3858	0.0612

Table A3.7 (continued). Mass data (*m/z* values and their relative intensities) for the DART-HRMS analysis of *L. virosa* flower. Ten replicates of one sample were averaged where the corresponding spectrum appears in Figure 3.4B.

m/z	Rel. Int. %	*m/z*	Rel. Int. %	*m/z*	Rel. Int. %	*m/z*	Rel. Int. %
569.4958	0.0687	589.4759	0.4809	610.5460	0.2179	632.5361	0.1042
569.5660	0.0294	590.3959	0.0839	611.5360	0.0404	633.5161	0.0621
569.6358	0.0599	590.4859	0.1049	612.4760	0.1484	633.5961	0.1306
570.4058	0.0553	591.3559	0.0431	612.5460	0.0056	633.6961	0.0315
570.5458	0.1187	591.4961	0.3294	613.3660	0.0561	634.4661	0.0373
571.4458	0.2256	592.4959	0.1302	613.5060	0.0790	634.5461	0.0836
572.3758	0.1181	592.5759	0.0330	614.4160	0.0132	635.5461	0.0378
572.4458	0.0398	592.6759	0.0381	614.4960	0.0337	635.6161	0.2656
572.5658	0.0184	593.5159	0.1259	615.5060	0.1332	636.3961	0.0280
573.4558	0.1725	594.5159	0.1067	615.6460	0.0479	636.5661	0.0242
573.5758	0.0254	597.3661	0.0037	616.5160	0.0950	637.5661	0.0491
574.4460	0.0922	597.4460	0.0850	617.5160	0.2146	638.5761	0.1421
575.5060	0.7925	597.5259	0.0228	617.6460	0.0190	638.6861	0.2157
576.5158	0.2770	598.4561	0.0575	618.5260	0.1723	639.5661	0.1578
577.5258	0.3265	598.5959	0.0687	618.6762	0.0048	640.4761	0.0653
578.5260	0.1356	599.5061	0.1714	619.4560	0.0609	640.5661	0.0596
579.5260	0.2123	600.3861	0.0501	619.5360	0.1140	641.4861	0.1144
580.4360	0.1728	600.5061	0.0908	619.6660	0.0117	642.4863	0.0993
581.3658	0.1026	601.3761	0.0832	619.7560	0.0298	643.4261	0.0830
581.4460	0.0394	601.5259	0.0394	620.3960	0.0045	643.4963	0.0104
581.5358	0.0343	601.5961	0.0038	620.4560	0.0863	644.4960	0.0034
582.2957	0.0069	602.3861	0.0349	620.5360	0.0309	645.4862	0.0269
582.3759	0.0262	602.5261	0.0234	620.6660	0.1093	646.4960	0.0070
582.5159	0.0462	603.5360	0.1250	621.6660	0.2800	646.6162	0.1500
583.4557	0.0975	603.6260	0.0538	623.4659	0.0106	647.6360	0.1308
583.5859	0.0483	604.4660	0.0319	623.5659	0.1408	648.6360	0.2514
585.4759	0.1774	604.5458	0.1300	624.4759	0.0790	649.5960	0.1603
585.5859	0.0078	604.6560	0.0131	624.5459	0.0665	649.6760	0.0473
586.3959	0.0675	605.4660	0.1776	625.4861	0.1530	650.5460	0.0404
586.4857	0.0620	605.5460	0.1013	626.5259	0.0225	650.6060	0.2830
586.5559	0.0620	606.4060	0.1035	627.5061	0.0149	651.5462	0.0983
587.4909	0.1556	606.5360	0.0777	627.5861	0.0182	652.4860	0.0262
587.5859	0.0392	607.5060	0.3054	628.5061	0.0070	652.5462	0.0669
588.4059	0.0349	608.4510	0.0108	629.5059	0.0506	653.4162	0.0631
588.5059	0.0946	608.5260	0.1773	630.4961	0.0360	653.5660	0.0697
588.6059	0.0071	609.5160	0.1614	631.5059	0.0952	654.5662	0.0616

Table A3.7 (continued). Mass data (*m/z* values and their relative intensities) for the DART-HRMS analysis of *L. virosa* flower. Ten replicates of one sample were averaged where the corresponding spectrum appears in Figure 3.4B.

m/z	Rel. Int. %	*m/z*	Rel. Int. %	*m/z*	Rel. Int. %	*m/z*	Rel. Int. %
655.4762	0.0501	680.4763	0.0099	708.6463	0.0311	740.4664	0.0032
656.4962	0.0032	680.5963	0.2446	709.5963	0.0883	740.5366	0.0172
657.5062	0.0335	681.4563	0.0048	710.6063	0.1095	740.6364	0.0110
658.5062	0.0337	681.5963	0.1403	711.6063	0.0849	741.4664	0.0023
659.5262	0.0071	682.4563	0.0422	712.6063	0.0662	741.5264	0.0087
659.6162	0.0928	683.4163	0.0155	713.5865	0.0764	741.6266	0.0082
660.5362	0.0397	683.4863	0.0047	714.5863	0.0812	742.3564	0.0034
660.6317	0.0854	684.5063	0.0387	715.6063	0.0543	742.6164	0.0104
661.5562	0.1875	685.4962	0.0309	716.5963	0.0116	743.6164	0.0065
662.5662	0.1674	688.5764	0.0408	717.5965	0.0759	744.6166	0.0053
663.5562	0.0786	689.4762	0.0030	718.6763	0.0030	745.6266	0.0120
663.6262	0.1517	689.6462	0.0307	719.6565	0.0100	746.5464	0.0169
664.4662	0.0071	690.4762	0.0121	720.7365	0.0059	746.6264	0.0357
665.4161	0.0686	690.6564	0.0485	721.5363	0.0297	747.6265	0.0333
665.5961	0.3062	691.6662	0.0817	721.6263	0.0415	748.6463	0.0356
666.4161	0.0565	692.6462	0.1047	722.6365	0.0431	749.6365	0.0238
666.6461	0.3035	693.6164	0.0645	722.7963	0.0310	750.6863	0.0331
666.7161	0.0111	694.6064	0.0386	723.6465	0.0314	750.8165	0.0140
667.4561	0.0050	694.7462	0.1781	724.6665	0.0378	751.5965	0.0436
667.5861	0.0551	695.6264	0.0908	725.6065	0.0517	751.6863	0.0131
667.7161	0.0807	695.7464	0.0538	725.6665	0.0056	752.6065	0.0545
668.4806	0.0076	696.5964	0.0076	726.6565	0.0337	752.6765	0.0028
668.5761	0.0167	696.6562	0.1219	727.5744	0.0376	753.6165	0.0220
669.5863	0.0319	697.4664	0.0059	728.5964	0.0607	753.6665	0.0117
670.5161	0.0026	697.6262	0.1006	729.5964	0.0322	754.6465	0.0393
673.6463	0.0265	700.5264	0.0159	732.6864	0.0394	755.6265	0.0086
674.6263	0.0658	703.6464	0.0541	733.4764	0.0058	756.6265	0.0142
675.6761	0.1741	704.6564	0.0396	733.7864	0.0075	757.6265	0.0051
676.5261	0.0080	705.6664	0.0565	734.6864	0.0191	766.6665	0.0022
676.6763	0.0963	705.7564	0.0444	735.4864	0.0026	767.6067	0.0147
677.5463	0.0758	706.3963	0.0031	735.6764	0.0228	768.5766	0.0445
677.6263	0.0083	706.5863	0.0560	736.5164	0.0140	769.6066	0.0247
677.7063	0.2583	706.6563	0.0514	736.6164	0.0150	769.7011	0.0068
678.5961	0.1232	707.6463	0.0336	737.5064	0.0069	770.6064	0.0229
678.7263	0.0998	708.4363	0.0031	737.6364	0.0095	771.6364	0.0075
679.5963	0.2458	708.5863	0.0748	738.6364	0.0097	772.6366	0.0158

Table A3.7 (continued). Mass data (*m/z* values and their relative intensities) for the DART-HRMS analysis of *L. virosa* flower. Ten replicates of one sample were averaged where the corresponding spectrum appears in Figure 3.4B.

				L. virosa **flower**			
m/z	Rel. Int. %	*m/z*	Rel. Int. %	*m/z*	Rel. Int. %	*m/z*	Rel. Int. %
773.6364	0.0043	779.6366	0.0020	790.6167	0.0186	810.6266	0.0170
775.6164	0.0036	779.7066	0.0138	792.6067	0.0340	831.7269	0.0057
776.6166	0.0065	780.7066	0.0101	793.6067	0.0045	833.7469	0.0173
776.6866	0.0103	781.6166	0.0272	794.6167	0.0045	837.5867	0.0040
777.6166	0.0185	782.6766	0.0225	798.4367	0.0088	857.7568	0.0030
778.6266	0.0284	784.6668	0.0028	798.6567	0.0043	867.5870	0.0033
778.6966	0.0062	788.6167	0.0031	809.6066	0.0225		

Table A3.8 Mass data (*m/z* values and their relative intensities) for the DART-HRMS analysis of *L. virosa* resin. Ten replicates of one sample were averaged where the corresponding spectrum appears in Figure 3.4B.

L. virosa resin								
m/z	Rel. Int. %	*m/z*	Rel. Int. %	*m/z*	Rel. Int. %	*m/z*	Rel. Int. %
61.0339	0.7124	94.0641	0.8176	115.1040	1.4447	134.2543	0.1316
61.1041	0.0043	94.1741	0.0409	115.2442	0.2043	135.1043	19.1216
62.0639	0.0470	95.0841	1.9881	116.0742	8.7260	135.2443	0.0423
67.0540	0.1254	96.0541	9.8180	116.1442	0.3302	135.9943	0.1394
68.0538	0.1347	97.0341	17.9665	116.2242	0.2752	136.0643	0.9455
68.9640	0.5185	97.0941	1.1207	117.0642	14.9564	136.1343	1.9620
69.0440	2.2074	97.9941	0.0463	117.2442	0.0422	136.2843	0.1675
70.0640	1.4948	98.0841	1.9964	118.0842	2.9964	136.4043	0.1179
71.0640	1.7818	99.0541	23.7888	118.2042	0.1826	137.0743	0.8315
72.0840	6.1101	99.1841	0.0027	119.0842	0.4167	137.1243	1.1149
72.2040	0.2915	100.0041	0.0828	120.0742	0.6144	137.2143	0.0152
74.0640	2.2216	100.0841	3.6358	120.2042	0.1153	138.0843	0.4751
75.0440	3.0884	100.2341	0.1340	122.0742	0.2106	138.1643	0.4580
76.0640	0.2077	101.0641	20.6625	123.0942	7.1162	139.0054	0.7713
77.0440	1.2866	101.1841	0.1273	123.2942	0.1219	139.1043	1.9631
78.0440	0.0526	102.0741	2.5669	124.0642	0.4730	139.2243	0.0070
79.0440	0.7682	104.0741	1.6473	125.0942	1.7632	139.2643	0.2560
80.0540	0.9257	104.1443	0.0199	125.2144	0.0444	140.0843	2.9004
81.0540	2.1750	104.2343	0.0075	126.0642	36.3376	140.2543	0.1375
81.1442	0.0039	105.0641	1.0985	126.1542	2.3627	140.3143	0.1938
82.0642	0.3156	106.0641	0.3994	127.0442	94.0547	141.1043	1.7822
82.9442	0.0354	108.0640	6.4785	127.1142	6.4677	142.1043	3.6325
83.0840	0.9001	109.0340	2.5335	127.2342	0.5891	142.1843	1.0908
84.0640	1.1861	109.0942	2.8434	127.9777	0.0876	143.0343	0.7645
85.0342	42.2101	109.2042	0.0297	128.0844	9.5947	143.0943	3.1594
85.0942	1.8611	110.0742	18.3547	128.1843	0.3096	144.0843	7.3841
86.0740	28.3835	110.2142	0.4300	128.2243	0.2054	144.2443	0.1281
86.1742	0.4200	111.0540	3.9270	128.9841	0.0217	145.0543	79.5103
86.9739	0.0036	111.1140	1.9436	129.0641	18.3875	145.2243	0.5873
88.0741	0.4268	111.2342	0.2225	129.1391	0.6163	145.9868	0.0116
88.2041	0.0194	112.0742	1.2598	130.0643	11.4386	146.0843	5.1643
90.0641	0.0324	112.1542	0.4297	130.1543	1.7785	146.2443	0.0428
90.1641	0.0029	113.0542	6.8637	131.2243	0.0985	146.9943	0.0136
91.0541	0.6604	114.0842	3.1716	132.1041	1.4199	147.0743	2.8866
92.0641	0.0669	114.2242	0.4389	134.0843	0.0202	148.0745	0.9315
93.0641	5.2372	115.0542	6.5265	134.1943	0.0140	149.0165	0.0271

Table A3.8 (continued). Mass data (*m/z* values and their relative intensities) for the DART-HRMS analysis of *L. virosa* resin. Ten replicates of one sample were averaged where the corresponding spectrum appears in Figure 3.4B.

				L. virosa resin			
m/z	Rel. Int. %	*m/z*	Rel. Int. %	*m/z*	Rel. Int. %	*m/z*	Rel. Int. %
149.1142	0.3672	166.2344	0.0695	189.2345	0.2437	206.2044	0.1023
149.9942	0.0376	167.0944	3.4622	189.4045	0.0113	207.0746	0.0400
150.0942	4.4773	167.2544	0.0356	190.1244	1.6009	207.3046	0.0567
150.1542	0.5056	168.2544	0.0705	190.2244	0.0040	208.1146	4.1789
150.2342	0.1484	168.9844	0.0167	191.3244	0.0871	208.2096	0.0748
150.3142	0.0966	169.1144	2.8344	192.1044	1.9339	209.2746	0.0095
151.2342	0.8687	170.0943	1.5581	192.1644	0.9082	210.1046	0.3126
152.1144	1.2620	170.1643	0.9929	193.0844	0.5696	210.3596	0.0182
152.2444	0.0396	171.1543	9.0636	193.1544	0.1416	211.1345	2.6482
153.0844	4.1420	171.3143	0.2915	194.0944	19.4882	211.3145	0.0316
154.0844	2.1755	172.1243	2.3745	194.9975	0.0133	212.1045	1.7322
154.1544	0.6215	173.1143	2.1399	196.2794	0.1162	212.3345	0.0595
155.1044	2.9497	174.1143	1.4456	197.1144	0.6771	213.1145	0.7475
155.2644	0.0310	176.0945	0.0387	197.3344	0.0019	213.2095	0.1058
156.1042	1.6298	178.0945	1.3781	198.1044	22.5370	214.1245	0.9891
156.1744	1.1605	178.1694	0.0892	198.2444	0.0311	214.2545	0.5507
156.2744	0.0523	180.0845	54.5224	199.1044	0.7586	215.1145	0.8193
157.0544	0.0357	180.2345	0.1073	199.1744	3.1130	215.1895	0.7426
157.1242	2.0297	181.0032	0.0416	199.3844	0.0376	215.3545	0.2166
157.2644	0.2483	181.1045	3.1129	199.4046	0.0699	216.1245	9.0045
158.1044	5.4861	181.2345	0.0426	200.1244	4.8650	216.1945	0.1883
158.1844	0.9673	182.0143	0.0276	200.1844	1.0751	217.0770	1.2803
159.0544	0.0536	182.1045	5.7978	201.0394	2.5797	217.1745	0.6434
159.1244	0.9510	182.9989	0.0032	201.1444	1.4410	217.3645	0.1561
160.0944	1.3988	183.0945	5.8730	201.3044	0.2731	218.1345	2.9566
160.1744	0.2670	183.1945	0.2232	202.1244	1.5260	220.1145	0.3831
161.0844	0.4107	184.1145	1.5810	202.2846	0.2153	220.1745	0.0497
162.0844	4.8159	185.1145	2.3072	203.1144	0.0397	220.3347	0.1996
162.2244	0.2356	185.2145	0.2702	203.1746	1.9114	222.1245	2.7791
163.0644	44.0975	185.3245	0.0572	203.3346	0.2133	224.1147	0.0735
163.1344	5.1191	186.1145	2.4210	204.1146	0.7496	224.2545	0.4678
163.2644	0.0129	187.1245	2.7307	204.1844	0.7790	225.2547	0.0116
164.0844	3.4792	188.0945	1.4758	205.1046	4.4487	226.1247	0.2001
164.1644	0.1974	188.1645	1.0463	205.3346	0.0039	227.1347	1.4111
165.2744	0.0083	189.0356	0.8609	205.4046	0.0065	228.1247	0.0582
166.0944	0.8362	189.1345	1.0446	206.1146	1.5839	228.1947	1.1783

Table A3.8 (continued). Mass data (*m/z* values and their relative intensities) for the DART-HRMS analysis of *L. virosa* resin. Ten replicates of one sample were averaged where the corresponding spectrum appears in Figure 3.4B.

				L. virosa resin			
m/z	Rel. Int. %	*m/z*	Rel. Int. %	*m/z*	Rel. Int. %	*m/z*	Rel. Int. %
229.1047	1.4943	247.2248	0.7507	271.0847	4.2146	288.1348	0.6505
229.2045	1.1053	248.1346	1.0527	271.1597	0.0286	288.2448	1.1915
230.1047	6.3898	248.2548	0.6008	271.2347	0.8827	289.1048	4.2089
230.1847	1.4637	248.3297	0.0750	272.1349	0.5321	289.2348	0.7576
230.3547	0.1506	248.4046	0.1774	272.2547	1.2047	289.4048	0.1540
231.1247	0.9418	250.1548	0.5458	272.4649	0.2617	289.4748	0.0023
231.2147	0.5388	252.1247	0.3567	273.0848	0.6734	290.1748	0.6728
232.1346	0.9315	252.1847	0.3704	273.2446	1.1007	290.2748	0.5021
232.2346	0.1393	252.2647	0.2074	274.1248	0.1937	291.0948	0.1231
233.1346	0.6037	254.2747	0.0033	274.1548	0.0990	291.1948	0.5094
233.2246	0.4905	255.0847	0.8123	274.2648	0.8427	291.2750	0.1409
234.1346	3.5518	255.2247	2.1887	274.4148	0.3312	291.4148	0.2275
234.2046	0.2774	257.2447	1.2794	275.1046	0.3094	292.1148	0.3797
234.3546	0.2151	258.1647	0.0336	275.2046	0.0191	292.1948	0.0577
236.1046	0.2990	258.2547	0.7412	275.2648	0.5395	292.3148	0.5597
236.1746	0.7208	258.4347	0.1410	276.1648	0.6470	293.2947	0.0608
237.1146	0.1275	259.1047	0.6880	276.2748	0.9012	294.2147	0.1867
237.1846	0.0603	259.1947	7.1764	277.2148	0.9589	294.2949	0.4862
238.1146	0.2983	259.2647	0.1258	277.4548	0.0525	295.2347	0.0096
238.1946	0.2011	259.4247	0.2398	277.5248	0.0309	296.1649	0.1555
238.3846	0.1275	260.1147	0.4076	278.1248	0.2783	296.2549	0.8224
241.1046	0.0313	260.1947	0.6897	278.2148	0.6303	296.3447	0.0011
241.1846	1.4813	260.2547	1.0684	278.2948	0.4324	296.4747	0.1952
242.1048	0.0772	261.1147	0.5152	279.4048	0.0501	296.5247	0.0569
242.1846	0.6135	261.2247	0.6948	280.1448	0.1656	298.4049	0.1158
243.1046	1.5618	261.4647	0.1570	280.2446	0.6189	298.5049	0.0313
243.1648	0.6721	262.1847	0.6696	281.2448	3.3893	299.1949	0.0016
243.2498	0.4358	262.2547	0.1364	282.1548	0.0050	299.2749	0.3641
243.4048	0.1443	264.1249	0.0134	282.2648	1.1134	300.4249	0.0495
244.1148	0.3227	264.2447	0.1582	282.5246	0.0661	302.1449	0.0154
244.1946	0.8473	266.1447	0.3938	286.1348	0.0132	302.2149	0.0280
245.1246	0.0170	266.2547	0.2543	286.2148	0.0136	302.3049	0.4502
245.2246	0.5003	267.2647	0.5508	286.2748	0.1978	303.1249	0.1004
246.1148	0.6017	268.2847	0.2902	287.1248	0.0698	303.3049	0.4674
246.2446	0.4677	270.1247	0.0164	287.2248	0.6672	304.1549	0.3033
247.1246	1.5820	270.3849	0.0015	287.4748	0.1683	304.2349	0.8102

Table A3.8 (continued). Mass data (*m/z* values and their relative intensities) for the DART-HRMS analysis of *L. virosa* resin. Ten replicates of one sample were averaged where the corresponding spectrum appears in Figure 3.4B.

				L. virosa resin			
m/z	Rel. Int. %	*m/z*	Rel. Int. %	*m/z*	Rel. Int. %	*m/z*	Rel. Int. %
305.1549	0.0434	324.2650	0.1667	344.2651	0.0874	361.2352	0.2189
305.2349	0.1117	325.1150	0.0432	344.3951	0.1071	361.3250	0.2991
305.3149	0.3251	325.2850	0.0309	346.1751	0.0025	362.1652	0.1977
306.1649	1.1018	326.1850	0.0182	347.2851	0.1063	362.2650	0.1137
306.2749	0.5739	326.2950	0.0102	347.3651	0.1386	362.3750	0.3135
306.3549	0.2144	329.3150	0.1834	348.1851	0.0933	363.1752	0.0555
307.2749	0.1203	330.1650	3.2693	348.2949	0.2159	363.2452	0.1112
307.3449	0.0044	330.3350	0.0761	348.3751	0.2914	364.1952	0.0915
308.1360	0.0426	331.2250	0.8706	349.2151	0.0061	364.2550	0.1059
308.2349	0.0184	331.2950	0.7665	349.3351	0.2514	365.2750	0.0040
308.3315	0.3108	332.2150	0.3612	350.1649	0.1588	365.4150	0.0210
309.2849	0.0030	332.2950	0.3595	350.2351	0.0435	366.1952	0.0347
310.1349	0.1152	332.3550	0.1976	350.3151	0.0271	366.2652	0.0119
310.2449	0.4485	333.1750	0.0266	350.3751	0.3082	366.2950	0.0289
315.2248	0.0243	333.3450	0.2455	351.3351	0.2244	366.4150	0.2863
315.2998	0.2186	334.1550	0.2678	352.3251	0.0957	367.3352	0.0963
315.4448	0.0542	334.2350	0.1098	353.3451	0.1157	368.2052	0.0041
316.2250	0.0699	334.3350	0.5019	354.1251	0.1293	368.3350	0.0422
316.3048	0.4697	335.2049	0.1501	354.1951	0.0435	369.3452	0.6979
317.2348	0.2350	335.3249	0.1649	354.2651	0.0315	369.5650	0.0053
317.3150	0.3007	336.1849	0.1505	354.3351	0.4283	370.1351	0.1684
318.2248	0.0284	336.3251	0.8686	355.0751	0.1211	370.2150	0.3367
318.2950	0.5331	336.4749	0.1228	355.3550	0.0723	370.3352	0.0161
319.2348	0.0444	337.3451	0.2377	356.1950	61.0486	371.1052	0.5228
319.3050	0.3450	338.1951	0.0186	357.2050	11.2963	371.3152	1.1704
319.4450	0.1521	338.2649	0.0186	358.2152	0.2195	371.5852	0.1397
320.1648	0.1254	338.3449	11.4925	358.3650	0.0645	371.6750	0.0013
320.2350	0.0615	338.4849	0.0312	359.2250	0.0361	371.7551	0.0120
320.3148	0.4308	338.6049	0.1590	359.2952	1.0006	371.8352	0.0013
321.2350	0.0541	339.3251	2.4868	359.5150	0.0435	372.1152	0.7698
321.3150	0.1611	340.3449	0.4743	359.5850	0.1096	372.3152	0.4930
322.1748	0.1480	341.3149	1.1918	360.0950	0.0226	372.8352	0.0113
322.2450	0.0532	342.1451	12.8975	360.1550	0.1640	372.9152	0.0113
322.3248	0.3197	342.3149	0.0832	360.3150	0.5790	373.1052	0.0545
323.2548	0.1509	343.1649	2.9910	361.0493	0.0129	374.0952	0.0247
324.1750	0.2059	343.3351	0.0623	361.1550	0.0268	375.1052	0.0292

Table A3.8 (continued). Mass data (*m/z* values and their relative intensities) for the DART-HRMS analysis of *L. virosa* resin. Ten replicates of one sample were averaged where the corresponding spectrum appears in Figure 3.4B.

				***L. virosa* resin**			
m/z	Rel. Int. %	*m/z*	Rel. Int. %	*m/z*	Rel. Int. %	*m/z*	Rel. Int. %
375.1752	0.0086	394.3353	0.0457	416.4452	0.0030	441.3754	0.0233
375.3152	0.0498	395.3653	0.1091	417.3753	0.0575	442.3854	0.2503
376.1451	0.0706	396.3753	0.0393	419.3253	0.1229	443.3854	0.1176
376.2551	0.0106	397.3852	0.4093	420.2553	0.0326	444.4054	0.0383
376.3351	0.4976	398.2152	0.0103	420.3153	0.0643	445.3754	0.0080
376.5751	0.0397	398.3950	0.0891	421.2753	0.0011	445.4454	0.0250
377.3351	0.1320	398.5452	0.0147	421.3453	0.0059	449.3254	0.0052
377.4251	0.0367	399.3652	0.2387	422.2053	0.0629	449.3954	0.0212
377.5251	0.0399	400.3552	0.0672	422.3453	0.0698	450.2154	0.0479
378.1851	0.0986	403.3652	0.0240	422.4851	0.0153	450.3454	0.0172
378.2651	0.0691	403.4452	0.0123	423.2753	0.0222	451.2254	0.0160
379.1751	0.0119	404.1552	0.0109	423.3753	0.1703	451.3454	0.0236
379.2651	0.0845	404.2952	0.0016	424.2053	0.0058	451.4254	0.0995
379.3451	0.0662	404.3752	0.0167	424.2653	0.0171	452.4854	0.0212
380.2051	0.0943	405.2752	0.1686	424.3753	0.0666	453.3554	0.0280
380.2851	0.0241	405.3752	0.0375	424.4453	0.0345	454.2154	0.0241
380.3451	0.0588	405.4552	0.0243	424.4753	0.0048	454.3454	0.0153
381.3451	0.0072	406.1952	0.0335	425.3753	0.0865	454.4956	0.0034
382.4351	0.0073	406.2852	0.2347	426.3853	0.0077	455.3556	0.0189
383.3651	0.2465	406.3854	0.0946	427.3953	0.1798	456.3754	0.0045
384.3051	0.0371	407.2652	0.0444	428.3955	0.3552	457.3754	0.0152
384.3751	0.0712	407.3652	0.0357	429.3853	0.2013	458.3853	0.0120
386.4053	0.0132	407.4652	0.0533	430.3853	0.0591	459.3855	0.0121
387.3353	0.0227	408.1952	0.0324	431.3853	0.0120	460.4155	0.0204
388.1351	0.0703	408.3752	0.1165	432.1853	0.0069	461.3755	0.0080
390.1353	0.0077	408.4554	0.0370	432.3955	0.0145	464.2255	0.0018
391.1753	0.0437	409.3852	0.9391	433.1855	0.0216	464.3855	0.0087
391.2951	0.4605	410.2252	0.0355	435.2253	0.0036	465.2255	0.0124
391.4851	0.0066	410.3854	0.2687	436.3353	0.0795	465.3955	0.0080
392.1851	0.0059	411.3852	1.2938	437.1955	0.0140	465.4855	0.0641
392.2853	0.2576	411.6954	0.0152	437.2753	0.0036	466.2355	0.0540
393.2652	0.0169	412.3852	0.3360	437.3455	0.0085	466.3355	0.1361
393.3451	0.0110	413.3754	0.0540	438.2154	0.0223	466.4055	0.0558
393.4453	0.0181	414.3854	0.0459	438.3552	0.0350	466.5055	0.0468
394.1853	0.0601	415.3754	0.0365	439.3652	0.0754	467.3955	0.2021
394.2653	0.0091	416.3652	0.1952	440.3654	0.0296	468.3955	0.0525

Table A3.8 (continued). Mass data (*m/z* values and their relative intensities) for the DART-HRMS analysis of *L. virosa* resin. Ten replicates of one sample were averaged where the corresponding spectrum appears in Figure 3.4B.

				L. virosa resin			
m/z	Rel. Int. %	*m/z*	Rel. Int. %	*m/z*	Rel. Int. %	*m/z*	Rel. Int. %
469.4055	0.0892	502.4155	0.0148	552.4959	0.0152	605.5460	0.0921
470.4155	0.0083	503.4155	0.0167	552.5857	0.0023	606.5360	0.0356
471.4955	0.0032	504.4555	0.0099	554.4057	0.0039	608.5260	0.0184
474.3855	0.0205	505.4955	0.0485	554.4957	0.0025	610.5460	0.0364
476.4055	0.0387	507.5155	0.0273	555.4559	0.0136	611.5360	0.0167
477.4355	0.0159	508.2355	0.0047	556.2459	0.0059	612.3560	0.0036
479.2956	0.0259	508.3557	0.0074	559.5459	0.0174	612.5460	0.0106
479.4854	0.0623	508.5257	0.0053	561.5658	0.0356	613.5060	0.0091
480.2454	0.0157	509.5257	0.0061	562.4358	0.0030	615.5060	0.0696
480.3254	0.0058	510.4157	0.0039	562.5158	0.0205	616.5160	0.0222
480.4954	0.0463	510.5357	0.0205	563.5358	0.0053	617.5160	0.2133
481.3254	0.0077	512.2057	0.0057	564.5458	0.0106	618.5260	0.0735
481.3954	0.0104	516.4257	0.0144	565.5258	0.0129	619.5360	0.0861
481.4956	0.0129	519.4057	0.0096	573.4558	0.0061	625.3961	0.0032
482.2154	0.0773	521.4056	0.0062	575.5060	0.3357	626.3359	0.0052
482.3354	0.0133	521.5256	0.0571	576.5158	0.1118	627.3361	0.0041
482.4756	0.0221	524.2756	0.0039	577.5258	0.1712	628.2761	0.0041
482.5256	0.0039	528.4256	0.0083	578.5260	0.0995	632.5361	0.0220
483.3856	0.0853	531.4756	0.0304	579.5260	0.1283	633.5161	0.0174
483.5356	0.0126	532.4158	0.0036	580.5258	0.0326	634.5461	0.0694
485.4056	0.0114	533.4407	0.0041	582.2957	0.0045	635.5461	0.0280
486.3854	0.0534	533.5258	0.0036	584.3959	0.0030	636.5661	0.0440
487.3854	0.0202	534.4858	0.0255	585.4759	0.0041	637.5661	0.0197
488.3956	0.0729	535.5358	0.0318	589.4759	0.0152	650.5460	0.0106
489.3756	0.0150	536.2558	0.0068	591.4961	0.0220	675.6761	0.0954
491.3756	0.0212	536.5358	0.0189	594.5159	0.0114	676.6763	0.0205
493.3056	0.0095	537.3958	0.0027	597.5259	0.0114	697.6262	0.0036
493.3856	0.0180	537.5058	0.0376	598.5959	0.0152	708.6463	0.0136
493.5156	0.0694	538.3158	0.0057	599.5061	0.2701	712.6063	0.0044
494.3656	0.0059	538.5058	0.0181	600.3861	0.0030	743.6164	0.0099
495.3856	0.0173	539.3658	0.0011	600.5061	0.0820	848.7569	0.0099
495.4456	0.0521	545.4757	0.0129	601.5259	0.3087	853.7170	0.0243
496.3256	0.0495	547.4657	0.0027	601.8059	0.0361	854.7268	0.0174
498.3256	0.0063	548.4657	0.1003	602.5261	0.1141	855.7368	0.0940
499.4256	0.0041	549.4959	0.0664	603.5360	0.2544	856.7468	0.0601
500.4255	0.0447	551.5057	0.0725	604.5458	0.1013	857.7568	0.0601

Table A3.8 (continued). Mass data (*m/z* values and their relative intensities) for the DART-HRMS analysis of *L. virosa* resin. Ten replicates of one sample were averaged where the corresponding spectrum appears in Figure 3.4B.

	L. virosa **resin**								
m/z	Rel. Int. %	*m/z*	Rel. Int. %	*m/z*	Rel. Int. %	*m/z*	Rel. Int. %
858.7570	0.0235	877.7269	0.0356	883.7571	0.0615	898.7670	0.0621
859.7668	0.0121	878.7369	0.0265	884.7571	0.0417	899.7770	0.0296
872.7669	0.0273	878.9070	0.0129	885.7771	0.0265	900.7970	0.0356
873.7669	0.0189	879.7369	0.1355	886.7871	0.0121	901.7970	0.0129
874.7669	0.0424	880.7371	0.0706	895.7370	0.0144	902.7970	0.0182
875.7769	0.0243	881.7469	0.1122	896.7570	0.0356	912.7569	0.0083
876.7869	0.0227	882.7471	0.0455	897.7570	0.0318		

Table A3.9 Mass data (*m/z* values and their relative intensities) for the DART-HRMS analysis of *L. virosa* leaf. Ten replicates of one sample were averaged where the corresponding spectrum appears in Figure 3.4B.

						L. virosa leaf		
m/z	Rel. Int. %	*m/z*	Rel. Int. %	*m/z*	Rel. Int. %	*m/z*	Rel. Int. %
67.0540	0.7454	86.0740	5.7982	102.0741	1.7797	119.0842	4.6495
67.1240	0.0121	86.1742	0.3543	102.1641	0.2434	120.0742	2.3631
68.0538	0.1011	87.0539	12.9080	103.0541	6.6356	120.2042	0.0929
68.9640	2.0296	87.1641	0.4761	103.1443	1.8051	121.0842	8.4130
69.0440	4.7702	88.0741	1.6945	104.0741	7.0855	122.0742	0.7699
69.1440	0.1896	88.1441	0.0827	104.1443	0.1540	122.2242	0.1046
70.0640	6.9897	88.2041	0.0672	104.2343	0.1380	123.0942	10.1989
70.1340	0.8426	89.0641	53.6069	105.0641	4.3390	123.2242	0.0349
71.0640	3.2002	89.1741	1.2905	105.1443	0.1159	123.2942	0.0615
71.1540	0.2993	89.2541	1.1775	105.1843	0.4484	124.0642	1.0931
72.0140	0.2860	90.0641	5.5087	106.0641	1.3984	124.1844	0.2743
72.0840	3.2613	90.1641	0.0158	107.0841	14.6083	125.0942	8.4995
72.1540	0.0435	91.0541	7.7225	108.0640	1.7689	125.2144	1.4086
72.2040	0.1586	91.1241	0.7991	109.0340	2.5524	126.0642	2.9841
73.0640	12.5788	92.0641	1.4647	109.0942	22.2814	126.1542	1.2894
73.1840	0.9735	93.0641	9.3396	109.2042	0.2180	127.0442	43.2376
74.0640	6.8508	93.1341	2.0996	110.0742	2.7741	127.1142	9.5924
74.1340	0.5554	94.0641	0.7459	110.2142	0.5794	127.2342	1.1638
75.0440	6.5345	94.1741	0.0493	111.0540	4.8162	128.0844	2.6043
75.1140	0.7347	95.0241	0.5440	111.1140	12.6583	128.1843	0.1885
76.0640	0.9550	95.0841	21.4255	111.2342	1.3469	128.2243	0.1206
77.0440	0.7770	95.1541	0.0024	112.0742	1.9476	129.0641	11.5672
78.0440	0.3790	96.0541	2.0518	112.1542	0.7945	129.1391	1.0567
79.0440	5.1788	97.0341	16.9433	113.0542	8.4270	130.0643	8.8233
79.1242	0.0566	97.0941	16.7854	114.0842	2.3617	130.1543	1.6989
80.0540	5.2936	97.2241	1.8660	114.2242	0.9382	130.2343	0.4751
81.0540	4.9516	97.2841	1.1708	115.0542	7.3034	131.0643	4.0198
81.1442	0.0412	97.9941	0.0256	115.1040	5.0082	131.2243	0.9234
82.0642	0.6270	98.0841	1.7035	115.2442	0.9188	132.1041	6.1989
83.0240	1.6711	99.0541	21.7555	116.0742	58.8242	133.0643	4.8283
83.0840	8.0210	99.1841	3.1153	116.2242	1.6864	133.2543	0.3011
84.0640	6.6958	100.0041	0.2719	117.0642	11.3390	134.0843	1.4209
84.1542	0.0507	100.0841	1.4818	117.1642	0.1912	134.1943	0.0904
85.0342	41.7694	100.2341	0.3833	117.2442	0.9786	134.2543	0.1542
85.0942	9.1746	101.0641	18.0107	118.0842	5.2742	135.1043	35.8102
85.1642	2.4411	101.1841	1.4625	118.2042	0.6472	135.2443	0.6714

Table A3.9 (continued). Mass data (*m/z* values and their relative intensities) for the DART-HRMS analysis of *L. virosa* leaf. Ten replicates of one sample were averaged where the corresponding spectrum appears in Figure 3.4B.

L. virosa leaf							
m/z	Rel. Int. %	*m/z*	Rel. Int. %	*m/z*	Rel. Int. %	*m/z*	Rel. Int. %
135.9943	0.7061	148.1544	0.2629	165.0844	4.1933	184.1145	1.1684
136.0643	1.5787	149.0165	2.1212	165.1794	2.5526	185.1145	4.3437
136.1343	2.8812	149.1142	6.3845	165.2744	0.5244	185.2145	0.8688
136.2143	0.0185	149.9942	0.0609	166.0944	2.1597	186.1145	1.3364
136.4043	0.2040	150.0942	0.9346	166.1944	0.8473	187.1245	3.6718
137.0743	11.4520	150.1542	1.0652	166.2344	0.1250	188.0945	1.0843
137.1243	11.5760	150.2342	0.3110	167.0944	5.1223	188.1645	0.9696
137.2143	0.1790	150.3142	0.2820	167.1744	0.1817	188.2445	0.1838
137.2843	1.4707	151.1042	4.7857	167.2544	0.7275	189.1345	3.2198
138.0843	0.9660	151.2342	0.7586	167.3344	0.5305	189.2345	0.1159
138.1643	1.4588	152.1144	2.2843	167.9944	0.0623	189.3145	0.0378
139.0054	1.3440	153.0844	10.6830	168.0944	1.5788	190.1244	3.6685
139.1043	6.3327	154.0844	1.1369	168.1744	0.5581	190.2244	0.3253
139.2643	0.9178	154.1544	0.6539	168.2544	0.2452	191.1644	10.8922
140.0843	1.1658	155.1044	10.3284	169.1144	5.0420	191.3244	1.5427
140.2143	0.0766	156.1042	1.7193	169.2044	0.4572	192.1644	1.1979
140.2543	0.0761	156.1744	0.5243	170.0943	1.6336	193.0844	0.7378
140.3143	0.0449	156.2744	0.1643	170.1643	0.5382	193.1544	3.5028
141.1043	6.1236	157.0544	0.2728	171.1543	9.1444	194.0944	1.5833
141.2043	0.4262	157.1242	6.3594	172.1243	1.9057	194.1944	0.1433
142.1043	1.4166	157.1944	0.1823	173.1143	6.3475	195.0946	4.3830
142.1843	0.8623	157.2644	1.1400	174.1143	1.3633	195.1845	2.8121
143.0343	0.4412	158.1044	1.5646	174.9843	0.0027	196.0946	1.6264
143.0943	6.9152	158.2544	0.0338	175.1245	4.0693	196.2794	0.1675
143.1743	0.4570	159.1244	5.8237	176.0945	0.9188	197.1144	8.8982
144.0843	3.4648	160.0944	1.3149	176.1694	0.3540	197.2244	0.1439
144.1743	0.4133	161.0844	3.3368	177.1443	6.4129	197.3344	0.4531
144.2443	0.0550	161.1644	0.3406	178.0945	0.7833	198.1044	29.9832
145.0543	62.1230	161.2344	0.3430	178.1694	0.3428	198.2444	0.0378
145.2243	1.8394	162.0844	3.4825	179.0845	6.8302	199.1744	8.1836
146.0843	4.5773	162.2244	0.6121	179.1743	0.3987	199.3844	0.0666
146.1643	0.3244	163.0644	37.0864	180.0845	50.2760	200.1244	0.8614
146.2443	0.0856	163.1344	10.5187	180.2345	0.1038	200.1844	1.9005
147.0743	9.2754	163.2644	0.3873	181.1045	10.7219	200.2346	0.2941
147.2345	0.2071	164.0844	1.5915	182.1045	2.4550	201.1444	2.7135
148.0745	1.0020	164.1644	1.4294	183.0945	8.8296	201.3044	0.4510

Table A3.9 (continued). Mass data (*m/z* values and their relative intensities) for the DART-HRMS analysis of *L. virosa* leaf. Ten replicates of one sample were averaged where the corresponding spectrum appears in Figure 3.4B.

				L. virosa leaf			
m/z	Rel. Int. %	*m/z*	Rel. Int. %	*m/z*	Rel. Int. %	*m/z*	Rel. Int. %
202.1244	1.3672	215.2645	0.0827	234.2796	0.0355	254.2747	0.2374
202.2846	0.3153	215.3245	0.2337	234.3546	0.1936	254.3047	0.1096
203.1746	4.2798	215.3545	0.3452	235.1746	3.7200	254.3547	0.0449
203.3346	0.1561	216.1245	1.5188	236.1746	1.1517	255.0847	0.1184
204.1146	0.0703	216.1945	0.2711	237.1146	0.1868	255.2247	10.8902
204.1844	0.9464	216.3345	0.1060	237.1846	4.1255	256.2447	1.7157
205.1046	2.2484	217.1745	3.7947	238.1946	1.3504	256.3447	0.0378
205.1946	3.7771	218.1345	1.3178	238.3846	0.1556	257.2447	50.8453
205.2646	0.0555	219.1845	8.1508	239.1446	0.8546	258.2547	8.1804
205.3346	0.1141	220.1145	0.2109	239.2346	6.9514	258.4347	0.7340
205.4046	0.0205	220.1745	1.2141	240.2146	1.4310	259.1947	10.9923
206.1146	1.4421	220.3347	0.3432	241.1846	6.4119	259.4247	0.6647
206.2044	0.5615	221.1845	3.2379	242.1048	0.0615	260.1947	1.0652
207.1546	4.3058	222.1245	0.3274	242.1846	0.9323	260.2547	0.5028
207.3046	0.0867	222.2045	0.3120	242.2846	0.7423	261.1147	0.9703
208.1146	0.6455	223.1247	4.2756	243.1648	1.4869	261.2247	5.8651
208.2096	0.7388	224.1147	0.8139	243.2498	1.3738	261.4647	0.4652
209.1346	4.2934	224.2545	0.6718	243.4048	0.5293	262.1847	0.7042
209.2746	0.2414	225.1447	3.4135	244.1148	0.0544	262.2547	0.3161
210.1046	0.8722	226.1247	0.7447	244.1946	1.0185	263.1347	1.5094
210.1646	0.4838	226.2547	0.7727	245.2246	2.5902	263.2347	6.5495
210.2246	0.4881	227.1347	2.0332	246.1148	0.9981	264.1249	0.2526
210.3596	0.1320	227.4147	0.0646	246.2446	0.4449	264.2447	0.9210
211.0245	0.0310	228.1947	1.4967	247.2248	2.1570	265.1547	1.0668
211.1345	5.8447	229.1047	1.2742	248.1346	0.6194	265.2449	4.6287
211.2445	0.2244	229.2045	4.3597	248.2548	0.4603	266.1447	0.5732
212.1045	1.6621	230.1047	0.2824	248.3297	0.1658	266.2547	0.6929
212.1845	0.2113	230.1847	1.2147	248.4046	0.1330	267.1547	1.7717
212.2245	0.0686	230.3547	0.3421	249.1646	1.7705	267.2647	1.2346
212.3345	0.2204	231.1247	0.1918	250.1548	0.6054	268.1149	0.5384
213.0145	0.0469	231.2147	2.2759	251.1648	3.2354	268.2047	0.8597
213.1145	0.7146	232.1346	0.9751	252.1847	0.6679	268.2847	0.2407
213.2095	3.0592	233.1346	1.9897	252.2647	0.0736	269.2147	4.0359
214.1245	0.5642	233.2246	1.2178	253.1847	4.0156	270.1247	0.0678
214.2545	2.0634	234.1346	0.0496	254.1145	0.0662	270.2049	0.5636
215.1895	2.4279	234.2046	0.6724	254.1847	0.7326	270.3849	0.1821

Table A3.9 (continued). Mass data (*m/z* values and their relative intensities) for the DART-HRMS analysis of *L. virosa* leaf. Ten replicates of one sample were averaged where the corresponding spectrum appears in Figure 3.4B.

L. virosa leaf							
m/z	Rel. Int. %	*m/z*	Rel. Int. %	*m/z*	Rel. Int. %	*m/z*	Rel. Int. %
271.0847	1.1777	286.1348	0.0298	300.4249	0.2230	318.2950	0.2712
271.1597	0.2082	286.2748	0.9743	301.0949	0.0283	319.2348	0.7400
271.2347	7.4824	287.0648	0.0709	301.2049	3.2204	319.4450	0.0483
272.2547	2.8511	287.2248	1.5136	301.2949	0.5634	320.2350	0.2661
272.4649	0.3057	287.3848	0.0497	302.2149	0.4624	320.3148	0.1050
273.1548	0.3997	287.4748	0.1561	302.3049	0.1300	321.2350	0.6631
273.2446	1.5811	288.2448	0.9597	302.4149	0.2171	321.3150	0.0023
274.2648	3.2795	289.1048	0.1980	303.2249	0.2168	322.2450	0.2990
274.4148	0.0917	289.1748	0.4139	303.3049	0.2868	323.2548	1.1600
275.1046	0.0242	289.2348	1.2586	304.2349	0.5036	323.3570	0.3392
275.2046	4.5066	289.4048	0.1219	305.2349	0.5997	324.2650	0.5894
275.2648	3.4137	289.4748	0.1928	305.3149	0.1001	325.1950	0.4088
276.1648	0.2520	290.1748	0.2720	306.2749	0.1661	325.2850	1.6630
276.2748	0.8862	290.2748	0.1836	307.1949	1.8319	326.2950	0.8915
277.1146	0.1843	291.1948	4.8966	307.2749	0.3852	327.1950	0.5890
277.2148	41.2851	291.4148	0.1890	307.3449	0.2753	327.2850	1.3432
277.4548	0.3835	292.1148	0.0526	308.2349	0.4932	328.2250	0.1104
277.5248	1.1050	292.1948	0.3500	309.2149	2.7961	328.3248	0.8362
278.2148	8.4645	292.3148	0.1861	309.2849	2.1134	329.1050	0.0536
279.1546	0.9788	293.2148	6.6358	310.2449	1.4517	329.2350	3.1563
279.2348	65.0575	294.2147	1.1120	311.2349	0.2793	329.3150	0.7319
280.1448	0.4881	294.2949	0.2512	311.2749	2.6365	330.1150	0.0169
280.2446	10.6433	295.2347	8.9567	312.2749	1.4718	330.1650	0.5767
280.3648	0.3924	296.2549	28.5176	313.1149	0.2060	330.3350	0.6799
281.2448	14.0126	296.4747	0.3163	313.2149	0.2579	331.2250	0.8173
282.1548	0.0266	296.5247	0.9942	313.2749	3.6806	331.2950	1.2782
282.2648	2.7034	297.2449	10.0726	314.2448	1.3442	332.2150	0.5686
282.5246	0.1178	298.2749	10.4950	315.1148	0.5675	332.2950	0.3872
283.0948	0.0460	298.4049	0.1620	315.2248	0.8189	333.2350	0.2491
283.1848	0.5490	298.5049	0.8699	315.2998	0.5329	333.3450	0.3268
283.2648	9.1266	299.0949	0.0352	315.4448	0.1984	334.2350	0.0684
284.1548	0.2456	299.1949	0.2388	316.1150	0.0179	334.3350	0.1905
284.2648	1.3427	299.2749	3.9152	316.2250	0.1151	335.2049	0.2601
284.3648	0.1655	300.1949	0.0307	316.3048	0.3866	335.3249	0.1837
285.1048	0.3166	300.2947	2.8931	317.2348	0.6159	336.1849	0.0412
285.2748	3.2903	300.3749	0.0662	318.2248	0.0824	336.2549	0.1572

Table A3.9 (continued). Mass data (*m/z* values and their relative intensities) for the DART-HRMS analysis of *L. virosa* leaf. Ten replicates of one sample were averaged where the corresponding spectrum appears in Figure 3.4B.

L. virosa leaf							
m/z	Rel. Int. %	*m/z*	Rel. Int. %	*m/z*	Rel. Int. %	*m/z*	Rel. Int. %
336.3251	0.5910	353.2651	0.7151	369.3452	4.3046	379.3451	1.0169
336.4749	0.1245	353.3451	0.2665	369.4852	0.0361	380.2051	0.0203
337.2651	0.6945	354.3351	1.1505	369.5650	0.3838	380.2851	0.0202
337.3451	0.6154	355.0751	0.7819	370.3352	1.4889	380.3451	0.1702
338.2649	0.0428	355.1950	0.1899	371.1052	5.8727	381.3451	0.2266
338.3449	10.6728	355.2950	1.2628	371.3152	91.4659	381.4153	0.7820
338.4849	0.4651	355.3550	0.1817	371.5852	1.2111	382.2951	0.3180
338.6049	0.4224	355.4350	0.0552	371.6750	0.6222	382.3551	0.1277
339.3251	2.6203	356.0750	0.1112	371.7551	0.6240	382.4351	0.4159
340.3449	0.8415	356.1950	0.0113	371.8352	0.2916	383.3651	2.7658
340.4251	0.0202	356.3550	0.4809	372.1152	3.1019	384.3051	0.0151
341.3149	1.5644	357.0750	0.0591	372.2352	0.2186	384.3751	0.7393
342.3149	0.4792	357.2950	0.6869	372.3152	22.9632	385.3151	1.3263
343.1649	0.1724	357.3850	0.1271	372.6450	0.1156	385.4851	0.1842
343.2351	0.5239	358.2152	0.0269	372.8352	0.4591	386.3351	0.6063
343.3351	0.2625	358.2950	0.1312	372.9152	0.2762	386.4053	0.1356
344.1751	0.0205	358.3650	0.1845	373.1052	1.5561	387.2853	0.0757
344.2651	0.4101	359.2250	0.1420	373.1752	0.1149	387.3353	0.7136
344.3951	0.0229	359.2952	0.9122	373.2452	0.7016	387.6051	0.0264
345.1849	0.1476	360.2252	0.1134	373.3152	2.9724	388.1351	0.3113
345.2749	0.7830	360.3150	0.5107	374.0952	0.3650	388.2653	0.1575
346.1751	2.1626	361.2352	0.1213	374.2652	0.3210	388.3451	8.4317
346.2749	0.3354	361.3250	0.5775	374.3252	0.5373	389.1553	0.1937
347.1649	0.4967	362.1652	0.0745	375.1052	0.4067	389.2653	0.0710
347.2851	0.5058	362.2650	0.1337	375.2452	0.1439	389.3453	1.9074
347.3651	0.0531	362.3750	0.2409	375.3152	0.6218	390.1353	0.0142
348.1851	0.0912	363.2452	0.2505	376.1451	0.0543	390.3351	0.3525
348.2949	0.5925	364.1952	0.0642	376.2551	0.0282	391.2951	2.5477
349.2151	0.2777	364.2550	0.1990	376.3351	0.2065	391.3901	0.3802
349.3351	0.5429	365.2750	0.9575	376.5751	0.0146	391.4851	0.4807
350.2351	0.0833	365.4150	2.1004	377.2551	0.0665	392.2853	0.6938
350.3151	0.1322	366.2652	0.1081	377.3351	0.5344	393.3451	1.6435
350.3751	0.1409	366.2950	0.2110	377.4251	0.2519	393.4453	1.5709
351.2451	0.3271	366.4150	0.6390	377.5251	0.0876	394.1853	0.0180
351.3351	0.7487	367.3352	1.2400	378.2651	0.2368	394.3353	0.4925
352.3251	0.5224	368.3350	0.4180	378.3351	0.0723	395.3653	3.1883

Table A3.9 (continued). Mass data (*m/z* values and their relative intensities) for the DART-HRMS analysis of *L. virosa* leaf. Ten replicates of one sample were averaged where the corresponding spectrum appears in Figure 3.4B.

				***L. virosa* leaf**			
m/z	Rel. Int. %	*m/z*	Rel. Int. %	*m/z*	Rel. Int. %	*m/z*	Rel. Int. %
396.2853	0.0897	412.2954	0.0261	431.4753	0.0355	453.4654	0.8113
396.3753	1.3711	412.3852	1.4372	432.3153	0.1274	454.3454	0.0426
397.3852	8.7273	413.0454	0.0169	432.3955	0.2976	454.4956	0.5374
398.2152	0.0378	413.3754	1.9093	433.3253	0.1994	455.3556	0.9418
398.3950	1.9397	414.3854	1.2907	433.4003	0.3272	455.4354	0.0327
398.5452	0.0338	414.6152	0.0894	433.4753	0.0256	455.4954	0.1077
399.2252	0.0703	415.3004	0.2893	434.3353	0.0158	456.3754	0.2018
399.3652	1.2426	415.3754	0.5603	434.3955	0.1068	456.5156	0.6504
400.3552	0.0710	416.2354	0.0615	435.3553	0.3261	457.3754	1.2375
400.4452	1.5107	416.3652	0.3117	435.4655	0.3531	457.4954	0.4681
401.3252	1.7201	416.4452	0.0396	437.3455	0.3552	458.2354	0.0282
401.4652	0.4041	417.3753	0.1290	437.4755	0.9043	458.3853	0.4535
402.3352	1.6695	417.4553	0.3229	438.3552	0.3958	459.3053	0.1773
403.2952	0.1273	418.2253	0.0225	438.4852	0.3550	459.3855	0.5322
403.3652	0.5359	418.3653	0.0769	439.3652	3.8921	459.4855	0.0315
404.2952	0.0233	418.4553	0.0168	440.3654	1.7026	460.3053	0.1073
404.3752	0.0390	419.3253	1.3654	441.3754	2.9894	460.4155	0.1863
405.3752	1.0604	420.3153	0.1335	442.3854	0.9883	460.4955	0.0412
405.4552	0.0933	421.3453	0.6919	442.4554	0.2635	461.3755	0.0455
406.2852	0.0493	421.4653	0.9483	443.3854	1.4003	461.4255	0.5038
406.3854	0.2157	422.3453	0.2488	444.2354	0.0620	462.1355	0.1198
407.3652	2.5359	422.4851	0.3831	444.2954	0.0752	462.4455	0.0112
408.3752	1.7865	423.3753	2.3152	444.4054	0.5612	463.3855	0.8969
408.4554	0.0686	424.2653	0.0370	445.2154	3.5551	464.3855	0.0490
409.2052	0.0755	424.3753	1.3632	445.3754	1.2596	465.4855	1.0817
409.3852	54.0622	424.5353	0.0374	446.2254	1.1867	466.5055	0.2051
410.2252	0.2406	425.3753	7.9042	446.3854	0.7638	467.4655	0.6665
410.2952	0.0179	426.2253	0.0845	447.2254	0.0345	468.4955	0.3983
410.3854	14.1632	426.3853	2.3747	447.3254	0.0135	469.4055	0.2287
411.1252	0.1388	427.3953	7.6420	447.3854	0.6176	470.4155	0.0113
411.1952	0.0397	428.3955	2.3486	448.3854	0.0169	470.5055	0.3835
411.3852	7.0249	429.3853	3.7848	449.4354	0.3202	471.3255	0.0463
411.6254	0.2707	430.2353	0.0169	449.5154	0.2210	471.3855	0.2269
411.6954	0.6644	430.3853	0.7942	451.4254	1.0194	471.4955	0.3039
412.1252	0.0666	430.5553	0.0542	452.4854	0.2565	472.3455	0.0480
412.2052	0.0842	431.3853	0.7604	453.3554	0.0104	472.3855	0.0297

Table A3.9 (continued). Mass data (*m/z* values and their relative intensities) for the DART-HRMS analysis of *L. virosa* leaf. Ten replicates of one sample were averaged where the corresponding spectrum appears in Figure 3.4B.

				L. virosa leaf			
m/z	Rel. Int. %	*m/z*	Rel. Int. %	*m/z*	Rel. Int. %	*m/z*	Rel. Int. %
473.3755	0.1615	493.3056	0.0315	521.5256	0.7790	563.6158	0.0259
474.3855	0.4633	493.5156	0.6023	526.5658	0.0158	564.5458	0.0146
474.4655	0.1047	495.4456	0.2589	527.5256	0.0817	565.5258	0.1033
475.3855	0.1203	498.5356	0.1799	531.3158	0.0227	566.5358	0.1179
476.3155	0.1271	499.4256	0.0449	531.4756	0.0679	567.3858	0.0352
476.4055	0.1241	500.4255	0.0140	533.5258	0.4830	569.3858	0.0352
476.4955	0.0191	502.4155	0.1117	535.4458	0.0248	575.5060	0.0819
477.4355	0.0248	503.3255	0.1571	535.5358	0.4105	577.5258	0.0833
477.5455	0.1912	503.4155	0.0912	536.5358	0.2087	578.5260	0.0463
478.4355	0.0303	504.2857	0.0706	537.5058	0.5602	579.5260	0.1312
478.5455	0.0135	505.4955	0.2375	537.6158	0.0653	583.3759	0.0207
479.4854	0.6986	507.2155	0.1435	538.5058	0.0668	585.3859	0.0310
480.4954	0.4051	507.3155	0.0527	547.3357	0.0496	591.3559	0.0289
481.4956	0.3039	507.5155	0.7211	548.3459	0.0310	591.5859	0.0917
482.5256	0.4019	508.2355	0.0093	549.4959	0.1379	592.5759	0.0113
483.3856	0.1079	508.3557	0.0149	550.5657	0.3245	593.6659	0.0135
483.5356	0.0447	508.5257	0.2078	551.5057	0.4667	621.6660	0.3343
484.5456	0.4062	509.5257	0.3434	552.4959	0.0463	638.6861	0.2819
485.4056	0.1247	510.5357	0.3308	552.5857	0.0846	647.6360	0.0102
486.3854	0.2312	512.5757	0.0473	553.3957	0.0331	649.6760	0.1662
486.4556	0.0104	516.4257	0.0294	553.4957	0.0248	663.6262	0.0130
487.3854	0.1761	517.4457	0.6652	554.5659	0.0674	665.5961	0.1467
487.5256	0.1173	518.4357	0.0947	555.5357	0.0766	666.7161	0.2811
488.3956	0.1228	518.5157	0.1531	557.5359	0.2998	667.7161	0.0338
488.4656	0.0704	519.4957	0.6833	559.5459	0.1118	677.7063	0.0365
489.3756	0.0124	520.3356	0.0310	561.5658	0.1929	691.6662	0.0121
491.4856	0.2203	520.4056	0.0124	563.5358	0.0792	694.7462	0.0821

Table A3.10 Mass data (*m/z* values and their relative intensities) for the DART-HRMS analysis of *L. virosa* seed. Ten replicates of one sample were averaged where the corresponding spectrum appears in Figure 3.4B.

				***L. virosa* seed**			
m/z	Rel. Int. %	*m/z*	Rel. Int. %	*m/z*	Rel. Int. %	*m/z*	Rel. Int. %
61.0339	0.0540	84.9540	1.5340	99.0541	8.0281	114.2242	0.3842
62.0639	0.0211	85.0342	6.6669	99.1841	0.2638	114.2842	0.0159
63.9941	0.0013	85.0942	5.2269	99.9741	0.4427	115.0542	3.9089
65.0541	0.1728	85.1642	1.2244	100.0041	0.2495	115.1040	3.4285
67.0540	0.7067	86.0740	2.5861	100.0841	1.6704	115.2442	0.5582
67.1240	0.0132	86.1742	0.1879	100.2341	0.2457	116.0742	4.4396
68.0538	0.2258	86.9739	0.1786	101.0641	10.5764	116.1442	0.3794
68.9640	2.0743	87.0539	7.9539	101.1841	0.5253	116.2242	0.3651
69.0440	2.2852	87.1641	0.5548	102.0741	2.0447	117.0642	6.7608
69.1440	0.0171	88.0741	2.4599	102.1641	0.5136	117.1642	0.0237
70.0640	3.9662	88.1441	0.1166	103.0541	2.9276	117.2442	0.5902
70.1340	0.1884	88.2041	0.0419	103.1443	1.3502	118.0842	4.1920
71.0640	2.0901	89.0641	47.1292	104.0741	7.8757	118.2042	0.3712
71.1540	0.0254	89.1741	1.4786	104.1443	0.1365	119.0842	2.6028
72.0140	0.7004	89.2541	0.7072	104.2343	0.0892	120.0742	1.4033
72.0840	7.1025	90.0641	13.2610	105.0641	2.6448	120.2042	0.0834
72.2040	0.3579	90.1641	0.2743	105.1443	0.1924	121.0842	5.6576
73.0640	12.4416	90.9639	0.0088	105.1843	0.2353	122.0742	0.6594
73.1840	0.8386	91.0541	7.8696	106.0641	0.8375	122.2242	0.0174
74.0640	10.7760	91.1241	0.5334	107.0841	11.4656	123.0942	6.8313
74.1340	0.7992	92.0641	2.7568	107.1543	0.6739	123.2942	0.1438
75.0440	5.9828	93.0641	19.7785	108.0640	1.4479	124.0642	1.8736
75.1140	1.0052	93.1341	3.8696	108.1542	0.3483	124.1844	0.2344
76.0640	0.9046	94.0641	1.1155	109.0340	0.0749	125.0942	5.6321
77.0440	0.5228	94.1741	0.1124	109.0942	14.3183	125.2144	0.5501
78.0440	0.1618	95.0241	0.6149	109.2042	0.3314	126.0642	5.1648
79.0440	2.4665	95.0841	13.7120	110.0742	3.1577	126.1542	0.6843
79.1242	0.0381	96.0541	4.3881	110.2142	0.5162	127.0442	10.0990
80.0540	1.6704	96.1291	0.0831	111.0540	2.6034	127.1142	8.5092
81.0540	3.4058	97.0341	2.6297	111.1140	10.2602	127.2342	1.2948
81.1442	0.1729	97.0941	10.0175	111.2342	0.8564	128.0844	2.1383
82.0642	0.8069	97.1741	0.3336	112.0742	5.0939	128.2243	0.3198
82.9442	2.3093	97.2241	0.5709	112.1542	0.9442	129.0641	4.0289
83.0240	0.5367	97.2841	0.5470	113.0542	6.5723	129.1391	3.8286
83.0840	11.2725	97.9941	3.9093	113.1642	0.1384	130.0643	5.4490
84.0640	4.9945	98.0841	3.1402	114.0842	4.2307	130.1543	1.8839

Table A3.10 (continued). Mass data (*m/z* values and their relative intensities) for the DART-HRMS analysis of *L. virosa* seed. Ten replicates of one sample were averaged where the corresponding spectrum appears in Figure 3.4B.

				L. virosa seed				

m/z	Rel. Int. %	*m/z*	Rel. Int. %	*m/z*	Rel. Int. %	*m/z*	Rel. Int. %
130.2343	0.0938	144.1743	1.3300	160.1744	0.2362	176.1694	0.4294
131.0643	5.0999	145.0543	13.6654	161.0844	3.1651	177.1443	4.1164
131.2243	1.0271	145.1243	3.4205	162.0844	1.5544	178.0945	0.2119
132.1041	4.5749	145.2243	0.9942	162.2244	0.1518	178.1694	0.7782
133.0643	4.5939	146.0843	3.9264	163.0644	8.1584	179.0845	8.2755
133.2543	0.0155	146.1643	27.7545	163.1344	5.0646	180.0845	11.7015
134.0843	0.9482	146.2443	0.4380	163.2644	0.0204	180.1645	0.9841
134.2543	0.1196	146.9943	0.0103	164.0844	1.1635	181.1045	2.5610
135.1043	16.1556	147.0743	4.0793	164.1644	0.8203	181.1945	1.5888
135.2443	0.4013	147.1843	0.9405	165.0844	1.9239	182.1045	1.0212
135.9943	0.7307	148.0745	2.7810	165.1794	1.7071	182.1943	0.5247
136.0643	12.9754	149.0165	1.5047	165.2744	0.4425	183.0945	3.1162
136.1343	1.4914	149.1142	2.3303	166.0944	2.2487	183.1945	1.7119
136.2143	0.0960	149.9942	0.2772	166.1944	0.3969	184.1145	0.3409
136.2843	0.2449	150.0942	0.3063	166.2344	0.0545	184.2045	0.5132
136.4043	0.2103	150.1542	0.4860	167.0944	2.4922	185.1145	2.5977
137.0743	76.7042	150.2342	0.0430	167.1744	0.0799	185.2145	2.1164
137.1243	6.2730	150.3142	0.0244	167.2544	0.7016	186.1145	0.6948
137.2143	0.1511	151.1042	3.4742	167.3344	0.4696	187.1245	1.8087
137.2843	1.1153	151.9942	0.0588	168.0944	0.9564	188.0945	0.5790
137.9843	0.0644	152.1144	1.2338	168.1744	0.3304	188.1645	0.2272
138.0843	5.8481	152.2444	0.0356	168.2544	0.1562	188.2445	0.0543
138.1643	1.2116	153.0844	9.9724	168.9844	0.0140	189.1345	1.3040
139.0054	2.3318	154.0844	0.6352	169.1144	4.4557	189.2345	0.0285
139.1043	6.8633	154.1544	0.6810	169.2044	0.3222	189.3145	0.0153
139.2243	0.0423	155.1044	5.5304	170.0943	0.9779	190.1244	1.8067
139.2643	0.7339	156.1042	1.0608	170.1643	1.5213	190.2244	0.1467
140.0843	1.2995	156.1744	0.1503	171.1543	7.6265	191.1644	2.4204
140.2543	0.0445	156.2744	0.1551	171.3143	0.2637	191.3244	0.4151
140.3143	0.0341	157.1242	10.4160	172.1243	1.0058	192.1044	0.6801
141.1043	4.5283	157.2644	1.1936	173.0243	0.0092	192.1644	2.2001
142.1043	0.9877	158.1044	0.8871	173.1143	2.7424	193.0844	0.5314
142.1843	0.0670	158.1844	1.4251	174.1143	2.1282	193.1544	1.9720
143.0343	0.0313	159.0544	0.0090	174.9843	0.1058	194.0944	0.4489
143.0943	4.0868	159.1244	3.7571	175.1245	2.0759	194.1944	0.2570
144.0843	2.0561	160.0944	0.9000	176.0945	0.2234	195.0946	0.3958

Table A3.10 (continued). Mass data (*m/z* values and their relative intensities) for the DART-HRMS analysis of *L. virosa* seed. Ten replicates of one sample were averaged where the corresponding spectrum appears in Figure 3.4B.

				L. virosa **seed**			
m/z	Rel. Int. %	*m/z*	Rel. Int. %	*m/z*	Rel. Int. %	*m/z*	Rel. Int. %
195.1845	2.6859	211.0245	0.1096	229.1047	0.6116	245.2246	2.5288
195.2744	0.1679	211.1345	2.7755	229.2045	1.8294	246.1148	1.6194
196.0946	0.7771	212.1045	0.5035	230.1847	0.6314	246.2446	0.2363
196.2794	0.0567	212.1845	0.4768	230.3547	0.1089	247.2248	0.9345
197.1144	2.3132	212.3345	0.1252	231.1247	0.0844	248.1346	0.1802
197.3344	0.3033	213.0145	0.0678	231.2147	0.8233	248.2548	0.2522
198.1044	11.4001	213.1145	0.3641	232.1346	0.1062	248.4046	0.0342
199.1744	4.4171	213.2095	1.1862	232.2346	0.3107	249.1646	0.3915
199.3844	0.0423	214.1245	0.2016	233.1346	0.0602	249.2648	0.1210
200.1244	0.0817	214.2545	0.9710	233.2246	0.6022	250.1548	0.2680
200.1844	0.9465	215.1145	0.0796	234.1346	1.0743	251.1048	0.0520
200.2346	0.2567	215.1895	1.1344	234.2046	0.9301	251.1648	0.8073
201.1444	1.2714	215.3245	0.1392	234.3546	0.2210	252.1247	28.4194
201.2244	0.0396	215.3545	0.0815	235.0846	0.5877	252.2647	0.1507
201.3044	0.2429	216.1245	0.4932	235.1746	1.7316	253.1047	3.2901
202.1244	0.8354	216.1945	0.6032	236.1046	0.4419	253.1847	1.3601
202.2846	0.2225	216.3345	0.0116	236.1746	0.7241	254.1145	2.7115
203.1746	1.5314	217.0770	6.2648	237.1146	2.2429	254.1847	0.7363
203.3346	0.1621	217.1745	2.3569	237.1846	1.2915	254.2747	0.4604
204.1146	0.0657	218.1345	0.8922	238.1146	0.0629	255.0847	0.0527
204.1844	0.4317	219.1845	1.5228	238.1946	0.4659	255.1347	0.1662
205.1046	1.6868	220.1145	0.2408	238.3846	0.0425	255.2247	4.5787
205.1946	1.1447	220.1745	0.5053	239.1446	0.6163	256.2447	0.7370
205.3346	0.0145	220.3347	0.1156	239.2346	1.4025	257.0847	0.4817
206.1146	1.1088	221.1845	0.9326	240.2146	0.3865	257.2447	8.3380
206.2044	0.1896	222.1245	0.1065	241.1046	0.3488	258.0947	0.0735
207.1546	1.2243	222.2045	0.1140	241.1846	1.2938	258.2547	1.4501
208.1146	0.3716	223.1247	1.4956	242.1846	0.4298	258.4347	0.2015
208.2096	0.6340	224.1147	0.3914	242.2846	0.4568	259.1047	0.2394
209.1346	1.2235	224.2545	0.2521	243.1046	0.2166	259.1947	0.3473
209.2146	0.5912	225.1447	1.6835	243.1648	1.1123	259.2647	0.5695
209.2746	0.1243	226.1247	0.8393	243.2498	0.0773	259.4247	0.0515
210.1046	0.6949	226.2547	0.1106	243.4048	0.1498	260.1147	0.0476
210.1646	0.0632	227.1347	1.1617	244.1148	0.1627	260.1947	0.0567
210.2246	0.4572	227.4147	0.0386	244.1946	0.7245	260.2547	0.2893
210.3596	0.0827	228.1947	2.0964	245.1246	0.0290	261.1147	0.0173

Table A3.10 (continued). Mass data (*m/z* values and their relative intensities) for the DART-HRMS analysis of *L. virosa* seed. Ten replicates of one sample were averaged where the corresponding spectrum appears in Figure 3.4B.

				L. virosa seed			
m/z	Rel. Int. %	*m/z*	Rel. Int. %	*m/z*	Rel. Int. %	*m/z*	Rel. Int. %
261.2247	0.8060	277.1146	0.4541	291.2750	0.0351	313.1149	0.1845
261.4647	0.0758	277.2148	0.9661	291.4148	0.1492	313.2749	1.7408
262.1847	0.3462	277.4548	0.0334	292.1148	0.0153	314.2448	2.9041
263.1347	0.0364	277.5248	0.0242	292.1948	0.0136	315.1148	0.0695
263.2347	12.6853	278.2148	0.5930	292.3148	0.1343	315.2998	1.3067
264.1249	0.0224	278.2948	0.1441	293.2148	0.3590	315.4448	0.1244
264.2447	1.8749	279.1546	1.4501	293.2947	0.2439	316.1150	0.0123
265.2449	1.5339	279.2348	21.8238	294.2147	0.0553	316.3048	0.8271
266.1447	0.2326	280.1448	0.2227	294.2949	0.1651	317.2348	0.1040
266.2547	0.5885	280.2446	5.3412	295.2347	2.3962	317.3150	0.2477
267.1547	0.2296	281.2448	40.2757	296.2549	1.4834	318.2950	0.3409
267.2647	0.7698	282.1548	0.0820	296.4747	0.1803	319.3050	0.2063
268.1149	1.8357	282.2648	7.6867	296.5247	0.0553	319.4450	0.0143
268.2047	0.8202	282.5246	0.4411	297.2449	14.1026	320.2350	0.0356
268.2847	0.1523	283.0948	0.0082	298.2749	64.1160	320.3148	0.1730
269.1347	0.0045	283.2648	4.7962	298.5049	0.9660	321.2350	0.0477
269.2147	1.4572	284.1548	0.0114	299.0949	0.0480	321.3150	0.1327
270.1247	0.0159	284.2648	0.6929	299.2749	12.4504	322.2450	0.0946
270.2049	0.2685	285.1048	0.2442	300.2947	4.0846	322.3248	0.1682
270.3849	0.0127	285.2748	2.0674	300.4249	0.1725	323.2548	0.2795
271.0847	0.1289	286.1348	0.0978	301.0949	0.2582	324.2650	0.5203
271.1597	0.1077	286.2748	0.6013	301.2949	0.7237	325.1150	0.0306
271.2347	1.6591	287.1248	0.0254	302.3049	0.4821	325.2850	0.4807
272.1349	0.0638	287.2248	0.4332	303.3049	0.2659	326.2950	0.4210
272.2547	0.9198	287.4748	0.0754	304.2349	0.3602	327.2850	0.5762
272.4649	0.0852	288.2448	0.3864	305.2349	0.1291	328.3248	0.4872
273.0848	0.0386	288.3648	0.0110	305.3149	0.0330	329.1050	0.0222
273.1548	0.0522	289.1048	0.0245	306.1649	0.0084	329.3150	0.4817
273.2446	0.8553	289.2348	0.3351	306.2749	0.6021	330.2350	0.0486
274.1548	0.0014	289.3250	0.0303	307.2749	0.2479	330.3350	3.4693
274.2648	1.0049	289.4048	0.1170	308.3315	0.2897	331.2950	0.6087
274.4148	0.0412	289.4748	0.0420	309.2849	0.5339	332.2150	0.0746
275.1046	0.0160	290.1748	0.0664	309.3549	0.1157	332.2950	0.2325
275.2648	0.6973	290.2748	0.1985	310.2449	1.3228	332.3550	0.0222
276.1648	0.0488	290.4048	0.0231	311.2749	1.1855	333.1750	0.0199
276.2748	0.1863	291.1948	0.2955	312.2749	0.8454	333.2350	0.0862

Table A3.10 (continued). Mass data (*m/z* values and their relative intensities) for the DART-HRMS analysis of *L. virosa* seed. Ten replicates of one sample were averaged where the corresponding spectrum appears in Figure 3.4B.

L. virosa seed							
m/z	Rel. Int. %	*m/z*	Rel. Int. %	*m/z*	Rel. Int. %	*m/z*	Rel. Int. %
333.3450	0.1215	355.3550	0.5252	371.4052	0.3662	382.4351	0.1030
334.1550	0.0140	356.0750	0.1442	371.5852	0.1852	383.3651	4.2288
334.2350	0.0184	356.2850	0.2860	371.6750	0.1478	384.3751	1.0820
334.3350	0.1613	356.3550	0.4785	371.7551	0.0817	385.2151	0.0064
335.3249	0.1085	357.0750	0.0740	371.8352	0.0032	385.3151	0.5033
336.1849	0.0444	357.2050	0.0525	372.1152	1.4614	386.3351	0.5182
336.3251	0.5641	357.2950	0.5199	372.3152	1.2691	386.4053	0.0472
336.4749	0.0545	357.3850	0.0626	372.4152	0.3084	387.3353	0.1470
337.2651	1.1002	358.2152	0.0224	372.4902	0.0773	388.1351	0.0687
338.3449	18.1445	358.3650	2.4126	372.6450	0.1643	388.2653	0.1900
338.6049	0.1250	359.2952	0.1074	372.8352	0.1250	388.3451	0.0735
339.1849	0.0068	359.3850	0.4905	372.9152	0.0953	388.4351	0.0700
339.3251	3.9656	359.5150	0.0558	373.1052	0.8292	388.5351	0.0696
340.3449	0.9387	359.5850	0.0143	373.2452	0.2489	389.1553	0.0367
341.3149	0.6624	360.1550	0.2342	373.3152	0.4699	389.2653	0.3830
342.3149	0.5524	360.3150	0.3286	373.4052	0.1135	389.3453	0.0884
343.1649	0.0486	361.2352	0.1254	374.0952	0.1607	390.1353	0.0431
343.2351	0.0136	361.3250	0.1946	374.2652	0.0633	390.3351	0.1149
343.3351	0.2860	362.2650	0.0432	374.3252	0.2950	391.2951	1.0438
344.1751	0.0217	362.3750	0.1342	375.1052	0.0680	392.2853	0.3458
344.2651	0.2152	363.1752	0.0169	375.3152	0.1159	393.3451	0.4353
345.2749	0.3502	363.2452	0.0721	376.3351	0.1018	393.4453	0.0445
346.2749	0.2233	364.1952	0.0125	377.1851	0.0147	394.3353	0.1727
347.2851	0.1854	364.2550	0.0749	377.3351	0.3204	395.1953	0.0096
348.2949	0.3159	365.2750	0.2648	377.4251	0.0224	395.3653	4.9364
349.3351	0.1685	365.4150	0.3829	377.5251	0.0264	396.3753	1.9697
350.3151	0.0408	366.4150	0.4124	378.2651	0.1658	397.2152	0.0194
350.3751	0.0802	367.3352	0.4369	378.3351	0.0163	397.3852	17.0081
351.3351	0.1835	368.2052	0.0096	379.3451	0.4523	398.2152	0.0745
352.1751	0.0103	368.3350	0.1702	380.3451	0.0816	398.3950	4.5322
352.3251	0.4378	369.3452	0.9785	381.1951	0.0103	398.5452	0.1894
353.2651	0.4942	369.4852	0.0323	381.2851	0.0088	399.2252	0.0779
354.3351	0.8405	369.5650	0.0308	381.3451	0.3558	399.3652	1.6337
355.0751	0.2852	370.3352	0.8348	381.4153	0.0499	400.2352	0.0071
355.1950	0.0512	371.1052	3.7514	382.2951	0.0572	400.3552	0.1364
355.2950	1.3045	371.3152	0.8282	382.3551	0.2075	400.4452	0.9943

Table A3.10 (continued). Mass data (*m/z* values and their relative intensities) for the DART-HRMS analysis of *L. virosa* seed. Ten replicates of one sample were averaged where the corresponding spectrum appears in Figure 3.4B.

				L. virosa seed			
m/z	Rel. Int. %	*m/z*	Rel. Int. %	*m/z*	Rel. Int. %	*m/z*	Rel. Int. %
401.3252	0.1489	419.3253	0.3355	446.3854	0.9481	474.3855	0.1975
401.4652	0.2059	420.3153	0.0313	447.3854	0.8980	474.4655	0.0698
402.3352	0.3177	421.3453	0.1152	448.3854	0.2111	475.3855	0.1635
403.3652	0.1856	422.3453	0.0499	449.3954	0.0657	476.4055	0.1655
404.1552	0.0219	422.4851	0.0160	449.4354	0.0660	476.4955	0.0126
404.2952	0.0830	423.3753	0.3373	451.4254	0.2394	477.4355	0.0258
404.3752	0.0471	424.3753	0.4178	452.4854	0.0194	478.4355	0.0365
405.3752	0.3408	424.4753	0.0081	453.3554	0.0315	479.3754	0.0466
406.2852	0.0580	425.3753	2.3606	453.4654	0.1399	479.4854	0.1236
406.3854	0.0370	426.3853	0.8463	455.3556	0.0255	480.4954	0.0792
407.2652	0.0132	426.4653	0.0379	455.4354	0.1551	481.3954	0.0194
407.3652	0.6501	427.3953	4.2791	456.3754	0.0050	481.4956	0.0715
407.4652	0.0153	428.3955	1.9093	457.3754	0.1336	482.4756	0.0643
408.3752	0.5062	429.3853	2.9241	458.3853	0.0625	482.5256	0.0158
408.4554	0.0757	430.3853	1.5907	459.3855	0.2057	483.3856	0.4545
409.3852	7.0897	431.3853	2.9249	459.4855	0.0093	484.3956	0.0392
410.2252	0.0118	432.1853	0.0097	460.4155	0.0576	485.4056	0.0500
410.3854	1.6805	432.3153	0.0068	461.3755	0.2428	486.4556	0.1469
411.3852	3.5408	432.3955	1.1194	461.4255	0.0422	487.3854	0.0430
411.6254	0.1282	433.3253	0.0789	462.1355	0.0408	488.3956	0.0366
411.6954	0.1572	433.4003	0.2070	463.3855	0.3834	488.4656	0.0184
412.2954	0.0090	434.3955	0.0704	464.3855	0.0369	489.3756	0.0955
412.3852	1.0362	435.3553	0.0811	465.3955	0.0780	491.3756	0.0820
413.3754	10.1016	436.3353	0.0349	465.4855	0.0732	491.4856	0.0393
414.3854	3.3966	437.3455	0.0088	466.4055	0.0054	493.3856	0.0256
414.6152	0.1360	438.3552	0.0937	466.5055	0.0382	493.5156	0.0673
415.3004	0.0122	438.4852	0.0264	467.3955	0.4958	494.3656	0.0184
415.3754	1.1633	439.3652	0.2579	467.4655	0.1120	495.2656	0.0074
416.2354	0.0122	440.3654	0.1251	468.3955	0.1082	495.3856	0.0385
416.3652	0.4947	441.3754	0.4230	468.4955	0.0518	495.4456	0.0648
416.4452	0.0514	442.3054	0.0587	469.4055	0.7123	498.5356	0.0354
417.3753	0.3076	442.3854	0.2462	470.4155	0.2670	499.4256	0.0059
417.4553	0.0708	442.4554	0.1999	470.5055	0.0224	500.4255	0.0609
418.2953	0.0110	443.3854	0.5035	471.3855	0.0262	502.4155	0.0713
418.3653	0.1620	444.4054	0.4396	471.4955	0.0227	503.4155	0.2490
418.4553	0.0271	445.3754	0.8157	472.3855	0.0280	504.4555	0.0610

Table A3.10 (continued). Mass data (*m/z* values and their relative intensities) for the DART-HRMS analysis of *L. virosa* seed. Ten replicates of one sample were averaged where the corresponding spectrum appears in Figure 3.4B.

				L. virosa **seed**			
m/z	Rel. Int. %	*m/z*	Rel. Int. %	*m/z*	Rel. Int. %	*m/z*	Rel. Int. %
505.3955	0.0977	548.4657	0.0361	589.5959	0.0135	631.5059	0.0420
505.4955	0.0446	549.4959	0.0073	591.4961	0.0298	632.5361	0.0257
505.5755	0.0101	550.5657	0.0418	591.5859	0.0227	633.5161	0.0518
507.5155	0.1378	551.5057	0.1453	592.5759	0.0246	633.5961	0.0135
508.5257	0.0545	552.4959	0.0082	593.5159	0.0245	633.6961	0.0054
509.5257	0.0918	552.5857	0.0404	594.5159	0.0918	634.5461	1.7415
510.5357	0.0543	554.4957	0.0082	597.5259	0.0508	635.5461	0.6117
511.4357	0.0126	554.5659	0.0440	598.4561	0.0272	635.7061	0.0395
514.4157	0.0200	557.4459	0.0054	598.5959	0.0168	636.5661	0.4370
515.4257	0.0751	557.5359	0.0109	599.5061	2.3412	637.5661	0.0948
516.4257	0.1099	558.4457	0.0082	600.5061	0.7886	638.5761	0.1805
517.4457	0.0152	559.4459	0.0086	601.5259	1.0807	638.6861	0.0245
518.4357	0.0397	559.5459	0.0283	601.8059	0.0116	639.5661	0.0507
519.4057	0.0177	561.4957	0.0821	602.5261	0.3889	640.5661	0.0082
519.4957	0.3701	561.5658	0.0455	602.6261	0.0077	647.4762	0.0484
521.5256	0.0962	562.5158	0.0708	603.5360	0.5177	647.6360	0.0050
522.4256	0.0068	563.5358	0.0295	604.5458	0.1782	648.5160	0.0077
525.4256	0.0152	564.5458	0.0168	605.5460	0.0800	649.5960	0.0054
526.4156	0.0402	566.5358	0.0269	606.5360	0.0270	650.5460	0.1688
526.5658	0.0379	567.5358	0.0135	606.6260	0.0126	650.6060	0.0122
527.5256	0.0282	569.5660	0.0101	608.5260	0.0059	650.6862	0.0762
528.4256	0.0283	570.5458	0.0172	610.5460	0.6705	651.5462	0.0260
531.4756	0.0888	573.4558	0.0077	611.5360	0.1410	652.5462	0.0244
532.4158	0.0109	573.5758	0.0135	612.5460	0.0182	654.5662	0.0082
533.4407	0.0619	575.5060	1.4509	613.5060	0.0059	659.5262	0.0050
533.5258	0.0910	576.5158	0.5056	615.5060	0.6503	662.5662	0.0054
534.4858	0.0704	577.5258	0.4546	615.6460	0.0161	663.4662	0.0093
535.5358	0.0822	578.5260	0.1378	616.5160	0.3225	666.6461	0.0064
536.5358	0.0405	579.5260	0.1093	617.5160	1.8979	675.6761	0.5756
537.5058	0.1291	580.6060	0.0143	618.5260	0.6217	676.5261	0.0082
538.5058	0.0409	582.5159	0.0064	618.6762	0.0162	676.6763	0.2871
539.4958	0.0168	583.5859	0.0109	619.5360	0.2569	678.5961	0.0636
541.5057	0.0101	584.5759	0.0101	619.7560	0.0367	678.7263	0.0059
544.5257	0.0454	586.5559	0.0109	620.5360	0.0283	679.5963	0.0050
545.4757	0.0194	588.5059	0.0059	620.6660	0.0068	680.5963	0.0068
547.4657	0.0431	589.4759	0.0230	621.6660	0.0172	692.6462	0.0145

Table A3.10 (continued). Mass data (*m/z* values and their relative intensities) for the DART-HRMS analysis of *L. virosa* seed. Ten replicates of one sample were averaged where the corresponding spectrum appears in Figure 3.4B.

				L. virosa seed			
m/z	Rel. Int. %	*m/z*	Rel. Int. %	*m/z*	Rel. Int. %	*m/z*	Rel. Int. %
693.6164	0.0235	755.6265	0.0068	876.7869	0.0869	902.7970	0.0773
694.6064	0.0511	756.6265	0.0054	876.9069	0.0077	912.7569	0.2745
695.6264	0.0054	768.5766	0.0064	877.7269	0.4592	914.7771	0.1289
696.6562	0.0064	769.6066	0.0082	878.0569	0.0118	930.8371	0.0104
706.5863	0.0450	770.6064	0.0064	878.7369	0.3892	954.8371	0.0129
708.5863	0.0064	771.6364	0.0222	878.9070	0.0118	956.8473	0.0348
709.5963	0.0091	781.6166	0.0077	879.0569	0.0346	969.7873	0.1040
710.6063	0.0068	782.6766	0.0054	879.7369	1.8300	970.7773	0.0376
711.6063	0.0054	788.6167	0.0220	880.7371	1.0044	974.7874	0.0238
712.6063	0.0140	792.6067	0.0045	881.7469	0.9173	978.7674	0.0064
725.6065	0.0059	848.7569	0.0209	882.7471	0.3511	997.8173	0.0237
727.5744	0.0050	853.7170	0.1275	883.7571	0.2824	998.8173	0.0059
728.5964	0.0233	854.7268	0.1162	884.7571	0.1815	1000.7873	0.0285
729.5964	0.0152	855.7368	0.7408	885.7771	0.0728	1003.8073	0.0091
744.6166	0.0168	856.7468	0.4346	886.7871	0.0253	1007.8273	0.0544
750.6863	0.2286	857.7568	0.2758	895.7370	0.1255	1014.7875	0.0702
750.8165	0.0145	858.7570	0.0719	896.7570	1.3694	1015.7774	0.0691
751.6863	0.0872	859.7668	0.0073	897.7570	0.9361	1016.7974	0.0961
752.6065	0.0327	872.7669	0.6344	898.7670	1.1901	1017.8074	0.0369
752.6765	0.0161	873.7669	0.3907	899.7770	0.4842		
753.6165	0.0297	874.7669	0.3742	900.7970	0.3825		
754.6465	0.0077	875.7769	0.1459	901.7970	0.1233		

Table A3.11 Mass data (*m/z* values and their relative intensities) for the DART-HRMS analysis of *L. virosa* powder. Ten replicates of one sample were averaged where the corresponding spectrum appears in Figure 3.4B.

				***L. virosa* powder**			
m/z	Rel. Int. %	*m/z*	Rel. Int. %	*m/z*	Rel. Int. %	*m/z*	Rel. Int. %
67.0540	0.0915	97.9941	0.2566	117.1642	0.0362	136.1343	2.3151
68.0538	0.4620	98.0841	6.2641	117.2442	0.1103	136.2843	0.6641
68.9640	0.4710	99.0541	15.8119	118.0842	2.3742	136.4043	0.3367
69.0440	5.4648	99.1841	0.0519	118.2042	0.4227	137.0743	0.1747
69.9240	0.0029	100.0041	0.1701	120.0742	0.6884	137.1243	2.3634
70.0640	3.2572	100.0841	8.2065	120.2042	0.0841	137.2143	0.3179
71.0640	1.1877	100.2341	0.1697	121.0842	0.0192	138.0843	0.0664
72.0840	5.6395	101.0641	2.5728	122.0742	1.0414	138.1643	1.3218
72.2040	0.3040	101.1841	0.0332	123.0942	4.5710	139.0054	0.2113
74.0640	8.3488	102.0741	5.5849	123.2942	0.4476	139.1043	2.6977
75.0440	0.0020	103.0541	0.9896	124.0642	0.0472	139.2243	0.0130
76.0640	0.0155	104.0741	0.2199	125.0942	2.5435	139.2643	1.2109
78.0440	0.0671	105.0641	0.5438	125.2144	0.3534	140.0043	0.0355
79.0440	0.2900	106.0641	1.6841	126.0642	2.9513	140.0843	2.7948
79.1242	0.0331	108.0640	0.6365	126.1542	4.0776	140.2543	0.2015
80.0540	3.1414	109.0340	0.6567	127.0442	14.8742	140.3143	0.5514
81.0540	3.3352	109.0942	6.2717	127.1142	5.9727	141.1043	4.5154
81.1442	0.0270	109.2042	0.2047	127.2342	0.5952	142.1043	2.2199
82.0642	0.6916	110.0742	4.6543	127.9777	0.0120	142.1843	1.1046
82.9442	0.0481	110.2142	0.8173	128.0844	6.6791	143.0343	0.2813
83.0840	1.1460	111.0540	0.2933	128.1843	0.4707	143.0943	3.5541
84.0640	2.2921	111.1140	6.8019	128.2243	0.3157	144.0843	2.5015
85.0342	9.5262	111.2342	0.5365	128.9841	0.0072	144.1743	0.6760
85.0942	0.6394	112.0742	1.0677	129.0641	10.5962	144.2443	0.0047
86.0740	3.7819	112.1542	3.5187	129.1391	2.1749	145.0543	28.6853
86.1742	0.1469	113.0542	1.0723	129.2141	0.1228	145.1243	0.5454
88.0741	1.4994	114.0842	9.4677	130.0643	4.2342	145.2243	0.2195
88.2041	0.1557	114.2242	1.8811	130.1543	2.1852	146.0843	2.9081
92.0641	0.1778	115.0542	0.8270	130.2343	0.2943	146.2443	0.3198
93.0641	0.2584	115.1040	2.2004	132.1041	0.7041	147.0743	1.0618
94.0641	2.1646	115.2442	0.2651	134.0843	0.4504	148.0745	0.3290
94.1741	0.1985	115.9642	0.0477	134.2543	0.0341	148.1544	0.7813
95.0841	5.0377	116.0742	7.6371	135.1043	19.8757	149.0165	4.3787
96.0541	3.9080	116.1442	1.1872	135.2443	0.0227	149.1142	0.8283
97.0341	4.6933	116.2242	0.5568	135.9943	1.1585	150.0942	2.1242
97.0941	1.0223	117.0642	13.4530	136.0643	1.5342	150.2342	0.8167

Table A3.11 (continued). Mass data (*m/z* values and their relative intensities) for the DART-HRMS analysis of *L. virosa* powder. Ten replicates of one sample were averaged where the corresponding spectrum appears in Figure 3.4B.

L. virosa powder							
m/z	Rel. Int. %	*m/z*	Rel. Int. %	*m/z*	Rel. Int. %	*m/z*	Rel. Int. %
150.3142	0.0318	170.1643	1.0740	189.0356	0.2109	205.1946	0.0473
151.2342	5.9926	170.3143	0.0149	189.1345	0.9584	206.1146	0.6728
152.1144	0.2165	171.1543	33.2692	189.2345	0.0255	206.2044	0.2891
153.0844	4.3892	171.3143	0.4829	190.1244	2.5187	207.0746	0.6066
154.0844	0.3157	172.1243	7.0894	190.2244	0.4915	207.3046	0.0299
154.1544	2.2351	173.1143	3.6570	191.3244	0.0654	208.1146	0.4433
155.1044	5.3609	174.1143	2.8777	192.1044	0.0811	208.2096	0.8612
156.1042	3.2174	174.2843	0.0621	192.1644	0.9445	210.1046	0.0282
156.1744	0.9642	176.0945	0.0657	193.0844	0.0456	210.3596	0.1543
156.2744	0.5567	176.1694	0.0908	193.1544	0.1277	211.0245	0.2206
157.0544	0.0462	178.0945	0.1185	194.0944	1.2371	211.1345	2.6155
157.1242	3.4598	178.1694	0.2802	194.1944	1.2889	212.1045	0.1301
157.2644	0.5598	178.2443	0.0040	195.0946	2.4652	212.3345	0.6170
158.1044	3.0021	179.0845	0.3235	195.2744	1.1218	213.1145	0.5372
158.1844	0.1198	179.2145	0.0106	196.0946	0.3105	213.2095	0.8921
159.0544	0.3477	180.0845	8.8305	196.2794	0.0547	214.1245	1.0257
159.1244	2.5621	180.1645	0.2723	197.1144	1.3704	214.2545	2.4861
160.0944	2.2209	180.2345	0.0125	197.3344	0.0384	215.1145	0.6371
160.2342	0.0206	181.0032	0.0081	198.1044	8.9061	215.1895	1.7869
161.0844	1.6153	181.1045	0.8706	198.1746	3.5736	215.3245	0.0135
162.0844	3.5243	181.1945	0.0840	199.1044	0.2343	215.3545	0.4016
162.2244	0.4874	182.0143	0.0027	199.1744	9.1603	216.1245	0.3635
163.0644	8.2385	182.1045	0.2127	199.3844	0.0674	216.1945	2.0783
163.1344	6.5624	182.1943	0.1335	199.4046	0.1613	216.3345	0.0325
164.0844	0.4276	183.0945	1.5358	200.1244	0.3302	217.0770	2.4858
164.1644	1.7637	183.1945	2.7084	200.1844	3.3628	217.1745	2.9858
165.0844	0.2261	184.1145	1.1974	201.0394	0.4223	217.3645	0.8181
165.2744	0.1096	184.2045	2.4425	201.1444	1.7380	218.1345	2.2751
166.0944	0.3801	185.0245	0.1628	201.3044	0.1467	220.1145	0.0340
167.0944	2.4698	185.1145	3.6448	202.1244	1.7004	220.1745	0.0959
167.2544	0.2911	185.2145	1.5164	202.2846	0.8399	220.3347	0.0591
168.0944	0.0058	186.1145	3.2468	203.1144	0.0459	221.1845	0.0321
168.2544	2.1989	187.1245	2.1398	203.1746	22.0089	222.1245	0.1270
168.9844	0.0874	188.0945	0.3213	203.3346	0.8323	222.2045	1.2910
169.1144	3.6983	188.1645	1.1772	204.1146	0.1390	224.1147	0.0359
170.0943	2.4136	188.2445	0.4694	204.1844	4.0136	224.2545	0.4063

Table A3.11 (continued). Mass data (*m/z* values and their relative intensities) for the DART-HRMS analysis of *L. virosa* powder. Ten replicates of one sample were averaged where the corresponding spectrum appears in Figure 3.4B.

				L. virosa **powder**			
m/z	Rel. Int. %	*m/z*	Rel. Int. %	*m/z*	Rel. Int. %	*m/z*	Rel. Int. %
225.0447	1.1568	243.2498	0.0809	261.1147	0.5003	277.2148	1.6860
225.2547	0.0587	243.4048	0.5856	261.2247	1.4938	277.2948	2.0614
226.1247	0.3069	244.1148	0.1387	261.4647	0.5656	277.4548	0.3536
227.1347	1.6651	244.1946	3.1816	262.1847	1.3696	277.5248	0.2529
227.4147	0.0075	245.1246	0.0574	262.2547	0.0279	278.1248	0.1581
228.1247	0.0314	245.2246	1.1086	263.3849	0.0076	278.2148	1.3752
228.1947	27.5222	246.1148	0.1883	264.1249	0.0222	278.2948	1.5125
229.1047	0.8987	246.2446	1.1992	264.2447	1.3023	279.1546	0.4129
229.2045	5.8131	247.1246	0.5395	265.1547	0.0049	279.2348	0.1519
230.1047	0.1623	247.2248	1.9699	266.1447	0.1156	279.4048	0.3631
230.1847	2.8125	248.1346	0.3397	266.2547	0.1739	280.1448	0.3302
230.3547	0.6247	248.2548	1.7239	267.2647	3.9819	280.2446	2.7823
231.1247	0.8107	248.3297	0.3061	268.1149	0.0314	281.1448	0.0402
231.2147	1.7005	248.4046	0.4735	268.2847	1.7926	281.2448	2.6025
231.3247	0.8422	249.0646	0.6628	269.2147	0.0137	282.1548	0.1692
232.1346	0.2082	249.3148	0.0077	270.3849	0.1377	282.2648	13.1777
232.2346	2.4554	250.1548	1.0621	271.0847	5.0152	282.5246	0.1280
233.1346	18.0193	251.1048	0.0068	271.1597	0.0236	285.1048	0.5223
233.2246	2.6695	252.1247	0.0489	271.2347	3.1545	286.1348	0.0734
234.1346	1.2020	252.1847	0.3838	272.0547	0.2299	286.2148	0.0167
234.2046	2.7630	252.2647	0.1634	272.1349	0.2412	286.2748	0.9119
234.3546	0.9191	254.3047	0.0042	272.2547	3.4675	287.0648	0.0342
235.1746	0.0885	255.0847	0.1250	272.4649	0.5774	287.1248	0.0937
236.1046	0.0264	255.1347	0.0893	273.0848	0.1204	287.2248	2.4615
236.1746	1.9959	255.2247	2.5163	273.1548	0.0186	287.4748	0.2100
237.1146	0.4275	257.0847	0.2615	273.2446	5.6209	288.1348	0.0746
237.1846	0.2096	257.2447	9.9473	274.1248	0.0445	288.2448	3.8648
238.1146	0.1309	258.0947	0.0089	274.1548	0.0397	289.1048	0.6532
238.1946	0.4585	258.2547	2.6433	274.2648	3.7285	289.2348	2.1219
238.3846	0.5329	258.4347	0.6130	274.4148	1.4711	289.4048	0.8519
241.1046	0.0459	259.1047	0.5426	275.1046	0.3641	289.4748	0.4913
241.1846	8.6071	259.1947	35.7501	275.2648	2.0026	290.1748	0.0942
242.1048	0.1500	259.4247	1.5590	276.0946	0.0630	290.2748	2.1742
242.1846	2.3154	260.1147	0.4097	276.1648	0.1175	290.4048	0.0871
243.1046	1.3866	260.1947	2.2763	276.2748	2.8756	291.0948	0.3923
243.1648	1.7026	260.2547	3.3113	277.1146	6.0978	291.1948	0.1675

Table A3.11 (continued). Mass data (*m/z* values and their relative intensities) for the DART-HRMS analysis of *L. virosa* powder. Ten replicates of one sample were averaged where the corresponding spectrum appears in Figure 3.4B.

m/z	Rel. Int. %	*m/z*	Rel. Int. %	*m/z*	Rel. Int. %	*m/z*	Rel. Int. %
291.2750	1.7280	307.3449	0.8436	325.1150	0.0444	346.2749	0.0031
291.4148	0.7274	308.1360	0.0050	325.2850	0.0694	347.1649	0.0150
292.1148	0.1638	308.2349	0.0196	326.2950	0.2372	347.2851	0.2987
292.3148	2.0515	308.3315	1.5356	327.2850	2.0289	347.3651	0.6749
293.2947	0.0807	309.2849	0.0576	328.3248	3.3759	348.1851	0.0270
294.1098	0.0396	310.1349	0.0071	329.3150	2.6834	348.2949	0.1023
294.2147	0.0983	310.2449	1.5672	330.3350	0.3957	348.3751	1.3721
294.2949	1.7419	311.2749	5.1238	331.0950	0.1064	349.1101	0.0055
295.2347	0.1168	313.2749	0.0336	331.2950	1.3020	349.2151	0.0039
296.1649	0.0283	315.1148	0.0417	332.0950	0.0149	349.3351	1.0818
296.2549	1.0873	315.2248	0.0233	332.2150	0.0132	350.1649	0.0438
296.4747	0.3819	315.2998	0.6644	332.2950	0.0243	350.3151	0.0154
296.5247	0.1557	315.4448	0.2121	332.3550	1.5637	350.3751	1.2643
298.4049	0.5163	316.1150	0.0200	333.0950	0.0294	351.3351	0.5729
298.5049	0.1334	316.2250	0.0130	333.1750	0.0206	352.3251	0.4637
299.0949	0.0159	316.3048	1.5519	333.3450	1.0215	353.3451	0.2913
299.1949	0.0115	317.1250	0.0247	334.1550	0.0571	354.3351	3.5432
299.2749	0.8752	317.2348	0.0344	334.2350	0.0119	355.0751	0.4677
300.4249	0.0801	317.3150	1.5713	334.3350	1.6722	355.3550	2.5497
301.0949	0.0246	318.1048	0.0191	335.2049	0.0519	356.0750	0.0175
302.1449	0.0712	318.2950	1.9470	335.3249	0.7825	356.3550	0.8802
302.3049	1.7430	319.2348	0.0317	336.1849	0.0238	357.2950	0.0310
302.4149	0.1651	319.3050	1.2376	336.3251	3.2954	357.3850	0.0114
303.1249	0.1238	319.4450	0.7633	336.4749	0.6791	358.3650	0.9279
303.2249	0.0362	320.1648	0.0375	337.3451	0.8876	359.1350	0.0018
303.3049	2.0692	320.2350	0.0146	338.1951	0.0057	359.2250	0.0029
304.1549	0.0495	320.3148	1.9561	338.3449	53.2644	359.2952	0.0107
304.2349	3.5304	321.1550	0.0139	338.6049	0.7691	359.5150	0.0137
305.1549	0.1393	321.2350	0.0265	339.1049	0.0492	359.5850	0.0060
305.2349	0.1282	321.3150	0.8125	339.3251	10.1331	360.1550	0.1885
305.3149	1.7211	322.1748	0.0410	340.3449	2.2717	360.3150	0.3934
306.1649	0.1250	322.2450	0.0303	341.3149	2.6261	361.1550	0.0293
306.2749	1.0713	322.3248	1.2630	342.3149	2.0742	361.3250	1.1148
306.3549	1.5869	323.2548	0.1519	343.1649	0.0072	362.1652	0.0503
307.1149	0.0054	324.1750	0.1000	343.3351	0.1662	362.2650	0.0137
307.2749	0.3757	324.2650	0.4614	344.3951	0.2594	362.3750	0.8417

Table A3.11 (continued). Mass data (*m/z* values and their relative intensities) for the DART-HRMS analysis of *L. virosa* powder. Ten replicates of one sample were averaged where the corresponding spectrum appears in Figure 3.4B.

				L. virosa powder			
m/z	Rel. Int. %	*m/z*	Rel. Int. %	*m/z*	Rel. Int. %	*m/z*	Rel. Int. %
363.1752	0.0469	376.3351	0.3383	393.4453	0.0168	410.3854	0.0175
363.2452	0.0331	376.5751	0.0747	394.1853	0.0350	411.1952	0.0646
364.1952	0.0447	377.1851	0.0122	394.2653	0.0112	411.3852	0.2234
364.2550	0.0328	377.3351	0.0587	394.3353	0.0257	411.6254	0.0080
365.1752	0.0022	377.4251	0.0332	395.3653	0.0031	411.6954	0.0148
365.2750	0.2324	377.5251	0.0049	396.3753	0.0282	412.2052	0.0487
365.4150	0.0603	378.1851	0.0049	397.3852	0.0691	412.3852	0.0253
366.1952	0.0207	378.2651	0.0395	398.2152	0.0023	413.3754	0.0060
366.4150	1.2805	379.1751	0.0032	398.3950	0.0173	414.3854	0.0069
367.3352	0.3030	379.2651	0.0127	399.3652	1.2099	415.3754	0.0506
368.3350	0.1465	379.3451	0.2909	400.3552	0.2718	416.3652	0.1988
369.3452	2.7462	380.2051	0.0317	400.4452	0.0325	418.2253	0.0679
369.4252	0.0479	380.3451	0.0298	401.2252	1.6649	418.3653	0.0150
369.4852	0.0326	381.3451	0.0180	401.3252	0.2220	419.1853	0.4211
369.5650	0.0570	382.2951	0.0076	403.1952	0.0783	419.3253	1.6768
370.3352	0.7905	382.3551	0.0212	403.2952	0.0531	420.2553	0.0260
371.1052	3.2860	382.4351	0.0174	404.1552	0.0163	420.3153	0.5109
371.3152	30.6043	383.2951	0.0015	404.2952	0.0311	421.3453	0.0297
371.5852	0.8122	383.3651	0.2566	404.3752	0.0398	421.4653	0.0206
371.6750	0.0670	383.4453	0.0160	405.1952	0.0109	422.2053	0.0209
371.7551	0.0449	384.1251	0.0038	405.2752	0.4303	422.3453	0.0483
371.8352	0.0326	384.2751	0.0046	405.3752	0.1585	422.4851	0.0134
372.1152	2.9842	384.3051	0.0387	405.4552	0.0199	423.1753	0.0153
372.3152	4.9478	384.3751	0.0230	406.1952	0.0271	423.2753	0.0031
372.6450	0.0067	385.4851	0.0191	406.2852	1.2038	423.3753	0.0042
372.8352	0.1967	387.2253	0.0431	406.3854	0.4040	424.2053	0.0014
372.9152	0.1263	387.3353	0.1400	407.2652	0.0171	424.3753	0.0183
373.1052	1.0132	387.6051	0.0129	407.3652	0.0105	425.3753	0.0125
373.3152	0.2508	388.1351	0.3787	408.1952	0.0022	427.3953	0.0480
374.0952	0.0944	390.3351	0.0099	408.3752	0.0331	427.4753	0.0114
374.3252	0.0420	391.1753	0.0613	408.4554	0.0026	428.3955	0.0124
375.1052	0.1677	391.2951	1.5858	409.2052	0.0076	428.4953	0.0092
375.2452	0.0190	391.4851	0.2506	409.2752	0.0148	429.3853	0.0351
375.3152	0.3113	392.2853	0.8783	409.3852	0.0398	429.4853	0.0040
376.1451	0.1222	393.1853	0.0452	409.4654	0.0202	430.3853	0.0018
376.2551	0.0031	393.3451	0.4208	410.2252	0.0260	431.2253	0.0069

Table A3.11 (continued). Mass data (*m/z* values and their relative intensities) for the DART-HRMS analysis of *L. virosa* powder. Ten replicates of one sample were averaged where the corresponding spectrum appears in Figure 3.4B.

m/z	Rel. Int. %	*m/z*	Rel. Int. %	*m/z*	Rel. Int. %	*m/z*	Rel. Int. %
431.3053	0.0069	453.3554	0.0176	481.4956	0.0031	519.1457	1.1493
431.4753	0.0044	453.4654	0.0095	482.2154	0.0062	525.4256	0.0040
433.4753	0.0031	454.2154	0.0040	482.3354	0.0068	528.4256	0.0092
434.2653	0.0198	454.3454	0.0060	483.3856	0.0680	531.4058	0.0038
434.3955	0.0153	455.3556	0.0236	484.2254	0.0038	532.4158	0.0350
435.2253	0.1315	457.3754	0.0130	484.3956	0.0114	533.5258	0.0035
435.3553	0.0929	458.3853	0.0044	486.3854	0.1166	534.4858	0.0035
435.4655	0.0165	459.4855	0.0029	487.3854	0.0324	536.1858	4.0692
436.3353	0.0224	460.4155	0.1035	487.5256	0.0016	536.3158	0.0018
437.1955	0.0130	460.4955	0.0114	488.3956	0.0187	536.3858	0.0246
438.2154	0.0026	461.4255	0.0517	488.4656	0.0183	536.5358	0.0287
438.3552	0.0170	462.1355	0.3658	489.1956	0.0064	536.6058	0.0231
439.3652	0.0137	462.2055	0.0059	489.3756	0.0180	537.1858	1.4782
439.4554	0.0114	463.3855	0.0031	491.2156	0.0073	537.3958	0.1598
441.2154	0.0048	464.2255	0.0053	491.3756	0.0018	537.5058	0.1397
441.3754	0.0147	464.3855	0.0086	492.2256	0.0017	537.6158	0.0121
442.3854	0.0145	465.3955	0.0144	493.3056	0.0035	538.1758	1.0425
443.3854	0.0373	465.4855	0.0029	493.3856	0.0038	538.3158	0.0176
443.4754	0.0212	466.2355	0.0040	495.2656	0.0018	538.3858	0.1126
444.4054	0.0092	466.3355	0.0136	495.3856	0.0143	538.5058	0.0153
445.1154	0.7059	467.3955	0.0251	495.4456	0.0038	539.3658	0.0128
445.3754	0.0174	468.3955	0.0099	496.3256	0.0026	545.4757	0.0033
446.3854	0.0149	469.1855	0.0047	497.3956	0.0017	548.4657	0.0297
447.2254	0.0071	469.4055	0.0284	499.2156	0.0408	552.3859	0.0092
448.2054	0.0160	470.4155	0.0133	499.4256	0.0054	553.3957	0.0468
448.3254	0.0107	473.3755	0.0017	500.4255	0.0073	553.4957	0.0079
448.3854	0.0123	474.3855	0.0214	502.4155	0.0628	554.2359	0.0035
449.2154	0.0169	474.4655	0.0107	503.4155	0.0130	554.4057	0.0169
449.3254	0.0044	475.3855	0.0034	505.3955	0.0057	555.4559	0.0046
449.3954	0.0233	476.4955	0.0026	509.5257	0.0015	557.2457	0.0374
449.5154	0.0084	479.2956	0.0099	510.5357	0.0029	559.4459	0.0026
450.2154	0.7481	479.3754	0.0107	511.4357	0.0226	565.5258	0.0220
450.3454	0.1015	479.4854	0.0033	515.4257	0.0040	568.3858	0.0029
450.5154	0.0060	480.2454	0.0016	516.4257	0.0076	569.3858	0.0046
451.3454	0.0478	481.3254	0.0157	517.4457	0.0031	569.4958	0.0029
451.4254	0.0577	481.3954	0.0051	518.4357	0.0135	570.4058	0.0053

Table A3.11 (continued). Mass data (*m/z* values and their relative intensities) for the DART-HRMS analysis of *L. virosa* powder. Ten replicates of one sample were averaged where the corresponding spectrum appears in Figure 3.4B.

L. virosa **powder**							
m/z	Rel. Int. %	*m/z*	Rel. Int. %	*m/z*	Rel. Int. %	*m/z*	Rel. Int. %
571.4458	0.0035	663.6262	0.0137	676.6763	0.1398	1000.7873	0.0033
586.3959	0.0035	664.5662	0.0046	677.7063	0.0349		
612.3560	0.0092	673.6463	0.0026	680.5963	0.0029		
627.3361	0.0170	675.6761	0.3560	708.6463	0.1592		

Table A3.12 Mass data (*m/z* values and their relative intensities) for the DART-HRMS analysis of *L. virosa* tincture. Ten replicates of one sample were averaged where the corresponding spectrum appears in Figure 3.4B.

				L. virosa **tincture**			
m/z	Rel. Int. %	*m/z*	Rel. Int. %	*m/z*	Rel. Int. %	*m/z*	Rel. Int. %
55.0539	0.4970	85.0342	22.8336	102.0741	0.2782	123.0942	1.2548
57.0539	0.4844	85.0942	0.0360	103.0541	2.3055	124.0642	1.6116
58.0639	0.0058	85.1642	0.0139	103.1443	0.1964	124.1844	0.0395
59.0541	2.9723	86.0740	16.7892	104.0741	16.3730	125.0942	2.8790
60.0541	0.2543	86.1742	0.2899	104.1443	0.5671	125.2144	0.0237
60.1541	0.0254	87.0539	6.7747	104.2343	0.1046	126.0642	15.3962
61.0339	3.4185	87.1641	0.0636	105.0641	0.4006	127.0442	50.7053
61.1041	0.0059	88.0741	0.1885	105.1843	0.0056	127.1142	0.2813
62.0639	1.9033	89.0641	0.8807	106.0641	0.1486	127.2342	0.1648
65.0541	13.2232	90.0641	3.2696	107.0841	0.0470	127.9777	0.0231
66.0441	0.1654	90.1641	0.0320	108.0640	2.6654	128.0844	5.4905
67.0540	0.0403	91.0541	0.6253	108.1542	0.1048	128.2243	0.0726
68.0538	0.1585	91.1241	0.0054	109.0340	7.2498	128.9841	0.0105
69.0440	3.8341	92.0641	0.0074	109.0942	0.5405	129.0641	3.8215
70.0640	14.3307	93.0641	86.2202	110.0742	4.0597	130.0643	15.8839
70.1340	0.7894	93.1341	3.0504	110.2142	0.0543	130.2343	0.1916
71.0640	2.1893	94.0641	4.0943	111.0540	11.0583	131.0643	1.9277
72.0140	0.0267	94.1741	0.2941	111.1140	0.2617	131.2243	0.1562
72.0840	20.6334	95.0241	0.2574	111.2342	0.0097	132.1041	4.8741
72.1540	0.1622	95.0841	0.2603	112.0742	12.3242	133.0643	0.6116
72.2040	0.2536	96.0541	5.1887	113.0542	2.9993	133.2543	0.0168
73.0640	3.1015	96.1291	0.0432	114.0842	2.4637	134.0843	1.2902
74.0640	0.4162	97.0341	16.6866	114.2242	0.0584	134.1943	0.0557
74.1340	0.0252	97.0941	0.7141	115.0542	1.5215	134.2543	0.0969
75.0440	3.4158	97.1741	0.0155	115.1040	0.2458	135.1043	0.4114
75.1140	7.0032	97.2241	0.0086	115.2442	0.0391	136.0643	10.5194
76.0640	0.9824	97.2841	0.0019	116.0742	63.9511	136.2143	0.2406
77.0440	0.0316	97.9941	0.1586	116.2242	0.7743	136.4043	0.0165
78.0440	0.0026	98.0841	2.1062	117.0642	16.1067	137.0743	4.9197
79.0440	1.0473	99.0541	81.1174	117.2442	0.1261	137.1243	0.2140
80.0540	0.7430	99.1841	0.3019	118.0842	6.2852	137.2143	0.0054
81.0540	7.5924	100.0841	2.3445	118.2042	0.1919	137.2843	0.0278
82.0642	0.3183	100.2341	0.0189	120.0742	0.2514	138.0843	1.2663
83.0240	0.0551	100.9841	0.0811	120.2042	0.0112	139.0054	0.6395
83.0840	0.1352	101.0641	1.7797	121.0842	0.2578	139.1043	0.8009
84.0640	8.9980	101.1841	0.0114	122.0742	0.4051	139.2243	0.0094

Table A3.12 (continued). Mass data (*m/z* values and their relative intensities) for the DART-HRMS analysis of *L. virosa* tincture. Ten replicates of one sample were averaged where the corresponding spectrum appears in Figure 3.4B.

m/z	Rel. Int. %	*m/z*	Rel. Int. %	*m/z*	Rel. Int. %	*m/z*	Rel. Int. %
139.2643	0.0214	158.9742	0.0024	185.1145	0.9730	204.1146	0.9465
140.0843	2.7978	159.1244	0.2238	186.1145	1.8957	205.1046	0.8544
140.3143	0.0168	160.0944	2.2477	186.9945	0.0024	205.1946	0.0475
141.1043	0.5322	161.0844	0.0580	187.1245	0.3647	205.2646	0.0152
142.1043	6.0176	162.0844	3.4184	188.0945	2.7316	205.3346	0.0291
142.1843	0.4240	162.2244	0.1010	189.0356	0.2187	206.1146	2.0027
143.0343	1.1083	163.0644	13.9876	189.1345	0.5880	207.0746	1.5373
143.0943	3.1876	163.1344	0.2104	189.2345	0.0800	207.1546	1.1181
144.0843	4.2536	164.0844	1.2235	189.3145	0.0570	208.1146	1.1963
144.1743	0.0418	165.0844	1.0008	190.1244	1.5002	208.2096	0.0159
144.2443	0.0164	165.1794	0.0708	190.2244	0.0881	209.1346	1.0262
145.0543	28.9691	165.2744	0.0123	191.0678	1.7260	209.2746	0.0321
145.1243	4.0350	166.0944	2.8014	191.1644	1.8296	210.1046	1.1305
145.2243	0.1484	167.0944	1.4094	191.3244	0.1389	210.3596	0.0095
145.9868	0.0102	167.2544	0.0635	192.1044	1.6900	211.1345	1.0502
146.0843	4.2452	168.0944	1.6169	192.1644	0.6455	211.3145	0.0054
146.9943	0.0084	168.2544	0.1018	193.0844	0.6471	212.1045	4.4881
147.0743	1.8850	169.1144	0.0483	193.1544	0.0039	212.3345	0.0524
148.0745	0.4206	170.0943	3.7552	194.0944	1.6141	213.1145	0.9010
149.0165	0.0610	172.1243	2.6222	195.0946	0.9444	213.7345	0.0022
149.1142	0.1607	173.1143	3.1302	196.0946	2.2276	214.0245	0.0019
150.0942	1.5240	174.1143	1.6024	196.2794	0.0480	214.1245	2.0795
150.1542	0.0340	175.1245	0.4022	197.1144	2.4647	215.1145	1.6819
150.2342	0.0134	176.0945	1.2612	197.3344	0.0277	215.3245	0.0261
150.3142	0.0069	177.0645	0.5933	198.1044	9.3761	215.3545	0.0237
151.0044	0.0056	177.1443	0.1084	199.1044	0.9456	216.1245	9.5868
151.1042	0.6425	178.0945	1.9071	199.1744	0.4416	216.3345	0.0822
152.1144	3.4801	179.0845	0.7912	200.1244	4.8005	217.0770	0.9010
153.0844	2.6211	180.0845	19.8471	201.0394	0.4178	217.1745	0.0869
154.0844	3.2666	181.0032	0.0025	201.1444	1.0689	217.3645	0.0047
155.1044	1.7963	181.1045	3.5200	201.3044	0.1424	218.0445	0.0021
156.1042	3.3575	182.1045	9.8869	202.1244	2.6696	218.1345	4.8940
156.2744	0.0504	182.9989	0.0045	202.2846	0.0892	219.1045	0.7868
157.1242	0.2044	183.0945	2.3289	203.1144	0.1272	220.1145	0.9025
157.2644	0.0204	184.0145	0.0020	203.1746	0.0621	220.3347	0.0774
158.1044	4.2224	184.1145	2.8952	203.3346	0.0104	221.1845	0.2926

Table A3.12 (continued). Mass data (*m/z* values and their relative intensities) for the DART-HRMS analysis of *L. virosa* tincture. Ten replicates of one sample were averaged where the corresponding spectrum appears in Figure 3.4B.

L. virosa tincture							
m/z	Rel. Int. %	*m/z*	Rel. Int. %	*m/z*	Rel. Int. %	*m/z*	Rel. Int. %
222.1245	0.7629	245.2246	0.1427	264.1249	0.5123	282.5246	0.0261
222.2947	0.0134	246.1148	1.3738	264.2447	0.1793	283.1848	0.1427
223.1247	0.7918	247.1246	0.6773	265.1547	0.3205	283.2648	0.4041
224.1147	1.5595	247.2248	0.0549	265.2449	0.0721	284.1548	0.4406
225.0447	0.3430	248.1346	1.9632	266.1447	1.3533	284.2648	0.0547
225.1447	0.8333	248.3297	0.0639	267.1547	0.2002	285.1048	0.2574
226.1247	0.9862	248.4046	0.0652	268.1149	4.9999	285.2748	0.1330
227.1347	0.4804	249.1646	0.2998	269.1347	0.7403	285.4148	0.0106
228.1247	0.4862	249.3148	0.0038	269.2147	0.2204	286.1348	0.3635
229.1047	0.6309	250.1548	0.6875	270.1247	0.9246	286.2748	0.0347
230.1047	4.2047	251.1648	0.4516	270.3849	0.0085	287.0648	0.0128
230.3547	0.0095	252.1247	0.9141	271.0847	1.7881	287.1248	0.3079
231.1247	0.4258	253.1047	0.8273	271.2347	0.1512	287.2248	0.0422
231.2147	0.0088	253.1847	0.3170	272.1349	0.8805	287.3048	0.0094
231.3247	0.0450	254.1145	1.0812	272.2547	0.0181	287.4748	0.0049
232.1346	2.4978	254.3047	0.0601	272.4649	0.0088	288.1348	1.0782
233.1346	0.5801	254.3547	0.0384	273.1548	0.1092	288.2448	0.1757
234.1346	5.4924	255.1347	0.0771	274.1248	0.4592	289.1048	1.5971
234.3546	0.0984	255.2247	0.0215	274.1548	0.0022	289.2348	0.2652
235.0846	0.7656	256.1447	0.7706	274.2648	0.0170	289.4748	0.0078
235.1746	0.2178	256.3447	0.0083	274.4148	0.0156	290.1748	0.9671
236.1046	1.1032	257.1647	0.0174	275.2046	0.3360	290.4048	0.0055
237.1146	0.5688	257.2447	0.0153	275.3848	0.0104	291.1948	0.4795
237.1846	0.0131	258.1647	0.3976	276.1648	0.7560	291.4148	0.0714
238.1146	0.9690	258.2547	0.0406	277.2148	1.9076	292.1148	0.4337
238.3846	0.0083	258.4347	0.0052	277.4548	0.0490	293.2148	0.8491
239.1446	0.3185	259.1047	0.1996	277.5248	0.0314	294.1098	0.3192
240.1246	0.8302	259.1947	0.0564	278.1248	1.1789	294.2147	0.2425
241.1046	0.2199	260.1147	1.1505	279.1546	0.2077	295.2347	1.1662
241.1846	0.2945	260.2547	0.0559	279.2348	2.5207	296.1649	0.5884
242.1048	0.8377	261.1147	1.2422	280.1448	0.6817	296.2549	0.4288
242.2846	0.0018	261.2247	0.0272	280.2446	0.5291	296.4747	0.0249
243.1046	1.1077	261.4647	0.0095	281.1448	0.0939	296.5247	0.0140
243.4048	0.0012	262.1847	1.1012	281.2448	2.0730	297.2449	1.9047
244.1148	0.6675	263.1347	0.4322	282.1548	0.5165	298.1649	0.1813
245.1246	0.5666	263.2347	0.7366	282.2648	0.5706	298.2749	0.6465

Table A3.12 (continued). Mass data (*m/z* values and their relative intensities) for the DART-HRMS analysis of *L. virosa* tincture. Ten replicates of one sample were averaged where the corresponding spectrum appears in Figure 3.4B.

				L. virosa tincture			
m/z	Rel. Int. %	*m/z*	Rel. Int. %	*m/z*	Rel. Int. %	*m/z*	Rel. Int. %
298.4049	0.0210	314.1548	0.3399	330.2350	0.0432	345.1849	0.4377
298.5049	0.0827	314.2448	0.3708	330.3350	0.1805	346.1751	0.2806
299.0949	0.0163	315.1148	0.0390	331.2250	0.0786	347.1649	0.0719
299.1949	0.3376	315.2248	0.1870	331.2950	0.1893	347.2851	0.0616
299.2749	0.3447	315.4448	0.0140	332.2150	0.3155	348.1851	0.1655
300.0949	0.3432	316.1150	0.2008	332.2950	0.1298	348.2949	0.2035
300.1949	0.2421	316.2250	0.0766	332.3550	0.0219	349.2151	0.0859
300.2947	0.0254	316.3048	0.0080	333.0950	0.0346	349.3351	0.0210
300.3749	0.0175	317.1250	0.0673	333.1750	0.1030	350.1649	0.2781
300.4249	0.0522	317.2348	0.0463	333.2350	0.0036	350.3151	0.0619
301.0949	0.2466	318.1048	0.1187	333.3450	0.0014	350.3751	0.0322
301.2949	0.0018	318.2248	0.1028	334.1550	0.3051	351.1751	0.0947
302.1449	0.3641	319.2348	0.1312	334.3350	0.0291	352.1751	0.2430
302.3049	0.0325	319.4450	0.0098	335.2049	0.1908	352.2451	0.0178
302.4149	0.0077	320.1648	0.2574	336.1849	0.2791	352.3251	0.0096
303.1249	0.1556	321.1550	0.0322	336.4749	0.0144	353.1851	0.0947
303.3049	0.0034	321.2350	0.1311	337.2049	0.1807	353.2651	0.0817
304.1549	0.4068	322.1748	0.3484	338.1951	0.2028	354.1951	0.1371
304.2349	0.0582	322.2450	0.0373	338.2649	0.0656	354.2651	0.1633
304.3649	0.0045	323.1750	0.1827	338.3449	0.1823	354.3351	0.0161
305.1549	0.3228	323.2548	0.1528	338.4251	0.0060	355.1950	0.0372
305.2349	0.0088	324.1750	0.6387	338.4849	0.0065	355.2950	0.2003
306.1649	0.9700	324.2650	0.0437	338.6049	0.0286	356.1950	0.1296
306.2749	0.0922	325.1150	0.3213	339.1849	0.1121	356.2850	0.0841
307.1149	0.3207	325.1950	0.0627	339.3251	0.0167	356.3550	0.0024
307.1949	0.1688	325.2850	0.1976	340.2651	0.1544	357.2050	0.1242
307.2749	0.1466	326.1850	0.6579	340.3449	0.0145	357.2950	0.0945
308.1360	0.5117	326.2950	0.0718	341.1349	0.0300	357.3850	0.0208
308.2349	0.0016	327.1950	0.1386	341.2149	0.1150	358.2950	0.0049
309.2149	0.4180	327.2850	0.1775	341.3149	0.0885	358.3650	0.0773
309.2849	0.2916	328.1300	0.1257	342.1451	0.7480	359.2250	0.1942
310.1349	0.2021	328.2250	0.1661	343.1649	0.2582	359.2952	0.0034
310.2449	0.1673	328.3248	0.1081	343.2351	0.0365	359.3850	0.0020
311.2349	0.3547	329.2350	0.1032	343.3351	0.0731	359.5150	0.0098
312.1649	0.3177	329.3150	0.0449	344.1751	1.3761	360.1550	0.5086
313.2749	0.4723	330.1650	0.2162	344.3951	0.0700	360.3150	0.0369

Table A3.12 (continued). Mass data (*m/z* values and their relative intensities) for the DART-HRMS analysis of *L. virosa* tincture. Ten replicates of one sample were averaged where the corresponding spectrum appears in Figure 3.4B.

				L. virosa tincture			
m/z	Rel. Int. %	*m/z*	Rel. Int. %	*m/z*	Rel. Int. %	*m/z*	Rel. Int. %
361.1550	0.0606	372.1152	0.0824	384.2751	0.0067	398.2952	0.0282
361.2352	0.1699	372.2352	0.1118	384.3051	0.0548	398.4752	0.0083
361.3250	0.0130	372.3152	0.5768	385.2151	0.1000	399.2252	0.0666
362.1652	0.2301	372.8352	0.0036	385.3151	0.0309	399.3652	0.0126
362.2650	0.1457	373.1752	0.1101	385.4851	0.0060	400.1552	0.0455
362.3750	0.0376	373.2452	0.0031	386.2153	0.1523	400.2352	0.0766
363.1752	0.1174	373.3152	0.0731	386.3351	0.1103	400.3552	0.0641
363.2452	0.0402	373.4052	0.0024	387.2253	0.0486	401.2252	0.0842
364.1952	0.1965	374.1652	0.1279	387.2853	0.0026	401.3252	0.1034
364.2550	0.0742	374.2652	0.1659	387.3353	0.0030	401.4652	0.0102
365.1752	0.0236	375.1752	0.0757	388.1351	0.1541	402.2252	0.0344
365.2750	0.0905	375.2452	0.0015	388.2653	0.0946	402.3352	0.1680
365.4150	0.0099	375.3152	0.0288	388.3451	0.1361	403.1952	0.0460
366.1952	0.0864	376.1451	0.1067	388.4351	0.0241	403.2952	0.0182
366.2652	0.0121	376.3351	0.0026	388.5351	0.0086	403.3652	0.0070
366.2950	0.0779	377.1851	0.1477	389.2653	0.1310	404.1552	0.2877
367.2050	0.0811	377.2551	0.0070	390.1353	0.0218	405.1952	0.0340
367.2750	0.0361	377.4251	0.0193	390.2551	0.0717	405.2752	0.0566
367.3352	0.0105	377.5251	0.0089	390.3351	0.0162	405.4552	0.0042
368.1252	0.0599	378.1851	0.2553	391.2951	0.0170	406.1952	0.0895
368.2052	0.1326	379.1751	0.0728	391.3901	0.0053	406.2852	0.0715
368.2652	0.0186	379.2651	0.0115	392.1851	0.1687	406.3854	0.0101
368.3350	0.0180	379.3451	0.0221	392.2853	0.0053	407.1754	0.0326
369.2150	0.1349	380.2051	0.1621	393.1853	0.0440	407.2652	0.0448
369.3452	0.0356	380.2851	0.0493	393.2652	0.0153	408.4554	0.0025
369.4252	0.0015	381.1951	0.0993	393.3451	0.0313	409.2052	0.0396
369.4852	0.0020	381.2851	0.0021	394.1853	0.1813	409.2752	0.0295
369.5650	0.0069	381.4153	0.0040	394.2653	0.0387	409.3852	0.0730
370.2150	0.2042	382.1951	0.0641	394.3353	0.0374	410.2252	0.1204
370.3352	0.0998	382.2951	0.1433	395.1953	0.1061	410.3854	0.0166
371.1052	0.0634	382.4351	0.0025	396.2053	0.1314	411.1952	0.0088
371.3152	2.0783	383.1951	0.0528	396.2853	0.1452	411.2952	0.0460
371.5852	0.0658	383.2951	0.0224	397.2152	0.0604	411.3852	0.0068
371.6750	0.0327	383.3651	0.0034	397.2950	0.0448	412.1252	0.0026
371.7551	0.0078	384.1251	0.0461	397.3852	0.0266	412.2052	0.0231
371.8352	0.0012	384.2051	0.0440	398.2152	0.1365	412.2954	0.0840

Table A3.12 (continued). Mass data (*m/z* values and their relative intensities) for the DART-HRMS analysis of *L. virosa* tincture. Ten replicates of one sample were averaged where the corresponding spectrum appears in Figure 3.4B.

				L. virosa tincture				

m/z	Rel. Int. %	*m/z*	Rel. Int. %	*m/z*	Rel. Int. %	*m/z*	Rel. Int. %
412.3852	0.0170	425.3753	0.0102	439.2903	0.0149	458.2354	0.0777
413.2152	0.0568	425.4553	0.0055	439.3652	0.0130	458.3853	0.0128
413.3052	0.0173	426.3153	0.1520	439.4554	0.0013	459.1855	0.0037
414.2154	0.0578	427.2253	0.0033	440.2054	0.0131	459.3053	0.0247
414.3154	0.1205	427.2953	0.0237	441.2154	0.0070	460.3053	0.0652
414.3854	0.0183	427.4753	0.0018	441.2954	0.0095	460.4955	0.0032
414.6152	0.0046	428.2353	0.0238	441.3754	0.0034	461.3055	0.0222
415.1554	0.0310	428.2953	0.1189	441.4754	0.0061	461.4255	0.0041
415.2254	0.0721	428.4953	0.0150	442.3054	0.1555	462.2055	0.0441
415.3004	0.0210	429.2353	0.0083	442.3854	0.1099	462.3053	0.0551
415.3754	0.0167	429.3053	0.0338	443.2954	0.0282	463.3153	0.0124
416.2354	0.0845	430.2353	0.0122	443.3854	0.0261	464.2255	0.0367
416.3652	0.0670	430.3053	0.0481	444.2954	0.2452	464.3155	0.0020
417.1753	0.0182	430.3853	0.0035	445.3054	0.0366	465.2255	0.0016
417.2553	0.0015	431.2253	0.0102	445.4454	0.0032	465.3255	0.0064
417.3053	0.0127	431.3053	0.0203	446.3054	0.1410	465.3955	0.0016
417.3753	0.0031	431.3853	0.0088	447.3254	0.0264	466.2355	0.0435
417.4553	0.0074	432.1853	0.0242	448.2054	0.0585	466.3355	0.0242
418.2253	0.0979	432.3153	0.0856	448.3254	0.0016	466.5055	0.0041
418.2953	0.0669	432.3955	0.0076	449.2154	0.0022	467.3255	0.0080
418.3653	0.0013	433.2555	0.0526	449.3254	0.0095	467.3955	0.0020
418.4553	0.0148	433.3253	0.0019	449.3954	0.0083	468.3955	0.0020
419.1853	0.0066	434.1953	0.0213	450.2154	0.0733	469.3353	0.0076
419.3253	0.0438	434.2653	0.0150	450.3454	0.0457	469.4055	0.0016
420.2553	0.0287	434.3353	0.0279	450.5154	0.0057	470.4155	0.0111
420.3153	0.0216	434.3955	0.0027	451.2254	0.0177	470.5055	0.0050
421.2753	0.0511	435.2253	0.0516	451.3454	0.0138	471.2455	0.0142
422.2053	0.0822	435.3553	0.0176	452.4854	0.0031	471.3255	0.0011
422.3453	0.0474	435.4655	0.0013	453.3554	0.0124	471.3855	0.0063
422.4851	0.0025	436.3353	0.0303	454.2154	0.0502	472.2555	0.0263
423.1753	0.0399	437.1955	0.0313	454.4956	0.0074	472.3455	0.0351
423.2753	0.0179	437.2753	0.0071	455.2856	0.0146	473.2255	0.0038
424.2653	0.0850	437.3455	0.0011	455.3556	0.0033	473.3755	0.0040
424.3753	0.0216	438.2154	0.0328	456.2854	0.0259	474.3855	0.1072
425.2053	0.0115	438.3552	0.0119	457.2256	0.0024	475.3855	0.0106
425.2853	0.0725	439.2154	0.0248	457.3054	0.0149	476.3155	0.0502

Table A3.12 (continued). Mass data (*m/z* values and their relative intensities) for the DART-HRMS analysis of *L. virosa* tincture. Ten replicates of one sample were averaged where the corresponding spectrum appears in Figure 3.4B.

L. virosa tincture							
m/z	Rel. Int. %	*m/z*	Rel. Int. %	*m/z*	Rel. Int. %	*m/z*	Rel. Int. %
476.4055	0.0017	494.2256	0.0169	515.4257	0.0033	538.5058	0.0050
477.1957	0.0151	494.3656	0.0126	516.3457	0.0128	539.3658	0.0035
477.2955	0.0045	495.3056	0.0086	517.3257	0.0068	540.4358	0.0054
478.3255	0.0162	496.3256	0.0070	518.3457	0.0057	541.3457	0.0051
478.4355	0.0032	497.3256	0.0055	518.5157	0.0026	542.3357	0.0011
479.2154	0.0116	498.3256	0.0327	519.3457	0.0061	542.4157	0.0032
479.2956	0.0056	498.5356	0.0035	520.3356	0.0020	544.3857	0.0076
479.3754	0.0110	499.2156	0.0054	521.2156	0.0036	545.3257	0.0059
480.2454	0.0155	499.3256	0.0059	521.3356	0.0046	545.4057	0.0025
481.3254	0.0091	500.3455	0.0210	521.4056	0.0028	546.2857	0.0046
482.2154	0.0069	501.2257	0.0066	521.5256	0.0031	546.3157	0.0013
482.4756	0.0011	501.3255	0.0028	522.2656	0.0023	546.4557	0.0037
482.5256	0.0030	502.3355	0.0193	522.4256	0.0018	547.3357	0.0022
483.3156	0.0117	502.4155	0.0093	523.2456	0.0068	547.4657	0.0022
483.5356	0.0019	503.3255	0.0132	523.3256	0.0027	548.3459	0.0091
484.2254	0.0298	503.4155	0.0017	525.3358	0.0062	549.2757	0.0033
484.3956	0.0045	504.2857	0.0260	526.2056	0.0102	550.3757	0.0028
484.5456	0.0047	504.4555	0.0059	526.4156	0.0048	550.5657	0.0024
485.3354	0.0089	505.3255	0.0075	526.5658	0.0026	551.3759	0.0038
485.4056	0.0016	506.2555	0.0365	527.2156	0.0026	552.3859	0.0085
486.2256	0.0255	507.3155	0.0035	527.3456	0.0032	552.4959	0.0038
486.3254	0.0018	507.5155	0.0022	527.4256	0.0024	552.5857	0.0020
486.3854	0.1250	508.3557	0.0147	528.3458	0.0112	553.2157	0.0019
487.3854	0.0396	508.5257	0.0027	529.2658	0.0052	553.3157	0.0021
487.5256	0.0224	509.2255	0.0095	529.4156	0.0020	554.4957	0.0033
488.2556	0.0178	509.3255	0.0067	531.3158	0.0041	555.3859	0.0028
488.3956	0.0097	509.4055	0.0040	532.2258	0.0020	556.2459	0.0014
488.5456	0.0058	509.5257	0.0025	532.3358	0.0093	556.3659	0.0061
489.1956	0.0129	510.4157	0.0014	533.2707	0.0031	556.4359	0.0028
489.3756	0.0075	511.3257	0.0080	533.5258	0.0016	558.3759	0.0059
490.3254	0.0388	512.2057	0.0103	534.3656	0.0090	559.3359	0.0052
491.2156	0.0132	512.5757	0.0019	535.4458	0.0015	560.3459	0.0061
491.3056	0.0040	513.3357	0.0036	536.1858	0.0030	560.4159	0.0058
492.3356	0.0124	514.3357	0.0203	536.3158	0.0027	561.2359	0.0022
493.3056	0.0144	514.4157	0.0019	537.5058	0.0037	562.2558	0.0016
493.3856	0.0106	515.2357	0.0045	538.3158	0.0129	562.3458	0.0040

Table A3.12 (continued). Mass data (*m/z* values and their relative intensities) for the DART-HRMS analysis of *L. virosa* tincture. Ten replicates of one sample were averaged where the corresponding spectrum appears in Figure 3.4B.

|							
				***L. virosa* tincture**			
m/z	Rel. Int. %	*m/z*	Rel. Int. %	*m/z*	Rel. Int. %	*m/z*	Rel. Int. %
562.4358	0.0035	574.4460	0.0026	590.3959	0.0048	618.3960	0.0033
563.3558	0.0027	575.4260	0.0031	594.3759	0.0027	618.5260	0.0019
564.2758	0.0038	576.3458	0.0081	595.3559	0.0026	619.3860	0.0019
564.3558	0.0022	577.3458	0.0019	599.5061	0.0021	620.3260	0.0027
566.3758	0.0031	577.5258	0.0035	600.3861	0.0025	620.3960	0.0022
566.5358	0.0027	578.3660	0.0024	601.5259	0.0025	624.4759	0.0017
567.3858	0.0031	578.5260	0.0028	603.5360	0.0154	626.3359	0.0017
568.3858	0.0057	584.3959	0.0036	604.5458	0.0100	632.4161	0.0025
570.4058	0.0035	585.3859	0.0027	606.4060	0.0049	634.3261	0.0022
571.3958	0.0024	586.3959	0.0048	608.3760	0.0026	634.4661	0.0016
572.3758	0.0055	588.4059	0.0024	612.3560	0.0026	638.5761	0.0022
572.4458	0.0019	589.3959	0.0019	617.5160	0.0032		
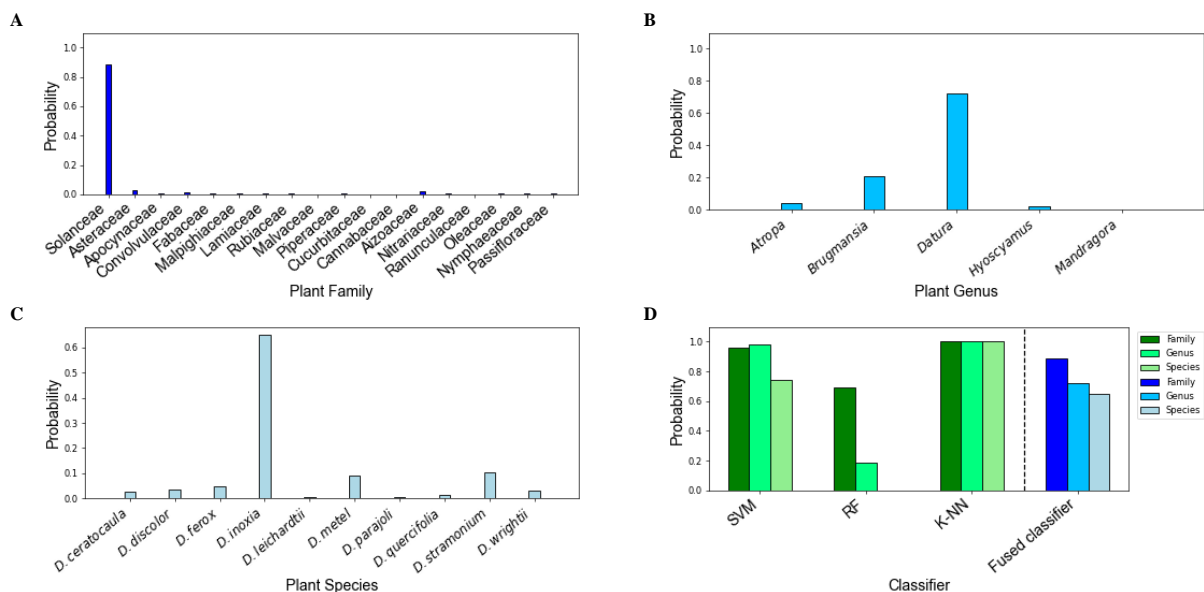
Figure A3.2 Identification result for *D. innoxia* seed analyzed by DART-HRMS in our laboratory. Panels A-C present three bar plots displaying the probabilities for identification of the family, genus and species levels acquired using the fused classifier; (D) Bar plot showing the probabilities associated with the identification of the family, genus, and species by the embedded classifiers (i.e., SVM, RF, K-NN and the fused classifier) in the hierarchical classification tree. DoPP identified the material as Solanceae, *Datura*, and *innoxia* with probabilities of 0.88, 0.72, and 0.65 for the averaged spectra of three DART-HRMS replicates.
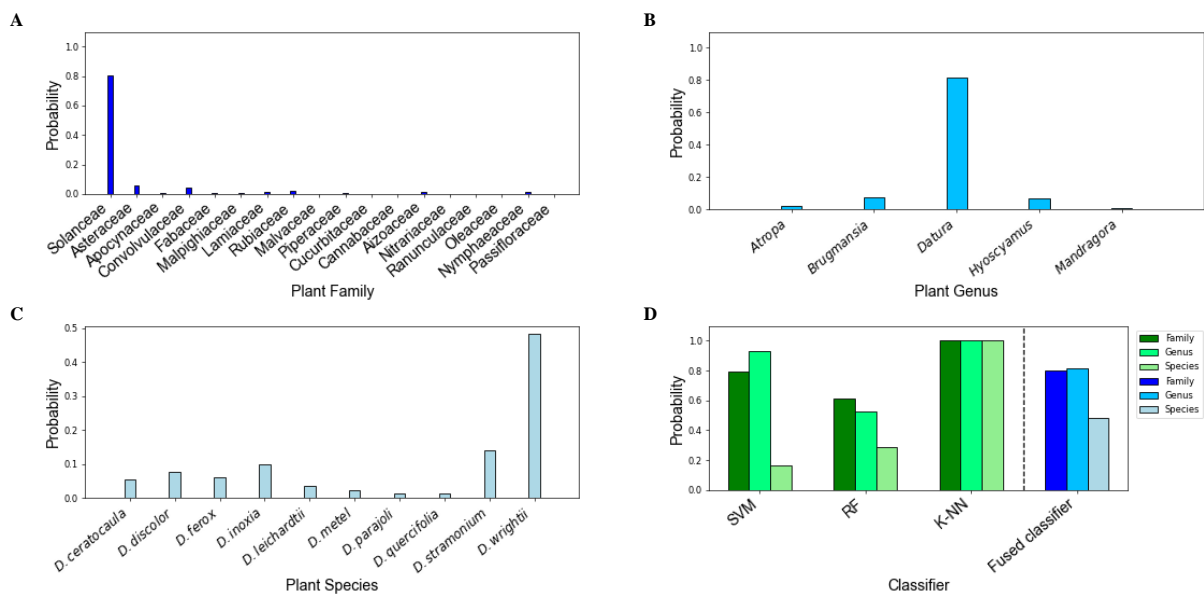
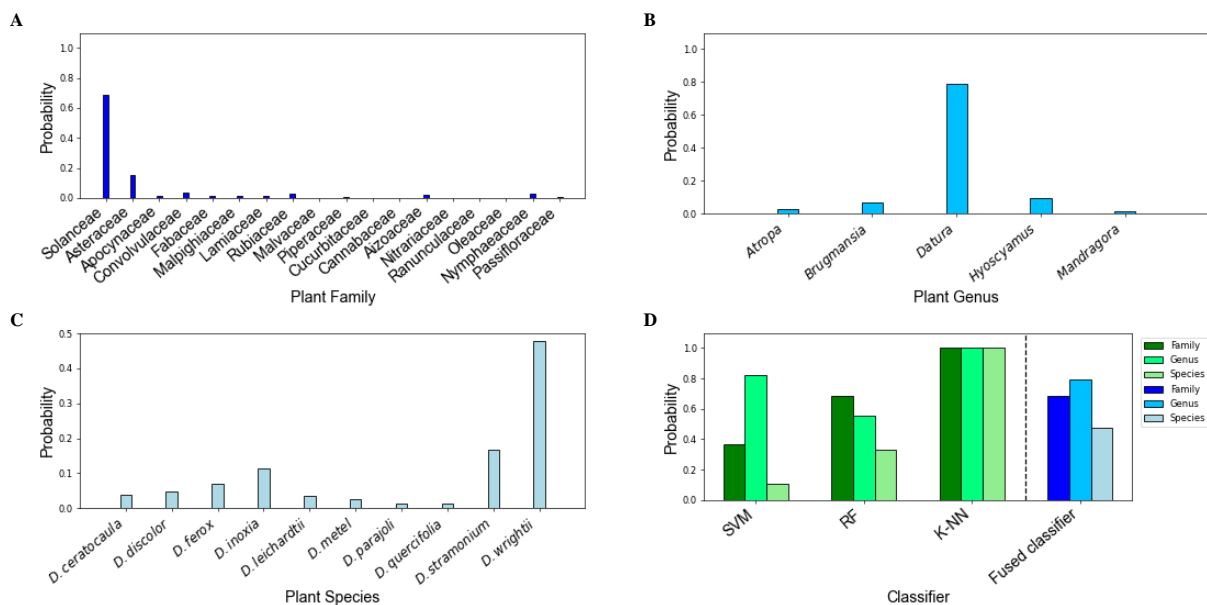**Figure A3.3** Identification result for *D. wrightii* seed analyzed by DART-HRMS in our laboratory. Panels A-C present three bar plots displaying the probabilities for identification of the family, genus and species levels respectively, acquired using the fused classifier; (D) Bar plot showing the probabilities associated with the identification of the family, genus, and species by the embedded classifiers (i.e., SVM, RF, K-NN and the fused classifier) in the hierarchical classification tree. DoPP identified the material as Solanceae, *Datura*, and *wrightii* with probabilities of 0.80, 0.82, and 0.48 for the averaged spectra of three DART-HRMS replicates.
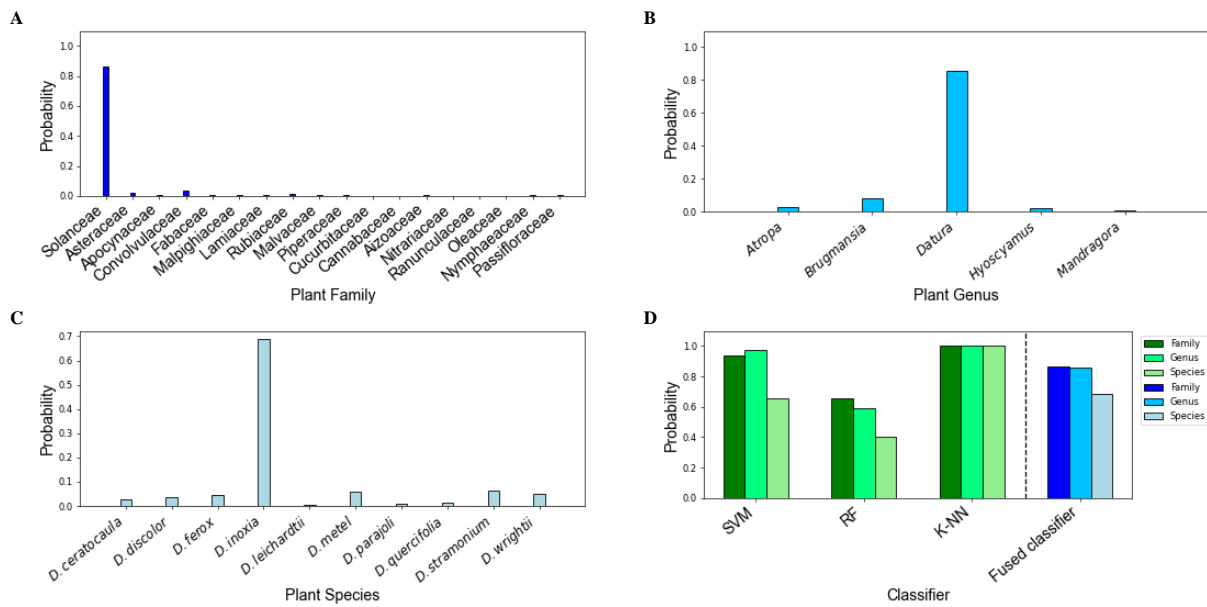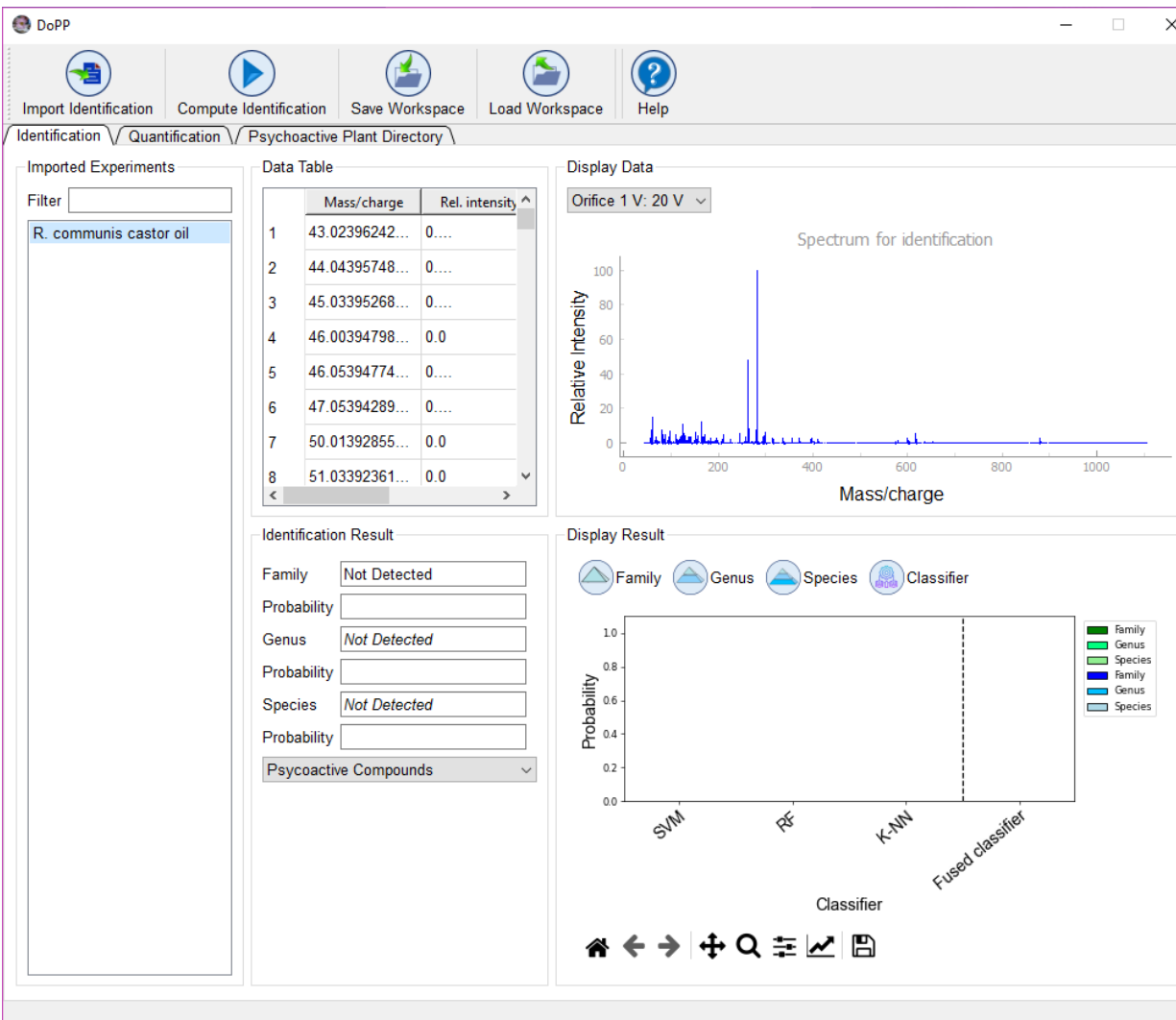
Figure A3.4 Identification result for *D. innoxia* seed analyzed by DART-HRMS in the ETEC laboratory. Panels A-C present three bar plots displaying the probabilities for identification of the family, genus and species levels acquired using the fused classifier; (D) Bar plot showing the probabilities associated with the identification of the family, genus, and species by the embedded classifiers (i.e., SVM, RF, K-NN and fused classifier) in the hierarchical classification tree. DoPP identified the material as Solanceae, *Datura*, and *innoxia* with probabilities of 0.86, 0.86, and 0.69 for the averaged spectra of three replicates.

Figure A3.5 Identification result for *D. wrightii* seed analyzed by DART-HRMS in the ETEC laboratory. Panels A-C present three bar plots displaying the probabilities for identification of the family, genus and species levels acquired using the fused classifier; (D) Bar plot showing the probabilities associated with the identification of the family, genus, and species by the embedded classifiers (i.e., SVM, RF, K-NN and fused classifier) in the hierarchical classification tree. DoPP identified the material as Solanceae, *Datura*, and *wrightii* with probabilities of 0.68, 0.79, and 0.48 for the averaged spectra of three replicates.

284

Figure A3.6 Identification result for *R. communis* castor oil (a species that is not represented in the database) analyzed by DART-HRMS. DoPP detected the material as an outlier and the sample is classified as "Not Detected".
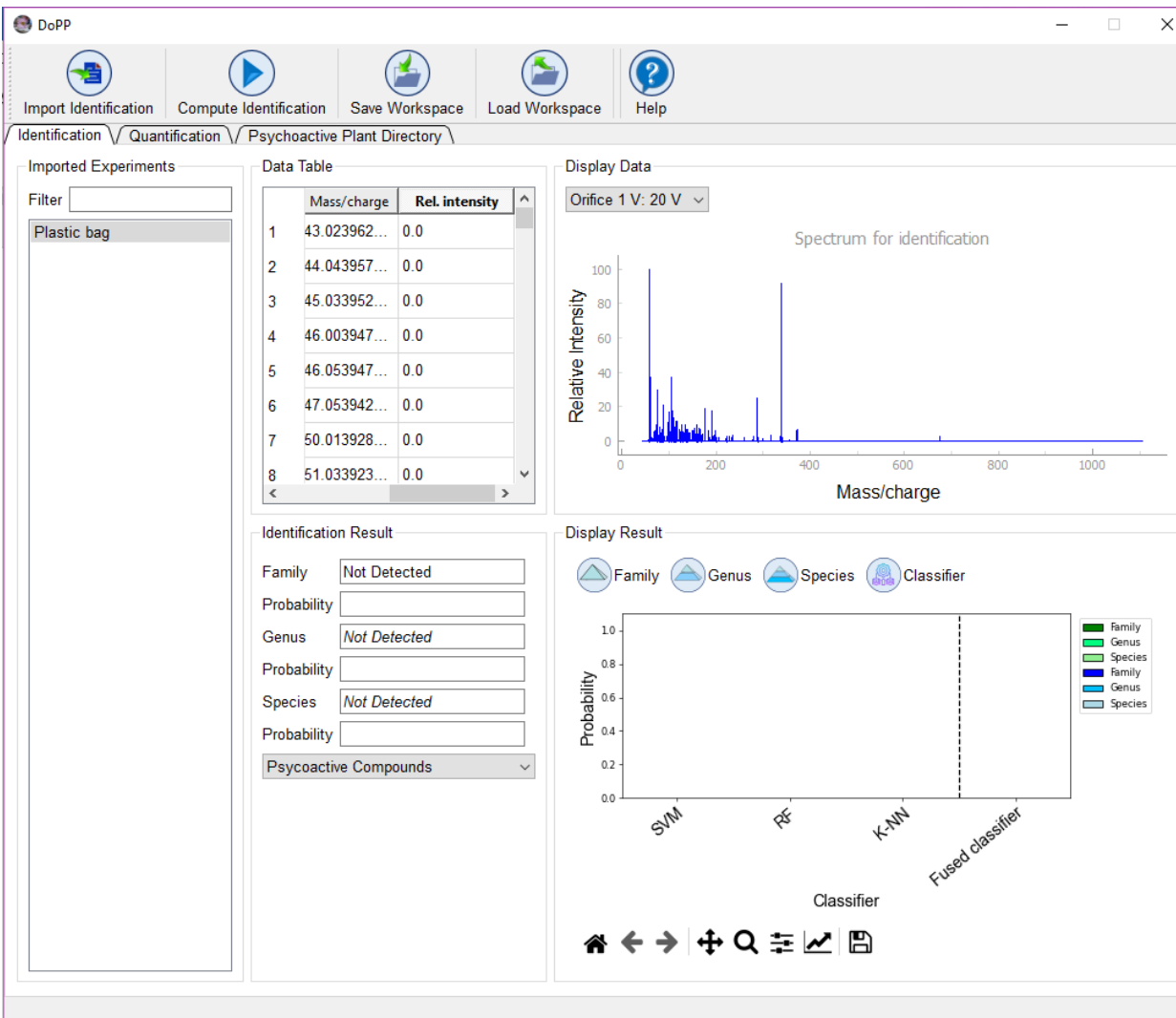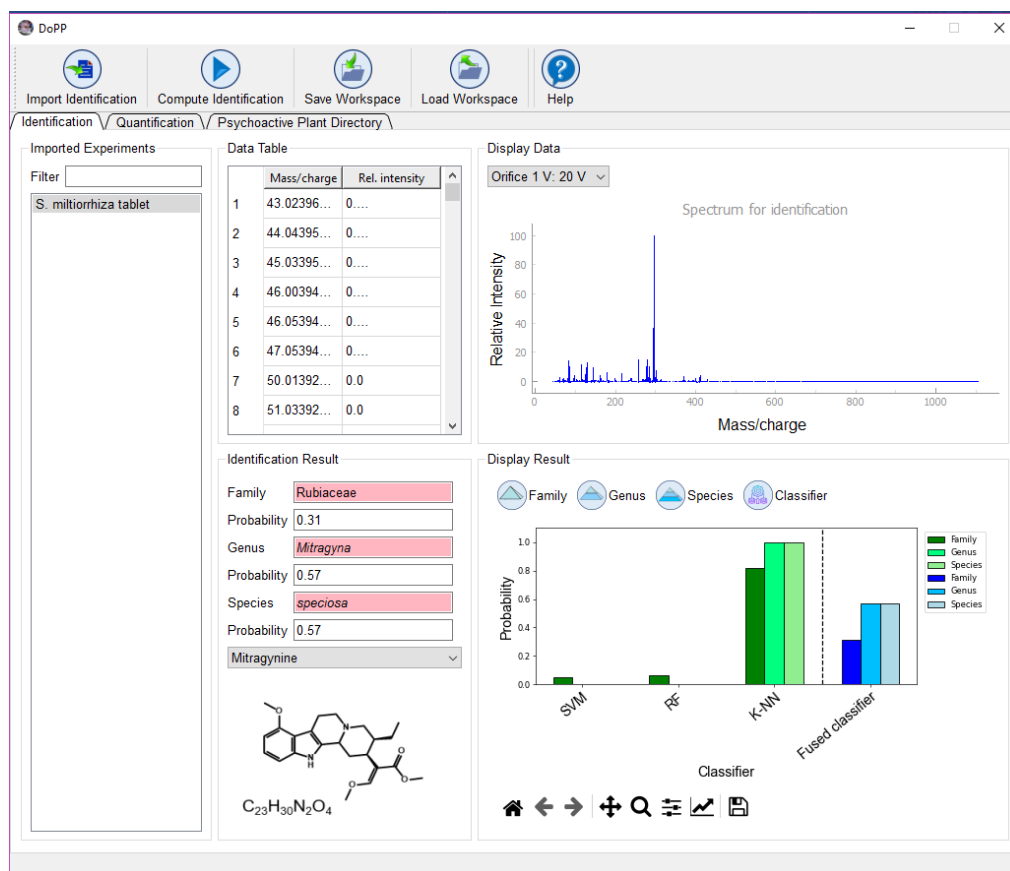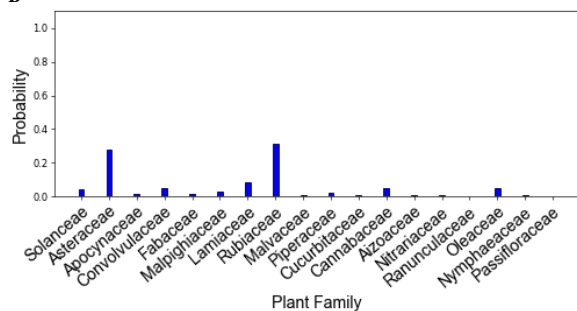
Figure A3.7 Identification result for plastic bag sample analyzed by DART-HRMS. DoPP detected the material as an outlier and presented the result as "Not Detected".
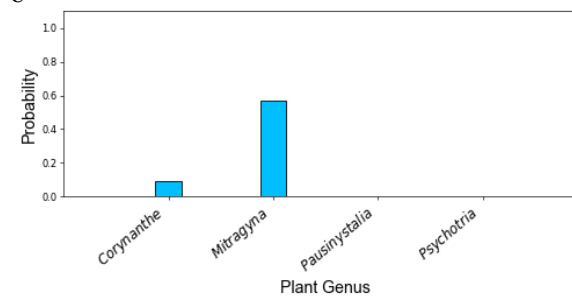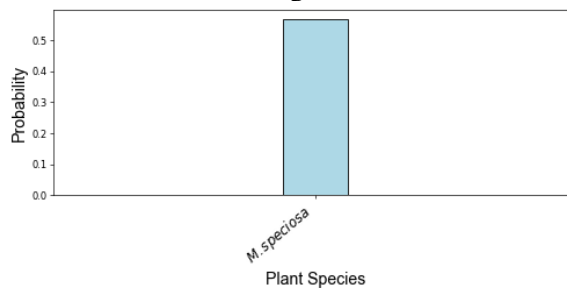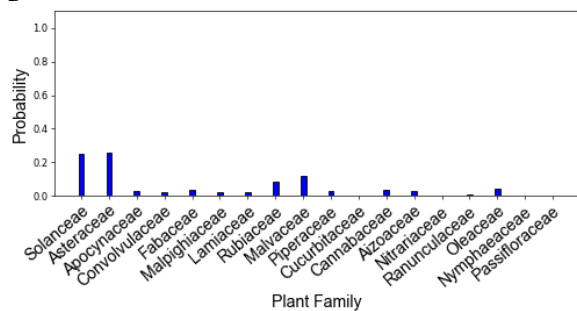
Figure A3.8 Identification result for a *Salvia miltiorrhiza* tablet (a species that is not represented in the database) analyzed by DART-HRMS. Panels B-D present three bar plots displaying the probabilities for identification of the family, genus and species levels acquired using the fused classifier. While DoPP shows a computed result in each level, the material is suggested to be non-assigned based on the appearance of the pink background color, since the family probability is 0.31, which is lower than the computed threshold (0.45) for Rubiaceae class.
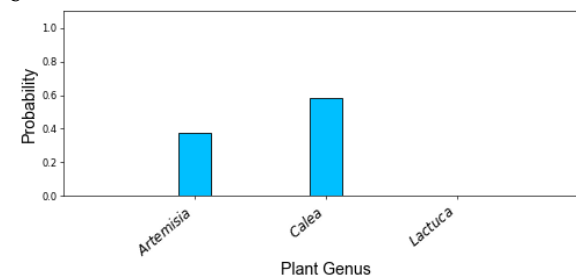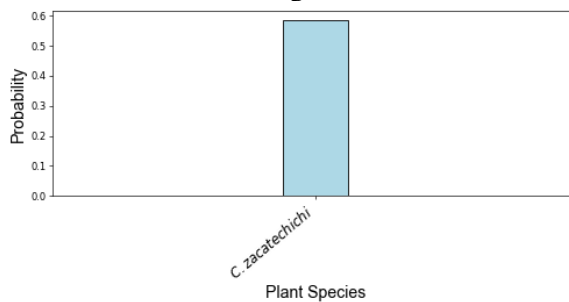
Figure A3.9 (A) Identification result for a *D. wrightii* spectrum that was not corrected for background following analysis by DART-HRMS. Panels B-D present three bar plots displaying the probabilities for identification of the family, genus and species levels acquired using the fused classifier. While DoPP shows a computed result at each level, it nevertheless suggests that the sample is unclassified, which is indicated by the appearance of the pink background color. This is because the probability for the family classification is lower than the threshold of 0.45 for the Asteraceae class (with a value of 0.26).

Table A4.1 Compounds detected via TD-GC-MS analysis of the *Dalbergia spp.* analyzed in this study. The first column presents the DART-HRMS measured masses of the 112 features utilized for SVM model creation. The "Molecular Formula" column lists the formula derived from the corresponding high-resolution mass shown in column 1. In the "Compound" column, the tentatively identified compound name (based on mass spectral fragmentation pattern matching using the NIST EI-MS database) is listed. The species listed in the fourth column represent those in which the indicated mass was detected in at least one individual in the listed species.

Measured Mass	Molecular Formula	Compound	Species
47.0511	$[C_2H_6O + H]^+$	Dimethyl ether	*D. occulta, D. oliveri, D. spruceana, D maritima, D. cochininchensis, D. maritima, D. occulta, D. melanoxylon, D. cearensis, D. madagascariensis, D. melanoxylon, D. latifolia, D. cearensis, D. stevensonii, D. normandii* and *D. decipularis*
57.0690	$[C_4H_8 + H]^+$	Cyclobutane	*D. stevensonii* and *D. normandii*
59.0482	$[C_3H_6O + H]^+$	Acetone	*D. baronii, D. cearensis, D. decipularis, D. stevensonii, D. cearensis, D. tucurensis, D. spruceana, D. maritima, D. occulta, D. madagascariensis, D. latifolia, D. melanoxylon, D. nigra, D. normandii, D. purprascens,* and *D. retusa*
59.0633	$[C_2H_6N_2 + H]^+$	Azomethane	*D. latifolia* and *D. retusa*
59.0928	-	-	-
59.1425	-	-	-
60.0644	$C_2H_8N_2^{+\cdot}$	1,2-Dimethylhydrazine	*D. cochinchinensis* and *D. decipularis*
61.0636	$[C_3H_8O + H]^+$	Isopropanol	*D. cochinchinensis*
61.0761	$[C_2H_8N_2 + H]^+$	1,2-Dimethylhydrazine	*D. cochinchinensis* and *D. decipularis*
65.0596	-	-	-
67.0713	-	-	-
69.0945	-	-	-
71.0863	$[C_5H_{10} + H]^+$	1-Pentene	*D. madagascariensis* and *D. melanoxylon*
73.0654	$[C_4H_8O + H]^+$	Isobutyraldehyde	*D. cearensis, D. decipularis,* and *D. stevensonii*
73.0900	-	-	-
74.0612	$[C_3H_7NO + H]^+$	Dimethylformamide	*D. baronii* and *D. occulta*
75.0310	-	-	-

Table A4.1 (continued). Compounds detected via TD-GC-MS analysis of the *Dalbergia spp.* analyzed in this study. The first column presents the DART-HRMS measured masses of the 112 features utilized for SVM model creation. The "Molecular Formula" column lists the formula derived from the corresponding high-resolution mass shown in column 1. In the "Compound" column, the tentatively identified compound name (based on mass spectral fragmentation pattern matching using the NIST EI-MS database) is listed. The species listed in the fourth column represent those in which the indicated mass was detected in at least one individual in the listed species.

Measured Mass	Molecular Formula	Compound	Species
75.0500	$[C_3H_6O_2 + H]^+$	Acetol	*D. baronii, D. cearensis, D. cochinchinensis, D. decipularis, D. stevensonii, D. tucurensis, D. spruceana, D. latifolia, D. maritima, D. madagascariensis, D. melanoxylon, D. nigra, D. normandii, D. oliveri, D. purprascens,* and *D. retusa*
76.0904	-	-	-
81.0717	$[C_6H_8 + H]^+$	1,4-Cyclohexadiene	*D. latifolia*
83.0848	$[C_6H_{10} + H]^+$	(*E,E*)-2,4-Hexadiene	*D. cearensis* and *D. decipularis*
83.1002	-	-	-
87.1684	-	-	-
89.0604	$[C_4H_8O_2 + H]^+$	Butyric Acid	*D. stevensonii*
90.2040	-	-	-
91.0457	-	-	-
93.0355	-	-	-
93.0710	$[C_7H_8 + H]^+$	Toluene	*D. baronii, D. cearensis, D. decipularis, D. tucurensis, D. spruceana, D. maritima, D. cochinchinensis, D. oliveri, D. occulta, D. madagascariensis, D. latifolia, D. melanoxylon, D. normandii, D. purprascens, D. retusa* and *D. nigra*
93.0893	-	-	-
93.1108	-	-	-
93.1259	-	-	-
93.1364	-	-	-
94.0671	-	-	-
97.0289	$[C_5H_4O_2 + H]^+$	3-Furaldehyde	*D. baronii, D. cearensis, D. stevensonii, D. tucurensis, D. spruceana, D. maritima, D. cochinchinensis, D. oliveri, D. occulta, D.*

Table A4.1 (continued). Compounds detected via TD-GC-MS analysis of the *Dalbergia spp.* analyzed in this study. The first column presents the DART-HRMS measured masses of the 112 features utilized for SVM model creation. The "Molecular Formula" column lists the formula derived from the corresponding high-resolution mass shown in column 1. In the "Compound" column, the tentatively identified compound name (based on mass spectral fragmentation pattern matching using the NIST EI-MS database) is listed. The species listed in the fourth column represent those in which the indicated mass was detected in at least one individual in the listed species.

Measured Mass	Molecular Formula	Compound	Species
			madagascariensis, D. latifolia, D. melanoxylon, D. normandii, D. purprascens, D. retusa, D. nigra and *D. decipularis*
97.0768	-	-	-
101.0602	-	-	-
103.0740	$[C_5H_{10}O_2 + H]^+$	Pentanoic Acid	*D. spruceana, D. madagascariensis, D. baronii, D. latifolia, D. melanoxylon* and *D. nigra*
107.0482	$[C_7H_6O + H]^+$	Benzaldehyde	*D. baronii, D. cearensis, D. decipularis, D. stevensonii, D. tucurensis, D. spruceana, D. maritima, D. cochinchinensis, D. oliveri, D. madagascariensis, D. latifolia, D. melanoxylon, D. normandii, D. purprascens, D. retusa* and *D. nigra*
109.1102	-	-	-
117.0358	-	-	-
117.0460	-	-	-
117.0856	-	-	-
127.0365	$[C_6H_6O_3 + H]^+$	Maltol	*D. occulta, D. madagascariensis, D. baronii, D. latifolia, D. normandii, D. retusa* and *D. nigra*
127.1223	-	-	-
128.1142	-	-	-
133.0632	$[C_9H_8O + H]^+$	(*E*)-Cinnamaldehyde	*D. baronii, D. cearensis, D. decipularis, D. stevensonii, D. tucurensis, D. spruceana, D. maritima, D. cochinchinensis, D. oliveri, D. occulta, D. madagascariensis, D. latifolia, D. melanoxylon, D. normandii, D. retusa* and *D. nigra*
133.0735	$[C_8H_8N_2 + H]^+$	5-Methylbenzimidazole	*D. madagascariensis* and *D. occulta*
133.1972	-	-	-
133.2250	-	-	-

Table A4.1 (continued). Compounds detected via TD-GC-MS analysis of the *Dalbergia spp.* analyzed in this study. The first column presents the DART-HRMS measured masses of the 112 features utilized for SVM model creation. The "Molecular Formula" column lists the formula derived from the corresponding high-resolution mass shown in column 1. In the "Compound" column, the tentatively identified compound name (based on mass spectral fragmentation pattern matching using the NIST EI-MS database) is listed. The species listed in the fourth column represent those in which the indicated mass was detected in at least one individual in the listed species.

Measured Mass	Molecular Formula	Compound	Species
135.0975	-	-	-
135.2787	-	-	-
136.0285	-	-	-
137.1189	-	-	-
137.1717	-	-	-
140.0446	$C_7H_8O_3^{+\bullet}$	3-Methoxycatechol	*D. baronii*, *D. cearensis*, *D. stevensonii*, *D. tucurensis*, *D. spruceana*, *D. maritima*, *D. cochinchinensis*, *D. oliveri*, *D. occulta*, *D. madagascariensis*, *D. latifolia*, *D. melanoxylon*. *D. normandii*, and *D. retusa*
141.1643	-	-	-
149.0441	-	-	-
149.1239	-	-	-
149.1350	-	-	-
151.1430	-	-	-
157.1264	$[C_9H_{16}O_2 + H]^+$	*trans*-3-Methyl-4-octanolide	*D. stevensonii*, *D. tucurensis*, *D. maritima*, *D. melanoxylon*, *D. purpascens*, and *D. nigra*
158.1294	$C_9H_{18}O_2^{+\bullet}$	Nonanoic acid	*D. stevensonii*, *D. tucurensis*, *D. cearensis*, *D. spruceana*, *D. maritima*, *D. cochinchinensis*, *D. occulta*, *D. madagascariensis*, *D. latifolia*, *D. melanoxylon*, *D. baronii* and *D. retusa*
159.1244	-	-	-
163.1281	-	-	-
167.0929	-	-	-
167.1136	-	-	-
167.1785	-	-	-
167.2440	-	-	-

Table A4.1 (continued). Compounds detected via TD-GC-MS analysis of the *Dalbergia spp.* analyzed in this study. The first column presents the DART-HRMS measured masses of the 112 features utilized for SVM model creation. The "Molecular Formula" column lists the formula derived from the corresponding high-resolution mass shown in column 1. In the "Compound" column, the tentatively identified compound name (based on mass spectral fragmentation pattern matching using the NIST EI-MS database) is listed. The species listed in the fourth column represent those in which the indicated mass was detected in at least one individual in the listed species.

Measured Mass	Molecular Formula	Compound	Species
169.1297	-	-	-
169.1437	-	-	-
171.1521	-	-	-
172.1404	-	-	-
174.1593	-	-	-
175.0952	-	-	-
177.1127	-	-	-
177.2715	-	-	-
178.1723	-	-	-
185.1574	-	-	-
188.1585	-	-	-
191.0655	-	-	-
191.1789	-	-	-
194.0935	-	-	-
195.1384	-	-	-
195.1652	-	-	-
195.1759	$[C_{13}H_{22}O + H]^+$	Geranylacetone	*D. decipularis* and *D. latifolia*
199.3238	-	-	-
205.1950	$[C_{15}H_{24} + H]^+$	β-Bisabolene	*D. cearensis*, *D. decipularis*, *D. stevensonii*, *D. tucurensis*, *D. baronii*, *D. madagascariensis*, *D. melanoxylon* and *D. purprascens*
205.2799	-	-	-
208.1097	-	-	-
221.1921	$[C_{15}H_{24}O + H]^+$	Humulenol II	*D. cearensis* and *D. baronii*
221.2777	-	-	-

Table A4.1 (continued). Compounds detected via TD-GC-MS analysis of the *Dalbergia spp.* analyzed in this study. The first column presents the DART-HRMS measured masses of the 112 features utilized for SVM model creation. The "Molecular Formula" column lists the formula derived from the corresponding high-resolution mass shown in column 1. In the "Compound" column, the tentatively identified compound name (based on mass spectral fragmentation pattern matching using the NIST EI-MS database) is listed. The species listed in the fourth column represent those in which the indicated mass was detected in at least one individual in the listed species.

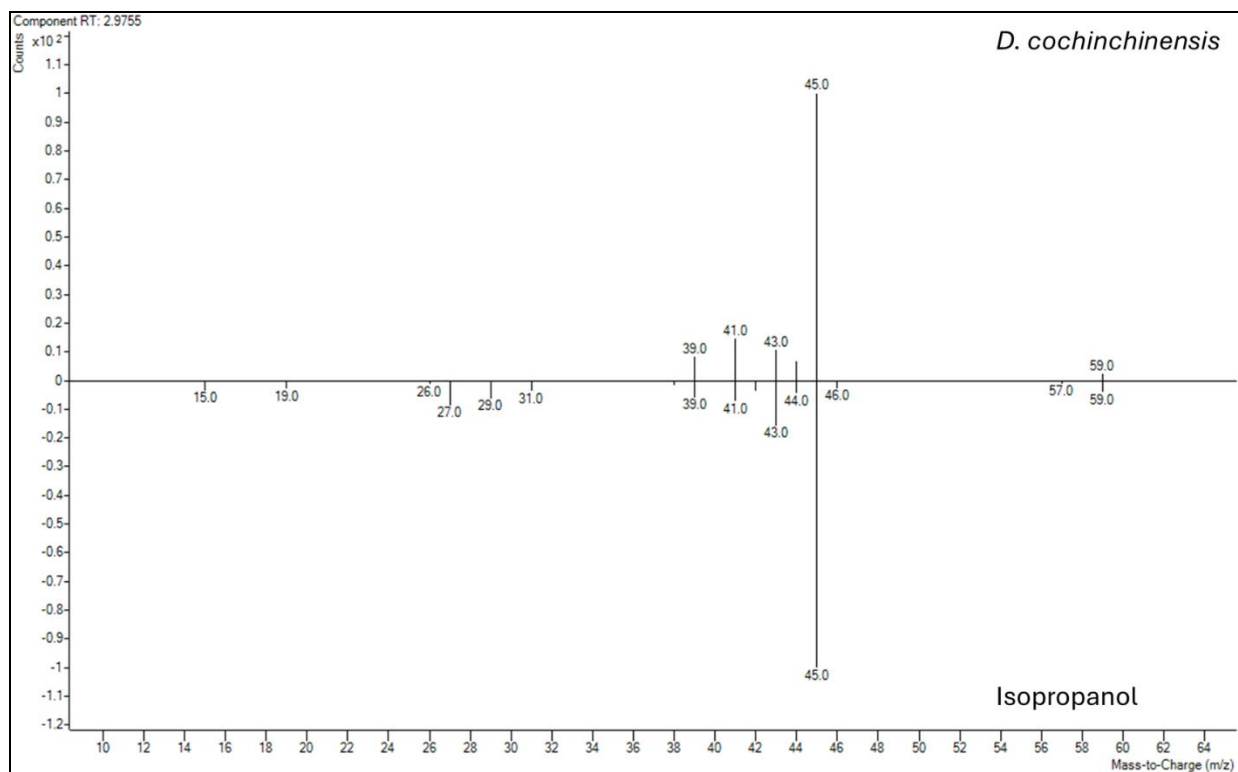| Measured Mass	Molecular Formula	Compound	Species
222.1846	-	-	-
222.2238	-	-	-
223.0606	-	-	-
225.1225	-	-	-
227.2774	$[C_{16}H_{34} + H]^+$	Hexadecane	*D. decipularis, D. stevensonii, D. cearensis, D. tucurensis, D. spruceana, D. maritima, D. cochinchinensis, D. oliveri, D. madagascariensis, D. latifolia, D. baronii, D. melanoxylon, D. purprascens,* and *D. nigra*
233.1612	-	-	-
233.1755	-	-	-
258.1060	-	-	-
277.2295	-	-	-
277.3491	-	-	-
277.5766	-	-	-
278.3430	-	-	-
279.2224	-	-	-
294.3706	-	-	-
294.5362	-	-	-
313.2388	-	-	-
371.1072	-	-	-
371.1186	-	-	-
371.3912	-	-	-
371.4867	-	-	-
372.1120	-	-	-

Figure A4.1 Head-to-tail plots showing the comparison of the EI mass spectral fragmentation pattern of isopropanol (bottom) from the NIST mass spectral library to that of the EI mass spectrum from *D. cochinchinensis* (top).
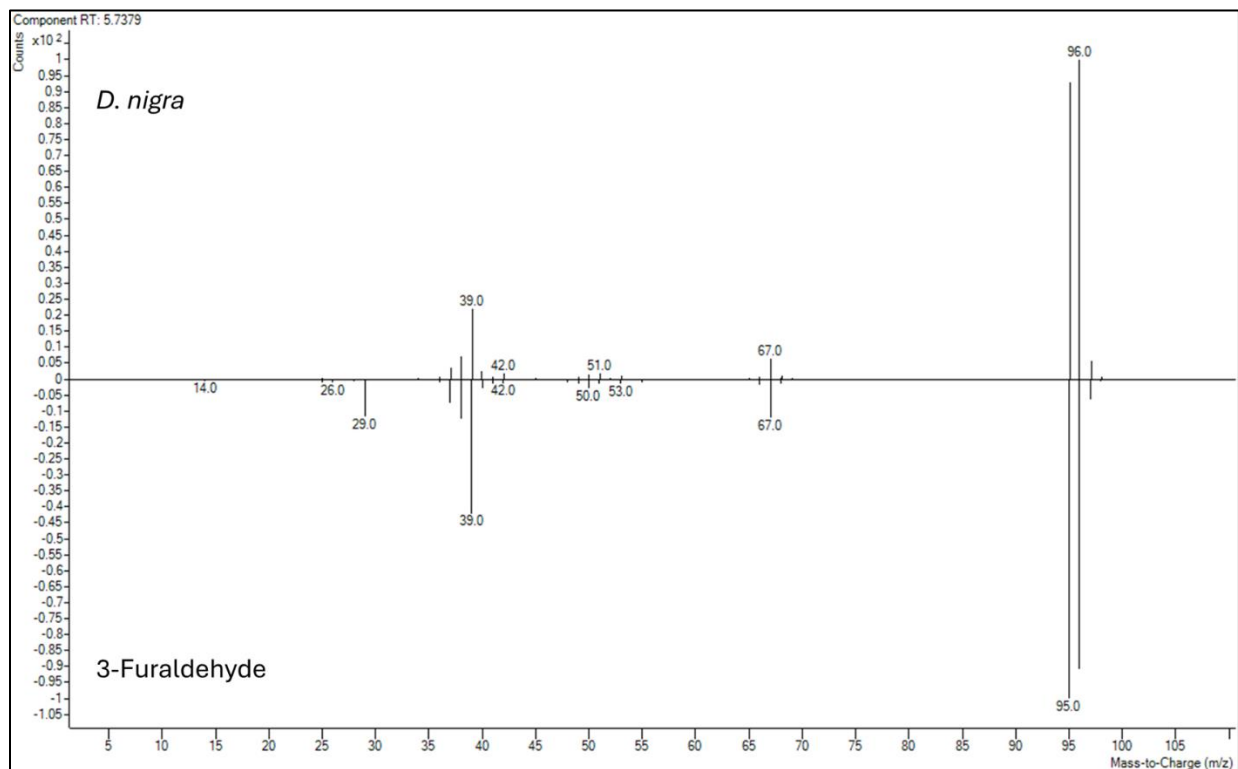

Figure A4.2 Head-to-tail plots showing the comparison of the EI mass spectral fragmentation pattern of 3-Furaldehydel (bottom) from the NIST mass spectral library to that of the EI mass spectrum from *D. nigra* (top).